



ADVANCES IN THE MOLECULAR BIOLOGY OF TRYPANOSOMATID PATHOGENS

EDITED BY: Gustavo Benaim, Alberto Enrique Paniz Mondolfi,
Juan David Ramírez and Emilia Mia Sordillo
PUBLISHED IN: *Frontiers in Cellular and Infection Microbiology*



frontiers

Frontiers eBook Copyright Statement

The copyright in the text of individual articles in this eBook is the property of their respective authors or their respective institutions or funders. The copyright in graphics and images within each article may be subject to copyright of other parties. In both cases this is subject to a license granted to Frontiers.

The compilation of articles constituting this eBook is the property of Frontiers.

Each article within this eBook, and the eBook itself, are published under the most recent version of the Creative Commons CC-BY licence.

The version current at the date of publication of this eBook is CC-BY 4.0. If the CC-BY licence is updated, the licence granted by Frontiers is automatically updated to the new version.

When exercising any right under the CC-BY licence, Frontiers must be attributed as the original publisher of the article or eBook, as applicable.

Authors have the responsibility of ensuring that any graphics or other materials which are the property of others may be included in the CC-BY licence, but this should be checked before relying on the CC-BY licence to reproduce those materials. Any copyright notices relating to those materials must be complied with.

Copyright and source acknowledgement notices may not be removed and must be displayed in any copy, derivative work or partial copy which includes the elements in question.

All copyright, and all rights therein, are protected by national and international copyright laws. The above represents a summary only. For further information please read Frontiers' Conditions for Website Use and Copyright Statement, and the applicable CC-BY licence.

ISSN 1664-8714

ISBN 978-2-88971-788-0

DOI 10.3389/978-2-88971-788-0

About Frontiers

Frontiers is more than just an open-access publisher of scholarly articles: it is a pioneering approach to the world of academia, radically improving the way scholarly research is managed. The grand vision of Frontiers is a world where all people have an equal opportunity to seek, share and generate knowledge. Frontiers provides immediate and permanent online open access to all its publications, but this alone is not enough to realize our grand goals.

Frontiers Journal Series

The Frontiers Journal Series is a multi-tier and interdisciplinary set of open-access, online journals, promising a paradigm shift from the current review, selection and dissemination processes in academic publishing. All Frontiers journals are driven by researchers for researchers; therefore, they constitute a service to the scholarly community. At the same time, the Frontiers Journal Series operates on a revolutionary invention, the tiered publishing system, initially addressing specific communities of scholars, and gradually climbing up to broader public understanding, thus serving the interests of the lay society, too.

Dedication to Quality

Each Frontiers article is a landmark of the highest quality, thanks to genuinely collaborative interactions between authors and review editors, who include some of the world's best academicians. Research must be certified by peers before entering a stream of knowledge that may eventually reach the public - and shape society; therefore, Frontiers only applies the most rigorous and unbiased reviews.

Frontiers revolutionizes research publishing by freely delivering the most outstanding research, evaluated with no bias from both the academic and social point of view. By applying the most advanced information technologies, Frontiers is catapulting scholarly publishing into a new generation.

What are Frontiers Research Topics?

Frontiers Research Topics are very popular trademarks of the Frontiers Journals Series: they are collections of at least ten articles, all centered on a particular subject. With their unique mix of varied contributions from Original Research to Review Articles, Frontiers Research Topics unify the most influential researchers, the latest key findings and historical advances in a hot research area! Find out more on how to host your own Frontiers Research Topic or contribute to one as an author by contacting the Frontiers Editorial Office: frontiersin.org/about/contact

ADVANCES IN THE MOLECULAR BIOLOGY OF TRYPANOSOMATID PATHOGENS

Topic Editors:

Gustavo Benaim, Fundación Instituto de Estudios Avanzados (IDEA), Venezuela
Alberto Enrique Paniz Mondolfi, Icahn School of Medicine at Mount Sinai, United States

Juan David Ramírez, Rosario University, Colombia

Emilia Mia Sordillo, Icahn School of Medicine at Mount Sinai, United States

Citation: Benaim, G., Mondolfi, A. E. P., Ramírez, J. D., Sordillo, E. M., eds. (2021). Advances in the Molecular Biology of Trypanosomatid Pathogens. Lausanne: Frontiers Media SA. doi: 10.3389/978-2-88971-788-0

Table of Contents

- 05 Editorial: Advances in the Molecular Biology of Trypanosomatid Pathogens: New Strategies Against Ancient Enemies**
Gustavo Benaim, Alberto E. Paniz-Mondolfi, Juan David Ramírez and Emilia Mia Sordillo
- 08 Genomic Diversification, Structural Plasticity, and Hybridization in Leishmania (Viannia) braziliensis**
Luz H. Patino, Marina Muñoz, Lissa Cruz-Saavedra, Carlos Muskus and Juan David Ramírez
- 25 Study on the Occurrence of Genetic Exchange Among Parasites of the Leishmania mexicana Complex**
Roman Telittchenko and Albert Descoteaux
- 36 Modulation of IMD, Toll, and Jak/STAT Immune Pathways Genes in the Fat Body of Rhodnius prolixus During Trypanosoma rangeli Infection**
Agustín Rolandelli, Adeisa E. C. Nascimento, Leticia S. Silva, Rolando Rivera-Pomar and Alessandra A. Guarneri
- 50 Prevalence of Genetically Complex Leishmania Strains With Hybrid and Mito-Nuclear Discordance**
Hirotomo Kato, Abraham G. Cáceres, Eduardo A. Gomez, Ahmed Tabbabi, Daiki Mizushima, Daisuke S. Yamamoto and Yoshihisa Hashiguchi
- 58 Repeat-Driven Generation of Antigenic Diversity in a Major Human Pathogen, Trypanosoma cruzi**
Carlos Talavera-López, Louisa A. Messenger, Michael D. Lewis, Matthew Yeo, João Luís Reis-Cunha, Gabriel Machado Matos, Daniella C. Bartholomeu, José E. Calzada, Azael Saldaña, Juan David Ramírez, Felipe Guhl, Sofía Ocaña-Mayorga, Jaime A. Costales, Rodion Gorchakov, Kathryn Jones, Melissa S. Nolan, Santuza M. R. Teixeira, Hernán José Carrasco, Maria Elena Bottazzi, Peter J. Hotez, Kristy O. Murray, Mario J. Grijalva, Barbara Burleigh, Edmundo C. Grisard, Michael A. Miles and Björn Andersson
- 72 All Roads Lead to Cytosol: Trypanosoma cruzi Multi-Strategic Approach to Invasion**
Gabriel Ferri and Martin M. Edreira
- 89 The Leishmania donovani LDBPK_220120.1 Gene Encodes for an Atypical Dual Specificity Lipid-Like Phosphatase Expressed in Promastigotes and Amastigotes; Substrate Specificity, Intracellular Localizations, and Putative Role(s)**
Amalia Papadaki, Olympia Tziouvara, Anastasia Kotopouli, Petrina Koumarianou, Anargyros Doukas, Pablo Rios, Isabelle Tardieux, Maja Köhn and Haralabia Boleti
- 111 Involvement of Leishmania Phosphatases in Parasite Biology and Pathogeny**
Anita Leocadio Freitas-Mesquita, André Luiz Araújo Dos-Santos and José Roberto Meyer-Fernandes

- 121** *Characterization and Follow-Up of Trypanosoma cruzi Natural Populations Refractory to Etiological Chemotherapy in Oral Chagas Disease Patients*
Arturo Muñoz-Calderón, Zoraida Díaz-Bello, Belkisyolé Alarcón de Noya, Oscar O. Noya-González and Alejandro G. Schijman
- 133** *Guide RNA Repertoires in the Main Lineages of Trypanosoma cruzi: High Diversity and Variable Redundancy Among Strains*
Fanny Rusman, Noelia Floridia-Yapur, Nicolás Tomasini and Patricio Diosque
- 147** *Development of a Fluorescent Assay to Search New Drugs Using Stable tdTomato-Leishmania, and the Selection of Galangin as a Candidate With Anti-Leishmanial Activity*
María Fernanda García-Bustos, Agustín Moya Álvarez, Cecilia Pérez Brandan, Cecilia Parodi, Andrea Mabel Sosa, Valeria Carolina Buttazzoni Zuñiga, Oscar Marcelo Pastrana, Paula Manghera, Pablo Alejandro Peñalva, Jorge Diego Marco and Paola Andrea Barroso
- 160** *The Complete Mitochondrial DNA of Trypanosoma cruzi: Maxicircles and Minicircles*
Francisco Callejas-Hernández, Alfonso Herreros-Cabello, Javier del Moral-Salmoral, Manuel Fresno and Núria Gironès
- 171** *Molecular and Functional Characteristics of DNA Polymerase Beta-Like Enzymes From Trypanosomatids*
Edio Maldonado, Sebastian Morales-Pison, Fabiola Urbina and Aldo Solari



Editorial: Advances in the Molecular Biology of Trypanosomatid Pathogens: New Strategies Against Ancient Enemies

Gustavo Benaim^{1,2*}, Alberto E. Paniz-Mondolfi^{1,3}, Juan David Ramírez⁴ and Emilia Mía Sordillo^{3,5}

¹ Laboratorio de Señalización Celular y Bioquímica de Parásitos, Instituto de Estudios Avanzados, Caracas, Venezuela,

² Instituto de Biología Experimental, Facultad de Ciencias, Universidad Central de Venezuela, Caracas, Venezuela,

³ Department of Pathology, Molecular, and Cell-Based Medicine, Icahn School of Medicine at Mount Sinai, New York, NY,

United States, ⁴ Grupo de Investigaciones Microbiológicas-UR (GIMUR), Departamento de Biología, Facultad de Ciencias Naturales, Universidad del Rosario, Bogotá, Colombia, ⁵ Institute for Health Sciences, Mount Sinai St Luke's & Mount Sinai West, New York, NY, United States

Keywords: trypanosomatids, Chagas, leishmaniasis, treatment, pathogenesis, genetics

Editorial on the Research Topic

Advances in the Molecular Biology of Trypanosomatid Pathogens

OPEN ACCESS

Edited and reviewed by:

Jeroen P. J. Saeij,
University of California, Davis,
United States

*Correspondence:

Gustavo Benaim
gbenaim@gmail.com

Specialty section:

This article was submitted to
Parasite and Host,
a section of the journal
Frontiers in Cellular and Infection
Microbiology

Received: 14 September 2021

Accepted: 20 September 2021

Published: 06 October 2021

Citation:

Benaim G, Paniz-Mondolfi AE,
Ramírez JD and Sordillo EM (2021)
Editorial: Advances in the Molecular
Biology of Trypanosomatid
Pathogens: New Strategies Against
Ancient Enemies.
Front. Cell. Infect. Microbiol. 11:777008.
doi: 10.3389/fcimb.2021.777008

INTRODUCTION

The Trypanosomatidae emerged as successful parasites of invertebrate and vertebrate hosts hundreds of millions of years ago. (Stevens et al., 2001) Infections by these important human pathogens cause diseases such as sleeping sickness or African trypanosomiasis (*Trypanosoma brucei*), Chagas disease (*Trypanosoma cruzi*) and cutaneous/visceral leishmaniasis that affect millions of people world-wide (Freitas Lidani et al. WHO-Leishmania, 2021). Once almost exclusively considered neglected tropical diseases, transmission of these infections is now recognized in economically-privileged countries such as the United States, which is endemic for McIlwee et al., 2018; WHO-Leishmania) as well as Chagas disease (Paniz-Mondolfi et al., 2020). The complex and varied life cycles of the Trypanosomatidae, plus their ability to inhabit diverse ecological niches and to infect a wide range of vertebrate and invertebrate hosts have contributed to their persistence and expansion despite efforts toward elimination by the scientific community, global agencies, and governments.

The contributions in this Research Topic utilize genomic, proteomic, transcriptomic and metabolomic methods in combination with traditional epidemiology to provide new insights into the biological mechanisms influencing disease spectrum and progression, pathogenesis, and potential new treatment approaches.

Disease transmission, clinical presentation and progression, and susceptibility to treatment are dependent on the pathogenicity, virulence, tissue tropism, and potential drug sensitivity of the infecting parasite. Several articles in this Research Topic demonstrate the genomic variability among currently circulating strains causing clinical disease and provide evidence for the existence of newly recognized hybrid strains. Luz H. Patino and colleagues assessed the genomic variability of circulating clinical isolates of *L. brasiliensis*, the agent of spundia, from different regions of South

America, comparing findings from Columbia and Bolivia to publicly available sequences for isolates from Brazil. Analysis of whole nuclear and mitochondrial maxicircle sequences demonstrated important genomic diversity and evidence of hybridization, indicating genomic plasticity in *Leishmania* that may be tied to clinical outcome. In their review, Hiroto Kato and colleagues summarize their recent country-wide studies in Ecuador and Peru; genetic analyses of kinetoplast and nuclear DNA using PCR-RFLP reveal the extent and distribution of *Leishmania* spp. causing infections in these countries. Notably, these authors also describe previously unknown hybrid species that appear to be associated with more severe clinical presentations and altered transmission dynamics. Evidence for genetic exchange in *Leishmania* parasites *in vitro* is provided by Roman Telittchenko and Albert Descoteaux, using promastigote lines of *L. amazonensis* and *L. mexicana* harboring integrated or episomal drug-resistance markers. Genetic exchange is described in both axenic promastigote cultures and infected macrophages. However, growth of the resulting hybrids was not sustained in subcultures, suggesting the recombination was unstable. Variability that can be associated with clinical presentation and outcome is also recognized within *T. cruzi* lineages. In their report, Callejas-Hernández et al. present results from sequencing of mitochondrial maxicircle and minicircle DNA from *T. cruzi* trypomastigotes of the Y and Bug2148 strains, finding conserved motifs in the maxicircles, but unexpected heterogeneity among minicircle sequences. Rusman and colleagues used deep-sequencing of the hypervariable regions of the minicircle kDNAs to highlight a previously undescribed repertoire of guide RNAs in the main lineages of *Trypanosoma cruzi*, demonstrating highly divergent gRNA repertoires among different parasite lineages, and even within those lineages. In addition to variable gRNA class redundancy, these authors found that gRNA classes of different strains may edit mitochondrial mRNAs from other lineages, suggesting a potential biparental inheritance of minicircles. Future studies are needed to shed light on the physiological implications of these findings.

Maldonado et al. reviewed the molecular mechanisms of DNA repair and the functional properties of DNA polymerase Beta-Like enzymes from trypanosomatids. Polymerase beta seems to play a role in kDNA replication as it associates with kinetoplast antipodal sites in some developmental stages in trypanosomatids and are relevant for cell replication. The authors summarized the main characteristics of trypanosomatid polymerase beta like enzymes and the further need to unveil key structural features for a comprehensive understanding of their role in mammal infection.

Understanding biochemical and metabolic events that influence parasite development in the vector and host are also essential to understanding the complexities underlying parasite life cycle, vector competency, host range, and their influence on the spectrum of clinical disease and outcomes. In the comprehensive review from the Meyer-Fernandes group (Freitas-Mesquita et al.), the expression of protein phosphatases in *Leishmania* parasites was revisited. Phosphatases play a role in adaptation to nutrient starvation during parasite passage through the sandfly midgut, and

are important to parasite virulence, *via* modulation of host cytokine production and impairment of the lytic potential of macrophages. Papadaki et al. address the differential gene expression of atypical lipid phosphatases (ALPs), which play a major role in the cell differentiation among *Leishmania* parasites. Focusing on the expression of LDBPK_220120.1 (ALP) in *L. donovani*, the cause of visceral leishmaniasis, these authors report the presence of its gene product in promastigotes and amastigotes, dual specificity for P-Tyr and PI(3)P, the regulatory influence of temperature and pH shifts, and its possible role in the transition between parasite stages to amastigotes in the mammalian cell.

To elucidate the potential impact of the regulation of parasite development in the insect vector on transmission to the mammalian host, Rolandelli and colleagues assessed immune pathways in *Rhodnius prolixus*, the triatomine vector of *Trypanosoma rangeli*. These authors detected differential modulation of the insect IMD, toll, and JAK-STAT pathways in insects with or without hemolymph infection in addition to gut infection, presenting an intriguing potential role for transmission to the mammalian host.

Once in a mammalian host, the parasite must establish infection. Ferri and Edreira reviewed the multi-strategic approach by *T. cruzi* to invasion, addressing the several strategies this parasite has developed to disrupt the host cell signaling machinery in order to gain access to the host cell cytoplasm. The authors highlight the role of the parasitophorous vacuole, from which the parasite escapes to the cytoplasm, and wherein differentiation and replication of the parasite take place. In recent years, ingestion of food contaminated by metacyclic trypomastigotes has triggered outbreaks of acute infection of Chagas disease by oral transmission. Muñoz-Calderón et al. characterized the genetic constitution of natural *T. cruzi* populations in individuals who had failed treatment with benznidazole 9 years earlier for infection acquired during an Oral Chagas Disease (OCD) outbreak at a rural school in Venezuela. Observed decreases in parasite loads and population variability indicated by Pre- and Post-Treatment intra-TcI *T. cruzi* clade I (TcI) diversity suggested the decrease might be a consequence of both natural evolution of the acute infection to the chronic phase and persistence of refractory populations due to treatment selection. One means used by *T. cruzi* to evade host immune response is antigenic variation.

Carlos Talavera-López and colleagues utilized high coverage single-molecule and deep sequence data to analyze genomes from 34 *T. cruzi* clade I (TcI) isolates and clones from different geographic locations against the Sylvio X10/1 TcI reference genome sequence, finding an unusual organizational structure for the region encoding surface molecules. These authors describe synteny of the core genomic regions, but flanked by unique, highly plastic multigene family clusters with abundant interspersed retrotransposons, apparently involved in recombination and generation of antigenic variation. Their comparative genomic analysis of the cohort of clinical TcI strains revealed multiple cases of such recombination events involving surface molecule genes, providing new insights into *T. cruzi* population structure and evasion of the host immune response.

Treatment of trypanosomatid infections remains an ongoing challenge. García-Bustos and colleagues have developed a rapid screening assay utilizing *Leishmania (Leishmania) amazonensis* expressing a red fluorescent protein encoded by pIRISAT/tDTomato to screen the anti-leishmania anti-parasitic activity of novel potential therapeutic compounds, and have identified the flavonoid galganin as a potential prospect for further investigation. Because of its low cost and speed, this new assay represents a cost-effective approach for resource-constrained countries for the identification of new agents or to detect antimonial resistance prior to treatment.

Advances in our knowledge of the molecular biology of the Trypanosomatidae will continue to enhance our understanding of parasite ecology, evolution, and pathogenesis, and enable our search for potential chemotherapeutic agents and immunomodulatory approaches to treatment and management of these neglected diseases.

REFERENCES

- McIlwee, B. E., Weis, S. E., and Hosler, (2018). Incidence of Endemic Human Cutaneous Leishmaniasis in the United States. *JAMA Dermatol.* 154, 1032–1039. doi: 10.1001/jamadermatol.2018.2133
- Paniz Mondolfi, A. E., Madigan, R., Perez-Garcia, L., and Sordillo, E. M. (2020). Chagas Disease Endemism in the United States. *Clin. Infect. Dis.* 70, 717–718. doi: 10.1093/cid/ciz465
- Stevens, J. R., Noyes, H. A., Schofield, C. J., and Gibson, W. (2001). The Molecular Evolution of Trypanosomatidae. *Adv. Parasitol.* 48, 1–56. doi: 10.1016/s0065-308x(01)48003-1
- WHO-Leishmania. (2021). *Leishmania*. Available at: <https://www.who.int/data/gho/data/indicators/indicator-details/GHO/status-of-endemicity-of-cutaneous-leishmaniasis>.

AUTHOR CONTRIBUTIONS

All authors listed have made a substantial, direct, and intellectual contribution to the work and approved it for publication.

FUNDING

This study was partially funded by the UK Research and Innovation, Global Challenges Research Fund (EP/T003782/1), the University of Glasgow Small Grants Fund and Scottish Funding Council.

ACKNOWLEDGMENTS

We thank the authors of this special issue for their valuable contributions.

Conflict of Interest: The authors declare that the research was conducted in the absence of any commercial or financial relationships that could be construed as a potential conflict of interest.

Publisher's Note: All claims expressed in this article are solely those of the authors and do not necessarily represent those of their affiliated organizations, or those of the publisher, the editors and the reviewers. Any product that may be evaluated in this article, or claim that may be made by its manufacturer, is not guaranteed or endorsed by the publisher.

Copyright © 2021 Benaim, Paniz-Mondolfi, Ramirez and Sordillo. This is an open-access article distributed under the terms of the Creative Commons Attribution License (CC BY). The use, distribution or reproduction in other forums is permitted, provided the original author(s) and the copyright owner(s) are credited and that the original publication in this journal is cited, in accordance with accepted academic practice. No use, distribution or reproduction is permitted which does not comply with these terms.



Genomic Diversification, Structural Plasticity, and Hybridization in *Leishmania (Viannia) braziliensis*

Luz H. Patino¹, Marina Muñoz¹, Lissa Cruz-Saavedra¹, Carlos Muskus²
and Juan David Ramírez^{1*}

¹ Grupo de Investigaciones Microbiológicas-UR (GIMUR), Departamento de Biología, Facultad de Ciencias Naturales, Universidad del Rosario, Bogotá, Colombia, ² Programa de Estudio y Control de Enfermedades Tropicales (PECET), Facultad de Medicina, Universidad de Antioquia, Medellín, Colombia

OPEN ACCESS

Edited by:

Herbert Leonel de Matos Guedes,
Federal University of Rio de Janeiro,
Brazil

Reviewed by:

Jose M. Requena,
Autonomous University of Madrid,
Spain
Isabel Mauricio,
New University of Lisbon, Portugal
Sarah Forrester,
University of York, United Kingdom

*Correspondence:

Juan David Ramírez
juand.ramirez@urosario.edu.co

Specialty section:

This article was submitted to
Parasite and Host,
a section of the journal
Frontiers in Cellular and Infection
Microbiology

Received: 10 July 2020

Accepted: 28 September 2020

Published: 16 October 2020

Citation:

Patino LH, Muñoz M,
Cruz-Saavedra L, Muskus C and
Ramírez JD (2020) Genomic
Diversification, Structural Plasticity,
and Hybridization in *Leishmania*
(*Viannia*) *braziliensis*.
Front. Microbiol. 10:582192.
doi: 10.3389/fcimb.2020.582192

Leishmania (Viannia) braziliensis is an important *Leishmania* species circulating in several Central and South American countries. Among *Leishmania* species circulating in Brazil, Argentina and Colombia, *L. braziliensis* has the highest genomic variability. However, genomic variability at the whole genome level has been only studied in Brazilian and Peruvian isolates; to date, no Colombian isolates have been studied. Considering that in Colombia, *L. braziliensis* is a species with great clinical and therapeutic relevance, as well as the role of genetic variability in the epidemiology of leishmaniasis, we analyzed and evaluated intraspecific genomic variability of *L. braziliensis* from Colombian and Bolivian isolates and compared them with Brazilian isolates. Twenty-one genomes were analyzed, six from Colombian patients, one from a Bolivian patient, and 14 Brazilian isolates downloaded from public databases. The results obtained of Phylogenomic analysis showed the existence of four well-supported clades, which evidenced intraspecific variability. The whole-genome analysis revealed structural variations in the somy, mainly in the Brazilian genomes (clade 1 and clade 3), low copy number variations, and a moderate number of single-nucleotide polymorphisms (SNPs) in all genomes analyzed. Interestingly, the genomes belonging to clades 2 and 3 from Colombia and Brazil, respectively, were characterized by low heterozygosity (~90% of SNP loci were homozygous) and regions suggestive of loss of heterozygosity (LOH). Additionally, we observed the drastic whole genome loss of heterozygosity and possible hybridization events in one genome belonging to clade 4. Unique/shared SNPs between and within the four clades were identified, revealing the importance of some of them in biological processes of *L. braziliensis*. Our analyses demonstrate high genomic variability of *L. braziliensis* in different regions of South America, mainly in Colombia and suggest that this species exhibits striking genomic diversity and a capacity of genomic hybridization; additionally, this is the first study to report whole-genome sequences of Colombian *L. braziliensis* isolates.

Keywords: DNA-seq, genomic variability, copy number variations, single-nucleotide polymorphisms, *Leishmania braziliensis*

INTRODUCTION

Leishmania (*Viannia*) *braziliensis* is the most important *Leishmania* species associated with cases of cutaneous leishmaniasis and muco-cutaneous leishmaniasis in several Central and South American countries (Ramirez et al., 2016; Patino et al., 2017). This species is characterized by its ability to cause distinct forms of tegumentary leishmaniasis in humans (Jirmanus et al., 2012; Meireles et al., 2017) and animals (De Oliveira et al., 2013; Brilhante et al., 2019), and also for its variable infectivity, virulence, and response to anti-leishmanial therapy (Rego et al., 2018; Patino et al., 2019a). In addition, it is considered a zoonotic parasite circulating in a wide range of mammalian and vector host species (Kuhls et al., 2013; Roque and Jansen, 2014), characteristics that can contribute to the generation and maintenance of genetic diversity within the species (Cupolillo et al., 2003; Bruna et al., 2019).

Several nuclear and mitochondrial DNA markers as well as different molecular techniques have been used with the purpose to evaluate inter- and intra-specific genetic variability of New/ Old world *Leishmania* species, such as *L. major*, *L. infantum*, *L. donovani*, *L. tropica*, *L. braziliensis*, *L. peruviana*, *L. guyanensis*, and *L. panamensis* (Cupolillo et al., 2003; Nolder et al., 2007; Kuhls et al., 2013; Restrepo et al., 2013; Marco et al., 2015; Restrepo et al., 2015; Fotouhi-Ardakani et al., 2016; Cysne-Finkelstein et al., 2018; Quaresma et al., 2018; Banu et al., 2019). This has suggested high intra-specific variability, especially for *L. braziliensis* from Brazil (Marlow et al., 2014), Argentina (Marco et al., 2015) and Colombia (Herrera et al., 2017). This variability is probably related to sand fly vector(s) and/or animal reservoir(s) involved in transmission cycles (Cupolillo et al., 2003) and with different clinical manifestations (Quaresma et al., 2018; Rego et al., 2018). However, few studies have examined this variability in whole genomes of New-World *Leishmania* species, such as *L. braziliensis* (Valdivia et al., 2015; Urrea et al., 2018; Bruna et al., 2019; Restrepo et al., 2019), because most of the research has focused on revealing the genome diversity of Old-World *Leishmania* species (Downing et al., 2011; Imamura et al., 2016; Ghouila et al., 2017; Franssen et al., 2020).

Two recent studies have used whole genome sequencing to reveal the genetic variability of *L. braziliensis*. One of them, published by Bruna et al. (2019) highlighted the tremendous genetic variability (~95,000–~131,000 SNPs) in 10 clinical isolates from forested and urbanized environments of Brazil and the existence of three distinct phylogenetic groups including one isolate from a forested environment that was characterized by moderate aneuploidy and reduced heterozygosity. The other study by Broeck et al. (2020) investigated the nuclear and mitochondrial genomes of *L. braziliensis* isolates from Peru and demonstrated genetic diversification and subsequent hybridization, this study highlights the origin of Andean/Amazonian *Leishmania* species (*L. peruviana* and *L. braziliensis*) and describes a possible meiotic recombination event between them, with uniparental inheritance of maxicircles but biparental inheritance of minicircles, which may be crucial for survival of the parasite in the wild. Considering the

close relatedness between *L. braziliensis* and *L. peruviana*, some authors have conducted genomic comparative analysis, which have identified a great number of interspecific SNP/indel differences between them as well as the presence of different gene and chromosome copy number variations supporting the classification of both organisms as closely related but distinct species (Valdivia et al., 2015; Broeck et al., 2020).

Despite these findings, knowledge about the genomic variability of *L. braziliensis* in other South American regions, such as Colombia, is limited. Different studies describe a high frequency of this species in Colombia; this being more frequent in rural (Perez-Franco et al., 2016; Patino et al., 2017) compared with urban populations (Ramirez et al., 2016; Ovalle-Bracho et al., 2019). In addition, Colombia has a large number of sand fly vectors and animal reservoirs, which are involved in the transmission cycle of the parasite (Valderrama-Ardila et al., 2010; Ferro et al., 2015). Considering the public health importance of leishmaniasis caused by *L. braziliensis* in Colombia and the role of genetic variability of the parasite in the epidemiology of the disease, the objective of this study was to perform a comprehensive analysis of whole genome sequencing (DNA-seq) to evaluate phylogenomic relationships among six Colombian clinical isolates and one Bolivian clinical isolate. We also determined phylogenomic relationships and genomic plasticity among these isolates and 14 publicly available *L. braziliensis* genomes from Brazil in terms of genome plasticity (chromosomes/genes) and single point mutations.

METHODS

Ethics Statement

All procedures were approved by the Ethics committee of the Universidad de Antioquia (number VRI3445/2010) in accordance with resolution number 36836. The patients included into the study read and signed the informed consent.

Population of Study

Twenty-one whole genomes were analyzed in this study, including six from Colombian clinical isolates and one Bolivian clinical isolate from patients who were attending in the 'Programa de Estudio y Control de Enfermedades Tropicales (PECET), Medellín-Colombia'. Also, 14 *L. braziliensis* genomic sequences reads, from Brazilian isolates publicly available from the DDBJ/ENA/GenBank database (<http://www.ebi.ac.uk/ena>) under accession codes PRJNA292004 (Alves-Ferreira et al., 2015) and PRJNA475480 (Bruna et al., 2019) were downloaded for respective comparison. The dataset was downloaded using the tools described in: <https://github.com/EnzoAndree/getENA>. The seven isolates included in this study were obtained from patients from different regions of Colombia and one from Bolivia, with nodular or ulcerative cutaneous lesions. The sampling was performed before patients underwent anti-Leishmanial therapy.

Parasite Culture and Identification

The parasites obtained from six Colombian clinical isolates and the Bolivian isolate were cultured axenically in Schneider's insect medium, which was supplemented with 10% (v/v) fetal bovine serum; the cultures were maintained at 26°C with 5% CO₂ as describe previously (Patino et al., 2020). Once the parasites were in late logarithmic growth phase, were recovered by centrifugation and submitted to DNA extraction. High Pure PCR Template Preparation Kit (Roche Life Science) was used for DNA extraction in accordance with the manufacturer's instructions. Later the concentration, quality and integrity of DNA were determined. To verify the quality of DNA, each sample was divided in two groups, the first used for species identification and the second for whole-genome sequencing.

Cytochrome b proteins (*Cytb*) and heat shock protein (*Hsp70*) were the genes selected to species identification through Sanger sequencing, as has been described previously (Ramirez et al., 2016; Patino et al., 2017). The amplification products were purified with EXOSAP (Affymetrix, USA) and sequenced using the dideoxy-terminal method in an automated capillary sequencer (AB3730; Applied Biosystem). Subsequently, sequences were subjected to a BLASTn similarity search for *Leishmania* sequences deposited in GenBank (Ramirez et al., 2016). Those isolates identified as *L. braziliensis* were selected for whole-genome sequencing.

Genomic Sequencing

HiSeq X-Ten system (Illumina) was used to sequence the whole-genome DNA, later mate-paired libraries were built and finally subjected to paired-end sequencing (2 × 150-bp read length producing a median coverage at least of 40x per sample). Reads with adapter contamination, >10% uncertain nucleotides, or >50% low-quality nucleotides (base quality < 5) were discarded (Yan et al., 2013).

DNA Mapping

The paired-end Illumina reads of six Colombian clinical isolates, one Bolivian clinical isolate and of the fourteen Brazilian genomes (data downloaded from European Nucleotide Archive) were mapped to the reference MHOMBR75/M2904_2019 *L. braziliensis* genome sequence assembly (<http://tritrypdb.org>) using the SMALT program (version 0.7.4) (www.sanger.ac.uk/resources/software/smalt/). Exhaustive search option (–x and –y of 0.8), a sliding step of 3 and a reference hash index of 13 bases were the parameters using during the mapping. To prevent the mapping of non-*Leishmania* reads to the reference sequences, we used an identity threshold of $\gamma = 0.8$. SAMtools (version 0.1.18) and Picard (version 1.85) were used to no-mapping read exclusion, sorting, file merging and elimination of PCR duplicates (Imamura et al., 2016). The reads corresponding to the mitochondrial genome were extracted and assembled under the same pipeline described for nuclear genome but using maxicircle sequence from novel long read assembly of *L. braziliensis* M2904 (available in tritrypdb).

Phylogenomic Analysis

SNPs alignments from whole nuclear and mitochondrial (maxicircle) genomes unphased and phased (see “Phasing of heterozygous SNP sites” section), were used to evaluate the phylogenomic relationship among *L. braziliensis* isolates and between each sequence generated by each isolate during the phasing. FastTree double precision version 2.1.10. (Price et al., 2009) was used to build a based-maximum-likelihood phylogenetic tree. The robustness of the nodes was evaluated using the Bootstrap method (BT, with 1,000 replicates). The obtained tree was visualized using the interactive tool Interactive Tree Of Life V4 (<http://itol.embl.de>) (Letunic and Bork, 2019). To detect recombination signatures in the analyzed genomes, phylogenetic networks were built in SplitsTree5 (Huson and Bryant, 2006) using the Neighbor-Net method. We included MHOMBR75/M2904_2019 *L. braziliensis* as genome sequence (REF) and used as outgroup the *L. guyanensis* genome assembly from European Nucleotide Archive accession number SRR8179913 (Lguy_SRR8179913) (<http://www.ebi.ac.uk/ena>) and the *L. panamensis* genome assembly from TriTrypDB <http://tritrypdb.org>: LPPSC1 (LpW).

Somy Analysis and Gene Copy Number Variations

The chromosomal somy was estimated calculating initially the median read depth of each chromosome (di). Positions with read depth of >1 standard deviation were removed and the di recalculated. Later, we calculated the median depth (dm) of whole genome (35 chromosomes) and the somy (S-value) of each chromosome, for that we used the formula previously described $S = 3 \times di/dm$ (Patino et al., 2019a). The ranges of somy (mono-di-tri-tetra and penta somy) were defined, as previously described (Dumetz et al., 2017).

To evaluate the gene copy number variations (CNVs), we calculated and related the average haploid depth per gene without somy effect (d_{HG}) and the full cell depth with somy effect (d_{FG}) using the formula: ($d_{FG} = S \times d_{HG}$). The statistical significance used in this study was set at a z-score cutoff of >2 and an adjusted p-value (Student's t-test) of <0.05. Heatmaps were created using the Heatmap3 package in R (Zhao et al., 2014). Finally, we used the Gene Ontology enrichment analyses from TriTrypDB tools (<http://tritrypdb.org>) to evaluate the genes with CNVs. *P-values* were adjusted for multiple testing with Benjamini-Hochberg method with a false-discovery rate (FDR) of <0.05. The GO terms were submitted to REVIGO (Supek et al., 2011).

SNP Estimations and Analysis

Initially, the reads were mapped to the reference MHOMBR75/M2904_2019 *L. braziliensis* genome sequence assembly using the SMALT program (version 0.7.4), different options of this program were used to search random mapping of multiple hit reads and obtained optimal alignments. The merging and sorting of bam files and marking duplicated reads were implemented with the Picard program (version 1.85) (<http://broadinstitute.github.io/picard/>) as described previously (Dumetz et al., 2017).

The SNPs were called with the population-based Unified Genotyper method in the Genome Analysis Toolkit (GATK) (version 3.4; <https://software.broadinstitute.org/gatk/>), where SNPs were called among all the samples simultaneously. Later, we realigned around indels to remove these and retrieved only the SNPs. GATK Variant Filtration was used to filter Low-quality SNPs, according to the following criteria: $QD < 2.0 \parallel MQ < 40 \parallel FS > 60.0 \parallel ReadPosRankSum < -8.0$. The SNP quality cutoff was set at 3000. Later, the Integrative Genomic Viewer program (IGV_2_3_47) was used to visualize all SNPs identified and the SnpEff program (version v4.1) to classify the SNPs based on their functional impact (Dumetz et al., 2017). Once the SNPs were independently detected, these were extracted from nuclear and mitochondrial alignments of *L. braziliensis* genomes using snp-sites program (Page et al., 2016). Based on the total number of SNPs and using snp-distans program (<https://github.com/tseemann/snp-distans>), we generated a pairwise distance matrix; the results obtained were graphically represented. Lastly, we selected the SNPs that have a potential effect on gene function (high and moderate impact); from this selection, we identified the unique/shared SNPs between and within the clades and between the Colombian genomes, the data were included in an Excel matrix, which was used to perform the comparative analysis. Finally, to measure nucleotide diversity (π), we used the DnaSP software v.5.0.

Heterozygosity/Homozygosity Analysis

From allele frequency estimation data, we determined the Homozygous and heterozygous variants. Allele shifts of < 0.33 or > 0.66 were considered as homozygous variants while allele shifts between 0.33 and 0.66 as heterozygous variants (Tihon et al., 2017). Once homozygous and heterozygous variants were identified, these were counted using an Excel matrix. Later, the heterozygosity/homozygosity for each chromosome from each sample was extracted and calculated using the variant call formats through a Perl script. The identified heterozygous and homozygous SNPs for each chromosome per sample were plotted using the packages: Stringr, Ape, and Phangorn in R (Paradis et al., 2004; Schliep et al., 2019; Wickham, 2019).

Phasing of Heterozygous SNP Sites

Heterozygous SNPs were phased using BEAGLE v5.1 (<https://faculty.washington.edu/browning/beagle/beagle.html>) over 30 iterations. The algorithm also imputes missing genotypes from identity-by-state segments found in the data (Schwabl et al.,

2019). A custom Perl script was used to retrieve the sequence from the phased region and replace consensus bases with SNPs, generating thus two sequences for each isolate (denote as A and B), substituting base predictions for each haplotype into each sequence. This was conducted with whole genome data and by chromosome.

RESULTS

Identification of *Leishmania* Species

The **Table 1** and **Figure 1A** describe the clinical characteristics and geographical distribution of the Colombian/Bolivian isolates analyzed in this study. The amplification and Sanger sequencing of *Cytb* and *Hsp70* genes identified that the isolates herein included corresponded to *L. braziliensis* (**Supplementary Table S1**).

Phylogenomic Analysis

Two alignments were used to conduct phylogenomic analyses for 21 genome sequences. The first corresponded to single nucleotide polymorphisms (SNPs) from nuclear genome (1,320,593 nucleotide positions). The second corresponded to SNPs from mitochondrial genomes (167 nucleotide positions). For both cases MHOM/BR75/M2904_2019 *L. braziliensis* genome as the reference and *L. guyanensis* (Lguy_SRR8179913) and *L. panamensis* LP-PSC1 (LpW) genomes as outgroups. The approximately-maximum-likelihood phylogenetic trees built in FastTree double precision version 2.1.10 (Price et al., 2009) allowed initially to confirm that all the genomes evaluated were closely related to the reference genome and evidencing that the genomes analyzed here corresponding to *L. braziliensis* (**Figures 1B, C**). In addition, tree topologies (**Figures 1B, C**) describe the presence of four subpopulations clustered in well-supported nodes (with bootstrap ≥ 90.0). Clade 1 (highlighted in purple) included most of the Brazilian genomes (Lb1979381, Lb1980022, Lb1980024, Lb1980025, Lb7293733, Lb7293734, Lb7293735, Lb7293736, Lb7293738, Lb7293739, Lb7293740, and Lb7293741), clade 2 (highlighted in sky blue) two Colombian genomes (Lb7616 and Lb7864), clade 3 (highlighted in red) the remaining Brazilian genomes (Lb7293737 and Lb7293742), and clade 4 (highlighted in yellow) included the remaining Colombian genomes (Lb7529, Lb7740, Lb8025, and Lb8102) and the Bolivian genome (Lb7933). Interestingly, the two Colombian genomes belong to clade 2, collected from Vaupés and Antioquia were

TABLE 1 | Clinical characteristic of each Colombian clinical isolate analyzed in the study.

| Database accession number | Genome ID | Gender | Age (years) | Origin | Number of lesions | Lesion type | Treatment |
|---------------------------|-----------|--------|-------------|-----------|-------------------|-------------|---------------------------|
| ERS4385934 | Lb7616 | Male | 20 | Vaupés | 3 | Ulcerative | Glucantime intralesional |
| ERS4385933 | Lb7864 | Male | 16 | Antioquia | 1 | Nodular | ND |
| ERS4385937 | Lb7529 | Male | 22 | Meta | 1 | Ulcerative | Glucantime systemic |
| ERS4385938 | Lb7740 | Male | 57 | Meta | 1 | Ulcerative | Glucantime intralesional |
| ERS4385939 | Lb7933 | Male | 31 | Bolivia | 1 | Nodular | Thermotherapy |
| ERS4385935 | Lb8025 | Male | 36 | Meta | 1 | Ulcerative | Miltefosine/thermotherapy |
| ERS4385936 | Lb8102 | Male | 49 | Guajira | 9 | Ulcerative | Glucantime systemic |

ND, No Data.

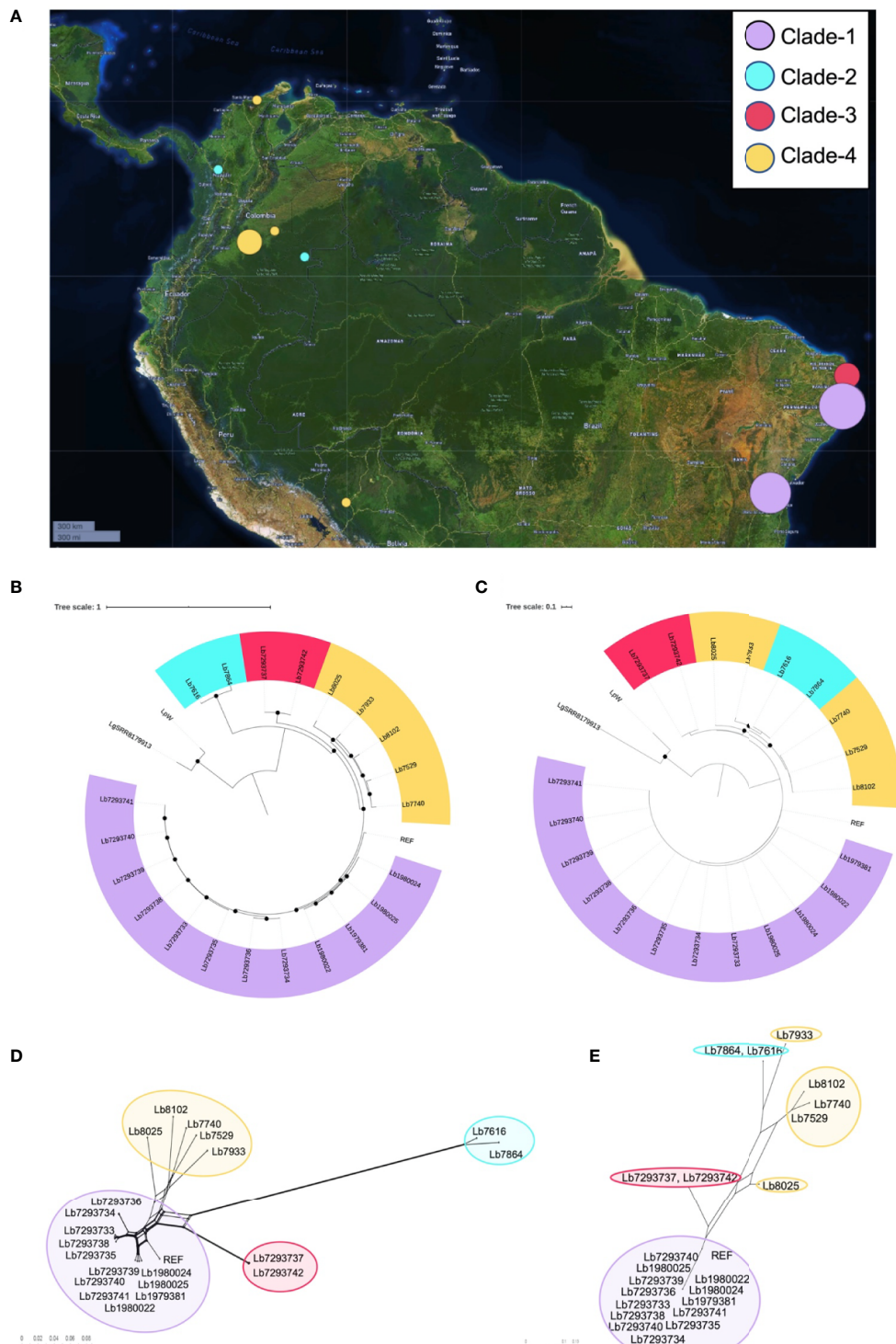


FIGURE 1 | Geographical distribution of genomes included in the study and *Leishmania braziliensis* phylogenomic relationships among nuclear and mitochondrial genomes. **(A)** Geographical location of the *L. braziliensis* genomes analyzed. The map was built using Microreact online tool (<https://microreact.org/showcase>) based on the GPS coordinates of each isolation (QGIS Geographic Information System, Open Source Geospatial Foundation Project, <http://qgis.osgeo.org>). Phylogenomic analysis based on whole nuclear genome **(B)** and mitochondrial genome: maxicircle **(C)**. MHOM/BR75/M2904_2019 *L. braziliensis* (REF) was included as reference genome and Lguy_SRR8179913 (*L. guyanensis*) and LpW (*L. panamensis*) were used as outgroup. Black dots represent well-supported nodes (Bootstrap ≥ 90). **(D, E)** represent the phylogenetic network (Neighbor-Net) constructed in SplitsTree 5, based on nuclear and mitochondrial (maxicircle) genomes respectively.

closer to the Brazilian genomes belonging to clade 3 than to genomes of clade 4, which included the other Colombian genomes collected from other regions of the country (Meta and Guajira). These findings were additionally supported by phylogenetic tree topologies obtained in SplitsTree5 (Huson and Bryant, 2006) (using neighbor-net method), where the members of these Clades were consistently clustered together and the four divergent between them (**Figures 1D, E**). The profiles were consistent between nuclear and mitochondrial analyses except for three remarkable events of clustering change that were defined as swapping events. These events were present in two relatively distant sub-clades within clade 4 (sub-clade 1 formed by Lb8025 and Lb7933 and sub-clade 2 by Lb7529, Lb7740, and Lb8102) (**Supplementary Figure S1**). Remarkably, one of the isolates that formed a possible subclade (Lb7933) was from Bolivia. Finally, we did not observe any relationship between the clustering patterns with the clinical or therapeutic characteristics of each genome analyzed.

Evaluation of Chromosome and Gene CNVs

We analyzed and compared the chromosome copy numbers in the 21 genomes included in this study. The results revealed that in some genomes the karyotype remained unchanged, most of the chromosomes presented a *S* value between 2.5 and 3.5, which indicate its trisomic state, with the consistent exception of chromosome 31, however, in other genomes we observed a moderate aneuploidy. In clade 1, the Lb7293740 genome presented six chromosomes (12, 18, 22, 29, 33, and 34) with extra copies, while the Lb7293733 genome presented three chromosomes (8, 26, and 27) with extra copies. Additionally, we observed that in one clade 4 genome (Lb8102), there was an extra copy of chromosome 2 compared with the other genomes of the same clade (**Figure 2**). We confirmed the accuracy of some value obtained by not observing discordance in the allele frequency counts for each predicted heterozygous SNP and the value obtained between the read depths and allele frequencies.

To evaluate the genes with CNVs and compared their occurrence in the genomes analyzed, we observed that the genome with the highest number of genes with CNVs was Lb8025 (147 genes), and the genomes with the lowest numbers were Lb7293737 and Lb7293742 (83 and 80 genes, respectively) (**Figure 3A**). The genes that presented the highest CNVs were found in the Lb8025 genome and encoded: β -tubulin, heat shock protein 83-1 and amastin protein. The genes that exhibit CNVs in the Lb7293737 and Lb7293742 genomes were mainly associated with cell adhesion (e.g. amastin and GP63 leishmanolysin), cell transport (e.g. ABC transporter and glucose transporter 3) and cytoskeletal proteins (e.g. β -tubulin). Additionally, we observed 25 genes with CNVs that were shared between all the genomes analyzed, 22 (88%) of which had known functions and three of which (12%) were annotated as hypothetical proteins. The genes with known function encoded to heat shock protein 83 and 70, α - and β -tubulin, amastin, zinc transporter, and NADH-dependent fumarate reductase (**Supplementary Table S2**). Finally, the Gene Ontology enrichment analysis revealed that the genes with CNVs

were mainly associated with cellular zinc ion homeostasis, response to stress, response to stimulus, and protein folding (**Figure 3B**).

SNPs Estimations

Comparison of each genome with the reference *L. braziliensis* sequence revealed a significant difference in the total number of SNPs per genome in each clade analyzed. The genomes of clade 1 contain between 42,617 and 68,989 SNPs, the genomes in clade 2 contain ~ 423,200 SNPs and the genomes belonging to clades 3 and 4 contain between 104,316 and 150,639 SNPs (**Supplementary Table S3**). Of the total number of SNPs identified ~20% had a potential effect on gene function (high and moderate impact). The genomes with the highest number of SNPs with functional impact were Lb7616 (54,640) and Lb7864 (53,576), belonging to clade 2, followed by the clade 4 genomes (~23,000 SNPs) (**Figure 4A**). Considering the SNP density between the genomes analyzed, we observed that this density was variable, ranging from less than 1 SNP/Kb in genomes belonging to cluster 1, 3 and 4 to 1.7 SNPs/Kb in genomes belonging to cluster 2. The least polymorphic genomes were Lb1980024 and Lb1980025 belonging to cluster 1 (0.23 and 0.24 SNPs/Kb, respectively), and the genomes with greatest variability were the Lb7616 and Lb7864 genomes belonging to cluster 2 (1.7 SNPs/Kb) (**Figure 4B**). Additionally, we evaluated and compared the nucleotide diversity between Colombian and Brazilian genomes and observed a low diversity in Brazilian genomes ($\pi = 0.072$) compared with the Colombian genomes ($\pi = 0.30$).

When we analyzed all genomes for SNP variants, we identify ~ 85% were synonymous variants; however, some variants had high functional impact (e.g. stop_gained and stop_lost) (**Table 2**). The SNPs associated to stop gained were identified in both genes encoding hypothetical proteins and in genes encoding to known function proteins such as surface proteins (amastin surface protein and phosphoglycans), multidrug resistance proteins, transporter proteins (pteridine transporter, ABC1 transporter, and iron/zinc transporter protein), and cytoskeletal proteins (β -tubulin), while the SNPs associated to stop lost were identified mainly in genes encoding hypothetical proteins and some of them in genes encoding transmembrane proteins (Meckelin transmembrane protein 67 putative) or transporter proteins (pteridine transporter) (**Supplementary Table S4**).

The next step was to evaluate the shared SNPs (with high and moderate functional impact) within and between each clade. The comparison of genomes within each clade revealed that the genomes of clade 2 had the highest number of shared SNPs (26,282) compared with clades 1, 3, and 4, where the number of SNPs shared was 1,173 and 9,703, and 5,520, respectively (**Figure 4C**). Fifty-two percent of shared SNPs in each clade were in genes encoding to hypothetical protein, and the remaining 48% were in genes encoding to proteins with known function. The comparison between the four clades allowed to identify 463 SNPs shared with known function (**Figure 4C**). Most of them identified in genes encoding transporter proteins (ABC

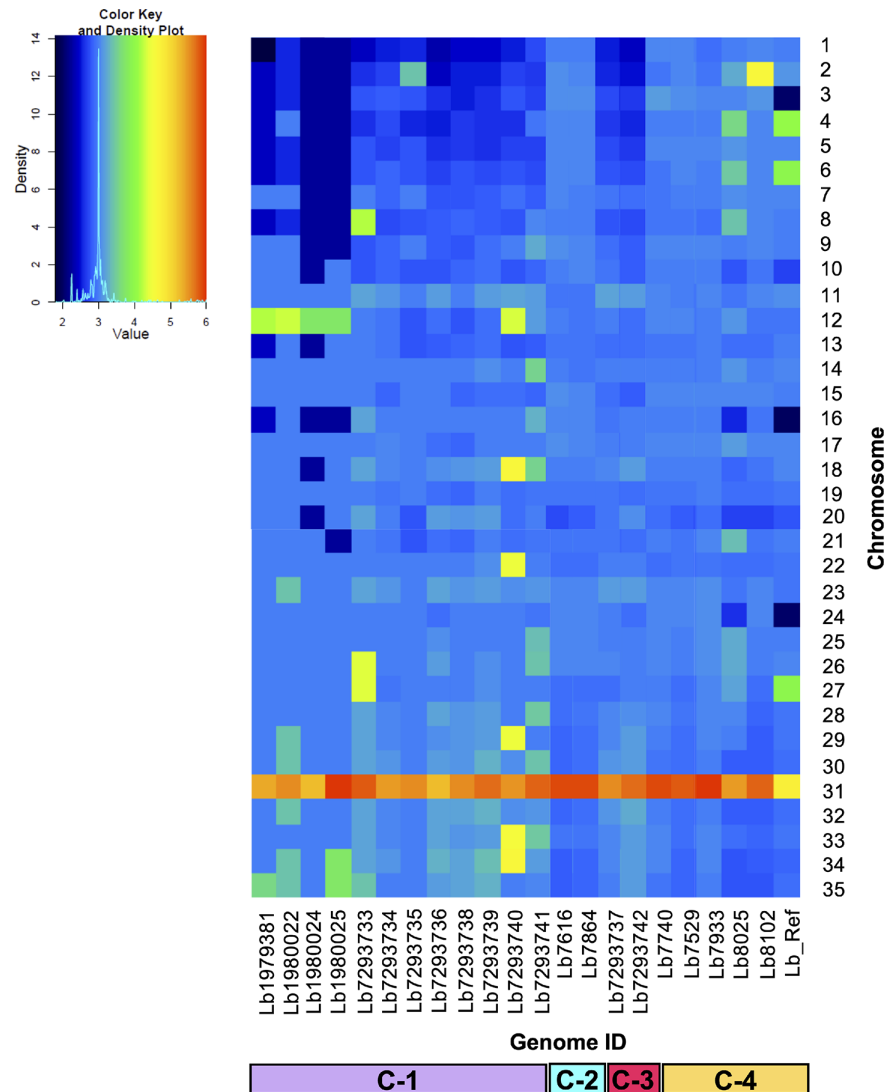


FIGURE 2 | Dynamic of copy number between the 21 *Leishmania braziliensis* genomes analyzed. The heatmap shows the copy number of the 35 chromosomes (y-axis) for the 21 genomes analyzed, included the reference genome (Lb_Ref) (x-axis). Trisomic (3, blue), tetrasomic (4, green), pentasomic (5, orange).

transporter, nucleoside transporter, zinc transporter, and sugar transporter), host-pathogen interaction-associated proteins (amastin surface protein), kinetoplast-associated protein, or intracellular degradation-associated proteins (ubiquitin-conjugating enzyme putative) (**Supplementary Table S5**). Regarding the shared SNPs between the clades, we observed a high number of shared SNPs between clade 2 and clade 3 (5,095) followed by the clades 2 and 4 (3,591) and clades 3 and 4 (3,145); additionally, we observed that the genomes belonging to clade 1 presented a low number of shared SNPs with the other clades (clades 1 and 2: 669; clades 1 and 3: 689; clades 1 and 4: 692) (**Figure 4C**).

Lastly, we evaluated the unique/shared SNPs (with high and moderate functional impact) between the Colombian genomes

included in the study. To analyze the unique SNPs in each genome, we observed that Lb7864 and Lb7616 were the genomes with the lowest number of SNPs (3 and 181, respectively), which represent less than 1% of the total, compared with the other genomes analyzed where the number of unique SNPs ranged between 9 and 13% (**Figure 4D**). Regarding the shared SNPs, the results revealed 7,512 SNPs between the genomes analyzed, 48% of them in genes encoding proteins associated with hypothetical function and the remaining 52% in genes with known function (**Figure 4D**). Later, we made a pairwise comparison considering not only the SNPs with high and moderate functional impact but also those located in genes with known function. The results revealed that the genomes with the highest number of shared SNPs between them were the genomes Lb7864 and Lb7616

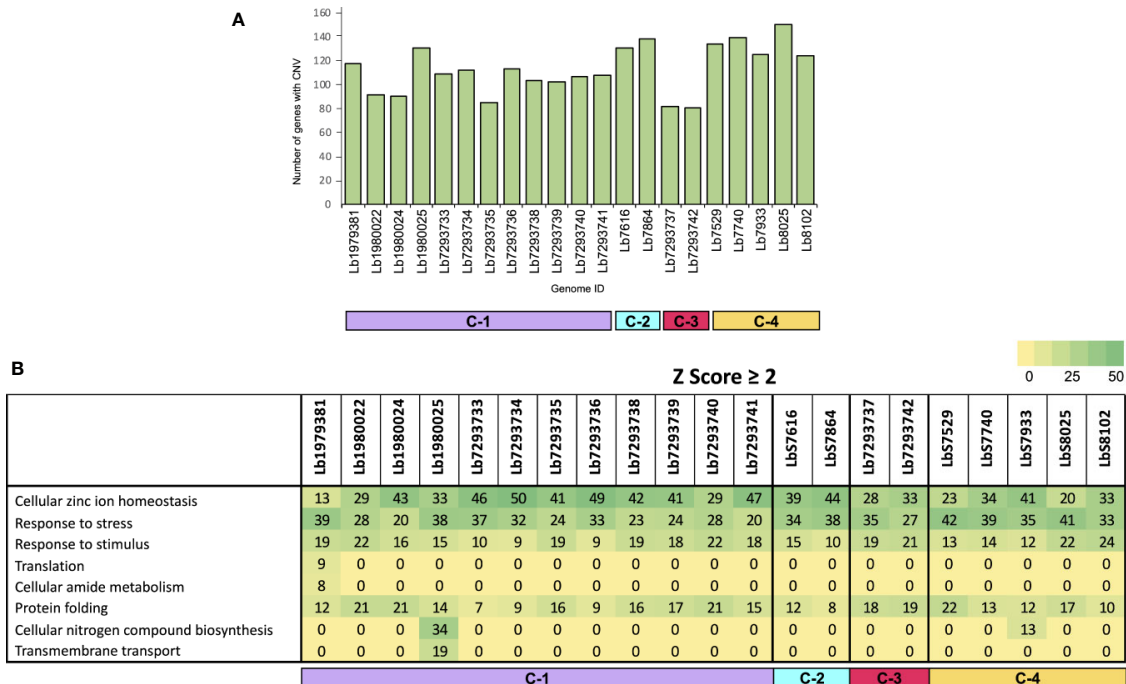


FIGURE 3 | Genes with copy number variation (CNV) and gene ontology enrichment analyses. **(A)** The bar graph represents the number of genes that presented CNVs in the 21 genomes included in the study. **(B)** The table represents the number of genes with CNVs in each genome analyzed, that were involved in different biological processes.

(26,763 SNPs), followed by the genomes Lb7529, Lb8025, and Lb7740, which presented a number of shared SNPs ranging from 7,700 to 7,897 (**Supplementary Table S6**).

LOH and Hybridization in *L. braziliensis*

Finally, of the SNPs with high and moderate functional impact, 73% were homozygous and 27% heterozygous. The most interesting result was the whole genome loss of heterozygosity (LOH) observed in some genomes (**Figure 5**). One Colombian genome (Lb7864) and two Brazilian genomes (Lb7293737 and Lb7293742) presented LOH in all 35 chromosomes (**Supplementary Figure S2** and **Supplementary Table S7**). To explain graphically these results, we selected one of the largest chromosomes comprising the *L. braziliensis* genome (Chromosome 35) and compared the heterozygosity/homozygosity (blue/green, respectively) along this chromosome among seven genomes (**Figure 5**). **Figures 5A–C** represent the Brazilian genomes and clearly show the absence of heterozygous SNPs (blue color) along chromosome 35 in the Lb7293737 and Lb7293742 genomes compared with Lb7293738 genome. Panels D–F represent Colombian genomes and show the high levels of homozygous SNPs (green color) in the Lb7616 and Lb7864 genomes (**Figure 5**).

In contrast, we identified one genome of clade 4 (Lb8025) to be highly heterozygous throughout the genome (99% heterozygous SNPs) (**Supplementary Table S7**). This finding, which was consistent in all chromosomes (**Figure 5G** and **Supplementary Figure S2**), together with the divergence observed when compared with the others belonging to the

same clade (**Supplementary Figure S3**), suggest a possible event of hybridization. With the purpose to analyze this possible event, we selected the genomes closely related to Lb8025 (Lb7933, Lb8102, Lb7529, and Lb7740) (**Figure 1**) and reconstructed haplotypes of each of them from both nuclear and mitochondrial genomes and by chromosome through phasing the genotype calls. The results obtained when analyzing the topologies of trees from the nuclear (**Figure 6A**) and mitochondrial genomes (**Figure 6B**) and the results obtained by chromosome (**Supplementary Figure S4**) showed that across the genome, the haplotype A and the haplotype B of Lb8025 (Lb8025-A and Lb8025-B) are grouped in distinct clusters, which contrast with the observed in the other genomes analyzed. This is a strong genomic evidence of hybridization with alleles from independent ancestries.

DISCUSSION

To understand the genetic heterogeneity of *L. braziliensis*, we used DNA-seq technology and bioinformatic analyses to investigate the genetic structure and the phylogenomic relationships among *L. braziliensis* genomes from Colombian/Bolivian clinical isolates and among genomes of Brazilian *L. braziliensis* isolates archived in public databases. The phylogenetic analysis of nuclear and mitochondrial genomes revealed the presence of two different *L. braziliensis* populations in Colombia (clade 2 and clade 4) (**Figures 1B–E**). We considered that the presence of these clades within

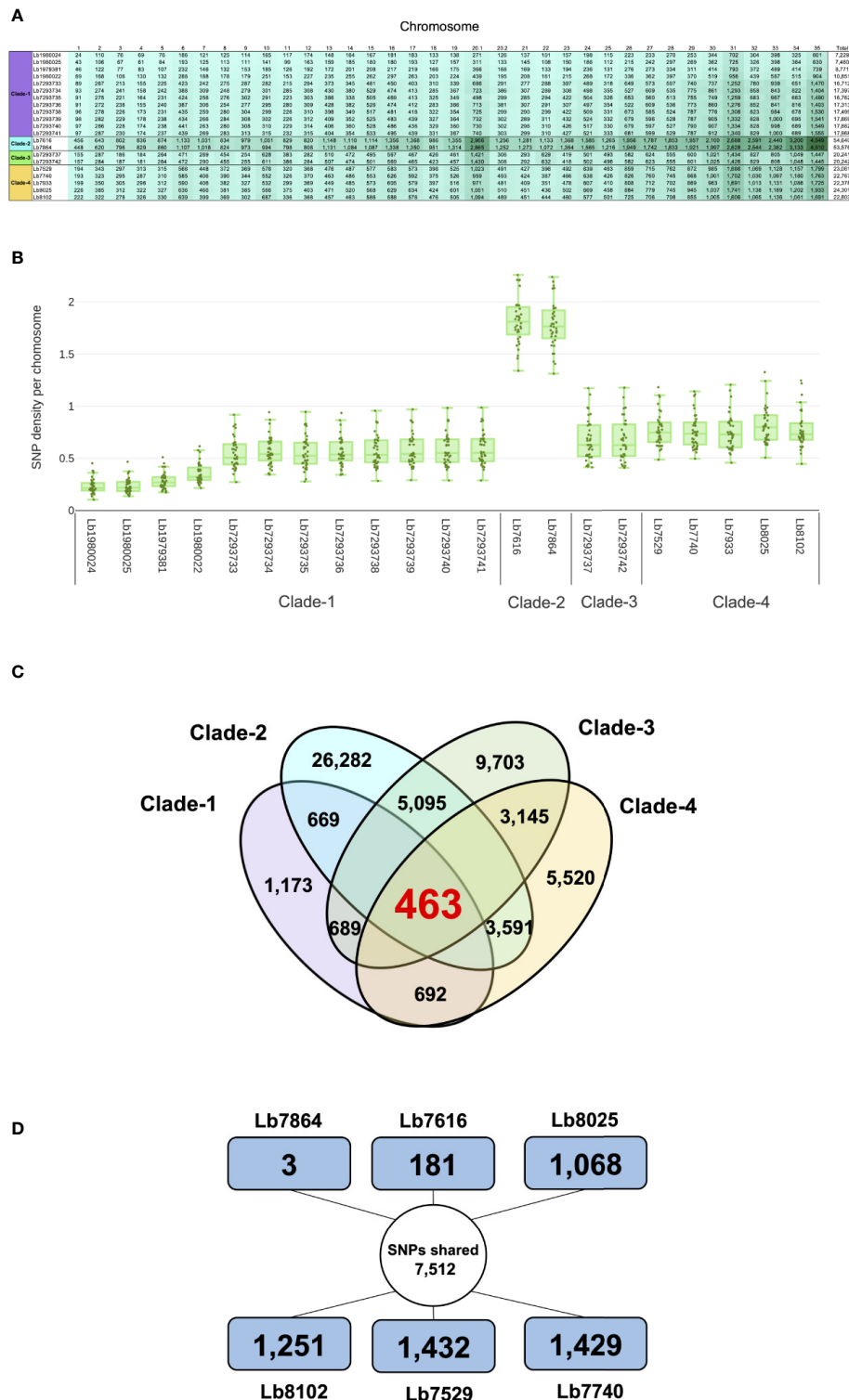


FIGURE 4 | Overview of SNPs identified in *L. braziliensis* genomes. **(A)** Number of SNPs per chromosome, that have a potential effect on gene function (high and moderate impact) in each of the genomes analyzed. The clade is indicated at left. **(B)** SNP density of 21 *L. braziliensis* genomes analyzed. **(C)** Number of SNPs unique and shared between and within the four clades identified. The colors represent each clade: clade 1 (Purple), clade 2 (sky blue), clade 3 (green) and clade 4 (light orange). **(D)** Summary of the number of SNPs unique and shared between the six Colombian genomes analyzed, the external square represents the unique SNPs and the inner circle the shared SNPs.

TABLE 2 | Number of SNPs with potential effect on gene function, in each genome analyzed.

| Database accession number | Genome ID | Number of Stop_lost | Number of Stop_gained | Synonymous variant |
|---------------------------|-----------|---------------------|-----------------------|--------------------|
| SRR1979381 | Lb1979381 | 8 | 23 | 8722 |
| SRR1980022 | Lb1980022 | 9 | 28 | 10793 |
| SRR1980024 | Lb1980024 | 6 | 18 | 6294 |
| SRR1980025 | Lb1980025 | 4 | 21 | 7420 |
| SRR7293733 | Lb7293733 | 15 | 44 | 16626 |
| SRR7293734 | Lb7293734 | 11 | 56 | 17298 |
| SRR7293735 | Lb7293735 | 15 | 45 | 16677 |
| SRR7293737 | Lb7293737 | 11 | 57 | 7059 |
| SRR7293738 | Lb7293738 | 13 | 46 | 17413 |
| SRR7293739 | Lb7293739 | 15 | 49 | 17777 |
| SRR7293740 | Lb7293740 | 15 | 51 | 17788 |
| SRR7293741 | Lb7293741 | 15 | 49 | 17866 |
| ERS4385934 | Lb7616 | 30 | 121 | 54407 |
| ERS4385933 | Lb7864 | 35 | 118 | 53348 |
| SRR7293736 | Lb7293736 | 16 | 57 | 17213 |
| SRR7293742 | Lb7293742 | 18 | 56 | 20139 |
| ERS4385937 | Lb7529 | 19 | 57 | 22943 |
| ERS4385938 | Lb7740 | 20 | 60 | 22647 |
| ERS4385939 | Lb7933 | 20 | 55 | 22264 |
| ERS4385935 | Lb8025 | 18 | 58 | 24183 |
| ERS4385936 | Lb8102 | 19 | 61 | 22691 |

Colombia can be associated with (i): the geographical localization of each clade; clade 4 genomes are located outside of mountain ecosystems (east Andes), while the clade 2 genome (Lb7864) occurs in Colombian mountain ecosystems (central cordillera) (**Figure 1A**), indicating that the Andes might generate intra-species diversification, as has been proposed for different arthropods, such as bees (Dick et al., 2004), butterflies (De-Silva et al., 2016; Chazot et al., 2018), arachnids (Salgado-Roa et al., 2018), Triatominae (Gomez-Palacio and Triana, 2014; Monsalve et al., 2016), *Lutzomyia* species (Gonzalez et al., 2014; Ferro et al., 2015) and plants, such as *Phlegmariurus* (Testo et al., 2019). (ii): Constant human displacement due to violence, armed conflict, or the deployment of military troops from areas of high endemicity (Ore et al., 2015). This could promote the distribution of this parasite to other geographical regions, as has been observed for *L. guyanensis*, which broke out of its native geographical distribution and is now detected in two different habitats (Ferro et al., 2011; Ramirez et al., 2016). Finally, (iii): migration of animal reservoirs or sand fly vectors responsible for transmission of the parasite within the national territory. *L. braziliensis* is associated with a wide variety of sand fly vectors (Bejarano et al., 2002; Testa et al., 2002; Ovallos et al., 2013; Ovalle-Bracho et al., 2019).

Another interesting finding was associated with the clear swapping event (incongruence in the tree topologies) identified in clade 4, when tree topology of nuclear genome was compared with the mitochondrial genome (**Figure 1** and **Supplementary Figure S1**). This finding was mainly observed in the Lb8025 genome, which may represent evidence of introgression, probably by interspecific hybridization, phenomena that has been described as a possible way for rapid evolution, which is key in species responses to environmental change or as a strategy of parasites to escape from Muller's ratchet (irreversible accumulation of deleterious mutations) (Harrison and Larson, 2014; Messenger and Miles, 2015). This was expected because of

recent evidence of hybridization and meiosis-like behavior in *Leishmania* and other trypanosomatids, such as *Trypanosoma cruzi* (Inbar et al., 2019; Schwabl et al., 2019; Broeck et al., 2020). We were able to identify a potential hybrid; however, considered that additional studies are necessary to understand not only the population structure but also to describe the evolutionary forces that possibly have promoted it. Therefore, studies that involved a larger population size from different countries, as well as crosses in sandflies should be performed.

When we then evaluated the somy value; observed that the Brazilian genomes had high karyotype instability compared with the Colombian/Bolivian genomes, of which only two of the seven genomes showed somy change (Lb8102 and Lb8025 genomes) (**Figure 2**). Aneuploidy is considered one of the most important processes for *Leishmania* adaptation; therefore, these results indicate that Colombian strains could be changing to adapt to the eco-epidemiological conditions of the country as the Brazilian strains and that the amplification of some chromosomes may provide fitness advantages during host adaptation, which is consistent with the observed in other *Leishmania* species (*L. donovani*, *L. major*, *L. tropica*, *L. infantum*, and *L. amazonensis*) (Dumetz et al., 2017; Iantorno et al., 2017; Bussotti et al., 2018; Patino et al., 2019b). Additionally, the somy dynamic observed reveals changes in an individualized manner, suggesting that environment-independent intrinsic genetic factors can affect *Leishmania* karyotypic adaptation, as has been described in Old-World *Leishmania* species (Bussotti et al., 2018). Despite moderate karyotype heterogeneity observed in the Colombian/Bolivian genomes, we highlight an interesting somy dynamic observed in the Lb8025 genome (**Figure 2**), in which the genetic content was doubled in various chromosomes. This, together with the possible introgression event (**Figure 1** and **Supplementary Figure S1**), the elevated heterozygosity (**Figure 5G**,

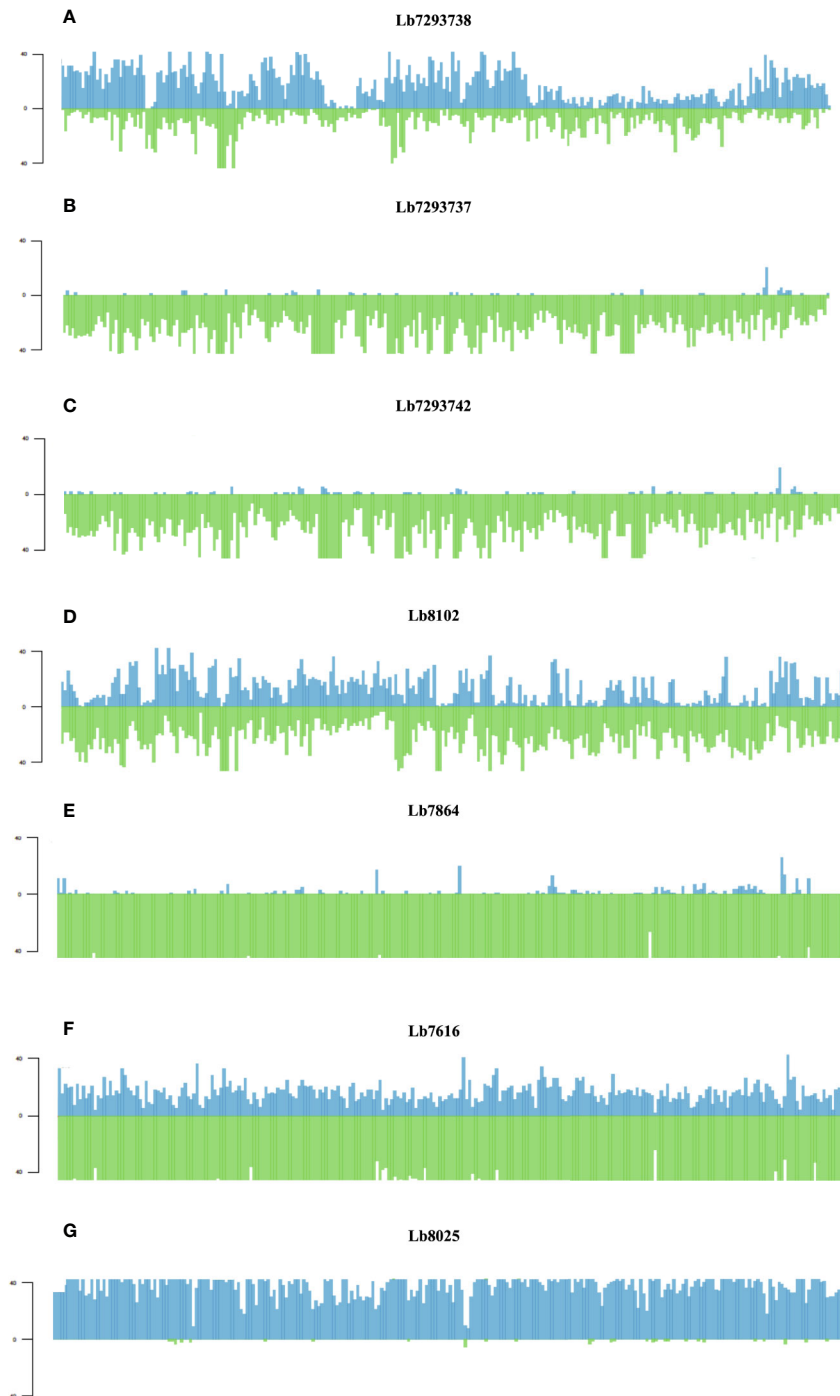


FIGURE 5 | Homozygosity/heterozygosity profile of chromosome 35 in *L. braziliensis* Colombian/Brazilian genomes. The distribution of homozygous (green color) and heterozygous (blue color) SNPs along chromosome 35. The X axis represents 10 kb windows of chromosome 35 and the Y axis indicates the total number of SNPs. Each panel represents a different genome; **(A–C)** represent the Brazilian genomes and **(D–G)** the Colombian genomes.

Supplementary Figure S2, and Supplementary Table S7), the divergence compared with other genomes of the same clade (Supplementary Figure S3), and the grouping of each haplotype in two different clusters (Figure 6 and Supplementary Figure

S4) indicate that this strain is a hybrid (via intra or interspecific hybridization or genomic recombination). The genetic exchange product of hybridization event could generate evolutionary advantages that can impact vector permissiveness, the

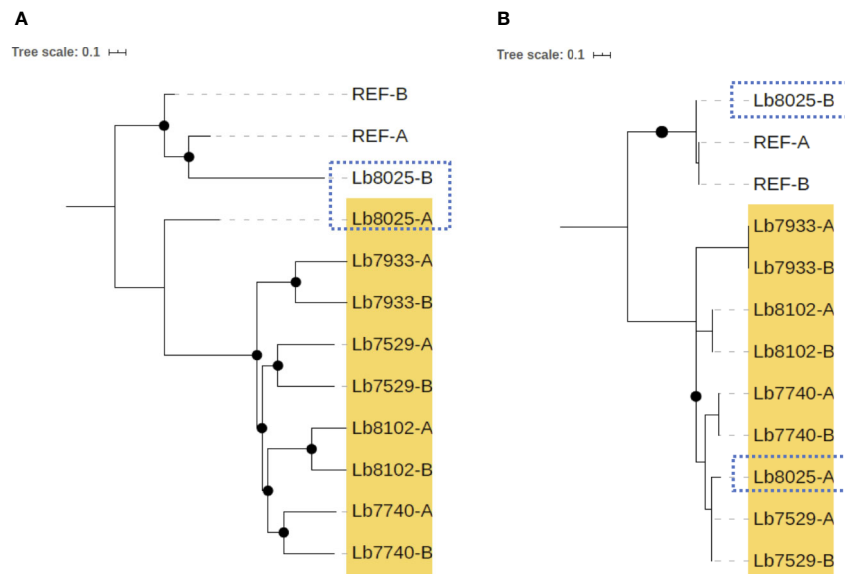


FIGURE 6 | Phylogenetic reconstruction based on genomic SNP alignments for phased haplotypes belonging to Clade 4. The trees represent phylogenetic analysis from whole nuclear **(A)** and mitochondrial (maxicircle) **(B)** single-nucleotide polymorphism (SNP) alignments based on phased haplotypes of five genome sequences belonging clade 4 (highlighted in yellow). MHOM/BR75/M2904_2019 *L. braziliensis* (REF) was included as reference genome. Black dots represent well-supported nodes (Bootstrap ≥ 90) and the dotted squares show the location of Lb8025 haplotypes.

adaptation to different environments/niches, to increase or alter the virulence and generate recombinant progeny that are capable of widespread clonal propagation. Likewise, the pathological implications of hybrid genotypes in human infections, could promote the spread of virulent strains to affect the transmissibility and the resistance to chemotherapeutics (Cortes et al., 2012; Ramirez et al., 2012; Messenger and Miles, 2015).

Another evaluated parameter was local copy number variation (CNV). The results did not reveal important intraspecies variations in the numbers of genes with CNV (**Figure 3A**) either in genomes collected within or outside of Colombia. Of the genes showing CNV in all analyzed genomes (25 in total), we highlight those involved in stress resistance, infectivity and virulence (Heat shock protein 70 and 83, α and β tubulin, amastin, and zinc transporter) (**Supplementary Table S2**); curiously, these genes were previously reported in other studies (Rastrojo et al., 2013; Bifeld and Clos, 2015; Bussotti et al., 2018; Urrea et al., 2018; Restrepo et al., 2019). These results together with the ontology enrichment analysis (**Figure 3B**), indicate that these genes may drive or be the result of rapid adaptation in *L. braziliensis*, results previously described in other *Leishmania* species (Rogers et al., 2011; Bussotti et al., 2018; Urrea et al., 2018) and suggest that genome plasticity in *L. braziliensis* not only at the level of whole chromosome but also of specific regions promotes important processes associated with the replication, infectivity, and virulence.

Likewise, the local copy number variation may represent an evolutionarily important adaptation, to confer a degree of plasticity in the regulation and functional expression of genes

or gene clusters involved in drug resistance, adaptation to different environmental, including survival in a variety of mammalian hosts and phenotypic diversity as has been observed in other species (*L. donovani*, *L. tropica*, *L. infantum*, and *L. panamensis*) (Laffitte et al., 2016; Iantorno et al., 2017; Sinha et al., 2018; Patino et al., 2020).

Our final strategy to evaluate genomic variability among *L. braziliensis* genomes involved analysis of nucleotide-level variations (SNPs). Comparing the number of SNPs found in this study (42,617 to 435,529; $n = 21$) (**Supplementary Table S3**) and the recent report in *L. braziliensis* isolates from Peru (Broeck et al., 2020), with the number of variants described in other Old/ New World *Leishmania* species, such as *L. donovani* (3,549 SNPs; $n = 17$) (Downing et al., 2011); *L. infantum* (17,333 SNPs; $n = 12$) (Rogers et al., 2014) (~3,000 SNPs; $n = 20$) (Teixeira et al., 2017), *L. amazonensis*/*L. mexicana* vs. *L. infantum* (~21,000 SNPs; $n = 2$) (Valdivia et al., 2017), *L. panamensis*; (~62,000 SNPs; $n = 22$) (Patino et al., 2020), *L. amazonensis* vs. reference genome of *L. mexicana* (~40,000 SNPs) (Patino et al., 2019b) and *L. peruviana* vs. reference genome of *L. braziliensis* (~112,000 SNPs; $n = 2$) (Valdivia et al., 2015), we can confirm that *L. braziliensis*, is the *Leishmania* (*Viannia*) species with the highest genetic variability circulating in some regions of South America (Brazil, Colombia and Perú). Additionally, to analyze the genetic variability of *L. braziliensis* between the Colombian and Brazilian isolates, we observed that Colombian genomes were much more diverse ($\pi = 0.30$; $n = 7$), than the Brazilian genomes ($\pi = 0.072$; $n = 14$) (**Supplementary Table S3**). This diversity is advantageous for the parasite because it favors survival in diverse ecological systems/niches, determines the distribution of the observed clinical forms

of the disease, and influences the anti-leishmanial therapy response; aspects that enable this species to be a successful human pathogen. Despite our results, we consider that additional studies, with a greater number of Colombian samples, are necessary to understand the reasons why *L. braziliensis* is such a highly diverse species.

To evaluate unique/shared SNPs among the four identified clades, we identified a high number of unique SNPs (**Figure 4C**), mainly in the clades with low heterozygosity (**Figure 5** and **Supplementary Table S7**) (genomes belonging to clades 2 and 3). Consistently, we observed a low number of shared SNPs among the four clades (463 SNPs) (**Figure 4C**). The analysis of shared SNPs between clades revealed the low similarity between the genomes belonging to clade 1 and the genomes belonging to other clades, contrary to observed with the genomes of clades 2, 3, and 4, which presented a high similarity between them (high number of shared SNPs), those results confirm the close relationship between the Colombian genomes with some Brazilian genomes (**Figure 4C**). Finally, we analyzed the unique/shared SNPs, but in this case between the six Colombian genomes. The results revealed in some genomes a low number of unique SNPs and a high number of shared SNPs (**Figure 4D**; **Supplementary Table S6**); two of the genomes (Lb7864 and Lb7616) had 99.5% of identity, and this close inter-strain relationship could indicate a recent shared ancestor between them.

In addition to the findings associated with the elevated number of SNPs in the genomes herein analyzed, we highlight the drastic whole genome loss of heterozygosity (LOH) observed in some Brazilian/Colombian genomes (specifically in those belonging to clades 2 and 3) (**Figure 5** and **Supplementary Table S7**). This large-scale of LOH, has been observed in fungi (*Candida albicans* and *Saccharomyces cerevisiae*) as a mechanism for introducing diversity into a population and as a strategy to survive in stressful conditions (response to treatment, DNA damage and host passage) (Dunkel and Morschhauser, 2011; Hirakawa et al., 2015; Wertheimer et al., 2016; Hoffert and Strome, 2019). In *Leishmania*, studies published to date, reveal LOH to short scale (loss of some heterozygous SNPs in a block) (Samarasinghe et al., 2018) or low-level heterozygosity (Downing et al., 2011; Rogers et al., 2014) mainly in Old World *Leishmania* parasites (*L. infantum*, *L. major* and *L. donovani*). Therefore, this is the first study using Colombian clinical isolates and next generation sequencing to identify patterns of homozygosity in the whole genome of one of the most important New World *Leishmania* species, *L. braziliensis*. This pattern of diversity could be explained by a substantial bottleneck of adaptation that occurred in an environment/niche-dependent manner, which favored and fixed certain genotypes in the population and promoted the stochastic loss of others, as has been described for *T. brucei* (Oberle et al., 2010) and recently for *T. terrestris* (Perez et al., 2019). Another possible hypothesis for these findings is associated with gene conversion, which may have produced unidirectional transfer of genetic material between members of the same species sharing the same ecological niche. This would contribute to the genetic diversity and

possible evolutionary success of the species, as has been suggested for this and other *Leishmania* species (*L. donovani* complex) (Mauricio et al., 2007; Rougeron et al., 2009), as well as other eukaryotic organisms (*Theileria parva* and *Saccharomyces cerevisiae*) (Qi et al., 2009; Henson et al., 2012; Sriswasdi et al., 2016). The structure of the *L. braziliensis* genome is complex, and additional studies are needed to unveil the existence of homozygous and heterozygous strains and the exact mechanism by which *Leishmania* can fix its heterozygosity including the biological consequences of this plasticity.

In conclusion, the findings in this study demonstrate the high intra-species genetic diversity of *L. braziliensis* in Colombia and the occurrence of distinct phylogenetic groups in the sampled regions. The genomic changes, until date unknown in *L. braziliensis*, such as moderate changes in copy number, CNVs, the introgression event, the increase of the heterozygosity and the duplication of genetic content in various chromosomes, identified in the Lb8025 genome (Potential hybrid), as well as the high number of homozygous SNPs (most of them unique for each clade) and the whole genome LOH, identified in Colombian/Brazilian genomes, suggest a striking genomic plasticity of this species, which could be genomic strategies used by *L. braziliensis* to favor its survival and adaptation to different ecological niches. These genomic findings can influence *L. braziliensis* epidemiology and future clinical and therapeutic outcomes.

Although our study was focused to analyze and compare the genomic structure of Colombian/Bolivian isolates with Brazilian isolates, we consider that there are necessary additional studies that include genomes from other regions of South America where *L. braziliensis* is endemic. This at the end will permit not only to make a broader comparative genomic analysis of our Colombian isolates with genomes from other regions but also to expand the knowledge about of genetic variability of this species in South America.

DATA AVAILABILITY STATEMENT

The datasets presented in this study can be found in online repositories. The names of the repository/repositories and accession number(s) can be found at: <https://www.ebi.ac.uk/ena>, ERS4385933, ERS4385934, ERS4385935, ERS4385936, ERS4385937, ERS4385938 and ERS4385939.

ETHICS STATEMENT

The studies involving human participants were reviewed and approved by: This study was approved by the Ethics Committee of the Universidad de Antioquia (number VRI3445/2010) in accordance with resolution number 36836. Written informed consent was obtained from the patients from which the strains were isolated. The patients/participants provided their written informed consent to participate in this study.

AUTHOR CONTRIBUTIONS

LP conceived and designed the study, analyzed and interpreted the data, and prepared the manuscript. MM interpreted the data and critically revised the manuscript and made important suggestions. LC-S critically revised the manuscript and made important suggestions. CM critically revised the manuscript and made important suggestions. JR conceived and designed the study and revised the manuscript. All authors contributed to the article and approved the submitted version.

FUNDING

This work was funded by DIRECCIÓN DE INVESTIGACIÓN E INNOVACIÓN from Universidad del Rosario. JR is a Latin American fellow in Biomedical Sciences, supported by The Pew Charitable Trusts.

ACKNOWLEDGMENTS

We thank the Colombian Science, Technology, and Innovation Ministry (MinCiencias) for sponsoring PhD training in Colombia, within the framework of the National Program for Promoting Research Training (sponsorship calls 647). We are also grateful to the Programa de Control y Estudio de Enfermedades Tropicales (PECET) for assistance with sampling and to Dr. Hideo Imamura for assistance with the analyses. We thank the High Computing Cluster (CENTAURO) Service from Universidad del Rosario. We thank Jeremy Allen, PhD, from Edanz Group (www.edanzediting.com/ac) for editing a draft of this manuscript.

REFERENCES

- Alves-Ferreira, E. V., Toledo, J. S., De Oliveira, A. H., Ferreira, T. R., Ruy, P. C., Pinzan, C. F., et al. (2015). Differential Gene Expression and Infection Profiles of Cutaneous and Mucosal *Leishmania braziliensis* Isolates from the Same Patient. *PLoS Negl. Trop. Dis.* 9, e0004018. doi: 10.1371/journal.pntd.0004018
- Banu, S. S., Meyer, W., Ferreira-Paim, K., Wang, Q., Kuhls, K., Cupolillo, E., et al. (2019). A novel multilocus sequence typing scheme identifying genetic diversity amongst *Leishmania donovani* isolates from a genetically homogeneous population in the Indian subcontinent. *Int. J. Parasitol.* 49, 555–567. doi: 10.1016/j.ijpara.2019.02.010
- Bejarano, E. E., Uribe, S., Rojas, W., and Dario Velez, I. (2002). Phlebotomine sand flies (Diptera: Psychodidae) associated with the appearance of urban leishmaniasis in the city of Sincelejo, Colombia. *Mem. Inst. Oswaldo Cruz.* 97, 645–647. doi: 10.1590/S0074-02762002000500010
- Bifeld, E., and Clos, J. (2015). The genetics of *Leishmania* virulence. *Med. Microbiol. Immunol.* 204, 619–634. doi: 10.1007/s00430-015-0422-1
- Brilhante, A. F., Lima, L., Zampieri, R. A., Nunes, V. L. B., Dorval, M. E. C., Malavazi, P., et al. (2019). *Leishmania* (Viannia) *braziliensis* type 2 as probable etiological agent of canine cutaneous leishmaniasis in Brazilian Amazon. *PLoS One* 14, e0216291. doi: 10.1371/journal.pone.0216291
- Broeck, F. V. D., Savill, N. J., Imamura, H., Sanders, M., Maes, I., Cooper, S., et al. (2020). Ecological divergence and hybridization of Neotropical *Leishmania* parasites. doi: 10.1073/pnas.1920136117

SUPPLEMENTARY MATERIAL

The Supplementary Material for this article can be found online at: <https://www.frontiersin.org/articles/10.3389/fcimb.2020.582192/full#supplementary-material>

SUPPLEMENTARY FIGURE 1 | Tree comparison of phylogenetic reconstruction from nuclear and mitochondrial alignments for *Leishmania braziliensis* genomes. Phylogenetic tree built based on a distance matrix, derived from nuclear SNPs (A) and mitochondrial (maxicircle) SNPs (B), shared among 21 clinical isolates of *L. braziliensis*. Tree topologies were compared to identify swapping events, characterized by changes in clustering patterns. Colors indicate similarity to most common node. A score of 1 denotes the subtree structure of the node is identical to the subtree structure of its best corresponding node. This comparison was performed using Phylo.io interactive tool (<http://phylo.io/>). Lguy_SRR8179913 (*L. guyanensis*) and LpW (*L. panamensis*) were used as outgroup and MHOM/BR75/M2904_2019 *L. braziliensis* (REF) as reference genome.

SUPPLEMENTARY FIGURE 2 | Homozygosity/heterozygosity profile to all 35 chromosomes in *L. braziliensis* Colombian/Brazilian genomes. The figure represents the distribution of homozygous (green color) and heterozygous (blue color) SNPs along chromosome. The X axis represents 10 kb windows of chromosome and the Y axis indicates the total number of SNPs. Each panel represents a different genome.

SUPPLEMENTARY FIGURE 3 | Phylogenetic network based on nuclear SNPs alignments for the five genomes belonging Cluster-4. Neighbour-joining network based on genome-wide SNPs for the five genomes belonging clade 4. MHOM/BR75/M2904_2019 *L. braziliensis* (REF) was used as reference genome. The network was constructed using SplitsTree 5.

SUPPLEMENTARY FIGURE 4 | Phylogenetic reconstruction based on genomic SNP variation of phased haplotypes belonging Clade 4 per chromosome. The trees represent phylogenetic analysis, per chromosome, of nuclear single-nucleotide polymorphism (SNP) alignments based on phased haplotypes of five genome sequences belonging clade 4 (highlighted in yellow). MHOM/BR75/M2904_2019 *L. braziliensis* (REF) was included as reference genome. Black dots represent well-supported nodes (Bootstrap ≥ 90) and the dotted squares show the ubication of Lb8025 haplotypes.

- Bruna, S., Rezende, A. M., de Melo Neto, O. P., de Brito, M. E. F., and Brandao Filho, S. P. (2019). Identification of divergent *Leishmania* (Viannia) *braziliensis* ecotypes derived from a geographically restricted area through whole genome analysis. *PLoS Negl. Trop. Dis.* 13, e0007382. doi: 10.1371/journal.pntd.0007382
- Bussotti, G., Gouzou, E., Cortes Boite, M., Kherachi, I., Harrat, Z., Eddakir, N., et al. (2018). *Leishmania* Genome Dynamics during Environmental Adaptation Reveal Strain-Specific Differences in Gene Copy Number Variation, Karyotype Instability, and Telomeric Amplification. *mBio* 9. doi: 10.1128/mBio.01399-18
- Chazot, N., De-Silva, D. L., Willmott, K. R., Freitas, A. V. L., Lamas, G., Mallet, J., et al. (2018). Contrasting patterns of Andean diversification among three diverse clades of Neotropical clearwing butterflies. *Ecol. Evol.* 8, 3965–3982. doi: 10.1002/ece3.3622
- Cortes, S., Esteves, C., Mauricio, I., Maia, C., Cristovao, J. M., Miles, M., et al. (2012). In vitro and in vivo behaviour of sympatric *Leishmania* (V.) *braziliensis*, *L. (V.) peruviana* and their hybrids. *Parasitology* 139, 191–199. doi: 10.1017/S0031182011001909
- Cupolillo, E., Brahim, L. R., Toaldo, C. B., De Oliveira-Neto, M. P., De Brito, M. E., Falqueto, A., et al. (2003). Genetic polymorphism and molecular epidemiology of *Leishmania* (Viannia) *braziliensis* from different hosts and geographic areas in Brazil. *J. Clin. Microbiol.* 41, 3126–3132. doi: 10.1128/jcm.41.7.3126-3132.2003
- Cysne-Finkelstein, L., Silva-Almeida, M., Pereira, B. A. S., Dos Santos Charret, K., Bertho, A. L., Bastos, L. S., et al. (2018). Evidence of Subpopulations with

- Distinct Biological Features Within a *Leishmania* (*Viannia*) *braziliensis* Strain. *Protist* 169, 107–121. doi: 10.1016/j.protis.2017.11.004
- De Oliveira, G. M., Madeira Mde, F., Oliveira, F. S., Pires, M. Q., and Pacheco Rda, S. (2013). Canine Cutaneous Leishmaniasis: Dissemination and Tissue Tropism of Genetically Distinct *Leishmania* (*Viannia*) *braziliensis* Populations. *Vet. Med. Int.* 2013, 982183. doi: 10.1155/2013/982183
- De-Silva, D. L., Elias, M., Willmott, K., Mallet, J., and Day, J. J. (2016). Diversification of clearwing butterflies with the rise of the Andes. *J. Biogeogr.* 43, 44–58. doi: 10.1111/jbi.12611
- Dick, C. W., Roubik, D. W., Gruber, K. F., and Bermingham, E. (2004). Long-distance gene flow and cross-Andean dispersal of lowland rainforest bees (Apidae: Euglossini) revealed by comparative mitochondrial DNA phylogeography. *Mol. Ecol.* 13, 3775–3785. doi: 10.1111/j.1365-294X.2004.02374.x
- Downing, T., Imamura, H., Decuyper, S., Clark, T. G., Coombs, G. H., Cotton, J. A., et al. (2011). Whole genome sequencing of multiple *Leishmania donovani* clinical isolates provides insights into population structure and mechanisms of drug resistance. *Genome Res.* 21, 2143–2156. doi: 10.1101/gr.123430.111
- Dumetz, F., Imamura, H., Sanders, M., Seblova, V., Myskova, J., Pescher, P., et al. (2017). Modulation of Aneuploidy in *Leishmania donovani* during Adaptation to Different In Vitro and In Vivo Environments and Its Impact on Gene Expression. *MBio* 8. doi: 10.1128/mBio.00599-17
- Dunkel, N., and Morschhauser, J. (2011). Loss of heterozygosity at an unlinked genomic locus is responsible for the phenotype of a *Candida albicans* sap4Delta sap5Delta sap6Delta mutant. *Eukaryot. Cell.* 10, 54–62. doi: 10.1128/EC.00281-10
- Ferro, C., Marin, D., Gongora, R., Carrasquilla, M. C., Trujillo, J. E., Rueda, N. K., et al. (2011). Phlebotomine vector ecology in the domestic transmission of American cutaneous leishmaniasis in Chaparral, Colombia. *Am. J. Trop. Med. Hyg.* 85, 847–856. doi: 10.4269/ajtmh.2011.10-0560
- Ferro, C., Lopez, M., Fuya, P., Lugo, L., Cordovez, J. M., and Gonzalez, C. (2015). Spatial Distribution of Sand Fly Vectors and Eco-Epidemiology of Cutaneous Leishmaniasis Transmission in Colombia. *PLoS One* 10, e0139391. doi: 10.1371/journal.pone.0139391
- Fotouhi-Ardakani, R., Dabiri, S., Ajdari, S., Alimohammadian, M. H., Alaeenovin, E., Taleshi, N., et al. (2016). Assessment of nuclear and mitochondrial genes in precise identification and analysis of genetic polymorphisms for the evaluation of *Leishmania* parasites. *Infect. Genet. Evol.* 46, 33–41. doi: 10.1016/j.meegid.2016.10.011
- Franssen, S. U., Durrant, C., Stark, O., Moser, B., Downing, T., Imamura, H., et al. (2020). Global genome diversity of the *Leishmania donovani* complex. *Elife* 9. doi: 10.7554/eLife.51243
- Ghouila, A., Guerfali, F. Z., Atri, C., Bali, A., Attia, H., Sghaier, R. M., et al. (2017). Comparative genomics of Tunisian *Leishmania* major isolates causing human cutaneous leishmaniasis with contrasting clinical severity. *Infect. Genet. Evol.* 50, 110–120. doi: 10.1016/j.meegid.2016.10.029
- Gomez-Palacio, A., and Triana, O. (2014). Molecular evidence of demographic expansion of the chagas disease vector *Triatoma dimidiata* (Hemiptera, Reduviidae, Triatominae) in Colombia. *PLoS Negl. Trop. Dis.* 8, e2734. doi: 10.1371/journal.pntd.0002734
- Gonzalez, C., Paz, A., and Ferro, C. (2014). Predicted altitudinal shifts and reduced spatial distribution of *Leishmania infantum* vector species under climate change scenarios in Colombia. *Acta Trop.* 129, 83–90. doi: 10.1016/j.actatropica.2013.08.014
- Harrison, R. G., and Larson, E. L. (2014). Hybridization, introgression, and the nature of species boundaries. *J. Hered.* 105 (Suppl 1), 795–809. doi: 10.1093/jhered/esu033
- Henson, S., Bishop, R. P., Morzaria, S., Spooner, P. R., Pelle, R., Poveda, L., et al. (2012). High-resolution genotyping and mapping of recombination and gene conversion in the protozoan *Theileria parva* using whole genome sequencing. *BMC Genomics* 13, 503. doi: 10.1186/1471-2164-13-503
- Herrera, G., Hernandez, C., Ayala, M. S., Florez, C., Teheran, A. A., and Ramirez, J. D. (2017). Evaluation of a Multilocus Sequence Typing (MLST) scheme for *Leishmania* (*Viannia*) *braziliensis* and *Leishmania* (*Viannia*) *panamensis* in Colombia. *Parasit. Vectors* 10, 236. doi: 10.1186/s13071-017-2175-8
- Hirakawa, M. P., Martinez, D. A., Sakthikumar, S., Anderson, M. Z., Berlin, A., Gujja, S., et al. (2015). Genetic and phenotypic intra-species variation in *Candida albicans*. *Genome Res.* 25, 413–425. doi: 10.1101/gr.174623.114
- Hoffert, K. M., and Strome, E. D. (2019). Single-Gene Deletions Contributing to Loss of Heterozygosity in *Saccharomyces cerevisiae*: Genome-Wide Screens and Reproducibility. *G3 (Bethesda)* 9, 2835–2850. doi: 10.1534/g3.119.400429
- Huson, D. H., and Bryant, D. (2006). Application of phylogenetic networks in evolutionary studies. *Mol. Biol. Evol.* 23, 254–267. doi: 10.1093/molbev/msj030
- Iantorno, S. A., Durrant, C., Khan, A., Sanders, M. J., Beverley, S. M., Warren, W. C., et al. (2017). Gene Expression in *Leishmania* Is Regulated Predominantly by Gene Dosage. *mBio* 8. doi: 10.1128/mBio.01393-17
- Imamura, H., Downing, T., Van Den Broeck, F., Sanders, M. J., Rijal, S., Sundar, S., et al. (2016). Evolutionary genomics of epidemic visceral leishmaniasis in the Indian subcontinent. *Elife* 5. doi: 10.7554/eLife.12613
- Inbar, E., Shaik, J., Iantorno, S. A., Romano, A., Nzulu, C. O., Owens, K., et al. (2019). Whole genome sequencing of experimental hybrids supports meiosis-like sexual recombination in *Leishmania*. *PLoS Genet.* 15, e1008042. doi: 10.1371/journal.pgen.1008042
- Jirmanus, L., Glesby, M. J., Guimaraes, L. H., Lago, E., Rosa, M. E., Machado, P. R., et al. (2012). Epidemiological and clinical changes in American tegumentary leishmaniasis in an area of *Leishmania* (*Viannia*) *braziliensis* transmission over a 20-year period. *Am. J. Trop. Med. Hyg.* 86, 426–433. doi: 10.4269/ajtmh.2012.11-0378
- Kuhls, K., Cupolillo, E., Silva, S. O., Schweynoch, C., Boite, M. C., Mello, M. N., et al. (2013). Population structure and evidence for both clonality and recombination among Brazilian strains of the subgenus *Leishmania* (*Viannia*). *PLoS Negl. Trop. Dis.* 7, e2490. doi: 10.1371/journal.pntd.0002490
- Laffitte, M. N., Leprohon, P., Papadopolou, B., and Ouellette, M. (2016). Plasticity of the *Leishmania* genome leading to gene copy number variations and drug resistance. *F1000Res* 5, 2350. doi: 10.12688/f1000research.9218.1
- Letunic, I., and Bork, P. (2019). Interactive Tree Of Life (iTOL) v4: recent updates and new developments. *Nucleic Acids Res.* 47, W256–W259. doi: 10.1093/nar/gkz239
- Marco, J. D., Barroso, P. A., Locatelli, F. M., Cajal, S. P., Hoyos, C. L., Nevot, M. C., et al. (2015). Multilocus sequence typing approach for a broader range of species of *Leishmania* genus: describing parasite diversity in Argentina. *Infect. Genet. Evol.* 30, 308–317. doi: 10.1016/j.meegid.2014.12.031
- Marlow, M. A., Boite, M. C., Ferreira, G. E., Steindel, M., and Cupolillo, E. (2014). Multilocus sequence analysis for *Leishmania braziliensis* outbreak investigation. *PLoS Negl. Trop. Dis.* 8, e2695. doi: 10.1371/journal.pntd.0002695
- Mauricio, I. L., Gaunt, M. W., Stothard, J. R., and Miles, M. A. (2007). Glycoprotein 63 (gp63) genes show gene conversion and reveal the evolution of Old World *Leishmania*. *Int. J. Parasitol.* 37, 565–576. doi: 10.1016/j.ijpara.2006.11.020
- Meireles, C. B., Maia, L. C., Soares, G. C., Teodoro, I. P. P., Gadelha, M., Da Silva, C. G. L., et al. (2017). Atypical presentations of cutaneous leishmaniasis: A systematic review. *Acta Trop.* 172, 240–254. doi: 10.1016/j.actatropica.2017.05.022
- Messenger, L. A., and Miles, M. A. (2015). Evidence and importance of genetic exchange among field populations of *Trypanosoma cruzi*. *Acta Trop.* 151, 150–155. doi: 10.1016/j.actatropica.2015.05.007
- Monsalve, Y., Panzera, F., Herrera, L., Triana-Chavez, O., and Gomez-Palacio, A. (2016). Population differentiation of the Chagas disease vector *Triatoma maculata* (Erichson 1848) from Colombia and Venezuela. *J. Vector Ecol.* 41, 72–79. doi: 10.1111/jvec.12196
- Nolder, D., Roncal, N., Davies, C. R., Llanos-Cuentas, A., and Miles, M. A. (2007). Multiple hybrid genotypes of *Leishmania* (*viannia*) in a focus of mucocutaneous leishmaniasis. *Am. J. Trop. Med. Hyg.* 76, 573–578.
- Oberle, M., Balmer, O., Brun, R., and Roditi, I. (2010). Bottlenecks and the maintenance of minor genotypes during the life cycle of *Trypanosoma brucei*. *PLoS Pathog.* 6, e1001023. doi: 10.1371/journal.ppat.1001023
- Ore, M., Saenz, E., Cabrera, R., Sanchez, J. F., De Los Santos, M. B., Lucas, C. M., et al. (2015). Outbreak of Cutaneous Leishmaniasis in Peruvian Military Personnel Undertaking Training Activities in the Amazon Basin 2010. *Am. J. Trop. Med. Hyg.* 93, 340–346. doi: 10.4269/ajtmh.15-0107
- Ovalle-Bracho, C., Londono-Barbosa, D., Salgado-Almario, J., and Gonzalez, C. (2019). Evaluating the spatial distribution of *Leishmania* parasites in Colombia from clinical samples and human isolates, (1999 to 2016). *PLoS One* 14, e0214124. doi: 10.1371/journal.pone.0214124

- Ovallos, F. G., Silva, Y. R., Fernandez, N., Gutierrez, R., Galati, E. A., and Sandoval, C. M. (2013). The sandfly fauna, anthropophily and the seasonal activities of *Pintomyia spinicrassa* (Diptera: Psychodidae: Phlebotominae) in a focus of cutaneous leishmaniasis in northeastern Colombia. *Mem. Inst. Oswaldo Cruz.* 108. doi: 10.1590/S0074-02762013000300007
- Page, A. J., Taylor, B., Delaney, A. J., Soares, J., Seemann, T., Keane, J. A., et al. (2016). SNP-sites: rapid efficient extraction of SNPs from multi-FASTA alignments. *Microb. Genom.* 2, e000056. doi: 10.1099/mgen.0.000056
- Paradis, E., Claude, J., and Strimmer, K. (2004). APE: Analyses of Phylogenetics and Evolution in R language. *Bioinformatics* 20, 289–290. doi: 10.1093/bioinformatics/btg412
- Patino, L. H., Mendez, C., Rodriguez, O., Romero, Y., Velandia, D., Alvarado, M., et al. (2017). Spatial distribution, Leishmania species and clinical traits of Cutaneous Leishmaniasis cases in the Colombian army. *PLoS Negl. Trop. Dis.* 11, e0005876. doi: 10.1371/journal.pntd.0005876
- Patino, L. H., Imamura, H., Cruz-Saavedra, L., Pavia, P., Muskus, C., Mendez, C., et al. (2019a). Major changes in chromosomal copy number, gene expression and gene dosage driven by Sb(III) in *Leishmania braziliensis* and *Leishmania panamensis*. *Sci. Rep.* 9, 9485. doi: 10.1038/s41598-019-45538-9
- Patino, L. H., Muskus, C., Munoz, M., and Ramirez, J. D. (2019b). Genomic analyses reveal moderate levels of ploidy, high heterozygosity and structural variations in a Colombian isolate of *Leishmania (Leishmania) amazonensis*. *Acta Trop.* 203, 105296. doi: 10.1016/j.actatropica.2019.105296
- Patino, L. H., Munoz, M., Muskus, C., Mendez, C., and Ramirez, J. D. (2020). Intraspecific Genomic Divergence and Minor Structural Variations in *Leishmania (Viannia) panamensis*. *Genes (Basel)* 11. doi: 10.3390/genes11030252
- Perez, S. D., Grummer, J. A., Fernandes-Santos, R. C., Jose, C. T., Medici, E. P., and Marcili, A. (2019). Phylogenetics, patterns of genetic variation and population dynamics of *Trypanosoma terrestris* support both coevolution and ecological host-fitting as processes driving trypanosome evolution. *Parasit. Vectors* 12, 473. doi: 10.1186/s13071-019-3726-y
- Perez-Franco, J. E., Cruz-Barrera, M. L., Robayo, M. L., Lopez, M. C., Daza, C. D., Bedoya, A., et al. (2016). Clinical and Parasitological Features of Patients with American Cutaneous Leishmaniasis that Did Not Respond to Treatment with Meglumine Antimoniate. *PLoS Negl. Trop. Dis.* 10, e0004739. doi: 10.1371/journal.pntd.0004739
- Price, M. N., Dehal, P. S., and Arkin, A. P. (2009). FastTree: computing large minimum evolution trees with profiles instead of a distance matrix. *Mol. Biol. Evol.* 26, 1641–1650. doi: 10.1093/molbev/msp077
- Qi, J., Wijeratne, A. J., Tomsho, L. P., Hu, Y., Schuster, S. C., and Ma, H. (2009). Characterization of meiotic crossovers and gene conversion by whole-genome sequencing in *Saccharomyces cerevisiae*. *BMC Genomics* 10, 475. doi: 10.1186/1471-2164-10-475
- Quaresma, P. F., De Brito, C. F. A., Rugani, J. M. N., Freire, J. M., Baptista, R. P., Moreno, E. C., et al. (2018). Distinct genetic profiles of *Leishmania (Viannia) braziliensis* associate with clinical variations in cutaneous-leishmaniasis patients from an endemic area in Brazil. *Parasitology* 145, 1161–1169. doi: 10.1017/S0031182018000276
- Ramirez, J. D., Gohl, F., Messenger, L. A., Lewis, M. D., Montilla, M., Cucunuba, Z., et al. (2012). Contemporary cryptic sexuality in *Trypanosoma cruzi*. *Mol. Ecol.* 21, 4216–4226. doi: 10.1111/j.1365-294X.2012.05699.x
- Ramirez, J. D., Hernandez, C., Leon, C. M., Ayala, M. S., Florez, C., and Gonzalez, C. (2016). Taxonomy, diversity, temporal and geographical distribution of Cutaneous Leishmaniasis in Colombia: A retrospective study. *Sci. Rep.* 6, 28266. doi: 10.1038/srep28266
- Rastrojo, A., Carrasco-Ramiro, F., Martin, D., Crespo, A., Reguera, R. M., Aguado, B., et al. (2013). The transcriptome of *Leishmania major* in the axenic promastigote stage: transcript annotation and relative expression levels by RNA-seq. *BMC Genomics* 14, 223. doi: 10.1186/1471-2164-14-223
- Rego, F. D., Da Rocha Lima, A., Pereira, A. A. S., Quaresma, P. F., Pascoal-Xavier, M. A., Shaw, J. J., et al. (2018). Genetic variant strains of *Leishmania (Viannia) braziliensis* exhibit distinct biological behaviors. *Parasitol. Res.* 117, 3157–3168. doi: 10.1007/s00436-018-6014-4
- Restrepo, C. M., De La Guardia, C., Sousa, O. E., Calzada, J. E., Fernandez, P. L., and Leonart, R. (2013). AFLP polymorphisms allow high resolution genetic analysis of American Tegumentary Leishmaniasis agents circulating in Panama and other members of the *Leishmania* genus. *PLoS One* 8, e73177. doi: 10.1371/journal.pone.0073177
- Restrepo, C. M., Llanes, A., De La Guardia, C., and Leonart, R. (2015). Genome-wide discovery and development of polymorphic microsatellites from *Leishmania panamensis* parasites circulating in central Panama. *Parasit. Vectors* 8, 527. doi: 10.1186/s13071-015-1153-2
- Restrepo, C. M., Llanes, A., Cedeno, E. M., Chang, J. H., Alvarez, J., Rios, M., et al. (2019). Environmental Conditions May Shape the Patterns of Genomic Variations in *Leishmania panamensis*. *Genes (Basel)* 10. doi: 10.3390/genes10110838
- Rogers, M. B., Hilley, J. D., Dickens, N. J., Wilkes, J., Bates, P. A., Depledge, D. P., et al. (2011). Chromosome and gene copy number variation allow major structural change between species and strains of *Leishmania*. *Genome Res.* 21, 2129–2142. doi: 10.1101/gr.122945.111
- Rogers, M. B., Downing, T., Smith, B. A., Imamura, H., Sanders, M., Svobodova, M., et al. (2014). Genomic confirmation of hybridisation and recent inbreeding in a vector-isolated *Leishmania* population. *PLoS Genet.* 10, e1004092. doi: 10.1371/journal.pgen.1004092
- Roque, A. L., and Jansen, A. M. (2014). Wild and synanthropic reservoirs of *Leishmania* species in the Americas. *Int. J. Parasitol. Parasites Wildl.* 3, 251–262. doi: 10.1016/j.ijppaw.2014.08.004
- Rougeron, V., De Meeus, T., Hide, M., Waleckx, E., Bermudez, H., Arevalo, J., et al. (2009). Extreme inbreeding in *Leishmania braziliensis*. *Proc. Natl. Acad. Sci. U. S. A.* 106, 10224–10229. doi: 10.1073/pnas.0904420106
- Salgado-Roa, F. C., Pardo-Diaz, C., Lasso, E., Arias, C. F., Solferini, V. N., and Salazar, C. (2018). Gene flow and Andean uplift shape the diversification of *Gasteracantha cancriformis* (Araneae: Araneidae) in Northern South America. *Ecol. Evol.* 8, 7131–7142. doi: 10.1002/ecs3.4237
- Samarasinghe, S. R., Samaranyake, N., Kariyawasam, U. L., Siriwardana, Y. D., Imamura, H., and Karunaweera, N. D. (2018). Genomic insights into virulence mechanisms of *Leishmania donovani*: evidence from an atypical strain. *BMC Genomics* 19, 843. doi: 10.1186/s12864-018-5271-z
- Schliep, K., Paradis, E., De Oliveira Martins, L., Potts, A., and Whit, T. W. (2019). *Phylogenetic Reconstruction and Analysis. Package "phangorn"*. Available at: <https://academic.oup.com/bioinformatics/article/27/4/592/198887>.
- Schwabl, P., Imamura, H., Van Den Broeck, F., Costales, J. A., Maiguashca-Sanchez, J., Miles, M. A., et al. (2019). Meiotic sex in Chagas disease parasite *Trypanosoma cruzi*. *Nat. Commun.* 10, 3972. doi: 10.1038/s41467-019-11771-z
- Sinha, R., Malar, C. M., Raghwan, S., Das, S., Shadab, M., et al. (2018). Genome Plasticity in Cultured *Leishmania donovani*: Comparison of Early and Late Passages. *Front. Microbiol.* 9, 1279. doi: 10.3389/fmicb.2018.01279
- Sriswasdi, S., Takashima, M., Manabe, R., Ohkuma, M., Sugita, T., and Iwasaki, W. (2016). Global deceleration of gene evolution following recent genome hybridizations in fungi. *Genome Res.* 26, 1081–1090. doi: 10.1101/gr.205948.116
- Supek, F., Bosnjak, M., Skunca, N., and Smuc, T. (2011). REVIGO summarizes and visualizes long lists of gene ontology terms. *PLoS One* 6, e21800. doi: 10.1371/journal.pone.0021800
- Teixeira, D. G., Monteiro, G. R. G., Martins, D. R. A., Fernandes, M. Z., Macedo-Silva, V., Ansaldi, M., et al. (2017). Comparative analyses of whole genome sequences of *Leishmania infantum* isolates from humans and dogs in northeastern Brazil. *Int. J. Parasitol.* 47, 655–665. doi: 10.1016/j.ijpara.2017.04.004
- Testa, J. M., Montoya-Lerma, J., Cadena, H., Oviedo, M., and Ready, P. D. (2002). Molecular identification of vectors of *Leishmania* in Colombia: mitochondrial introgression in the *Lutzomyia townsendi* series. *Acta Trop.* 84, 205–218. doi: 10.1016/s0001-706x(02)00187-0
- Testo, W. L., Sessa, E., and Barrington, D. S. (2019). The rise of the Andes promoted rapid diversification in Neotropical *Phlegmariurus* (Lycopodiaceae). *New Phytol.* 222, 604–613. doi: 10.1111/nph.15544
- Tihon, E., Imamura, H., Van Den Broeck, F., Vermeiren, L., Dujardin, J. C., and Van Den Abbeele, J. (2017). Genomic analysis of Isometamidium Chloride resistance in *Trypanosoma congolense*. *Int. J. Parasitol. Drugs Drug Resist.* 7, 350–361. doi: 10.1016/j.ijpdr.2017.10.002
- Urrea, D. A., Duitama, J., Imamura, H., Alzate, J. F., Gil, J., Munoz, N., et al. (2018). Genomic Analysis of Colombian *Leishmania panamensis* strains with different level of virulence. *Sci. Rep.* 8, 17336. doi: 10.1038/s41598-018-35778-6

- Valderrama-Ardila, C., Alexander, N., Ferro, C., Cadena, H., Marin, D., Holford, T. R., et al. (2010). Environmental risk factors for the incidence of American cutaneous leishmaniasis in a sub-Andean zone of Colombia (Chaparral, Tolima). *Am. J. Trop. Med. Hyg.* 82, 243–250. doi: 10.4269/ajtmh.2010.09-0218
- Valdivia, H. O., Reis-Cunha, J. L., Rodrigues-Luiz, G. F., Baptista, R. P., Baldeviano, G. C., Gerbasi, R. V., et al. (2015). Comparative genomic analysis of *Leishmania* (Viannia) *peruviana* and *Leishmania* (Viannia) *braziliensis*. *BMC Genomics* 16, 715. doi: 10.1186/s12864-015-1928-z
- Valdivia, H. O., Almeida, L. V., Roatt, B. M., Reis-Cunha, J. L., Pereira, A. A., Gontijo, C., et al. (2017). Comparative genomics of canine-isolated *Leishmania* (*Leishmania*) *amazonensis* from an endemic focus of visceral leishmaniasis in Governador Valadares, southeastern Brazil. *Sci. Rep.* 7, 40804. doi: 10.1038/srep40804
- Wertheimer, N. B., Stone, N., and Berman, J. (2016). Ploidy dynamics and evolvability in fungi. *Philos. Trans. R Soc. Lond. B Biol. Sci.* 371. doi: 10.1098/rstb.2015.0461
- Wickham, H. (2019). *Simple, Consistent Wrappers for Common String Operations: Package "stringr"*. Available at: <https://joss.theoj.org/papers/10.21105/joss.01686.pdf>.
- Yan, L., Yang, M., Guo, H., Yang, L., Wu, J., Li, R., et al. (2013). Single-cell RNA-Seq profiling of human preimplantation embryos and embryonic stem cells. *Nat. Struct. Mol. Biol.* 20, 1131–1139. doi: 10.1038/nsmb.2660
- Zhao, S., Guo, Y., Sheng, Q., and Shyr, Y. (2014). Advanced heat map and clustering analysis using heatmap3. *BioMed. Res. Int.* 2014, 986048. doi: 10.1155/2014/986048

Conflict of Interest: The authors declare that the research was conducted in the absence of any commercial or financial relationships that could be construed as a potential conflict of interest.

Copyright © 2020 Patino, Muñoz, Cruz-Saavedra, Muskus and Ramírez. This is an open-access article distributed under the terms of the Creative Commons Attribution License (CC BY). The use, distribution or reproduction in other forums is permitted, provided the original author(s) and the copyright owner(s) are credited and that the original publication in this journal is cited, in accordance with accepted academic practice. No use, distribution or reproduction is permitted which does not comply with these terms.



Study on the Occurrence of Genetic Exchange Among Parasites of the *Leishmania mexicana* Complex

Roman Telittchenko and Albert Descoteaux*

Institut national de la recherche scientifique, Centre Armand-Frappier Santé Biotechnologie, Laval, QC, Canada

OPEN ACCESS

Edited by:

Juan David Ramírez,
Rosario University, Colombia

Reviewed by:

Isabel Mauricio,
New University of Lisbon, Portugal
Luz Patino,
Universidad del Rosario, Colombia

*Correspondence:

Albert Descoteaux
albert.descoteaux@inrs.ca

Specialty section:

This article was submitted to
Parasite and Host,
a section of the journal
Frontiers in Cellular
and Infection Microbiology

Received: 16 September 2020

Accepted: 10 November 2020

Published: 07 December 2020

Citation:

Telittchenko R and Descoteaux A
(2020) Study on the Occurrence of
Genetic Exchange Among Parasites of
the *Leishmania mexicana* Complex.
Front. Cell. Infect. Microbiol. 10:607253.
doi: 10.3389/fcimb.2020.607253

In *Leishmania*, genetic exchange has been experimentally demonstrated to occur in the sand fly vector and in promastigote axenic cultures through a meiotic-like process. No evidence of genetic exchange in mammalian hosts have been reported so far, possibly due to the fact that the *Leishmania* species used in previous studies replicate within individual parasitophorous vacuoles. In the present work, we explored the possibility that residing in communal vacuoles may provide conditions favorable for genetic exchange for *L. mexicana* and *L. amazonensis*. Using promastigote lines of both species harboring integrated or episomal drug-resistance markers, we assessed whether genetic exchange can occur in axenic cultures, in infected macrophages as well as in infected mice. We obtained evidence of genetic exchange for *L. amazonensis* in both axenic promastigote cultures and infected macrophages. However, the resulting products of those putative genetic events were unstable as they did not sustain growth in subsequent sub-cultures, precluding further characterization.

Keywords: genetic exchange, *Leishmania*, host-pathogen relationship, macrophage, drug resistance, intracellular pathogen

INTRODUCTION

Protozoan parasites of the genus *Leishmania* are the causative agents of a spectrum of diseases known as leishmaniasis that range from self-healing cutaneous lesions to destructive mucocutaneous infections and visceral pathologies. *Leishmania* has a distinct life cycle which consists of two specific environments. The first is that of the sand fly insect vector in which the parasites multiply within the alimentary tract under the promastigote form and the second is the infected mammalian or human hosts where the parasites replicate as amastigotes within the phagolysosomal compartment of host phagocytes. Currently, there are 20 known species of parasites that are associated with human disease. However, there is still a considerable amount of debate of whether this diversity is due to recombinational events or due to gradual accumulation of mutations during clonal division (Tibayrenc and Ayala, 2013; Rougeron et al., 2017).

In eukaryotic pathogenic organisms, sex is one of the main mechanisms that allows the spread of pathogenicity, resistance, and virulence genes (Heitman, 2010). Due to very strong linkage disequilibrium observed in *Leishmania*, it has been argued that the reproductive mode of *Leishmania* is predominantly clonal (Tibayrenc and Ayala, 2013). However, there is much evidence indicating that genetic exchange is part of the biology of *Leishmania* parasites, as

evidenced by the occurrence of hybrids in nature. These natural hybrids were described at the intraspecific level for *L. tropica*, *L. donovani*, *L. infantum*, and *L. brasiliensis* (Chargui et al., 2009; Rougeron et al., 2009; Gelanew et al., 2014; Rogers et al., 2014; Iantorno et al., 2017). There were also reports of hybrids that originated from crosses between parasites of the *Viannia* subgenus, such as *L. braziliensis* and *L. guyanensis*, which are one of the most common ones described (Bonfante-Garrido et al., 1992; Belli et al., 1994; Dujardin et al., 1995; Banuls et al., 1997; Cupolillo et al., 1997; Delgado et al., 1997; Banuls et al., 1999; Torrico et al., 1999; Nolder et al., 2007; Cortes et al., 2012; Jennings et al., 2014; Kato et al., 2016; Kato et al., 2019). Natural hybrids were also reported for *Leishmania* species of the *Leishmania* subgenus such as *L. major* and *L. arabica*, *L. major* and *L. infantum*, as well as *L. donovani* and *L. infantum* (Evans et al., 1987; Kelly et al., 1991; Ravel et al., 2006; Volf et al., 2007; Odiwuor et al., 2011; Seblova et al., 2015; Cortes et al., 2019).

Using two strains of *L. major* harboring distinct integrated drug-resistance markers, Akopyants and colleagues experimentally demonstrated the existence of genetic exchange in the invertebrate stage of the parasite (Akopyants et al., 2009). By infecting sand flies and dissecting them 13–16 days post-infection, the double drug-resistant progeny of this cross was further demonstrated to be actual genomic hybrids by confirming the presence of at least one set of allelic markers from each parent (Akopyants et al., 2009). In another study from the same group, it was further shown that crosses in the invertebrate stage between *L. major* parasites coming from 4 distinct geographical locations are able to produce hybrid progeny, which also suggests that there are no intraspecies barriers when it comes to exchanging genetic information (Inbar et al., 2013). Another interesting finding, was that hybrid formation was observed in both the natural *P. duboscqi* vector and in the unnatural but permissive *L. longipalpis* and, by isolating the parasites from infected sand flies 3–18 days post-infection, it was further ruled out that genetic exchange takes place between parasites when they are in the nectomonad form (Inbar et al., 2013). In addition, a study based on microscopy and flow cytometry allowed to visualize evidence of genetic exchange between two strains of *L. donovani* expressing two different fluorescent molecules (RFP and GFP) which were present in the same vector (*P. perniciosus* or *L. longipalpis*) and gave rise to yellow promastigote progeny; however, these putative hybrids could not be recovered from the sand flies and grown in culture for further analyses (Sadlova et al., 2011). There was also a study which demonstrated hybrid formation in sand flies between two *L. infantum* strains expressing different fluorescent as well as different drug-resistance markers (Calvo-Alvarez et al., 2014) and another paper demonstrated formation of hybrid parasite strains in sand flies between two entirely different species, namely *L. major* and *L. infantum* (Romano et al., 2014). Finally, the ability of *L. tropica* to exchange genetic information in an intraspecific manner in an infected insect vector as well as in axenic culture has also been recently demonstrated using whole genome sequencing (Inbar et al., 2019; Louradour et al., 2020).

Despite the fact that hybrid parasites could be isolated both in nature and in laboratory conditions from infected sand flies and axenic cultures, the mechanism by which they reproduce is still poorly understood. This is partially due to the fact that this is not an obligate mode of reproduction of the parasite; however, recent genome sequencing data from 44 hybrids generated between and within *L. infantum*, *L. tropica*, and *L. major* suggest that *Leishmania* reproduces via a meiotic-like mechanism (Inbar et al., 2019). Apart from one study using *L. major* (Akopyants et al., 2009), it is still not widely known whether or not genetic exchange can occur within an infected mammalian host, although there is a study that has shown previously by DNA quantification that infected macrophages could harbor 4N amastigotes suggesting that genetic exchange is possible in mammalian host cells (Kreutzer et al., 1994). Here, we explored the possibility of intraclonal and interspecific genetic exchange among parasites of the *L. mexicana* complex, which unlike other *Leishmania* species, replicate in spacious communal vacuoles that may provide an environment favorable to genetic exchange (Case et al., 2016).

MATERIALS AND METHODS

Ethics Statement

All animal handling was performed in accordance with the protocols 1806–01 and 1806–02, which were approved by the *Comité Institutionnel de Protection des Animaux* of the INRS-Centre Armand-Frappier Santé Biotechnologie. These protocols respect procedures on animal practice as instructed by the Canadian Council on Animal Care, described in the Guide to the Care and Use of Experimental Animals.

Plasmids and Constructs

The plasmid pLaLPG2-HYG from which the *LPG2::ΔHYG* targeting construct was used to create Hygromycin B-resistant parasites was kindly provided by Drs. Valeria M. Borges and Leonardo Paiva Farias (Fiocruz Bahia - Instituto Gonçalo Moniz, Brazil) (Figure 1). The plasmid pCR2.1-Ld-rDNA-pr-αIRNEOαIR-GFP from which the Ld-rDNA-NEO-GFP targeting sequence was used to create G418-resistant parasites was kindly provided by Dr. Barbara Papadopolou (Université Laval, Canada) (Figure 1). The plasmid pKS-NEO-DsRed was provided by Dr. David L. Sacks (National Institute of Allergy and Infectious Diseases, USA) (Kimblin et al., 2008). The pLeish-HYG-GFP construct was created the following way: a *SacI* fragment containing the *GFP* gene was excised from the plasmid pXG-GFP⁺ (Ha et al., 1996), blunted, and inserted into the *EcoRV* site of pLeish-HYG (unpublished), yielding pLeish-HYG-GFP.

Parasites

Both *L. amazonensis* LV79 (MPRO/BR/72/M1841) and *L. mexicana* (MNYC/BZ/62/M379) were passaged in mice to maintain their virulence. Amastigotes recovered from ear dermis lesions of infected C57BL/6 mice were differentiated

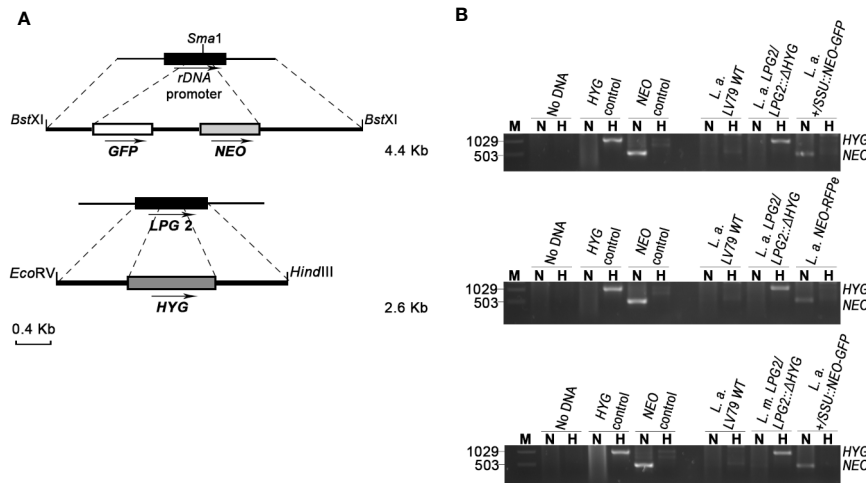


FIGURE 1 | Generation of drug-resistant *Leishmania* parasites. **(A)** L.d-rDNA-NEO-GFP and LPG2::ΔHYG targeting constructs were used for the integration into the ribosomal RNA locus or in one allele of LPG2, respectively. For the L.d-rDNA-NEO-GFP construct, the NEO-GFP resistance cassette (white and gray boxes) was inserted in the SmaI site of the ribosomal RNA locus (black rectangle). The dashed lines delimit the regions of recombination between the target genes and targeting constructs. Arrows indicate orientation. **(B)** PCR products for drug resistance markers HYG and NEO of *L. amazonensis* and *L. mexicana* parental strains. The size of HYG and NEO resistance genes is 1,029 and 503 bp long, respectively. The pLeish-HYG-GFP and the pKS-NEO-DsRed constructs were used as controls for the HYG and NEO genes, respectively. *L. a.* LV79 WT is a DNA sample used to show that our wild type parasites do not harbor any drug-resistance markers in their genomes. *L. amazonensis* LPG2/LPG2::ΔHYG, *L. amazonensis* +/SSU::NEO-GFP, *L. mexicana* LPG2/LPG2::ΔHYG and *L. amazonensis* NEO-DsRede are controls used to validate the presence of HYG and NEO resistance genes. No DNA sample was loaded as negative control. M, molecular DNA ladder; H, Hygromycin; N, G418.

into promastigotes in *Leishmania* medium (M199-1X (Sigma) with 10% heat-inactivated fetal bovine serum (FBS), 100 μ M hypoxanthine, 3 μ M bioppterin, 40 mM HEPES at pH 7.4, 5 μ M hemin, 1 μ M biotin, and Penicillin-Streptomycin) in a 26°C incubator. For the generation of *L. amazonensis* LPG2/LPG2::ΔHYG and *L. mexicana* LPG2/LPG2::ΔHYG, log-phase *L. amazonensis* and *L. mexicana* promastigotes were electroporated with the LPG2::ΔHYG targeting construct (excised as a 2.6-kb EcoRVI-HindIII-BglII fragment from pLaLPG2KO-HYG) in 0.2 cm electroporation cuvettes, at 0.45 kV and 500 μ F of high capacitance as previously described in similar protocols (Descoteaux et al., 1994; Turco et al., 1994). After electroporation, promastigotes were grown in drug-free *Leishmania* medium for 24 h. Following this incubation, *L. amazonensis* LPG2/LPG2::ΔHYG parasites were selected in the presence of 35 μ g/ml Hygromycin B (Sigma) and *L. mexicana* LPG2/LPG2::ΔHYG parasites were selected in the presence of 70 μ g/ml Hygromycin B (Sigma) respectively. For the generation of *L. amazonensis* +/SSU::NEO-GFP, *L. amazonensis* promastigotes were electroporated with the L.d-rDNA-NEO-GFP targeting construct (excised as a 4.25-kb BstXI fragment from pCR2.1-L.d-rDNA-pr- α IRNEO α IR-GFP). After electroporation, the parasites were grown in drug free medium for 24 h and then grown in *Leishmania* medium containing 20 μ g/ml G418 (Life Technologies). *L. amazonensis* NEO-DsRede parasites were obtained by electroporating *L. amazonensis* promastigotes with the plasmid pKS-NEO-DsRed. Parasites were grown in drug free medium for 24 h and then grown in medium containing 20 μ g/ml G418. The same method was used to obtain *L. mexicana* pKS-NEO-DsRede and they were maintained in *Leishmania* medium

containing 40 μ g/ml of G418. *L. amazonensis* HYG-GFPe promastigotes were generated by electroporating *L. amazonensis* with the plasmid pLeish-HYG-GFP. Parasites were grown in drug-free medium for 24 h and then grown in medium containing 35 μ g/ml Hygromycin B

Mammalian Cell Culture

Bone marrow-derived macrophages (BMM) were differentiated from the bone marrow of 6- to 8-week old C57BL/6 mice as previously described (Descoteaux and Matlashewski, 1989). BMM were differentiated for 7 days in complete DMEM [containing L-glutamine (Life Technologies), 10% v/v heat inactivated fetal bovine serum (FBS) (Life Technologies), 10 mM HEPES (Bioshop) at pH 7.4, and penicillin-streptomycin (Life Technologies)] supplemented with 15% v/v L929 cell-conditioned medium (LCM) as a source of macrophage colony-stimulating factor-1. To render the BMM quiescent prior to experiments, cells were transferred to tissue culture-treated 6- or 24-well plates or T25 tissue culture flasks for 24 h in complete DMEM without LCM. The cells were kept in a humidified 37°C incubator with 5% CO₂. The number of macrophages used per container are as following: 2.2 X 10⁶ BMMs per well of a 6-well plate, 0.3 X 10⁶ BMMs per well of 24-well plate and 25 X 10⁶ BMMs in T-25 flasks.

Transwell Experiments

For genetic exchange transwell experiments, donor parasites (*L. amazonensis* NEO-dsRede) were relocated to the insert chamber containing 0.4 μ m pores in a polycarbonate membrane (Corning) and the recipient parasites (*L. amazonensis* LPG2/

LPG2::ΔHYG) were added to the wells. The plates were then either incubated at 26°C or pre-incubated at 34°C for 4 h, as done previously (Hassani et al., 2011), and then transferred to 26°C. The parasites were collected at 24, 72, 96, and 120 h post-incubation. Each parental strain was equally divided into 3 wells of a 6-well plate and were grown in the presence of antibiotics. Two wells were used as controls containing either 35 µg/ml of Hygromycin B or 20 µg/ml of G418 and the last well contained both drugs in the medium. The parasites were kept in such conditions up to 3 weeks. Each parental strain was also grown separately and were under the same conditions as a control.

Parasite Co-Culture Experiments

As described (Louradour et al., 2020), stationary phase promastigotes of two parental strains were mixed and distributed into 96-well plates up to a total volume of 100 µl in each well. One million parasites of each strain were added in the wells. Three days later, each co-culture from the 96-well plate was transferred to a single well of a 24-well plate containing 900 µl of *Leishmania* medium containing either 35 µg/ml Hygromycin B and 20 µg/ml G418 if both parental strains were *L. amazonensis* or 60 µg/ml Hygromycin B and 40 µg/ml G418 if one of the parental strains was *L. amazonensis* and the other was *L. mexicana*. Each line was cultured individually in *Leishmania* medium supplemented with either Hygromycin B or G418 or both drugs as controls. When double drug-resistant parasite cultures were growing in wells (growth was observed between 19 and 28 days), the cells were passaged in *Leishmania* medium at a dilution of 1:10. DNA was then extracted from double drug-resistant parasites and was used for PCR reactions.

In Vitro Infections

Metacyclic promastigotes were isolated from promastigote cultures in the late stationary phase by means of a density gradient centrifugation (Spath and Beverley, 2001). Specifically, 2 ml of 40% w/v Ficoll PM400 (GE healthcare) were added to the bottom of a 15 ml tube, followed by a 5 ml layer of 10% Ficoll PM400 in M199-1x and topped by late stationary phase promastigotes resuspended in 5 ml of DMEM with no FBS (Arango Duque et al., 2019). Metacyclic promastigotes were collected from the DMEM-10% Ficoll interphase after spinning the gradient for 10 min. The percentage of isolated metacyclic parasites from the interphase generally varied from 12–18% of the input population. Metacyclic promastigotes were then opsonized with the serum of C57BL/6 mice for 30 min, washed 3 times with PBS and resuspended in cold complete DMEM (cDMEM). The parasites were then fed to macrophages adhered in T-25 flasks (Sarstedt) (Ratio 3:1 for single infections, ratio 6:1 for mix infections). The cells were then incubated at 4°C for 10 min (Arango Duque et al., 2019) to synchronize phagocytosis. The internalization of parasites was triggered by transferring the cells to 34°C (Arango Duque et al., 2019). Two hours post-internalization, the cells were washed three times with warmed cDMEM to remove non-internalized promastigotes. Infected BMM were incubated for 120 and 192 h. Next, the amastigotes were isolated from infected macrophages by resuspending those in cDMEM containing

0.05% of SDS. Shortly, the macrophages resuspended in 2ml of cDMEM containing SDS are incubated at 37°C for 3 min. Then, the resulting supernatant is resuspended in 10 ml of cDMEM and spun at 3,000 rpm. After the spin, the supernatant was discarded. The amastigotes were resuspended in *Leishmania* medium and separated into 3 separate conditions. The conditions were: *Leishmania* medium containing 20 µg/ml of G418 or *Leishmania* medium containing 32 µg/ml of Hygromycin B or *Leishmania* medium containing both drugs. The parasites were left for incubation at 26°C for up to 3 weeks to select for double drug-resistant parasites. If applicable, the double drug-resistant parasites were passaged at a dilution of 1/10 and their DNA was then extracted and was used for PCR reactions. Double drug-resistant parasites were also passaged in infected BMM for 3 days as well. For parasite survival, cells were washed with PBS and fixed and stained with fixative and staining solutions of the Hema 3 stain set (Fisher Scientific). This process was done for 2, 48, 120, and 192 h timepoints.

Alternatively, the infections were done in 6-well plates instead of T-25 flasks. Three wells were used for mixed infection for each timepoint (120 and 192 h) and two wells were reserved for infection with each parental strain alone. Once the amastigotes were obtained, they were plated in 96-well plates in 100 µl of drug free *Leishmania* medium as described in the parasite co-culture section. The amastigotes were plated at 5 million parasites per well. Three days later, each well was transferred to a well of 24-well plate that contained 900 µl with antibiotics. Pure parental cultures were used as controls as previously described. If applicable, the double drug-resistant parasites were passaged at a dilution of 1/10 and their DNA was then extracted from double drug-resistant parasites and was used for PCR reactions.

In Vivo Infections and Parasite Recovery

C57BL/6 mice (6–8 weeks old) were infected with 1×10^5 metacyclic promastigotes (5×10^4 of each line) of either *L. amazonensis* *LPG2/LPG2::ΔHYG* + *L. amaz* +/SSU::NEO-GFP or *L. mexicana* *LPG2/LPG2::ΔHYG* + *L. amaz* +/SSU::NEO-GFP into the ear dermis with an insulin syringe (29 G). Mice infected separately with each line were used as controls. At 9 weeks post-infection, mice were euthanized under CO₂ asphyxiation and by cerebral dislocation as well. The infected ears were then collected and disinfected in 70% ethanol for 10 min and air dried for 10 min. Then, they were separated into dorsal and ventral leaflets and cut up into small pieces with surgical scissors. The cut-up ears were loaded in 2.0 ml tubes containing zirconium beads (Benchmark Scientific Inc.) and resuspended in 1 ml of *Leishmania* medium and vortexed for a 1 min and 30 s. The resulting suspension was then transferred to 100 µm cell strainers placed over 50 ml Falcon tubes and filtered to isolate the amastigotes. The remaining tissue in the cell strainer was smashed with a sterile 10 ml syringe plunger and washed two times with *Leishmania* medium. The resulting cell suspension was spun at 3,200 RPM at 4°C for 10 min. The amastigotes were then separated in three T-25 flasks and left in unconditioned *Leishmania* medium for 24 h. Lastly, the antibiotics were added to each flask according to each condition and were incubated at 26°C for three weeks. The conditions were Hygromycin only, G418 only or both drugs.

DNA Extraction and PCR Confirmation of Double-Resistant Parasites

For genotyping analyses, total DNA was extracted from parasites by using a phenol/chloroform treatment as previously described (Medina-Acosta and Cross, 1993). All of the PCR amplifications were done in 50 μ l total volume containing 100 ng of parasite DNA and 10pmol of each primer. The following primer pairs were used: for Hygromycin B 5'-ATGAAAAGCCTGA ACTCACC-3' (Forward), 5'-CTATTCCTTTGCCCTCGG-3' (Reverse) that were previously described (Romano, 2014); for G418 5'-CCACGACGGGCGTTTCCTTGCGCAGCTGTGC-3' (Forward), 5'-GTCAGCCCATTTCG CCAAGCTCTTCAGC-3' (Reverse) which were custom made. The resulting DNA products were then verified by electrophoresis on 1.2% Agarose gel and subsequently viewed by staining the samples with ethidium bromide.

Live Microscopy

BMMs were plated at the bottom of 6 well-plate with a coverslip attached to the bottom of the wells. The cells were kept in the 34°C incubator for 24 h without LCM to render them quiescent. They were then infected with metacyclic parasites of each line separately as a positive control or with a combination of two. Non-infected cells were used as a negative control. The samples were then viewed with 63X objective lens LSM780 system confocal microscope (Carl Zeiss microimaging). The images were taken and processed with the ZEN 2012 Software (Carl Zeiss) and subsequently mounted into the figures via Adobe Photoshop 2019.

RESULTS

Generation of Drug-Resistant Strains of *L. amazonensis* and *L. mexicana*

To investigate the possibility that formation of hybrids and genetic exchange may occur among parasites of the *L. mexicana* complex, we used *L. amazonensis* LV79 and *L. mexicana* M379 expressing either episomal or integrated genes encoding resistance to Hygromycin B (*HYG*) or to G418 (*NEO*). To this end, we generated one line of *L. amazonensis* and one line of *L. mexicana* in which the *HYG* resistance gene was integrated in one allele of the *LPG2* gene (*L. amazonensis* *LPG2/LPG2::ΔHYG* and *L. mexicana* *LPG2/LPG2::ΔHYG*) (Figure 1A), one line of *L. amazonensis* in which a *NEO-GFP* construct was integrated into the ribosomal RNA locus (*L. amazonensis* *+SSU::NEO-GFP*) (Figure 1A), one line of *L. amazonensis* and one line of *L. mexicana* with an episomal *NEO-DsRed* plasmid (*L. amazonensis* *NEO-DsRede* and *L. mexicana* *NEO-DsRede*), and one line of *L. amazonensis* with an episomal *HYG-GFP* plasmid (*L. amazonensis* *HYG-GFPe*). We confirmed the presence/absence of both resistance genes in each line by PCR analysis using specific primers against *HYG* and *NEO* (Figure 1B), and we ensured that these drug-resistant recombinant parasites retained the ability to infect and replicate within bone marrow-derived macrophages (BMMs) over a period of 196 h (Figure 2).

Drug Resistance is not Transferred in *In Vitro* Cultures of Promastigotes in the Absence of Cell-To-Cell Contact

Evidence indicate that DNA can be transferred from cell-to-cell through extracellular vesicles (Elzanowska et al., 2020). In addition, erythrocytes infected with *Plasmodium falciparum* can transfer parasite DNA to other infected cells via the release of extracellular vesicles (Regev-Rudzki et al., 2013). Whereas no such mechanism has been described in *Leishmania*, it was recently reported that the *Leishmania* RNA virus 1 (LRV1) exploits the *Leishmania* exosomal pathway as a mode of transmission from one promastigote to another (Atayde et al., 2019). This led us to verify the hypothesis that extracellular vesicles released in the culture medium may serve as a vehicle to transfer genetic material, including episomes harboring a drug-resistance gene among promastigotes. To this end, we used transwells (0.4 μ m pores) to physically separate *L. amazonensis* *NEO-DsRede* promastigotes from *L. amazonensis* *LPG2/LPG2::ΔHYG* promastigotes. We incubated the transwell plates either at 26°C or we pre-incubated them at 34°C for 4 h and then transferred the plates to 26°C. Such a transient increase in temperature has been previously shown to enhance the secretion of extracellular vesicles by *Leishmania* promastigotes (Hassani et al., 2011). Promastigotes co-incubated in transwells at either 26 or 34°C were collected after 24, 72, 96, and 120 h and assessed for their capacity to grow in the presence of both hygromycin and G418. Both *L. amazonensis* *NEO-DsRede* and *L. amazonensis* *LPG2/LPG2::ΔHYG* were viable and resistant to G418 and hygromycin, respectively, up to 120 h of co-incubation in the transwells. However, no double drug-resistant parasites were recovered from 9 independent experiments performed in

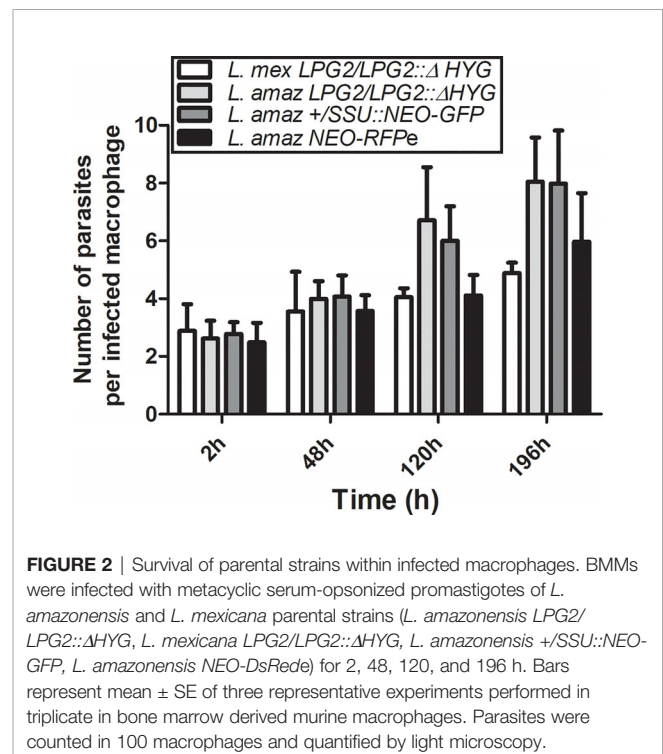


FIGURE 2 | Survival of parental strains within infected macrophages. BMMs were infected with metacyclic serum-opsonized promastigotes of *L. amazonensis* and *L. mexicana* parental strains (*L. amazonensis* *LPG2/LPG2::ΔHYG*, *L. mexicana* *LPG2/LPG2::ΔHYG*, *L. amazonensis* *+SSU::NEO-GFP*, *L. amazonensis* *NEO-DsRede*) for 2, 48, 120, and 196 h. Bars represent mean \pm SE of three representative experiments performed in triplicate in bone marrow derived murine macrophages. Parasites were counted in 100 macrophages and quantified by light microscopy.

triplicate, indicating that exchange of genetic information through extracellular vesicles among *L. amazonensis* promastigotes, if it occurs, is a very rare event.

Genetic Exchange Among *L. amazonensis* and *L. mexicana* Promastigotes in Axenic Cultures

A recent study revealed that some strains of *L. tropica*, but not *L. major*, form hybrids in promastigote axenic cultures (Louradour et al., 2020). This finding prompted us to evaluate the occurrence of genetic crosses among *L. amazonensis* and *L. mexicana* promastigotes in *in vitro* co-cultures. Following the experimental protocol described by Louradour et al. we co-cultured combinations of stationary phase promastigotes with integrated drug-resistance genes as depicted in **Table 1** (Louradour et al., 2020). We also performed co-culture experiments using promastigotes harboring episomes (**Table 1**). Each co-culture was distributed into 96-well plates in drug-free medium. Three days later, the parasites were transferred into 24-well plates and cultured in selective medium (hygromycin B and G418) and left for up to 40 days in a 26°C incubator. Individual single drug-resistant lines were used as controls and had gone through the same process. After 40 days of incubation, we did not obtain double drug-resistant parasites except for the co-cultures of *L. amazonensis*-LPG2/LPG2::ΔHYG and *L. amazonensis*-NEO-DsRede (**Table 1**). We obtained promastigote populations resistant to both G418 and hygromycin B in 3 separate wells. However, only one out of 3 grew sufficiently to allow for DNA isolation and PCR analysis, which revealed the presence of both *HYG* and *NEO* genes (**Figure 3**). However, we were unable to further characterize these double-drug-resistant parasites as they perished in subsequent sub-cultures. These results suggest that genetic exchange in axenic cultures among those two drug-resistant lines may occur and results in transient/unstable double drug-resistant promastigotes.

Unstable Genetic Exchange in Infected Macrophages

The fact that *L. amazonensis* and *L. mexicana* replicate within communal parasitophorous vacuoles led us to verify the possibility that these intracellular replicative niches provide

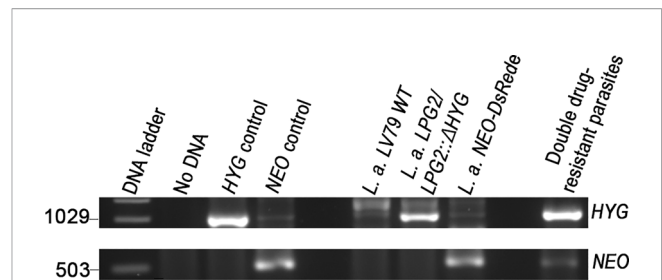


FIGURE 3 | Molecular genotype characterization of double drug-resistant parasites isolated from axenic cultures. PCR amplification of genes encoding antibiotic resistance. The size of *HYG* and *NEO* resistance genes is 1,029 and 503 bp long. The pLeish-HYG-GFP and the pKS-NEO-DsRede constructs were used as controls for the *HYG* and *NEO* genes, respectively. *L. a.* LV79 WT is a DNA sample used to show that our wild type parasites do not express any drug-resistance markers. *L. amazonensis* LPG2/LPG2::ΔHYG and *L. amazonensis* NEO-DsRede are controls used to validate the presence of *HYG* and *NEO* resistance genes within the appropriate parental strains. No DNA sample was loaded as negative control.

conditions propitious for genetic exchange. To this end, we infected BMMs with the following four combinations of drug-resistant parasites: *L. amazonensis* LPG2/LPG2::ΔHYG + *L. amazonensis* +/SSU::NEO-GFP; *L. amazonensis* LPG2/LPG2::ΔHYG + *L. amazonensis* NEO-DsRede; *L. mexicana* LPG2/LPG2::ΔHYG + *L. amazonensis* +/SSU::NEO-GFP, and *L. mexicana* LPG2/LPG2::ΔHYG + *L. amazonensis* NEO-DsRede. Similar to single infection, parasites in mixed infections replicated up to 192 h post-infection and induced the formation of communal PVs (**Figure 4A**). To confirm that these communal PVs harbored both drug-resistant *Leishmania* lines, we performed live cell imaging on BMMs co-infected with either *L. amazonensis* HYG-GFP + *L. amazonensis* NEO-DsRede or *L. amazonensis* HYG-GFP + *L. mexicana* NEO-DsRede. In both cases, we observed the two drug-resistant parasite lines within the same communal vacuoles, at 48 and 72 h post-infection (**Figure 4B**). At 120 and 192 h post-infection, we lysed the infected BMM and cultured the recovered parasites in medium containing hygromycin B and G418 in a similar fashion as the axenic parasite cultures done in plates. As shown in **Table 2**, we failed to recover any double drug-resistant parasites from these co-infection experiments. Next, we modified our experimental approach to perform co-infection experiments on a larger scale, with the following 3 combinations of drug-resistant promastigotes: *L. amazonensis* LPG2/LPG2::ΔHYG + *L. amazonensis* +/SSU::NEO-GFP, *L. amazonensis* LPG2/LPG2::ΔHYG + *L. amazonensis* NEO-DsRede, and *L. mexicana* LPG2/LPG2::ΔHYG + *L. amazonensis* +/SSU::NEO-GFP (**Table 3**). We co-infected BMMs with each combination and we used each individual drug-resistant line as controls. Out of a total of 28 infections, we obtained double drug-resistant parasite populations out of 2 separate infections, which arose from the co-infections with *L. amazonensis* LPG2/LPG2::ΔHYG + *L. amazonensis* +/SSU::NEO-GFP (**Table 3**). We detected the presence of both *NEO* and *HYG* drug-resistance genes in these double drug-resistant parasite populations by PCR analysis (**Figure 5**). We were able to

TABLE 1 | Crosses used in axenic cultures.

| Crosses in axenic cultures | No. of wells with crosses | % Yield of double drug-resistant parasites |
|--|---------------------------|--|
| <i>L. amaz</i> LPG2/LPG2::ΔHYG × <i>L. amaz</i> +/SSU::NEO-GFP | 192 | 0/192 (0%) |
| <i>L. amaz</i> LPG2/LPG2::ΔHYG × <i>L. amaz</i> NEO-DsRede | 192 | 3/192 (1.56%) |
| <i>L. mex.</i> LPG2/LPG2::ΔHYG × <i>L. amaz</i> +/SSU::NEO-GFP | 96 | 0/96 (0%) |
| <i>L. mex</i> LPG2/LPG2::ΔHYG × <i>L. amaz</i> NEO-DsRede | 96 | 0/96 (0%) |

Demonstrates the number of wells tested and percentage of isolated double drug-resistant parasites.

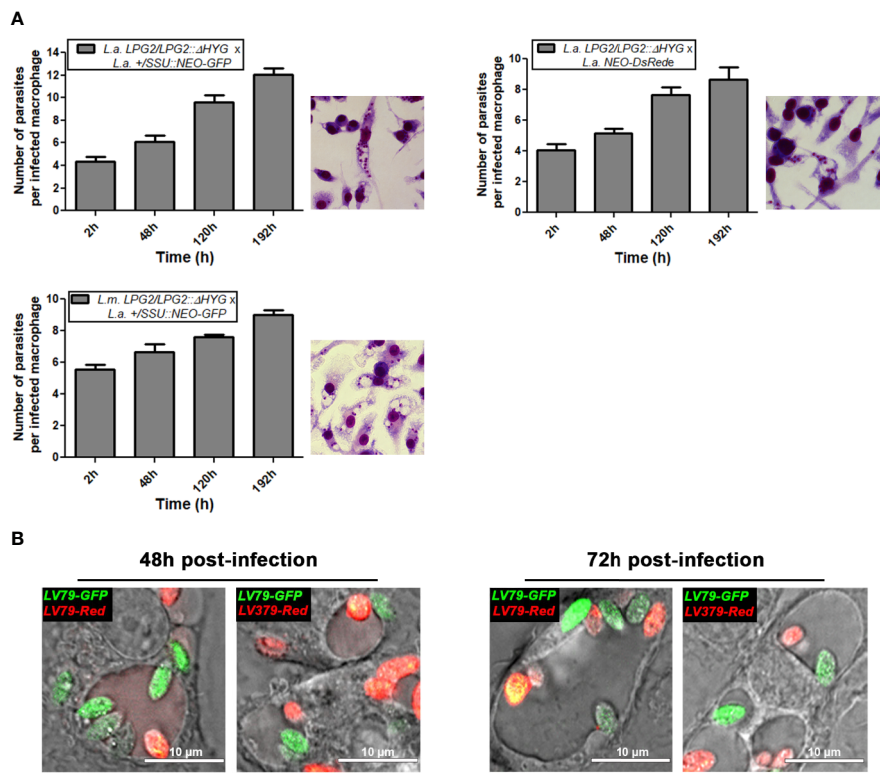


FIGURE 4 | Survival of mating crosses within infected macrophages and visualization of both parental strains within the same vacuole. **(A)** BMMs were infected with metacyclic serum-opsonized promastigote crosses of *L. mexicana* complex parental parasite strains (*L. amazonensis* LPG2/LPG2::ΔHYG + *L. amazonensis* +/SSU::NEO-GFP; *L. amazonensis* LPG2/LPG2::ΔHYG + *L. amazonensis* NEO-DsRede; *L. mexicana* LPG2/LPG2::ΔHYG + *L. amazonensis* +/SSU::NEO-GFP for 2, 48, 120, and 196 h. Bars represent mean ± SE of three representative experiments performed in triplicate in bone marrow derived murine macrophages. Parasites were counted in 100 macrophages and quantified by light microscopy. Macrophages were stained with HEMA 3 kit. Representative pictures from each cross are shown. **(B)** Live microscopy analysis of *L. amazonensis* and *L. mexicana* parasite strains expressing different fluorescent markers. Representative pictures of both parental strains within the same communal vacuole at 48 and 72 h are shown. LV79-GFP, *L. amazonensis* HYG-GFP; LV79-DsRed, *L. amazonensis* NEO-DsRede; M379-DsRed, *L. mexicana* NEO-DsRede.

TABLE 2 | Crosses used in *in vitro* infections done in wells.

| Crosses 120 h post-infection | No. of wells with crosses | % Yield of double drug-resistant parasites |
|--|---------------------------|--|
| <i>L. amaz</i> LPG2/LPG2::ΔHYG × <i>L. amaz</i> +/SSU::NEO-GFP | 89 | 0/89 (0%) |
| <i>L. amaz</i> LPG2/LPG2::ΔHYG × <i>L. amaz</i> NEO-DsRede | 34 | 0/34 (0%) |
| <i>L. mex.</i> LPG2/LPG2::ΔHYG × <i>L. amaz</i> +/SSU::NEO-GFP | 63 | 0/63 (0%) |
| <i>L. mex</i> LPG2/LPG2::ΔHYG × <i>L. amaz</i> NEO-DsRede | 63 | 0/63 (0%) |
| Crosses 192 h post-infection | | |
| <i>L. amaz</i> LPG2/LPG2::ΔHYG × <i>L. amaz</i> +/SSU::NEO-GFP | 72 | 0/72 (0%) |
| <i>L. amaz</i> LPG2/LPG2::ΔHYG × <i>L. amaz</i> NEO-DsRede | 72 | 0/72 (0%) |
| <i>L. mex.</i> LPG2/LPG2::ΔHYG × <i>L. amaz</i> +/SSU::NEO-GFP | 69 | 0/69 (0%) |
| <i>L. mex</i> LPG2/LPG2::ΔHYG × <i>L. amaz</i> NEO-DsRede | 66 | 0/66 (0%) |

Demonstrates the number of wells tested and percentage of isolated double drug-resistant parasites.

maintain one of this double drug-resistant population in culture for 3 weeks; however, after the third week, this population lost the *NEO* resistance gene and has ultimately perished afterwards (**Figure 5A**). For the second occurrence of double drug-resistant parasites, we isolated 3 separate populations which contained both the *HYG* and *NEO* genes as assessed by PCR analysis (**Figure 5B**), whereas the third population had only the *HYG* resistance gene and died upon further passages (**Figure 5B**). The two double drug-resistant populations were maintained for a week and died upon additional passages. These results suggest that genetic exchange may take place in infected macrophages and result in transient/unstable double drug-resistant parasites.

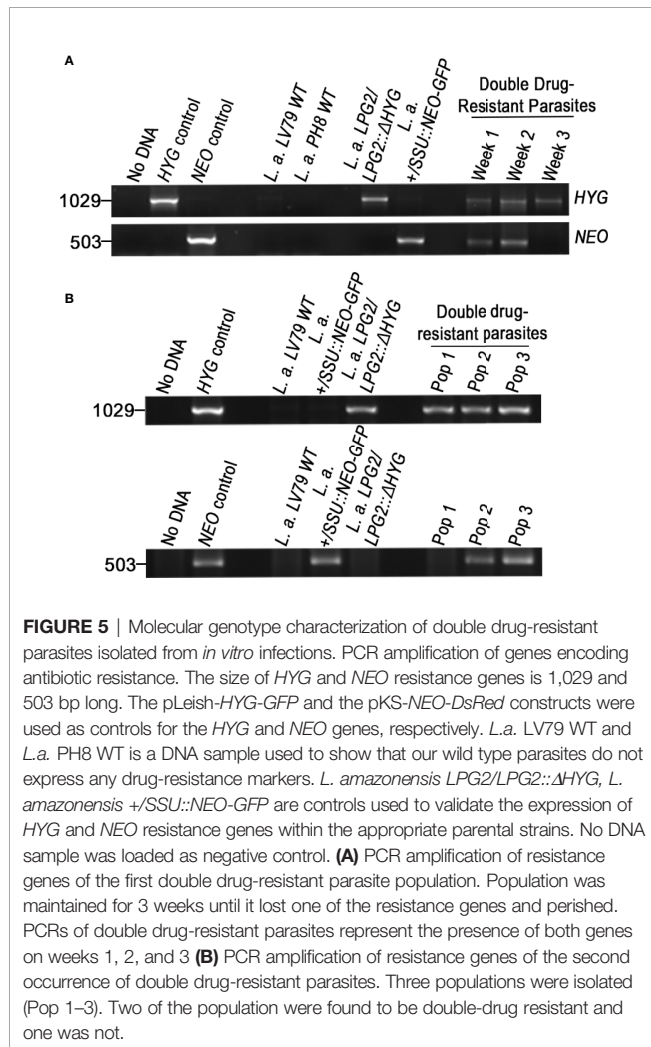
Absence of Detectable Genetic Exchange in *In Vivo* Infections

To determine whether mammalian hosts provide an environment favorable for genetic exchange for the species of the *L. mexicana* complex, we inoculated mice into the ear dermis with two combinations of single drug-resistant parasites, namely *L. amazonensis* LPG2/LPG2::ΔHYG + *L. amazonensis* +/SSU::NEO-GFP and *L. mexicana* LPG2/LPG2::ΔHYG + *L.*

TABLE 3 | Crosses used in *in vitro* infections done in flasks.

| Cross | No. of infections | No. of times parent 1 was isolated | No. of times parent 2 was isolated | No. of times double drug-resistant parasites were isolated | % Recovery |
|--|-------------------|------------------------------------|------------------------------------|--|------------|
| <i>L. amaz</i> LPG2/LPG2::ΔHYG × <i>L. amaz</i> +/SSU::NEO-GFP | 14 | 14 | 14 | 2 | 14% |
| <i>L. amaz</i> LPG2/LPG2::ΔHYG × <i>L. amaz</i> NEO-DsRed | 10 | 10 | 10 | 0 | 0% |
| <i>L. mex.</i> LPG2/LPG2::ΔHYG × <i>L. amaz</i> +/SSU::NEO-GFP | 4 | 4 | 4 | 0 | 0% |

Data includes the number of mating crosses executed in flasks and parasite strains that were isolated from each infection. Percentage indicates the total number of times that double-drug resistant parasites were isolated.



amazonensis +/SSU::NEO-GFP (Table 4). Mice infected with single drug-resistant lines were used as a control. Nine weeks post-infection, we recovered parasites from lesions and we cultured them in the presence of either hygromycin B, G418, or both. As shown in Table 4, we recovered each single drug-resistant line that was co-inoculated or inoculated alone as controls. However, we did not succeed in isolating double drug-resistant parasites from cutaneous lesions, indicating that genetic exchange does not occur to a detectable level within the

mammalian host for *Leishmania* species residing in communal parasitophorous vacuoles.

DISCUSSION

For decades, the occurrence of natural *Leishmania* hybrids has been described among clinical and field isolates, indicating that genetic exchange is part of the biology of these parasites. Experimental genetic crosses among *Leishmania* cells were initially reported to occur exclusively in the sand fly vector (Akopyants et al., 2009; Sadlova et al., 2011; Inbar et al., 2013; Calvo-Alvarez et al., 2014; Romano et al., 2014; Inbar et al., 2019). However, recent evidence revealed that experimental genetic crosses also occur in axenic promastigote cultures, indicating that mating competent forms are present in these populations (Louradour et al., 2020). The fact that studies on the experimental generation of hybrids have been performed with *Leishmania* species living in tight individual parasitophorous vacuoles may have precluded the detection of genetic exchange within mammalian host cells. In this study, we sought to determine whether genetic exchange occurs among species of the *L. mexicana* complex, which replicate within communal parasitophorous vacuoles. Using promastigotes expressing drug-selectable markers, we obtained evidence of intraclonal genetic exchange for *L. amazonensis* in both axenic promastigote cultures and infected macrophages. However, the resulting products of those genetic events were unstable as they did not sustain growth in subsequent sub-cultures.

The study of experimental genetic exchange in *Leishmania* consists in mixing strains carrying distinct drug-resistance markers and/or fluorescent markers integrated into their genomes and the subsequent selection and analysis of double drug-resistant parasites (Akopyants et al., 2009; Sadlova et al., 2011; Inbar et al., 2013; Calvo-Alvarez et al., 2014; Romano et al., 2014; Inbar et al., 2019; Louradour et al., 2020). Whole genome sequencing revealed that these double drug-resistant parasites are full genomic hybrids predominantly resulting from a mechanism resembling meiosis (Inbar et al., 2019). Whether other forms of genetic exchange take place in *Leishmania* had not received much attention. Hence, we tested whether the transfer of genetic material can occur without direct contact between *Leishmania* promastigotes, as previously reported for *P. falciparum* via cell-derived extravesicular vesicles (Regev-Rudzki et al., 2013). Our

TABLE 4 | Crosses used in *in vivo* infections.

| Cross | No. of infected mice | No. of times parent 1 was isolated | No. of times parent 2 was isolated | No. of times double drug-resistant parasites were isolated | % Recovery |
|--|----------------------|------------------------------------|------------------------------------|--|------------|
| <i>L. amaz</i> LPG2/LPG2::ΔHYG × <i>L. amaz</i> +/SSU::NEO-GFP | 13 | 13 | 13 | 0 | 0% |
| <i>L. mex.</i> LPG2/LPG2::ΔHYG × <i>L. amaz</i> +/SSU::NEO-GFP | 6 | 6 | 6 | 0 | 0% |

Data includes the number of infected mice with each cross and parasite strains that were isolated from each infection. Percentage indicates the total number of times that double drug-resistant parasites were isolated.

attempts to detect the transfer of an episome from one line of *L. amazonensis* to another in transwell experiments were unsuccessful, suggesting that physical contact is required for genetic exchange among *Leishmania* promastigotes. Our results also suggest that in contrast to the *Leishmania* virus LRV-1 (Atayde et al., 2019), episomal DNA is not transferred through extracellular vesicles or other released material.

The recent report that genetic crosses take place in axenic cultures of *L. tropica* (Louradour et al., 2020) prompted us to explore the possibility that genetic exchange occur among *L. amazonensis* and *L. mexicana* promastigotes in axenic cultures. In contrast to the *L. tropica* strains used by Louradour and colleagues (Louradour et al., 2020), we obtained only a few populations of double drug-resistant *L. amazonensis* promastigotes which turned out to be unstable. The fact that those populations did not sustain sub-cultures precluded further analyses. Clearly, not all species or strains of *Leishmania* are equal in terms of capacity to generate mating-competent forms *in vitro*. Hence, whereas Louradour and colleagues were successful in recovering hybrids from *L. tropica* axenic co-cultures, no hybrids were obtained when both parental strains were *L. major* (Louradour et al., 2020). In the case of *L. amazonensis*, it is possible that strains other than the one we used are more efficient in generating mating-competent forms in axenic cultures. Future studies will be aimed at investigating this important issue.

It is well established that hybrid formation among *Leishmania* promastigotes takes place in the sand fly (Akopyants et al., 2009; Sadlova et al., 2011; Inbar et al., 2013; Calvo-Alvarez et al., 2014; Romano et al., 2014; Inbar et al., 2019; Louradour et al., 2020). Failure to detect genetic exchange in the mammalian host suggests that amastigotes do not generate mating competent forms or that they are less prone to recombination. It is also possible that the phagolysosomal environment is not as conducive to genetic exchange as the sand fly midgut. However, it was reported previously that amastigotes undergo nuclear fusion within infected macrophages suggesting that genetic exchange may indeed be possible within infected hosts (Kreutzer et al., 1994). Alternatively, the fact that the *Leishmania* species used so far to study genetic exchange replicate within individual parasitophorous vacuoles (*L. major*, *L. tropica*, *L. donovani*, *L. infantum*) may have limited the probabilities of genetic exchange among amastigotes. With this in mind, we hypothesized that replication within a communal vacuole may provide amastigotes with conditions propitious to genetic

exchange, as reported for *Chlamydia* (Jeffrey et al., 2013). The recovery of double-drug resistant promastigote populations from macrophages co-infected with *L. amazonensis* LPG2/LPG2::ΔHYG + *L. amazonensis* +/SSU::NEO-GFP and the detection of both the *HYG* and *NEO* genes in these cultures suggest that intraclonal genetic exchange may occur within communal parasitophorous vacuoles. However, the inability to grow these *L. amazonensis* double drug-resistant populations over several passages and to clone double drug-resistant parasites precluded further characterization of these progeny and thus determine whether or not these parasites were genuine hybrids. Previous studies revealed that not all hybrid progeny is as viable as their parental counterparts. Hence, Sadlova et al. observed *L. donovani* hybrids in infected sand flies, but all of their attempts to grow them in culture have failed. This led to the conclusion that although *L. donovani* parasites are able to exchange genetic information, the hybrids produced were not viable (Sadlova et al., 2011). Finally, there was also a report which explored the possibility of genetic exchange between *L. major* and *L. turanica* in infected sand flies; however, it was reported that such events do not take place between these parasite species (Chajbullinova et al., 2012).

As described for *L. major* (Akopyants et al., 2009), we were unable to recover double drug-resistant parasites from mice co-infected with *L. amazonensis* and *L. mexicana*. However, based on our results with *in vitro* infections, we cannot rule out that genetic exchange do not take place in mammalian hosts infected with those species/strains. An important factor to consider is the number of *in vivo* infections we performed. Indeed, studies on genetic exchange done in the insect vector required hundreds of sand flies to be infected. Hence, Akopyants et al. used 102 sand flies to study genetic exchange between *L. major* parasites, Sadlova et al. infected 121 sandflies to study this phenomenon for *L. donovani*, whereas Romano et al. used 446 sandflies to study these events among strains of *L. infantum* (Akopyants et al., 2009; Sadlova et al., 2011; Romano et al., 2014). Another important factor to take into consideration is the ability of the *L. amazonensis* and *L. mexicana* strains we used in our study to generate mating competent forms, as evidenced in the study of Louradour and colleagues using *L. tropica* and *L. major* (Louradour et al., 2020).

In summary, we provide evidence of possible intraclonal genetic exchange among *L. amazonensis* parasites in axenic cultures and within mammalian host cells. However, the double drug-resistant parasites obtained in our studies were

unstable and could not be further characterized. Future studies will be required to identify strains of *L. amazonensis* and *L. mexicana* with higher capacity to generate mating competent forms and use these strains for studies in macrophages and in mice on a larger scale.

DATA AVAILABILITY STATEMENT

The raw data supporting the conclusions of this article will be made available by the authors, without undue reservation.

ETHICS STATEMENT

The animal study was reviewed and approved by Comité Institutionnel de Protection des Animaux of the INRS-Centre Armand-Frappier Santé Biotechnologie.

AUTHOR CONTRIBUTIONS

RT and AD conceived and designed the study, contributed to the data analysis, and drafted and revised the manuscript. RT performed the experiments. RT and AD wrote and revised the

manuscript. All authors contributed to the article and approved the submitted version.

FUNDING

This work was supported by the Canadian Institutes of Health Research (CIHR) grant PJT-156416 to AD. AD is the holder of the Canada Research Chair on the Biology of intracellular parasitism. The funders had no role in study design, data collection and interpretation, decision to publish, or preparation of the manuscript.

ACKNOWLEDGMENTS

We thank Dr. David L. Sacks (National Institute of Allergy and Infectious Diseases, USA) for providing the plasmid pKS-NEO-*dsRed*, Dr Barbara Papadopoulou (Université Laval, Canada) for providing the plasmid pCR2.1-L.d-rDNA-pr- α IRNEO α IR-GFP, and Drs Leonardo Paiva Farias (Fiocruz Bahia, Brazil) for providing the pLaLPG2-HYG construct and J. Tremblay for assistance in immunofluorescence experiments. We thank Matthias Govaerts and Olivier Séguin for their technical help during this study.

REFERENCES

- Akopyants, N. S., Kimblin, N., Secundino, N., Patrick, R., Peters, N., Lawyer, P., et al. (2009). Demonstration of genetic exchange during cyclical development of *Leishmania* in the sand fly vector. *Science* 324 (5924), 265–268. doi: 10.1126/science.1169464
- Arango Duque, G., Jardim, A., Gagnon, E., Fukuda, M., and Descoteaux, A. (2019). The host cell secretory pathway mediates the export of *Leishmania* virulence factors out of the parasitophorous vacuole. *PLoS Pathog.* 15 (7), e1007982. doi: 10.1371/journal.ppat.1007982
- Atayde, V. D., da Silva Lira Filho, A., Chaparro, V., Zimmermann, A., Martel, C., Jaramillo, M., et al. (2019). Exploitation of the *Leishmania* exosomal pathway by *Leishmania* RNA virus 1. *Nat. Microbiol.* 4 (4), 714–723. doi: 10.1038/s41564-018-0352-y
- Banuls, A. L., Guerrini, F., Le Pont, F., Barrera, C., Espinel, I., Guderian, R., et al. (1997). Evidence for hybridization by multilocus enzyme electrophoresis and random amplified polymorphic DNA between *Leishmania braziliensis* and *Leishmania panamensis*/guyanensis in Ecuador. *J. Eukaryot. Microbiol.* 44 (5), 408–411. doi: 10.1111/j.1550-7408.1997.tb05716.x
- Banuls, A. L., Jonquieres, R., Guerrini, F., Le Pont, F., Barrera, C., Espinel, I., et al. (1999). Genetic analysis of leishmania parasites in Ecuador: are *Leishmania* (Viannia) panamensis and *Leishmania* (V.) Guyanensis distinct taxa? *Am. J. Trop. Med. Hyg.* 61 (5), 838–845. doi: 10.4269/ajtmh.1999.61.838
- Belli, A. A., Miles, M. A., and Kelly, J. M. (1994). A putative *Leishmania* panamensis/*Leishmania* braziliensis hybrid is a causative agent of human cutaneous leishmaniasis in Nicaragua. *Parasitology* 109 (Pt 4), 435–442. doi: 10.1017/s0031182000080689
- Bonfante-Garrido, R., Melendez, E., Barroeta, S., de Alejos, M. A., Momen, H., Cupolillo, E., et al. (1992). Cutaneous leishmaniasis in western Venezuela caused by infection with *Leishmania* venezuelensis and *L. braziliensis* variants. *Trans. R. Soc. Trop. Med. Hyg.* 86 (2), 141–148. doi: 10.1016/0035-9203(92)90544-m
- Calvo-Alvarez, E., Alvarez-Velilla, R., Jimenez, M., Molina, R., Perez-Pertejo, Y., Balana-Fouce, R., et al. (2014). First evidence of intraclonal genetic exchange in trypanosomatids using two *Leishmania* infantum fluorescent transgenic clones. *PLoS Negl. Trop. Dis.* 8 (9), e3075. doi: 10.1371/journal.pntd.0003075
- Case, E. D., Smith, J. A., Ficht, T. A., Samuel, J. E., and de Figueiredo, P. (2016). Space: A Final Frontier for Vacuolar Pathogens. *Traffic* 17 (5), 461–474. doi: 10.1111/tra.12382
- Chajbullinova, A., Votycka, J., Sadlova, J., Kvapilova, K., Seblova, V., Kreisinger, J., et al. (2012). The development of *Leishmania turanica* in sand flies and competition with *L. major*. *Parasit. Vectors* 5:219. doi: 10.1186/1756-3305-5-219
- Chargui, N., Amro, A., Haouas, N., Schonian, G., Babba, H., Schmidt, S., et al. (2009). Population structure of Tunisian *Leishmania* infantum and evidence for the existence of hybrids and gene flow between genetically different populations. *Int. J. Parasitol.* 39 (7), 801–811. doi: 10.1016/j.ijpara.2008.11.016
- Cortes, S., Esteves, C., Mauricio, I., Maia, C., Cristovao, J. M., Miles, M., et al. (2012). In vitro and in vivo behaviour of sympatric *Leishmania* (V.) braziliensis, *L. (V.) peruviana* and their hybrids. *Parasitology* 139 (2), 191–199. doi: 10.1017/S0031182011001909
- Cortes, S., Albuquerque-Wendt, A., Maia, C., Carvalho, M., Lima, I. A., de Freitas, L. A. R., et al. (2019). Elucidating in vitro and in vivo phenotypic behaviour of *L. infantum*/*L. major* natural hybrids. *Parasitology* 146 (5), 580–587. doi: 10.1017/S0031182018001993
- Cupolillo, E., Grimaldi, G. Jr., and Momen, H. (1997). Genetic diversity among *Leishmania* (Viannia) parasites. *Ann. Trop. Med. Parasitol.* 91 (6), 617–626. doi: 10.1080/00034989760716
- Delgado, O., Cupolillo, E., Bonfante-Garrido, R., Silva, S., Belfort, E., Grimaldi Junior, G., et al. (1997). Cutaneous leishmaniasis in Venezuela caused by infection with a new hybrid between *Leishmania* (Viannia) braziliensis and *L. (V.) guyanensis*. *Mem. Inst. Oswaldo Cruz* 92 (5), 581–582. doi: 10.1590/s0074-02761997000500002
- Descoteaux, A., and Matlashewski, G. (1989). c-fos and tumor necrosis factor gene expression in *Leishmania* donovani-infected macrophages. *Mol. Cell Biol.* 9 (11), 5223–5227. doi: 10.1128/mcb.9.11.5223
- Descoteaux, A., Garraway, L. A., Ryan, K. A., Garrity, L. K., Turco, S. J., and Beverley, S. M. (1994). "Identification of genes by functional complementation in protozoan parasite *Leishmania*" in *Methods in Molecular Genetics (Molecular Microbiology Techniques)*. Molecular Biology Techniques. 3. Eds. K. W. Adolph (San Diego: Academic Press), p. 22–48.
- Dujardin, J. C., Banuls, A. L., Llanos-Cuentas, A., Alvarez, E., DeDoncker, S., Jacquet, D., et al. (1995). Putative *Leishmania* hybrids in the Eastern Andean valley of Huanuco, Peru. *Acta Trop.* 59 (4), 293–307. doi: 10.1016/0001-706x(95)00094-u
- Elzanowski, J., Semira, C., and Costa-Silva, B. (2020). DNA in extracellular vesicles: biological and clinical aspects. *Mol. Oncol.* doi: 10.1002/1878-0261.12777

- Evans, D. A., Kennedy, W. P., Elbihari, S., Chapman, C. J., Smith, V., and Peters, W. (1987). Hybrid formation within the genus *Leishmania*? *Parasitologia* 29 (2-3), 165–173.
- Gelanew, T., Hailu, A., Schonian, G., Lewis, M. D., Miles, M. A., and Yeo, M. (2014). Multilocus sequence and microsatellite identification of intra-specific hybrids and ancestor-like donors among natural Ethiopian isolates of *Leishmania donovani*. *Int. J. Parasitol.* 44 (10), 751–757. doi: 10.1016/j.ijpara.2014.05.008
- Ha, D. S., Schwarz, J. K., Turco, S. J., and Beverley, S. M. (1996). Use of the green fluorescent protein as a marker in transfected *Leishmania*. *Mol. Biochem. Parasitol.* 77 (1), 57–64. doi: 10.1016/0166-6851(96)02580-7
- Hassani, K., Antoniak, E., Jardim, A., and Olivier, M. (2011). Temperature-induced protein secretion by *Leishmania mexicana* modulates macrophage signalling and function. *PLoS One* 6 (5), e18724. doi: 10.1371/journal.pone.0018724
- Heitman, J. (2010). Evolution of eukaryotic microbial pathogens via covert sexual reproduction. *Cell Host Microbe* 8 (1), 86–99. doi: 10.1016/j.chom.2010.06.011
- Iantorno, S. A., Durrant, C., Khan, A., Sanders, M. J., Beverley, S. M., Warren, W. C., et al. (2017). Gene Expression in *Leishmania* Is Regulated Predominantly by Gene Dosage. *mBio* 8 (5), e01393–17. doi: 10.1128/mBio.01393-17
- Inbar, E., Akopyants, N. S., Charmoy, M., Romano, A., Lawyer, P., Elnaïem, D. E., et al. (2013). The mating competence of geographically diverse *Leishmania* major strains in their natural and unnatural sand fly vectors. *PLoS Genet.* 9 (7), e1003672. doi: 10.1371/journal.pgen.1003672
- Inbar, E., Shaik, J., Iantorno, S. A., Romano, A., Nzulu, C. O., Owens, K., et al. (2019). Whole genome sequencing of experimental hybrids supports meiosis-like sexual recombination in *Leishmania*. *PLoS Genet.* 15 (5), e1008042. doi: 10.1371/journal.pgen.1008042
- Jeffrey, B. M., Suchland, R. J., Eriksen, S. G., Sandoz, K. M., and Rockey, D. D. (2013). Genomic and phenotypic characterization of *in vitro*-generated *Chlamydia trachomatis* recombinants. *BMC Microbiol.* 13:142. doi: 10.1186/1471-2180-13-142
- Jennings, Y. L., de Souza, A. A., Ishikawa, E. A., Shaw, J., Lainson, R., and Silveira, F. (2014). Phenotypic characterization of *Leishmania* spp. causing cutaneous leishmaniasis in the lower Amazon region, western Para state, Brazil, reveals a putative hybrid parasite, *Leishmania* (Viannia) guyanensis x *Leishmania* (Viannia) shawi shawi. *Parasite* 21, 39. doi: 10.1051/parasite/2014039
- Kato, H., Caceres, A. G., and Hashiguchi, Y. (2016). First Evidence of a Hybrid of *Leishmania* (Viannia) *braziliensis*/L. (V.) *peruviana* DNA Detected from the Phlebotomine Sand Fly *Lutzomyia tejadai* in Peru. *PLoS Negl. Trop. Dis.* 10 (1), e0004336. doi: 10.1371/journal.pntd.0004336
- Kato, H., Gomez, E. A., Seki, C., Furumoto, H., Martini-Robles, L., Muzzio, J., et al. (2019). PCR-RFLP analyses of *Leishmania* species causing cutaneous and mucocutaneous leishmaniasis revealed distribution of genetically complex strains with hybrid and mito-nuclear discordance in Ecuador. *PLoS Negl. Trop. Dis.* 13 (5), e0007403. doi: 10.1371/journal.pntd.0007403
- Kelly, J. M., Law, J. M., Chapman, C. J., Van Eys, G. J., and Evans, D. A. (1991). Evidence of genetic recombination in *Leishmania*. *Mol. Biochem. Parasitol.* 46 (2), 253–263. doi: 10.1016/0166-6851(91)90049-c
- Kimblin, N., Peters, N., Debrabant, A., Secundino, N., Egen, J., Lawyer, P., et al. (2008). Quantification of the infectious dose of *Leishmania* major transmitted to the skin by single sand flies. *Proc. Natl. Acad. Sci. U.S.A.* 105 (29), 10125–10130. doi: 10.1073/pnas.0802331105
- Kreutzer, R. D., Yemma, J. J., Grogl, M., Tesh, R. B., and Martin, T. I. (1994). Evidence of sexual reproduction in the protozoan parasite *Leishmania* (Kinetoplastida: Trypanosomatidae). *Am. J. Trop. Med. Hyg.* 51 (3), 301–307. doi: 10.4269/ajtmh.1994.51.301
- Louradour, I., Ferreira, T. R., Ghosh, K., Shaik, J., and Sacks, D. (2020). In Vitro Generation of *Leishmania* Hybrids. *Cell Rep.* 31 (2), 107507. doi: 10.1016/j.celrep.2020.03.071
- Medina-Acosta, E., and Cross, G. A. (1993). Rapid isolation of DNA from trypanosomatid protozoa using a simple 'mini-prep' procedure. *Mol. Biochem. Parasitol.* 59 (2), 327–329. doi: 10.1016/0166-6851(93)90231-l
- Nolder, D., Roncal, N., Davies, C. R., Llanos-Cuentas, A., and Miles, M. A. (2007). Multiple hybrid genotypes of *Leishmania* (viannia) in a focus of mucocutaneous Leishmaniasis. *Am. J. Trop. Med. Hyg.* 76 (3), 573–578. doi: 10.4269/ajtmh.2007.76.573
- Odiwuor, S., De Doncker, S., Maes, I., Dujardin, J. C., and Van der Auwera, G. (2011). Natural *Leishmania donovani*/*Leishmania aethiopica* hybrids identified from Ethiopia. *Infect. Genet. Evol.* 11 (8), 2113–2118. doi: 10.1016/j.meegid.2011.04.026
- Ravel, C., Cortes, S., Pratlong, F., Morio, F., Dedet, J. P., and Campino, L. (2006). First report of genetic hybrids between two very divergent *Leishmania* species: *Leishmania infantum* and *Leishmania major*. *Int. J. Parasitol.* 36 (13), 1383–1388. doi: 10.1016/j.ijpara.2006.06.019
- Regev-Rudski, N., Wilson, D. W., Carvalho, T. G., Sisquella, X., Coleman, B. M., Rug, M., et al. (2013). Cell-cell communication between malaria-infected red blood cells via exosome-like vesicles. *Cell* 153 (5), 1120–1133. doi: 10.1016/j.cell.2013.04.029
- Rogers, M. B., Downing, T., Smith, B. A., Imamura, H., Sanders, M., Svobodova, M., et al. (2014). Genomic confirmation of hybridisation and recent inbreeding in a vector-isolated *Leishmania* population. *PLoS Genet.* 10 (1), e1004092. doi: 10.1371/journal.pgen.1004092
- Romano, A., Inbar, E., Debrabant, A., Charmoy, M., Lawyer, P., Ribeiro-Gomes, F., et al. (2014). Cross-species genetic exchange between visceral and cutaneous strains of *Leishmania* in the sand fly vector. *Proc. Natl. Acad. Sci. U.S.A.* 111 (47), 16808–16813. doi: 10.1073/pnas.1415109111
- Rougeron, V., De Meeus, T., Hide, M., Waleckx, E., Bermudez, H., Arevalo, J., et al. (2009). Extreme inbreeding in *Leishmania braziliensis*. *Proc. Natl. Acad. Sci. U.S.A.* 106 (25), 10224–10229. doi: 10.1073/pnas.0904420106
- Rougeron, V., De Meeus, T., and Banuls, A. L. (2017). Reproduction in *Leishmania*: A focus on genetic exchange. *Infect. Genet. Evol.* 50, 128–132. doi: 10.1016/j.meegid.2016.10.013
- Sadlova, J., Yeo, M., Seblova, V., Lewis, M. D., Mauricio, I., Volf, P., et al. (2011). Visualisation of *Leishmania donovani* fluorescent hybrids during early stage development in the sand fly vector. *PLoS One* 6 (5), e19851. doi: 10.1371/journal.pone.0019851
- Seblova, V., Myskova, J., Hlavacova, J., Votupka, J., Antoniou, M., and Volf, P. (2015). Natural hybrid of *Leishmania infantum*/L. *donovani*: development in *Phlebotomus tobbi*, *P. perniciosus* and *Lutzomyia longipalpis* and comparison with non-hybrid strains differing in tissue tropism. *Parasit. Vectors* 8, 605. doi: 10.1186/s13071-015-1217-3
- Spath, G. F., and Beverley, S. M. (2001). A lipophosphoglycan-independent method for isolation of infective *Leishmania* metacyclic promastigotes by density gradient centrifugation. *Exp. Parasitol.* 99 (2), 97–103. doi: 10.1006/expr.2001.4656
- Tibayrenc, M., and Ayala, F. J. (2013). How clonal are *Trypanosoma* and *Leishmania*? *Trends Parasitol.* 29 (6), 264–269. doi: 10.1016/j.pt.2013.03.007
- Torrico, M. C., De Doncker, S., Arevalo, J., Le Ray, D., and Dujardin, J. C. (1999). In vitro promastigote fitness of putative *Leishmania* (Viannia) *braziliensis*/*Leishmania* (Viannia) *peruviana* hybrids. *Acta Trop.* 72 (1), 99–110. doi: 10.1016/s0001-706x(98)00076-x
- Turco, S., Descoteaux, A., Ryan, K., Garraway, L., and Beverley, S. (1994). Isolation of virulence genes directing GPI synthesis by functional complementation of *Leishmania*. *Braz. J. Med. Biol. Res.* 27 (2), 133–138.
- Volf, P., Benkova, I., Myskova, J., Sadlova, J., Campino, L., and Ravel, C. (2007). Increased transmission potential of *Leishmania major*/*Leishmania infantum* hybrids. *Int. J. Parasitol.* 37 (6), 589–593. doi: 10.1016/j.ijpara.2007.02.002

Conflict of Interest: The authors declare that the research was conducted in the absence of any commercial or financial relationships that could be construed as a potential conflict of interest.

Copyright © 2020 Telittchenko and Descoteaux. This is an open-access article distributed under the terms of the Creative Commons Attribution License (CC BY). The use, distribution or reproduction in other forums is permitted, provided the original author(s) and the copyright owner(s) are credited and that the original publication in this journal is cited, in accordance with accepted academic practice. No use, distribution or reproduction is permitted which does not comply with these terms.



Modulation of IMD, Toll, and Jak/STAT Immune Pathways Genes in the Fat Body of *Rhodnius prolixus* During *Trypanosoma rangeli* Infection

Agustín Rolandelli^{1*}, Adeisa E. C. Nascimento², Leticia S. Silva², Rolando Rivera-Pomar¹ and Alessandra A. Guarneri^{2*}

OPEN ACCESS

Edited by:

Alberto Enrique Paniz Mondolfi,
Icahn School of Medicine at Mount
Sinai, United States

Reviewed by:

Anderson Sa-Nunes,
University of São Paulo, Brazil
Elisa Azuara-Liceaga,
Universidad Autónoma de la Ciudad
de México, Mexico

*Correspondence:

Agustín Rolandelli
arolandelli@
comunidad.unnoba.edu.ar
Alessandra A. Guarneri
alessandra.guarneri@fiocruz.br

Specialty section:

This article was submitted to
Parasite and Host,
a section of the journal
Frontiers in Cellular and Infection
Microbiology

Received: 24 August 2020

Accepted: 30 November 2020

Published: 18 January 2021

Citation:

Rolandelli A, Nascimento AEC,
Silva LS, Rivera-Pomar R and
Guarneri AA (2021) Modulation of
IMD, Toll, and Jak/STAT Immune
Pathways Genes in the Fat Body of
Rhodnius prolixus During
Trypanosoma rangeli Infection.
Front. Cell. Infect. Microbiol. 10:598526.
doi: 10.3389/fcimb.2020.598526

¹ Centro de Bioinvestigaciones (CeBio), Centro de Investigaciones y Transferencia del Noroeste de la Provincia de Buenos Aires (CIT-NOBA), Universidad Nacional del Noroeste de la Provincia de Buenos Aires (UNNOBA)—Consejo Nacional de Investigaciones Científicas y Técnicas (CONICET), Pergamino, Argentina, ² Vector Behaviour and Pathogen Interaction Group, Instituto René Rachou, Fundação Oswaldo Cruz (FIOCRUZ), Belo Horizonte, Brazil

Trypanosoma rangeli is the second most common American trypanosome that infects man. It is vectored by triatomines from the genus *Rhodnius*, in which it invades the hemolymph and infects the salivary glands, avoiding the bug immune responses. In insects, these responses are initiated by well conserved pathways, mainly the IMD, Toll, and Jak/STAT. We hypothesize that long-term infection with *T. rangeli* in the gut or hemolymph of *Rhodnius prolixus* triggers different systemic immune responses, which influence the number of parasites that survive inside the vector. Thus, we investigated groups of insects with infections in the gut and/or hemolymph, and evaluated the parasite load and the expression in the fat body of transcription factors (*Rp-Relish*, *Rp-Dorsal*, and *Rp-STAT*) and inhibitors (*Rp-Cactus* and *Rp-Caspar*) of the IMD, Toll, and Jak/STAT pathways. We detected lower parasite counts in the gut of insects without hemolymph infection, compared to hemolymph-infected groups. Besides, we measured higher parasite numbers in the gut of bugs that were first inoculated with *T. rangeli* and then fed on infected mice, compared with control insects, indicating that hemolymph infection increases parasite numbers in the gut. Interestingly, we observed that genes from the three immune pathways were differentially modulated, depending on the region parasites were present, as we found (1) *Rp-Relish* downregulated in gut-and/or-hemolymph-infected insects, compared with controls; (2) *Rp-Cactus* upregulated in gut-infected insect, compared with controls and gut-and-hemolymph-infected groups; and (3) *Rp-STAT* downregulated in all groups of hemolymph-infected insects. Finally, we uncovered negative correlations between parasite loads in the gut and *Rp-Relish* and *Rp-Cactus* expression, and between parasite counts in the hemolymph and *Rp-Relish* levels, suggesting an association between parasite numbers and the IMD and Toll pathways. Overall, our findings reveal new players in *R. prolixus*–*T. rangeli* interactions that could be key for the capacity of the bug to transmit the pathogen.

Keywords: trypanosomatids, vector-parasite interactions, immune response, parasite load, kissing bugs

INTRODUCTION

Trypanosoma rangeli is a protozoan parasite vectored by triatomine bugs, especially those from the genus *Rhodnius*, and is able to infect humans and other mammals. However, in contrast to *Trypanosoma cruzi*, the etiologic agent of Chagas disease, *T. rangeli* is considered unable to elicit pathology in mammals, though it is detrimental to its insect vector (Watkins, 1971; Guarneri and Lorenzo, 2017). In addition, both parasites share biological characteristics, antigens, geographical distribution, as well as insect and vertebrate hosts, which can compromise the correct diagnosis of *T. cruzi* infection due to crossed serological reactions (Vieira C. B. et al., 2018).

Rhodnius prolixus is considered one of the most efficient *T. cruzi* and *T. rangeli* vector in South America. It is a classical model organism in which basic concepts of insect physiology were initially established by Professor Sir Vincent B. Wigglesworth, with a relatively rapid life cycle and easy to breed in the laboratory, compared with other triatomine species (Vieira et al., 2016; Azambuja et al., 2017). In addition, *R. prolixus* is the only triatomine with its full genome sequenced to date, making it an ideal model to investigate arthropod-parasite interactions in a non-dipteran blood feeding insect vector (Mesquita et al., 2015).

The interactions between *T. rangeli* and *R. prolixus* begin when parasites are ingested as blood trypomastigotes, when the triatomine feeds on infected hosts (Hecker et al., 1990). After ingestion, the parasites transform into epimastigotes in the digestive tract and eventually cross the intestinal epithelium, reaching the hemocoel and hemolymph. Finally, *T. rangeli* invades and multiplies in the salivary glands, where it differentiates into metacyclic trypomastigotes, which are the infective forms transmitted during blood-meal to new vertebrate hosts (Guarneri and Lorenzo, 2017).

In order to establish the infection, *T. rangeli* must overcome the barriers imposed by the triatomine immune response in both the digestive tract and hemocoel. In insects, this response is initiated by host pattern receptor proteins (PRPs), which recognize pathogen associated molecular patterns (PAMPs) on the surface of pathogens and elicit different well conserved immune pathways: the immune deficiency (IMD), the Toll and the Janus kinase/Signal Transducers, and Activators of Transcription (Jak/STAT) (Salcedo-Porras and Lowenberger, 2019). Apparently, each of them acts in different types of infection, and induces the expression of certain subset of antimicrobial peptides (AMPs): Gram-negative bacteria trigger the IMD pathway, Gram-positive bacteria and fungi initiate the Toll pathway, and viruses activate the Jak/STAT pathway (Salcedo-Porras et al., 2019). Nevertheless, studies in ticks, lice, and hemipterans point to a deviation from the paradigm of a complete conservation of immune pathways in arthropods, emphasizing the need to investigate immune responses in different subphyla (Kim et al., 2011; Palmer and Jiggins, 2015; Shaw et al., 2018; Nishide et al., 2019).

Most of the key molecules for the IMD, Toll, and Jak/STAT pathways are present in the genome and many transcriptomes of

R. prolixus (Ribeiro et al., 2014; Mesquita et al., 2015; Ons et al., 2016; Latorre-Estivalis et al., 2017; Zumaya-Estrada et al., 2018). The gene encoding the protein *Relish* (*Rp-Relish*), a conserved transcription factor (TF) related to the IMD pathway, was identified in *R. prolixus* genome; while its inhibitory protein *Caspar* (*Rp-Caspar*) was not detected until a recent deeper analysis using BLAST complemented with hidden Markov model profiles (Mesquita et al., 2015; Salcedo-Porras et al., 2019). Moreover, the coding sequences for the NF- κ B TF *Dorsal* (*Rp-Dorsal*) and its inhibitor protein *Cactus* (*Rp-Cactus*) of the Toll pathway were detected in *R. prolixus* by suppressive subtractive hybridization technique and by transcriptome analysis, respectively (Ursic-Bedoya and Lowenberger, 2007; Ursic-Bedoya et al., 2009; Ribeiro et al., 2014). In addition, a transcript coding for the TF *STAT* (*Rp-STAT*) of the Jak/STAT pathway was also observed in transcriptomes from the *R. prolixus* digestive tract (Ribeiro et al., 2014). Furthermore, AMPs, such as lysozymes, defensins and prolixicin, have also been isolated from *R. prolixus* digestive tract and fat body (Lopez et al., 2003; Ursic-Bedoya et al., 2008; Ursic-Bedoya et al., 2011).

AMPs are mainly synthesized by fat body cells, which release them into the hemolymph for systemic delivery; or by epithelial cells for local secretion (Vieira et al., 2016; Azambuja et al., 2017; Salcedo-Porras and Lowenberger, 2019). Remarkably, there are several reports that investigate the induction of AMPs, which are the main effector molecules of the IMD, Toll, and Jak/STAT immune pathways, in *R. prolixus* challenged with different microorganisms (Castro et al., 2012; Vieira et al., 2014; Mesquita et al., 2015; Vieira et al., 2015; Vieira et al., 2016; Azambuja et al., 2017; Salcedo-Porras et al., 2019). Nevertheless, there are very few studies that investigate the immune pathways triggered by pathogens that lead to the production of those AMPs, or whether there are differences in the pathways activated according to the type, route and duration of infection. In this regard, *Rp-Relish* was found to regulate certain AMPs in response to Gram-negative and Gram-positive bacteria, in the fat body of *R. prolixus* (Salcedo-Porras et al., 2019). Furthermore, other report demonstrated that *Rp-Relish* controls defensins and lysozymes expression; and its repression led to an increase in the population of the symbiotic bacteria *Rhodococcus rhodnii*. Strikingly, the same study revealed that silencing *Rp-Relish* or *Rp-Dorsal* did not influence in *T. cruzi* loads detected 1 or 2 weeks after the infection (Mesquita et al., 2015). However, in a recent report, a reduction in *T. cruzi* loads was evidenced in the midgut of *R. prolixus* treated with the drug IMD-0354, which blocks I κ B α phosphorylation and thus prevents nuclear translocation of NF- κ B TFs (*Rp-Relish* and *Rp-Dorsal*), indicating the importance of these pathways in the anti-parasitic innate immune responses (Vieira C. S. et al., 2018).

Several studies demonstrate that oral infection with *T. rangeli* modulates systemic immune responses in *R. prolixus*, even without (or before) the penetration of parasites into the hemolymph (Gomes et al., 2003; Garcia et al., 2004b; Whitten et al., 2007; Figueiredo et al., 2008). In addition to *T. rangeli*, *T. cruzi* (which do not infect the hemolymph) also modulates the systemic immune responses when infecting the digestive tract

(Vieira et al., 2016; Favila-Ruiz et al., 2018). Furthermore, the growth of the native microbiota in the gut following a blood meal elicits the up-regulation of *Rp-Relish* in the fat body (Mesquita et al., 2015). These evidences support a significant role of systemic immune responses in controlling localized microbial infection. Accordingly, in this work we measured the expression of TFs (*Rp-Relish*, *Rp-Dorsal*, and *Rp-STAT*) and inhibitors (*Rp-Cactus* and *Rp-Caspar*) of the IMD, Toll, and Jak/STAT immune pathways in the triatomine's fat body, the main organ that synthesizes and release in the hemolymph inducible humoral immune factors to establish a systemic response. Furthermore, we analyzed parasite loads in the gut and hemolymph of *R. prolixus* with different forms of infection with *T. rangeli*, and we evaluated whether there was a correlation between the parasite counts and the expression of these immune genes. We hypothesize that long-term infection with *T. rangeli* in the digestive tract or hemolymph of *R. prolixus* triggers different systemic immune responses, which influences the number of parasites that survive in both regions of the insect body.

MATERIALS AND METHODS

Insect Rearing

Rhodnius prolixus were obtained from a colony maintained by the Vector Behavior and Pathogen Interaction Group at René Rachou Institute (FIOCRUZ, Minas, Brazil), which was established from insects collected in Honduras around 1990. The colony was maintained under controlled temperature ($26 \pm 1^\circ\text{C}$), relative humidity ($65 \pm 10\%$), and natural illumination cycle. Insects were consistently fed on diverse sources of blood that included mice, chicken, and a membrane feeder offering citrated rabbit blood at 37°C . Mice and chickens were anesthetized with intraperitoneal injections of ketamine (150 mg/kg; Cristália, Brazil) plus xylazine (10 mg/kg; Bayer, Brazil), and ketamine (20 mg/kg; Cristália, Brazil) plus detomidine (0.3 mg/kg; Syntec, Brazil), respectively. *Rhodnius prolixus* 4th instar nymphs starved for 30 days were used in all experiments.

Trypanosoma rangeli Culture

Trypanosoma rangeli CHOACHI strain used in this study was originally isolated from naturally infected *R. prolixus* (Schottelius, 1987). The epimastigote forms used to infect insects were cultured by twice weekly passages at 27°C in liver-infusion tryptose (LIT) medium, supplemented with fetal bovine serum 15%, 100 units/ml penicillin, and 100 $\mu\text{g/ml}$ streptomycin. In order to maintain the strain infectivity, parasites were passed through triatomines and mice every 3 months (Rodrigues et al., 2016).

Insect Infections

Insects were infected as recently described (Guarneri, 2020). For oral infection, sixty-day old male *Swiss Webster* mice were used. *Trypanosoma rangeli*-infected mice were generated through the bite of 5th instar nymphs containing trypomastigote forms in their salivary glands and were used at 14 days post infection (pi).

Mice parasitemia was confirmed immediately before starting the experiments ($2.5\text{--}5 \times 10^3$ parasites/ml).

For intracoelomic inoculation, *T. rangeli* epimastigotes were obtained from 10 day cultures, and resuspended in sterile PBS (0.15 M NaCl in 0.01 M sodium phosphate, pH 7.4) in a concentration of 5×10^4 parasites/ml. *Rhodnius prolixus* nymphs were inoculated through the thoracic pleura with 1 μl of PBS + LIT or PBS + the parasite suspension, using a 50 μl syringe (Hamilton Company, NV, USA, needle $13 \times 3.3; \frac{1}{2}''$) connected to a dispenser (model 705, Hamilton Company, NV, USA).

Experimental Design 1

To simulate a natural infection with the parasite, *R. prolixus* nymphs were randomly separated and fed on healthy or *T. rangeli*-infected mice (oral infection). Each insect was allowed to ingest 20–30 μl of blood, which resulted in ingestion of approximately 50–150 trypomastigotes. A week later, both groups of insects were randomly divided and inoculated in the hemocoel with 1 μl of PBS + LIT or PBS + parasite suspension (5×10^4 epimastigotes/ml). The inoculation was performed since *T. rangeli* does not always invade the hemocoel in the natural course of the insect infection (Ferreira et al., 2010). One week after inoculation (2 weeks after oral infection), hemolymph samples were taken by cutting off the terminal segment of a hind leg and collecting a drop of hemolymph on a microscope slide to check the status of infection. Thus, five experimental groups representing different forms of *T. rangeli* infection were generated: (1) insects without parasites in gut or hemolymph (G–H–, control group); (2) insects with parasites in the gut, but not in the hemolymph (G+H–); (3) insects that were only infected by inoculation in the hemolymph (G–H+); (4) insects with parasites in the gut and further inoculated with parasites in the hemolymph (G+H+); and (5) insects that were only gut-infected, but with parasites in hemolymph by “natural” crossing from the intestinal lumen (G+H+Nat). Two weeks after the inoculation all groups of insects were fed on healthy mice. Finally, a week later (4 weeks since the beginning of the experiment; 3 weeks after inoculations) parasite counts and gene expression were determined in individual insects.

The experimental design was repeated three times (three biological replicates), and insects used in subsequent experiments came from all the three biological replicates ($n = 26\text{--}28$ insects per group for parasite counts, with 8–10 insects from each replicate; and $n = 8\text{--}10$ insects per group for gene expression, with 2–4 insects from each replicate), except for the G+H+Nat group that only appeared in two of the replicates ($n = 12$ insects for parasite counts, with eight and four insects from each replicate; and $n = 8$ insects for gene expression, with four insects from each replicate).

Experimental Design 2

This design was only used to determine whether hemolymph infection could alter the parasite load in the gut of *R. prolixus* orally infected with *T. rangeli*. For this reason, the experiment was performed based on the first experimental design, but insects

were first inoculated in the hemocoel and then orally infected. Accordingly, *R. prolixus* nymphs were fed on healthy mice. A week later, insects were randomly divided and inoculated with 1 μ l of PBS + parasite suspension containing 50 or 500 parasites, or the same volume of PBS + LIT. Thus, four experimental groups were obtained: insects infected by inoculation with PBS + 50 epimastigotes (H+50), insects infected by inoculation with PBS + 500 epimastigotes (H+500), and their respective PBS + LIT inoculated control groups (H–50 and H–500, without hemolymph infection). Two weeks after the inoculation, all groups of insects were orally infected by feeding 20–30 μ l of blood on *T. rangeli*-infected mice. One week later (4 weeks since the beginning of the experiment) parasite counts were determined. Two biological replicates were performed for this experiment, and 4–5 insects per group from each replicate were used for parasite counts.

After the inoculation, the survival of the insect was >95% in each of the experimental group, in all biological replicates, in both experimental designs.

Quantification of Parasite Loads

Parasite Loads in the Hemolymph

2 μ l of hemolymph samples from individual insects were taken by cutting off the terminal segment of the right hind leg and gently pressing the abdomen. Samples were immediately diluted in 18 μ l of anticoagulant solution (0.01 M ethylenediamine tetra-acetic acid, 0.1 M glucose, 0.062 M sodium chloride, 0.03 M trisodium citrate, 0.026 M citric acid, pH 4.6), in a proportion of 1:10 hemolymph:anticoagulant (Mello et al., 1995). Parasite loads were estimated by directly counting in a Neubauer chamber.

Parasite Loads in the Gut

After hemolymph extraction, the cuticle of the insects was cut laterally and the entire digestive tract (anterior midgut, posterior midgut and rectum) was carefully removed with tweezers under a stereo microscope. Each digestive tract was washed three times in PBS and then transferred to a 0.5 ml plastic tube, where it was homogenized in 20 μ l of PBS. Afterward, parasite loads were estimated by directly counting in a Neubauer chamber.

Fat Body Isolation, RNA Extraction, and cDNA Synthesis

After gut removal, the thin layer of abdominal fat body beneath the dorsal and ventral cuticle was dissected and immediately transferred to a 1.5-ml tube containing 1 ml of TRIzol reagent (Thermo Fisher Scientific, MA, USA). Fat body RNA was extracted from individual insects following the manufacturer's recommendations, concentrations were determined using a Qubit 2.0 Fluorometer (Thermo Fisher Scientific, MA, USA), and RNA integrity was checked by agarose gel electrophoresis. Afterward, DNase treatment was carried out in 20- μ l reactions with RNase-free DNase I (TransGen Biotech, Beijing, China) for 15 min at 37°C, using 1 μ g of total RNA. Then, cDNA synthesis was performed in 20- μ l reactions containing 500 ng of DNase treated RNA using the EasyScript Reverse Transcriptase (TransGen Biotech, Beijing, China) with anchored Oligo(dT)₁₈

Primer, following the manufacturer's instructions. The subsequent cDNA was diluted 1:2 with DEPC water.

Real-Time Quantitative Polymerase Chain Reaction

Real-time quantitative polymerase chain reactions (RT-qPCR) were conducted using an Applied Biosystems 7500 Real-Time PCR System (Thermo Fisher Scientific, Waltham, MA, USA). Primers were designed for: α -Actin (housekeeping), *Rp-Relish*, *Rp-Dorsal*, *Rp-Caspar*, and *Rp-STAT*. Primers for *Rp-Cactus* were retrieved from the literature (Vieira C. S. et al., 2018). RT-qPCR efficiency for each primer pair was determined using the slope of a linear regression mode. The sequences, amplicon length and RT-qPCR efficiency of each of the primer pair are shown in **Table 1**. The identity of each of the amplicons was confirmed by Sanger sequencing (Standard-Seq, Macrogen, Seoul, Rep. of Korea).

All RT-qPCR reactions contained 1 μ l (~12.5 ng) of cDNA, 0.3 μ l of each primer (10 mM), 5 μ l of iTaq Universal SYBR Green Supermix (Bio-Rad Laboratories, CA, USA), and 3.4 μ l of DEPC water in a final volume of 10 μ l. The RT-qPCR conditions used were: 95°C for 5 min; 35 cycles of: 95°C for 15 s, 55°C for 30 s and 72°C for 30 s; followed by a melting curve analysis to confirm the specificity of the reaction. No-template controls and no-RT controls were included to verify the absence of exogenous DNA, primer-dimers formation and/or contamination. Reactions on each sample and controls were run in duplicate. Relative differences in transcripts levels were calculated considering the amplification efficiency of each primer pair using the Pfaffl method (Pfaffl, 2001), with α -Actin as reference gene. All data were normalized relative to values recorded for non-infected control insects (G–H– group).

Statistical Analysis

Shapiro-Wilk normality test was applied for assessing normality in the data set. The non-parametric Mann-Whitney U test was used for comparison between two experimental groups. One-way ANOVA followed by Bonferroni multiple-comparison *post-hoc* test was performed to analyze differences between three or more experimental groups. Correlation analyses were carried out using

TABLE 1 | Primer sequences, amplicon lengths, and RT-qPCR efficiencies.

| Gene | Primer sequence (5' to 3') | Amplicon length (bp) | RT-qPCR efficiency (%) |
|------------------|---|----------------------|------------------------|
| α -Actin | Fw-GACTTGGCTGGTCGTGATCT Rv-ACCATCAGGCAATTCGTAGG | 201 | 95.81% |
| <i>Rp-Relish</i> | Fw-CCGCATGGACCATTAACCTG Rv-AGGTTCACTTCTTACACTTCTTC | 167 | 108.55% |
| <i>Rp-Caspar</i> | Fw-GATGGTAGTGTATTGACGAATG Rv-CGGTGACAGTGATCTTGC | 196 | 106.28% |
| <i>Rp-Dorsal</i> | Fw-GTCATTGTTCTGGTTCAGTAGC Rv-GGCGTTCGGAATGAAATAGC | 181 | 91.25% |
| <i>Rp-Cactus</i> | Fw-GTGCTGGTGCTTGACGAAA Rv-GGAGTCGGACGATACCTCAA | 154 | 96.84% |
| <i>Rp-STAT</i> | Fw-GGCACCGAATCAGTAATGG Rv-AAAGCATTATCCAGGTTACC | 173 | 94.17% |

the Spearman correlation test. P values of < 0.05 were considered statistically significant.

RESULTS

T. rangeli Numbers in the Gut of *R. prolixus* Are Higher When the Hemolymph Is Infected

First, we investigated whether there were differences in parasite loads in the gut or hemolymph of *R. prolixus* with different forms of infection with *T. rangeli*. As detailed in Methods section (Experimental design 1), we analyzed five different groups of long-term infected insects: (1) without gut or hemolymph infection (G–H–); (2) without parasites in the gut, but infected in the hemolymph by inoculation (G–H+); (3) with parasites in the gut, but not in the hemolymph (G+H–); (4) with parasites in the gut and further inoculated with parasites in the hemolymph (G+H+); and (5) with parasites in the gut and in the hemolymph, but by “natural” crossing from the intestinal lumen (G+H+Nat).

We found significant differences in the number of parasites present in the gut of insects that were orally infected but differed in the presence of *T. rangeli* in the hemolymph (Figure 1A, ANOVA,

$p < 0.001$). Specifically, we detected lower parasite loads in G+H– insects compared to G+H+ or G+H+Nat (Figure 1A, Bonferroni's *post-hoc* test, $p < 0.001$ for all mentioned comparisons). Conversely, when we analyzed *T. rangeli* numbers in the hemolymph of inoculated or spontaneous infected insects, we found similar parasite loads, regardless of the presence of *T. rangeli* in the gut (Figure 1B, ANOVA, $p > 0.05$). These results suggest that *T. rangeli* numbers in the digestive tract of *R. prolixus* could be affected by the presence of the parasite in the hemolymph. In line with this, we observed a positive correlation between parasite numbers in the gut and the hemolymph (Figure 1C, Spearman $r = 0.55$, $p < 0.001$). Indeed, this positive correlation was maintained when we analyzed the G+H+ and G+H+Nat groups of insects separately (Supplementary Figure 1), indicating higher parasite loads in the gut of *R. prolixus* when *T. rangeli* numbers are also elevated in the hemolymph.

Hemolymph Infection Increases *T. rangeli* Numbers in the Gut of Orally Infected *R. prolixus*

To further support the hypothesis that the presence of *T. rangeli* in the hemolymph could affect the parasite numbers in the gut, we first inoculated insect hemocoel with PBS + 50 or 500 epimastigotes

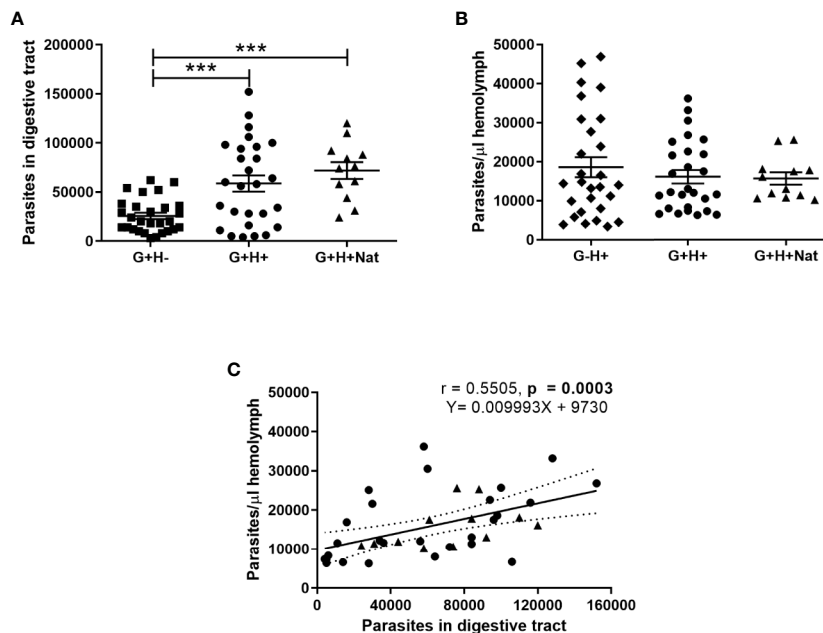


FIGURE 1 | *T. rangeli* loads in the gut and hemolymph of *R. prolixus* with different forms of infection. **(A, B)** Parasite numbers in **(A)** digestive tract and **(B)** hemolymph. Each point represents the numbers of parasites found in individual insects. Error bars represent the mean \pm SEM. Asterisks correspond to significant differences (***) $p < 0.001$ obtained by one-way ANOVA followed by Bonferroni multiple-comparison *post-hoc* test. **(C)** Correlation between *T. rangeli* numbers in gut and hemolymph. Each point represents the numbers of parasites measured in the gut and in the hemolymph of individual insects. The regression line calculated from the data and its 95% confidence intervals are also represented (continuous and curved dotted lines, respectively). G+H–: insects with parasites in the gut, but not in the hemolymph (represented by squares); G–H+: insects that were only infected in the hemolymph by inoculation (represented by diamonds); G+H+: insects with parasites in the gut and further inoculated with parasites in the hemolymph (represented by circles); and G+H+Nat: insects that were only gut-infected, but with parasites in the hemolymph by “natural” crossing from the intestinal lumen (represented by triangles). Each experimental group contained insects from three biological replicates ($n = 26$ – 28), with 8–10 insects from each replicate (except for $n = 12$ in the G+H+Nat group, composed of eight and four insects from two replicates).

(H+50 and H+500, respectively) or with PBS + LIT (H–50 and H–500, respectively), and then we proceeded with the oral infection (Experimental design 2 of the Methods section). Afterward, we evaluated the parasite loads in the gut and in the hemolymph of the different experimental groups (Figure 2). We evidenced higher parasite numbers in the gut of the H+50 and H+500 groups compared to insects from their respective mock-inoculated control groups (Figure 2A, ANOVA, $p < 0.001$; Bonferroni's *post-hoc* test, $p < 0.01$ for H–50 vs. H+50 and for H–500 vs. H+500). Besides, we found no differences in *T. rangeli* loads in the gut between insects that were inoculated with different parasite doses (Figure 2A, Bonferroni's *post-hoc* test, $p > 0.05$ for H+50 vs. H+500). Moreover, we detected similar numbers of parasites in the hemolymph between insects inoculated with 50 or 500 epimastigotes (Figure 2B, Mann-Whitney U test, $p > 0.05$). These results indicate that the parasite load achieved in the hemolymph was similar regardless of the inoculation dose used, but that *T. rangeli* infection in the hemolymph increased the parasite numbers in the gut of orally infected *R. prolixus*.

Differential Expression of IMD, Toll, and Jak/STAT Immune Pathway Genes in *R. prolixus* With Different Forms of *T. rangeli* Infection

As the vector immune response is directly involved in parasite killing and is critical for determining the ability of the parasite to establish the infection, we next investigated whether there were differences in the expression of IMD, Toll, and Jak/STAT immune pathway genes in the fat body of *R. prolixus* with different forms of *T. rangeli* infection. We evidenced that the expression of the TFs *Rp-Relish* and *Rp-STAT* and the inhibitor *Rp-Cactus* differed significantly between the groups of insects analyzed (Figure 3, ANOVA, $p < 0.01$ for the three genes). Particularly related to the IMD pathway, we found the TF *Rp-Relish* downregulated in the G+H–, G–H+, and G+H+Nat groups compared to uninfected insects (Figure 3A, Bonferroni's *post-hoc* test, $p < 0.05$ for all mentioned comparisons), and similar levels of the inhibitor *Rp-Caspar* between the different experimental groups (Figure 3D, ANOVA, $p > 0.05$). Moreover, regarding the Toll pathway, we

measured similar expression of the TF *Rp-Dorsal* between the different groups of insects (Figure 3B, ANOVA, $p > 0.05$). Nevertheless, we evidenced higher levels of the inhibitor *Rp-Cactus* in G+H– insects compared to the G–H– (control insects), G+H+ and G+H+Nat groups (Figure 3E, Bonferroni's *post-hoc* test, $p < 0.05$ for G+H– vs. G–H–, $p < 0.01$ for G+H– vs. G+H+ and $p < 0.001$ for G+H– vs. G+H+Nat). Furthermore, concerning the STAT pathway, we observed a lower expression of the TF *Rp-STAT* in the G–H+, G+H+, and G+H+Nat groups when compared to uninfected insects (Figure 3C, Bonferroni's *post-hoc* test, $p < 0.05$ for G+H+ vs. G–H– and $p < 0.01$ for G–H+ vs. G–H– and G+H+Nat vs. G–H–). Overall, these data demonstrate that key components of the IMD, Toll, and Jak/STAT immune pathways are differentially modulated in *R. prolixus* when *T. rangeli* infects the gut, the hemolymph or both regions of the insect vector.

Correlation Between Parasite Loads and the Expression of Immune Pathway Genes in the Fat Body of *R. prolixus* Infected With *T. rangeli*

We next evaluated whether there is a correlation between the expression of the IMD, Toll, and Jak/STAT pathway genes and the parasite counts in the gut (Figure 4) and the hemolymph (Figure 5) of *T. rangeli*-infected insects (Supplementary Figures 2–6 for correlations analyzing each group of insects separately). We found no association between *Rp-Dorsal* (Figure 4B, Spearman $r = 0.05$, $p > 0.05$), *Rp-STAT* (Figure 4C, Spearman $r = 0.08$, $p > 0.05$) or *Rp-Caspar* (Figure 4D, Spearman $r = 0.08$, $p > 0.05$) and parasite loads in the gut. Nevertheless, we did find a negative correlation between the number of parasites in that organ and the expression of the TF *Rp-Relish* (Figure 4A, Spearman $r = -0.61$, $p = 0.001$) and the inhibitor *Rp-Cactus* (Figure 4E, Spearman $r = -0.52$, $p < 0.01$). Furthermore, we observed no association between *T. rangeli* numbers in the hemolymph and the expression of *Rp-Dorsal* (Figure 5B, Spearman $r = -0.26$, $p > 0.05$), *Rp-STAT* (Figure 5C, Spearman $r = 0.07$, $p > 0.05$), *Rp-Caspar* (Figure 5D, Spearman $r = -0.11$, $p > 0.05$) or *Rp-Cactus* (Figure 5E, Spearman $r = -0.11$, $p > 0.05$), while we detected a negative correlation between

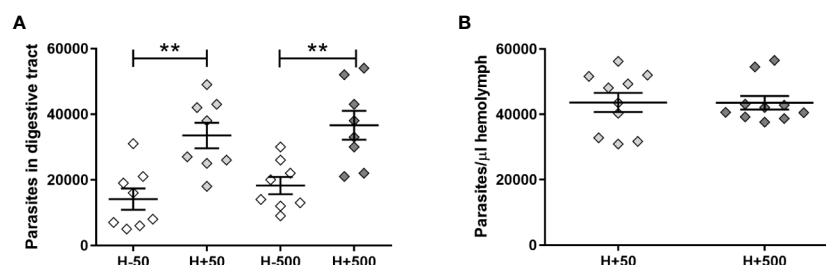


FIGURE 2 | *T. rangeli* loads in the gut and hemolymph of hemolymph-infected *R. prolixus* that were later orally infected. Parasite numbers in (A) digestive tract and (B) hemolymph. Each point represents the numbers of parasites found in individual insects. Error bars represent the mean ± SEM. Data was analyzed using one-way ANOVA followed by Bonferroni multiple-comparison *post-hoc* test (A) or Mann-Whitney U test (B). Asterisks correspond to significant differences (** $p < 0.01$). H+50: insects infected in the hemolymph by inoculation with 50 epimastigotes; H+500: insects infected in the hemolymph by inoculation with 500 epimastigotes; H–50 and H–500: control groups with PBS + LIT intracoeleomic inoculation. Two weeks after the inoculation all groups of insects were orally infected, and parasite counts were determined one week later. Each experimental group contained insects from two biological replicates ($n = 8–10$), with four to five insects from each replicate.

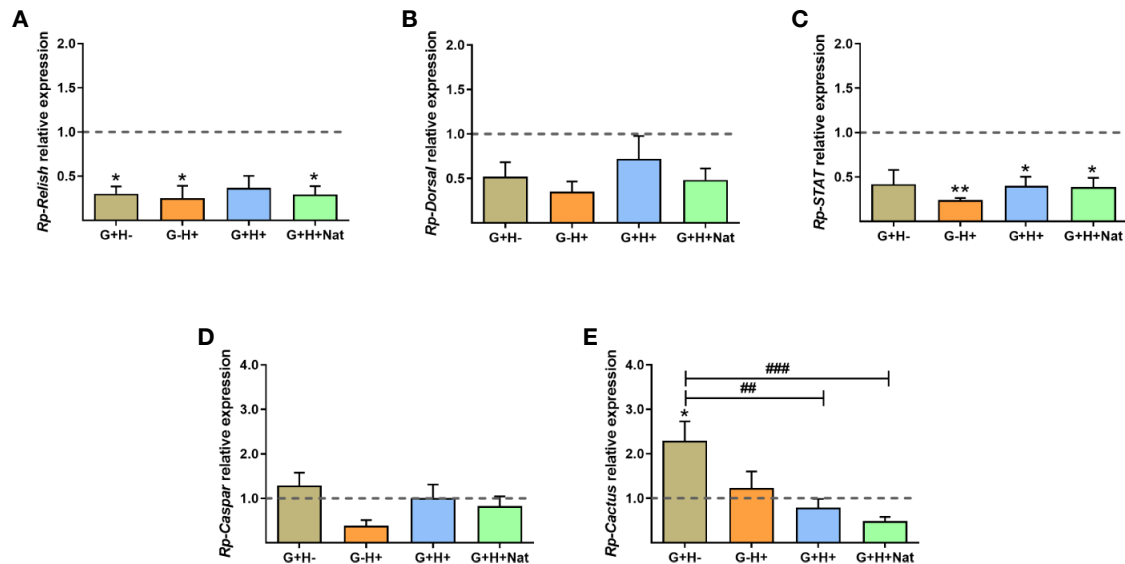


FIGURE 3 | Expression of IMD, Toll, and Jak/STAT immune pathway genes in the fat body of *R. prolixus* with different forms of *T. rangeli* infection. Relative mRNA abundance of the transcription factors **(A)** *Rp-Relish*, **(B)** *Rp-Dorsal*, and **(C)** *Rp-STAT*, and the inhibitors **(D)** *Rp-Caspar* and **(E)** *Rp-Cactus*. All RT-qPCR data were analyzed with the Pfaffl Method, using α -Actin as reference gene and normalizing to the gene expression of control insects (represented by the dotted line). Error bars represent the mean \pm SEM. Asterisks correspond to significant differences (* $p < 0.05$ and ** $p < 0.01$) as compared to control, and numerals correspond to significant differences (## $p < 0.01$ and ### $p < 0.001$) between the selected experimental groups, obtained by one-way ANOVA followed by Bonferroni multiple-comparison *post-hoc* test. G+H-: insects with parasites in the gut, but not in the hemolymph; G-H+: insects that were only infected in the hemolymph by inoculation; G+H+: insects with parasites in the gut and further inoculated with parasites in the hemolymph; and G+H+Nat: insects that were only gut-infected, but with parasites in hemolymph by "natural" crossing from the intestinal lumen. Each experimental group contained insects from three biological replicates ($n = 8-10$), with two to four insects from each replicate (except for two replicates in the G+H+Nat group, composed of four insects each).

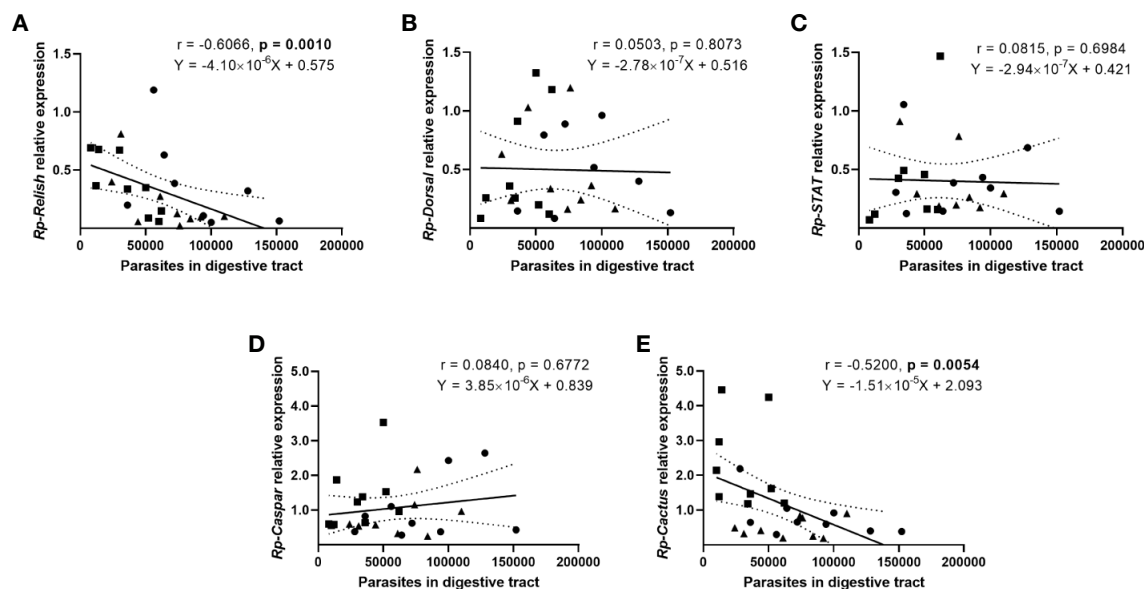


FIGURE 4 | Correlation between the parasite load in the gut and the expression of IMD, Toll, and Jak/STAT immune pathway genes in *R. prolixus* with different forms of *T. rangeli* infection. Correlation between *T. rangeli* numbers in the gut and the relative mRNA abundance of the transcription factors **(A)** *Rp-Relish*, **(B)** *Rp-Dorsal*, and **(C)** *Rp-STAT*, and the inhibitors **(D)** *Rp-Caspar* and **(E)** *Rp-Cactus*. Each point represents the gene expression and the numbers of parasites measured in the fat body of individual insects ($n = 25-27$), from a total of three biological replicates composed of 8-10 insects each. Squares represent insects with parasites in the gut, but not in the hemolymph (G+H-); circles represent insects with parasites in the gut and further inoculated with parasites in the hemolymph (G+H+); and triangles represent insects that were only gut-infected, but with parasites in hemolymph by "natural" crossing from the intestinal lumen (G+H+Nat). Each graph includes the regression line calculated from the data and its 95% confidence intervals (continuous and curved dotted lines, respectively).

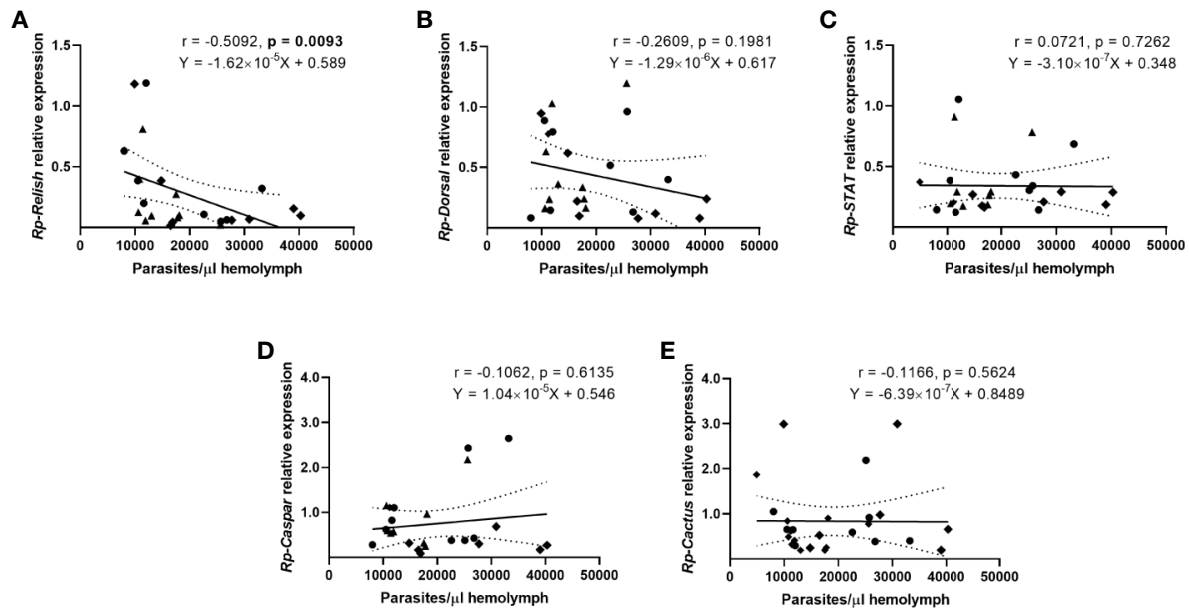


FIGURE 5 | Correlation between the parasite load in the hemolymph and the expression of IMD, Toll, and Jak/STAT immune pathway genes in *R. prolixus* with different forms of *T. rangeli* infection. Correlation between *T. rangeli* numbers in the hemolymph and the relative mRNA abundance of the transcription factors **(A)** *Rp-Relish*, **(B)** *Rp-Dorsal*, and **(C)** *Rp-STAT*, and the inhibitors **(D)** *Rp-Caspar* and **(E)** *Rp-Cactus*. Each point represents the gene expression and the numbers of parasites measured in the fat body of individual insects ($n = 25$ – 27), from a total of three biological replicates composed of 8–10 insects each. Diamonds represent insects that were only infected in the hemolymph by inoculation (G+H+); circles represent insects with parasites in the gut and further inoculated with parasites in the hemolymph (G+H+); and triangles represent insects that were only gut-infected, but with parasites in hemolymph by "natural" crossing from the intestinal lumen (G+H+Nat). Each graph includes the regression line calculated from the data and its 95% confidence intervals (continuous and curved dotted lines, respectively).

parasite counts and the expression of *Rp-Relish* in the same samples (**Figure 5A**, Spearman $r = -0.51$, $p < 0.01$). Taken together, our results indicate a relationship between *T. rangeli* loads in the gut and the hemolymph of *R. prolixus* with the expression of critical genes that modulate different immune pathways during infection.

DISCUSSION

Several reports in which *R. prolixus* was infected with *T. rangeli* have revealed that the ability of the parasite to reach the hemolymph, modulate the immune response and establish the infection in the salivary glands is dependent on the parasite strain and developmental form (short vs. long epimastigotes) (Grisard et al., 1999; Machado et al., 2001; Whitten et al., 2001; Whitten et al., 2007; Figueiredo et al., 2008; Ferreira et al., 2010; Cosentino-Gomes et al., 2014; Vieira et al., 2015). In this regard, and taking into consideration that insects are more susceptible to strains isolated from the same geographic region, we used for our experiments the CHOACHI strain of *T. rangeli*, which was isolated from naturally infected *R. prolixus* in Colombia and is able to complete its lifecycle inside the vector (Machado et al., 2001; Ferreira et al., 2010). Furthermore, to simulate the natural infection with the parasite, we used *T. rangeli*-infected mice to perform gut infections, and a low dose (50 epimastigotes) of cultured parasites for intracoeleomic infections, which were

previously passed through triatomines and mice to maintain the strain infectivity. We also discriminated and analyzed a group of insects that were only gut-infected and presented hemolymph infection by spontaneous crossing of parasites from the intestinal lumen (G+H+Nat group), which implies a more physiological approach for our experiments. Correspondingly, and in agreement with a previous report (Ferreira et al., 2010), we found similar results between insects that were orally infected and later inoculated with parasites in the hemolymph (G+H+) and the G+H+Nat group, suggesting that our protocol could be used to mimic the effects of the *T. rangeli* in the natural course of infection, at least during the evaluated period.

Independently of the way insects were infected, we measured similar numbers of parasites in the hemolymph of individuals with systemic infection, indicating that parasite loads in the caelomatic cavity were not affected by the presence of *T. rangeli* in the gut during long-term infections. Comparable numbers of parasites in the hemolymph were found in other studies using an initial dose of 10 or 100 parasites, which showed that the load of *T. rangeli* reaches a plateau of about 10^7 – 10^8 parasites/ml, suggesting that similar results could be achieved after 2 weeks of intracoeleomic infection by the inoculation of 10, 50, 100, or 500 parasites (Mello et al., 1995; Ferreira et al., 2010). In addition, and similar to a previous study using the CHOACHI strain, we detected high parasite numbers in the gut of insects 4 weeks after they fed on infected mice (Ferreira et al., 2018). Nevertheless, infections of *R. prolixus* with culture epimastigotes from Macias

and H14 strains showed that, during short-term infections, the parasite predominantly colonized the anterior midgut of the bug and its numbers decreased over time, while in long-term infections and after the bug's molting, the parasite infected the posterior midgut (Gomes et al., 2003; Vieira et al., 2015). Although we dissected the entire digestive tract, the parasite numbers we counted were higher than in those last reports. These discrepancies could be related to differences in infection's methodology, since the mentioned studies were performed using artificial blood feeding and different *T. rangeli* strains that were maintained exclusively in culture, which may impact parasite infectivity.

Strikingly, we found significantly higher parasite loads in the gut of insects that also had hemolymph infection, in comparison with insects without systemic infection, suggesting that the presence of *T. rangeli* in the hemolymph could influence parasite numbers in the gut during long-term infections. In line with this, we showed a positive correlation between the number of parasites in the hemolymph and in the gut. To confirm the hypothesis that the presence of parasites in the hemolymph could modulate the size of the population in the gut, we inoculated the insects' hemocoel with parasites and then performed the oral infection. Through this approach, we observed higher parasite loads in the gut of insects with hemolymph infection compared to the PBS + LIT inoculated groups. Overall, we evidenced for the first time that the presence of *T. rangeli* in the hemolymph affects the infection of the digestive tract, enhancing parasite numbers. Thus, we support the notion that this has significance on the course of natural infections and reinfections.

During an infection, the insect immune system recognizes pathogens' antigens as non-self, initiating several responses against the microbe, which are mainly triggered by the Toll, IMD and Jak/STAT immune pathways (Salcedo-Porras and Lowenberger, 2019). Several reports in different insect species have shown that the presence of parasites in the digestive tract stimulates the production of AMPs by the fat body and their systemic secretion in the hemolymph, even without the invasion into the hemocoel (Boulanger et al., 2001; Hao et al., 2001; Boulanger et al., 2002; Boulanger et al., 2004). Afterward, AMPs can diffuse throughout the insect body, establishing a systemic response that seems to diminish parasite loads in the digestive tract in response to oral infection (Boulanger et al., 2004). The opposite seems to occur in the case of *T. rangeli* infection in triatomines. The oral infection of *R. prolixus* with *T. rangeli* impacts the systemic immune responses by suppressing the prophenoloxidase activating pathway in the hemolymph, and inhibiting microaggregation reactions and phagocytic activity of hemocytes, which apparently facilitates parasite growth in the hemolymph (Gomes et al., 2003; Garcia et al., 2004b; Figueiredo et al., 2008). Besides, *T. rangeli* infection also modulates differentially the production of AMPs and nitric oxide in the gut and in the fat body of *R. prolixus*, varying over time as parasites multiply and the infection is established (Whitten et al., 2007; Vieira et al., 2015). Thus, in this study, we hypothesized that there are differences in the systemic modulation of immune pathways in *R. prolixus* during a long-term infection with

T. rangeli in the gut or in the hemolymph, and these differences could influence in the number of parasites that survive in both regions of the triatomine body.

There are few studies on the immune pathways elicited in *R. prolixus* during pathogen infection, and it is assumed that these pathways function as in other model insects (Mesquita et al., 2015; Zumaya-Estrada et al., 2018; Salcedo-Porras and Lowenberger, 2019). Recently, the NF- κ B TF *Rp-Relish* of the IMD pathway was found to differentially regulate the expression of AMPs in response to Gram-negative and Gram-positive bacteria (Salcedo-Porras et al., 2019). In addition, when *Rp-Relish* expression was silenced, the population of the symbiotic bacteria *Rhodococcus rhodnii* increased in the insect gut (Mesquita et al., 2015). However, it was reported that silencing *Rp-Relish* or the NF- κ B TF *Rp-Dorsal* of the Toll pathway did not influence in *T. cruzi* loads in *R. prolixus* gut (Mesquita et al., 2015). Conversely, *T. cruzi* and *T. rangeli* infections modulate the expression of AMPs that are thought to be regulated by the Toll and IMD pathways, indicating that these pathways are functional during parasitic infections (Vieira et al., 2015; Vieira et al., 2016). In this regard, our results suggest a decreased activity of the IMD pathway in *R. prolixus* during long-term infections with *T. rangeli*. Accordingly, we demonstrated a ~70%–75% downregulation of the TF *Rp-Relish* and no changes in the expression of the inhibitor *Rp-Caspar* of the IMD pathway in insects with oral and/or systemic infection, in comparison with uninfected controls. Besides, we found an inverse correlation between the numbers of parasites in the gut and the expression of *Rp-Relish*, suggesting that higher numbers of *T. rangeli* in the digestive tract could increase the systemic repression of the IMD pathway in orally infected *R. prolixus*. Moreover, we detected an inverse correlation between parasite counts in the hemolymph and the expression of this TF, pointing that the activation of the IMD pathway could be reduced by higher parasite loads in the hemolymph of insects with systemic infection.

Regarding the Toll pathway, we found no differences in *Rp-Dorsal* expression between the groups of insects analyzed, but a ~2- to 4-fold higher levels of the inhibitor *Rp-Cactus* in the G+H– group, compared to controls and insects with both oral and systemic infection, suggesting a downregulation of this pathway in gut-only infected insects, which could be reverted when *T. rangeli* also infects the hemolymph. This differential expression of *Rp-Cactus* between the G+H– compared to the G+H+ and G+H+Nat groups of insects could be related to the differences in parasite loads found between insect with or without hemolymph infection. Accordingly, we found a negative correlation between *Rp-Cactus* expression and parasite loads in the gut, indicating that when there are low parasite counts in the gut, the expression of *Rp-Cactus* is high (as in the G+H– group); or when the parasite numbers in the gut are high, the expression of *Rp-Cactus* is lower (as in G+H+ and G+H+Nat groups). Supporting our findings, another study demonstrated that the phenoloxidase activity and *Rp-Prolixicin*, *Rp-Lysozyme A*, *Rp-Lysozyme B*, and *Rp-Defensin B* gene expression (AMPs induced by the activation of immune pathways) are suppressed in the digestive tract of *R. prolixus* after oral infection with this

parasite, indicating a systemic down-regulation of the immune pathways by *T. rangeli* infection (Vieira et al., 2015). In addition, studies on *Anopheles gambiae*, *Glossina morsitans*, *Phlebotomus papatasi*, and *Aedes aegypti* infected with different parasites (*Plasmodium* sp., *Trypanosoma* sp. and *Leishmania* sp.) showed that the expression of *Relish* and *Cactus* regulates infection prevalence and intensity, highlighting the importance of the IMD and Toll pathways in anti-parasitic immune responses in vectors (Meister et al., 2005; Frolet et al., 2006; Hu and Aksoy, 2006; Antonova et al., 2009; Louradour et al., 2019). In this regard, a recent report demonstrated a reduction in *T. cruzi* loads in the midgut of *R. prolixus* treated with the drug IMD-0354, which impedes the activation of NF- κ B TFs (Vieira C. S. et al., 2018).

The TF *Rp-STAT* was first sequenced in transcriptome analyses from the digestive tract of non-infected *R. prolixus* (Ribeiro et al., 2014). Afterward, several members of the Jak/STAT pathway were identified in transcriptome analyses of *Triatoma infestans*, *Triatoma dimidiata*, and *Triatoma pallidipennis*, and in the genome of *R. prolixus*, suggesting that this pathway is functional in triatomines (Mesquita et al., 2015; Zumaya-Estrada et al., 2018). Nevertheless, as far as we know, the expression and function of this pathway in triatomines during microbial infection has not been studied. In this work, we did not find any correlation between parasite loads and the expression of *Rp-STAT*, suggesting that the Jak/STAT pathway is not modulated by *T. rangeli* numbers in *R. prolixus*. Strikingly, in comparison with uninfected insects, we determined a ~60%–75% lower expression of *Rp-STAT* in all groups of insects with hemolymph infection, suggesting that *T. rangeli* reduces the Jak/STAT pathway activity when infecting the hemocoel, independently of the presence of parasites in the gut. This downregulation of *Rp-STAT* could be needed for the parasite to proliferate and increase its number in the hemolymph after the hemocoel infection. Besides, it could also be related to the higher *T. rangeli* numbers found in the gut of hemolymph infected insects, as the systemic repression of the Jak/STAT pathway could influence in the parasite loads in the gut. In agreement with this hypothesis, STAT knockdown by RNAi increased the number of *Plasmodium vivax* in the midgut of *Anopheles aquasalis*, and enhanced *Plasmodium berghei* and *Plasmodium falciparum* infection in the digestive tract of *A. gambiae* (Gupta et al., 2009; Bahia et al., 2011). Further studies are needed to also confirm the anti-parasitic role of this pathway during *T. rangeli* and *R. prolixus* interactions.

It is worth mentioning that, to date, no study has examined whether IMD, Toll, and Jak/STAT immune pathway genes are modulated in *R. prolixus* by *T. rangeli* infection. Nevertheless, we are aware that gene expression of regulatory factors in immune pathways does not necessarily reflect the activation of these pathways, as they are often regulated by post-transcriptional modifications. However, to our knowledge, specific antibodies to detect the cellular localization of these proteins or the phosphorylation status are not available yet for *R. prolixus*. Furthermore, a larger-scale gene expression analysis will be important to reveal whether there is a global modulation in

each of the immune pathways' genes (receptors, signaling cascade components) besides their TFs/inhibitors. On the other hand, compared to *Drosophila melanogaster*, in which the expression of certain AMPs (i.e. the AMP *Drosomycin* for the Toll pathway or the AMP *Diptericin* for the IMD pathway) directly reflects the activity of specific immune pathways, the specificity of AMPs expression triggered by each of the immune pathways are unknown in *R. prolixus* (Lemaitre et al., 1997; Khush et al., 2001; Michel et al., 2001; Gottar et al., 2002; Rutschmann et al., 2002; Tauszig-Delamasure et al., 2002; Hanson et al., 2019; Lin et al., 2019). In fact, to date only two studies reported modulation of AMPs after silencing *Rp-Relish*, with discrepancies between them (Mesquita et al., 2015; Salcedo-Porras et al., 2019). In addition, there is no information regarding AMPs expression after silencing genes of the Toll or Jak/STAT pathway in *R. prolixus*, which does not allow the comparison with the mentioned reports on the IMD pathway. Consequently, we considered that measuring the expression of TFs and negative regulators that are specific for each of the immune pathways would be a feasible way to evaluate how these pathways are modulated in *R. prolixus*.

The aim of this work was to analyze the systemic modulation of immune pathways in *R. prolixus* during long-term infection with *T. rangeli* as a mean to uncover which immune pathways play a role during the different phases of the infection in the insect. Accordingly, we demonstrated a relationship between parasite counts in the digestive tract/hemolymph and gene expression in the fat body, but local immune responses in the digestive tract of triatomines or triggered by hemocytes also play important roles in controlling microbial infections at different sites (Mello et al., 1995; Whitten et al., 2001; de Oliveira and de Souza, 2003; Garcia et al., 2004a; Castro et al., 2012; Vieira et al., 2014; Mesquita et al., 2015; Vieira et al., 2016; Favila-Ruiz et al., 2018; Vieira C. S. et al., 2018). In fact, it was shown that oral infection with *T. rangeli* modulates AMPs and NOS expression in the gut of *R. prolixus*; and systemic infections increase hemocyte numbers, hemocyte microaggregation, ROS and NOS levels in the hemolymph, and the activity of the prophenoloxidase (proPO) system (Whitten et al., 2001; Garcia et al., 2004a; Whitten et al., 2007; Vieira et al., 2015). Thus, additional studies analyzing which immune pathways are modulated in the digestive tract/hemocytes of *R. prolixus* during *T. rangeli* infection and whether there is an association between these pathways and parasite loads will yield valuable information to complement the present and mentioned reports.

It should be noted that in the present study we analyzed individual insects, and thus inherent high variability between samples are expected for parasite loads and gene expression. In line with this, we consider that the main source of variation came from the inter-individual genetic differences in the population of parasites and insects. Although we worked with only one strain of *T. rangeli* (CHOACHI) and a single colony of *R. prolixus*, the individuals forming those populations are not genetic clones. Thus, while all insects were infected at the same time and under similar conditions, the numbers of parasites infecting each individual, the immune responses elicited, and the course of

the infection will depend on the specific interactions between the insects and the parasites infecting it. In this regard, previous reports analyzing individual insects using the same colony of *R. prolixus* and *T. rangeli* strain have demonstrated this variation (Ferreira et al., 2010; Ferreira et al., 2015; Ferreira et al., 2018). In addition, during the oral feeding, we allowed the insects to ingest 20–30 μ l of blood, which resulted in ingestion of approximately 50–150 trypomastigotes for the infections. These differences in the initial dose of ingested parasites per insect may also contribute to the variance observed in our results. Another source of variation came from the spontaneous infection of the hemolymph in orally infected insects, as we cannot control whether or when the parasite crosses the gut epithelium to the hemocoel. Thus, although we were able to discriminate insects with spontaneous infection in the hemolymph (G+H+Nat group), probably the passage from the gut occurred at different time in different insects, influencing in the results obtained within this group of insects and between other groups. Finally, for the case of the association found between parasite loads and gene expression, the data correspond to individual insects infected in the gut or the hemolymph, independently of other types of infection. Hence, it is likely that whether insects are infected in other sites would influence in the results of the correlations. Accordingly, we showed the correlation for all groups of insects separately in **Supplementary Figures 2–6**. However, in this latter analysis, the numbers of individual drop considerably in each correlation (<10 insects per group), and we believe that the information of more insects is needed to get robust conclusions from these results.

Another limitation of this work is that only one timepoint was chosen for the experiments. *Trypanosoma rangeli* is a parasite that produce chronic systemic infections in *Rhodnius* (colonizing the gut, hemolymph and salivary gland of the insect) (Guarneri and Lorenzo, 2017). It is unclear how and when *T. rangeli* spontaneously cross the gut epithelium and colonizes the hemolymph; and it is a process that occurs in a very low percentage (2%–13%) of orally infected insects (Hecker et al., 1990; de Oliveira and de Souza, 2001; Ferreira et al., 2010; Ferreira et al., 2015). When hemolymph invasion happens, the development of the parasite in the insect is usually slow, as it takes approximately 3 weeks after entering in the hemolymph to produce metacyclic forms in the salivary glands (Ferreira et al., 2010; Paim et al., 2013). Therefore, we chose the period of 4 weeks to make our measurements because we wanted that all developmental forms were established. However, future research with a temporal kinetics will be very interesting to complement our findings, as it would uncover how the immune pathways are modulated by parasite loads during the entire infection and how the dynamics in parasite loads in the gut or hemolymph influence in the number of *T. rangeli* presents in other regions of the insect body, shedding more light into the communication between the gut and the hemolymph along the course of the infection. Thus, even though we could not show the modulation of the immune system over time, our results revealed important features of the *T. rangeli*–*R. prolixus* interaction. The fact that the parasite can sustain distinct immunomodulation in long-term infections, depending on the site of infection, indicates that these differences are crucial to complete its entire biological cycle

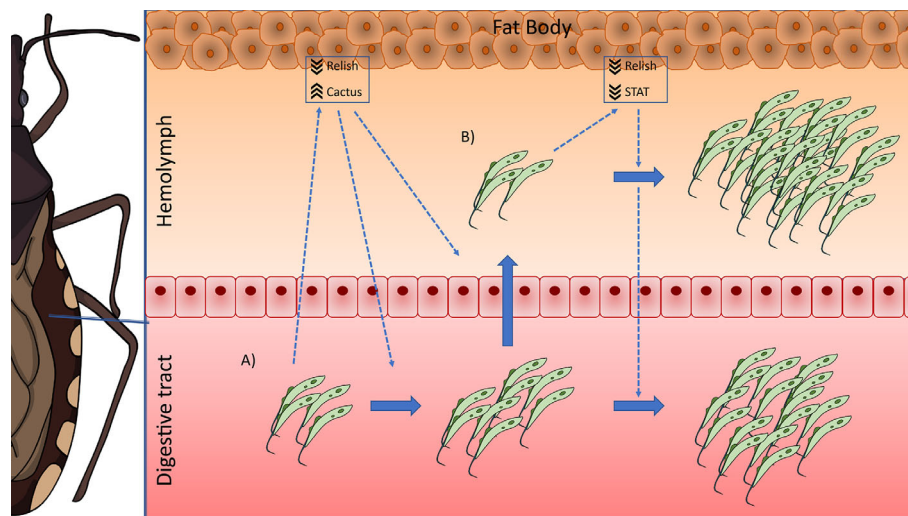


FIGURE 6 | IMD, Toll, and Jak/STAT immune pathway genes modulation in *R. prolixus* during long-term infection with *T. rangeli*. Possible scenario: **(A)** When *T. rangeli* infects the digestive tract of *R. prolixus*, it causes a systemic decrease in the activation of the Toll (by upregulating the levels of the inhibitor *Rp-Cactus*) and IMD (by downregulating the TF *Rp-Relish*) immune pathways, which allows the setting of the infection. This modulation of the immune response would also trigger the multiplication of the first parasites that reach the hemocoel, which proliferate and establish the infection in the hemolymph. **(B)** During hemolymph infection, the systemic inhibition of the IMD pathway remains (downregulation of *Rp-Relish*) but not the repression in the Toll pathway (*Rp-Cactus* levels return to basal); and the systemic activity of the Jak/STAT immune pathway is now also diminished (downregulation of the TF *Rp-STAT*). In consequence, parasite loads in the hemolymph and the digestive tract increase.

inside the insect. Moreover, taking into consideration that most of the infected insects will not develop a systemic infection, the fact that gut only-infected bugs maintain two immune activation pathways reduced (Toll and IMD, as suggested by our results) in a long-term infection may be important for the maintenance of stable populations with a high number of parasites in the intestinal tract, which could increase the chances of hemolymph invasion (Hecker et al., 1990; de Oliveira and de Souza, 2001; Ferreira et al., 2010; Ferreira et al., 2015; Ferreira et al., 2018). Similarly, the sustained repression of two immune pathways (IMD and Jak/STAT) in hemolymph-infected *R. prolixus* during long-term infection may be responsible for the high parasite loads found in that region of the insect body, which could facilitate the infection of the salivary glands (Mello et al., 1995; Ferreira et al., 2010).

Based on our results, we postulate the following possible scenario in *R. prolixus* during long-term infections with *T. rangeli*: when the parasite infects the digestive tract of the insect, it causes a systemic decrease in the activation of the Toll (by upregulating the levels of the inhibitor *Rp-Cactus*) and IMD (by downregulating the TF *Rp-Relish*) immune pathways, which allows the setting of the infection. This modulation of the immune response would also trigger the multiplication of the first parasites that reach the hemocoel, which proliferate and establish the infection in the hemolymph. During that process, the systemic inhibition of the IMD pathway remains (downregulation of *Rp-Relish*) but not the repression in the Toll pathway (*Rp-Cactus* levels return to basal); and the systemic activity of the Jak/STAT immune pathway is now also diminished (downregulation of the TF *Rp-STAT*). In consequence, parasite loads in the hemolymph and digestive tract increase (Figure 6). Our studies open new and challenging questions: Which are the effector mechanisms triggered by each immune pathway to modify *T. rangeli* loads? Is the downregulation of the Jak/STAT pathway necessary for the parasite to invade the salivary glands? Can we inhibit the parasite to infect the hemolymph after an oral infection by upregulating the activation of these immune pathways? RNAi/CRISPR experiments targeting the transcription factors and inhibitors of the IMD, Toll, and Jak/STAT pathways will follow suit to understand the immunological processes involved in *T. rangeli*–*R. prolixus* interaction.

DATA AVAILABILITY STATEMENT

The original contributions presented in the study are included in the article/supplementary material. Further inquiries can be directed to the corresponding authors.

ETHICS STATEMENT

The animal study was reviewed and approved by the Ethics Committee in Animal Experimentation (CEUA/FIOCRUZ) under the protocol number LW-8/17. This protocol adheres to the guidelines of National Council for Animal Experimentation

Control (CONCEA/MCT), which is the maximum ethics committee of the Brazilian government.

AUTHOR CONTRIBUTIONS

AR and AG designed the study. AR, AN, and LS were in charge of insect rearing, trypanosome culture, insect infections, and dissections. AR performed the quantification of parasite loads and qRT-PCRs. AR and AG analyzed the data and wrote the original draft of the manuscript. RR-P reviewed and edited the manuscript. All authors contributed to the article and approved the submitted version.

FUNDING

This work was supported by project grants from Universidad Nacional del Noroeste de la Provincia de Buenos Aires (SIB 0615/2019 to AR), Roemmers Foundation (FAJR 2018 to AR), Agencia Nacional de Promoción de Ciencia y Tecnología (PICT-2014-1554 to RR-P), and by travel grants from Universidad Nacional del Noroeste de la Provincia de Buenos Aires (SIDT N° 402/2018 and N° 458/2019 to AR). This work was also supported by Fundação de Amparo à Pesquisa do Estado de Minas Gerais (FAPEMIG, grant numbers CRA-APQ-00569-15 and CRA-PPM-00162-17), Instituto Nacional de Ciência e Tecnologia em Entomologia Molecular (INCTEM/CNPq, grant number 465678/2014-9). This study was financed in part by the Coordenação de Aperfeiçoamento de Pessoal de Nível Superior – Brasil (CAPES) – Finance Code 001.

ACKNOWLEDGMENTS

AR was supported by a postdoctoral fellowship from the Consejo Nacional de Investigaciones Científicas y Técnicas (CONICET, Argentina). AG was supported by CNPq productivity grant. We would like to thank Newmar Pinto Marlière (FIOCRUZ), Agustina Pascual (CeBio), and Maria José Delgado (CeBio) for excellent technical assistance and insightful comments. In addition, we are grateful with Lillian Rainer Butler (University of Maryland School of Medicine) for her help in the design of Figure 6. Finally, we thank the Instituto Nacional de Tecnología Agropecuaria (INTA-Pergamino) for having facilitated the use of its ABIPRISM 7500 Sequence Detection System to perform the RT-qPCR experiments.

SUPPLEMENTARY MATERIAL

The Supplementary Material for this article can be found online at: <https://www.frontiersin.org/articles/10.3389/fcimb.2020.598526/full#supplementary-material>

REFERENCES

- Antonova, Y., Alvarez, K. S., Kim, Y. J., Kokoza, V., and Raikhel, A. S. (2009). The role of NF-kappaB factor REL2 in the *Aedes aegypti* immune response. *Insect Biochem. Mol. Biol.* 39 (4), 303–314. doi: 10.1016/j.ibmb.2009.01.007
- Azambuja, P., Garcia, E. S., Wanek, P. J., Vieira, C. S., Figueiredo, M. B., Gonzalez, M. S., et al. (2017). *Rhodnius prolixus*: from physiology by Wigglesworth to recent studies of immune system modulation by *Trypanosoma cruzi* and *Trypanosoma rangeli*. *J. Insect Physiol.* 97, 45–65. doi: 10.1016/j.jinsphys.2016.11.006
- Bahia, A. C., Kubota, M. S., Tempone, A. J., Araujo, H. R., Guedes, B. A., Orfano, A. S., et al. (2011). The JAK-STAT pathway controls *Plasmodium vivax* load in early stages of *Anopheles aquasalis* infection. *PLoS Negl. Trop. Dis.* 5 (11), e1317. doi: 10.1371/journal.pntd.0001317
- Boulanger, N., Ehret-Sabatier, L., Brun, R., Zachary, D., Bulet, P., and Imler, J. L. (2001). Immune response of *Drosophila melanogaster* to infection with the flagellate parasite *Crithidia* spp. *Insect Biochem. Mol. Biol.* 31 (2), 129–137. doi: 10.1016/S0965-1748(00)00096-5
- Boulanger, N., Brun, R., Ehret-Sabatier, L., Kunz, C., and Bulet, P. (2002). Immunopeptides in the defense reactions of *Glossina morsitans* to bacterial and *Trypanosoma brucei* infections. *Insect Biochem. Mol. Biol.* 32 (4), 369–375. doi: 10.1016/S0965-1748(02)00029-2
- Boulanger, N., Lowenberger, C., Volf, P., Ursic, R., Sigutova, L., Sabatier, L., et al. (2004). Characterization of a defensin from the sand fly *Phlebotomus duboscqi* induced by challenge with bacteria or the protozoan parasite *Leishmania major*. *Infect. Immun.* 72 (12), 7140–7146. doi: 10.1128/IAI.72.12.7140-7146.2004
- Castro, D. P., Moraes, C. S., Gonzalez, M. S., Ratcliffe, N. A., Azambuja, P., and Garcia, E. S. (2012). *Trypanosoma cruzi* immune response modulation decreases microbiota in *Rhodnius prolixus* gut and is crucial for parasite survival and development. *PLoS One* 7 (5), e36591. doi: 10.1371/journal.pone.0036591
- Cosentino-Gomes, D., Rocco-Machado, N., and Meyer-Fernandes, J. R. (2014). *Rhodnius prolixus*: modulation of antioxidant defenses by *Trypanosoma rangeli*. *Exp. Parasitol.* 145, 118–124. doi: 10.1016/j.exppara.2014.08.002
- de Oliveira, M. A., and de Souza, W. (2001). An electron microscopic study of penetration by *Trypanosoma rangeli* into midgut cells of *Rhodnius prolixus*. *J. Invertebr. Pathol.* 77 (1), 22–26. doi: 10.1006/jipa.2000.4988
- de Oliveira, M. A., and de Souza, W. (2003). Further morphological studies on the behavior of *Trypanosoma rangeli* in the hemocytes of *Rhodnius prolixus*. *Parasitol. Int.* 52 (4), 299–307. doi: 10.1016/j.parint.2003.08.002
- Favila-Ruiz, G., Jimenez-Cortes, J. G., Cordoba-Aguilar, A., Salazar-Schettino, P. M., Gutierrez-Cabrera, A. E., Perez-Torres, A., et al. (2018). Effects of *Trypanosoma cruzi* on the phenoloxidase and prophenoloxidase activity in the vector *Meccus pallidipennis* (Hemiptera: Reduviidae). *Parasit. Vectors* 11 (1), 434. doi: 10.1186/s13071-018-3016-0
- Ferreira, L. L., Lorenzo, M. G., Elliot, S. L., and Guarneri, A. A. (2010). A standardizable protocol for infection of *Rhodnius prolixus* with *Trypanosoma rangeli*, which mimics natural infections and reveals physiological effects of infection upon the insect. *J. Invertebr. Pathol.* 105 (1), 91–97. doi: 10.1016/j.jip.2010.05.013
- Ferreira, L., Pereira, M. H., and Guarneri, A. A. (2015). Revisiting *Trypanosoma rangeli* Transmission Involving Susceptible and Non-Susceptible Hosts. *PLoS One* 10 (10), e0140575. doi: 10.1371/journal.pone.0140575
- Ferreira, R. C., Teixeira, C. F., de Sousa, V. F. A., and Guarneri, A. A. (2018). Effect of temperature and vector nutrition on the development and multiplication of *Trypanosoma rangeli* in *Rhodnius prolixus*. *Parasitol. Res.* 117 (6), 1737–1744. doi: 10.1007/s00436-018-5854-2
- Figueiredo, M. B., Genta, F. A., Garcia, E. S., and Azambuja, P. (2008). Lipid mediators and vector infection: *Trypanosoma rangeli* inhibits *Rhodnius prolixus* hemocyte phagocytosis by modulation of phospholipase A2 and PAF-acetylhydrolase activities. *J. Insect Physiol.* 54 (12), 1528–1537. doi: 10.1016/j.jinsphys.2008.08.013
- Frolet, C., Thoma, M., Blandin, S., Hoffmann, J. A., and Levashina, E. A. (2006). Boosting NF-kappaB-dependent basal immunity of *Anopheles gambiae* aborts development of *Plasmodium berghei*. *Immunity* 25 (4), 677–685. doi: 10.1016/j.immuni.2006.08.019
- Garcia, E. S., Machado, E. M., and Azambuja, P. (2004a). Effects of eicosanoid biosynthesis inhibitors on the prophenoloxidase-activating system and microaggregation reactions in the hemolymph of *Rhodnius prolixus* infected with *Trypanosoma rangeli*. *J. Insect Physiol.* 50 (2–3), 157–165. doi: 10.1016/j.jinsphys.2003.11.002
- Garcia, E. S., Machado, E. M., and Azambuja, P. (2004b). Inhibition of hemocyte microaggregation reactions in *Rhodnius prolixus* larvae orally infected with *Trypanosoma rangeli*. *Exp. Parasitol.* 107 (1–2), 31–38. doi: 10.1016/j.exppara.2004.03.015
- Gomes, S. A., Feder, D., Garcia, E. S., and Azambuja, P. (2003). Suppression of the prophenoloxidase system in *Rhodnius prolixus* orally infected with *Trypanosoma rangeli*. *J. Insect Physiol.* 49 (9), 829–837. doi: 10.1016/S0022-1910(03)00133-1
- Gottar, M., Gobert, V., Michel, T., Belvin, M., Duyk, G., Hoffmann, J. A., et al. (2002). The *Drosophila* immune response against Gram-negative bacteria is mediated by a peptidoglycan recognition protein. *Nature* 416 (6881), 640–644. doi: 10.1038/nature734
- Grisard, E. C., Steindel, M., Guarneri, A. A., Eger-Mangrich, I., Campbell, D. A., and Romanha, A. J. (1999). Characterization of *Trypanosoma rangeli* strains isolated in Central and South America: an overview. *Mem. Inst. Oswaldo Cruz* 94 (2), 203–209. doi: 10.1590/S0074-0276199900200015
- Guarneri, A. A., and Lorenzo, M. G. (2017). Triatomine physiology in the context of trypanosome infection. *J. Insect Physiol.* 97, 66–76. doi: 10.1016/j.jinsphys.2016.07.005
- Guarneri, A. A. (2020). Infecting Triatomines with Trypanosomes. *Methods Mol. Biol.* 2116, 69–79. doi: 10.1007/978-1-0716-0294-2_5
- Gupta, L., Molina-Cruz, A., Kumar, S., Rodrigues, J., Dixit, R., Zamora, R. E., et al. (2009). The STAT pathway mediates late-phase immunity against *Plasmodium* in the mosquito *Anopheles gambiae*. *Cell Host. Microbe* 5 (5), 498–507. doi: 10.1016/j.chom.2009.04.003
- Hanson, M. A., Dostalova, A., Ceroni, C., Poidevin, M., Kondo, S., and Lemaitre, B. (2019). Synergy and remarkable specificity of antimicrobial peptides in vivo using a systematic knockout approach. *Elife* 8. doi: 10.7554/eLife.44341
- Hao, Z., Kasumba, I., Lehane, M. J., Gibson, W. C., Kwon, J., and Aksoy, S. (2001). Tsetse immune responses and trypanosome transmission: implications for the development of tsetse-based strategies to reduce trypanosomiasis. *Proc. Natl. Acad. Sci. U.S.A.* 98 (22), 12648–12653. doi: 10.1073/pnas.221363798
- Hecker, H., Schwarzenbach, M., and Rudin, W. (1990). Development and interactions of *Trypanosoma rangeli* in and with the reduviid bug *Rhodnius prolixus*. *Parasitol. Res.* 76 (4), 311–318. doi: 10.1007/bf00928185
- Hu, C., and Aksoy, S. (2006). Innate immune responses regulate trypanosome parasite infection of the tsetse fly *Glossina morsitans morsitans*. *Mol. Microbiol.* 60 (5), 1194–1204. doi: 10.1111/j.1365-2958.2006.05180.x
- Khush, R. S., Leulier, F., and Lemaitre, B. (2001). *Drosophila* immunity: two paths to NF-kappaB. *Trends Immunol.* 22 (5), 260–264. doi: 10.1016/S1471-4906(01)01887-7
- Kim, J. H., Min, J. S., Kang, J. S., Kwon, D. H., Yoon, K. S., Strycharz, J., et al. (2011). Comparison of the humoral and cellular immune responses between body and head lice following bacterial challenge. *Insect Biochem. Mol. Biol.* 41 (5), 332–339. doi: 10.1016/j.ibmb.2011.01.011
- Latorre-Estivalis, J. M., Robertson, H. M., Walden, K. K., Ruiz, J., Goncalves, L. O., Guarneri, A. A., et al. (2017). The molecular sensory machinery of a Chagas disease vector: expression changes through imaginal moult and sexually dimorphic features. *Sci. Rep.* 7:40049. doi: 10.1038/srep40049
- Lemaitre, B., Reichhart, J. M., and Hoffmann, J. A. (1997). *Drosophila* host defense: differential induction of antimicrobial peptide genes after infection by various classes of microorganisms. *Proc. Natl. Acad. Sci. U.S.A.* 94 (26), 14614–14619. doi: 10.1073/pnas.94.26.14614
- Lin, S. J. H., Fulzele, A., Cohen, L. B., Bennett, E. J., and Wasserman, S. A. (2019). Bombardier Enables Delivery of Short-Form Bomanins in the *Drosophila* Toll Response. *Front. Immunol.* 10:3040. doi: 10.3389/fimmu.2019.03040
- Lopez, L., Morales, G., Ursic, R., Wolff, M., and Lowenberger, C. (2003). Isolation and characterization of a novel insect defensin from *Rhodnius prolixus*, a vector of Chagas disease. *Insect Biochem. Mol. Biol.* 33 (4), 439–447. doi: 10.1016/S0965-1748(03)00008-0
- Louradour, I., Ghosh, K., Inbar, E., and Sacks, D. L. (2019). CRISPR/Cas9 Mutagenesis in *Phlebotomus papatasi*: the Immune Deficiency Pathway

- Impacts Vector Competence for *Leishmania major*. *mBio* 10 (4). doi: 10.1128/mBio.01941-19
- Machado, P. E., Eger-Mangrich, I., Rosa, G., Koerich, L. B., Grisard, E. C., and Steindel, M. (2001). Differential susceptibility of triatomines of the genus *Rhodnius* to *Trypanosoma rangeli* strains from different geographical origins. *Int. J. Parasitol.* 31 (5–6), 632–634. doi: 10.1016/s0020-7519(01)00150-3
- Meister, S., Kanzok, S. M., Zheng, X. L., Luna, C., Li, T. R., Hoa, N. T., et al. (2005). Immune signaling pathways regulating bacterial and malaria parasite infection of the mosquito *Anopheles gambiae*. *Proc. Natl. Acad. Sci. U.S.A.* 102 (32), 11420–11425. doi: 10.1073/pnas.0504950102
- Mello, C. B., Garcia, E. S., Ratcliffe, N. A., and Azambuja, P. (1995). *Trypanosoma cruzi* and *Trypanosoma rangeli*: interplay with hemolymph components of *Rhodnius prolixus*. *J. Invertebr. Pathol.* 65 (3), 261–268. doi: 10.1006/jipa.1995.1040
- Mesquita, R. D., Vionette-Amaral, R. J., Lowenberger, C., Rivera-Pomar, R., Monteiro, F. A., Minx, P., et al. (2015). Genome of *Rhodnius prolixus*, an insect vector of Chagas disease, reveals unique adaptations to hematophagy and parasite infection. *Proc. Natl. Acad. Sci. U.S.A.* 112 (48), 14936–14941. doi: 10.1073/pnas.1506226112
- Michel, T., Reichhart, J. M., Hoffmann, J. A., and Royet, J. (2001). *Drosophila* Toll is activated by Gram-positive bacteria through a circulating peptidoglycan recognition protein. *Nature* 414 (6865), 756–759. doi: 10.1038/414756a
- Nishide, Y., Kageyama, D., Yokoi, K., Jouraku, A., Tanaka, H., Futahashi, R., et al. (2019). Functional crosstalk across IMD and Toll pathways: insight into the evolution of incomplete immune cascades. *Proc. Biol. Sci.* 286 (1897), 20182207. doi: 10.1098/rspb.2018.2207
- Ons, S., Lavore, A., Sterkel, M., Wulff, J. P., Sierra, I., Martinez-Barnette, J., et al. (2016). Identification of G protein coupled receptors for opsins and neurohormones in *Rhodnius prolixus*. Genomic and transcriptomic analysis. *Insect Biochem. Mol. Biol.* 69, 34–50. doi: 10.1016/j.ibmb.2015.05.003
- Paim, R. M., Pereira, M. H., Araujo, R. N., Gontijo, N. F., and Guarneri, A. A. (2013). The interaction between *Trypanosoma rangeli* and the nitrophorins in the salivary glands of the triatomine *Rhodnius prolixus* (Hemiptera: Reduviidae). *Insect Biochem. Mol. Biol.* 43 (3), 229–236. doi: 10.1016/j.ibmb.2012.12.011
- Palmer, W. J., and Jiggins, F. M. (2015). Comparative Genomics Reveals the Origins and Diversity of Arthropod Immune Systems. *Mol. Biol. Evol.* 32 (8), 2111–2129. doi: 10.1093/molbev/msv093
- Pfaffl, M. W. (2001). A new mathematical model for relative quantification in real-time RT-PCR. *Nucleic Acids Res.* 29 (9), e45. doi: 10.1093/nar/29.9.e45
- Ribeiro, J. M., Genta, F. A., Sorgine, M. H., Logullo, R., Mesquita, R. D., Paiva-Silva, G. O., et al. (2014). An insight into the transcriptome of the digestive tract of the bloodsucking bug, *Rhodnius prolixus*. *PLoS Negl. Trop. Dis.* 8 (1), e2594. doi: 10.1371/journal.pntd.0002594
- Rodrigues, J., Lorenzo, M. G., Martins-Filho, O. A., Elliot, S. L., and Guarneri, A. A. (2016). Temperature and parasite life-history are important modulators of the outcome of *Trypanosoma rangeli*–*Rhodnius prolixus* interactions. *Parasitology* 143 (11), 1459–1468. doi: 10.1017/S0031182016001062
- Rutschmann, S., Kilinc, A., and Ferrandon, D. (2002). Cutting edge: the toll pathway is required for resistance to gram-positive bacterial infections in *Drosophila*. *J. Immunol.* 168 (4), 1542–1546. doi: 10.4049/jimmunol.168.4.1542
- Salcedo-Porras, N., and Lowenberger, C. (2019). The innate immune system of kissing bugs, vectors of chagas disease. *Dev. Comp. Immunol.* 98, 119–128. doi: 10.1016/j.dci.2019.04.007
- Salcedo-Porras, N., Guarneri, A., Oliveira, P. L., and Lowenberger, C. (2019). *Rhodnius prolixus*: Identification of missing components of the IMD immune signaling pathway and functional characterization of its role in eliminating bacteria. *PLoS One* 14 (4), e0214794. doi: 10.1371/journal.pone.0214794
- Schottelius, J. (1987). Neuraminidase fluorescence test for the differentiation of *Trypanosoma cruzi* and *Trypanosoma rangeli*. *Trop. Med. Parasitol.* 38 (4), 323–327.
- Shaw, D. K., Tate, A. T., Schneider, D. S., Levashina, E. A., Kagan, J. C., Pal, U., et al. (2018). Vector Immunity and Evolutionary Ecology: The Harmonious Dissonance. *Trends Immunol.* 39 (11), 862–873. doi: 10.1016/j.it.2018.09.003
- Tauszig-Delamasure, S., Bilak, H., Capovilla, M., Hoffmann, J. A., and Imler, J. L. (2002). *Drosophila* MyD88 is required for the response to fungal and Gram-positive bacterial infections. *Nat. Immunol.* 3 (1), 91–97. doi: 10.1038/ni747
- Ursic-Bedoya, R. J., and Lowenberger, C. A. (2007). *Rhodnius prolixus*: identification of immune-related genes up-regulated in response to pathogens and parasites using suppressive subtractive hybridization. *Dev. Comp. Immunol.* 31 (2), 109–120. doi: 10.1016/j.dci.2006.05.008
- Ursic-Bedoya, R. J., Nazzari, H., Cooper, D., Triana, O., Wolff, M., and Lowenberger, C. (2008). Identification and characterization of two novel lysozymes from *Rhodnius prolixus*, a vector of Chagas disease. *J. Insect Physiol.* 54 (3), 593–603. doi: 10.1016/j.jinsphys.2007.12.009
- Ursic-Bedoya, R., Buchhop, J., and Lowenberger, C. (2009). Cloning and characterization of Dorsal homologues in the hemipteran *Rhodnius prolixus*. *Insect Mol. Biol.* 18 (5), 681–689. doi: 10.1111/j.1365-2583.2009.00909.x
- Ursic-Bedoya, R., Buchhop, J., Joy, J. B., Durvasula, R., and Lowenberger, C. (2011). Prolixin: a novel antimicrobial peptide isolated from *Rhodnius prolixus* with differential activity against bacteria and *Trypanosoma cruzi*. *Insect Mol. Biol.* 20 (6), 775–786. doi: 10.1111/j.1365-2583.2011.01107.x
- Vieira, C. S., Waniek, P. J., Mattos, D. P., Castro, D. P., Mello, C. B., Ratcliffe, N. A., et al. (2014). Humoral responses in *Rhodnius prolixus*: bacterial feeding induces differential patterns of antibacterial activity and enhances mRNA levels of antimicrobial peptides in the midgut. *Parasit. Vectors* 7:232. doi: 10.1186/1756-3305-7-232
- Vieira, C. S., Mattos, D. P., Waniek, P. J., Santangelo, J. M., Figueiredo, M. B., Gumiel, M., et al. (2015). *Rhodnius prolixus* interaction with *Trypanosoma rangeli*: modulation of the immune system and microbiota population. *Parasit. Vectors* 8, 135. doi: 10.1186/s13071-015-0736-2
- Vieira, C. S., Waniek, P. J., Castro, D. P., Mattos, D. P., Moreira, O. C., and Azambuja, P. (2016). Impact of *Trypanosoma cruzi* on antimicrobial peptide gene expression and activity in the fat body and midgut of *Rhodnius prolixus*. *Parasit. Vectors* 9, 119. doi: 10.1186/s13071-016-1398-4
- Vieira, C. B., Praca, Y. R., Bentes, K., Santiago, P. B., Silva, S. M. M., Silva, G. D. S., et al. (2018). Triatomines: Trypanosomatids, Bacteria, and Viruses Potential Vectors? *Front. Cell Infect. Microbiol.* 8, 405. doi: 10.3389/fcimb.2018.00405
- Vieira, C. S., Moreira, O. C., Batista, K. K. S., Ratcliffe, N. A., Castro, D. P., and Azambuja, P. (2018). The NF-kappaB Inhibitor, IMD-0354, Affects Immune Gene Expression, Bacterial Microbiota and *Trypanosoma cruzi* Infection in *Rhodnius prolixus* Midgut. *Front. Physiol.* 9, 1189. doi: 10.3389/fphys.2018.01189
- Watkins, R. (1971). Histology of *Rhodnius prolixus* infected with *Trypanosoma rangeli*. *J. Invertebr. Pathol.* 17 (1), 59–66. doi: 10.1016/0022-2011(71)90126-1
- Whitten, M. M., Mello, C. B., Gomes, S. A., Nigam, Y., Azambuja, P., Garcia, E. S., et al. (2001). Role of superoxide and reactive nitrogen intermediates in *Rhodnius prolixus* (Reduviidae)/*Trypanosoma rangeli* interactions. *Exp. Parasitol.* 98 (1), 44–57. doi: 10.1006/expr.2001.4615
- Whitten, M., Sun, F., Tew, I., Schaub, G., Soukou, C., Nappi, A., et al. (2007). Differential modulation of *Rhodnius prolixus* nitric oxide activities following challenge with *Trypanosoma rangeli*, *T. cruzi* and bacterial cell wall components. *Insect Biochem. Mol. Biol.* 37 (5), 440–452. doi: 10.1016/j.ibmb.2007.02.001
- Zumaya-Estrada, F. A., Martinez-Barnette, J., Lavore, A., Rivera-Pomar, R., and Rodriguez, M. H. (2018). Comparative genomics analysis of triatomines reveals common first line and inducible immunity-related genes and the absence of Imd canonical components among hemimetabolous arthropods. *Parasit. Vectors* 11 (1), 48. doi: 10.1186/s13071-017-2561-2

Conflict of Interest: The authors declare that the research was conducted in the absence of any commercial or financial relationships that could be construed as a potential conflict of interest.

Copyright © 2021 Rolandelli, Nascimento, Silva, Rivera-Pomar and Guarneri. This is an open-access article distributed under the terms of the Creative Commons Attribution License (CC BY). The use, distribution or reproduction in other forums is permitted, provided the original author(s) and the copyright owner(s) are credited and that the original publication in this journal is cited, in accordance with accepted academic practice. No use, distribution or reproduction is permitted which does not comply with these terms.



Prevalence of Genetically Complex *Leishmania* Strains With Hybrid and Mito-Nuclear Discordance

Hiroto Kato^{1*}, Abraham G. Cáceres^{2,3}, Eduardo A. Gomez⁴, Ahmed Tabbabi¹, Daiki Mizushima¹, Daisuke S. Yamamoto¹ and Yoshihisa Hashiguchi⁴

¹ Division of Medical Zoology, Department of Infection and Immunity, Jichi Medical University, Tochigi, Japan, ² Sección de Entomología, Instituto de Medicina Tropical “Daniel A. Carrión” y Departamento Académico de Microbiología Médica, Facultad de Medicina Humana, Universidad Nacional Mayor de San Marcos, Lima, Peru, ³ Laboratorio de Entomología, Instituto Nacional de Salud, Lima, Peru, ⁴ Departamento de Parasitología y Medicina Tropical, Facultad de Ciencias Médicas, Universidad Católica de Santiago de Guayaquil, Guayaquil, Ecuador, ⁵ Department of Parasitology, Kochi Medical School, Kochi University, Kochi, Japan

OPEN ACCESS

Edited by:

Emilia Mia Sordillo,
Icahn School of Medicine at
Mount Sinai, United States

Reviewed by:

Isabel Mauricio,
New University of Lisbon,
Portugal
Celio Geraldo Freire-de-Lima,
Federal University of Rio de Janeiro,
Brazil

*Correspondence:

Hiroto Kato
hirok@jichi.ac.jp

Specialty section:

This article was submitted to
Parasite and Host,
a section of the journal
Frontiers in Cellular and
Infection Microbiology

Received: 02 November 2020

Accepted: 14 January 2021

Published: 24 February 2021

Citation:

Kato H, Cáceres AG, Gomez EA,
Tabbabi A, Mizushima D,
Yamamoto DS and Hashiguchi Y
(2021) Prevalence of Genetically
Complex *Leishmania* Strains With
Hybrid and Mito-Nuclear Discordance.
Front. Cell. Infect. Microbiol. 11:625001.
doi: 10.3389/fcimb.2021.625001

Approximately 20 *Leishmania* species are known to cause cutaneous, mucocutaneous, and visceral disorders in humans. Identification of the causative species in infected individuals is important for appropriate treatment and a favorable prognosis because infecting species are known to be the major determinant of clinical manifestations and may affect treatments for leishmaniasis. Although *Leishmania* species have been conventionally identified by multilocus enzyme electrophoresis, genetic analysis targeting kinetoplast and nuclear DNA (kDNA and nDNA, respectively) is now widely used for this purpose. Recently, we conducted countrywide epidemiological studies of leishmaniasis in Ecuador and Peru to reveal prevalent species using PCR-RFLP targeting nDNA, and identified unknown hybrid parasites in these countries together with species reported previously. Furthermore, comparative analyses of kDNA and nDNA revealed the distribution of parasites with mismatches between these genes, representing the first report of mito-nuclear discordance in protozoa. The prevalence of an unexpectedly high rate (~10%) of genetically complex strains including hybrid strains, in conjunction with the observation of mito-nuclear discordance, suggests that genetic exchange may occur more frequently than previously thought in natural *Leishmania* populations. Hybrid *Leishmania* strains resulting from genetic exchanges are suggested to cause more severe clinical symptoms when compared with parental strains, and to have increased transmissibility by vectors of the parental parasite species. Therefore, it is important to clarify how such genetic exchange influences disease progression and transmissibility by sand flies in nature. In addition, our aim was to identify where and how the genetic exchange resulting in the formation of hybrid and mito-nuclear discordance occurs.

Keywords: *Leishmania*, hybrid, mito-nuclear discordance, genetic exchange, Ecuador, Peru

INTRODUCTION

Human leishmaniasis is caused by approximately 20 species of the genus *Leishmania* belonging to the subgenera *Leishmania* (*Leishmania*), *Leishmania* (*Viannia*), and *Leishmania* (*Mundinia*) (Paranaíba et al., 2017; Ruiz-Postigo et al., 2020). The clinical presentation is varied, ranging from a localized cutaneous lesion to a potentially fatal visceral disorder, and the infecting parasite species is the major determinant of the outcome (Ruiz-Postigo et al., 2020). Importantly, several *L. braziliensis* complex species, such as *Leishmania* (*Viannia*) *braziliensis* and *L. (V.) guyanensis*, are associated with a risk of metastasizing destructive mucosal lesions after healing of the primary cutaneous lesion (Ruiz-Postigo et al., 2020). In addition, for cutaneous leishmaniasis, variability in disease severity and susceptibility to treatment may be associated with the infecting parasite species, although the characteristic cutaneous lesions caused by each infecting species have yet to be determined. Therefore, identification of the causative *Leishmania* species is important for appropriate treatment and a favorable prognosis.

Leishmania species have been classified by multilocus enzyme electrophoresis (MLEE) as the reference protocol (Rioux et al., 1990; Cupolillo et al., 1994). This method requires parasite isolation in culture, which is time-consuming and associated with risks of contamination with bacteria and fungi on sample collection, and interfusion of other cultures during long-term cultivation. Recently, the application of molecular biological techniques using samples directly obtained from patients' lesions has facilitated rapid and efficient identification of the parasite species. Kinetoplast DNA (kDNA) is a unique mitochondrial structure found in trypanosomatid parasites, containing 20–50 copies of maxicircle DNA and approximately 10,000 copies of minicircle DNA (Simpson, 1986). Because of the multicopy property, kDNA is widely used as a target for detection and identification of *Leishmania* species. Although minicircle DNA is more sensitive for detection, it is heterogeneous in sequence. Therefore, maxicircle genes, such as cytochrome *b* (*cyt b*), cytochrome *c* oxidase subunits, and NADH dehydrogenase subunits, are preferentially used as targets for species identification; *cyt b* gene sequence analysis is widely used and accepted as a reliable marker for this purpose (Luyo-Acero et al., 2004; Asato et al., 2009; Kato et al., 2010; Kato et al., 2011; Leelayoova et al., 2013; Kato et al., 2016a; Kato et al., 2019a). Similarly, among nuclear DNA (nDNA) targets, internal transcribed spacer (ITS) regions of ribosomal RNA and heat shock protein 70 (*hsp70*) are commonly used for species identification, due to their sensitivity for detection of interspecific sequence divergence (da Silva et al., 2010; Talmi-Frank et al., 2010; de Almeida et al., 2011; Fraga et al., 2012; Montalvo et al., 2012). Generally, genetic analysis of a single target is considered acceptable for reliable identification at the species level; however, analysis of multiple targets may increase accuracy. Furthermore, analysis of single targets may not detect strains that are the product of recombination between different species.

Recently, countrywide surveillances were performed in Ecuador and Peru using *cyt b* gene analysis, and geographic

distributions of *Leishmania* species were identified (Kato et al., 2010; Kato et al., 2016a; Kato et al., 2019a). Furthermore, comparative analyses of kDNA and nDNA revealed the prevalence of genetically complex *Leishmania* including hybrids and strains with mismatches between these genes, known as mito-nuclear discordance, at an unexpectedly high rate (~10%) in these countries (Kato et al., 2019b; Tabbabi et al., 2020). In this review, we describe the genetic complexity of *Leishmania* strains found in Ecuador and Peru that showed hybrid and mito-nuclear discordance characteristics, and discuss where and how such genetic exchange occurs, and its influence on disease severity and expansion of potential vector species.

LEISHMANIASIS IN ECUADOR AND PERÚ, AND IDENTIFICATION OF CAUSATIVE SPECIES BASED ON CYTOCHROME B GENE ANALYSIS

Ecuador is a relatively small country located on the Equator in northwestern South America. The country includes four ecological regions, each with a unique biodiversity and ecosystem: the Pacific coast subtropical areas, Andean highlands, Amazonian rainforest, and Galapagos Islands. Leishmaniasis is endemic in the first three regions (Hashiguchi et al., 2017). Up to the present, eight *Leishmania* species: *L. (V.) guyanensis*, *L. (V.) panamensis*, *L. (V.) braziliensis*, *L. (V.) naiffi*, *L. (V.) lainsoni*, *L. (L.) mexicana*, *L. (L.) amazonensis*, and *L. (L.) major*-like, have been recorded as responsible for cutaneous leishmaniasis (CL) and mucocutaneous leishmaniasis (MCL) (Kato et al., 2016a; Hashiguchi et al., 2017; Kato et al., 2019b) (Figure 1). On the Pacific coast, *L. (V.) guyanensis* is the dominant causative agent, and infections by *L. (V.) panamensis* and *L. (V.) braziliensis* also have been reported. In addition, the distribution of *L. (L.) amazonensis* has been recorded in certain areas, although infection by it has not been reported recently (Kato et al., 2016a; Hashiguchi et al., 2017). In Amazonian areas, CL and MCL caused by *L. (V.) guyanensis* and *L. (V.) braziliensis* have been widely recorded, and CL caused by *L. (V.) naiffi* and *L. (V.) lainsoni* was recently reported in several areas (Kato et al., 2013; Kato et al., 2016a; Kato et al., 2016b). In the Andean highlands, areas endemic for CL are limited to the mid-southwestern part of Ecuador, and *L. (L.) mexicana* is currently the major causative species, whereas infection by *L. (L.) major*-like was reported previously (Kato et al., 2016a; Hashiguchi et al., 2017; Hashiguchi et al., 2018) (Figure 1). In addition, a hybrid of *L. (V.) guyanensis* and *L. (V.) braziliensis* was recorded in southern parts (Bañuls et al., 1997). The observed variety in species and hybrids that cause CL in this relatively small country may reflect the extensive ecological and biological diversities, including among sand fly vectors and reservoir animals. In Ecuador, CL is the most frequently observed form of leishmaniasis, most commonly presenting as an ulcer, followed by popular, nodular, and atypical forms, including diffuse and disseminated lesions, and recidiva cutis (Hashiguchi et al., 2016; Hashiguchi et al., 2017).

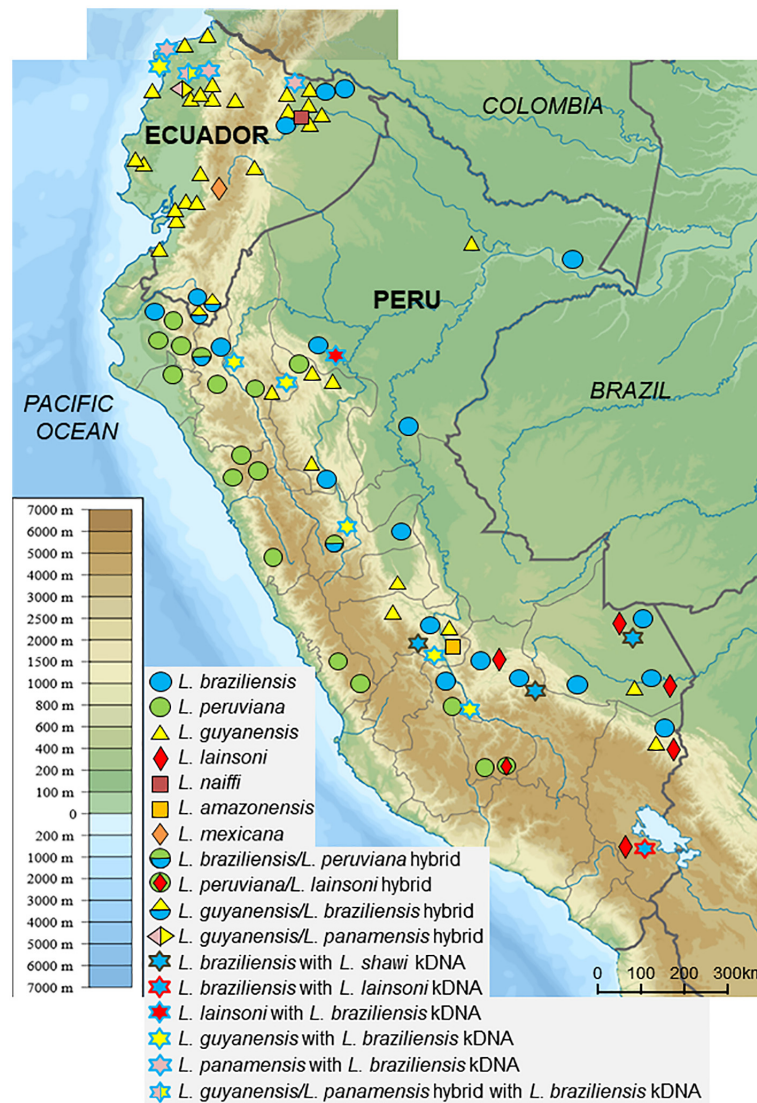


FIGURE 1 | Geographic distribution of *Leishmania* species in Ecuador and Peru. *Leishmania* species in clinical samples were identified by sequence analysis of kinetoplast DNA and PCR-RFLP and sequence analyses of nuclear DNA. (Adapted from maps available at https://commons.wikimedia.org/wiki/File:Peru_physical_map.svg and https://commons.wikimedia.org/wiki/File:Ecuador_relief_location_map.svg).

The characteristic presenting symptoms have not been defined for all infecting species, however, diffuse and disseminated forms of leishmaniasis are caused by *L. (L.) mexicana* and *L. (V.) guyanensis*, respectively (Hashiguchi et al., 2017).

Peru, a larger country located to the south of Ecuador, similarly includes Pacific coast, Andean highland, and Amazonian rainforest regions. Peru is one of the most highly endemic countries for CL, which occurs throughout the country from highlands to lowlands. In contrast, MCL is endemic to Amazonian areas (Kato et al., 2010; Kato et al., 2019a). Six *Leishmania* species and several hybrids have been recorded as responsible for leishmaniasis (Kato et al., 2010; Kato et al., 2019a; Tabbabi et al., 2020) (**Figure 1**). Of these, the main causative agents are *L. (V.) peruviana*, *L. (V.) braziliensis*, and *L. (V.)*

guyanensis, mainly circulating in the Andean highlands, tropical rainforest, and northern to central rainforest areas, respectively (Kato et al., 2010; Kato et al., 2019a) (**Figure 1**). In addition to the three dominant species, *L. (V.) lainsoni* and *L. (L.) amazonensis* have been reported to be cause disease in lower rainforest areas, and *L. (V.) shawi* was recently identified as a rare and sporadic species responsible for CL based on *cyt b* gene sequence analysis (Kato et al., 2010; Kato et al., 2019a) (**Figure 1**). Furthermore, a hybrid of *L. (V.) braziliensis* and *L. (V.) peruviana* first recorded in 1995 in a central area, was recently reported in northern Peru (Dujardin et al., 1995; Koarashi et al., 2016; Kato et al., 2019a) (**Figure 1**). Unlike Ecuador, CL is highly endemic throughout Andean areas in Peru. Additionally, the cutaneous lesions of patients in the Peruvian Andes were

commonly larger and more severe when compared with those of patients in the Ecuadorian Andes (Hashiguchi et al., 2018).

COMPARATIVE NUCLEAR AND KINETOPLAST DNA ANALYSES REVEAL GENETICALLY COMPLEX *LEISHMANIA* STRAINS WITH HYBRID AND MITO-NUCLEAR DISCORDANCE

Sequence analysis targeting kDNA and nDNA is a powerful and reliable tool for the identification of infecting *Leishmania* species; however, it requires costly reagents and equipment. Therefore, cost-effective alternatives are preferable for more practical use applicable in less-equipped laboratories/countries. Of these, PCR-restriction fragment length polymorphism (RFLP) analysis is a promising candidate. In addition, PCR-RFLP allows analysis of heterozygous multicopy regions. For this purpose, nDNA is considered to be a more suitable target than kDNA, due to the potential effect of polymorphisms in the kDNA sequences of both minicircle and maxicircle genes on restriction fragment patterns. To date, ITS regions of ribosomal RNA and the *hsp70* gene have been widely used as targets due to their sensitivity, specificity, and reliability (Garcia et al., 2004; Rotureau et al., 2006; Spanakos et al., 2008; Fraga et al., 2012; Khanra et al., 2012; Fraga et al., 2013; Mouttaki et al., 2014). In addition, PCR-RFLP analyses targeting leishmanial mannose phosphate isomerase (*mpi*) and 6-phosphogluconate dehydrogenase (*pgd*) genes, both of which have been used for multilocus sequence typing (MLST), were recently established, and their reliability for species identification was confirmed (Kato et al., 2019b).

In recent studies, PCR-RFLP analyses of nDNA were applied to 92 and 134 clinical samples from Ecuador and Peru, respectively, and the results were compared with those obtained by kDNA sequence analyses (Kato et al., 2019b; Tabbabi et al., 2020). Interestingly, results that were consistent between the two analyses were obtained only for about 90% of samples each, from Ecuador and Peru (90.2 and 87.3%, respectively). On the other hand, five Ecuadorian samples showed hybrid patterns by PCR-RFLP, and were identified as hybrid strains of *L. (V.) guyanensis/L. (V.) braziliensis* and *L. (V.) guyanensis/L. (V.) panamensis* (Kato et al., 2019b). Similarly, six Peruvian samples showing hybrid RFLP patterns were identified as hybrids of *L. (V.) braziliensis/L. (V.) peruviana* and *L. (V.) peruviana/L. (V.) lainsoni* (Tabbabi et al., 2020) (Figure 1). Furthermore, these studies unexpectedly identified strains showing incompatibility between kDNA and nDNA, known as mito-nuclear discordance, which had not been reported previously in protozoa, in five Ecuadorian (5.4%) and eleven Peruvian (8.2%) samples (Kato et al., 2019b; Tabbabi et al., 2020). These samples were identified as hybrids of *L. (V.) guyanensis/L. (V.) panamensis* with *L. (V.) braziliensis* kDNA, *L. (V.) guyanensis* with *L. (V.) braziliensis* kDNA, and *L. (V.) panamensis* with *L. (V.) braziliensis* kDNA in Ecuador, and of

L. (V.) guyanensis with *L. (V.) braziliensis* kDNA, *L. (V.) braziliensis* with *L. (V.) shawi* kDNA, *L. (V.) braziliensis* with *L. (V.) lainsoni* kDNA, and *L. (V.) lainsoni* with *L. (V.) braziliensis* kDNA, in Peru. Interestingly, strains with mito-nuclear discordance were detected from geographically separate areas, rather than from delimited areas in both countries (Figures 1 and 2). The distribution of unexpectedly high rates of hybrid or mito-nuclear discordance strains in both Ecuador and Peru indicates that the genetic structure of *Leishmania* is more complex than expected. In addition, these results suggest that interspecific genetic exchange occurs at a certain frequency in nature. It is important to note that all strains with mito-nuclear discordance are associated with *L. (V.) braziliensis*, suggesting that the species may have characteristics promoting genetic exchange with other species.

WHERE AND HOW DOES GENETIC EXCHANGE OCCUR?

Hybrids of *Leishmania* species such as *L. (V.) braziliensis/L. (V.) guyanensis*, *L. (L.) infantum/L. (L.) major*, and *L. (L.) donovani/L. (L.) aethiopica* have been reported in other countries (Delgado et al., 1997; Ravel et al., 2006; Odiwuor et al., 2011). Recently, genome-scale analyses provided evidence of meiotic-like recombination between *Leishmania* species, resulting in full-genome hybrids (Van den Broeck et al., 2020). Interestingly, this study also showed that the mitochondrial genome of hybrid strains consisted of homogeneous uniparental maxicircles, whereas minicircles originated from both parental species (Van den Broeck et al., 2020).

The mechanisms of genetic exchange in *Leishmania* resulting in the formation of hybrid and mito-nuclear discordance, and where and how they occur, are still unclear. In Peru, the natural hybridization between *L. (V.) braziliensis* and *L. (V.) peruviana* is hypothesized to be associated with a massive migration of people and animals between highland and lowland areas, due to the deterioration and recovery of the political and security situation (Kato et al., 2016c; Van den Broeck et al., 2020). A resulting increased risk for infection by multiple *Leishmania* species in humans and animals, is thought to give rise to the emergence and establishment of hybrid strains. A hybrid of *Leishmania* can be generated experimentally in sand fly vectors by co-infecting them with two different strains of the same *Leishmania* species (Akopyants et al., 2009; Sadlova et al., 2011; Calvo-Álvarez et al., 2014), and *in vitro* by co-culture of different strains of *L. (L.) tropica* promastigotes, a stage in the sand fly vector lifecycle (Louradour et al., 2020). In addition, direct evidence of sexual recombination in natural populations was provided by whole genome sequencing of *Leishmania* isolated from sand flies (Rogers et al., 2014). The midgut adhesion molecule of sand flies is believed to be a major determinant of parasite-vector specificity by supporting species-specific parasite attachment and their growth (Kamhawi et al., 2004). Therefore, interspecific hybrid formation is considered to occur within sand flies if the

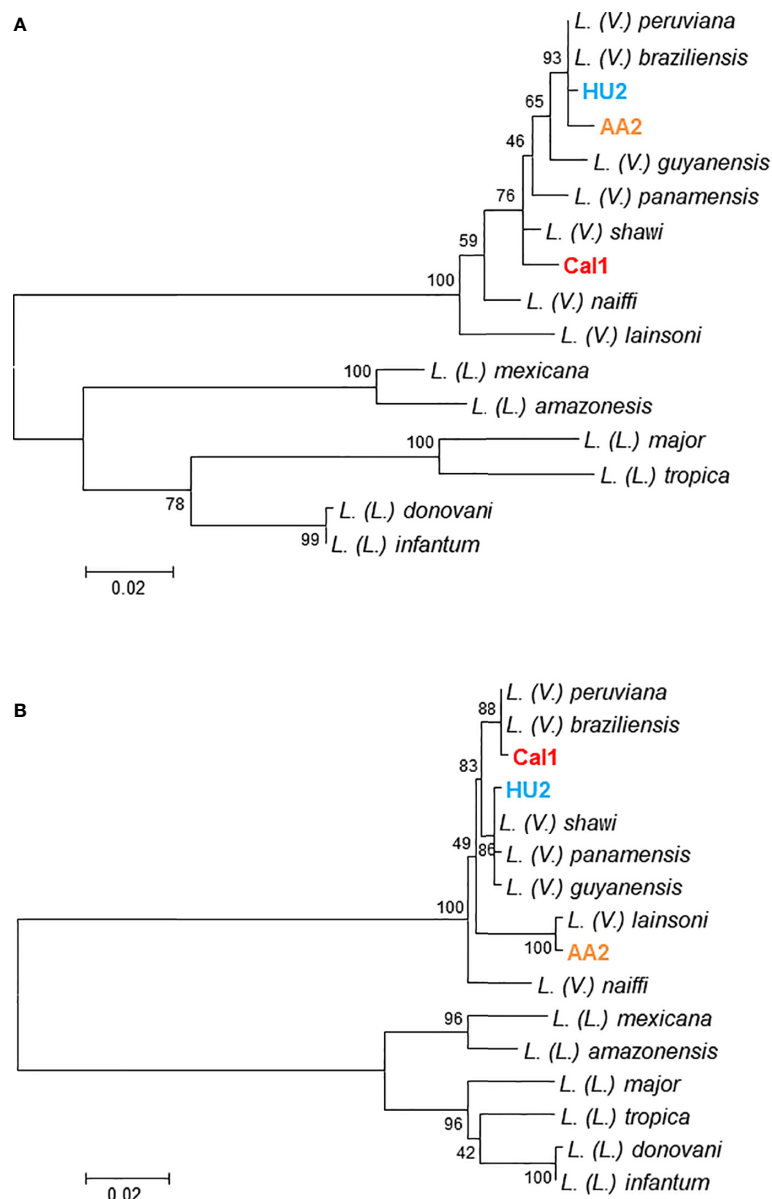


FIGURE 2 | Discordance between cytochrome *b* and mannose phosphate isomerase gene sequences in clinical samples. Leishmanial cytochrome *b* (**A**) and mannose phosphate isomerase (**B**) genes were determined from clinical samples of patients with cutaneous leishmaniasis (HU2, AA2, and Cal1), and phylogenetic analyses were performed by the maximum likelihood method together with those sequences from 13 *Leishmania* species. The scale bar represents 0.02% divergence. Bootstrap values are shown above or below branches. Parasites were identified as *Leishmania* (*Viannia*) *guyanensis* with *L. (V.) braziliensis* kDNA, *L. (V.) lainsoni* with *L. (V.) braziliensis* kDNA, and *L. (V.) shawi* with *L. (V.) braziliensis* kDNA in clinical samples, HU2, AA2, and Cal1, respectively.

two parasite species share the midgut molecule for their attachment, which may be possible between closely-related species such as *L. (V.) braziliensis* and *L. (V.) peruviana*, and *L. (V.) guyanensis* and *L. (V.) panamensis*. However, genetic exchange will not occur between more distantly-related *Leishmania* species within a sand fly, when its affinities differ for those *Leishmania* species. Therefore, the potential for genetic exchange within reservoirs with subsequent hybrid formation should be considered.

MITO-NUCLEAR DISCORDANCE

In addition to hybrid species, recent studies have reported the presence of *Leishmania* strains showing discordance between kDNA and nDNA at a relatively high rate; this represents the first report of mito-nuclear discordance in protozoan parasites (Kato et al., 2019b; Tabbabi et al., 2020). It is not known where and how such incompatibility occurs, or whether the mechanism is the same as for the hybrid formation of nDNA.

Mitochondrial and nuclear genomes co-exist in each cell; however, the rate of evolution of mitochondrial DNA (mtDNA) is more rapid than that of nDNA (Toews and Brelsford, 2012). Incompatibility between mtDNA and nDNA has been reported in various organisms including mammals, birds, reptiles, amphibians, fish, insects, and yeasts (Toews and Brelsford, 2012). It has also been reported in helminth parasites, between *Schistosoma turkestanicum* populations (Lawton et al., 2017), between *Taenia solium* lineages (Yanagida et al., 2014), and between *T. saginata* and *T. asiatica* (Yamane et al., 2012; Yamane et al., 2013; Sato et al., 2018). Mito-nuclear discordance is considered to result from various processes such as adaptive introgression of mtDNA, demographic disparities, sex-biased asymmetries, hybrid zone movement, an intracellular bacteria, *Wolbachia* infection in insects, and human actions (Toews and Brelsford, 2012). It is well known that mitochondria play essential roles in cellular energy production, cellular proliferation, and many other metabolic functions (McBride et al., 2006). Although mitochondria contain their own DNA independently, the interaction between mitochondrial and nuclear genomes is important for biological functions of the cell (McBride et al., 2006; Ali et al., 2019). Therefore, it is considered that exchange of kDNA possibly affects pathogenicity and transmission potential by sand flies of *Leishmania* protozoa, as suggested in a hybrid strain (Cortes et al., 2012). Further studies that involve isolating parasite strains with mito-nuclear discordance are expected to elucidate these issues and provide further insight into the mechanism of genetic exchange between *Leishmania* protozoa.

CONCLUDING REMARKS

This review describes the genetic exchange that results in the establishment of hybrid strains and mito-nuclear discordance in

Leishmania under natural conditions. Formation of a hybrid strain was suggested to increase the severity of disease when compared with parental species in an experimental animal model (Cortes et al., 2012). In addition, hybrid strains can increase the potential for sand fly transmission (Volf et al., 2007; Seblova et al., 2015). It is not yet well-established whether strains showing mito-nuclear discordance have increased pathogenicity or vector range. Isolation of strains with mito-nuclear discordance and further studies on the infection in animals and sand flies will be necessary to clarify these issues. Since mitochondria are organelles that are essential for cell energy supply, differentiation, and growth, (McBride et al., 2006), the genetic exchange resulting in mito-nuclear discordance could affect disease progression, as well as modify the potential for transmission by sand flies. Finally, the development of hybrids and strains with mito-nuclear discordance may have biological significance for parasite evolution and adaptation.

AUTHOR CONTRIBUTIONS

All authors listed have made a substantial, direct, and intellectual contribution to the work and approved it for publication.

FUNDING

This study was financially supported by the Ministry of Education, Culture and Sports, Science and Technology (MEXT) of Japan (Grant No. 17H01685).

REFERENCES

- Akopyants, N. S., Kimblin, N., Secundino, N., Patrick, R., Peters, N., Lawyer, P., et al. (2009). Demonstration of genetic exchange during cyclical development of *Leishmania* in the sand fly vector. *Science* 324, 265–268. doi: 10.1126/science.1169464
- Ali, A. T., Boehme, L., Carbajosa, G., Seitan, V. C., Small, K. S., and Hodgkinson, A. (2019). Nuclear genetic regulation of the human mitochondrial transcriptome. *eLife* 8, e41927. doi: 10.7554/eLife.41927
- Asato, Y., Oshiro, M., Myint, C. K., Yamamoto, Y., Kato, H., Marco, J. D., et al. (2009). Phylogenetic analysis of the genus *Leishmania* by cytochrome *b* gene sequencing. *Exp. Parasitol.* 121, 352–361. doi: 10.1016/j.exppara.2008.12.013
- Bañuls, A. L., Guerrini, F., Le Pont, F., Barrera, C., Espinel, I., Guderian, R., et al. (1997). Evidence for hybridization by multilocus enzyme electrophoresis and random amplified polymorphic DNA between *Leishmania braziliensis* and *Leishmania panamensis/guyanensis* in Ecuador. *J. Eukaryot. Microbiol.* 44, 408–411. doi: 10.1111/j.1550-7408.1997.tb05716.x
- Calvo-Álvarez, E., Álvarez-Velilla, R., Jiménez, M., Molina, R., Pérez-Pertejo, Y., Balaña-Fouce, R., et al. (2014). First evidence of intraclonal genetic exchange in trypanosomatids using two *Leishmania infantum* fluorescent transgenic clones. *PLoS Negl. Trop. Dis.* 8, e3075. doi: 10.1371/journal.pntd.0003075
- Cortes, S., Esteves, C., Maurício, I., Maia, C., Cristovão, J. M., Miles, M., et al. (2012). *In vitro* and *in vivo* behavior of sympatric *Leishmania* (V.) *braziliensis*, *L.* (V.) *peruviana* and their hybrids. *Parasitology* 139, 191–199. doi: 10.1017/S0031182011001909
- Cupolillo, E., Grimaldi, G., and Momen, H. (1994). A general classification of New World *Leishmania* using numerical zymotaxonomy. *Am. J. Trop. Med. Hyg.* 50, 296–311. doi: 10.4269/ajtmh.1994.50.296
- da Silva, L. A., de Sousa, C., dos, S., da Grac, G. C., Porrozzio, R., and Cupolillo, E. (2010). Sequence analysis and PCR RFLP profiling of the *hsp70* gene as a valuable tool for identifying *Leishmania* species associated with human leishmaniasis in Brazil. *Infect. Genet. Evol.* 10, 77–83. doi: 10.1016/j.meegid.2009.11.001
- de Almeida, M. E., Steurer, F. J., Koru, O., Herwaldt, B. L., Pieniazek, N. J., and da Silva, A. J. (2011). Identification of *Leishmania* spp. by molecular amplification and DNA sequencing analysis of a fragment of rRNA internal transcribed spacer 2. *J. Clin. Microbiol.* 49, 3143–3149. doi: 10.1128/JCM.01177-11
- Delgado, O., Cupolillo, E., Bonfante-Garrido, R., Silva, S., Belfort, E., Júnior, G. G., et al. (1997). Cutaneous leishmaniasis in Venezuela caused by infection with a new hybrid between *Leishmania* (*Viannia*) *braziliensis* and *L.* (V.) *guyanensis*. *Mem. Inst. Oswaldo Cruz* 92, 581–582. doi: 10.1590/s0074-02761997000500002
- Dujardin, J. C., Bañuls, A. L., Llanos-Cuentas, A., Alvarez, E., DeDoncker, S., Jacquet, D., et al. (1995). Putative *Leishmania* hybrids in the Eastern Andean valley of Huanuco, Peru. *Acta Trop.* 59, 293–307. doi: 10.1016/0001-706x(95)00094-u

- Fraga, J., Veland, N., Montalvo, A. M., Praet, N., Boggild, A. K., Valencia, B. M., et al. (2012). Accurate and rapid species typing from cutaneous and mucocutaneous leishmaniasis lesions of the New World. *Diagn. Microbiol. Infect. Dis.* 74, 142–150. doi: 10.1016/j.diagmicrobio.2012.06.010
- Fraga, J., Montalvo, A. M., Maes, L., Dujardin, J. C., and Van der Auwera, G. (2013). *HindII* and *SduI* digests of heat-shock protein 70 PCR for *Leishmania* typing. *Diagn. Microbiol. Infect. Dis.* 77, 245–247. doi: 10.1016/j.diagmicrobio.2013.07.023
- Garcia, L., Kindt, A., Bermudez, H., Llanos-Cuentas, A., De Doncker, S., Arevalo, J., et al. (2004). Culture-independent species typing of neotropical *Leishmania* for clinical validation of a PCR-based assay targeting heat shock protein 70 genes. *J. Clin. Microbiol.* 42, 2294–2297. doi: 10.1128/jcm.42.5.2294-2297.2004
- Hashiguchi, Y., Gomez, E. L., Kato, H., Martini, L. R., Velez, L. N., and Uezato, H. (2016). Diffuse and disseminated cutaneous leishmaniasis: clinical cases experienced in Ecuador and a brief review. *Trop. Med. Health* 44, 2. doi: 10.1186/s41182-016-0002-0
- Hashiguchi, Y., Velez, L. N., Villegas, N. V., Mimori, T., Gomez, E. A. L., and Kato, H. (2017). Leishmaniasis in Ecuador: Comprehensive review and current status. *Acta Trop.* 166, 299–315. doi: 10.1186/s41182-016-0002-0
- Hashiguchi, Y., Gomez, E. A. L., Cáceres, A. G., Velez, L. N., Villegas, N. V., Hashiguchi, K., et al. (2018). Andean cutaneous leishmaniasis (Andean-CL, uta) in Peru and Ecuador: the causative *Leishmania* parasites and clinico-epidemiological features. *Acta Trop.* 177, 135–145. doi: 10.1016/j.actatropica.2017.09.028
- Kamhawi, S., Ramalho-Ortigao, M., Pham, V. M., Kumar, S., Lawyer, P. G., Turco, S. J., et al. (2004). A role for insect galectins in parasite survival. *Cell* 119, 329–341. doi: 10.1016/j.cell.2004.10.009
- Kato, H., Cáceres, A. G., Mimori, T., Ishimaru, Y., Sayed, A. S., Fujita, M., et al. (2010). Use of FTA cards for direct sampling of patient's lesions in the ecological study of cutaneous leishmaniasis. *J. Clin. Microbiol.* 48, 3661–3665. doi: 10.1128/JCM.00498-10
- Kato, H., Watanabe, J., Mendoza Nieto, I., Korenaga, M., and Hashiguchi, Y. (2011). *Leishmania* species identification using FTA card sampling directly from patients' cutaneous lesions in the state of Lara, Venezuela. *Trans. R. Soc. Trop. Med. Hyg.* 105, 561–567. doi: 10.1016/j.trstmh.2011.05.009
- Kato, H., Calvopiña, M., Criollo, H., and Hashiguchi, Y. (2013). First human cases of *Leishmania (Viannia) naiffi* infection in Ecuador and identification of its suspected vector species. *Acta Trop.* 128, 710–713. doi: 10.1016/j.actatropica.2013.09.001
- Kato, H., Gomez, E. A., Martini-Robles, L., Muzzio, J., Velez, L., Calvopiña, M., et al. (2016a). Geographic distribution of *Leishmania* species in Ecuador based on the cytochrome *b* gene sequence analysis. *PLoS Negl. Trop. Dis.* 10, e0004844. doi: 10.1371/journal.pntd.0004844
- Kato, H., Bone, A. E., Mimori, T., Hashiguchi, K., Shiguango, G. F., Gonzales, S. V., et al. (2016b). First human cases of *Leishmania (Viannia) lainsoni* infection and a search for the vector sand flies in Ecuador. *PLoS Negl. Trop. Dis.* 10, e0004728. doi: 10.1371/journal.pntd.0004728
- Kato, H., Cáceres, A. G., and Hashiguchi, Y. (2016c). First evidence of a hybrid of *Leishmania (Viannia) braziliensis*/L. (V.) *peruviana* DNA detected from the *Phlebotomine* sand fly *Lutzomyia tejadai* in Peru. *PLoS Negl. Trop. Dis.* 10, e0004336. doi: 10.1371/journal.pntd.0004336
- Kato, H., Cáceres, A. G., Seki, C., Silupu Garcia, C. R., Holguin Mauricci, C., Castro Martinez, S. C., et al. (2019a). Further insight into the geographic distribution of *Leishmania* species in Peru by cytochrome *b* and mannose phosphate isomerase gene analyses. *PLoS Negl. Trop. Dis.* 13, e0007496. doi: 10.1371/journal.pntd.0007496
- Kato, H., Gomez, E. A., Seki, C., Furumoto, H., Martini-Robles, L., Muzzio, J., et al. (2019b). PCR-RFLP analyses of *Leishmania* species causing cutaneous and mucocutaneous leishmaniasis revealed distribution of genetically complex strains with hybrid and mito-nuclear discordance in Ecuador. *PLoS Negl. Trop. Dis.* 13, e0007403. doi: 10.1371/journal.pntd.0007403
- Khanra, S., Datta, S., Mondal, D., Saha, P., Bandopadhyay, S. K., Roy, S., et al. (2012). RFLPs of ITS, ITS1 and hsp70 amplicons and sequencing of ITS1 of recent clinical isolates of Kala-azar from India and Bangladesh confirms the association of *L. tropica* with the disease. *Acta Trop.* 124, 229–234. doi: 10.1016/j.actatropica.2012.08.017
- Koarashi, Y., Cáceres, A. G., Zuniga, S. M. F., Palacios, F. E. E., Celis, T. A., Abanto, A. J. L., et al. (2016). Identification of causative *Leishmania* species in Giemsa-stained smears prepared from patients with cutaneous leishmaniasis in Peru using PCR-RFLP. *Acta Trop.* 158, 83–87. doi: 10.1016/j.actatropica.2016.02.024
- Lawton, S. P., Bowen, L. I., Emery, A. M., and Majoros, G. (2017). Signatures of mito-nuclear discordance in *Schistosoma turkestanicum* indicate a complex evolutionary history of emergence in Europe. *Parasitol* 144, 1752–1762. doi: 10.1017/S0031182017000920
- Leelayoova, S., Siripattanapong, S., Hitakarun, A., Kato, H., Tan-ariya, P., Siriwasatien, P., et al. (2013). Multilocus characterization and phylogenetic analysis of *Leishmania siamensis* isolated from autochthonous visceral leishmaniasis cases, southern Thailand. *BMC Microbiol.* 13:60. doi: 10.1186/1471-2180-13-60
- Louradour, I., Ferreira, T. R., Ghosh, K., Shaik, J., and Sacks, D. (2020). *In vitro* generation of *Leishmania* hybrids. *Cell Rep.* 31, 107507. doi: 10.1016/j.celrep.2020.03.071
- Luyo-Acero, G. E., Uezato, H., Oshiro, M., Takei, K., Kariya, K., Katakura, K., et al. (2004). Sequence variation of the cytochrome *b* gene of various human infecting members of the genus *Leishmania* and their phylogeny. *Parasitol* 128, 483–491. doi: 10.1017/s0031182004004792
- McBride, H. M., Neuspiel, M., and Wasiak, S. (2006). Mitochondria: more than just a powerhouse. *Curr. Biol.* 16, R551–R560. doi: 10.1016/j.cub.2006.06.054
- Montalvo, A. M., Fraga, J., Maes, I., Dujardin, J. C., and Van der Auwera, G. (2012). Three new sensitive and specific heat shock protein 70 PCRs for global *Leishmania* species identification. *Eur. J. Clin. Microbiol. Infect. Dis.* 31, 1453–1461. doi: 10.1007/s10096-011-1463-z
- Mouttaki, T., Morales-Yuste, M., Merino-Espinosa, G., Chiheb, S., Fellah, H., Martin-Sanchez, J., et al. (2014). Molecular diagnosis of cutaneous leishmaniasis and identification of the causative *Leishmania* species in Morocco by using three PCR-based assays. *Parasitol. Vectors* 7:420. doi: 10.1186/1756-3305-7-420
- Odiwuor, S., De Doncker, S., Maes, I., Dujardin, J. C., and Van der Auwera, G. (2011). Natural *Leishmania donovani/Leishmania aethiopica* hybrids identified from Ethiopia. *Infect. Genet. Evol.* 11, 2113–2118. doi: 10.1016/j.meegid.2011.04.026
- Paranaíba, L. F., Pinheiro, L. J., Torrecilhas, A. C., Macedo, D. H., Menezes-Neto, A., Tafuri, W. L., et al. (2017). *Leishmania enriettii* (Muniz & Medin): A highly diverse parasite is here to stay. *PLoS Pathog.* 13, e1006303. doi: 10.1371/journal.ppat.1006303
- Ravel, C., Cortes, S., Pratlong, F., Morio, F., Dedet, J. P., and Campino, L. (2006). First report of genetic hybrids between two very divergent *Leishmania* species: *Leishmania infantum* and *Leishmania major*. *Int. J. Parasitol.* 36, 1383–1388. doi: 10.1016/j.ijpara.2006.06.019
- Rioux, J. A., Lanotte, G., Serres, E., Pratlong, F., Bastien, P., and Perieres, J. (1990). Taxonomy of *Leishmania*. Use of isoenzymes. Suggestions for a new classification. *Ann. Parasitol. Hum. Comp.* 65, 111–125. doi: 10.1051/parasite/1990653111
- Rogers, M. B., Downing, T., Smith, B. A., Imamura, H., Sanders, M., Svobodova, M., et al. (2014). Genomic confirmation of hybridisation and recent inbreeding in a vector-isolated *Leishmania* population. *PLoS Genet.* 10, e1004092. doi: 10.1371/journal.pgen.1004092
- Rotureau, B., Ravel, C., Couppie, P., Pratlong, F., Nacher, M., Dedet, J. P., et al. (2006). Use of PCR-restriction fragment length polymorphism analysis to identify the main new world *Leishmania* species and analyze their taxonomic properties and polymorphism by application of the assay to clinical samples. *J. Clin. Microbiol.* 44, 459–467. doi: 10.1128/JCM.44.2.459-467.2006
- Ruiz-Postigo, J. A., Grouta, L., and Jaina, S. (2020). Global leishmaniasis surveillance 2017–2018, and first report on 5 additional indicators. *World Health Organ. Wkly. Epidemiol. Rec.* 25, 265–280.
- Sadlova, J., Yeo, M., Seblova, V., Lewis, M. D., Mauricio, I., Volf, P., et al. (2011). Visualisation of *Leishmania donovani* fluorescent hybrids during early stage development in the sand fly vector. *PLoS One* 6, e19851. doi: 10.1371/journal.pone.0019851
- Sato, M. O., Sato, M., Yanagida, T., Waikagul, J., Pongvongsa, T., Sako, Y., et al. (2018). *Taenia solium*, *Taenia saginata*, *Taenia asiatica*, their hybrids and other helminthic infections occurring in a neglected tropical diseases' highly endemic area in Lao PDR. *PLoS Negl. Trop. Dis.* 12, e0006260. doi: 10.1371/journal.pntd.0006260
- Seblova, V., Myskova, J., Hlavacova, J., Votpyka, J., Antoniou, M., and Volf, P. (2015). Natural hybrid of *Leishmania infantum/L. donovani*: development in

- Phlebotomus tobbi*, *P. perniciosus* and *Lutzomyia longipalpis* and comparison with non-hybrid strains differing in tissue tropism. *Parasitol. Vectors* 8, 605. doi: 10.1186/s13071-015-1217-3
- Simpson, L. (1986). Kinetoplast DNA in trypanosomid flagellates. *Int. Rev. Cytol.* 99, 119–179. doi: 10.1016/s0074-7696(08)61426-6
- Spanakos, G., Piperaki, E. T., Menounos, P. G., Tegos, N., Flemetakis, A., and Vakalis, N. C. (2008). Detection and species identification of Old World *Leishmania* in clinical samples using a PCR-based method. *Trans. R. Soc. Trop. Med. Hyg.* 102, 46–53. doi: 10.1016/j.trstmh.2007.05.019
- Tabbabi, A., Cáceres, A. G., Bustamante Chauca, T. P., Seki, C., Choochartpong, Y., Mizushima, D., et al. (2020). Nuclear and kinetoplast DNA analyses reveal genetically complex *Leishmania* strains with hybrid and mito-nuclear discordance in Peru. *PLoS Negl. Trop. Dis.* 14, e0008797. doi: 10.1371/journal.pntd.0008797
- Talmi-Frank, D., Nasereddin, A., Schnur, L. F., Schonian, G., Toz, S. O., Jaffe, C. L., et al. (2010). Detection and identification of Old World *Leishmania* by high resolution melt analysis. *PLoS Negl. Trop. Dis.* 4, e581. doi: 10.1371/journal.pntd.0000581
- Toews, D. P., and Brelsford, A. (2012). The biogeography of mitochondrial and nuclear discordance in animals. *Mol. Ecol.* 21, 3907–3930. doi: 10.1111/j.1365-294X.2012.05664.x
- Van den Broeck, F., Savill, N. J., Imamura, H., Sanders, M., Maes, I., Cooper, S., et al. (2020). Ecological divergence and hybridization of Neotropical *Leishmania* parasites. *Proc. Natl. Acad. Sci. U. S. A.* 117, 25159–25168. doi: 10.1073/pnas.1920136117
- Volf, P., Benkova, I., Myskova, J., Sadlova, J., Campino, L., and Ravel, C. (2007). Increased transmission potential of *Leishmania major/Leishmania infantum* hybrids. *Int. J. Parasitol.* 37, 589–593. doi: 10.1016/j.ijpara.2007.02.002
- Yamane, K., Suzuki, Y., Tachi, E., Li, T., Chen, X., Nakao, M., et al. (2012). Recent hybridization between *Taenia asiatica* and *Taenia saginata*. *Parasitol. Int.* 61, 351–355. doi: 10.1016/j.parint.2012.01.005
- Yamane, K., Yanagida, T., Li, T., Chen, X., Dekumyoy, P., Waikagul, J., et al. (2013). Genotypic relationships between *Taenia saginata*, *Taenia asiatica* and their hybrids. *Parasitology* 140, 1595–1601. doi: 10.1017/S0031182013001273
- Yanagida, T., Carod, J. F., Sako, Y., Nakao, M., Hoberg, E. P., and Ito, A. (2014). Genetics of the pig tapeworm in Madagascar reveal a history of human dispersal and colonization. *PLoS One* 9, e109002. doi: 10.1371/journal.pone.0109002

Conflict of Interest: The authors declare that the research was conducted in the absence of any commercial or financial relationships that could be construed as a potential conflict of interest.

Copyright © 2021 Kato, Cáceres, Gomez, Tabbabi, Mizushima, Yamamoto and Hashiguchi. This is an open-access article distributed under the terms of the Creative Commons Attribution License (CC BY). The use, distribution or reproduction in other forums is permitted, provided the original author(s) and the copyright owner(s) are credited and that the original publication in this journal is cited, in accordance with accepted academic practice. No use, distribution or reproduction is permitted which does not comply with these terms.



Repeat-Driven Generation of Antigenic Diversity in a Major Human Pathogen, *Trypanosoma cruzi*

Carlos Talavera-López^{1,2*}, Louisa A. Messenger³, Michael D. Lewis³, Matthew Yeo³, João Luís Reis-Cunha⁴, Gabriel Machado Matos⁵, Daniella C. Bartholomeu⁴, José E. Calzada⁶, Azael Saldaña⁶, Juan David Ramírez⁷, Felipe Guhl⁸, Sofía Ocaña-Mayorga⁹, Jaime A. Costales⁹, Rodion Gorchakov¹⁰, Kathryn Jones¹⁰, Melissa S. Nolan¹⁰, Santuza M. R. Teixeira¹¹, Hernán José Carrasco¹², Maria Elena Bottazzi¹⁰, Peter J. Hotez¹⁰, Kristy O. Murray¹⁰, Mario J. Grijalva^{9,13}, Barbara Burleigh¹⁴, Edmundo C. Grisard¹⁵, Michael A. Miles³ and Björn Andersson^{1*}

OPEN ACCESS

Edited by:

Julius Lukes,
Academy of Sciences of the Czech
Republic (ASCR), Czechia

Reviewed by:

Carlos A. Buscaglia,
Consejo Nacional de Investigaciones
Científicas y Técnicas (CONICET),
Argentina
Anzhelika Butenko,
Academy of Sciences of the Czech
Republic (ASCR), Czechia

*Correspondence:

Björn Andersson
bjorn.andersson@ki.se
Carlos Talavera-López
ct5@sanger.ac.uk

Specialty section:

This article was submitted to
Parasite and Host,
a section of the journal
Frontiers in Cellular
and Infection Microbiology

Received: 06 October 2020

Accepted: 22 January 2021

Published: 03 March 2021

Citation:

Talavera-López C, Messenger LA, Lewis MD, Yeo M, Reis-Cunha JL, Matos GM, Bartholomeu DC, Calzada JE, Saldaña A, Ramírez JD, Guhl F, Ocaña-Mayorga S, Costales JA, Gorchakov R, Jones K, Nolan MS, Teixeira SMR, Carrasco HJ, Bottazzi ME, Hotez PJ, Murray KO, Grijalva MJ, Burleigh B, Grisard EC, Miles MA and Andersson B (2021) Repeat-Driven Generation of Antigenic Diversity in a Major Human Pathogen, *Trypanosoma cruzi*. *Front. Cell. Infect. Microbiol.* 11:614665. doi: 10.3389/fcimb.2021.614665

¹ Department of Cell and Molecular Biology, Karolinska Institutet, Stockholm, Sweden, ² European Bioinformatics Institute, Wellcome Sanger Institute, Hinxton, United Kingdom, ³ Faculty of Infectious and Tropical Diseases, London School of Hygiene and Tropical Medicine, London, United Kingdom, ⁴ Departamento de Parasitologia, Universidade Federal de Minas Gerais, Belo Horizonte, Brazil, ⁵ Departamento de Biologia Celular, Embriologia e Genética, Universidade Federal Santa Catarina, Florianópolis, Brazil, ⁶ Departamento de Parasitología, Instituto Conmemorativo Gorgas de Estudios de la Salud, Ciudad de Panamá, Panamá, ⁷ Grupo de Investigaciones Microbiológicas-UR (GIMUR), Departamento de Biología, Facultad de Ciencias Naturales, Universidad del Rosario, Bogotá, Colombia, ⁸ Grupo de Investigaciones en Microbiología y Parasitología Tropical (CIMPAT), Tropical Parasitology Research Center, Universidad de Los Andes, Bogotá, Colombia, ⁹ Centro de Investigación para la Salud en América Latina (CISAL), Escuela de Ciencias Biológicas, Pontificia Universidad Católica del Ecuador, Quito, Ecuador, ¹⁰ Sabin Vaccine Institute and Texas Children's Hospital Center for Vaccine Development, National School of Tropical Medicine, Department of Pediatrics - Tropical Medicine, Baylor College of Medicine, Houston, TX, United States, ¹¹ Departamento de Bioquímica e Imunologia, Universidade Federal de Minas Gerais, Belo Horizonte, Brazil, ¹² Laboratorio de Biología Molecular de Protozoarios, Instituto de Medicina Tropical, Facultad de Medicina, Universidad Central de Venezuela, Caracas, Venezuela, ¹³ Department of Biomedical Sciences, Heritage College of Osteopathic Medicine, Infectious and Tropical Disease Institute, Ohio University, Athens, OH, United States, ¹⁴ Department of Immunology and Infectious Diseases, T.H. Chan School of Public Health, Harvard University, Boston, MA, United States, ¹⁵ Departamento de Microbiologia, Imunologia e Parasitologia, Universidade Federal Santa Catarina, Florianópolis, Brazil

Trypanosoma cruzi, a zoonotic kinetoplastid protozoan parasite, is the causative agent of American trypanosomiasis (Chagas disease). Having a very plastic, repetitive and complex genome, the parasite displays a highly diverse repertoire of surface molecules, with pivotal roles in cell invasion, immune evasion and pathogenesis. Before 2016, the complexity of the genomic regions containing these genes impaired the assembly of a genome at chromosomal level, making it impossible to study the structure and function of the several thousand repetitive genes encoding the surface molecules of the parasite. We here describe the genome assembly of the Sylvio X10/1 genome sequence, which since 2016 has been used as a reference genome sequence for *T. cruzi* clade I (Tcl), produced using high coverage PacBio single-molecule sequencing. It was used to analyze deep Illumina sequence data from 34 *T. cruzi* Tcl isolates and clones from different geographic locations, sample sources and clinical outcomes. Resolution of the surface molecule gene distribution showed the unusual duality in the organization of the parasite genome, a synteny of the core genomic region with related protozoa flanked by unique and highly plastic multigene family clusters encoding surface antigens. The presence of abundant interspersed retrotransposons in these multigene family clusters suggests that these

elements are involved in a recombination mechanism for the generation of antigenic variation and evasion of the host immune response on these TcI strains. The comparative genomic analysis of the cohort of TcI strains revealed multiple cases of such recombination events involving surface molecule genes and has provided new insights into *T. cruzi* population structure.

Keywords: *Trypanosoma cruzi*, genome sequence, antigenic variation, population genetics, parasitology, microbial genomics, tropical medicine, pathology of infectious diseases

INTRODUCTION

Trypanosoma cruzi is a kinetoplastid protozoan and the etiologic agent of Chagas disease, considered one of the most important human parasitic disease in Latin America. The Global Burden of Disease Study 2013 reported that almost 7 million people live with Chagas disease in the Western Hemisphere (GBD 2013 Mortality and Causes of Death Collaborators, 2015), with the expectation that up to one third will progress to develop chronic chagasic cardiomyopathy (CCC) or other life-threatening symptoms. In 2015, 5,742,167 people were estimated to be infected with *T. cruzi* in 21 Latin American countries and around 13% of the Latin American population is at risk of contracting *T. cruzi* infection due to domicile infestation of triatomine bugs or due to non-vectorial transmission *via* blood transfusion, organ transplant, oral, congenital or accidental infection (“WHO | 6 February 2015, Vol. 90, 6 (pp. 33–44)” 2015). Human Chagas disease is not restricted to Latin America. The migration of infected humans to non-endemic areas has made it a new public health threat in other geographic areas such as North America, Europe and Asia (Bern, 2015). Also, sylvatic *T. cruzi* transmission cycles, often associated with human disease, have been described in areas formerly considered as free from this disease such as in Texas (USA) (Bern, 2015).

The acute phase of the disease frequently lacks specific symptoms, is often undiagnosed and usually resolves in a few weeks in immunocompetent individuals but may be fatal in around 5% of diagnosed cases. Without successful treatment, a *T. cruzi* infection is normally carried for life. The disease progresses to either a chronic indeterminate phase that is asymptomatic, or to a chronic symptomatic phase with severe clinical syndromes such as cardiomyopathy, megaesophagus and/or megacolon (Rassi et al., 2010); meningoencephalitis may occur, especially in immunocompromised patients (Bern, 2015). The current prolonged chemotherapy (benznidazole or nifurtimox) is mostly effective only in the acute phase, particularly because severe side effects may interrupt treatment of adults in the chronic phase. There is currently no effective treatment for advanced chagasic cardiomyopathy (Morillo et al., 2015), and there is an urgent need to identify new potential drug and vaccine targets (Pecoul et al., 2016).

T. cruzi infection is a zoonosis, and the parasite has a complex life cycle; where transmission to humans occurs most frequently by contamination with infected feces from triatomine insect vectors (Subfamily Triatominae). The parasite evades the

immune responses with the aid of multiple surface molecules from three large diverse gene families (Trans-Sialidases, Mucins and Mucin-Associated Surface Proteins - MASPs), which are also involved in cell invasion and possibly pathogenicity (Schenkman et al., 1994; Frasc, 2000; Yoshida and Cortez, 2008; Osorio et al., 2012).

Six distinct genetic clades of *T. cruzi* have been recognized, named TcI to TcVI (Discrete Typing Units or DTU-I to VI). The first genome sequence for *T. cruzi* was produced using Sanger sequencing technology from a hybrid, highly polymorphic, TcVI strain. The resultant genome sequence, while extremely useful for the core regions of the genome, was highly fragmented, especially in repetitive regions (El-Sayed et al., 2005). This sequence has been improved using enhanced scaffolding algorithms, but many repetitive regions remain unresolved (Weatherly et al., 2009). Subsequently, FLX 454 Titanium and Illumina sequencing were used to sequence a less polymorphic TcI strain (Sylvio X10/1), which allowed the first comparative genomic studies of *T. cruzi*, but correct assembly of repetitive regions was still impossible (Franzén et al., 2011; Franzén et al., 2012). The thousands of related genes that code for the surface proteins are generally located in large multigene family clusters of the *T. cruzi* genome (Kim et al., 2005), in the form of extremely repetitive segments with multiple gene copies and pseudogenes. These multigene family clusters are distinct from the core regions of the genome, defined as regions that share gene content and synteny with the genomes of other trypanosomatids (Llewellyn et al., 2009). The repetitive nature of the tandem arrays, and the length of the repeats, made correct assembly impossible using short and medium-sized sequence reads. The available *T. cruzi* genome sequences were therefore incomplete and inaccurate in these important regions, making it impossible to study the complex surface gene families in contrast to conserved core genomic regions (Berná et al., 2018).

We made a near-complete reconstruction of the majority (~98.5% of the estimated genome size) of the *T. cruzi* TcI Sylvio X10/1 genome available in Genbank and TriTrypDB in 2016, and it was described in a preprint made available in June 2018 (Talavera-López et al., 2018). This sequence has served as a main genome sequence for *T. cruzi* clade 1, since it was made public. We were able to decipher the majority of the organization of *T. cruzi* surface protein coding gene repertoire from the TcI Sylvio X10/1 strain, revealing large numbers of evenly spaced retrotransposons, which may play a role in generating genomic structural diversity and antigenic variation. This study has been followed by several others using similar approaches and parasite

strains (Callejas-Hernández et al., 2018; Reis-Cunha et al., 2018; Schwabl et al., 2019).

The population structure of *T. cruzi* is complex, and there is a high degree of genetic and phenotypic variation. The current TcI to TcVI clades are based on biochemical and molecular markers (Zingales et al., 2012), although there is substantial diversity even within these six groups (Llewellyn et al., 2009). The TcI clade is widespread and can be found across the American continent, and has been associated with CCC (Ramírez et al., 2010) and sudden death (Bern et al., 2011; Montgomery et al., 2014), among other clinical manifestations. In conjunction with the Sylvio X10/1 genome sequence, we generated Illumina whole-genome sequencing data for 34 *T. cruzi* TcI isolates and clones from different geographic locations for comparative analyses. These data was used to carry out population genetics studies, where strains from different environments and geographic locations were compared. We found patterns of active recombination possibly associated with the generation of new surface molecule variants. These studies contributed to answering longstanding questions on the biology of Chagas disease and host-parasite interaction in general. The availability of the close to complete repertoire of genes encoding surface molecules allows further research on virulence and pathogenesis, as well as the identification of drug targets and vaccine candidates, focused on shared and conserved motifs present within these variable families.

MATERIALS AND METHODS

Genome Sequencing and Assembly

The *Trypanosoma cruzi* Sylvio X10/1 strain was isolated from an acute human case of Chagas disease in Brazil. Total genomic DNA of this TcI strain was obtained from culture epimastigotes as formerly described¹¹ and used to produce PacBio CCS data according to standard protocols from the Genomic Facility of Science for Life Laboratory (Sweden) and Pacific Biosciences (USA). Genomic DNA was sequenced to a depth of 210X using the PacBio platform, supplying raw reads with an average length of 5.8 Kb. These reads were corrected by means of the PBcR v8.3 pipeline with the MHAP algorithm (Berlin et al., 2015) using the auto-correction parameters described to merge haplotypes and skipping the assembly step, producing a total of 1,216 contigs (NG50 = 62 Kb). Illumina sequences at an average coverage of approximately 120X, with a mean read length of 101 bp were added. The reads were trimmed from adaptors and filtered using the Nsoni utility (<https://github.com/Victorian-Bioinformatics-Consortium/nesoni>), which is now part of Tail Tools (<https://github.com/Monash-RNA-Systems-Biology-Laboratory/tail-tools>) in order to remove bases with a quality score < 20 and length < 75.

Later, the assembly was scaffolded using the corrected PacBio reads with the SSPACE-Long scaffolder yielding 310 scaffolds (NG50 = 788 Kb); 118 gaps were filled using Illumina reads with GapFiller and corrected PacBio reads with PBJelly2. Finally, the core regions of these scaffolds were aligned against the core

regions of the TcVI CL Brener reference genome using ABACAS (<http://abacas.sourceforge.net>), producing 47 scaffolds, henceforth designated as chromosomes. The quality of the new assembly was assessed with FRCbam with the Illumina paired end reads generated at the Genomic Facility of Science for Life Laboratory (Sweden) using the same genomic DNA extraction used for PacBio sequencing. The final genome size was 41382871 bp in 47 scaffolds. The number of gaps was 1005, and they are indicated by rows of Ns in the sequence.

Annotation of the *Trypanosoma cruzi* Sylvio X10/1 Genome

The genome sequence was annotated using a new kinetoplastid genome annotation pipeline combining homology-based gene model transfer with *de novo* gene prediction. To allow for the sensitive identification of partial genes, input sequences were split at stretches of undefined bases, effectively creating a set of 'pseudocontigs', each of which does not contain any gaps. Gene finding was then performed on both the original sequences and the pseudocontigs using AUGUSTUS, which also calls partial genes at the boundaries of each pseudocontig. The minimum ORF length that was considered for annotation was 50 amino acids to allow for the identification of short peptides that were supported by a contig at least twice the length of a read. AUGUSTUS models were trained on 800 genes randomly sampled from the 41 Esmeraldo-type (TcII) *T. cruzi* CL Brener chromosomes in GeneDB. Protein-DNA alignments of reference proteins against the new *T. cruzi* sequences, generated using Exonerate, were additionally used to improve the accuracy of the gene prediction. In addition, the RATT software was used to transfer highly conserved gene models from the *T. cruzi* CL Brener annotation to the target. A non-redundant set of gene models was obtained by merging the results of both RATT and AUGUSTUS and, for each maximal overlapping set of gene models, selecting the non-overlapping subset that maximizes the total length of the interval covered by the models, weighted by varying levels of *a priori* assigned confidence. Spurious low-confidence protein coding genes with a reading direction in disagreement with the directions of the polycistronic transcriptional units were removed automatically. The result of this integration process was then merged with ncRNA annotations produced by specific tools such as ARAGORN and Infernal. Finally, protein-DNA alignments with frame shifts produced by BLAST were used in a computational approach to identify potential pseudogenes in the remaining sequence.

Downstream of the structural annotation phase, gene models were automatically assigned IDs and further extended with product descriptions and GO terms, both transferred from CL Brener orthologs and inferred from Pfam protein domain hits and represented as feature attributes or Sequence Ontology-typed subfeatures tagged with appropriate evidence codes. This annotation pipeline has been implemented in the Companion web server. The assembled genome was scanned for small RNAs using INFERNAL against the curated RFAM database using cmsearch with a minimum e-value of 1×10^{-10} , a GC-bias of 0 and a minimum alignment length of 10 nt. This annotation

process has been implemented into the web-based annotation pipeline COMPANION (Steinbiss et al., 2016) from the Wellcome Trust Sanger Institute.

Repetitive sequences were annotated using RepeatMasker with the NCBI+ search engine and LTRHarvest. Using the genomic coordinates of the repetitive elements, the genome was split in windows of 10 Kb to identify VIPER and LITc retroelements adjacent to surface molecule genes (i.e: transsialidases, mucins and MASP). A one-sided Fisher's exact test was used to evaluate if the retroelements were enriched in genomic segments containing surface molecule genes.

Identification of Single Nucleotide Polymorphism (SNP) and Insertion/Deletion Events (Indels)

An improved short-read mapping strategy was used to assign the reads to their target sequences with high accuracy, especially in regions rich in simple and low complexity repeats, by taking advantage of the statistical read placement implemented in the Stampy read mapper to accurately call genomic variants from the mapped reads. Reads from all 34 *T. cruzi* TcI isolates (SRA BioProject accession number: PRJNA325924) were mapped against the assembled *T. cruzi* Sylvio X10/1 genome using a two-step mapping process to improve the mapping of Illumina data to highly repetitive regions: First, reads were mapped using BWA MEM with default parameters; later, the BAM file produced by BWA was remapped with Stampy (v1.23) using the *-bamkeepgoodreads* option. The final mapping file was sorted and filtered for PCR duplicates using Picard Tools v1.137. Variants were called using FreeBayes with a minimum per-base quality of 30, minimum mapping quality of 30 and minimum coverage of 15 bases. Variants that were found in a potentially misassembled region were excluded from the analysis. Additionally, genomic variants were called using FermiKit—which is an assembly-based variant caller—to validate the genomic variants observed in subtelomeric regions. A consensus of the two methods was used as a final set of variants for downstream analyses. Haplotypes were phased using Beagle r1399. The phased markers were used for downstream analyses with SNPrelate and VCFtools and the functional effect of the identified variants was predicted using SnpEff.

Identification of Genomic Structural Variants (SV)

Genomic structural variants were identified within TcI isolates, using a consensus of different methods: Delly2, Lumpy, FermiKit and FindTranslocations (<https://github.com/vezzi/FindTranslocations.git>) using both raw reads and realigned BAM files. For each method, an SV must had a depth of coverage > 10 reads and a mapping quality of > 30. Later, a consensus was created with all the SV that were supported by all the methods. SVs that were supported by FermiKit and at least one of the mapping-based methods were also included but labeled as 'Low Confidence'. SVs identified by only one method were not included. Breakpoint analysis was done with custom Python

scripts and their functional effect was predicted using SnpEff. Analyses of copy number variation (CNV) were done using the BAM files for each sample with the *Control-FREEC* package. Determination of the fixation index (*Fst*) using VCFtools was carried out for the *T. cruzi* CG and FcHc clones obtained from human TcI isolates from Colombia (**Supplementary Table 1**). For each strain, replicate clones from the original sample were isolated and cultured under the same conditions, and five of the replicates from each sample were sequenced in the Illumina HiSeq 2500 run.

RESULTS

Genome Sequence of *Trypanosoma cruzi* Sylvio X10/1

The final Sylvio X10/1 (TcI) genome assembly reconstructed 98.5% of the genome size, as previously estimated by analyzing gene content, and was contained in 47 chromosomes (**Figure 1A**) assembled from 210 X PacBio sequence data and a previous Illumina data set (**Table 1**). We tentatively refer to these as chromosomes in this paper, even though more verification of the complete karyotype is needed. Reads corresponding to mitochondrial DNA, kDNA, were removed by homology searches and were thus not included in the analysis. Comparison with the available short read assembly of the TcVI strain CL Brener revealed conserved core syntenic blocks composed of stretches of homologous sequences separated by non-syntenic regions (**Figure 1B** and **Supplementary Table 2**) that corresponded to regions that were in some cases initially not reconstructed in the hybrid TcVI strain, but have been partially resolved in later versions of this genome sequence. The non-syntenic regions mostly contained surface molecule gene arrays, and other repeated regions. In some cases, we found possible other gene-rich regions that were expanded in longer CL Brener chromosomes (**Figure 1B**). The length of the PacBio reads and the high coverage allowed the reconstruction of long stretches of repetitive sequences in the Sylvio X10/1 genome that could previously not be resolved using shorter read data for this genome.

The coverage of genomic regions coding for surface molecules was similar to that of known non-repetitive regions, which supported the correct reconstruction of these areas with a limited amount of assembly errors. To further investigate the quality of the new assembly, Illumina short reads were mapped and analyzed with FRC_bam, which revealed assembly artefacts related to low coverage, wrong paired-end read orientation, and higher than expected sequencing coverage in regions with long stretches of simple repeats. Coverage data based on mapping Illumina reads to the final genome sequence is presented in **Supplementary Figures 1 and 2**.

Repetitive elements comprised 18.43% of the TcI Sylvio X10/1 genome, 2.18% of which could not be classified using the repeat databases. LINE retroelements of the R1/Jockey group (3.63%) and VIPER LTRs (2.87%) were found to be the most prevalent types of retroelements, covering 6.89% of the genome, which is

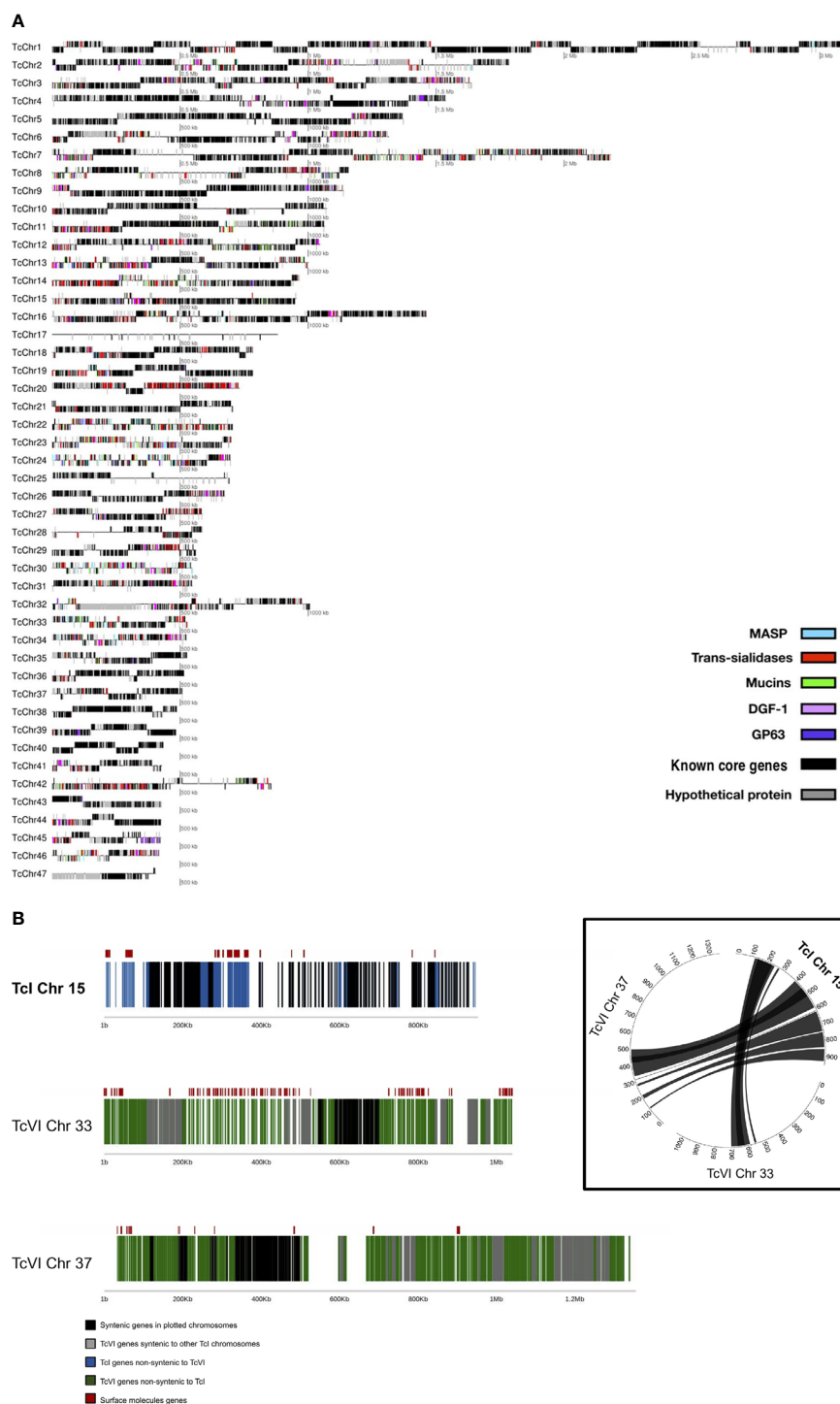


FIGURE 1 | (A) Distribution of surface molecule gene tandem arrays in the 47 chromosomes of the TcI Sylvio X10/1 genome. In this image, each line corresponds to an assembled putative chromosome drawn in proportion to its size, where genes corresponding to the largest *T. cruzi* multigene families are represented by colored boxes, hypothetical genes are represented by gray boxes and known core genes as black boxes. The position of the gene boxes above or below the line corresponds to the direction of transcription. **(B)** Comparison of chromosome 15 from the TcI Sylvio X10/1 assembly with TcVI CL Brener chromosomes containing syntenic blocks. The TcI (Sylvio X10/1) chromosome is depicted with black boxes indicating genes that have a CL Brener homolog, and blue boxes showing genes with no synteny with CL Brener. For TcVI (CL Brener) green boxes indicate genes that have no Sylvio X10/1 homolog. The red boxes above these lines show the location of complete genes coding for large surface molecule gene family members. In the circle plot, the lines between chromosomes represent regions of synteny between orthologous genes.

TABLE 1 | *Trypanosoma cruzi* Sylvio X10/1 strain (Tc-I) genome assembly.

| Metric | Value |
|------------------------------|----------|
| Genome size | 41.3 Mbp |
| Number of scaffolds | 47 |
| Percentage of reconstruction | 98.5% |
| Longest scaffold | 3.1 Mbp |
| Shortest scaffold | 404 Kb |
| NG50 | 1.0 Mbp |
| N50 | 1.1 Mbp |

much higher than the 2.57% estimated from the previously published Sylvio X10/1 draft assembly using short reads (Franzén et al., 2012).

Although retrotransposons were found to be present throughout the genome, the frequency of VIPER and LITc elements was markedly higher in multigene family-rich regions and they were found within one kilobase of pseudogenes, hypothetical proteins and surface molecule gene tandem arrays (One-sided Fisher exact test, p -value $< 1.32 \times 10^{-16}$). This distribution indicates that these elements may contribute to increased recombination activity in the gene family clusters by providing a source of microhomology. We do not have experimental evidence for the activity of these retroelements in *T. cruzi* and it is unknown if they directly affect gene expression.

Simple and low complexity repeats were observed surrounding surface molecule coding sequences and were also more abundant in the multigene family regions (2.18%), extending up to 4 Kb, compared to core regions (0.98%) where they were much shorter (10–120 bp). The most prevalent type of simple repeat had the (C)_n motif (11.7%), (TG)_n repeat motif (5.6%) and (CA)_n repeat motif (5.1%); each variable in length. The microhomology of these simple subtelomeric repeats may facilitate recombination resulting in new surface molecule variants, as described in other parasitic protozoa, including *Trypanosoma brucei* and *Plasmodium falciparum* (Hall et al., 2013; Claessens et al., 2014). However, it is noteworthy to mention that such subtelomeric regions are far less complex and shorter in *T. brucei* (African, virulent) and *T. rangeli* (Stoco et al., 2014) (American, non-virulent).

Based on our annotation approach, a total of 19,096 genes were identified in the TcI Sylvio X10/1 haploid genome sequence. The public CL Brener genome assembly has 11,106 annotated genes in one haplotype, 10,596 in the other, and 3,397 in smaller contigs. We have previously estimated the total gene content of CL Brener, based on read coverage, to approximately 22,570 for the haploid genome (Arner et al., 2007). This is mostly due to the larger size of the multigene family clusters in the TcVI hybrid genome. The genome sequence was longer and less fragmented than the version generated previously using short-read sequencing of the same strain (Franzén et al., 2011), which indicated resolution of additional regions of the genome. About 24.1% ($n = 4,602$) of the total annotated genes were truncated, mostly due to the introduction of premature stop codons, and 67% of these were located within surface molecule gene arrays, sharing motifs of the complete genes.

The new assembly allowed an improved analysis of the *T. cruzi* surface molecule gene repertoire. While the regions can be described as large gene arrays that contain genes from different surface molecule gene families, the genes of each of the three major surface molecules families were mostly organized as multiple smaller groups or tandem arrays within the larger regions. After genome annotation, the total number of such smaller arrays were: trans-sialidases, 312, with 2,048 complete gene copies and 201 pseudogenes; mucins 98, with 2,466 complete copies and 111 pseudogenes; MASPs 264, with 1,888 complete copies and 245 pseudogenes. These three surface molecule gene families comprised 16.02 Mbp (39.04%) of the TcI Sylvio X10/1 genome and presented a high level of sequence diversity (**Figure 1A**). Sequence strand switches often delimited the surface molecule tandem arrays. Commonly, these arrays had two to four complete copies immediately followed by two or more truncated copies with motifs similar to the complete gene. The intergenic spaces between arrays were rich in simple and low complexity repeats with no identifiable regulatory elements. The VIPER and LITc retrotransposon elements, in clusters of two to four copies, were found in the proximity of, or inside, tandem arrays containing trans-sialidases, mucins and MASP genes. As the surface molecule genes are known to evolve rapidly and be highly variable (Andersson, 2011), the enrichment of VIPER and LITc elements in these regions supports the hypothesis that they may be involved in generating new surface molecule gene variants *via* recombination mediated by sequence homology.

Both Ser/Thr kinases and DEAD-box RNA helicase genes were found at both extremes of 34 (10.81%) trans-sialidase arrays located in chromosomes 1, 2, and 8. Searches against the RFAM database identified 1,618 small RNAs in the TcI Sylvio X10/1 genome. These were mostly ribosomal RNAs with the 5S rDNA subunit being the most common (31.9%) followed by ACA Box snoRNAs (30.9%), SSU rDNA (12.2%) and LSU rDNA (10.2%) subunits. We also found hits to telomerase RNA component (TERC), Catabolite Repression Control sequester (CrcZ), Protozoa Signal Recognition Particle RNAs, spliceosomal RNA subunits and miRNAs. The putative miRNAs identified in Sylvio X10/1 belong to the MIR2118 and MIR1023 families, previously not found in protozoan parasites. The functional relevance of these predicted small RNAs will need to be further validated *in vitro*. The miRNA segments were located in both strands within 1 Kb of genes coding for DEAD-box RNA helicases surrounding surface molecule gene tandem arrays.

Genomic Variation Within The *Trypanosoma cruzi* TcI Clade

Intra-TcI genomic diversity was examined among 34 samples from six countries: United States, Mexico, Panama, Colombia, Venezuela and Ecuador, derived from a range of triatomine vectors and human patients of different clinical stages (**Table 2** and **Supplementary Table 1**). Our hybrid variant calling strategy, combined with removal of repeat elements and repeated genes, allowed us to identify genomic variants in the core and multigene family clusters in a reliable fashion (See methods).

TABLE 2 | Genomic variants identified among the *Trypanosoma cruzi* TcI isolates.

| GROUP | SNPs | INDELs | DELETION | DUPLICATION | TRANSLOCATION |
|--------------|--------|--------|----------|-------------|---------------|
| Colombia* | 158565 | 59520 | 439 | 1231 | 4140 |
| Colombiana** | 105023 | 30697 | 23 | 86 | 273 |
| Venezuela | 77232 | 70086 | 43 | 183 | 614 |
| Ecuador | 122122 | 84201 | 40 | 164 | 354 |
| Panama | 620499 | 238833 | 225 | 605 | 2060 |
| Texas | 101771 | 78499 | 69 | 303 | 978 |

*FcHc and CG clones from Colombia.

**TcI Colombiana strain.

A total of 1,031,785 SNPs and 279,772 INDELs shorter than 50 bp were called for all sequenced TcI isolates relative to the Sylvio X10/1 genome. INDELs presented an average density of 5.3 variants per Kb and SNPs 24.1 variants per Kb. An individual *T. cruzi* TcI isolate was found to contain an average of 61,000 SNPs and 6,820 INDELs with a density of 31.8 variants per Kb. However, these measures fluctuated depending on the geographical and biological source of the sample. Core regions had an average SNP density of 0.4 variants per Kb, in contrast with surface molecule multigene family clusters where approx. 10 variants per Kb were found. It was not surprising that the bulk of the genomic variants were located in the multigenic family clusters regions in all the isolates, with fewer differences in the core regions. Although several studies using single gene markers have identified heterogeneity in the TcI clade (Llewellyn et al., 2009; Guhl and Ramírez, 2011), the extent of this variation had not previously been assessed genome-wide.

The majority of INDELs (96%) were found in intergenic or noncoding regions, and 81% of these were located in surface molecule multigene family regions. INDELs within coding sequences were exclusively found to cause frameshifts turning the affected coding sequence into a pseudogene. This distribution of INDELs is a genomic signature that has been associated with non-allelic homologous recombination due to unequal crossing over (Parks et al., 2015) or microhomology-mediated end joining (Sfeir and Symington, 2015; Weckselblatt et al., 2015) (Table 3). However, these repair mechanisms, or something similar, have not yet been shown to be present in *T. cruzi*. Short insertions were more prevalent than short deletions, a pattern common to all the analyzed TcI genomes when compared to Sylvio X10/1.

In the subtelomeric regions, short insertions (1–3 bp) occurred within the upstream and downstream portions of the coding sequences and usually involved the addition of one or more cytosines or guanines. Single-base pair deletions of an adenine or thymine were also observed within these regions, but at a lower frequency. Longer deletions (5–20 bp) and insertions (8–10 bp) were observed within trans-sialidases, Retrotransposon Hot Spot (RHS), pseudogenes and, at a lower frequency, L1Tc retroelements.

Population Genomics of the *Trypanosoma cruzi* TcI Clade

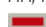

We used the short genomic variants to analyze the population genomics of the *T. cruzi* TcI clade, and where possible taking into account the different sample sources (insect vector or human host), clinical outcome of the infected patients and geographic locations (Supplementary Table 1). This sampling strategy allowed comparison of parasite population structure in different environments. Interestingly, a Bayesian PCA analysis using INDELs and IBD-based hierarchical clustering using only SNPs from core regions for all the samples showed a mostly geography-specific population structure (Figures 2A, B).

The analysis of the variation between two Colombian TcI isolates made it possible to compare parasites from a HIV-positive patient with fatal cardiomyopathy (CG) and from an acute chagasic patient infected by oral transmission (FcHc). To increase accuracy, repeat elements, repeated genes and repeated surface molecule family genes were excluded from this analysis, while core regions and non-repeated, unique surface molecule genes and other genes were kept, in order to have markers outside the core regions. The latter were selected by lower sequence similarity to known surface molecule genes. A total of 158,565 well-supported SNPs, called by both GATK and FreeBayes, was selected from these clones, and used to calculate global and per-site population genetic statistics. These samples displayed distinctive behavior in a global analysis of genomic diversity by separating into two well-defined clusters, as can be seen in Figures 2A, B. Linkage Disequilibrium (LD) analyses were performed genome-wide for both groups using the r^2 statistic; revealing a fluctuating pattern of LD across the entire genome with large blocks of low r^2 values—implying a recombinatorial process—present at distinctive chromosomal locations that were specific to each group of clones. Particularly, CG clones had less genetic diversity than FcHc clones (Figure 3A) and displayed a trend toward LD, whereas FcHc clones presented a more dynamic LD pattern. Values of r^2

TABLE 3 | Patterns of INDELs and their associated mechanisms of origin.

| INDEL type | Example | Mechanism | Frequency* |
|----------------|--------------------------------------|-----------|------------|
| HR - deletion | GCATAAA aa AAAGC | NAHR | 756 411 |
| HR - insertion | CACA AAAA AAAAAGCTAC | NAHR | 521 002 |
| TR - mixed | ACACAC acac ACACACACAC | NAHR | 118 432 |
| Non-repetitive | TAGCAC ag tGACTTCACAGCCTG | NHEJ-like | 28 389 |
| Long | CGGCTAGACCCAGGTACAGTCA | MMEJ | 32 666 |
| Insertion | | | |
| Long Deletion | GCacactgacacgacactgacacactgaaA | MMEJ | 31 712 |

HR, Homopolymer run; TR, Tandem Repeat.

 = Deletion = Insertion

*For all the 34 TcI genomes compared against Sylvio X10/1.

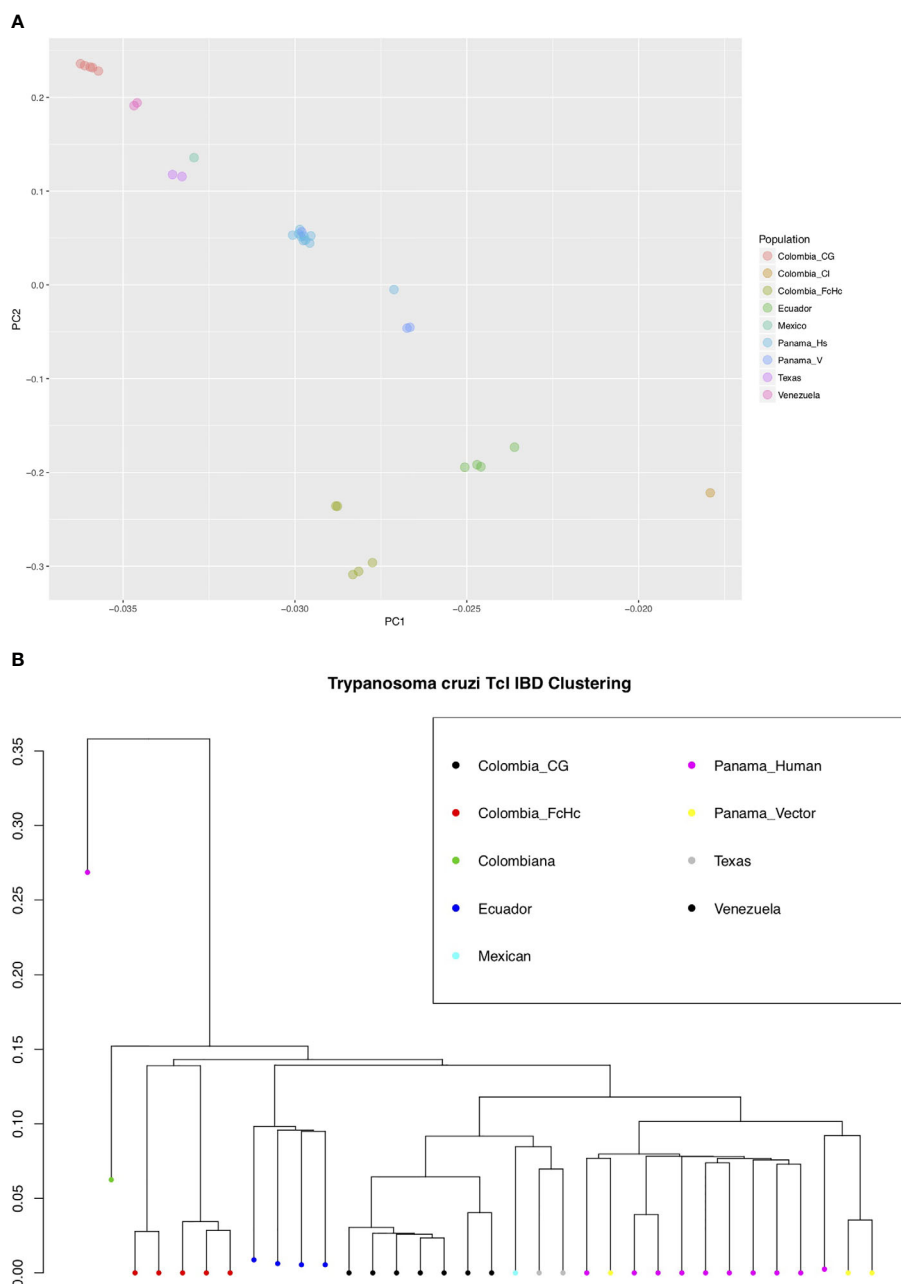


FIGURE 2 | (A) Bayesian principal component analysis (PCA) of *T. cruzi* TcI strains using INDELs. The percentage of variance for PC1 was 46.2 and for PC2 28.6. **(B)** Identity by Descent (IBD) dendrogram of *T. cruzi* TcI strains using SNPs, calculated using 1000 bootstraps. Both analyses, using different markers, support the population structure of the analyzed TcI samples. Notably, the highly virulent TcI Colombiana and the Panamanian TcI H1 from a chronic patient are presented as outliers [(B), far left].

near zero were more common in LD sliding windows containing genes coding for surface molecules and r^2 values closer to one were present exclusively in core regions rich in housekeeping genes, indicating that these regions are more stable. For the CG and FcHc clones we calculated a global Fixation index (F_{st}) value of -0.9377958 and -0.1162212, respectively (Figure 3B). These values are consistent with genetic differentiation in

recombination hotspots in the multigene family regions. The global Tajima's D value for the CG clones was 1.373 and 0.9906 for FcHc clones, suggesting the presence of multiple alleles at variable frequencies in both populations (Figure 3C). This pattern was more evident in the multigene family regions, which is consistent with balancing selection of surface molecules. The values for each set of clones were calculated

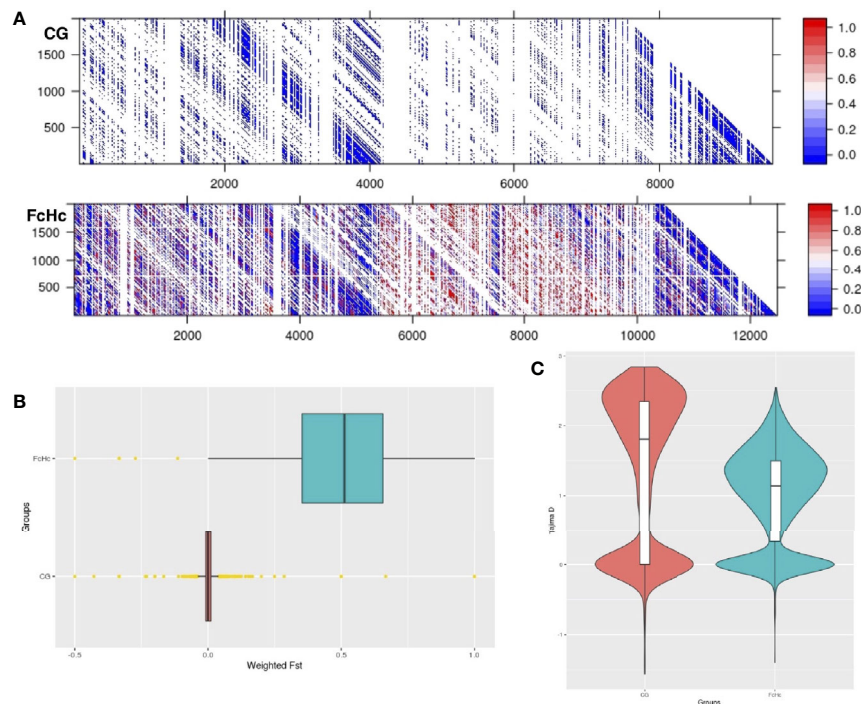


FIGURE 3 | (A) Linkage disequilibrium matrix (r^2) of chromosome 2 for the Colombian CG and FcHc clones. LD values range from 0 (recombination) to 1 (no recombination). **(B)** Genome-wide F_{st} distribution in 10 Kb bins displaying a state of panmixia for the CG clones and moderate genetic differentiation in the FcHc clones, yellow dots represent outlier bins. The differences in chromosome length are caused by missing sequences in these strains, that resulted in regions with no mapping that were removed from the analysis. **(C)** Distribution of subtelomeric Tajima's D selection test in both groups displaying overall balancing selection ($D > 0$) in these regions for both clones.

separately, from different sets of SNPs, which makes a direct comparison in smaller regions difficult. We were only able to detect the larger patterns described above.

Analyses of genomic variation between samples isolated from humans and vectors from Mexico, Panama and Ecuador revealed that the global genetic differentiation among samples isolated from vectors was $F_{st} = 0.1289547$ whereas for samples isolated from humans the observed was $F_{st} = -0.05521983$. The patterns of linkage disequilibrium between human and vector derived isolates were similar to those observed in the Colombian clones. Estimates of the Tajima's D statistic revealed a distinctive pattern of selection between the two groups. Balancing selection was detected specifically in regions containing tandem gene arrays coding for surface molecules in all the samples derived from vectors, regardless of their geographical origin; whereas selective sweeps were present in the same regions in human-derived samples. Large genomic areas (> 50 Kb) containing surface molecule genes displayed negative Tajima's D values in human-derived isolates, in contrast with the pattern observed in vector-derived isolates with long genomic stretches (> 70 Kb) of positive Tajima's D values and short genomic blocks (< 5 Kb) with negative values. We speculate that these patterns may be caused by selection pressure from the immune system in human-derived strains, which is absent in strains that have grown in insects for extended times.

Genome Structural Variation

Genomic structural variants, such as deletions, tandem and interspersed duplications, genomic inversions and chromosomal break-ends, were observed ubiquitously throughout the genomes of the analyzed TcI strains. The most common type of intrachromosomal structural variant observed was tandem duplications followed by deletions larger than 50 Kb (Table 2). Chromosomal break-ends, similar to the unbalanced chromosomal translocations observed in many eumetazoans, were the most abundant type of structural rearrangement and they were only present in surface molecule multigene family regions that were statistically enriched with retroelements and simple repeats. The recombination breakpoints were found to occur at simple repeats and retrotransposons of the VIPER and LITc class.

The detected recombination events were found to involve fragments ranging between 20–150 Kb in length and in most cases contained fragments or even complete coding sequences for surface molecule genes, such as trans-sialidases, mucins and MASP genes and other surface glycoproteins (gp63/gp85). Housekeeping genes did not appear to have been affected by these genomic rearrangements. We detected several instances where rearrangements resulted in altered or longer coding sequences by superimposing fragments—or the entire coding sequence—on genes of the same family located in a different

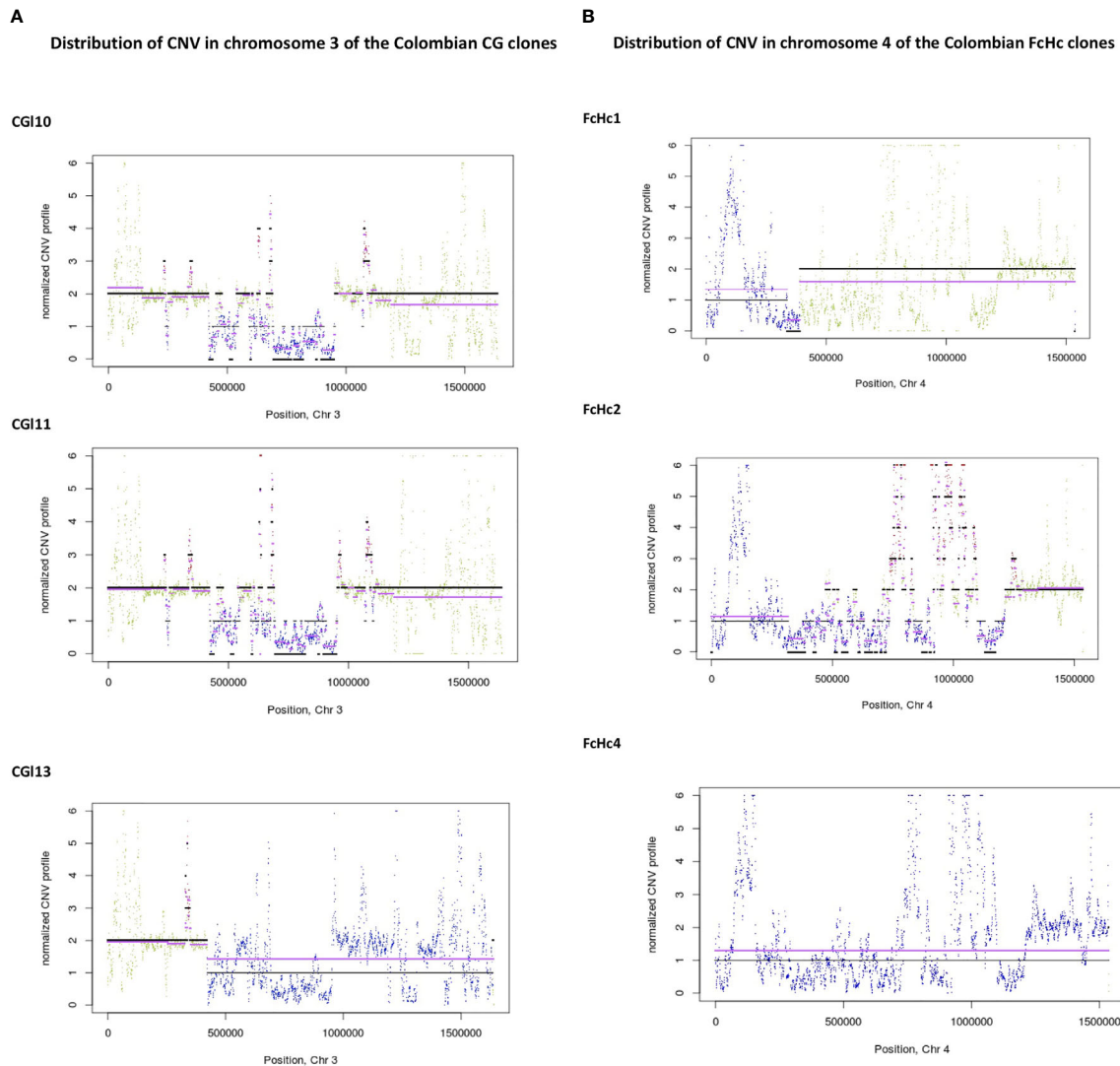


FIGURE 4 | Distribution of CNV changes in chromosome 3 of the Colombian (A) CG clones and (B) FcHc clones. Black lines represent the reference genome sequence and cyan lines represent the sample under study. Each sliding window for CNV evaluation is represented as a dot. A drastic change in CNV can be noted in the FcHc clones whereas the CG clones seem to be less affected.

genomic location. This was found to have occurred both in the Colombian and the Texas isolates by recombination between trans-sialidases from different chromosomes. The biological relevance of the new altered gene sequences is not known.

Retroelements could be found within or near genomic regions containing surface molecule gene tandem arrays and L1Tc fragments or their entire sequence were also found near all the observed rearrangements, where they were inserted into regions containing simple repeats composed by AT dimers. Data on the genomic positions for repeat elements have been listed in **Supplementary Tables 3–5**.

Multiple such examples of the generation of possible new surface molecule gene variants were identified in TcI. It is a possibility that the parasite uses specific molecular mechanisms of recombination that can rapidly generate surface molecule

diversity, allowing it to increase the genomic plasticity required to adapt to changing environments and evade immune responses during short and long-term infections in various host species.

The sizes of the tandem duplications ranged from 6 to 75 Kb and mainly involved tandem arrays coding for surface molecules, mostly trans-sialidases and mucins, but also Dispersed Gene Family 1 (DGF-1) and several hypothetical proteins. The breakpoints of these duplications were surrounded by simple repeats and retroelements in multigene family regions. A tandem duplication event could involve between four and 25 copies of a specific gene when in the surface multigene family regions, whereas in core regions the number was between two and eight. We observed that large deletions occurring in multigene family regions were surrounded by simple repeats of the type (T)_n and (AT)_n and retrotransposons of the L1Tc class, containing

surface molecule gene tandem arrays. Deletions in these genomic regions tended to be shorter (4–12 Kb) and sample-specific.

Distribution of Copy Number Variation (CNV) Within the TcI clade

CNV varied extensively between *T. cruzi* TcI strains. There have been previous attempts to assess CNV in the *T. cruzi* genome (Minning et al., 2011), but these studies were performed using DNA tiling microarrays with probes designed using the TcVI CL Brener strain assembly, in which multigenefamily regions are more difficult to study.

The distribution of CNV in the genomes of the studied TcI samples involved segments of an average size of 5 Kb. We observed blocks of segmental CNV within a chromosome with a pattern that was unique to each sample. Notably, the Colombian clones presented individual profiles of CNV (Figures 4A, B and Supplementary Figures 3–8) despite being derived from the same clinical isolates.

Sequence blocks affected by segmental CNVs contained retrotransposons of the VIPER and L1Tc class, as well as surface molecule genes surrounded by simple repeats. The isolate-specific nature of these CNV events demonstrates the high level of within-clade diversity of the TcI samples. The distribution of CNV across the *T. cruzi* genome reinforces the dynamic nature of the multigene family clusters and the surface molecule gene families.

DISCUSSION

Complete reconstruction of the *T. cruzi* genome to encompass the subtelomeric regions and surface molecule multigene family clusters proved to be difficult to achieve using short reads, due to sequencing library preparation biases and a genome architecture that is rich in long stretches of simple repeats, large repetitive gene families and multiple retrotransposons. In 2016, we used long PacBio sequencing reads to provide the most complete genome sequence of a *T. cruzi* strain to date and this reference genome was made public through Genbank and TriTrypDB. This allowed us to perform a detailed analysis of the repertoire of complex genes families that encode cell surface molecules, considered to be involved in cell invasion and evasion of the host immune response. We could clearly see the duality in the organisation of the parasite genome, comprised of a core genomic component with few repetitive elements and a slow evolutionary rate, resembling that of other related protozoa, and contrasting, highly plastic multigene family clusters encoding fast-evolving surface antigens, with abundant interspersed retrotransposons. The structural changes that generate and maintain diversity in *T. cruzi* surface molecules have certain mechanistic parallels in other protozoa such as those recently described in *Plasmodium falciparum* (Miles et al., 2016), but differing from the shorter, less repetitive genome of the non-virulent, human-infective *Trypanosoma rangeli*.

In order to overcome the limitations of short read mapping to a highly complex genome such as *T. cruzi*, we first mapped the reads against the repeat masked genome using 'bwa-mem' with

probabilistic read placement and multi-mapping probability assignment. The mapping results were subsequently submitted for statistical evaluation using Stampy (<https://genome.cshlp.org/content/21/6/936>). The Stampy algorithm assigns a probability for read-base misplacement and repeats. To evaluate the results we used two different variant callers (GATK + Freebayes) which also take into account these scores. For a variant to be considered, it needed to be reported by both variant calling methods and pass the filters. This strategy and the TcI reference genome made it possible to carry out the TcI population genomics study.

Early studies of the genetic diversity of *T. cruzi* using geographically disparate sampling and restricted comparisons of genetic diversity suggested a clonal population structure (Tibayrenc et al., 1990; Tibayrenc and Ayala, 1991); however, population genetics with an expanded set of markers have now challenged this view (Gaunt et al., 2003; Westenberger et al., 2005; Llewellyn et al., 2009). Nevertheless, there are still conflicting views as to which model best describes the population structure of *T. cruzi* (Messenger and Miles, 2015; Tibayrenc and Ayala, 2015). The newer Sylvio X10/1 genome sequence has enabled extensive genome-wide comparative population genomics analyses, which may shed light on this issue (Schwabl et al., 2019; Rose et al., 2020). Our comparative analyses of 34 *T. cruzi* isolates and clones from the TcI clade suggested many recombination events and population indices normally associated with genetic exchange between strains, which are more likely to be caused by the extensive repeat-driven recombination in the subtelomeric regions. The extent of variation in the multigene family clusters rich in surface antigen coding genes and the geographical clustering of strains based on geographic distribution indicates active, on-going adaptation to host and vectors. This need for phenotypic—and thus genomic—versatility may impel the active generation of sequence diversity in *T. cruzi*. Further analyses of the evolution of multigene family clusters will yield much more detailed understanding of diversity within and between the six currently recognised genetic lineages of *T. cruzi* (Andersson, 2011). We have shown how the genome architecture and dynamic multigene family clusters of *T. cruzi* may provide a mechanism to rapidly generate sequence diversity, required to escape the host immune response and adapt in response to new environments. It is the striking richness in simple repeat, retrotransposons and motif conservation in the multigene family clusters that renders these genomic areas susceptible to structural change, similar to yeast and other pathogens (Aksenova et al., 2013; de Jonge et al., 2013; Faino et al., 2016; Weatherly et al., 2016). Retrotransposons have been associated with the generation of complexity in genomic regions in mammals and plants and with control of gene expression (de Jonge et al., 2013; McConnell et al., 2013). In the case of *T. cruzi*, they appear to generate novel variants *via* mechanisms that exploit sequence homology. The presence of the simple repeats and retrotransposons near surface molecule coding genes provides the microhomology for both mechanisms to operate in such regions. Besides retrotransposons, the modular structure of the multigene families MASP and Trans-sialidase, where

different genes share conserved motifs, could also provide microhomology needed for this homologous recombination (El-Sayed et al., 2005; Weatherly et al., 2016). Our analysis of INDELs and chromosomal breakpoints in the subtelomeric regions confirmed that a mechanism similar to NAHR or MMEJ operates as source of sequence diversity, for example by transposition of trans-sialidase genes or pseudogenes to produce new sequence mosaics. The required recombination machinery is conserved in *T. cruzi* (Ramesh et al., 2005). Furthermore, these mechanisms would explain the higher amount of pseudogenes observed in the surface molecule regions.

Retrotransposons were first reported from *T. cruzi* in 1991 (Villanueva et al., 1991). The presence of these elements may also partly account for the previously reported widespread observation of copy number variation in different *T. cruzi* strains (Minning et al., 2011). Thus, we find that repeats near the surface molecule genes appear to drive recombination in *T. cruzi*. The apparent inability of *T. cruzi* to condense chromatin may facilitate transposition in a stochastic fashion, facilitating generation of sequence diversity in exposed regions of the genome. A similar process has been described in the neurons of mammals and insects (Erwin et al., 2014) but not in any other unicellular organism. Retrotransposons may also have an important role as gene transcription regulators: they may either silence or promote gene expression, due to their susceptibility to DNA methylation or by providing potential binding sites respectively, as observed previously (Elbarbary et al., 2016). This lack of a well-defined transcriptional regulation machinery in the *T. cruzi* genome may suggest a link to the requirement for retrotransposon closely associated with gene tandem arrays.

CONCLUSION

Here we describe the sequencing and assembly of the complete genome of the *Trypanosoma cruzi* TcI strain Sylvio X10/1, which was made public in 2016. This genome sequence enabled the first resolution of the complex multiple gene families that encode *T. cruzi* surface molecules, and provided a basis for *T. cruzi* population genomics. We discovered an extraordinary concentration of retrotransposons among the multigene family clusters and indications of repeat-driven recombination and generation of antigenic diversity, providing the mechanisms for *T. cruzi* to evade the host immune response, and to facilitate the adaption to new host and vectors. This genome will provide an invaluable resource to facilitate the prospective discovery of novel drug targets and vaccine candidates for Chagas disease.

DATA AVAILABILITY STATEMENT

The datasets presented in this study can be found in online repositories. The names of the repository/repositories and accession number(s) can be found below: <https://www.ncbi.nlm.nih.gov/genbank/>, ADWP000000000 and <https://www.ncbi.nlm.nih.gov/genbank/>, SRP076682.

AUTHOR CONTRIBUTIONS

CT-L and BA conceived and designed the study. CT-L designed and executed computational analyses. MY prepared Sylvio X10/1 genomic DNA for PacBio sequencing and performed manual annotation of surface molecule genes. JEC, AS, JR, FG, SO-M, JAC, ST, HC, RG, KJ, MB, PH, KM, MJG, and BB provided genomic DNA for TcI isolates. JR-C and DB created chromosome maps for surface molecules. MM, LM, ML, JR-C, GM, and EG contributed to the interpretation of the results. CT-L, EG, MM, and BA wrote the manuscript. All authors contributed to the article and approved the submitted version.

FUNDING

This research was funded by grants from the Knut and Alice Wallenberg Foundation, The Swedish Research Council and the European FP7 program, Contract No. 223034. LM was funded by a grant from the NIH (5R01AI107028); DB, EG, and ST were funded by grants from CNPq (Brazilian Government Agency). GM was a recipient of a CAPES/PRINT Program Scholarship.

ACKNOWLEDGMENTS

The authors wish to thank John Kuijpers and Lawrence Hon from Pacific Biosciences (PacBio) for providing the data for the Sylvio X10/1 genome and preliminary assembly results. We would also like to acknowledge Eric Dumonteil, University of the Yucatan, Mexico, and Ed Wozniak, Texas Department of State Health Services, for past work on parasite collection. This manuscript has been released as a preprint at Biorxiv (Talavera-Lopez et al., 2018).

SUPPLEMENTARY MATERIAL

The Supplementary Material for this article can be found online at: <https://www.frontiersin.org/articles/10.3389/fcimb.2021.614665/full#supplementary-material>

Supplementary Table 2 | A list of coordinates for the synteny analysis comparing the Sylvio X10/1 genome with CL Brener for all chromosomes.

Supplementary Table 3–5 | The tables list the genomic coordinates and identity of repeat elements of various types that have been identified in the Sylvio X10/1 genome sequence. The lists have been used for the annotation of the publically available genome sequence.

Supplementary Figure 1 | Results from mapping Illumina reads back to the completed genome sequence. The graphs show the overall coverage across the genome.

Supplementary Figure 2 | Results from mapping Illumina reads back to the completed genome sequence. The plots show coverage across each chromosome. Local variation in coverage indicate the presence of highly repeated regions.

Supplementary Figure 3–8 | Distribution of CNV changes in the Colombian CG clones and FcHc clones for all chromosomes.

REFERENCES

- Aksenova, A. Y., Greenwell, P. W., Dominska, M., Shishkin, A. A., Kim, J. C., Petes, T. D., et al. (2013). Genome Rearrangements Caused by Interstitial Telomeric Sequences in Yeast. *Proc. Natl. Acad. Sci. U.S.A.* 110 (49), 19866–19871. doi: 10.1073/pnas.1319313110
- Andersson, B. (2011). The Trypanosoma Cruzi Genome; Conserved Core Genes and Extremely Variable Surface Molecule Families. *Res. Microbiol.* 162 (6), 619–625. doi: 10.1016/j.resmic.2011.05.003
- Arner, E., Kindlund, E., Nilsson, D., Farzana, F., Ferella, M., Tammi, M. T., et al. (2007). Database of Trypanosoma cruzi repeated genes: 20,000 additional gene variants. *BMC Genomics* 8, 391. doi: 10.1186/1471-2164-8-391
- Berlin, K., Koren, S., Chin, C.-S., Drake, J. P., Landolin, J. M., and Phillippy, A. M. (2015). Assembling Large Genomes with Single-Molecule Sequencing and Locality-Sensitive Hashing. *Nat. Biotechnol.* no August 2014, 1–11. doi: 10.1038/nbt.3238
- Bern, C., Kjos, S., Yabsley, M. J., and Montgomery, S. P. (2011). Trypanosoma Cruzi and Chagas' Disease in the United States. *Clin. Microbiol. Rev.* 24 (4), 655–681. doi: 10.1128/CMR.00005-11
- Bern, C. (2015). Chagas' Disease. *New Engl. J. Med.* 373 (5), 456–466. doi: 10.1056/NEJMr1410150
- Berná, L., Rodríguez, M., Chiribao, M. L., Parodi-Talice, A., Pita, S., Rijo, G., et al. (2018). Expanding an expanded genome: long-read sequencing of Trypanosoma cruzi. *Microbial. Genomics* 4 (5), e000177. doi: 10.1099/mgen.0.000177
- Callejas-Hernández, F., Rastrojo, A., Poveda, C., Gironès, N., and Fresno, M. (2018). Genomic Assemblies of Newly Sequenced Trypanosoma Cruzi Strains Reveal New Genomic Expansion and Greater Complexity. *Sci. Rep.* 8 (1), 14631. doi: 10.1038/s41598-018-32877-2
- Claessens, A., Hamilton, W. L., Kekre, M., Otto, T. D., Faizullahbhoj, A., Rayner, J. C., et al. (2014). Generation of Antigenic Diversity in Plasmodium Falciparum by Structured Rearrangement of Var Genes during Mitosis. *PLoS Genet.* 10 (12), e1004812. doi: 10.1371/journal.pgen.1004812
- de Jonge, R., Bolton, M. D., Kombrink, A., van den Berg, G. C.M., Yadeta, K. A., et al. (2013). Extensive Chromosomal Reshuffling Drives Evolution of Virulence in an Asexual Pathogen. *Genome Res.* 23 (8), 1271–1282. doi: 10.1101/gr.152660.112
- Elbarbary, R. A., Lucas, B. A., and Maquat, L. E. (2016). Retrotransposons as Regulators of Gene Expression. *Science* 351 (6274), aac7247. doi: 10.1126/science.aac7247
- El-Sayed, N. M., Myler, P. J., Bartholomeu, D. C., Nilsson, D., Aggarwal, G., Tran, A.-N., et al. (2005). The Genome Sequence of Trypanosoma Cruzi, Etiologic Agent of Chagas Disease. *Science* 309 (5733), 409–415. doi: 10.1126/science.1112631
- Erwin, J. A., Marchetto, M. C., and Gage, F. H. (2014). Mobile DNA Elements in the Generation of Diversity and Complexity in the Brain. *Nat. Rev. Neurosci.* 15 (8), 497–506. doi: 10.1038/nrn3730
- Faino, L., Seidl, M. F., Shi-Kunne, X., Pauper, M., van den Berg, G. C. M., Wittenberg, A. H. J., et al. (2016). Transposons Passively and Actively Contribute to Evolution of the Two-Speed Genome of a Fungal Pathogen. *Genome Res.* 26 (8), 1091–1100. doi: 10.1101/gr.204974.116
- Franzén, O., Ochaya, S., Sherwood, E., Lewis, M. D., Llewellyn, M. S., Miles, M. A., et al. (2011). Shotgun Sequencing Analysis of Trypanosoma Cruzi I Sylvio X10/1 and Cruzi VI CL Brenner. *PLoS Neglect. Trop. Dis.* 5 (3), e984. doi: 10.1371/journal.pntd.0000984
- Franzén, O., Talavera-López, C., Ochaya, S., Butler, C. E., Messenger, L. A., Lewis, M. D., et al. (2012). Comparative Genomic Analysis of Human Infective Trypanosoma Cruzi Lineages with the Bat-Restricted Subspecies T. Cruzi Marinkellei. *BMC Genomics* 13 (January), 531. doi: 10.1186/1471-2164-13-531
- Frasch, A. C. (2000). Functional diversity in the trans-sialidase and mucin families in Trypanosoma cruzi. *Parasitol. Today* 16 (7), 282–286. doi: 10.1016/S0169-4758(00)01698-7
- Gaunt, M. W., Yeo, M., Frame, I. A., and Stothard, J. R. (2003). Mechanism of Genetic Exchange in American Trypanosomes. *Nature* 421 (6926), 936–939. doi: 10.1038/nature01438
- GBD 2013 Mortality and Causes of Death Collaborators (20159963). Global, Regional, and National Age-Sex Specific All-Cause and Cause-Specific Mortality for 240 Causes of Death-2013: A Systematic Analysis for the Global Burden of Disease Study 2013. *Lancet* 385, 117–171. doi: 10.1016/S0140-6736(14)61682-2
- Guhl, F., and Ramírez, J. D. (2011). Trypanosoma Cruzi I Diversity: Towards the Need of Genetic Subdivision? *Acta Tropica* 119 (1), 1–4. doi: 10.1016/j.actatropica.2011.04.002
- Hall, J. P.J., Wang, H., and Barry, J. D. (2013). Mosaic VSGs and the Scale of Trypanosoma Brucei Antigenic Variation. *PLoS Pathog.* 9 (7), e1003502. doi: 10.1371/journal.ppat.1003502
- Kim, D., Chiurillo, M. A., El-Sayed, N., Jones, K., Santos, M. R.M., Porcile, P. E., et al. (2005). Telomere and Subtelomere of Trypanosoma Cruzi Chromosomes Are Enriched in (pseudo)genes of Retrotransposon Hot Spot and Trans-Sialidase-like Gene Families: The Origins of T. Cruzi Telomeres. *Gene* 346 (February), 153–161. doi: 10.1016/j.gene.2004.10.014
- Llewellyn, M. S., Miles, M. A., Carrasco, H. J., Lewis, M. D., Yeo, M., Vargas, J., et al. (2009). Genome-Scale Multilocus Microsatellite Typing of Trypanosoma Cruzi Discrete Typing Unit I Reveals Phylogeographic Structure and Specific Genotypes Linked to Human Infection. *PLoS Pathog.* 5 (5), e1000410. doi: 10.1371/journal.ppat.1000410
- McConnell, M. J., Lindberg, M. R., Brennand, K. J., Piper, J. C., Voet, T., Cowing-Zitron, C., et al. (2013). Mosaic Copy Number Variation in Human Neurons. *Science* 342 (6158), 632–637. doi: 10.1126/science.1243472
- Messenger, L. A., and Miles, M. A. (2015). Evidence and Importance of Genetic Exchange among Field Populations of Trypanosoma Cruzi. *Acta Tropica* 151 (November), 150–155. doi: 10.1016/j.actatropica.2015.05.007
- Miles, A., Iqbal, Z., Vauterin, P., Pearson, R., Campino, S., Theron, M., et al. (2016). Indels, Structural Variation, and Recombination Drive Genomic Diversity in Plasmodium Falciparum. *Genome Res.* 26 (9), 1288–1299. doi: 10.1101/gr.203711.115
- Minning, T. A., Weatherly, D. B., Flibotte, S., and Tarleton, R. L. (2011). Widespread, Focal Copy Number Variations (CNV) and Whole Chromosome Aneuploidies in Trypanosoma Cruzi Strains Revealed by Array Comparative Genomic Hybridization. *BMC Genomics* 12 (1), 139. doi: 10.1186/1471-2164-12-139
- Montgomery, S. P., Starr, M. C., Cantey, P. T., Edwards, M. S., and Meymandi, S. K. (2014). Neglected Parasitic Infections in the United States: Chagas Disease. *Am. J. Trop. Med. Hygiene* 90 (5), 814–818. doi: 10.4269/ajtmh.13-0726
- Morillo, C. A., Marin-Neto, J. A., Avezum, A., Sosa-Estani, S., Rassi, A. Jr, Rosas, F., et al. (2015). Randomized Trial of Benznidazole for Chronic Chagas' Cardiomyopathy. *New Engl. J. Med.* 373 (14), 1295–1306. doi: 10.1056/NEJMoa1507574
- Osorio, L., Ríos, I., Gutiérrez, B., and González, J. (2012). Virulence Factors of Trypanosoma Cruzi: Who Is Who? *Microbes Infect. / Institut Pasteur* 14 (15), 1390–1402. doi: 10.1016/j.micinf.2012.09.003
- Parks, M. M., Lawrence, C. E., and Raphael, B. J. (2015). Detecting Non-Allelic Homologous Recombination from High-Throughput Sequencing Data. *Genome Biol.* 16 (April), 72. doi: 10.1186/s13059-015-0633-1
- Pecoul, B., Batista, C., Stobbaerts, E., Ribeiro, I., Vilasanjuan, R., Gascon, J., et al. (2016). The BENEFIT Trial: Where Do We Go from Here? *PLoS Neglect. Trop. Dis.* 10 (2), e0004343. doi: 10.1371/journal.pntd.0004343
- Ramesh, M. A., Malik, S.-B., and Logsdon, J. M. Jr (2005). A Phylogenomic Inventory of Meiotic Genes: Evidence for Sex in Giardia and an Early Eukaryotic Origin of Meiosis. *Curr. Biology: CB* 15 (2), 185–191. doi: 10.1016/S0960-9822(05)00028-X
- Ramírez, J. D., Guhl, F., Rendón, L. M., Rosas, F., Marin-Neto, J. A., and Morillo, C. A. (2010). Chagas Cardiomyopathy Manifestations and Trypanosoma Cruzi Genotypes Circulating in Chronic Chagasic Patients. *PLoS Neglect. Trop. Dis.* 4 (11), e899. doi: 10.1371/journal.pntd.0000899
- Rassi, A., Rassi, A., and Marin-Neto, J. A. (2010). Chagas Disease. *Lancet* 375 (9723), 1388–1402. doi: 10.1016/S0140-6736(10)60061-X
- Reis-Cunha, J. L., Baptista, R. P., Rodrigues-Luiz, G. F., Coqueiro-Dos-Santos, A., Valdivia, H. O., de Almeida, L. V., et al. (2018). Whole Genome Sequencing of Trypanosoma Cruzi Field Isolates Reveals Extensive Genomic Variability and Complex Aneuploidy Patterns within TcII DTU. *BMC Genomics* 19 (1), 816. doi: 10.1186/s12864-018-5198-4
- Rose, E., Carvalho, J. L., and Hecht, M. (2020). Mechanisms of DNA Repair in Trypanosoma Cruzi: What Do We Know so Far? *DNA Repair* 91-92 (July), 102873. doi: 10.1016/j.dnarep.2020.102873

- Schenkman, S., Eichinger, D., Pereira, M. E., and Nussenzweig, V. (1994). Structural and functional properties of Trypanosoma trans-sialidase. *Annu. Rev. Microbiol.* 48, 499–523. doi: 10.1146/annurev.mi.48.100194.002435
- Schwabl, P., Imamura, H., Van den Broeck, F., Costales, J. A., Maiguashca-Sánchez, J., Miles, M. A., et al. (2019). Meiotic Sex in Chagas Disease Parasite Trypanosoma Cruzi. *Nat. Commun.* 10 (1), 3972. doi: 10.1038/s41467-019-11771-z
- Sfeir, A., and Symington, L. S. (2015). Microhomology-Mediated End Joining: A Back-up Survival Mechanism or Dedicated Pathway? *Trends Biochem. Sci.* 40 (11), 701–714. doi: 10.1016/j.tibs.2015.08.006
- Steinbiss, S., Silva-Franco, F., Brunk, B., Foth, B., Hertz-Fowler, C., Berriman, M., et al. (2016). Companion: A Web Server for Annotation and Analysis of Parasite Genomes. *Nucleic Acids Res.* 44 (W1), W29–W34. doi: 10.1093/nar/gkw292
- Stoco, P. H., Wagner, G., Talavera-Lopez, C., Gerber, A., Zaha, A., Thompson, C. E., et al. (2014). Genome of the Avirulent Human-Infective Trypanosome—Trypanosoma Rangeli. *PLoS Neglect. Trop. Dis.* 8 (9), e3176. doi: 10.1371/journal.pntd.0003176
- Talavera-López, C., Reis-Cunha, J. L., Messenger, L. A., Lewis, M. D., Yeo, M., Bartholomeu, D. C., et al. (2018). Repeat-Driven Generation of Antigenic Diversity in a Major Human Pathogen, Trypanosoma Cruzi. *BioRxiv* 283531. doi: 10.1101/283531
- Tibayrenc, M., and Ayala, F. J. (1991). Towards a Population Genetics of Microorganisms: The Clonal Theory of Parasitic Protozoa. *Parasitol. Today* 7 (9), 228–232. doi: 10.1016/0169-4758(91)90234-F
- Tibayrenc, M., and Ayala, F. J. (2015). The Population Genetics of Trypanosoma Cruzi Revisited in the Light of the Predominant Clonal Evolution Model. *Acta Tropica* 151 (November), 156–165. doi: 10.1016/j.actatropica.2015.05.006
- Tibayrenc, M., Kjellberg, F., and Ayala, F. J. (1990). A Clonal Theory of Parasitic Protozoa: The Population Structures of Entamoeba, Giardia, Leishmania, Naegleria, Plasmodium, Trichomonas, and Trypanosoma and Their Medical and Taxonomical Consequences. *Proc. Natl. Acad. Sci. U. States America* 87 (7), 2414–2418. doi: 10.1073/pnas.87.7.2414
- Villanueva, M. S., Williams, S. P., Beard, C. B., Richards, F. F., and Aksoy, S. (1991). A New Member of a Family of Site-Specific Retrotransposons Is Present in the Spliced Leader RNA Genes of Trypanosoma Cruzi. *Mol. Cell. Biol.* 11 (12), 6139–6148. doi: 10.1128/MCB.11.12.6139
- Weatherly, D. B., Boehlke, C., and Tarleton, R. L. (2009). Chromosome Level Assembly of the Hybrid Trypanosoma Cruzi Genome. *BMC Genomics* 10 (June), 255. doi: 10.1186/1471-2164-10-255
- Weatherly, D. B., Peng, D., and Tarleton, R. L. (2016). Recombination-Driven Generation of the Largest Pathogen Repository of Antigen Variants in the Protozoan Trypanosoma Cruzi. *BMC Genomics* 17 (1), 729. doi: 10.1186/s12864-016-3037-z
- Weckselblatt, B., Hermetz, K. E., and Rudd, M. K. (2015). Unbalanced Translocations Arise from Diverse Mutational Mechanisms Including Chromothripsis. *Genome Res.* 25 (7), 937–947. doi: 10.1101/gr.191247.115
- Westenberger, S. J., Barnabé, C., Campbell, D. A., and Sturm, N. R. (2005). Two Hybridization Events Define the Population Structure of Trypanosoma Cruzi. *Genetics* 171 (2), 527–543. doi: 10.1534/genetics.104.038745
- WHO (2015). Available at: <http://www.who.int/wer/2015/wer9006/en/> (Accessed 6 February 2015).
- Yoshida, N., and Cortez, M. (2008). Trypanosoma cruzi: parasite and host cell signaling during the invasion process. *Subcellular Biochem.* 47, 82–91. doi: 10.1007/978-0-387-78267-6_6
- Zingales, B., a Miles, M., Campbell, D. A., Tibayrenc, M., Macedo, A. M., Teixeira, M. M. G., et al. (2012). The Revised Trypanosoma Cruzi Subspecific Nomenclature: Rationale, Epidemiological Relevance and Research Applications. *Infect. Genet. Evol.: J. Mol. Epidemiol. Evol. Genet. Infect. Dis.* 12 (2), 240–253. doi: 10.1016/j.meegid.2011.12.009

Conflict of Interest: The authors declare that the research was conducted in the absence of any commercial or financial relationships that could be construed as a potential conflict of interest.

Copyright © 2021 Talavera-López, Messenger, Lewis, Yeo, Reis-Cunha, Matos, Bartholomeu, Calzada, Saldaña, Ramírez, Guhl, Ocaña-Mayorga, Costales, Gorchakov, Jones, Nolan, Teixeira, Carrasco, Bottazzi, Hotez, Murray, Grijalva, Burleigh, Grisard, Miles and Andersson. This is an open-access article distributed under the terms of the Creative Commons Attribution License (CC BY). The use, distribution or reproduction in other forums is permitted, provided the original author(s) and the copyright owner(s) are credited and that the original publication in this journal is cited, in accordance with accepted academic practice. No use, distribution or reproduction is permitted which does not comply with these terms.



All Roads Lead to Cytosol: *Trypanosoma cruzi* Multi-Strategic Approach to Invasion

Gabriel Ferri¹ and Martin M. Edreira^{1,2,3*}

¹ CONICET-Universidad de Buenos Aires, IQUIBICEN, Ciudad de Buenos Aires, Argentina, ² Laboratorio de Biología Molecular de *Trypanosoma*, Departamento de Química Biológica, Facultad de Ciencias Exactas y Naturales, Universidad de Buenos Aires, Ciudad de Buenos Aires, Argentina, ³ Department of Pharmacology and Chemical Biology, School of Medicine, University of Pittsburgh, Pittsburgh, PA, United States

OPEN ACCESS

Edited by:

Gustavo Benaim,
Fundación Instituto de Estudios
Avanzados (IDEA), Venezuela

Reviewed by:

Marcel I. Ramirez,
Oswaldo Cruz Foundation
(Fiocruz), Brazil
Carlos A. Buscaglia,
Consejo Nacional de Investigaciones
Científicas y Técnicas (CONICET) y la
Universidad Nacional de General San
Martín, Argentina

*Correspondence:

Martin M. Edreira
mme2@pitt.edu

Specialty section:

This article was submitted to
Parasite and Host,
a section of the journal
Frontiers in Cellular and
Infection Microbiology

Received: 28 November 2020

Accepted: 27 January 2021

Published: 05 March 2021

Citation:

Ferri G and Edreira MM (2021)
All Roads Lead to Cytosol:
Trypanosoma cruzi Multi-Strategic
Approach to Invasion.
Front. Cell. Infect. Microbiol. 11:634793.
doi: 10.3389/fcimb.2021.634793

T. cruzi has a complex life cycle involving four developmental stages namely, epimastigotes, metacyclic trypomastigotes, amastigotes and bloodstream trypomastigotes. Although trypomastigotes are the infective forms, extracellular amastigotes have also shown the ability to invade host cells. Both stages can invade a broad spectrum of host tissues, in fact, almost any nucleated cell can be the target of infection. To add complexity, the parasite presents high genetic variability with differential characteristics such as infectivity. In this review, we address the several strategies *T. cruzi* has developed to subvert the host cell signaling machinery in order to gain access to the host cell cytoplasm. Special attention is made to the numerous parasite/host protein interactions and to the set of signaling cascades activated during the formation of a parasite-containing vesicle, the parasitophorous vacuole, from which the parasite escapes to the cytosol, where differentiation and replication take place.

Keywords: invasion, internalization, lysosome-mediated invasion, exocytic pathway, autophagic pathway, host signaling, host/parasite interaction

INTRODUCTION

Chagas Disease is a serious life-threatening disease caused by the protozoan parasite *Trypanosoma cruzi* and transmitted by blood-sucking triatomine insects from the Reduviidae family. In addition to an estimated of 6–8 million infected people and an alarming 50,000 deaths per year, 65–100 million people are living in areas at risk for infection (Lidani et al., 2019). This regional issue is now becoming global due to the migration of infected people to non-endemic countries, resulting in an estimated global economic burden of \$7.19 billion (Lee et al., 2013).

T. cruzi has a complex life cycle, involving an insect vector and a mammalian host. Typically, metacyclic trypomastigotes (MTs) gain access to the mammalian host through feces contamination at the insect bite wound. Upon internalization by the host cells close to the site of entry, MTs initially reside in a parasite-containing vesicle, the parasitophorous vacuole (TcPV), from which they escape to the host cell cytoplasm and differentiate into the proliferative amastigote form. After several rounds of replication, amastigotes differentiate into motile flagellated trypomastigotes, bloodstream (BSTs), or tissue culture-derived (TCTs) trypomastigotes, that are released into the

bloodstream, from where they could disseminate by infecting distant tissues or taken up by the triatomine vector during a bloodmeal (Monteón et al., 1996). Interestingly, although the parasite could potentially infect any nucleated cells, it has been demonstrated that different strains exhibit distinct tropism, measured as parasite load, for organs such as esophagus, liver, spleen, intestine, heart, and skeletal muscle, during acute phase of the infection, while tropism in the chronic phase has shown to be more homogeneous and restricted to intestine, skeletal muscle, and heart (Santi-Rocca et al., 2017). In this regard, it is worth to mention that adipocytes are also an important target cell during the acute phase of the disease, and may represent an important long-term reservoir for parasites during chronic infection (Combs et al., 2005). Additionally, it has been shown that amastigotes represent 10% of the parasites circulating in the blood of infected animals during the acute phase of infection (Andrews et al., 1987). Extracellular amastigotes (EAs), originated from premature rupture of infected cells or transformed from BSTs, are also infective and can disseminate in the infected hosts (Walker et al., 2014; Bonfim-Melo et al., 2018a).

In addition to a complex life cycle, *T. cruzi* has shown to be a remarkably heterogeneous taxon, that presents multiple strains with a high degree of genetic variability. This immense genetic diversity has been classified into six Discrete Typing Units (DTUs): the ancestral strains DTU-I and II, homozygote-derived hybrids DTU-III and IV, and heterozygote hybrids DTU-V and VI (Zingales et al., 2009). *T. cruzi*'s genome presents a conserved core of genes and extremely variable multigene surface proteins families (Berná et al., 2018). These multigene families are expanded in the genome, accordingly to its repetitive structure, and there is a rich source of diversity between different strains (De Pablos and Osuna, 2012). Among these families are the Trans-sialidase (TS) superfamily (about 1400 genes), the mucin family (about 860 genes), the Dispersed Gene Family-1 (DGF-1) family (565 genes) and the Mucin-Associated Surface Proteins (MASPs) family, which comprises around 1370 genes (El-Sayed et al., 2005; Kawashita et al., 2009). This incredible number of genes, coupled to tightly regulated post-transcriptional control of gene expression, are key players in the specific stage expression of the main surface constituents (Herrerros-Cabello et al., 2020). As a consequence of the great expansion of surface protein families, the parasite is able to interact with a large number of surface receptors on the different host cells, a fundamental requirement for invasion.

In the process of invasion, the parasite hijacks the host cellular functions with the ultimate goal of establishing the replicative niche. Several pathways, converging in the formation of the TcPV, have been implicated in host cell invasion (Barrias et al., 2013). In general, *T. cruzi* invasion can be divided into four major steps: 1) host cell recognition and adhesion, 2) parasite internalization, 3) TcPV formation and maturation, and 4) escape to the cytosol. In this review, we highlight the different host cell signaling pathways that the parasite exploits to promote internalization, TcPV formation and the establishment of a productive intracellular infection.

The focus will be first placed on three strategies that *T. cruzi* uses to hijack host cell signaling pathways to facilitate invasion:

1) Engagement of host cell surface receptors (Alba Soto and González Cappa, 2019); 2) Protein and molecule shedding, including microvesicles and other vesicles, such as exosomes (Borges et al., 2016; Watanabe Costa et al., 2016); and 3) Host cell plasma membrane mechanical wounding (Fernandes and Andrews, 2012). These events converge in preparing the cell for subsequent invasion. The display of redundant strategies is crucial because it guarantees an effective invasion by *T. cruzi*.

Second, attention will be placed on the strategies that lead to the internalization of the parasite. *T. cruzi* exploits three main mechanisms in the host cell to facilitate internalization: a) Ca^{2+} -dependent recruitment of lysosomes, b) Endocytosis, and c) Autophagy. As a result of the activation of these pathways, invading trypomastigotes end up localizing inside the TcPV. The mechanism for vacuolar escape is known to be lysosome- and pH- dependent, involving secretion of a porin-like/ complement 9-related factor TcTOX (Andrews, 1994). As an obligate intracellular parasite, ensuring cell integrity is essential for the establishment of a productive infection. Accordingly, signaling pathways are also manipulated to avoid apoptosis (Stahl et al., 2014).

Bidirectional signaling pathways are activated in both the parasite and the host cell during invasion. *T. cruzi* specific signal transduction pathways have recently been reviewed elsewhere (Schoijet et al., 2019). This review provides a general overview of the key parasite/host interactions and signaling pathways activated in the host cell during *T. cruzi* invasion, which are summarized in **Table 1** and **Figure 1**.

THE PRELUDE TO INVASION: HOST CELL RECOGNITION, ADHESION, AND ACTIVATION

Stage-Specific Surface Molecules

Early studies have shown that proteolytic treatment of trypomastigotes resulted in 90% inhibition of invasion, establishing a clear correlation between parasite surface proteins and infectivity (Andrews et al., 1984). Since then, several surface proteins have been identified and characterized. More recently, the first mass spectrometry-based exhaustive glycoproteome analysis of *T. cruzi* was completed, allowing the identification of 690 glycoproteins. Among them, 170 were exclusively identified in epimastigotes and 334 in trypomastigotes (Alves et al., 2017). In addition, it has been well established that every infective form of *T. cruzi* (MTs, TCTs and EAs) expresses on its surface a distinct set of stage-specific glycoproteins (Alba Soto and González Cappa, 2019). Several parasite stage-specific glycoprotein/host cell receptor interactions, and the corresponding signaling cascade activated in the host, are currently known (**Figure 1** and **Table 1**).

Metacyclic Trypomastigotes

- gp82

Among surface glycoproteins involved in the adhesion of *T. cruzi* to the host cell is gp82, a MT-specific virulence factor, member of the

TABLE 1 | Stage-specific proteins involved during invasion by *T. cruzi*.

| Stage | Molecule | Surface, secreted, or both | Signaling | Function | Ref. |
|--|------------|----------------------------|-----------------------------|--|--|
| <i>Metacyclic trypomastigotes (MTs)</i> | gp82 | Both | PLC, mTOR and PI3K | Ca ²⁺ and lysosome mobilization | (Teixeira and Yoshida, 1986; Cortez et al., 2014) |
| | gp90 | Both | | Inhibit gp82-mediated internalization | (Cordero et al., 2008; Martins et al., 2009; Rodrigues et al., 2017) |
| | gp35/50 | Both | | Ca ²⁺ elevation and actin cytoskeleton-dependent invasion | (Ramirez et al., 1993; Dorta et al., 1995; Ferreira et al., 2006) |
| | SAP | Secreted | | Enhance gp82-mediated internalization | (Baida et al., 2006; Zanforlin et al., 2013) |
| | TcSMP | Both | | Enhance gp82-mediated internalization | (Martins et al., 2015) |
| <i>Tissue-culture trypomastigotes (TCTs)</i> | TS and iTS | Both | PI3K/Akt and MAPK/Erk | Promotion of invasion and sialylation pattern | (Chuenkova et al., 2001; Butler et al., 2013; Campetella et al., 2020) |
| | Tc85 | Surface | ERK1/2 | Host cell attachment and invasion | (Magdesian et al., 2007; Mattos et al., 2014) |
| | TSSA | Surface | ERK1/2 | Host cell attachment and Ca ²⁺ signaling | (Cánepa et al., 2012a; Cámara et al., 2017) |
| | TcOPB | Secreted | PLC and Rac1 | Produces an unknown structure soluble factor that triggers Ca ²⁺ mobilization | (Caler et al., 1998; Motta et al., 2019) |
| <i>Extracellular amastigotes (EAs)</i> | Amastin | Surface | | Inhibit cell invasion | (Cruz et al., 2012) |
| | P21 | Secreted | ERK and PI3K | Phagocytosis and actin cytoskeleton remodeling | (Rodrigues et al., 2012; Teixeira T. L. et al., 2015) |
| | TcMVK | Secreted | P38/ERK and FAK/PAK | Protein glycosylation and cytoskeletal assembly | (Ferreira et al., 2016) |
| | Ssp-4 | Secreted | Rac1/WAVE2 and Cdc42/N-WASP | Associated with host cell invasion | (Florentino et al., 2018) |
| <i>TCTs and EAs</i> | TcPLA1 | Both | PKC | Lipid profile modification and amastigote development | (Wainszelbaum et al., 2001; Belaunzarán et al., 2007) |
| <i>All forms</i> | Cruzipain | Secreted | PI3K/Akt and MEK/ERK | Ca ²⁺ signaling | (Taketo et al., 1997; San Francisco et al., 2017) |

gp85/TS family (Teixeira and Yoshida, 1986; Cortez et al., 2012; Maeda et al., 2012). Gp82 is attached to the outer cell membrane of the parasite by a glycosylphosphatidylinositol (GPI) anchor, which is susceptible to cleavage by an endogenous phosphatidylinositol-specific phospholipase C (PI-PLC) and released into the extracellular medium (Bayer-Santos et al., 2013a). During the MTs invasion process, secreted, and/or surface-anchored gp82 molecules interact with a host receptor and trigger signaling pathways leading to intracellular Ca²⁺ and lysosome mobilization in the host cell (Manque et al., 2003). Gp82 mediates the mobilization of Ca²⁺ from thapsigargin-sensitive intracellular stores (Yoshida et al., 2000). The activation of PLC in the host cell generates diacylglycerol (DAG) and inositol 1,4,5-trisphosphate (IP3), which induces protein kinase C (PKC) and promotes the release of Ca²⁺ from IP3-sensitive compartments (Maeda et al., 2012). Mammalian target of rapamycin (mTOR) and phosphatidylinositol 3-kinase (PI3K) are also activated during MTs invasion. The elevation in the cytosolic Ca²⁺ concentration triggered by these pathways, promotes actin cytoskeleton disruption

and lysosome mobilization to the cell periphery, both events promoting the internalization of the parasite (Martins et al., 2011; Cortez et al., 2014). The lysosome-associated membrane protein 2 (LAMP-2) has been recently identified as the host cell receptor for gp82 (Rodrigues et al., 2019). In this work, Rodrigues et al. have shown that antibodies directed against LAMP-2, but not to LAMP-1, significantly inhibit MTs internalization. Moreover, co-immunoprecipitation assays demonstrated that gp82 binds to LAMP-2 protein in a receptor-mediated manner (Rodrigues et al., 2019).

- gp90

Another key MTs surface glycoprotein is gp90, also a member of the gp85/TS superfamily, which in opposition to gp82, has a negative effect on parasite invasion (Bubis et al., 2018). Early studies have shown an inverse correlation between gp90 expression levels and MTs infectivity (Málaga and Yoshida, 2001). Moreover, monoclonal antibodies confirmed low levels of gp90 in a highly invasive strain (CL), while high expression of

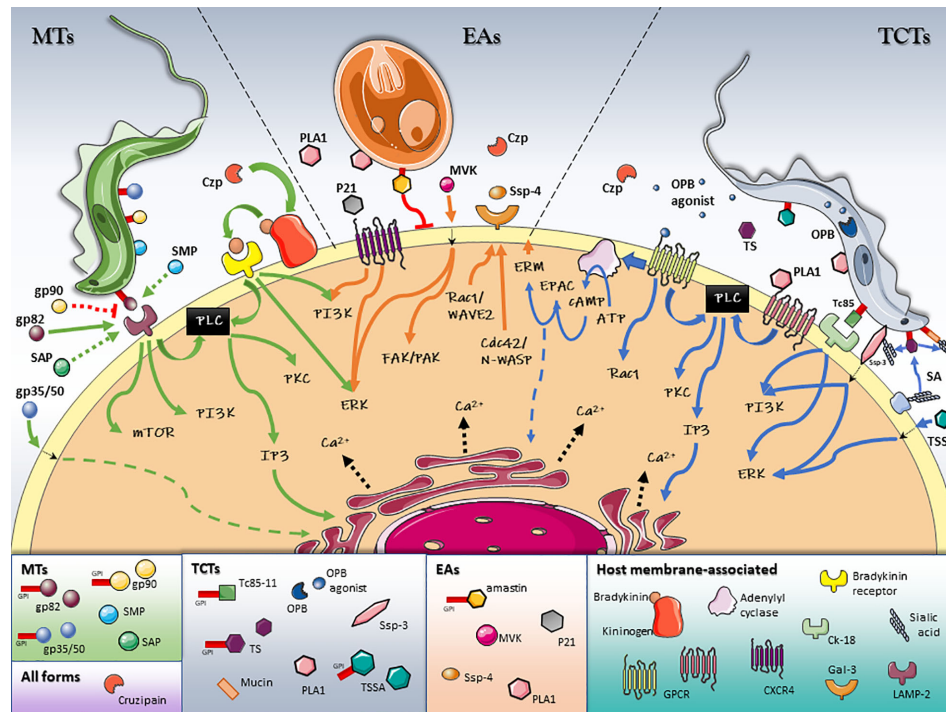


FIGURE 1 | Schematic model of *T. cruzi*/host cell protein interactions and activated signaling pathways during invasion. Stage-specific Surface Molecules expressed on the membrane of the parasite or shed into the extracellular medium, play an essential role in the recognition, adhesion and activation of signaling pathways that lead to a successful invasion of the host cell. Figures were created using images from Servier Medical Art Commons Attribution 3.0 Unported License. (<http://smart.servier.com>). Servier Medical Art by Servier is licensed under a Creative Commons Attribution 3.0 Unported License.

gp90 was observed in a poor invasive strain (G) (Ruiz et al., 1998). Although gp90 binds to the host cell, it fails to trigger cytosolic Ca^{2+} mobilization (Ruiz et al., 1998). The inhibition of host cell lysosome spreading has been recently proposed as the mechanism by which gp90 exerts its down-regulatory role (Rodrigues et al., 2017).

- gp35/50

Gp35/50 mucins are highly glycosylated proteins expressed by MTs forms of *T. cruzi* (Ramirez et al., 1993). Like gp82, gp35/50 has the ability to trigger intracellular Ca^{2+} elevation when binding to host cell (Dorta et al., 1995; Ruiz et al., 1998). However, gp35/50-mediated invasion induces actin recruitment, in contrast to gp82, that triggers signaling pathways leading to disassembly of F-actin (Ferreira et al., 2006). In addition, high level expression of gp35/50 was found to be inversely correlated to infectivity (Ruiz et al., 1998), although, when treatment of MTs with neuraminidase was applied before invasion assays, an increase in infectivity was observed, probably due to the fact that desialylated gp35/50 can interact with the host cell (Yoshida et al., 1997).

Cell-Derived Trypomastigotes

- Trans-sialidase

Among the different surface molecules involved in TCTs invasion is the unique *T. cruzi* trans-sialidase (TS), an important parasite virulence factor. Unable to synthesize sialic

acid (SA), TS enables TCTs to transfer terminal SA residues linked $\alpha 2,3$ to terminal β -galactopyranoses from host cell donor macromolecules to glycans of mucin-type proteins displayed on the parasite membrane (Schenkman et al., 1991; da Fonseca et al., 2019; Campetella et al., 2020). The generation of a sialylated surface plays a central role in promoting the evasion of immune responses, favoring survival and the establishment of the chronic disease (Nardy et al., 2016). In addition, the transference of SA to the parasite surface creates the Stage-Specific Epitope 3 (Ssp-3) that promotes invasion of the host cell (Schenkman et al., 1991). TS has also been postulated as counter-receptor for TCTs binding to $\alpha 2,3$ -sialyl receptors on the host cell, as a prelude to *T. cruzi* invasion (Ming et al., 1993). Signaling pathways implicated in TS mediated promotion of invasion includes the PI3K/AKT (Chuenkova et al., 2001; Butler et al., 2013) and the MAPK/ERK (mitogen-activated protein kinase/extracellular regulated kinase) pathways (Chuenkova and Pereira, 2001). Furthermore, shedding of TS into the bloodstream allows *T. cruzi* to manipulate the surface sialylation pattern of the target cell and different cell types distant from the site of infection. This soluble form of TS has been involved, among other processes, in host immunomodulation and haematological alterations, mainly by disruption of cell surface sialyl homeostasis (Campetella et al., 2020). Moreover, differential TS expression and gene dosage between different *T. cruzi* strains, have been reported. In a murine model, highly virulent strains of the parasite, belonging

to DTU-VI, expressed and shed high amounts of TS, whereas the opposite was observed in mice infected by the low-virulence DTU-I strains (Risso et al., 2004; Burgos et al., 2013). Intriguingly, a naturally occurring point mutation, the Y342H substitution, accounts for the lack of trans-sialylation activity that generates an inactive form of TS (iTS) (Cremona et al., 1995). Still, iTS behaves as a lectin-like protein, that maintains the ability to bind SA and β -galactose residues (Cremona et al., 1999). Experimental data strongly suggest that iTS confers alternative and/or complementary roles to TS in the parasite virulence and pathogenesis (Campetella et al., 2020).

- Tc85

Another TCTs surface molecule with affinity for the extracellular matrix is the Tc85 family (Giordano et al., 1999). Belonging to the gp85/TS superfamily, Tc85 proteins lack enzymatic activity and, although unable to transfer SA, they have been implicated in cell adhesion and invasion (Mattos et al., 2014). A Laminin-G like domain (LamG) at the C-terminus of gp85/TS seems to be responsible for binding different receptors present in the extracellular matrix and host cell surface (Teixeira A. A. R. et al., 2015). Two motifs in the LamG domain have been described: The FLY motif (VTvxNVxLYNRPLN), present at the C-terminus of Tc85 proteins, mediates the interaction with cytokeratins (Tonelli et al., 2010), and the TS9 motif that showed significant cell binding capacity (Teixeira A. A. R. et al., 2015). In particular, FLY has been implicated in cytokeratin remodeling, ERK1/2 signaling pathway activation and increased internalization (Magdesian et al., 2007). It was shown that the FLY interacts with the endothelium in an organ-dependent manner with significantly higher avidity for the heart vasculature (Tonelli et al., 2010). These results, and the fact that TS9 and FLY are separated from each other by approximately 100 amino acids in the primary sequence of the gp85/TS proteins, are in agreement with the idea that TS9 and FLY comprise a non-linear conformational binding site (Teixeira A. A. R. et al., 2015).

- TSSA

The trypomastigote small surface antigen (TSSA) is a small mucin-like protein from the TcMUC family of *T. cruzi* mucin genes, the main mucins on the surface of TCTs and the scaffolds of the Ssp-3 epitope (Buscaglia et al., 2004; Campo et al., 2006). Although TSSA is not a SA acceptor, it binds to mammalian cells and induces Ca^{2+} signaling (Cánepa et al., 2012a). There are four allelic variants (TSSA I-IV), each one corresponding to an ancestral DTU (I-IV), while in hybrid genomes (DTU V-VI) TSSA isoforms II and III can be found (Balouz et al., 2021). TSSAII showed higher adhesion to host cells than TSSAI. Furthermore, TSSAII elicited a much more rapid and sustained increase in intracellular Ca^{2+} and promoted a stronger stimulation of the ERK1/2 pathway, than TSSA I (Cánepa et al., 2012a). Mapping experiments and cell-binding assays revealed that at least two peptidic motifs are critical for the interaction of the “adhesive” TSSA variant to host cell surface receptor(s) prior to trypomastigote internalization. These observations were supported by the fact that transgenic trypomastigotes over-expressing the ‘adhesive’ TSSA displayed improved adhesion and infectivity towards non-macrophagic cell lines (Cámara et al., 2017).

Extracellular Amastigotes

- δ -Amastin

The amastin multi-gene family was originally identified by screening an amastigote cDNA library (Teixeira et al., 1994). In particular, δ -Amastin, a transmembrane glycoprotein highly expressed on the surface of intracellular amastigotes, has been implicated in EAs cell invasion and differentiation (Cruz et al., 2012). Although amastin is present in all sequenced *T. cruzi* strains (Cerqueira et al., 2008), transcript levels were found to be down-regulated in amastigotes of the G strain (Cruz et al., 2012; Kangussu-Marcolino et al., 2013). It was shown that recombinant δ -amastin binds to cells in a saturable and dose-dependent manner and was able to inhibit parasite internalization, suggesting a role for amastin in *T. cruzi* invasion (Cruz et al., 2012). Moreover, in transgenic EAs, the overexpression of amastin promoted liver tropism during *in vivo* infections in mice and accelerated amastigogenesis (Cruz et al., 2012). The involvement of amastins in *T. cruzi* virulence was also supported by knocking down δ -amastins in *Leshmania braziliensis*, which resulted in a decrease in survival and proliferation of intracellular parasites after *in vitro* macrophage infection and no detectable parasites after *in vivo* infections (de Paiva et al., 2015).

Protein Secretion and Extracellular Vesicles Cargo

Trypomastigotes (MTs and TCTs) and EAs shed a wide number of GPI-anchored surface proteins/glycoproteins such as members of the gp85/TS family, mucins and MASPs (Trocoli Torrecilhas et al., 2009; Cánepa et al., 2012b; Bayer-Santos et al., 2013b; Lantos et al., 2016; Watanabe Costa et al., 2016). These proteins are not secreted by the classical endoplasmic reticulum (ER)/Golgi-dependent secretion pathway, but instead, gradually released into milieu by the action of an endogenous PI-PLC (Andrews et al., 1988), or associated to extracellular vesicles (EVs) involved in host cell invasion, immunomodulation and pathogenesis (Borges et al., 2016; Torrecilhas et al., 2020).

EVs can be divided into: microvesicles or ectosomes (100 nm to 1 μ m), directly originated by budding from plasma membrane, and exosomes (30–100 nm), that are secreted following the fusion of multivesicular endosomes with the membrane at the flagellar pocket (Evans-Osses et al., 2015). Quantitative proteomic analysis revealed differences in protein content between these two populations of EVs (Bayer-Santos et al., 2013a). An interesting case is the trypomastigote excreted/secreted antigens (TESA), around 80 parasite proteins with the majority being highly immunogenic gp85s, associated with exosomal vesicles shed by MTs, TCTs, and intracellular amastigotes, used as a reagent in the diagnosis of the disease (Berrizbeitia et al., 2006; Bautista-López et al., 2017). Although EVs are secreted by all forms of *T. cruzi*, only those shed by infective forms are able to enhance internalization of host cells, by inducing intracellular Ca^{2+} mobilization (Moreira et al., 2019). Inoculation of EVs before infection in mice produced an increment of parasitemia in early days post-infection and more amastigote nests in mice hearts (Lovo-Martins et al., 2018). Moreover, it has been shown that vesicles from TCTs from the *T. cruzi* strains Colombiana (DTU I), YuYu (DTU I), Y (DTU II), and CL-14 (DTU VI) presented differences in their protein and α -galactosyl contents and were able to differentially modulate host's

immune responses and parasite invasion (Nogueira et al., 2015). Although all strains were capable of activating MAPKs like p38, JNK, and ERK 1/2, CL-14, and YuYu activated MAPKs *via* TLR2, while EVs from Colombiana and Y strains needed to be internalized to activate the MAPK pathway (Nogueira et al., 2015). Thus, the composition and effects of EVs on host cell seems to be strain-dependent.

In addition to glycoproteins, a substantial number of other molecules are released into the extracellular medium, like complement regulatory proteins (CRPs), cruzipain (Czp), peptidyl-prolyl cis-trans-isomerases, oligopeptidases and proteases, phospholipases A1 and C, P21, and amastigote specific proteins (Torrecilhas et al., 2012; Watanabe Costa et al., 2016).

Interesting examples are SAP (serine-, alanine-, and proline-rich protein) and TcSMP (*Trypanosoma cruzi* Surface Membrane Proteins), which have been involved in MTs invasion by binding to host cells and triggering Ca^{2+} signaling and lysosome mobilization (Baida et al., 2006; Zanforlin et al., 2013; Martins et al., 2015).

- SAP

Diverse paralogs of SAPs, with different cellular localization, are expressed in the different development stages of the parasite. In particular, SAP peptides were identified by mass spectrometry in vesicle and soluble-protein fractions from epimastigotes and MTs conditioned medium. Although, SAP transcript levels and protein expression in MTs were found to be twice as high as in epimastigotes, in agreement with their proposed role in cell adhesion and invasion (Zanforlin et al., 2013). In this regard, the fact that gp82 and SAP share the ability to induce Ca^{2+} signaling and lysosome mobilization, led to the hypothesis that both molecules display a synergistic effect in the process of MTs host-cell invasion (Baida et al., 2006; Zanforlin et al., 2013).

- TcSMP

Recently described, the TcSMP family, possesses two main features typical of surface proteins, an N-terminal signal peptide and a C-terminal hydrophobic sequence, predicted to be a transmembrane domain, rather than the most prevalent GPI anchoring (Martins et al., 2015). TcSMPs are expressed in all *T. cruzi* developmental stages, located at the surface and present in the secretome of epimastigotes and MTs. Similarly to SAP, TcSMPs have been shown to promote a weaker lysosome mobilization and parasite internalization than gp82, suggesting an auxiliary role in parasite invasion (Martins et al., 2015).

- TcPLA1

The membrane-associated phospholipase A1 (TcPLA1) can be also found in the extracellular medium of TCTs and EAs (Belaunzarán et al., 2007). Host cells exposed to the conditioned medium of EAs, TCTs, or recombinant TcPLA1, showed modified lipid profiles, with increased cellular concentrations of free fatty acids, diacylglycerol and lysophosphatidylcholine, that contributed to the concomitant activation of the PKC pathway (Belaunzarán et al., 2013). Remarkably, PKC has been previously implicated in parasite invasion, suggesting that Tc-PLA1 would participate in the events preceding host cell invasion (Watanabe Costa et al., 2016).

Peptidases

Peptidases, a class of hydrolytic enzymes responsible for breaking peptide bonds, has attracted the attention of distinct research groups because of their role in several crucial steps of the life cycle of the trypanosomatid parasites. The *T. cruzi* genome contains several families of peptidases that play central roles in diverse processes, such as adhesion and cell invasion (Alvarez et al., 2012; Rawlings et al., 2014).

- Cruzipain

Cruzipain (Czp), the most notorious cysteine peptidase, is expressed as a complex mixture of isoforms in all forms of *T. cruzi* and mainly located in lysosome-related organelles (Lima et al., 2012), have been shown to be required but not essential for invasion (San Francisco et al., 2017). Czp released by trypomastigote promotes invasion through its cysteine protease activity by producing bradykinin from membrane-bound kininogen on the surface of the host cell and triggering IP3-mediated Ca^{2+} signaling upon recognition by bradykinin B2 receptor (B_2R) (Scharfstein et al., 2000). More recently, a second cruzipain-mediated route, blocked by a cysteine protease inhibitor, thapsigargin and immunodepletion of Czp, but not by kinin receptor antagonists, was described for TCTs (Aparicio et al., 2004). Experimental data evidenced that this effect is mediated by a soluble trypomastigote-associated factor released by Czp (Aparicio et al., 2004).

- Oligopeptidase B

Oligopeptidase B (OPB), a serine endopeptidase from the prolyl oligopeptidase family, is conserved in trypanosomatids but not present in any mammalian genome (Motta et al., 2019). OPB has a cytosolic localization and there is not any strong evidence suggesting its secretion by the parasite. Instead, it has been involved in the cytoplasmatic processing of a trypomastigote-specific precursor that generates a soluble factor of unknown structure which is shed by TCTs (Burleigh et al., 1997).

Upon binding to the host cell receptor, the OPB-agonist induces PLC activation and an IP3-dependent release of Ca^{2+} from intracellular stores. This Ca^{2+} mobilization promotes lysosomal recruitment to the entry site and F-actin filaments disruption, both events associated with an increased parasite invasion (Burleigh et al., 1997; Caler et al., 1998). Surprisingly, even today, with genomes of several *T. cruzi* strains available, the identity of the precursor it is still unknown. However, the secretion of OPB cannot be ruled out since OPB activity has been found in trypomastigotes supernatants (Fernandes et al., 2005; Motta et al., 2019). *Trypanosoma brucei* and *Trypanosoma evansi* OPBs, are released into the extracellular milieu and contribute to pathogenesis by hydrolyzing host circulating factors (Motta et al., 2019). In the case of *T. cruzi*, hydrolyzed peptides would mimics ligands capable of activating GPCR and/or RTK (Motta et al., 2019).

EAs Specific Proteins

EAs are capable of invading mammalian cells in an actin-dependent mechanism, forming a phagocytic cup that engulfs the parasite (Mortara et al., 2005). Secreted proteins from EAs, such as P21, mevalonate kinase (TcMVK) and specific-surface

protein 4 (Ssp-4), mediate host cell signaling during the phagocytosis-like mechanism of invasion (Rodrigues et al., 2012; Ferreira et al., 2016; Florentino et al., 2018).

- P21

P21 is a 21kDa protein expressed in all developmental stages of *T. cruzi* and secreted by EAs to induce host cell invasion (da Silva et al., 2009). Evidence for this observation came from the use of a recombinant version of P21 (rP21) that bound to the CXCR4 chemokine receptor and promoted phagocytosis by induction of actin cytoskeleton polymerization and the modulation of the expression of actin-related genes in a PI3K-dependent manner (Rodrigues et al., 2012; Teixeira et al., 2017). In addition, in mice infections with the *T. cruzi* naturally attenuated TCC strain, rP21 lead to an exacerbated infection and parasite load in target organs (Brandán et al., 2019).

- TcMVK

MVK is a key enzyme involved in the early steps of the sterol isoprenoids biosynthesis pathway (Ferreira et al., 2016). In *T. cruzi*, TcMVK localizes to glycosomes, and may be also secreted into the extracellular milieu where it modulate host cell invasion, independently of its catalytic function. More precisely, TcMVK activates the actin-related kinases FAK (focal adhesion kinase) and PAK (p21-activated kinase), and the MAPK pathway components, ERK, and p38 to promote EAs internalization (Ferreira et al., 2016).

- Ssp-4

Ssp4 is a major surface GPI-anchored glycoprotein that is secreted by the EAs (Andrews et al., 1987). Although EAs Ssp-4 expression does not correlate with infectivity, glycosylation of Ssp-4 was associated with host cell invasion. It has been shown that only EAs from highly infective strains secreted a differentially glycosylated Ssp-4 into vesicle trails at the site of entry, contributing to Galectin-3 (Gal-3) recruitment and establishing a physical link between the parasite and the host cell surface (Florentino et al., 2018). Gal-3, a 31kDa β -galactoside-binding protein, is recruited to the site of EAs entry during cell invasion and participates in the intracellular trafficking of the parasite (Machado et al., 2014).

Plasma Membrane Damage

It has been proposed that flagellar motility of trypomastigotes strongly attached to the host cells surface through their posterior end produces membrane damage in the host cell. An active gliding motility of parasites firmly attached to host cells was evidenced using time-lapse phase-contrast live images of trypomastigotes interacting with a HeLa cells (Fernandes et al., 2011). Supporting evidence was also obtained from the analysis of scanning electron microscopy images of *T. cruzi* during early steps of invasion, showing parasites gliding under cells or in close contact with the plasma membrane at the cell periphery (Fernandes et al., 2011). Parasite-mediated membrane damage triggers Ca^{2+} -dependent fusion of lysosomes and internalization through Plasma Membrane Repair Mechanism (PMR), that will be discussed below.

HIJACKING HOST'S SIGNALING MACHINERY

To maintain homeostasis, host cells have a complex vesicular transport system, that consist of multiple connected networks with different levels of cross-talk (Salimi et al., 2020). *T. cruzi* has developed the ability of subverting and exploiting the most suitable mechanism at the time of invasion to gain access to the host cell (Figure 2). Three main mechanisms of internalization, involving several coordinated and integrated pathways, are used by the parasite to gain access to the target cell: 1) Ca^{2+} -mediated recruitment and fusion of lysosomes to the entry site (Figures 2.1–3), 2) Endocytosis of plasma membrane (Figures 2.4–7) and 3) Autophagy (Figure 2.8).

It is important to note that regardless of the parasite strain, the developmental stage, the repertoire of surface/secreted molecules expressed and the signaling cascades activated to prepare the host cell for invasion, all the internalization mechanisms lead to the biogenesis of TcPV (Batista et al., 2020). Moreover, despite the invasion mechanism as well, the acquisition of lysosome markers by the TcPV during the process of internalization has shown to be essential for intracellular retention of the parasite and the establishment of a successful infection (Andrade and Andrews, 2004).

Plasma Membrane Repair Mechanism

In order to maintain cellular homeostasis, membrane disruptions are rapidly resealed by a conserved PMR. Upon wounding, toxic levels of Ca^{2+} and oxidants from the extracellular milieu enter the cell. To avoid cell death, the damage is rapidly repaired by an extracellular Ca^{2+} -induced recruitment of intracellular vesicles (Blazek et al., 2015) (Figures 2.1–3). It has been shown that conventional lysosomal exocytosis mediates the resealing in primary skin fibroblasts (Reddy et al., 2001). After wounding, Ca^{2+} -dependent fusion of lysosomes to the host cell membrane was evidenced by the exposure of the luminal domain of lysosomal LAMP-1 and Synaptotagmin isoform VII (SytVII), a putative Ca^{2+} sensor in exocytosis (Sugita et al., 2001).

Moreover, a SytVII regulation of lysosome Ca^{2+} -dependent exocytosis was evident by a dramatic inhibitory effect on plasma membrane resealing by antibodies directed against the cytosolic domain of this protein (Reddy et al., 2001). In addition to the exposure of lysosomal luminal proteins on the surface of the cell, the lysosomal enzyme Acid Sphingomyelinase (ASM) is secreted during cell injury and promotes plasma membrane repair (Tam et al., 2010) (Figures 2.1–3).

Invasion assays in the presence the pore-forming bacterial toxin Streptolysin O (SLO) increased parasite internalization, while bromoenol lactone (BEL), a lysosomal exocytosis inhibitor, strongly restrained invasion by *T. cruzi* trypomastigotes. Moreover, PMR and *T. cruzi* internalization have been shown to depend on the secretion of ASM, the lysosomal enzyme responsible for catalysing the breakdown of sphingomyelin to ceramide and phosphorylcholine in the outer leaflet of the plasma membrane (Tam et al., 2010; Fernandes et al., 2011). Lysosomal cysteine proteases cathepsin B and L are also secreted and may participate

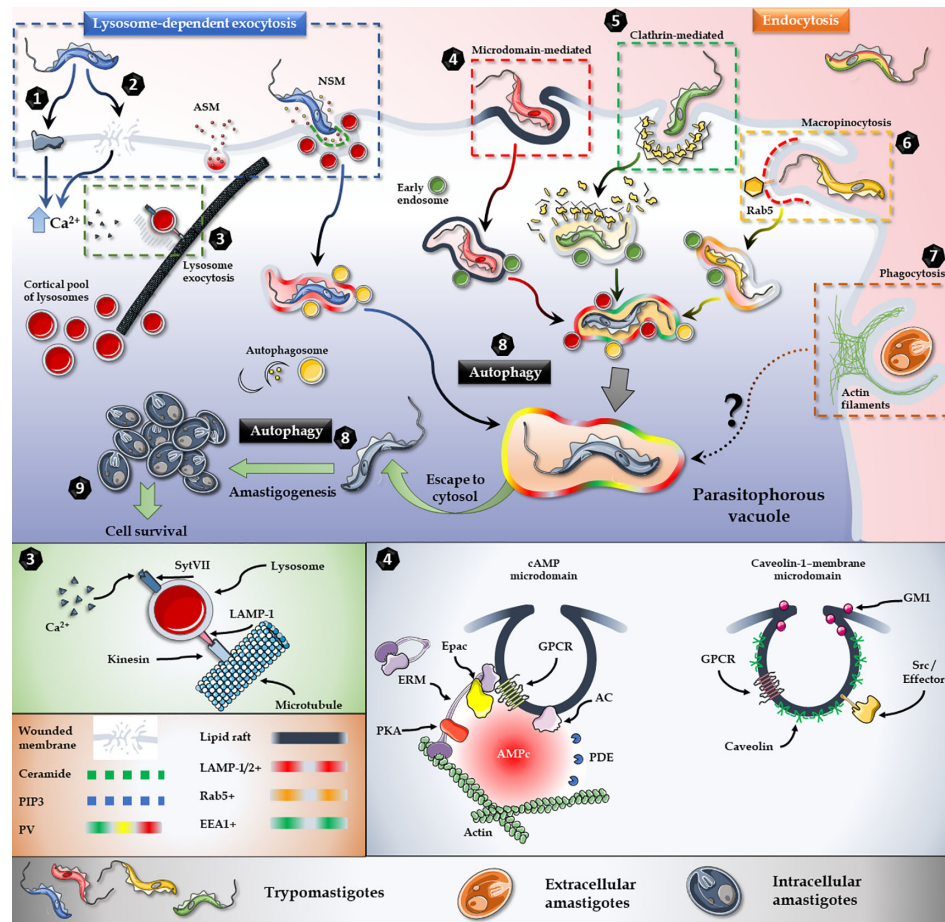


FIGURE 2 | *T. cruzi* invasion model. Lysosome exocytosis involves surface/secreted proteins (1) or micro-injuries (2) that trigger an elevation in the intracellular levels of Ca^{2+} and the microtubule/kinesin-mediated recruitment of lysosomes from surrounding areas to the parasite entry site (3). Host's Acid Sphingomyelinase (ASM) and a parasite Neutral Sphingomyelinase (NSM) are secreted to the extracellular milieu and participates in the breakdown of sphingomyelin to ceramide and phosphorylcholine in the outer leaflet of the plasma membrane (3). Endocytic mechanisms, such as lipid raft-dependent endocytosis (4), clathrin-mediated endocytosis (5) and macropinocytosis (6) also converge in the internalization of the parasite. Extracellular amastigotes, on the other hand, employ a phagocytosis-like mechanism for invasion (7). Moreover, autophagy is a key player during the invasion and also promotes trypomastigotes to amastigotes differentiation (8). In brief, regardless of the parasite stage, or the activated cascade, all internalization pathways culminate in the parasitophorous vacuole, from which parasite escapes to the cytoplasm and differentiates into amastigotes and proliferates (9). Figures were created using images from Servier Medical Art Commons Attribution 3.0 Unported License. (<http://smart.servier.com>). Servier Medical Art by Servier is licensed under a Creative Commons Attribution 3.0 Unported License.

in the repair process by facilitating membrane access of ASM (Castro-Gomes et al., 2016). As a result, surface staining with anti-ceramide monoclonal antibodies and EEA1 (early endosome-associated protein)-positive vesicles increased after treatment with extracellular ASM, suggesting that ceramide-enriched endocytic vesicles formation can facilitate trypomastigote entry. In the same line, inhibition of ASM reduced trypomastigote entry and this inhibition was reverted by the addition of extracellular sphingomyelinase (Fernandes et al., 2011). Proteomics studies have shown that trypomastigotes express and shed a neutral sphingomyelinase (Brossas et al., 2017) that might be contributing to the production of the required ceramide in the outer leaflet of the plasma membrane during host cell invasion by *T. cruzi*, although this hypothesis has not been yet explored. In accordance with the PMR-mediated invasion model, it was

recently reported that the parasite could modulate the expression of plasma membrane repair-related proteins and the fold of change depends on the number of parasites interacting with the host cell (Brígido et al., 2017) (Figures 2.1–3).

Ca^{2+} -Dependent Lysosome Exocytosis

Originally considered terminal degradative organelles, lysosomes have been found to participate in many other cellular processes (Pu et al., 2016). The involvement of lysosomes in these different processes depends on their sub-cellular distribution and their ability to move throughout the cytoplasm (Pu et al., 2016). Lysosomes distribute in a rather immobile perinuclear pool and a more dynamic pool in the cell periphery (Cabukusta and Neefjes, 2018). Living cells video microscopy during TCTs host cell invasion showed a directional microtubule/kinesin-mediated migration of

lysosomes from surrounding areas to the parasite entry site (Rodríguez et al., 1996). It was later demonstrated that TCTs use the cortical pool of lysosomes in the invasion process (Hissa and Andrade, 2015) (**Figures 2.1–3**).

Membrane-associated rafts enriched in cholesterol and ganglioside GM1 have been also implicated in adhesion and internalization of all infective forms of *T. cruzi* (Barrias et al., 2007; Fernandes et al., 2007). Immunofluorescence analysis demonstrated a colocalization of GM1, flotillin 1, and caveolin 1 in the nascent TcPV, supporting the fact that membrane rafts participate in *T. cruzi* invasion (Barrias et al., 2007). Consistently, cholesterol involvement in the recruitment of lysosomes was evidenced using methyl-beta cyclodextrin (M β CD), a cholesterol-removing agent used for lipid raft disruption. Noteworthy, LAMP-2 has shown to play a major role in cholesterol and caveolin traffic, membrane repair and *T. cruzi* invasion. Cells lacking LAMP-2 showed deficiency in cholesterol delivered to the plasma membrane and an altered caveolin-1 distribution, both phenomena being refractory to TCTs invasion (do Couto et al., 2020). Similarly, MTs internalization was significantly reduced in LAMP-2-depleted HeLa cells (Cortez et al., 2016).

In MTs invasion of HeLa cells, lysosome biogenesis/scattering was stimulated upon interaction of the parasites with the host cell and a reduction in the number of cortical lysosomes negatively affected MTs invasion (Cortez et al., 2016), as previously reported for TCTs invasion of cardiomyocytes (Hissa et al., 2012; Hissa and Andrade, 2015). However, in the HeLa model, the stimulation of lysosome biogenesis/scattering diminished TCTs ability for invasion, whereas rapamycin-promoted lysosome accumulation at the perinuclear region led to a higher TCTs invasion (Cortez et al., 2016). While these observations may result contradictory, it is important to consider that different parasite strains have been used in order to establish the different models of invasion. *T. cruzi* invasion, already showed to be a complex process when only taking into account the different stages of the invading parasite. This complexity gets even higher when considering different DTUs, strains, the repertoire of surface/secreted molecules, and signaling pathways activated in the host cell. In this regard, differential infectivity has been reported for trypomastigotes of different strains (Cortez et al., 2012; Santi-Rocca et al., 2017); thus, it is not unlikely that a particular mechanism of invasion is exploited depending on the strain and host cell/tissue. For example, in contrast to the results reported for TCTs, the absence of extracellular Ca²⁺ had no effect on MTs invasion, while the presence of the pore-forming bacterial toxin SLO decreased MTs internalization (Rodrigues et al., 2019), strongly suggesting a PMR-independent mechanism of invasion for MTs.

Ca²⁺ release from cellular compartments, such as the endoplasmic reticulum, is accompanied by an activation of PLC and an elevation of intracellular cAMP levels. It has been shown that cAMP is able to potentiate the Ca²⁺-dependent exocytosis of lysosomes and lysosome-mediated cell invasion by *T. cruzi* (Rodríguez et al., 1999). In mammalian cells, both cAMP effector pathways, i.e., Protein Kinase A (PKA) and Exchange protein activated directly by cAMP (Epac), are involved in Ca²⁺-triggered exocytic events

(Seino and Shibasaki, 2005). Moreover, members of this latter pathway, including Rap1, have been localized to late endosomes/lysosomes (Pizon et al., 1994), and Epac-mediated Rap activation has been involved in regulated exocytosis in human sperm (Miro-Moran et al., 2012), insulin secretion (Tengholm and Gylfe, 2017) and pancreatic amylase release (Sabbatini et al., 2008). Accordingly, it was recently shown that Epac1-mediated signaling represents the main mechanism for cAMP-dependent host cell invasion by *T. cruzi* (Musikant et al., 2017). Additionally, ERM proteins (ezrin, radixin and moesin), which are essential for the cell cortex function and architecture by linking plasma membrane to the underneath actin cytoskeleton (McClatchey, 2014), have been associated to *T. cruzi* invasion (Ferreira et al., 2017). Confocal microscopy studies have shown that ERM proteins are recruited to the EA invasion site, where they co-localize with F-actin, and that depletion of host ERM proteins inhibited *T. cruzi* invasion in HeLa cells (Ferreira et al., 2017). Remarkably, radixin was identified as a scaffolding unit for cAMP effectors in the spatial regulation of cAMP-Epac1-Rap-mediated signaling (Gloerich et al., 2010; Hochbaum et al., 2011). A link between radixin and cAMP-Epac-mediated TCTs invasion was recently evidenced by blocking invasion in pre-treated NRK host cells with a 15 amino acid permeable peptide spanning Epac's minimal ERM-binding domain (Musikant et al., 2017). This observation was consistent with a co-localization of a pool of Epac1 and radixin, as a requirement for invasion. Also, F-actin regulation is in part due to the activity of the focal adhesion kinase (FAK), a cytoplasmic protein tyrosine kinase (PTK) that participates during invasion by *T. cruzi* (Melo et al., 2014) (**Figure 2.4**). Both, inhibition of FAK autophosphorylation or knockdown of FAK expression by siRNA in cardiomyocytes, led to a reduction in *T. cruzi* internalization, hence showing a key role of the FAK-mediated pathway in this process (Melo et al., 2014). FAK inhibition was associated with ERK1/2 dephosphorylation and F-actin rearrangement, suggesting a crosstalk between this signaling cascade and the MEK/ERK pathway (Onofre et al., 2019). Likewise, the interaction between HeLa cells and EAs induced N-WASP-dependent actin polymerization via PI3K/AKT and ERK but not SFK (Src family kinases) (Bonfim-Melo et al., 2018a). In opposition, previous works on cardiomyocytes have shown that Src was required for TCTs internalization (Melo et al., 2014). However, observations are not conclusive since internalization experiments were done using PP1 as Src inhibitor, which also blocks TGF- β -mediated cellular responses in a Src-independent fashion (Ming et al., 1995; Yoshida and Cortez, 2008; Ferrão et al., 2015; Silva et al., 2019).

Endocytic Pathways

Endocytic processes can be divided into different classes: clathrin-mediated, caveolae-mediated, membrane microdomain-mediated, macropinocytosis and phagocytosis (Chou et al., 2011). Several of these endocytic pathways are exploited by *T. cruzi* for invasion (Barrias et al., 2013) (**Figures 2.4–7**). Moreover, lysosome-independent endocytosis has been proposed to be the main entry mechanism for TCTs (Burleigh, 2005; Cortez et al., 2016).

- Phagocytosis

Experimental evidence showed that approximately 20 to 25% of the internalized trypomastigotes were associated to lysosomes, while

50% of the invading parasites exploited an alternative PI3-kinase-dependent mechanism of invasion, involving a host cell plasma membrane-derived vacuole enriched in the lipid products of class I PI3-kinases, Phosphatidylinositol 3-Phosphate PI3P/Phosphatidylinositol 3,4-bisphosphate (P3,4P2) (Woolsey et al., 2003). In this endocytic mechanism of internalization, downstream of cell entry the EEA1 marker was never associated to the parasite-containing vacuoles, instead, a gradual lysosomal fusion was revealed by the acquisition of lysosomal markers such as LAMP-1 and fluid-phase endocytic tracers from the lysosomal compartment (Woolsey et al., 2003). However, Rab5, a marker for early endosomes, was found to associate to a fraction of *T. cruzi*-containing vacuoles during and immediately following internalization. Likewise, the remaining 20% to 30% of the *T. cruzi*-containing vacuoles were positive for EEA1, the Rab5 effector, indicating that early endocytic pathway of internalization took place as well. Interestingly, it has been shown that the Toll-Like Receptor 2 (TLR2) was required to activate PI3K and Rab5 binding to early endosomes in the Rab5/Rab7-endosome-dependent invasion mechanism (Maganto-Garcia et al., 2008). Accordingly, a strong activation of PI3K and PKB/AKT was detected when cells were incubated with trypomastigotes or their isolated membranes (Wilkowsky et al., 2001). Noteworthy, *T. cruzi*-infected human macrophages shed EVs that enhance host cell TLR-2-mediated invasion (Cronemberger-Andrade et al., 2020).

EAs employ a phagocytosis-like mechanism when invading non-professional phagocytic cells (Fernandes et al., 2013), with positive participation of Cdc42, N-WASP, WAVE2, and Rac1, and negative regulation of RhoA (Bonfim-Melo et al., 2018b) (Figure 2.7). Furthermore, EAs interaction with HeLa cells produced an increase in ERK1/2 phosphorylation, while pre-treatment of HeLa cells with an ERK1/2 inhibitor had a negative effect on internalization. This results demonstrated a key role for that PI3K/AKT and ERK pathway during *T. cruzi* EA invasion (Ferreira et al., 2019), probably through activation of proteins that regulate microfilament remodelling such as calpain, FAK and cortactin (Bonfim-Melo et al., 2018a).

- Clathrin-Mediated Endocytosis

Clathrin-mediated endocytosis in *T. cruzi* internalization was recently evidenced (Barrias et al., 2019) (Figure 2.5). Clathrin-containing vesicles and actin filaments were localized at sites of parasites attachment and internalization and around the nascent TcPV. Accordingly, specific inhibition of clathrin-coated pit formation impaired *T. cruzi* internalization (Barrias et al., 2019).

- Macropinocytosis

Macropinocytosis, an actin-driven process originally described as a mechanism of non-specific uptake of fluid into large cytoplasmic vesicles, has also been implicated in host cell invasion by *T. cruzi* (King and Kay, 2019) (Figure 2.6). The nascent macropinosome accumulates PI3P and active Rab5, that regulates the fusion of membranous organelles at early stages of endocytosis (Feliciano et al., 2011). Signaling patches involving PIP3, Ras, and Rac direct actin polymerization to the periphery of the macropinocytic cup (Kay et al., 2018). The involvement of macropinocytosis as a mechanism of entry for *T. cruzi* was demonstrated by blocking

parasite internalization using macropinocytosis inhibitors, such as amiloride, rottlerin and IPA3 (Barrias et al., 2012). In accordance, the stimulation of macropinocytic activity through activation of PKC by PMA, showed an increased internalization of parasites (Barrias et al., 2012). Moreover, colocalization at entry sites of trypomastigotes with the Rab5 effector rabankyrin 5, tyrosine kinases, Pak1 and actin microfilaments, confirmed macropinosomes formation (Barrias et al., 2012).

Autophagic Pathway

Autophagy as an alternative pathway of internalization for *T. cruzi* was evidenced in starved cells, where the induction of autophagy was a positive modulator of invasion (Figure 2.8). On the other hand, the disruption of mammalian autophagy led to a reduction in infectivity (Salassa and Romano, 2019). The autophagy pathway consists of several coordinated and consecutive events: initiation, elongation, maturation, and fusion of lysosomes to the autophagosome. Upon activation, autophagosome biogenesis is initiated with the induction and nucleation of the phagophore, a double-membrane structure that grows to engulf the autophagic cargo, and the recruitment of the core autophagy machinery (Dikic and Elazar, 2018). Lipidated LC3-II is required in autophagosome biogenesis, and since it forms a stable association with the membrane of autophagosomes it is used as a marker for autophagy (Tanida et al., 2008). The presence of LC3 in the membrane of the TcPV during the internalization process showed a connection between the TCTs and the host-cell autophagic pathway (Romano et al., 2009). Accordingly, infection was reduced in the absence of specific autophagy genes Atg5 or Beclin1, confirming the requirement of an autophagic-derived compartment in autophagy-mediated invasion (Romano et al., 2009). Moreover, starvation and rapamycin treatment induced an increase of LAMP-1 in *T. cruzi*-containing vesicles, indicating lysosomal association to TcPV and the consequent autolysosome formation were required for an increased internalization (Romano et al., 2009).

TcPV MATURATION AND ESCAPE TO CYTOSOL

Several proteins are recruited to the TcPV at different times during the biogenesis and maturation process (Batista et al., 2020). Within these proteins are the SNAREs, fusion proteins that regulate docking of granules and vesicles to target membranes including the plasma membrane (Wang et al., 2017). Vesicle associated membrane proteins 3 (VAMP3) and VAMP7, are consecutively recruited to the TcPV. VAMP3, usually present in recycling or early endosomes, is not essential for invasion, whereas SNARE complexes involving VAMP7, required for late endosome/lysosome fusion, are crucial in the establishment of *T. cruzi* infection (Cueto et al., 2017). Besides, early (Rab5, Rab22a, and Rab21 positive vesicles) and late (Rab7 and Rab39a) endocytic compartments, also recruited to the TcPV at early times post internalization, regulate the transit of the TcPV and promote fusion with lysosomes (Salassa et al.,

2020). TcPV maturation is characterized by an initial interaction with Rab5 and VAMP3-positive vesicles, followed by the recruitment of Rab7 and VAMP7, to finally fuse with lysosomes (Cueto et al., 2017; Salassa et al., 2020).

It is well established that fusion of lysosomes to the TcPV induces acidification that triggers the vacuole disruption and subsequent release of *T. cruzi* into the host cell cytosol (Ley et al., 1990). *T. cruzi* viability in the TcPV depends on a highly effective antioxidant defense machinery involving specialized antioxidant enzymes, such as peroxidases and superoxide dismutases (SODs), that protects the parasite against reactive oxygen and nitrogen species (Cardoso et al., 2016). Interestingly, oxidative stress has been shown to be an enhancer of *T. cruzi* infection in macrophages (Paiva et al., 2012). Although, a plausible hypothesis is that *T. cruzi* needs minimal levels of ROS, signaling for replication, while high levels of ROS are deleterious (Goes et al., 2016). Heavily sialylated LAMP-1 and 2, located in the inner coat of the TcPV, have been shown to protect the TcPV from lysis (Rubin-de-Celis et al., 2006). Additionally, LAMP-1 and 2 are essential to retain the intracellular parasite (Albertti et al., 2010) and avoid reversible invasion (Caradonna and Burleigh, 2011).

Under acidic conditions, the disruption of de TcPV occurs through the several *T. cruzi* proteins, such as secreted TS (Hall et al., 1992) and two pore-forming proteins, TcTOX (Andrews et al., 1990) and LYT1 (Manning-Cela et al., 2001). In TCTs, the expression of TS induces the escape from the TcPV by desialylation of LAMP-1 and 2, making membranes more susceptible to disruption by pore-forming proteins (Hall et al., 1992; Rubin-de-Celis et al., 2006). Pores are then formed by TcTOX and LYT1. Interestingly, TcTOX and LYT1 share similar characteristics: both are secreted, present cross-reactivity with C9 antibodies and have hemolytic activity at low PH. In fact, the molecular identity of TcTOX still remains unknown, and all available data suggest that LYT1 is TcTOX, or a TcTOX-like protein (Benabdellah et al., 2007; Friedrich et al., 2012).

Once in the cytoplasm, host cellular and metabolic pathways will be targeted by amastigotes in order to successfully replicate. Four to seven days post-invasion, amastigotes differentiate into the non-replicative infective trypomastigote form, that is released into the bloodstream (Caradonna et al., 2013; Li et al., 2016; Oliveira et al., 2020)

CONCLUDING REMARKS

Numerous works have endeavored to comprehend the molecular basis of *T. cruzi* invasion. Although some mechanisms involved in parasite/host interaction have been already described, a thorough understanding off the process would contribute to find new key players and provide a more diverse set of potential molecular targets against the disease. However, the evolution of this parasite has provided it with redundant and diverse molecular tools, able to interfere with multiple host cell pathways, to achieve a successful invasion.

The process of invasion begins with the recognition and adhesion of the parasite to the target cell. This interaction, reinforced by EVs and secreted proteins, leads to the activation of signaling pathways in the host cell that promote parasite internalization into an encasing vacuole, from which the parasite escapes to the cytosol where differentiation and replication take place.

Invasion has a pyramidal structure, in the base the diverse parasite/host protein interactions involved in internalization converge in the activation of a smaller set of signaling cascades and, regardless of the parasite strategy of internalization, all pathways end at the top of the pyramid with a parasite-containing vesicle to which lysosomes fuse to generate the parasitophorous vacuole. Little is known about the events that occur after TcPV is established, and a better understanding of this crucial mechanism may be the key to define new therapeutic targets against Chagas disease.

In this review, we address the several strategies *Trypanosoma cruzi*, the etiological agent of Chagas disease, has developed to subvert the host cell signaling pathways in order to gain access to the host cell cytoplasm, where replication and differentiation. Special attention is made to the numerous parasite/host protein interactions and the set of signaling cascades interfered during the formation of the parasitophorous vacuole. We first discuss the three strategies that *T. cruzi* exploits to trigger host cell signaling pathways to facilitate invasion: 1) Parasite surface/secreted proteins/host cell receptor interactions, 2) Protein shedding and 3) Host plasma membrane wounding. Later, strategies that lead to the internalization of the parasite, involving three main mechanisms: 1) Ca²⁺-dependent recruitment of lysosomes, 2) Endocytosis, and 3) Autophagy, are discussed. Finally, we examine the mechanisms by which the parasite escapes from the parasitophorous vacuole to establish a successful invasion. The topics discussed in this work were partially covered by other authors, however, we present a bigger picture, describing the complexity of the process considering genetic variability, strains, parasite/host interactions, signaling pathways activated and host cell. To our knowledge, this would be the more complete and updated review currently available.

AUTHOR CONTRIBUTIONS

GF and MME conceived, designed, and wrote the article. All authors contributed to the article and approved the submitted version.

FUNDING

This work was partially supported by the FIC-NIH award number R03TW009001.

ACKNOWLEDGMENTS

Authors would like to thank Dr. Daniel Altschuler from the University of Pittsburgh for his constant support.

REFERENCES

- Alba Soto, C. D., and González Cappa, S. M. (2019). "Trypanosoma cruzi Journey from the Insect Vector to the Host Cell," in *Chagas Disease: A Clinical Approach*. Eds. J. M. Altcheh and H. Freilij (Cham, Switzerland: Springer International Publishing), 25–59. doi: 10.1007/978-3-030-00054-7_2
- Alberti, L. A. G., Macedo, A. M., Chiari, E., Andrews, N. W., and Andrade, L. O. (2010). Role of Host Lysosomal Associated Membrane Protein (LAMP) in Trypanosoma Cruzi Invasion and Intracellular Development. *Microbes Infect.* 12 (10), 784–789. doi: 10.1016/j.micinf.2010.05.015
- Alvarez, V. E., Niemirówic, G. T., and Cazzulo, J. J. (2012). The Peptidases of Trypanosoma Cruzi: Digestive Enzymes, Virulence Factors, and Mediators of Autophagy and Programmed Cell Death. *Biochim. Biophys. Acta - Proteins Proteomics* 1824, 195–206. doi: 10.1016/j.bbapap.2011.05.011
- Alves, M. J. M., Kawahara, R., Viner, R., Colli, W., Mattos, E. C., Thaysen-Andersen, M., et al. (2017). Comprehensive Glycoproteomic Profiling of the Epimastigote and Trypomastigote Stages of Trypanosoma Cruzi. *J. Proteomics* 151, 182–192. doi: 10.1016/j.jprot.2016.05.034
- Andrade, L. O., and Andrews, N. W. (2004). Lysosomal Fusion Is Essential for the Retention of Trypanosoma Cruzi inside Host Cells. *J. Exp. Med.* 200 (9), 1135–1143. doi: 10.1084/jem.20041408
- Andrews, N. W., Katzin, A. M., and Colli, W. (1984). Mapping of Surface Glycoproteins of Trypanosoma Cruzi by Two-dimensional Electrophoresis: A Correlation with the Cell Invasion Capacity. *Eur. J. Biochem* 140, 599–604. doi: 10.1111/j.1432-1033.1984.tb08144.x
- Andrews, N. W., Hong, K. S., Robbins, E. S., and Nussenzweig, V. (1987). Stage-Specific Surface Antigens Expressed during the Morphogenesis of Vertebrate Forms of Trypanosoma Cruzi. *Exp. Parasitol.* 64, 474–484. doi: 10.1016/0014-4894(87)90062-2
- Andrews, N. W., Robbins, E., Ley, V., and Nussenzweig, V. (1988). Stage-Specific Surface Antigens during the Morphogenesis of Trypanosoma Cruzi: Developmentally Regulated Expression of a Glycosyl-Phosphatidylinositol Anchored Glycoprotein of Amastigotes. *Em Inst. Oswaldo Cruz* 83 (Suppl 1), 561–562. doi: 10.1590/s0074-02761988000500067
- Andrews, N. W., Abrams, C. K., Slatin, S. L., and Griffiths, G. (1990). A T. Cruzi-Secreted Protein Immunologically Related to the Complement Component C9: Evidence for Membrane Pore-Forming Activity at Low PH. *Cell* 61, 1277–1287. doi: 10.1016/0092-8674(90)90692-8
- Andrews, N. W. (1994). From Lysosomes into the Cytosol: The Intracellular Pathway of Trypanosoma Cruzi. *Braz. J. Med. Biol. Res.* 27 (2), 471–475.
- Aparicio, I. M., Scharfstein, J., and Lima, A. P. C. A. (2004). A New Cruzipain-Mediated Pathway of Human Cell Invasion by Trypanosoma Cruzi Requires Trypomastigote Membranes. *Infect. Immunity* 72, 5892–5902. doi: 10.1128/IAI.72.10.5892-5902.2004
- Baida, R. C. P., Carmo, M. S., Yoshida, N., Ferreira, D., Ferreira, A. T., El Sayed, N. M., et al. (2006). Molecular Characterization of Serine-, Alanine-, and Proline-Rich Proteins Of. *Society* 74 (3), 1537–1546. doi: 10.1128/IAI.74.3.1537
- Balouz, V., Bracco, L., Romer, G., Ricci, A. D., Agüero, F., and Buscaglia, C. (2021). Serological Approaches for Trypanosoma Cruzi Strain Typing. *Trends Parasitol.* 37, 214–225. doi: 10.1016/j.pt.2020.12.002
- Barrias, E. S., Dutra, J. M. F., De Souza, W., and Carvalho, T. M. U. (2007). Participation of Macrophage Membrane Rafts in Trypanosoma Cruzi Invasion Process. *Biochem. Biophys. Res. Commun.* 363 (3), 828–834. doi: 10.1016/j.bbrc.2007.09.068
- Barrias, E. S., Reignault, L. C., De Souza, W., and Carvalho, T. M. U. (2012). Trypanosoma Cruzi Uses Macropinocytosis as an Additional Entry Pathway into Mammalian Host Cell. *Microbes Infect.* 14 (14), 1340–1351. doi: 10.1016/j.micinf.2012.08.003
- Barrias, E. S., de Carvalho, T. M. U., and Souza, W. De (2013). Trypanosoma Cruzi: Entry into Mammalian Host Cells and Parasitophorous Vacuole Formation. *Front. Immunol* 4, 186. doi: 10.3389/fimmu.2013.00186
- Barrias, E., Reignault, L., de Carvalho, T. M. U., and de Souza, W. (2019). Clathrin Coated Pit Dependent Pathway for Trypanosoma Cruzi Internalization into Host Cells. *Acta Tropica* 199 (June), 105057. doi: 10.1016/j.actatropica.2019.105057
- Batista, M. F., Nájera, C. A., Meneghelli, I., and Bahia, D. (2020). The Parasitic Intracellular Lifestyle of Trypanosomatids: Parasitophorous Vacuole Development and Survival. *Front. Cell Dev. Biol.* 8, 396. doi: 10.3389/fcell.2020.00396
- Bautista-López, N. L., Ndao, M., Camargo, F. V., Nara, T., Annoura, T., Hardie, D. B., et al. (2017). Characterization and Diagnostic Application of Trypanosoma Cruzi Trypomastigote Excreted-Secreted Antigens Shed in Extracellular Vesicles Released from Infected Mammalian Cells. *J. Clin. Microbiol* 55, 744–758. doi: 10.1128/JCM.01649-16
- Bayer-Santos, E., Aguilar-Bonavides, C., Rodrigues, S. P., Maurício Cordero, E., Ferreira Marques, A., Varela-Ramirez, A., et al. (2013a). Proteomic Analysis of Trypanosoma Cruzi Secretome: Characterization of Two Populations of Extracellular Vesicles and Soluble Proteins. *J. Proteome Res.* 12 (2), 883–897. doi: 10.1021/pr300947g
- Bayer-Santos, E., Cunha-E-Silva, N. L., Yoshida, N., and Silveira, J. F. Da (2013b). Expression and Cellular Trafficking of GP82 and GP90 Glycoproteins during Trypanosoma Cruzi Metacyclogenesis. *Parasites Vectors* 6 (1), 1–10. doi: 10.1186/1756-3305-6-127
- Belaunzarán, M. L., Wainszelbaum, M. J., Lammel, E. M., Gimenez, G., Aloise, M. M., Florin-Christensen, J., et al. (2007). Phospholipase A1 from Trypanosoma Cruzi Infective Stages Generates Lipid Messengers That Activate Host Cell Protein Kinase C. *Parasitology* 134 (4), 491–502. doi: 10.1017/S0031182006001740
- Belaunzarán, M. L., Wilkowsky, S. E., Lammel, E. M., Giménez, G., Bott, E., Barbieri, M. A., et al. (2013). Phospholipase A1: A Novel Virulence Factor in Trypanosoma Cruzi. *Mol. Biochem. Parasitol.* 187, 77–86. doi: 10.1016/j.molbiopara.2012.12.004
- Benabdellah, K., González-Rey, E., and González, A. (2007). Alternative Trans-Splicing of the Trypanosoma Cruzi LYT1 Gene Transcript Results in Compartmental and Functional Switch for the Encoded Protein. *Mol. Microbiol.* 65 (6), 1559–1567. doi: 10.1111/j.1365-2958.2007.05892.x
- Berná, L., Rodríguez, M., Chiribao, M. L., Parodi-Tallice, A., Pita, S., Rijo, G., et al. (2018). Expanding an Expanded Genome: Long-Read Sequencing of Trypanosoma Cruzi. *Microbial Genomics* 4, e000177. doi: 10.1099/mgen.0.000177
- Berrizbeitia, M., Ndao, M., Bubis, J., Gottschalk, M., Aché, A., Lacouture, S., et al. (2006). Purified Excreted-Secreted Antigens from Trypanosoma Cruzi Trypomastigotes as Tools for Diagnosis of Chagas' Disease. *J. Clin. Microbiol.* 44, 291–296. doi: 10.1128/JCM.44.2.291-296.2006
- Blazek, A. D., Paleo, B. J., and Weisleder, N. (2015). Plasma Membrane Repair: A Central Process for Maintaining Cellular Homeostasis. *Physiology* 30, 438–448. doi: 10.1152/physiol.00019.2015
- Bonfim-Melo, A., Ferreira, E. R., Florentino, P. T. V., and Mortara, R. A. (2018a). Amastigote Synapse: The Tricks of Trypanosoma Cruzi Extracellular Amastigotes. *Front. Microbiol.* 9, 2018.01341 (JUN). doi: 10.3389/fmicb.2018.01341
- Bonfim-Melo, A., Ferreira, E. R., and Mortara, R. A. (2018b). Rac1/WAVE2 and Cdc42/N-WASP Participation in Actin-Dependent Host Cell Invasion by Extracellular Amastigotes of Trypanosoma Cruzi. *Front. Microbiol.* 9, 2018.00360 (FEB). doi: 10.3389/fmicb.2018.00360
- Borges, B. C., Uehara, I. A., Dias, L. O. S., Brígido, P. C., da Silva, C. V., and Silva, M. J. B. (2016). Mechanisms of Infectivity and Evasion Derived from Microvesicles Cargo Produced by Trypanosoma Cruzi. *Front. Cell. Infect. Microbiol* 6, 161. doi: 10.3389/fcimb.2016.00161
- Brandán, C. P., Mesias, A. C., Acuña, L., Teixeira, T. L., and Silva, C. V. Da (2019). Evaluation of Pathogen P21 Protein as a Potential Modulator of the Protective Immunity Induced by Trypanosoma Cruzi Attenuated Parasites. *Memorias Do Instituto Oswaldo Cruz* 114 (4), 1–7. doi: 10.1590/0074-02760180571
- Brígido, R. T. e., Tavares, P. C. B., dos Santos, M. A., de Gouveia Santos, J., de Souza, M. A., Goulart, I. M. B., et al. (2017). Trypanosoma Cruzi Modulates Gene Expression of Plasma Membrane Repair-Related Proteins. *Acta Tropica* 153–157. doi: 10.1016/j.actatropica.2016.06.008
- Brossas, J. Y., Gulin, J. E. N., Bisio, M. M. C., Chapelle, M., Marinach-Patrice, C., Bordessoules, M., et al. (2017). Secretome Analysis of Trypanosoma Cruzi by Proteomics Studies. *PLoS One* 12 (10), 1–16. doi: 10.1371/journal.pone.0185504
- Bubis, J., Martínez, J. C., Calabokis, M., Ferreira, J., Sanz-Rodríguez, C. E., Navas, V., et al. (2018). The Gene Product of a Trypanosoma Equiperdum Ortholog of the CAMP-Dependent Protein Kinase Regulatory Subunit Is a Monomeric Protein That Is Not Capable of Binding Cyclic Nucleotides. *Biochimie* 146, 166–180. doi: 10.1016/j.biochi.2017.12.010

- Burgos, J. M., Risso, M. G., Brenière, S. F., Barnabé, C., Campetella, O., and Leguizamón, M. S. (2013). Differential Distribution of Genes Encoding the Virulence Factor Trans-Sialidase along Trypanosoma Cruzi Discrete Typing Units. *PLoS One* 8 (3), 9–11. doi: 10.1371/journal.pone.0058967
- Burleigh, B. A., Caler, E. V., Webster, P., and Andrews, N. W. (1997). A Cytosolic Serine Endopeptidase from Trypanosoma Cruzi Is Required for the Generation of Ca²⁺ Signaling in Mammalian Cells. *J. Cell Biol.* 136 (3), 609–620. doi: 10.1083/jcb.136.3.609
- Burleigh, B. A. (2005). Host Cell Signaling and Trypanosoma Cruzi Invasion: Do All Roads Lead to Lysosomes? *Sci. STKE* 2005, pe36. doi: 10.1126/stke.2932005pe36
- Buscaglia, C. A., Campo, V. A., Noia, J. M. Di, Torrecilhas, A. C. T., De Marchi, C. R., Ferguson, M. A. J., et al. (2004). The Surface Coat of the Mammal-Dwelling Infective Trypomastigote Stage of Trypanosoma Cruzi Is Formed by Highly Diverse Immunogenic Mucins. *J. Biol. Chem.* 279, 15860–15869. doi: 10.1074/jbc.M314051200
- Butler, C. E., de Carvalho, T. M. U., Grisard, E. C., Field, R. A., and Tyler, K. M. (2013). Trans-Sialidase Stimulates Eat Me Response from Epithelial Cells. *Traffic* 14 (7), 853–869. doi: 10.1111/tra.12078
- Cabukusta, B., and Neefjes, J. (2018). Mechanisms of Lysosomal Positioning and Movement. *Traffic* 19, 761–769. doi: 10.1111/tra.12587
- Caler, E. V., Avalos, S. V. De, Haynes, P. A., Andrews, N. W., and Burleigh, B. A. (1998). Oligopeptidase B-Dependent Signaling Mediates Host Cell Invasion by Trypanosoma Cruzi. *EMBO J.* 17 (17), 4975–4986. doi: 10.1093/emboj/17.17.4975
- Cámara, M. de I. M., Cánepa, G. E., Lantos, A. B., Balouz, V., Yu, H., Chen, X., et al. (2017). The Trypomastigote Small Surface Antigen (TSSA) Regulates Trypanosoma Cruzi Infectivity and Differentiation. *PLoS Neglect. Trop. Dis.* 11 (8), 1–21. doi: 10.1371/journal.pntd.0005856
- Campetella, O., Buscaglia, C. A., Mucci, J., and Leguizamón, M. S. (2020). Parasite-Host Glycan Interactions during Trypanosoma Cruzi Infection: Trans-Sialidase Rides the Show. *Biochim. Biophys. Acta - Mol. Basis Dis.* 1866 (5), 165692. doi: 10.1016/j.bbdis.2020.165692
- Campo, V. A., Buscaglia, C. A., Di Noia, J. M., and Frasch, A. C. C. (2006). Immunoc characterization of the Mucin-Type Proteins from the Intracellular Stage of Trypanosoma Cruzi. *Microbes Infect.* 8, 401–409. doi: 10.1016/j.micinf.2005.07.008
- Cánepa, G. E., Degese, M. S., Budu, A., Garcia, C. R. S., Buscaglia, C. A., Cánepa, G. E., et al. (2012a). Involvement of TSSA (Trypomastigote Small Surface Antigen) in Trypanosoma Cruzi Invasion of Mammalian Cells. *Biochem. J.* 444 (2), 211–218. doi: 10.1042/BJ20120074
- Cánepa, G. E., Mesías, A. C., Yu, H., Chen, X., Buscaglia, C. A., Cánepa, G. E., et al. (2012b). Structural Features Affecting Trafficking, Processing, and Secretion of Trypanosoma Cruzi Mucins. *J. Biol. Chem.* 287 (31), 26365–26376. doi: 10.1074/jbc.M112.354696
- Caradonna, K. L., Engel, J. C., Jacobi, D., Lee, C. H., and Burleigh, B. A. (2013). Host Metabolism Regulates Intracellular Growth of Trypanosoma Cruzi. *Cell Host Microbe* 13, 108–117. doi: 10.1016/j.chom.2012.11.011
- Caradonna, K. L., and Burleigh, B. A. (2011). Mechanisms of Host Cell Invasion by Trypanosoma Cruzi. *Adv. Parasitol.* 76, 33–61. doi: 10.1016/B978-0-12-385895-5.00002-5
- Cardoso, M. S., Reis-Cunha, J. L., and Bartholomeu, D. C. (2016). Evasion of the Immune Response by Trypanosoma Cruzi during Acute Infection. *Front. Immunol.* 6, 2015.00659 (JAN). doi: 10.3389/fimmu.2015.00659
- Castro-Gomes, T., Corrotte, M., Tam, C., and Andrews, N. W. (2016). Plasma Membrane Repair Is Regulated Extracellularly by Proteases Released from Lysosomes. *PLoS One* 11, e0152583. doi: 10.1371/journal.pone.0152583
- Cerqueira, G. C., Bartholomeu, D. C., DaRocha, W. D., Hou, L., Freitas-Silva, D. M., Renato Machado, C., et al. (2008). Sequence Diversity and Evolution of Multigene Families in Trypanosoma Cruzi. *Mol. Biochem. Parasitol.* 157, 65–72. doi: 10.1016/j.molbiopara.2007.10.002
- Chou, L. Y. T., Ming, K., and Chan, W. C. W. (2011). Strategies for the Intracellular Delivery of Nanoparticles. *Chem. Soc. Rev.* 40, 233–245. doi: 10.1039/c0cs00003e
- Chuenkova, M. V., Furnari, F. B., Cavenee, W. K., and Pereira, M. A. (2001). Trypanosoma Cruzi Trans-Sialidase: A Potent and Specific Survival Factor for Human Schwann Cells by Means of Phosphatidylinositol 3-Kinase/Akt Signaling. *Proc. Natl. Acad. Sci. U. S. A.* 98 (17), 9936–9941. doi: 10.1073/pnas.161298398
- Chuenkova, M. V., and Pereira, M. A. (2001). The T. Cruzi Trans-Sialidase Induces PC12 Cell Differentiation via MAPK/ERK Pathway. *NeuroReport* 12 (17), 3715–3718. doi: 10.1097/00001756-200112040-00022
- Combs, T. P., Shankar Mukherjee, N., De Almeida, C. J. G., Jelicks, L. A., Schubert, W., Lin, Y., et al. (2005). The Adipocyte as an Important Target Cell for Trypanosoma Cruzi Infection. *J. Biol. Chem.* 280, 24085–24094. doi: 10.1074/jbc.M412802200
- Cordero, E. M., Gentil, L. G., Crisante, G., Ramírez, J. L., Yoshida, N., Añez, N., et al. (2008). Expression of GP82 and GP90 Surface Glycoprotein Genes of Trypanosoma Cruzi during in Vivo Metacyclogenesis in the Insect Vector Rhodnius Prolixus. *Acta Tropica* 105 (1), 87–91. doi: 10.1016/j.actatropica.2007.08.004
- Cortez, C., Martins, R. M., Alves, R. M., Silva, R. C., Bilches, L. C., Macedo, S., et al. (2012). Differential Infectivity by the Oral Route of Trypanosoma Cruzi Lineages Derived from Y Strain. *PLoS Neglect. Trop. Dis.* 6 (10), e1804. doi: 10.1371/journal.pntd.0001804
- Cortez, C., Sobreira, T. J., Maeda, F. Y., and Yoshida, N. (2014). The Gp82 Surface Molecule of Trypanosoma Cruzi Metacyclic Forms. *Subcellular Biochem.* 74, 137–150. doi: 10.1007/978-94-007-7305-9
- Cortez, C., Real, F., and Yoshida, N. (2016). Lysosome Biogenesis/Scattering Increases Host Cell Susceptibility to Invasion by Trypanosoma Cruzi Metacyclic Forms and Resistance to Tissue Culture Trypomastigotes. *Cell. Microbiol.* 18 (5), 748–760. doi: 10.1111/cmi.12548
- Cremona, M. L., Sánchez, D. O., Frasch, A. C. C., and Campetella, O. (1995). A Single Tyrosine Differentiates Active and Inactive Trypanosoma Cruzi Trans-Sialidases. *Gene* 160, 123–128. doi: 10.1016/0378-1119(95)00175-6
- Cremona, M. L., Campetella, O., Sánchez, D. O., and Frasch, A. C. C. (1999). Enzymically Inactive Members of the Trans-Sialidase Family from Trypanosoma Cruzi Display β -Galactose Binding Activity. *Glycobiology* 9, 581–587. doi: 10.1093/glycob/9.6.581
- Cronemberger-Andrade, A., Xander, P., Soares, R. P., Pessoa, N. L., Campos, M. A., Ellis, C. C., et al. (2020). Trypanosoma Cruzi-Infected Human Macrophages Shed Proinflammatory Extracellular Vesicles That Enhance Host-Cell Invasion via Toll-Like Receptor 2. *Front. Cell. Infect. Microbiol.* 10:2020.00099 (March). doi: 10.3389/fcimb.2020.00099
- Cruz, M. C., Souza-Melo, N., da Silva, C. V., DaRocha, W. D., Bahia, D., Araújo, P. R., et al. (2012). Trypanosoma Cruzi: Role of δ -Amastin on Extracellular Amastigote Cell Invasion and Differentiation. *PLoS One* 7 (12), e51804. doi: 10.1371/journal.pone.0051804
- Cueto, J. A., Vannrell, M. C., Salassa, B. N., Nola, S., Galli, T., Colombo, M. I., et al. (2017). Soluble N-Ethylmaleimide-Sensitive Factor Attachment Protein Receptors Required during Trypanosoma Cruzi Parasitophorous Vacuole Development. *Cell. Microbiol.* 19 (6), e12713. doi: 10.1111/cmi.12713
- da Fonseca, L. M., da Costa, K. M., de Sousa Chaves, V., Freire-De-Lima, C. G., Morrot, A., Mendonça-Prevato, L., et al. (2019). Theft and Reception of Host Cell's Sialic Acid: Dynamics of Trypanosoma Cruzi Trans-Sialidases and Mucin-like Molecules on Chagas' Disease Immunomodulation. *Front. Immunol.* 10, 2019.00164 (February). doi: 10.3389/fimmu.2019.00164
- da Silva, C. V., Kawashita, S. Y., Probst, C. M., Dallagiovanna, B., Cruz, M. C., da Silva, E. A., et al. (2009). Characterization of a 21 KDa Protein from Trypanosoma Cruzi Associated with Mammalian Cell Invasion. *Microbes Infect.* 11, 563–570. doi: 10.1016/j.micinf.2009.03.007
- De Pablos, L. M., and Osuna, A. (2012). Multigene Families in Trypanosoma Cruzi and Their Role in Infectivity. *Infect. Immun.* 80 (7), 2258–2264. doi: 10.1128/IAI.06225-11
- de Paiva, R. M. C., Grazielle-Silva, V., Cardoso, M. S., Nakagaki, B. N., Mendonça-Neto, R. P., Canavaci, A. M. C., et al. (2015). Amastin Knockdown in Leishmania Braziliensis Affects Parasite-Macrophage Interaction and Results in Impaired Viability of Intracellular Amastigotes. *PLoS Pathog.* 11 (12), e1005296. doi: 10.1371/journal.ppat.1005296
- Dikic, I., and Elazar, Z. (2018). Mechanism and Medical Implications of Mammalian Autophagy. *Nat. Rev. Mol. Cell Biol.* 19, 349–364. doi: 10.1038/s41580-018-0003-4
- do Couto, N. F., Pedersane, D., Rezende, L., Dias, P. P., Corbani, T. L., Bentini, L. C., et al. (2020). Correction: LAMP-2 Absence Interferes with Plasma Membrane

- Repair and Decreases T. Cruzi Host Cell Invasion. *PLoS Neglect. Trop. Dis.* 14 (9), e0008724. doi: 10.1371/journal.pntd.0008724
- Dorta, M. L., Ferreira, A. T., Oshiro, M. E. M., and Yoshida, N. (1995). Ca²⁺ Signal Induced by Trypanosoma Cruzi Metacyclic Trypomastigote Surface Molecules Implicated in Mammalian Cell Invasion. *Mol. Biochem. Parasitol.* 73 (1–2), 285–289. doi: 10.1016/0166-6851(94)00123-5
- El-Sayed, N. M., Myler, P. J., Bartholomeu, D. C., Nilsson, D., Aggarwal, G., Tran, A. N., et al. (2005). The Genome Sequence of Trypanosoma Cruzi, Etiologic Agent of Chagas Disease. *Science* 309 (5733), 409–415. doi: 10.1126/science.1112631
- Evans-Osses, I., Reichembach, L. H., and Ramirez, M. I. (2015). Exosomes or Microvesicles? Two Kinds of Extracellular Vesicles with Different Routes to Modify Protozoan-Host Cell Interaction. *Parasitol. Res.* 114, 3567–3575. doi: 10.1007/s00436-015-4659-9
- Feliciano, W. D., Yoshida, S., Straight, S. W., and Swanson, J. A. (2011). Coordination of the Rab5 Cycle on Macropinosomes. *Traffic* 12, 1911–1922. doi: 10.1111/j.1600-0854.2011.01280.x
- Fernandes, L. C., Bastos, I. M. D., Lauria-Pires, L., Rosa, A. C. O., Teixeira, A. R. L., Grellier, P., et al. (2005). Specific Human Antibodies Do Not Inhibit Trypanosoma Cruzi Oligopeptidase B and Cathepsin B, and Immunoglobulin G Enhances the Activity of Trypomastigote-Secreted Oligopeptidase B. *Microbes Infect.* 7, 375–384. doi: 10.1016/j.micinf.2004.11.009
- Fernandes, M. C., Cortez, M., Yoneyama, K. A. G., Straus, A. H., Yoshida, N., and Mortara, R. A. (2007). Novel Strategy in Trypanosoma Cruzi Cell Invasion: Implication of Cholesterol and Host Cell Microdomains. *Int. J. Parasitol.* 37 (13), 1431–1441. doi: 10.1016/j.ijpara.2007.04.025
- Fernandes, M. C., Cortez, M., Flannery, A. R., Tam, C., Mortara, R. A., and Andrews, N. W. (2011). Trypanosoma Cruzi Subverts the Sphingomyelinase-Mediated Plasma Membrane Repair Pathway for Cell Invasion. *J. Exp. Med.* 208 (5), 909–921. doi: 10.1084/jem.20102518
- Fernandes, M. C., Flannery, A. R., Andrews, N., and Mortara, R. A. (2013). Extracellular Amastigotes of Trypanosoma Cruzi Are Potent Inducers of Phagocytosis in Mammalian Cells. *Cell. Microbiol.* 15 (6), 977–991. doi: 10.1111/cmi.12090
- Fernandes, M. C., and Andrews, N. W. (2012). Host Cell Invasion by Trypanosoma Cruzi: A Unique Strategy That Promotes Persistence. *FEMS Microbiol. Rev.* 36, 734–747. doi: 10.1111/j.1574-6976.2012.00333.x
- Ferrão, P. M., D'Avila-Levy, C. M., Araujo-Jorge, T. C., Degraive, W. M., Gonçalves, A. Da S., Garzoni, L. R., et al. (2015). Cruzipain Activates Latent TGF- β from Host Cells during T. Cruzi Invasion. *PLoS One* 10 (5), 1–15. doi: 10.1371/journal.pone.0124832
- Ferreira, D., Cortez, M., Atayde, V. D., and Yoshida, N. (2006). Actin Cytoskeleton-Dependent and -Independent Host Cell Invasion by Trypanosoma Cruzi Is Mediated by Distinct Parasite Surface Molecules. *Infect. Immun.* 74 (10), 5522–5528. doi: 10.1128/IAI.00518-06
- Ferreira, É. R., Horjales, E., Bonfim-Melo, A., Cortez, C., Da Silva, C. V., De Groote, M., et al. (2016). Unique Behavior of Trypanosoma Cruzi Mevalonate Kinase: A Conserved Glycosomal Enzyme Involved in Host Cell Invasion and Signaling. *Sci. Rep.* 6 (April), 1–13. doi: 10.1038/srep24610
- Ferreira, E. R., Bonfim-Melo, A., Cordero, E. M., and Mortara, R. A. (2017). ERM Proteins Play Distinct Roles in Cell Invasion by Extracellular Amastigotes of Trypanosoma Cruzi. *Front. Microbiol.* 8, 2017.02230 (NOV). doi: 10.3389/fmicb.2017.02230
- Ferreira, B. L., Ferreira, E. R., Bonfim-Melo, A., Mortara, R. A., and Bahia, D. (2019). Trypanosoma Cruzi Extracellular Amastigotes Selectively Trigger the PI3K/Akt and Erk Pathways during HeLa Cell Invasion. *Microbes Infect.* 21 (10), 485–489. doi: 10.1016/j.micinf.2019.06.003
- Florentino, P. T. V., Real, F., Orikaza, C. M., da Cunha, J. P. C., Vitorino, F. N. L., Cordero, E. M., et al. (2018). A Carbohydrate Moiety of Secreted Stage-Specific Glycoprotein 4 Participates in Host Cell Invasion by Trypanosoma Cruzi Extracellular Amastigotes. *Front. Microbiol.* 9, 2018.00693 (APR). doi: 10.3389/fmicb.2018.00693
- Friedrich, N., Hagedorn, M., Soldati-Favre, D., and Soldati, T. (2012). Prison Break: Pathogens' Strategies To Egress from Host Cells. *Microbiol. Mol. Biol. Rev.* 76, 707–720. doi: 10.1128/mmbr.00024-12
- Giordano, R., Fouts, D. L., Tewari, D., Colli, W., Manning, J. E., and Alves, M. J. M. (1999). Cloning of a Surface Membrane Glycoprotein Specific for the Infective Form of Trypanosoma Cruzi Having Adhesive Properties to Laminin. *J. Biol. Chem.* 274 (6), 3461–3468. doi: 10.1074/jbc.274.6.3461
- Gloerich, M., Ponsioen, B., Vliem, M. J., Zhang, Z., Zhao, J., Kooistra, M. R., et al. (2010). Spatial Regulation of Cyclic AMP-Epac1 Signaling in Cell Adhesion by ERM Proteins. *Mol. Cell. Biol.* 30 (22), 5421–5431. doi: 10.1128/mcb.00463-10
- Goes, G. R., Rocha, P. S., Diniz, A. R. S., Aguiar, P. H. N., Machado, C. R., and Vieira, L. Q. (2016). Trypanosoma Cruzi Needs a Signal Provided by Reactive Oxygen Species to Infect Macrophages. *PLoS Negl. Trop. Dis.* 10 (4), e0004555. doi: 10.1371/journal.pntd.0004555
- Hall, B. F., Webster, P., Ma, A. K., Joiner, K. A., and Andrews, N. W. (1992). Desialylation of Lysosomal Membrane Glycoproteins by Trypanosoma Cruzi: A Role for the Surface Neuraminidase in Facilitating Parasite Entry into the Host Cell Cytoplasm. *J. Exp. Med.* 176 (2), 313–325. doi: 10.1084/jem.176.2.313
- Herreros-Cabello, A., Callejas-Hernández, F., Gironès, N., and Fresno, M. (2020). Trypanosoma cruzi genome: Organization, multi-gene families, transcription, and biological implications. *Genes (Basel)* 11, 1196. doi: 10.3390/genes11101196
- Hissa, B., Duarte, J. G., Kelles, L. F., Santos, F. P., del Puerto, H. L., Gazzinelli-Guimarães, P. H., et al. (2012). Membrane Cholesterol Regulates Lysosome-Plasma Membrane Fusion Events and Modulates Trypanosoma Cruzi Invasion of Host Cells. *PLoS Neglect. Trop. Diseases* 6, e1583. doi: 10.1371/journal.pntd.0001583
- Hissa, B., and Andrade, L. de O. (2015). Trypanosoma Cruzi Uses a Specific Subset of Host Cell Lysosomes for Cell Invasion. *Parasitol. Int.* 64 (2), 135–138. doi: 10.1016/j.parint.2014.11.005
- Hochbaum, D., Barila, G., Ribeiro-Neto, F., and Altschuler, D. L. (2011). Radixin Assembles CAMP Effectors Epac and PKA into a Functional CAMP Compartment: Role in CAMP-Dependent Cell Proliferation. *J. Biol. Chem.* 286 (1), 859–866. doi: 10.1074/jbc.M110.163816
- Kangussu-Marcolino, M. M., Paiva, R. M. C. De, Araújo, P. R., De Mendonça-Neto, R. P., Lemos, L., Bartholomeu, D. C., et al. (2013). Distinct Genomic Organization, mRNA Expression and Cellular Localization of Members of Two Amastin Sub-Families Present in Trypanosoma Cruzi. *BMC Microbiol.* 13, 10. doi: 10.1186/1471-2180-13-10
- Kawashita, S. Y., da Silva, C. V., Mortara, R. A., Burleigh, B. A., and Briones, M. R. S. (2009). Homology, Paralogy and Function of DGF-1, a Highly Dispersed Trypanosoma Cruzi Specific Gene Family and Its Implications for Information Entropy of Its Encoded Proteins. *Mol. Biochem. Parasitol.* 165 (1), 19–31. doi: 10.1016/j.molbiopara.2008.12.010
- Kay, R. R., Williams, T. D., and Paschke, P. (2018). Amplification of Pip3 Signalling by Macropinosytic Cups. *Biochem. J.* 475, 643–648. doi: 10.1042/BCJ20170785
- King, J. S., and Kay, R. R. (2019). The Origins and Evolution of Macropinosytosis. *Philos. Trans. R. Soc. B: Biol. Sci.* 374, 20180158. doi: 10.1098/rstb.2018.0158
- Lantos, A. B., Carlevaro, G., Araoz, B., Diaz, P. R., de los Milagros Camara, M., Buscaglia, C. A., et al. (2016). Sialic Acid Glycobiology Unveils Trypanosoma Cruzi Trypomastigote Membrane Physiology. *PLoS Pathog.* 12 (4), e1005559. doi: 10.1371/journal.ppat.1005559
- Lee, B. Y., Bacon, K. M., Bottazzi, M. E., and Hotez, P. J. (2013). Global Economic Burden of Chagas Disease: A Computational Simulation Model. *Lancet Infect. Dis.* 13 (4), 342–348. doi: 10.1016/S1473-3099(13)70002-1
- Ley, V., Robbins, E. S., Nussenzweig, V., and Andrews, N. W. (1990). The Exit of Trypanosoma Cruzi from the Phagosome Is Inhibited by Raising the PH of Acidic Compartments. *J. Exp. Med.* 171 (2), 401–413. doi: 10.1084/jem.171.2.401
- Li, Y., Shah-Simpson, S., Okrah, K., Trey Belew, A., Choi, J., Caradonna, K. L., et al. (2016). Transcriptome Remodeling in Trypanosoma Cruzi and Human Cells during Intracellular Infection. *PLoS Pathog.* 12, e1005511. doi: 10.1371/journal.ppat.1005511
- Lidani, K. C. F., Andrade, F. A., Bavia, L., Damasceno, F. S., Beltrame, M. H., Messias-Reason, I. J., et al. (2019). Chagas Disease: From Discovery to a Worldwide Health Problem. *Front. Public Health* 7 (6), 166. doi: 10.3389/fpubh.2019.00166
- Lima, L., Ortiz, P. A., da Silva, F. M., Alves, J. M. P., Serrano, M. G., Cortez, A. P., et al. (2012). Repertoire, Genealogy and Genomic Organization of Cruzipain and Homologous Genes in Trypanosoma Cruzi, T. Cruzi-like and Other Trypanosome Species. *PLoS One* 7, e38385. doi: 10.1371/journal.pone.0038385
- Lovo-Martins, M. I., Malvezi, A. D., Zanluchi, N. G., Lucchetti, B. F. C., Tatakahara, V. L. H., Mörking, P. A., et al. (2018). Extracellular Vesicles

- Shed By Trypanosoma Cruzi Potentiate Infection and Elicit Lipid Body Formation and PGE2 Production in Murine Macrophages. *Front. Immunol.* 9, 896. doi: 10.3389/fimmu.2018.00896
- Machado, F. C., Cruz, L., Da Silva, A. A., Cruz, M. C., Mortara, R. A., Roque-Barreira, M. C., et al. (2014). Recruitment of Galectin-3 during Cell Invasion and Intracellular Trafficking of Trypanosoma Cruzi Extracellular Amastigotes. *Glycobiology* 24 (2), 179–184. doi: 10.1093/glycob/cwt097
- Maeda, F. Y., Cortez, C., and Yoshida, N. (2012). Cell Signaling during Trypanosoma Cruzi Invasion. *Front. Immunol.* 3361. doi: 10.3389/fimmu.2012.00361
- Maganto-Garcia, E., Punzon, C., Terhorst, C., and Fresno, M. (2008). Rab5 Activation by Toll-Like Receptor 2 Is Required for Trypanosoma Cruzi Internalization and Replication in Macrophages. *Traffic* 9, 1299–1315. doi: 10.1111/j.1600-0854.2008.00760.x
- Magdesian, M. H., Tonelli, R. R., Fessel, M. R., Silveira, M. S., Schumacher, R. I., Linden, R., et al. (2007). A Conserved Domain of the Gp85/Trans-Sialidase Family Activates Host Cell Extracellular Signal-Regulated Kinase and Facilitates Trypanosoma Cruzi Infection. *Exp. Cell Res.* 313 (1), 210–218. doi: 10.1016/j.yexcr.2006.10.008
- Málaga, S., and Yoshida, N. (2001). Targeted Reduction in Expression of Trypanosoma Cruzi Surface Glycoprotein Gp90 Increases Parasite Infectivity. *Infect. Immun.* 69 (1), 353–359. doi: 10.1128/IAI.69.1.353-359.2001
- Manning-Cela, R., Cortés, A., González-Rey, E., Van Voorhis, W. C., Swindle, J., and González, A. (2001). LYT1 Protein Is Required for Efficient In Vitro Infection by Trypanosoma Cruzi. *Infect. Immun.* 69 (6), 3916–3235. doi: 10.1128/IAI.69.6.3916
- Manque, P. M., Neira, I., Atayde, V. D., Cordero, E., Ferreira, A. T., Da Silveira, J. F., et al. (2003). Cell Adhesion and Ca²⁺ Signaling Activity in Stably Transfected Trypanosoma Cruzi Epimastigotes Expressing the Metacyclic Stage-Specific Surface Molecule Gp82. *Infect. Immun.* 71, 1561–1565. doi: 10.1128/IAI.71.3.1561-1565.2003
- Martins, R. M., Covarrubias, C., Rojas, R. G., Silber, A. M., and Yoshida, N. (2009). Use of L-Proline and ATP Production by Trypanosoma Cruzi Metacyclic Forms as Requirements for Host Cell Invasion. *Infect. Immun.* 77 (7), 3023–3032. doi: 10.1128/IAI.00138-09
- Martins, R. M., Alves, R. M., Macedo, S., and Yoshida, N. (2011). Starvation and Rapamycin Differentially Regulate Host Cell Lysosome Exocytosis and Invasion by Trypanosoma Cruzi Metacyclic Forms. *Cell. Microbiol.* 13 (7), 943–954. doi: 10.1111/j.1462-5822.2011.01590.x
- Martins, N. O., de Souza, R. T., Cordero, E. M., Maldonado, D. C., Cortez, C., Marini, M. M., et al. (2015). Molecular Characterization of a Novel Family of Trypanosoma Cruzi Surface Membrane Proteins (TcSMP) Involved in Mammalian Host Cell Invasion. *PLoS Neglect. Trop. Dis.* 9 (11), 1–28. doi: 10.1371/journal.pntd.0004216
- Mattos, E. C., Tonelli, R. R., Colli, W., and Alves, M. J. M. (2014). The Gp85 Surface Glycoproteins from Trypanosoma Cruzi. *Sub Cellular Biochem.* 74, 151–180. doi: 10.1007/978-94-007-7305-9_7
- McClatchey, A. I. (2014). ERM Proteins at a Glance. *J. Cell Sci.* 127 (15), 3199–3204. doi: 10.1242/jcs.098343
- Melo, T. G., Tucci, A. R., Nogueira, A. R., Meirelles, M. de N. S. L., and Pereira, M. C. S. (2014). The Involvement of FAK and Src in the Invasion of Cardiomyocytes by Trypanosoma Cruzi. *Exp. Parasitol.* 139 (1), 49–57. doi: 10.1016/j.jexppara.2014.02.008
- Ming, M., Chuenkova, M., Ortega-Barria, E., and Pereira, M. E. A. (1993). Mediation of Trypanosoma Cruzi Invasion by Sialic Acid on the Host Cell and Trans-Sialidase on the Trypanosome. *Mol. Biochem. Parasitol.* 59, 243–252. doi: 10.1016/0166-6851(93)90222-J
- Ming, M., Ewen, M. E., and Pereira, M. E. A. (1995). Trypanosome Invasion of Mammalian Cells Requires Activation of the TGF β Signaling Pathway. *Cell* 82 (2), 287–296. doi: 10.1016/0092-8674(95)90316-X
- Miro-Moran, A., Jardim, I., Ortega-Ferrusola, C., Salido, G. M., Peña, F. J., Tapia, J. A., et al. (2012). Identification and Function of Exchange Proteins Activated Directly by Cyclic AMP (Epac) in Mammalian Spermatozoa. *PLoS One* 7, e37713. doi: 10.1371/journal.pone.0037713
- Monteón, V. M., Furuzawa-Carballeda, J., Alejandre-Aguilar, R., Aranda-Frausto, A., Rosales-Encina, J. L., and Reyes, P. A. (1996). American Trypanosomiasis: In Situ and Generalized Features of Parasitism and Inflammation Kinetics in a Murine Model. *Exp. Parasitol.* 83 (3), 267–274. doi: 10.1006/expr.1996.0074
- Moreira, L. R., Serrano, F. R., and Osuna, A. (2019). Extracellular Vesicles of Trypanosoma Cruzi Tissue-Culture Cell-Derived Trypomastigotes: Induction of Physiological Changes in Non-Parasitized Culture Cells. *PLoS Neglect. Trop. Dis.* 13 (2), 1–26. doi: 10.1371/journal.pntd.0007163
- Mortara, R. A., Andreoli, W. K., Tantwaki, N. N., Fernandes, A. B., Silva, C. V. Da, Fernandes, M. C. D. C., et al. (2005). Mammalian Cell Invasion and Intracellular Trafficking by Trypanosoma Cruzi Infective Forms. *Anais Da Academia Bras. Cienc.* 77, 77–94. doi: 10.1590/s0001-37652005000100006
- Motta, F. N., Azevedo, C. S., Neves, B. P., de Araújo, C. N., Grellier, P., de Santana, J. M., et al. (2019). Oligopeptidase B, a Missing Enzyme in Mammals and a Potential Drug Target for Trypanosomatid Diseases. *Biochimie* 167, 207–216. doi: 10.1016/j.biochi.2019.10.006
- Musikant, D., Ferri, G., Durante, I. M., Buscaglia, C. A., Altschuler, D. L., and Edreira, M. M. (2017). Host Epac1 Is Required for CAMP-Mediated Invasion by Trypanosoma Cruzi. *Mol. Biochem. Parasitol.* 211 (January), 67–70. doi: 10.1016/j.molbiopara.2016.10.003
- Nardy, A. F. F. R., Freire-de-Lima, C. G., Pérez, A. R., and Morrot, A. (2016). Role of Trypanosoma Cruzi Trans-Sialidase on the Escape from Host Immune Surveillance. *Front. Microbiol.* 7, 348. doi: 10.3389/fmicb.2016.00348
- Nogueira, P. M., Ribeiro, K., Silveira, A. C. O., Campos, J. H., Martins-Filho, O. A., Bela, S. R., et al. (2015). Vesicles from Different Trypanosoma Cruzi Strains Trigger Differential Innate and Chronic Immune Responses. *J. Extracellular Vesicles* 4 (1), 1–16. doi: 10.3402/jev.v4.28734
- Oliveira, A. E. R., Grazielle-Silva, V., Ferreira, L. R. P., and Teixeira, S. M. R. (2020). Close Encounters between Trypanosoma Cruzi and the Host Mammalian Cell: Lessons from Genome-Wide Expression Studies. *Genomics* 112, 990–997. doi: 10.1016/j.ygeno.2019.06.015
- Onofre, T. S., Rodrigues, J. P. F., and Yoshida, N. (2019). Depletion of Host Cell Focal Adhesion Kinase Increases the Susceptibility to Invasion by Trypanosoma Cruzi Metacyclic Forms. *Front. Cell. Infect. Microbiol.* 9:2019.00231 (JUN). doi: 10.3389/fcimb.2019.00231
- Paiva, C. N., Feijó, D. F., Dutra, F. F., Carneiro, V. C., Freitas, G. B., Alves, L. S., et al. (2012). Oxidative Stress Fuels Trypanosoma Cruzi Infection in Mice. *J. Clin. Invest.* 122 (7), 2531–2542. doi: 10.1172/JCI58525
- Pizon, V., Desjardins, M., Bucci, C., Parton, R. G., and Zerial, M. (1994). Association of Rap1a and Rap1b Proteins with Late Endocytic/Phagocytic Compartments and Rap2a with the Golgi Complex. *J. Cell Sci.* 107, 1661–1670.
- Pu, J., Guardia, C. M., Keren-Kaplan, T., and Bonifacino, J. S. (2016). Mechanisms and Functions of Lysosome Positioning. *J. Cell Sci.* 129, 4329–4339. doi: 10.1242/jcs.196287
- Ramirez, M. I., De Cassia Ruiz, R., Araya, J. E., Da Silveira, J. F., and Yoshida, N. (1993). Involvement of the Stage-Specific 82-Kilodalton Adhesion Molecule of Trypanosoma Cruzi Metacyclic Trypomastigotes in Host Cell Invasion. *Infect. Immun.* 61 (9), 3636–3641. doi: 10.1128/iai.61.9.3636-3641.1993
- Rawlings, N. D., Waller, M., Barrett, A. J., and Bateman, A. (2014). MEROPS: The Database of Proteolytic Enzymes, Their Substrates and Inhibitors. *Nucleic Acids Res.* 42, D503–D509. doi: 10.1093/nar/gkt953
- Reddy, A., Caler, E. V., and Andrews, N. W. (2001). Plasma Membrane Repair Is Mediated by Ca²⁺-Regulated Exocytosis of Lysosomes. *Cell* 106, 157–169. doi: 10.1016/S0092-8674(01)00421-4
- Risso, M. G., Garbarino, G. B., Mocetti, E., Campetella, O., Cappa, S. M. G., Buscaglia, C. A., et al. (2004). Differential Expression of a Virulence Factor, the Trans-Sialidase, by the Main Trypanosoma Cruzi Phylogenetic Lineages. *J. Infect. Dis.* 189 (12), 2250–2259. doi: 10.1086/420831
- Rodrigues, A. A., Clemente, T. M., dos Santos, M. A., Machado, F. C., Gomes, R. G. B., Moreira, H. H. T., et al. (2012). A Recombinant Protein Based on Trypanosoma Cruzi P21 Enhances Phagocytosis. *PLoS One* 7 (12), 1–9. doi: 10.1371/journal.pone.0051384
- Rodrigues, J. P. F., Santana, G. H. T., Juliano, M. A., and Yoshida, N. (2017). Inhibition of Host Cell Lysosome Spreading by Trypanosoma Cruzi Metacyclic Stage-Specific Surface Molecule Gp90 Downregulates Parasite Invasion. *Infect. Immun.* 85 (9), 1–10. doi: 10.1128/IAI.00302-17
- Rodrigues, J. P. F., Onofre, T. S., Barbosa, B. C., Ferreira, E. R., Bonfim-Melo, A., and Yoshida, N. (2019). Host Cell Protein LAMP-2 Is the Receptor for Trypanosoma Cruzi Surface Molecule Gp82 That Mediates Invasion. *Cell. Microbiol.* 21 (5), 1–11. doi: 10.1111/cmi.13003

- Rodríguez, A., Samoff, E., Rioult, M. G., Chung, A., and Andrews, N. W. (1996). Host Cell Invasion by Trypanosomes Requires Lysosomes and Microtubule/Kinesin-Mediated Transport. *J. Cell Biol.* 134 (2), 349–362. doi: 10.1083/jcb.134.2.349
- Rodríguez, A., Martínez, I., Chung, A., Berlot, C. H., and Andrews, N. W. (1999). CAMP Regulates Ca²⁺-Dependent Exocytosis of Lysosomes and Lysosome-Mediated Cell Invasion by Trypanosomes. *J. Biol. Chem.* 274 (24), 16754–16759. doi: 10.1074/jbc.274.24.16754
- Romano, P. S., Arboit, M. A., Vázquez, C. L., and Colombo, M. I. (2009). The Autophagic Pathway Is a Key Component in the Lysosomal Dependent Entry of Trypanosoma Cruzi into the Host Cell. *Autophagy* 5 (1), 6–18. doi: 10.4161/auto.5.1.7160
- Rubin-de-Celis, S. S. C., Uemura, H., Yoshida, N., and Schenkman, S. (2006). Expression of Trypomastigote Trans-Sialidase in Metacyclic Forms of Trypanosoma Cruzi Increases Parasite Escape from Its Parasitophorous Vacuole. *Cell. Microbiol.* 8 (12), 1888–1898. doi: 10.1111/j.1462-5822.2006.00755.x
- Ruiz, R. C., Favoreto, S., Dorta, M. L., Oshiro, M. E. M., Ferreira, A. T., Manque, P. M., et al. (1998). Infectivity of Trypanosoma Cruzi Strains Is Associated with Differential Expression of Surface Glycoproteins with Differential Ca²⁺ Signalling Activity. *Biochem. J.* 330 (1), 505–511. doi: 10.1042/bj3300505
- Sabbatini, M. E., Chen, X., Ernst, S. A., and Williams, J. A. (2008). Rap1 Activation Plays a Regulatory Role in Pancreatic Amylase Secretion. *J. Biol. Chem.* 283, 23884–23894. doi: 10.1074/jbc.M800754200
- Salassa, B. N., Cueto, J. A., Tudela, J. G., and Romano, P. S. (2020). Endocytic Rabs Are Recruited to the Trypanosoma Cruzi Parasitophorous Vacuole and Contribute to the Process of Infection in Non-Professional Phagocytic Cells. *Front. Cell. Infect. Microbiol.* 10, 2020.536985 (October). doi: 10.3389/fcimb.2020.536985
- Salassa, B. N., and Romano, P. S. (2019). Autophagy: A Necessary Process during the Trypanosoma Cruzi Life-Cycle. *Virulence* 10 (1), 460–469. doi: 10.1080/21505594.2018.1543517
- Salimi, L., Akbari, A., Jabbari, N., Mojarad, B., Vahhabi, A., Szafert, S., et al. (2020). Synergies in Exosomes and Autophagy Pathways for Cellular Homeostasis and Metastasis of Tumor Cells. *Cell Biosci.* 10, 64. doi: 10.1186/s13578-020-00426-y
- San Francisco, J., Barria, I., Gutiérrez, B., Neira, I., Muñoz, C., Sagua, H., et al. (2017). Decreased Cruzipain and Gp85/Trans-Sialidase Family Protein Expression Contributes to Loss of Trypanosoma Cruzi Trypomastigote Virulence. *Microbes Infect.* 19 (1), 55–61. doi: 10.1016/j.micinf.2016.08.003
- Santi-Rocca, J., Fernandez-Cortes, F., Chillón-Marinas, C., González-Rubio, M. L., Martín, D., and Fresno, M. (2017). A Multi-Parametric Analysis of Trypanosoma Cruzi Infection: Common Pathophysiologic Patterns beyond Extreme Heterogeneity of Host Responses. *Sci. Rep.* 7, 1–12. doi: 10.1038/s41598-017-08086-8
- Scharfstein, J., Schmitz, V., Morandi, V., Capella, M. M. A., Lima, A. P. C. A., Morrot, A., et al. (2000). Host Cell Invasion by Trypanosoma Cruzi Is Potentiated by Activation of Bradykinin B2 Receptors. *J. Exp. Med.* 192, 1289–1300. doi: 10.1084/jem.192.9.1289
- Schenkman, S., Jiang, M. S., Hart, G. W., and Nussenzweig, V. (1991). A Novel Cell Surface Trans-Sialidase of Trypanosoma Cruzi Generates a Stage-Specific Epitope Required for Invasion of Mammalian Cells. *Cell* 65, 1117–1125. doi: 10.1016/0092-8674(91)90008-M
- Schoijet, A. C., Sternlieb, T., and Alonso, G. D. (2019). Signal Transduction Pathways as Therapeutic Target for Chagas Disease. *Curr. Medicinal Chem.* 26, 6572–6589. doi: 10.2174/0929867326666190620093029
- Seino, S., and Shibasaki, T. (2005). PKA-Dependent and PKA-Independent Pathways for CAMP-Regulated Exocytosis. *Physiol. Rev.* 85 (4), 1303–1342. doi: 10.1152/physrev.00001.2005
- Silva, T. A., Ferreira, L. F. de C., de Souza Pereira, M. C., and Calvet, C. M. (2019). Differential Role of TGF- β in Extracellular Matrix Regulation during Trypanosoma Cruzi-Host Cell Interaction. *Int. J. Mol. Sci.* 20 (19), 4836. doi: 10.3390/ijms20194836
- Stahl, P., Schwarz, R. T., Debierre-Grockie, F., and Meyer, T. (2014). Trypanosoma Cruzi Parasites Fight for Control of the JAK-STAT Pathway by Disarming Their Host. *Jak-Stat* 3 (4), e1012964. doi: 10.1080/21623996.2015.1012964
- Sugita, S., Han, W., Butz, S., Liu, X., Fernández-Chacón, R., Lao, Y., et al. (2001). Synaptotagmin VII as a Plasma Membrane Ca²⁺ Sensor in Exocytosis. *Neuron* 30, 459–473. doi: 10.1016/S0896-6273(01)00290-2
- Taketo, M., Yokoyama, S., Kimura, Y., and Higashida, H. (1997). Ca²⁺ Release and Ca²⁺ Influx in Chinese Hamster Ovary Cells Expressing the Cloned Mouse B2 Bradykinin Receptor: Tyrosine Kinase Inhibitor-Sensitive and -Insensitive Processes. *Biochim. Biophys. Acta - Mol. Cell Res.* 1355 (1), 89–98. doi: 10.1016/S0167-4889(96)00126-7
- Tam, C., Idone, V., Devlin, C., Fernandes, M. C., Flannery, A., He, X., et al. (2010). Exocytosis of Acid Sphingomyelinase by Wounded Cells Promotes Endocytosis and Plasma Membrane Repair. *J. Cell Biol.* 189 (6), 1027–1038. doi: 10.1083/jcb.201003053
- Tanida, I., Ueno, T., and Kominami, E. (2008). LC3 and Autophagy. *Methods Mol. Biol.* 445, 77–88. doi: 10.1007/978-1-59745-157-4_4
- Teixeira, A. A. R., de Cássia Sardinha de Vasconcelos, V., Colli, W., Alves, M. J. M., and Giordano, R. J. (2015). Trypanosoma Cruzi Binds to Cytokeratin through Conserved Peptide Motifs Found in the Laminin-G-Like Domain of the Gp85/Trans-Sialidase Proteins. *PLoS Neglect. Trop. Dis.* 9 (9), e0004099. doi: 10.1371/journal.pntd.0004099
- Teixeira, S. M. R., Russell, D. G., Kirchhoff, L. V., and Donelson, J. E. (1994). A Differentially Expressed Gene Family Encoding 'amastin,' a Surface Protein of Trypanosoma Cruzi Amastigotes. *J. Biol. Chem.* 269 (32), 20509–20516. doi: 10.1016/S0021-9258(17)32022-7
- Teixeira, S. C., Lopes, D. S., Gimenes, S. N. C., Teixeira, T. L., Da Silva, M. S., Silva Brígido, R. T. E., et al. (2017). Mechanistic Insights into the Anti-Angiogenic Activity of Trypanosoma Cruzi Protein 21 and Its Potential Impact on the Onset of Chagasic Cardiomyopathy. *Sci. Rep.* 7, 44978. doi: 10.1038/srep44978
- Teixeira, T. L., Machado, F. C., Da Silva, A. A., Teixeira, S. C., Borges, B. C., Dos Santos, M. A., et al. (2015). Trypanosoma Cruzi P21: A Potential Novel Target for Chagasic Cardiomyopathy Therapy. *Sci. Rep.* 5, 1–10. doi: 10.1038/srep16877
- Teixeira, M. M. G., and Yoshida, N. (1986). Stage-Specific Surface Antigens of Metacyclic Trypomastigotes of Trypanosoma Cruzi Identified by Monoclonal Antibodies. *Mol. Biochem. Parasitol.* 18 (3), 271–282. doi: 10.1016/0166-6851(86)90085-X
- Tengholm, A., and Gylfe, E. (2017). CAMP Signalling in Insulin and Glucagon Secretion. *Diabetes Obes. Metab.* 19, 42–53. doi: 10.1111/dom.12993
- Tonelli, R. R., Giordano, R. J., Barbu, E. M., Torrecilhas, A. C., Kobayashi, G. S., Langley, R. R., et al. (2010). Role of the Gp85/Trans-Sialidases in Trypanosoma Cruzi Tissue Tropism: Preferential Binding of a Conserved Peptide Motif to the Vasculature in Vivo. *PLoS Neglect. Trop. Dis.* 4 (11), e864. doi: 10.1371/journal.pntd.0000864
- Torrecilhas, A. C., Schumacher, R. I., Alves, M. J. M., and Colli, W. (2012). Vesicles as Carriers of Virulence Factors in Parasitic Protozoan Diseases. *Microbes Infect.* 14 (15), 1465–1474. doi: 10.1016/j.micinf.2012.07.008
- Torrecilhas, A. C., Soares, R. P., Schenkman, S., Fernández-Prada, C., and Olivier, M. (2020). Extracellular Vesicles in Trypanosomatids: Host Cell Communication. *Front. Cell. Infect. Microbiol.* 10, 2020.602502. doi: 10.3389/fcimb.2020.602502
- Trocoli Torrecilhas, A. C., Tonelli, R. R., Pavanelli, W. R., da Silva, J. S., Schumacher, R. I., de Souza, W., et al. (2009). Trypanosoma Cruzi: Parasite Shed Vesicles Increase Heart Parasitism and Generate an Intense Inflammatory Response. *Microbes Infect.* 11 (1), 29–39. doi: 10.1016/j.micinf.2008.10.003
- Wainszelbaum, M., Isola, E., Wilkowsky, S., Cannata, J. J. B., Florin-Christensen, J., and Florin-Christensen, M. (2001). Lysosomal Phospholipase A1 in Trypanosoma Cruzi: An Enzyme with a Possible Role in the Pathogenesis of Chagas' Disease. *Biochem. J.* 355 (3), 765–770. doi: 10.1042/bj3550765
- Walker, D. M., Oghumu, S., Gupta, G., McGwire, B. S., Drew, M. E., and Satoskar, A. R. (2014). Mechanisms of Cellular Invasion by Intracellular Parasites: Mechanisms of Host Cell Invasion in Leishmania. *Cell Mol. Life Sci.* 71 (7), 1245–1263. doi: 10.1007/s00018-013-1491-1
- Wang, T., Li, L., and Hong, W. (2017). SNARE Proteins in Membrane Trafficking. *Traffic* 18, 767–775. doi: 10.1111/tra.12524
- Watanabe Costa, R., da Silveira, J. F., and Bahia, D. (2016). Interactions between Trypanosoma Cruzi Secreted Proteins and Host Cell Signaling Pathways. *Front. Microbiol.* 7:2016.00388 (MAR). doi: 10.3389/fmicb.2016.00388
- Wilkowsky, S. E., Barbieri, M. A., Stahl, P., and Isola, E. L. D. (2001). Trypanosoma Cruzi: Phosphatidylinositol 3-Kinase and Protein Kinase B Activation Is Associated with Parasite Invasion. *Exp. Cell Res.* 264 (2), 211–218. doi: 10.1006/excr.2000.5123

- Woolsey, A. M., Sunwoo, L., Petersen, C. A., Brachmann, S. M., Cantley, L. C., and Burleigh, B. A. (2003). Novel PI 3-Kinase-Dependent Mechanisms of Trypanosome Invasion and Vacuole Maturation. *J. Cell Sci.* 116 (17), 3611–3622. doi: 10.1242/jcs.00666
- Yoshida, N., Dorta, M. L., Ferreira, A. T., Oshiro, M. E. M., Mortara, R. A., Acosta-Serrano, A., et al. (1997). Removal of Sialic Acid from Mucin-like Surface Molecules of Trypanosoma Cruzi Metacyclic Trypomastigotes Enhances Parasite-Host Cell Interaction. *Mol. Biochem. Parasitol.* 84 (1), 57–67. doi: 10.1016/S0166-6851(96)02783-1
- Yoshida, N., Favoreto, S., Ferreira, A. T., and Manque, P. M. (2000). Signal Transduction Induced in Trypanosoma Cruzi Metacyclic Trypomastigotes during the Invasion of Mammalian Cells. *Braz. J. Med. Biol. Res.* 33, 269–278. doi: 10.1590/S0100-879X2000000300003
- Yoshida, N., and Cortez, M. (2008). Parasite and Host Cell Signaling during the Invasion Process. *Mol. Mech. Parasite Invasion* 47, 82–91. doi: 10.1007/978-0-387-78267-6_6
- Zanforlin, T., Bayer-Santos, E., Cortez, C., Almeida, I. C., Yoshida, N., and Silveira, J. F. Da. (2013). Molecular Characterization of Trypanosoma Cruzi SAP Proteins with Host-Cell Lysosome Exocytosis-Inducing Activity Required for Parasite Invasion. *PLoS One* 8 (12), e83864. doi: 10.1371/journal.pone.0083864
- Zingales, B., Andrade, S. G., Briones, M. R. S., Campbell, D. A., Chiari, E., Fernandes, O., et al. (2009). A New Consensus for Trypanosoma Cruzi Intraspecific Nomenclature: Second Revision Meeting Recommends TcI to TcVI. *Memorias Do Instituto Oswaldo Cruz* 104 (7), 1051–1054. doi: 10.1590/S0074-02762009000700021

Conflict of Interest: The authors declare that the research was conducted in the absence of any commercial or financial relationships that could be construed as a potential conflict of interest

Copyright © 2021 Ferri and Edreira. This is an open-access article distributed under the terms of the Creative Commons Attribution License (CC BY). The use, distribution or reproduction in other forums is permitted, provided the original author(s) and the copyright owner(s) are credited and that the original publication in this journal is cited, in accordance with accepted academic practice. No use, distribution or reproduction is permitted which does not comply with these terms.



The *Leishmania donovani* LDBPK_220120.1 Gene Encodes for an Atypical Dual Specificity Lipid-Like Phosphatase Expressed in Promastigotes and Amastigotes; Substrate Specificity, Intracellular Localizations, and Putative Role(s)

OPEN ACCESS

Edited by:

Juan David Ramirez,
Rosario University, Colombia

Reviewed by:

Jose M. Requena,
Autonomous University of Madrid,
Spain
Carolina Catta-Preta,
University of Glasgow,
United Kingdom

*Correspondence:

Haralabia Boleti
hboleti@pasteur.gr

[†]These authors have contributed
equally to this work

Specialty section:

This article was submitted to
Parasite and Host,
a section of the journal
Frontiers in Cellular and
Infection Microbiology

Received: 05 August 2020

Accepted: 25 January 2021

Published: 25 March 2021

Citation:

Papadaki A, Tziouvara O, Kotopoulis A,
Koumariannou P, Doukas A, Rios P,
Tardieux I, Köhn M and Boleti H (2021)
The *Leishmania donovani*
LDBPK_220120.1 Gene Encodes
for an Atypical Dual Specificity
Lipid-Like Phosphatase Expressed in
Promastigotes and Amastigotes;
Substrate Specificity, Intracellular
Localizations, and Putative Role(s).
Front. Cell. Infect. Microbiol. 11:591868.
doi: 10.3389/fcimb.2021.591868

Amalia Papadaki^{1†}, Olympia Tziouvara^{1†}, Anastasia Kotopoulis¹, Petrina Koumariannou^{1,2},
Anargyros Doukas¹, Pablo Rios^{3,4,5}, Isabelle Tardieux⁶, Maja Köhn^{3,4,5}
and Haralabia Boleti^{1,2*}

¹ Intracellular Parasitism Laboratory, Department of Microbiology, Hellenic Pasteur Institute, Athens, Greece, ² Light Microscopy Unit, Hellenic Pasteur Institute, Athens, Greece, ³ Genome Biology Unit, European Molecular Biology Laboratory, Heidelberg, Germany, ⁴ Signalling Research Centres BIOS and CIBSS, University of Freiburg, Freiburg, Germany, ⁵ Faculty of Biology, University of Freiburg, Freiburg, Germany, ⁶ Team «Biomechanics of Host Parasite Interactions», Institut for Advanced BioSciences, Univ. Grenoble Alpes, Inserm U1209 - CNRS UMR 5309, 38700 La Tronche, France

The intracellular protozoan parasites of the *Leishmania* genus are responsible for Leishmaniasis, vector borne diseases with a wide range of clinical manifestations. *Leishmania* (*L.*) *donovani* causes visceral leishmaniasis (kala azar), the most severe of these diseases. Along their biological cycle, *Leishmania* parasites undergo distinct developmental transitions including metacyclogenesis and differentiation of metacyclic promastigotes (MPs) to amastigotes. Metacyclogenesis inside the *phlebotomine* sandfly host's midgut converts the procyclic dividing promastigotes to non-dividing infective MPs eventually injected into the skin of mammalian hosts and phagocytosed by macrophages where the MPs are converted inside modified phagolysosomes to the intracellular amastigotes. These developmental transitions involve dramatic changes in cell size and shape and reformatting of the flagellum requiring thus membrane and cytoskeleton remodeling in which phosphoinositide (PI) signaling and metabolism must play central roles. This study reports on the LDBPK_220120.1 gene, the *L. donovani* ortholog of *LmjF.22.0250* from *L. major* that encodes a phosphatase from the "Atypical Lipid Phosphatases" (ALPs) enzyme family. We confirmed the expression of the LDBPK_220120.1 gene product in both *L. donovani* promastigotes and axenic amastigotes and showed that it behaves *in vitro* as a Dual Specificity P-Tyr and monophosphorylated [PI(3)P and PI(4)P] PI phosphatase and therefore named it LdTyrPIP_22 (*Leishmania donovani* Tyrosine PI Phosphatase, gene locus at chromosome 22). By immunofluorescence confocal microscopy we localized the

LdTyrPIP₂₂ in several intracellular sites in the cell body of *L. donovani* promastigotes and amastigotes and in the flagellum. A temperature and pH shift from 25°C to 37°C and from pH 7 to 5.5, induced a pronounced recruitment of LdTyrPIP₂₂ epitopes to the flagellar pocket and a redistribution around the nucleus. These results suggest possible role(s) for this P-Tyr/PI phosphatase in the regulation of processes initiated or upregulated by this temperature/pH shift that contribute to the developmental transition from MPs to amastigotes inside the mammalian host macrophages.

Keywords: *Leishmania* developmental transitions, atypical lipid phosphatase, phosphoinositide signaling and metabolism, P-Tyr/PI phosphatase, flagellar pocket, endocytosis/exocytosis

INTRODUCTION

Leishmania parasites, a class of trypanosomatid protozoans of the kinetoplastidae family, parasitize both invertebrate (sandflies of the genus *Phlebotomus* or *Lutzomyia*) and vertebrate hosts. When transmitted to the mammal host by the sandfly bite upon blood-feeding, *Leishmania* parasites are responsible for leishmaniasis, a wide spectrum of diseases, which are major public health threats in endemic areas (WHO/PAHO, 2020). The most severe and potentially fatal form of these diseases transmitted by *Leishmania* (*L.*) *donovani* is visceral leishmaniasis (kala-azar) (Burza et al., 2018; WHO/PAHO, 2020). Up to 1 million new cases of all forms of leishmaniasis occur annually in about 100 endemic countries and over 20,000 deaths are attributed annually to them (WHO/PAHO, 2020). The few anti-leishmania drugs available to date present serious limitations. They are associated with severe side effects/toxicity or teratogenicity, high cost or emergence/spread of drug-resistant parasites in the field (Ghorbani and Farhoudi, 2018). Therefore, there is an urgent need to develop new specific and safe anti-parasitic compounds. In such framework, the identification of molecular determinants along the complex life cycle of these parasites should enlarge the target repertoire for designing anti-parasitic strategies.

To achieve its complex life cycle in the hematophagous insect host and in the mammalian host, *Leishmania* spp. undergo a series of differentiation processes that give rise to distinct biological stages allowing tight adjustments in each of their hosts (e.g., the insect's luminal digestive tract and the interior of mammalian cells) that are significantly different in temperature, pH, nutrient availability and immune status

(Bates, 1994; Mauel, 1996; Sunter and Gull, 2017). The main *Leishmania* developmental forms are: 1) the flagellated promastigotes, living in the sandfly host vector's digestive tract (Bates, 1994; Dostalova and Volf, 2012) and eventually delivered into the mammalian host skin and 2) the ovoid amastigotes with a short mostly internal flagellum (Glaser et al., 1990; Gupta et al., 2001; Wheeler et al., 2015), propagating within macrophages of the vertebrate hosts inside a modified parasitophorous phagolysosome [(Desjardins and Descoteaux, 1997), reviewed by (Mauel, 1996; Handman and Bullen, 2002; Young and Kim, 2019)]. In the digestive tract of the insect, the dividing promastigotes go through several stages of differentiation the last step of which is called metacyclogenesis (Bates, 1994; Rogers et al., 2002; Bates, 2007). This developmental phase leads to the emergence of infectious metacyclics, short and slender flagellated forms never seen in division. They are highly motile and unattached to the insect's digestive track and have a flagellum at least twice the length of their cell body (Bates, 2007; Sunter and Gull, 2017). The metacyclic promastigotes are believed to be the only forms injected into the skin when an infected fly takes a blood meal. Metacyclogenesis can be mimicked *in vitro* by cultivating promastigotes under chemically defined conditions allowing the generation of intermediate differentiation forms as well as fully differentiated metacyclic *Leishmania* promastigotes (Bates et al., 1992; Zakai et al., 1998; Nayak et al., 2018). Conditions have also been defined to reproduce the developmental transition from metacyclic promastigotes (MPs) to amastigotes by shifting stationary phase promastigotes' cultures to 37°C and pH 5.5, mimicking thereby the conditions inside the parasitophorous phagolysosomes of mammalian macrophages (Doyle et al., 1991; Debrabant et al., 2004; Zilberstein, 2020).

The developmental transitions of metacyclogenesis and MP to amastigote enable *Leishmania* parasites to cope with the distinct microenvironments of their hosts by adjusting gene expression (Iantorno et al., 2017; Coutinho-Abreu et al., 2020) and consequently metabolism. These adaptations are reflected by the broad alterations in the absolute and relative RNA and protein levels and activity observed over metacyclogenesis and MP to amastigote transition [(De Pablos et al., 2016; Inbar et al., 2017) recently reviewed by (Karamysheva et al. (2020))]. In this context, changes in the phosphorylation state of many proteins carried out by specific kinases and phosphatases have already

Abbreviations: LdTyrPIP₂₂, *Leishmania donovani* Tyrosine and Phosphoinositide Phosphatase in chromosome 22; DSP, dual-specificity phosphatase; aDSP, atypical dual-specificity phosphatase; PTPs, Protein Tyrosine Phosphatases; P-Tyr, phosphotyrosine; P-Ser, phosphoserine; P-Thr, phosphothreonine; PI(s), phosphoinositide(s); ALPs, atypical lipid phosphatases; PIPs, PI phosphatases; wt, wild type; ORF, open reading frame; aa, amino acids; Ab, antibody; pAb, polyclonal antibody; mRFP1, monomeric red fluorescent protein; GFP, green fluorescent protein; PFA, paraformaldehyde; ATCC, American Type Culture Collection; MW, Molecular Weight; WB, western blot; h, hours; PI(3)P, phosphatidylinositol 3-phosphate; PI(4)P, phosphatidylinositol 4-phosphate; PI(3,5)P₂, phosphatidylinositol 3,5-bisphosphate; IF, immunofluorescence; FL, Fluorescence; BW, black and white; KO, knock out.

been highlighted (Nascimento et al., 2003; McNicoll et al., 2006; Nascimento et al., 2006; Zhou et al., 2006; Depledge et al., 2009; Morales et al., 2010; Tsigankov et al., 2013; Soulat and Bogdan, 2017) pointing to the importance of P-Tyr phosphatases (PTPs) in the differentiation process of *Leishmania* parasites although few proteins (0.4%) were found to be phosphorylated on tyrosine during the *L. donovani* promastigotes' differentiation to amastigotes *in vitro* (Tsigankov et al., 2013).

Besides the human homologs of PTPs expressed in *Leishmania* (Nascimento et al., 2006; Soulat and Bogdan, 2017), atypical Dual Specificity Phosphatases (aDSPs) with P-Tyr phosphatase activity have been detected in a phosphatome analysis of *Leishmania* genome sequences (Brenchley et al., 2007). These phosphatases seem to have no human homologs or to be very divergent from human homologs (Brenchley et al., 2007; Soulat and Bogdan, 2017). Moreover, another Bioinformatics study identified four *Leishmania* aDSPs as members of an "Atypical Lipid Phosphatase" family (ALPs) (Beresford et al., 2010), a group of enzymes found only in bacteria and lower eukaryotes. All ALPs share the characteristic structural P-loop feature (HCXXGKDR) of the catalytic site of PTPs, a signature also found in MptpB, a triple specificity (i.e., P-Tyr, P-Ser/P-Thr, and PI) phosphatase from *M. tuberculosis* (Beresford et al., 2007) and the LipA, a P-Tyr, and PI phosphatase from *Listeria monocytogens* (Kastner et al., 2011). Of note, both MptpB and LipA are secreted by the bacteria into their respective host cells where they subvert PI signaling, hence contributing to bacteria virulence (Beresford et al., 2007; Kastner et al., 2011). One of the *Leishmania* members of the ALP family encoded by the *LmjF.22.0250* gene was shown in the same study to dephosphorylate P-Tyr peptides and monophosphorylated PIs. Interestingly, the *LmjF.22.0250* gene transcript was later reported to be highly enriched during metacyclogenesis in the natural sandfly vector (Inbar et al., 2017). In the same line, *L. mexicana* parasites in which was ablated the *LmxM.22.0250* gene, orthologous to the *LmjF.22.0250*, showed severely impaired survival in primary mouse macrophages in an *in vitro* infection system (Kraeva et al., 2019), results supporting a strong contribution of this ALP to the parasite's fitness. Overall, the unique sequence- and biochemical- related features of ALPs, in addition to their acting as fitness determinants, make them attractive candidate targets for the development of specific antimicrobial inhibitors/drugs.

Herein, we report data from the biochemical characterization of the LdTyrPIP₂₂ protein (*Leishmania donovani* Tyrosine PI Phosphatase with gene locus at chromosome 22), encoded by the *LdBPK_220120* gene, the *L. donovani* ortholog of the *LmjF.22.0250* and *LmxM.22.0250* genes mentioned above. We found that the LdTyrPIP₂₂ sequence is highly conserved in all sequenced *Leishmania* spp. from the *Leishmania* and *Sauroleishmania* subgenera and detected the expression of the *LdBPK_220120* encoded protein in different morphological forms of cultured *L. donovani* promastigotes and axenic amastigotes. LdTyrPIP₂₂, when expressed in bacteria, dephosphorylates P-Tyr peptides and monophosphorylated PIs similarly to its *L. major* ALP ortholog. It is specifically distributed in distinct subcellular compartments in the promastigote and

amastigote cells and is recruited to the flagellar pocket upon a temperature shift from 25°C to 37°C, one of the main parameters that drive the developmental transition of the *Leishmania* MP to amastigote.

MATERIALS AND METHODS

Reagents and Antibodies

All chemicals used, unless otherwise stated, were of analytical grade and purchased from Sigma-Aldrich or Applichem. Specifically, Digitonin (D141-100MG), Triton-X 100 (X100-100ML) and Ponceau S (P3504-50G) were from Sigma-Aldrich. Nourseothricin (NTC-AB-102L0) was from Jena Biosciences. Restriction enzymes were purchased from Roche (New England Biolabs) and/or KAPA Biosystems. Taq DNA polymerase (R001A) and T4 ligase (2011B) were from TaKaRa. All primers used in the PCR reactions (synthesized by VBC Biotech) are listed in **Table S1**. DNase I (2270A) was from TaKaRa and RNase (10109134001) from Sigma Aldrich (Merck). One kb DNA ladder (N3232L) was from New England Biolabs (NEB), protein molecular mass standards (17-0446-01) were purchased from Amersham Biosciences and Nippon Genetics (Broad range:10–180 kDa, MWP03) while protein quantification reagent Bradford (B6916) and proteolytic inhibitors (P8465) were from Sigma-Aldrich. Fetal Bovine Serum (FBS) was from Thermo Fisher Scientific (10270106, Gibco) or Biosera (FB-1001/500). Bacto-tryptone (211705), Bacto Yeast extract (212750), and Bacto-agar (14050) were from BD Biosciences. The mouse monoclonal 6xHistidine epitope tag antibody (Ab) was from Acris Antibodies (SM1693PS), the α -tubulin (T5168) mouse monoclonal (mAb) was from Sigma, the rabbit polyclonal (pAb) α -Leish actin was kind gift from Dr Amogh Sahasrabudhe (Division of Molecular and Structural Biology Central Drug Research Institute Lucknow, India). The GAPDH pAb was a kind gift of Frédéric Bringaud (U. of Bordeaux/CNRS, France). The α -mRFP pAb was prepared by us as described by Papadaki et al. (2015). The α -A2 Ab was from Abcam (ab150344). The α -EF1a Ab clone CBP-KK1 (05-235) was purchased from Merck. All Fluorochrome-conjugated secondary Abs [Alexa Fluor[®] 546 (A-11030 or A-11035) and Alexa Fluor[®] 488 (A32723 or A32731)] were from Thermo Fisher Scientific. Goat anti-rabbit HRP (41460) and goat anti-mouse HRP (31230) were from Pierce while the α -mouse and α -rabbit Abs conjugated with CF488A were from Biotinum (20010 and 20012, respectively). Hoechst 33342 (H3570) and FM 4-64 FX fixable membrane stain (F34653) were purchased from Thermo Fisher Scientific.

Cell Culture

The murine monocytic cell line J774 was cultured in high glucose RPMI (1640) (Biosera LM1638) containing 10% (v/v) hiFBS [heat-inactivated (56°C, 30 min) fetal bovine serum], 1 U/ml penicillin and 0.1 mg/ml streptomycin. Cell counting was performed with a Neubauer hemocytometer.

L. donovani (strain LG13, MHOM/ET/0000/HUSSEN) promastigotes were cultured in RPMI 1640 containing 10% (v/v) hiFBS 1 U/ml penicillin, 0.1 mg/ml streptomycin (Gibco) and 10 mM Hepes (Gibco), at 25°C as previously described (Papadaki and Boleti, 2019). Cell counting was performed with a Malassez hemocytometer as described (Papadaki and Boleti, 2019). *L. donovani* axenic amastigotes were obtained according to modified published protocol (Barak et al., 2005; Zilberstein, 2020). Briefly, promastigotes at the stationary phase of growth, obtained after 8 days incubation at 25°C, pH 7, were harvested and resuspended in prewarmed (37°C) Medium 199 (pH of 5.5) containing 25% v/v FBS. Axenic amastigotes were obtained after 120 h incubation under these conditions (37°C, pH 5.5). Parasites incubated in the conditions inducing transformation of promastigotes to amastigotes (37°C, pH 5.5) were also analyzed after 24 h.

DNA Constructs and Cell Transfection

The gene encoding the LdTyrPIP₂₂ [1-258 amino acids (aa), GenBank®, accession No MF461274] was amplified by PCR from genomic *L. donovani* DNA (strain LG13) and inserted into the *Bgl*III site of the pLexsy-sat-*mrfp1* plasmid (Papadaki et al., 2015) to create the pLexsy-*ldtyrpip*₂₂-*mrfp1* plasmid. Secondly, the *ldtyrpip*₂₂ gene was cloned into the *Bgl*III/*Xho*I sites of the pTriEx1.1 vector (Invitrogen), in frame with the C-terminal His tag to produce the pTriEx1.1-*ldtyrpip*₂₂ and pTriEx1.1-N15-*ldtyrpip*₂₂ plasmids. N15 corresponds to the 15 additional aa (Met-Ala-Ile-Ser-Arg-Glu-Leu-Val-Asp-Pro-Asn-Ser-Gln-Ile-Ser) added to the N-terminus of LdTyrPIP₂₂ by expression from the second construct. All plasmid constructs were propagated in the *Escherichia coli* (*E. coli*) Top10F' strain for small (mini) and large scale (midi) plasmid DNA preparations. Two positive clones were selected and sequenced in each case (VBC-Biotech). The results showed 100% nucleotide sequence identity at the DNA level between the two clones. For recombinant protein production we used clones of *E. coli* BL21 (DE3) strain harboring the pTriEx1.1 based plasmids.

The transgenic promastigotes were generated based on minor modifications of a protocol previously described (Papadaki et al., 2015). Briefly, for episomal expression of LdTyrPIP₂₂-mRFP1, *Leishmania* promastigotes (2x10⁷ cells/ml) at the stationary phase of growth were transfected by electroporation with supercoiled circular pLexsy-sat-*ldtyrpip*₂₂-*mrfp1* plasmid. For electroporation, *Leishmania* promastigotes from a 10 ml culture were washed once and incubated (10 min, on ice) in 10 ml ice cold electroporation buffer (21 mM HEPES, pH 7.5, 0.7 mM Na₂HPO₄, 137 mM NaCl, 6 mM glucose, 5 mM KCl). Subsequently, they were centrifuged (1,000 g, 10 min), resuspended in 1 ml ice cold electroporation buffer and 400 µl of this suspension (2 x10⁸ cells/ml) were added in a 1.5 ml Eppendorf tube containing 20-50 µg plasmid DNA dissolved in 50 µl dH₂O. After mixing, the promastigotes/DNA suspension was transferred to chilled electroporation cuvette (Gene Pulser/Micro Pulser Electroporation cuvette 0.2 cm, 165-2086, BioRad) and electroporated (50 µF, 0.45 kV, pulse time ~ 4-5 msec). The electroporated promastigotes (8x10⁷ cells), after a 10 min incubation on ice, were transferred in 10 mL RPMI [20% (v/v)

hiFBS] and incubated for 16 h at 25°C before the addition of the antibiotic Nourcethricin. A pool of positive transgenic promastigotes was selected by the addition (once a week) of gradually increasing concentration (20-100 µg/ml) of Nourcethricin.

Overexpression and Purification of Recombinant LdTyrPIP₂₂-His Protein

The recombinant proteins used in the biochemical characterization of LdTyrPIP₂₂ were produced in *E. coli* as follows: A 4 L culture of BL21 (DE3) cells carrying the plasmid pTriEx1.1-rN15-*ldtyrpip*₂₂-His was induced overnight (~16 h) with 0.5 mM isopropyl β-D-thiogalactoside (IPTG) at 20°C and the cells were harvested by centrifugation (4,000 g, 15 min) 20 h later. Subsequently, the cell pellet was resuspended in lysis buffer (50 mM Tris, 300 mM NaCl, 30 mM imidazole, pH 8) with proteolytic inhibitors (Sigma, P 2714) and lysed by a freeze-thaw process repeated three times followed by 6-8 sonications (30-60 s, 100 W) each followed by a 30 s pause step of incubation in ice. The fusion rN15-LdTyrPIP₂₂-His protein was purified by nickel-affinity chromatography. The soluble fraction of the bacterial lysate was passed through a GE Healthcare (His Trap™ HP) His-binding column (ÄKTA-FPLC) with Ni²⁺ charged resin. The bound proteins, after been washed with lysis buffer, were eluted with 50 mM Tris, 300 mM NaCl (pH 8) and gradient concentration of imidazole up to 400 mM. As most of the proteins were eluted at fraction 1 (200 mM imidazole), this was used for a second purification step through a Talon column (Clontech Laboratories/A TaKaRa Bio company) packed with Co²⁺ charged resin. Finally, a total amount of ~1.6 mg of highly purified protein was obtained.

Generation of Antibodies

The fusion protein rN15-LdTyrPIP₂₂-His purified by Metal-Affinity Chromatography (Qiagen Ni-NTA Superflow resin) was injected into New Zealand white rabbits and BALB/c mice to raise polyclonal anti-sera, according to published protocols (Papadaki et al., 2015). All experimental procedures were approved by the Institutional Animal Bioethics Committee following the EU Directive 2010/63 and the National Law 2013/56. Purified rabbit anti-LdTyrPIP₂₂ pAb was obtained by low pH elution from immunoblots of purified rN15-LdTyrPIP₂₂-His, as previously described (Harlow and Lane, 1988).

Phosphatase Activity Assays

Initially, the rN15-LdTyrPIP₂₂-His phosphatase activity was assayed at 25°C and 37°C in a reaction buffer (100 mM Tris, 150 mM NaCl, 4mM DTT) containing 10 mM of the generic phosphatase substrate p-nitrophenyl phosphate (pNPP) and pH ranging from 4 to 8. The reaction (200 µl buffer with substrate) was initiated by the addition of enzyme and quenched after 60 min by addition of two volumes 0.5 N NaOH. The absorbance of the reaction product (*p*-nitrophenolate = *p*NP) in the supernatant was measured at λ=405 nm.

To study the kinetic parameters of rN15-LdTyrPIP₂₂-His, phosphatase assays were carried out three times in triplicates, in

a total volume of 60 μ l, containing reaction buffer (pH 6), enzyme (2 μ M), and pNPP (0.5–100 mM) at 25°C. The absorbance ($\lambda=405$ nm) was measured in Infinite M1000PRO plate reader (TECAN). Kinetic constants were determined by fitting the data to the Michaelis-Menten equation using GraphPad Prism Software 5.01 (GraphPad, San Diego, CA).

Substrate Specificity and Inhibition Assays

To determine the substrate specificity of rN15-LdTyrPIP₂₂-His a number of reactions were carried out using as substrates P-Tyr (1 mM) or P-Ser/P-Thr (60 μ M) peptides in reaction buffer (100 mM Tris, 150 mM NaCl, 4 mM DTT, pH 7) at 25°C (Table S2). The peptides were synthesized and purified according to standard procedures. Additionally, mono, bis, or trisphosphorylated PIs (100 μ M) (Avanti polar lipids or Echelon) (Table S2) were tested as plausible substrates of the recombinant LdTyrPIP₂₂ using the EnzChek® (Thermo Scientific) protocol (pH 7, 25°C) following the manufactures' instructions. The absorbance reading at 360 nm was performed with the X Infinite M1000PRO plate reader (TECAN).

The effect of inhibitors was evaluated in phosphatase assays where rN15-LdTyrPIP₂₂-His solutions (2 μ M) were pre-incubated (25 min, RT) with a) sodium orthovanadate (Na₃VO₄) concentrations ranging from 1–20 mM, b) 100 mM sodium fluoride (NaF) or c) with reaction buffer only (100 mM Tris, 150 mM NaCl, 4 mM DTT, pH 7). The phosphatase activities in the solutions were subsequently assayed using as substrate the pNPP (10 mM) and reading the absorbance at $\lambda=405$ nm (max absorbance of the chromogenic product pNP). Estimation of the product concentration was according to a standard curve generated with pNP samples of known concentration.

Preparation of Total Lysates from *Leishmania* Promastigotes

Promastigotes were resuspended in lysis buffer [20 mM Tris-HCl (pH 6.8), 0.1% SDS] (10⁸ parasites in 100 μ l lysis buffer), boiled for 5 min, cooled on ice and treated with DNase I (5–10 U/sample, 15 min, on ice) to remove DNA. Protein was estimated by the Bradford assay method. For further analysis by SDS-PAGE, 6X Laemmli sample buffer was added and the samples were either boiled for 5 min or incubated at 37°C for 30 min in the presence of proteolytic inhibitors.

Detergent-Based Protein Fractionation

Digitonin permeabilization of *L. donovani*-rLdTyrPIP₂₂-mRFP1 stationary phase *L. donovani* promastigotes is based on protocols previously described (Foucher et al., 2006; Doukas et al., 2019) with slight modifications. Briefly, *L. donovani* (wt or transgenic) promastigotes ($\sim 2 \times 10^9$) were harvested by centrifugation (1,000 g, 7 min, 4°C), washed twice in resuspension buffer (145 mM NaCl, 11 mM KCl, 75 mM Tris-HCl, pH 7.4) resuspended in 0.5 ml of the same buffer and supplemented with protease inhibitors. A stock of 100 mM digitonin solution in dH₂O was prepared. From this 100 mM digitonin solution were subsequently prepared by serial dilution solutions of 20 mM, 2 mM, 400 μ M and 40 μ M. Membrane

permeabilization and protein fractionation were achieved by adding 0.5 ml digitonin solution prewarmed at 37°C of progressively increased detergent concentrations (stepwise, four steps) to achieve digitonin concentrations of 20 μ M, 200 μ M, 1 mM, or 10 mM. In each step a soluble fraction and a corresponding pellet were recovered. The final pellet recovered after treatment with 10 mM digitonin (F5; enriched in plasma membrane, nuclei and cytoskeletal proteins), was further solubilized with 0.5 ml 1% (v/v) TritonX-100 (1 h, 4°C) and the soluble fraction (F5 S) was recovered from the insoluble fraction (F5 P) by centrifugation (20,000 g, 20 min, 4°C). The soluble fractions (F1-F4 and F5 S) were subjected to acetone precipitation by the addition of an acetone (prechilled at -20°C) volume equal to four sample volumes followed by 1h incubation at -20°C. The protein pellets recovered and the F5 P pellet were solubilized in Laemmli buffer, samples were boiled (5 min, 95°C) and further analyzed by SDS-PAGE and Western blot.

Protein Electrophoresis and Western Blotting

Proteins were separated by SDS-PAGE (12% gel) and transferred to Hybond-C nitrocellulose (Amersham) membrane using a wet blotting apparatus (BioRad). After protein transfer, Hybond-C membranes were stained with Ponceau S solution [0.5% (w/v) Ponceau S dissolved in 1% (v/v) acetic acid]. Nonspecific sites for Ab binding on the nitrocellulose membrane were blocked by incubation (1 h, RT) with Blocking buffer [Tris-buffered saline (TBS; 50 mM Tris-Cl, pH 7.5, 150 mM NaCl), 0.05% (v/v) Tween 20, 5% w/v BSA]. Incubation with the primary Abs was performed overnight (~ 16 h) at 4°C. The a-LdTyrPIP₂₂ mouse or rabbit pAbs were used at 1:1200 (serum) or ~ 1 μ g/ml (affinity purified) respectively diluted in [Tris-buffered saline, 0.1% (v/v) Tween 20 (TBST)]. Other Abs were used as indicated in figure legends. After three washes in TBST, the blots were incubated (1 h, RT) with HRP-labeled a-mouse or a-rabbit Abs used at 1:5,000 dilution. Following three washes in TBST and one final wash in TBS Ab reactivity was revealed either by the ECL plus system (Amersham) or by the chromogenic DAB method. In the former case, membranes were exposed to Kodak photographic films further developed with Kodak reagents. Reprobing with the a-mRFP1 pAb (0.5 μ g/ml) or a-EF1A (1:10,000) where required, was performed after stripping the membrane by incubation (30 min, RT) with a low pH buffer (25 mM glycine-HCl, 1% (w/v) SDS, pH 2) followed by washing and reblocking with the Blocking buffer. Apparent molecular weights of proteins detected with the specific Abs were assigned by using low (14–98 kDa, Amersham) or broad range molecular weight markers (10–180 kDa, Nippon).

Immunofluorescence Staining of *Leishmania* and Mammalian Cells and Confocal Imaging Analysis

L. donovani promastigotes were fixed with 2% (w/v) paraformaldehyde (PFA) (20 min, RT) in PBS, allowed to adhere to poly-L-lysine coated coverslips and treated with 50 mM NH₄Cl in PBS (10 min, RT) followed by PBS wash. Fixed cells were incubated (1 h, RT) first with primary Abs in blocking

buffer (PBS, 1% (w/v) BSA) and after extensive washing, the appropriate secondary Abs conjugated to Alexa Fluor[®] 546 and Alexa Fluor[®] 488 were added at a final concentration of 2 µg/ml in blocking buffer (1 h, RT). The secondary Abs were removed with extensive washing and the parasite DNA was stained (10 min, RT) either with 10 µg/ml propidium iodide solution in PBS containing 100 µg/ml RNase or with Hoechst 33342 (Mol. Probes H3570) at final concentration of 10 µg/ml. Coverslips were mounted with Mowiol 4-88 (10% (w/v) Mowiol-Calbiochem, 25% (v/v) glycerol, 100 mM Tris-HCl, pH 8.5) on microscope slides, sealed with nail polish, and stored at 4°C.

For the infection of macrophages, stationary phase *L. donovani* promastigotes, obtained after 8 days in culture without subculturing, were added to semi confluent cultures of J774 mouse macrophage cells grown on coverslips in multiwell dishes, at 20:1 parasite/macrophage ratio and the macrophages/parasites co culture were incubated at 37°C for 4 h. At the end of this period, the parasites were removed, the macrophages were washed once with prewarmed (37°C) fresh medium and were either processed for immunofluorescence confocal microscopy analysis or they were further incubated in fresh medium (RPMI, 10% v/v FBS, 1% w/v penicillin/streptomycin, 37°C) according to each experiment's specification. For immunofluorescence analysis, infected J744 macrophages were fixed (20 min, RT) with PFA [4% (w/v) in PBS]. The non-reacted PFA was neutralized with 50 mM NH₄Cl in PBS (10 min, RT) and the cells were stained with primary and secondary Abs or phalloidin-Alexa-546[®]. Coverslips were mounted as described in the previous paragraph.

Microscopic analysis of the *Leishmania* cells or the infected J744 macrophages was performed with the Leica TCS SP or SP8 confocal microscopes using the 63X apochromat lens. Image acquisition included collecting z stacks of 0.3 or 1 µm step size for parasites or infected macrophages respectively.

The extent of co localization between the LdActin and the LdTyrPIP₂₂ (green and red FL respectively) was measured using the 3D "Coloc" module of Imaris v9.2.1, which utilizes the algorithms introduced by Costes et al. for the automatic selection of thresholds of the image channels (Costes et al., 2004). We have used a third channel as a masking area for the entire analysis (created with the channel Arithmetic function "sqrt (ch1*ch2)", to exclude the background pixels of the dataset from the co localization analysis. The mask channel is used in conjunction with the automatic threshold function. This way Imaris "3D Coloc" can generate a new channel (the co localization channel), which only contains voxels representing the co localization between the red and green channels. Co localization was quantitated separately in the promastigotes' cell bodies and the flagella. Threshold 5 was used for analysis in the cell body and 2.9 for the entire promastigote and the flagellum.

Secretion Assay

L. donovani promastigotes in a stationary phase culture (50 ml) were enumerated with a Malassez hemocytometer or by measuring turbidity at OD₆₀₀ (Papadaki and Boleti, 2019) and were then harvested by centrifugation (1,000 g, 10 min, RT). The *Leishmania* cell pellet was resuspended for washing in the same

volume of RPMI and the cells were collected by centrifugation (1,000 g, 10 min, RT). Subsequently the promastigotes' pellet was resuspended in RPMI/10 mM Hepes (1/5th of the starter's culture volume) without FBS and the promastigotes were incubated at 25°C for 9 h or at 37°C for 6 h. At the end of the incubation period, the cells were separated from the culture supernatant by centrifugation, washed with PBS and stored (-20°C) until use. The culture supernatant was centrifuged (21,000 g, 20 min, 4°C) and filtered through a 0.2 µm filter to remove cell debris. Finally, the proteins in the culture supernatant were precipitated by adding 4 volumes of prechilled acetone (-20°C), vortexing and incubating overnight at -20°C. The precipitated proteins were collected by centrifugation at 14,000 g and recovered by decanting the supernatant. Acetone was allowed to evaporate from the uncapped tube at room temperature for 30 min. Appropriate volume of buffer for the downstream process was added and the sample was vortexed thoroughly to dissolve the protein pellet. Alternatively, the culture supernatant was concentrated through 10 kDa cutoff centrifugal filters (Merck) and the buffer was changed to 20 mM Tris-HCl, 150 mM NaCl, pH 9. The same buffer was used to equilibrate a Superdex 200 10/300 column which was subsequently used for analysis of the supernatant proteins according to molecular size. After fractionation, the samples were concentrated with the use of filters (10 kDa MW cutoff, Thermo Fischer) and stored at -20°C until analyzed by SDS-PAGE and WB.

Bioinformatics and Statistical Analysis

The algorithms used for identifying sequence similarities prediction (Blast) and multiple sequence alignment/editing were: 1) TriTrypDB BLAST¹ 2) ClustalW2²; 3) BioEdit Sequence Alignment Editor, version 7.0.9.0 (Ibis Biosciences). Signal P 3.0³) and NetPhos3.1b; 4) ExPASy ProScale Hphob./Kyte & Doolittle⁴; 5) NetPhos3.1b tool⁵ and GPS-Lipid⁶ were algorithms used to predict sites for post-translational modifications, signal sequence for secretion. The sequence used in this study to design primers for PCR amplifications of the *ldtyrPIP₂₂* gene from *L. donovani* is the ortholog *LINF_220007400* from *L. infantum* [(clone JPCM5 (MCAN/ES/98/LLM-877)] (TritypDB) (**Table S1**). To perform the Blast search for *ldtyrPIP₂₂* orthologs in *Leishmania* spp. genome, we used the *ldtyrPIP₂₂* sequence registered in GenBank as '*Leishmania donovani* tyrosine phosphoinositide phosphatase, LdTyrPIP₂₂' (accession No MF461274). The rooted phylogenetic tree analysis was based on the UPGMA method. Data for the Enzyme kinetics were analyzed using the GraphPad Prism Software 5.01 Michaelis-Menten model algorithm⁷. Graphs of enzyme activities were generated with the use of GraphPad. Standard deviations and t-test for statistical significance were calculated using the Excel's Formula and Data

¹ <http://tritypdb.org/tritypdb/>

² <http://www.ebi.ac.uk/Tools/msa/clustalw2/>

³ <http://www.cbs.dtu.dk/services/SignalP/>

⁴ <http://web.expasy.org/protscale/>

⁵ <http://www.cbs.dtu.dk/cgi-bin/webface2.fcgi?jobid=57C41FF500007612F0B128BD&wait=20>

⁶ <http://lipid.biocuckoo.org/>

tools. The Icy computational algorithm^{7,8} and the Adobe Photoshop CS6 Portable were used for image evaluation and processing, while for the co localization analysis, we used the 3D “Coloc” module of Imaris v9.2.1. The Fiji algorithm was used for quantification of the band intensities in the Western Blot digital images.

RESULTS

The *LDBPK_220120.1* Gene Product *LdTyrPIP₂₂* Is Highly Conserved Among the *Leishmania* and *Sauroleismania* Subgenera of *Leishmania* spp. and Shows High Homology to Pathogenic Bacteria Virulence Factors

Our interest on PI phosphatases in *Leishmania* spp. focused on a study identifying the *Leishmania major* *LmjF.22.0250* gene that encodes for a dual specificity PI and P-Tyr phosphatase (Beresford et al., 2010). This protein (LM1) contains the putative P-loop motif (HCXXGKDR[TA]G) of PTPs detected in the Mptpb triple specificity PI phosphatase from *M. tuberculosis* and in the LipA dual specificity P-Tyr and PI phosphatase from *L. monocytogenes* (Beresford et al., 2010). Moreover, a later study showing an increase in the levels of the *LmjF.22.0250* gene transcripts during metacyclogenesis in the natural sandfly vector (Inbar et al., 2017) prompted us to better characterize the structural and functional features of this phosphatase in the related *L. donovani* species, which causes in humans the potentially fatal disease of visceral leishmaniasis (Burza et al., 2018). We therefore cloned the *LmjF.22.0250* ortholog gene from *L. donovani* by a PCR approach using genomic DNA isolated from the *L. donovani* LG13 strain (MHOM/ET/0000/HUSSEN) (*Materials and Methods*; Gene Bank accession No MF461274). This was found to be 99.9% identical to the *LDBPK_220120.1* gene (777 bp) from the sequenced *L. donovani* Nepalese strain BPK282A1 registered in the TriTrypDB database with one base difference leading to substitution of Ala¹⁷¹ by a Thr¹⁷¹ (**Figure 1A**). The *LDBPK_220120.1* gene, from now on designated in our study as *ldtyrpip₂₂* (*Leishmania donovani* Tyrosine PI Phosphatase on chromosome 22), is located at positions 91159 to 91935 of chromosome 22. A Blast search using the full length *ldtyrpip₂₂* gene product from the *L. donovani*, strain LG13, identified orthologs in all *Leishmania* spp. genome sequences available in the TriTrypDB with exception the *L. braziliensis* strain M2904, MHOM/BR/75M2904 from the *Viania* subgenus. In this case a pseudogene (*LbrM.22.2.000240*) was retrieved by our search. Multiple sequence alignment indicated that the *LdTyrPIP₂₂* protein sequence (length 258 aa, calculated MW: 29081.69 Da, PI: 8.30) is highly conserved (81.34–99.22% identity) (**Figure 1**, **Table S2**) in several species of the

Leishmania and *Sauroleismania* subgenera of the *Leishmania* genus according to a recent classification of *Leishmania* spp. (Akhoundi et al., 2016; Akhoundi et al., 2017). The rooted phylogenetic tree (UPGMA) from a multiple sequence alignment of the *LdTyrPIP₂₂* orthologs from several *Leishmania* spp. (**Figure 1B**) highlighted the sequence similarities depicted in the representation of the ClustalW2 sequence analysis shown in **Figure 1A** and **Table S2**. Interestingly, no homologs were detected by this BLAST analysis in the closely related species of *Trypanosoma*.

With respect to its bacteria homologs (Beresford et al., 2010) from *M. tuberculosis* (Mptpb, GenBank: CCC62750.1), *L. monocytogenes* [lmo1800, NP_465325; lmo1935, NP_465459], *Yersinia pestis* KIM10+ (WP_002228183), and *Bacillus anthracis* strain Ames (NP_845680), the *LdTyrPIP₂₂* shows in its entire sequence length 19.4%, 29.6%, 36.1%, 27.4% and 32.4% aa sequence identity, respectively. In the P-loop active site-containing region the sequence identity is 73–91% with the respective protein sequences of the aforementioned bacterial homologs (**Figure S1**).

Finally, by applying several tools of bioinformatics, we searched for predicted structural motifs and post-translational modifications in the *LdTyrPIP₂₂* aa sequence. As the bacteria homologs of this putative phosphatase are secreted, we first analyzed by the SignalP 3.0 software for the presence of a eukaryotic secretion signal sequence motif in the N-terminus of *LdTyrPIP₂₂*. No such sequence was detected. However the absence of a secretion signal does not exclude the possibility that *LdTyrPIP₂₂* is secreted since a significant number of *Leishmania* proteins with no signal sequence motif are secreted via exosomes (Silverman et al., 2008; Dong et al., 2019) or ectosomes [recently reviewed by (de Souza and Barrias, 2020)]. Subsequently, we searched for putative phosphorylation sites using the NetPhos3.1b bioinformatics tool. Interestingly, the extreme C-terminal Ser residue of a series of Ser and Thr residues (TSSSS) was predicted to be phosphorylated with high score (0.970). Three more residues in the N-terminal half of the molecule, Ser⁷⁴, Ser¹¹⁶, and Tyr¹²⁷, were also predicted to be phosphorylated (scores 0.991, 0.973, and 0.945, respectively). This information, suggests that the *LdTyrPIP₂₂* may be post-translationally regulated by phosphorylation. Moreover, the *LdTyrPIP₂₂* sequence was checked for other possible post translational modifications. In this search, a putative palmitoylation site at Cys¹⁸² (S-Palmitoylation: Cluster C: FMLTNRCCVPPSCE) in the *LdTyrPIP₂₂* sequence was revealed by the GPS-Lipid algorithm with moderately high score (1.495 with cutoff 1.396).

Recombinant Bacterially Expressed r*LdTyrPIP₂₂*-His Acts as a PI and P-Tyr Dual Specificity Phosphatase

From the primary structure of *LdTyrPIP₂₂* was predicted that this protein must act as a PTP since it contains the characteristic P-loop motif sequence of the PTP catalytic center also described to be present in the sequence of the ALP enzyme family members (Beresford et al., 2010). To confirm the predicted PTP catalytic properties of *LdTyrPIP₂₂* we analyzed the enzyme kinetics and

⁷ https://www.graphpad.com/guides/prism/7/curve-fitting/reg_michaelis-menten_enzyme.htm

⁸ <http://icy.bioimageanalysis.org>

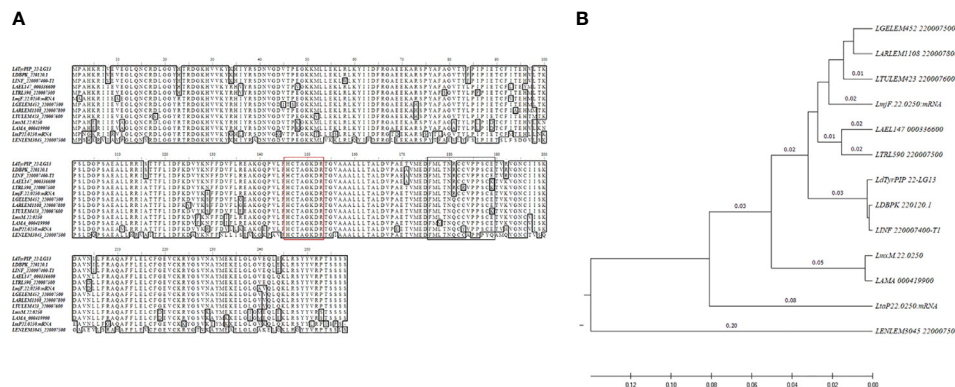


FIGURE 1 | Sequence comparison of the *LdTyrPIP₂₂* orthologs in *Leishmania* spp. **(A)** ClustalW multiple sequence alignment of the *ldtypip₂₂* gene product orthologs in *Leishmania* spp. The *L. donovani* (strain LG13, MHOM/ET/0000/HUSSEN) *LdTyrPIP₂₂* aa sequence (GenBank® accession No MF461274) was generated in this work. The aa sequences for the *L. donovani* *LDBPK_220120.1* gene product from the Nepalese strain BPK282A1 and from another eleven *Leishmania* spp. (Table S2) with genomes sequenced were obtained from the TritypDB database and were analyzed/edited using the software BioEdit Sequence Alignment Editor. The aa of the PTP P-loop motif are framed by a red box; The aa predicted as S-Palmitoylation site are framed by the black box. **(B)** Rooted phylogenetic tree (UPGMA) from a multiple sequence alignment of the *LdTyrPIP₂₂* orthologs from *Leishmania* spp.

the substrate specificity of a *LdTyrPIP₂₂* recombinant form expressed in bacteria. For this we constructed two plasmids encoding the full length protein (residues 1–777) with a polyHis tag at the C-terminus. In the first plasmid the initiation of translation of the insert begun at the ATG codon of the *ldtypip₂₂* sequence, whereas in the second plasmid translation was initiated at the pTriEx1.1 plasmid's ATG codon located 45 bp upstream the site where the *ldtypip₂₂* sequence was inserted. The second construction encodes for a polypeptide with an additional 15-mer at the N-terminus (pTriEx1.1-N15-*ldtypip₂₂*-His; Figure 2A). The recombinant protein produced from the first plasmid was mostly insoluble (Figure S2A). In contrast, the rN15-*LdTyrPIP₂₂*-His polypeptide produced from the second plasmid (Figure 2A), was mostly soluble (Figure S2B). The rN15-*LdTyrPIP₂₂*-His (281 aa, calculated MW 32062 Da), was subsequently purified by affinity chromatography on Ni²⁺ and/or Co²⁺ beads (Figure 2B, inset) and its enzymatic activity was assessed by monitoring the kinetics of dephosphorylation of the generic phosphatase substrate *p*NPP (Table 1, Figure 2B).

As expected, the rN15-*LdTyrPIP₂₂*-His specific activity [74.8 ± 1.01 nmol *p*NPP/min/mg (n=4)] estimated at 37°C and pH 6, was in the same range as the specific activity estimated for the *L. major* ortholog phosphatase (45.47 ± 1.52 nmol *p*NPP/min/mg) reported in the original publication describing the ALP family in bacteria and lower eukaryotes (Beresford et al., 2010). Finally, the catalytic activity of rN15-*LdTyrPIP₂₂*-His towards *p*NPP was shown to be optimal at pH 6 and 7 when measured at 25°C, while at 37°C the activity was found to be optimal at pH 6 (Figures 3A and S3C). Phosphatase activity was also detected at more acidic conditions (Figures 3A and S3C).

Apart from the *p*NPP substrate, we also compared the ability of rN15-*LdTyrPIP₂₂* to dephosphorylate a panel of PIs (Figure 2C) and peptides containing in their sequence P-Tyr or P-Ser/

Thr (Figures 2D, E; Table S3). Our results indicated that rN15-*LdTyrPIP₂₂*-His has a double substrate specificity. It dephosphorylated both monophosphorylated PIs [PI(3)P and PI(4)P] (Figure 2C) and P-Tyr containing peptides (Figure 2D), while it did not dephosphorylate any of the small number of P-Ser/P-Thr containing peptides tested (Figure 2E and Table S2). As control enzymes were used the bacterially expressed human phosphatase of regenerating liver-3 (PRL3) (Goldstein, 2001, Mc Parland et al., 2011) (Figure S3A) and the human protein-tyrosine phosphatase PTP1B (Wassef et al., 1985) (Figure S3B). The substrate selectivity of rN15-*LdTyrPIP₂₂* for P-Tyr was further confirmed by carrying out inhibition assays with the P-Tyr phosphatase inhibitor Na₃VO₄ and the P-Ser/P-Thr phosphatase inhibitor NaF using *p*NPP as substrate (10 mM) (Figure 3). Na₃VO₄ inhibited almost quantitatively the dephosphorylation of *p*NPP even at 1/10th of the substrate concentration (Figure 3B), whereas NaF showed no inhibitory effect even at a concentration 10 fold higher than the substrate's concentration (Figure 3C).

All the above described data confirmed that the recombinant bacterially expressed *LdTyrPIP₂₂* behaves as a dual specificity P-Tyr and PI phosphatase as expected from its sequence similarity to phosphatases from the ALP family (Beresford et al., 2010).

***LdTyrPIP₂₂* Is Expressed in *L. donovani* Promastigotes as Soluble, Membrane Bound and Insoluble Cytoskeleton Associated Forms**

To confirm the expression of the *LDBPK_220120.1* encoded *LdTyrPIP₂₂* protein in *L. donovani* cells and assess its abundance at different developmental stages of the parasite we used axenic *L. donovani* promastigote cultures growing at 25°C and pH 7 at the logarithmic (enriched in dividing cells) and

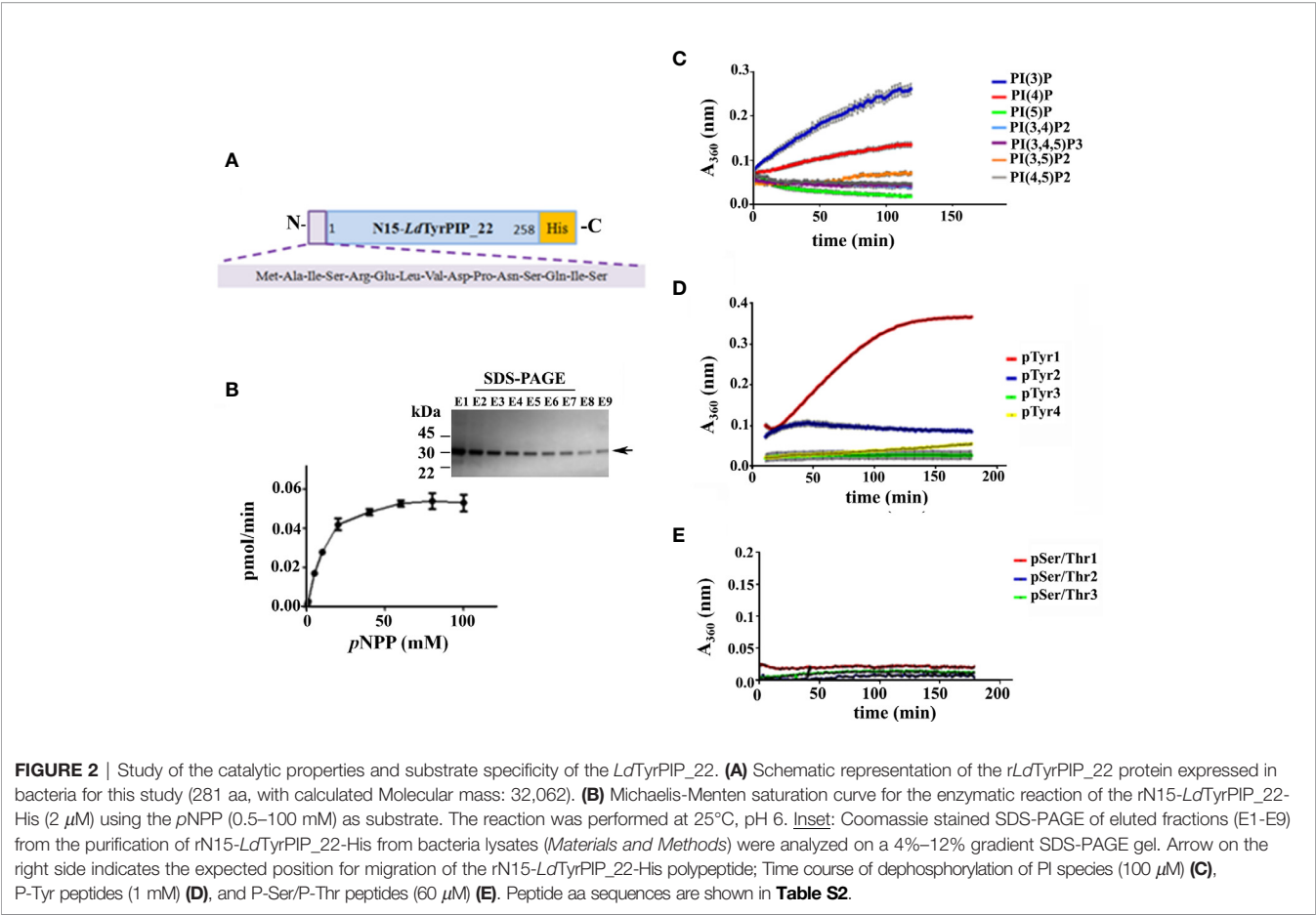


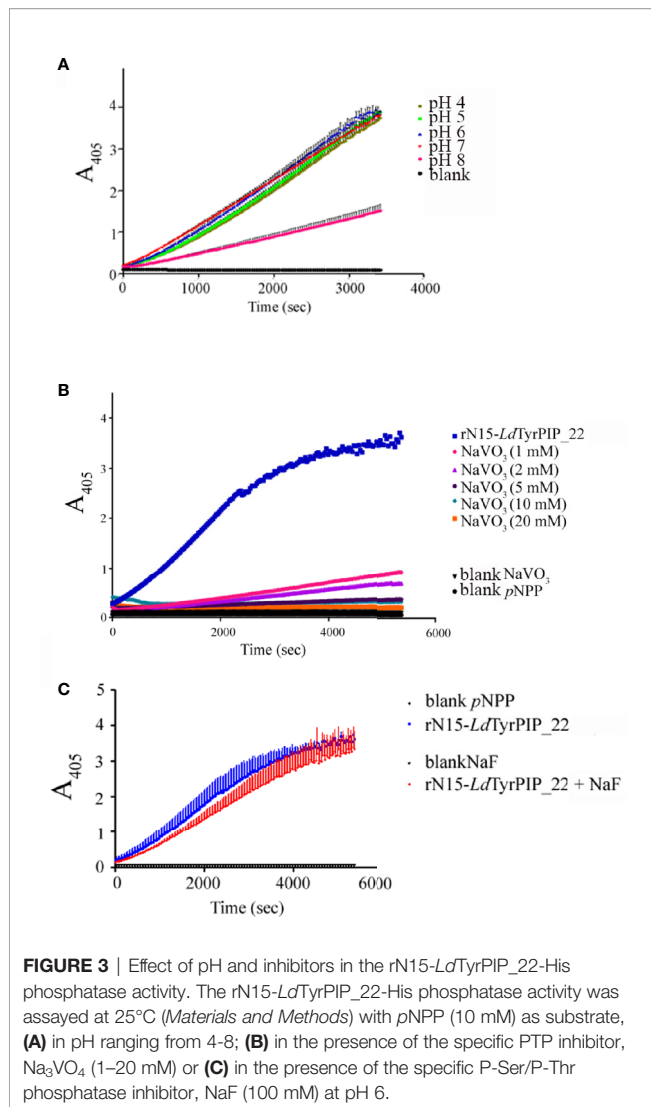
TABLE 1 | Kinetic parameters of *rN15-LdTyrPIP₂₂*-His (values are means \pm S.E.M.).

| Substrate | K _m (mM) | K _{cat} (s ⁻¹) | K _{cat} /K _m (M ⁻¹ × s ⁻¹) |
|-----------|---------------------|-------------------------------------|---|
| pNPP | 11,793 \pm 2,942 | 0,03124 \pm 0,004 | 2.65 \pm 0,280 |

stationary (enriched in non-dividing cells/metacyclis) phases of growth. We also used stationary phase promastigotes cultured for another 24 h at 37°C and pH 5.5, conditions mimicking the temperature and pH of the parasitophorous phagolysosome’s environment in mammalian macrophages (Mc Parland et al., 2011). For this, total lysates from these parasites were analyzed by Western Blot using *a-LdTyrPIP₂₂* specific polyclonal antibodies (pAbs) generated for this project (*Materials and Methods* and **Figure S4A**). The rabbit pAb detected in all three cases [i.e., logarithmic and stationary phase promastigotes growing at 25°C and pH 7 and promastigotes subjected to heat (37°C) and low pH (5.5) treatment] a protein species with apparent MW \sim 30 kDa (**Figure 4Aa**). Given that the calculated MW of *LdTyrPIP₂₂* is 29.1 kDa we consider that this \sim 30 kDa protein species corresponds to the nascent *LdTyrPIP₂₂* form. Occasionally we also detected a pair of bands migrating with lower mobility below the 35 kDa protein

size marker (**Figure S4B**). Quantification of the signal intensity of the \sim 30 kDa band detected by the specific *a-LdTyrPIP₂₂* rabbit pAb showed significantly higher levels in the logarithmically growing cells than in the stationary phase ones (**Figure 4Ad**).

To examine whether the *LdTyrPIP₂₂* protein could preferentially associate with certain subcellular compartments, we prepared subcellular fractions from transgenic *L. donovani* promastigotes expressing a chimeric *LdTyrPIP₂₂*-mRFP1 which would serve as an internal positive control for the specificity of the *a-LdTyrPIP₂₂* pAbs. The biochemical subcellular protein fractionation performed was based on a protocol using a stepwise permeabilization of promastigote membranes by incubating with gradually increasing concentrations of the natural detergent digitonin (Foucher et al., 2006) followed by an additional membrane solubilization step in which the final pellet [Fraction 5 (F5)] was treated with 1% (v/v) Triton X-100 [(Doukas et al., 2019), *Materials and Methods*]. This procedure allowed preparation of subcellular fractions enriched in soluble cytosolic proteins (Fractions F1 and F2), proteins associated with intracellular organelles (Fraction F3 and F4), endoplasmic reticulum (ER) (Fraction F4), pelicular membrane (Fraction F5s), and an insoluble



fraction (F5in, final insoluble pellet) enriched in nuclear/cytoskeleton proteins. We further analyzed these fractions by WB using the mouse a-LdTyrPIP₂₂ pAb that we generated (Figure S4A).

A band detected with apparent MW ~ 55 kDa (Figure 4Ba) probably corresponds to the recombinant LdTyrPIP₂₂-mRFP1 polypeptide (calculated MW 54.5 kDa) since it was also detected by the a-mRFP1 specific pAb (Figure 4Bb). Three more protein species were detected at the 30–35 kDa range with the a-LdTyrPIP₂₂ pAb (Figure 4Bc), not recognized by the a-mRFP1 pAb (Figure 4Bb). The lower size band of ~30 kDa most probably corresponds to the endogenous LdTyrPIP₂₂ form identified in the wt *L. donovani* total lysates by the rabbit a-LdTyrPIP₂₂ pAb (Figure 4Aa). The doublet just below 35 kDa could be assigned to proteolytic fragments of the LdTyrPIP₂₂-mRFP1 not recognized by the a-mRFP1 pAb under the specific conditions of the experiment. Interestingly, the recombinant full length LdTyrPIP₂₂-mRFP1 was detected in all subcellular fractions analyzed [F1–F5ins]. The three protein

species of lower size were detected in all fractions except the F5s (Figure 4Bc) a fraction shown before (Doukas et al., 2019) to be enriched in pelicular membrane proteins. The presence of LdTyrPIP₂₂-mRFP1 in the F5s fraction could represent a translocation artifact due to overexpression, as previously observed for other chimeric proteins tagged with fluorescent proteins (Moore and Murphy, 2009). Finally, a small fraction of the ~ 30 kDa species, assigned to the endogenous LdTyrPIP₂₂ and of the full length LdTyrPIP₂₂-mRFP1 were faintly detected in the F5ins fraction which is enriched in nuclear/cytoskeletal proteins (Foucher et al., 2006). Monomeric free mRFP1 (MW ~27 kDa), probably produced by proteolysis of the full length chimera LdTyrPIP₂₂-mRFP1, was only detected in fraction F5s (Figure 4Bc). In previously published work we have shown that free mRFP1⁹ produced in transgenic *L. tarentolae*-mRFP1 cells was mostly recovered in fractions F1 and F2 whereas ER-associated or pelicular membrane proteins were recovered in fractions F4 and F5s (Papadaki et al., 2015; Doukas et al., 2019). It is worth emphasizing that both a-LdTyrPIP₂₂ Abs (mouse and rabbit) detected the 30 kDa protein species (Figures 4Aa, Ba), a result that strengthens the assignment of this band to the endogenous LdTyrPIP₂₂ protein.

Since there is evidence for secretion of the bacteria ALP homologs of LdTyrPIP₂₂ (i.e., MptpB and LipA) (Koul et al., 2000; Kastner et al., 2011), we also investigated whether the LdTyrPIP₂₂ could be secreted by wt *L. donovani*. For this, we analyzed by WB the proteins in the extracellular medium of axenic *L. donovani* promastigotes growing at 25°C (temperature of the invertebrate host) at the stationary phase of growth or at 37°C (temperature of the mammalian host) following the two approaches described in the Materials and Methods. Despite repeated attempts we were not able to detect the LdTyrPIP₂₂ amongst the proteins collected from the extracellular medium of the *L. donovani* LG13 strain incubated without serum for 9 h at 25°C or for 6 h at 37°C (data not shown). These assays did not include however the challenging analysis of proteins that would be released by the amastigotes inside the infected macrophages.

Thus, the LdTyrPIP₂₂ protein, encoded by the LDBPK_220120.1 gene, is expressed in *L. donovani* promastigotes at the logarithmic and stationary phases of growth, as well as in promastigotes subjected to heat (37°C) and pH (5.5) stress for 24 h. Interestingly, the LdTyrPIP₂₂ was detected in several different subcellular fractions enriched in cytoplasmic, membrane or cytoskeleton associated proteins.

LdTyrPIP₂₂ Is Localized in Multiple Sites in *L. donovani* Promastigotes Growing at 25°C and pH 7

To study further the LdTyrPIP₂₂ subcellular distribution in *Leishmania* cells we performed immunofluorescence labeling and confocal microscopy analysis using our homemade mouse and rabbit a-LdTyrPIP₂₂ pAbs (Figure S4A, B) in combination with Abs recognizing other *Leishmania* proteins of known

⁹<https://www.fpbse.org/protein/mrfp1/>

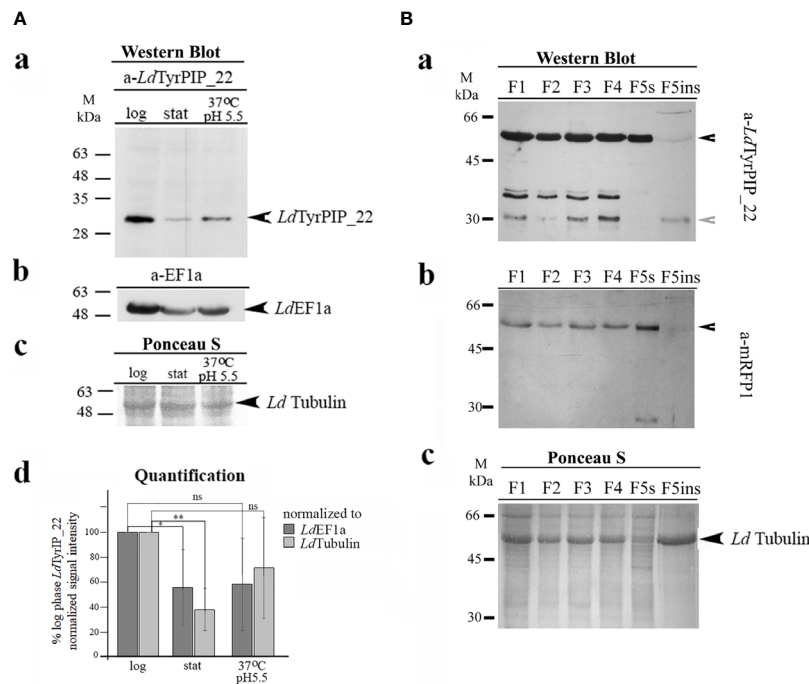


FIGURE 4 | Biochemical detection of the endogenous LdTyrPIP₂₂ forms in wt *L. donovani* (LG13) and in *L. donovani*-LdtyrPIP₂₂-mrp1 transgenic promastigotes. Subcellular distribution of LdTyrPIP₂₂ by detergent treatment. **(A)** Total lysates (40 µg protein/well) from logarithmic (log) and stationary (stat) phase cultures of promastigotes (~5X10⁶ cells), as well as from parasites after treatment of stationary phase promastigotes for 24 h at 37°C and pH 5.5, were analyzed by SDS-PAGE (12% w/v) and immunoblotted with the purified rabbit a-LdTyrPIP₂₂ pAb (2 µg/ml) (a). The membrane was then reblotted after stripping with the a-EF1a mAb (1:10,000). LdEF1a was used as loading indicator (b). The region of the membrane with tubulin stained with Ponceau-S is shown (c) as a 2nd loading indicator. (d) Quantification of the intensity of the LdTyrPIP₂₂ band signal for each condition was performed using the Fiji algorithm. The intensity of the LdTyrPIP₂₂ band signal for each condition was normalized to the intensity of the corresponding LdEF1a or LdTubulin band signals and expressed as % of the normalized LdTyrPIP₂₂ signal at the logarithmic phase in each experiment. The mean values from three independent experiments with standard deviations were plotted. ** (P ≤ 0.01), * (P ≤ 0.05) and ns (P > 0.05). **(B)** Protein fractions (F1-F5ins) from stationary phase *L. donovani*-LdtyrPIP₂₂-mrp1 transgenic promastigotes, produced by permeabilization of total cell pellet with digitonin and Triton X-100 (*Materials and Methods*) were analyzed by SDS-PAGE (12% w/v) and immunoblotted with the mouse a-LdTyrPIP₂₂ serum (1:1,200) (a) and subsequently, after stripping, with the purified a-mRFP1 (0.5 µg/ml) pAb (b). Ponceau-S of respective membrane regions (c), is shown as loading indicator. Black arrowhead indicate the protein bands corresponding rabbit to rLdTyrPIP₂₂-mRFP1 and grey arrowhead to band assigned to the endogenous LdTyrPIP₂₂. Molecular weights are indicated in kDa.

subcellular localization, including LdActin (Sahasrabudhe et al., 2004), LdTubulin, and GAPDH as a glycosome marker (Herman et al., 2008).

We first analyzed the LdTyrPIP₂₂ localization in axenic dividing and non-dividing promastigotes grown at 25°C using logarithmic or stationary phase promastigote cultures. Having at our disposal a-LdTyrPIP₂₂ Abs from two species, allowed us: 1) to ensure that the epitopes highlighted by each Ab belong to the endogenous LdTyrPIP₂₂ (**Figure S4B**) and 2) to perform co localization studies with other *Leishmania* proteins using specific primary Abs either from rabbit or mouse origin. For imaging of the parasites besides the TCS SP Leica confocal microscope we used the SP5 and SP8 Leica more advanced confocal models which allowed us to benefit from maximum optical resolution of the lenses and higher digital resolution in the image acquisition than the older TCS SP confocal microscope.

The localization pattern of LdTyrPIP₂₂ varied in parasites at different cell cycle dependent morphological stages (**Figure 5** and **Figure S5**). Depending on the cell cycle stage, axenic *Leishmania*

promastigotes obtain diverse morphologies most of which, with exception the procyclic and the metacyclic forms, coexist both in the exponential and stationary phases of growth (Wheeler et al., 2011). These morphologies, following nomenclature used for description of the flagellated promastigote forms observed in the midgut of sandflies (Sunter and Gull, 2017), could be assigned as: 1) dividing procyclic-like with short cell body (6.5–11.5 µm) and flagellum shorter than the cell body; 2) leptomonad-like with cell body between 6.5–11.5 µm and longer flagellum; 3) nectomonad-like with cell body longer than 12 µm and long flagellum and 4) the metacyclic-like with short (8 µm) and slender cell body and long flagellum (>2X longer than the cell body).

Interestingly, in dividing and non-dividing morphological forms of promastigotes in culture, LdTyrPIP₂₂ was localized at the periphery of the cell body (**Figure 5**, **Figures S5Ac, d, S6** and **S9**) in areas rich in LdActin (**Figures 5A–D** insets) and microtubules (**Figures S6**) or stained with the FM4-64 dye (**Figure S7**) (Vince et al., 2008). Occasionally, LdTyrPIP₂₂

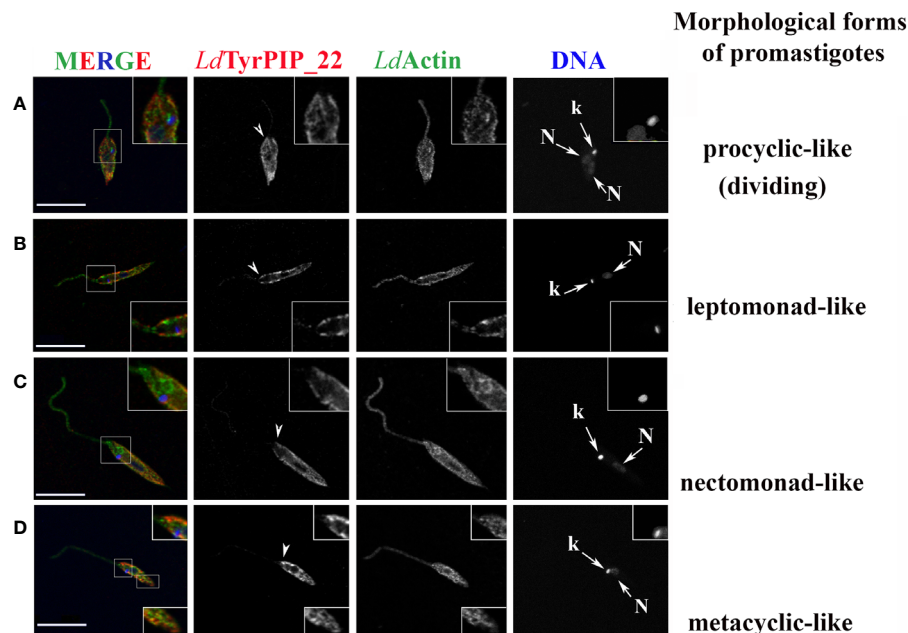


FIGURE 5 | Localization of *LdTyrPIP₂₂* in different cell cycle dependent morphological forms of cultured *L. donovani* promastigotes growing at 25°C, pH 7; co staining for *LdActin*. *L. donovani* promastigotes from logarithmic or stationary phase cultures were fixed (4% w/v PFA) and permeabilized with 0.1% (v/v) TritonX-100. They were then co stained by IF with the α -*LdTyrPIP₂₂* mouse pAb (1:250) and rabbit α -LeishActin pAb (1:1,000) followed by secondary Abs conjugated to Alexa Fluor®546 and Alexa Fluor® 488, respectively. Nuclear and kinetoplast DNA was stained with Hoechst 33342 (1:5,000). Representative images of different cell cycle dependent morphological forms of promastigotes were acquired by z-scanning performed at 0.3 μ m step size using the TCS SP8 Leica confocal microscope. A single z section with representative staining from each case is shown. Single FL images are shown in black and white (BW) for better contrast while images of the merged FL signals are shown in color. The molecule highlighted in the BW images with single color FL is indicated at the top in the same color as the respective FL signal. Arrowheads point to the flagellar pocket region/flagellum base. Small arrows point to the kinetoplast (k) and nucleus (N). Magnifications (1.5-2X) of framed areas are shown as insets. Scale bar size: 10 μ m.

epitopes were also detected in internal tubular/filament-like structures (**Figure 5D**, bottom inset, **Figures S5Ab, S7b**) which could be part of the tubular MTV endosome (Halliday et al., 2019; Wang et al., 2020) and at the posterior region of the cell body (**Figure 5A**, **Figure S7b**), area where internalized/endocytosed cargo accumulates in late endosomes (Ghedin et al., 2001; Fernandes et al., 2020). Lower intensity punctate staining was also observed along the entire flagellum in most parasites (**Figures 5B and S5Aa, c, d and S5Bb**). In this analysis, *LdActin* was detected both at the promastigote's cell body and along the flagellum with the labelling of the α -*LdActin* Ab more evident at the periphery of the cell body including the area where the flagellum buds. The pellicular membrane-associated actin has been described to be closely localized with the subpellicular microtubules (sMTs) (Sahasrabudde et al., 2004). Consistently, co staining with the *LdTyrPIP₂₂* rabbit pAb and a mouse Ab for *Leishmania* tubulin, highlighting the subpellicular microtubules, confirmed the localization of *LdTyrPIP₂₂* at the periphery of the promastigote's cell body (**Figure S6**) either subpellicularly or at the pellicular membrane.

Given the limitation of the optical resolution of confocal microscopes we cannot ascertain protein co-localization or distinguish between the subpellicular actin or microtubules and the pellicular membrane. However, quantification of the % of red

pixels in the cell body (corresponding to *LdTyrPIP₂₂* epitopes), overlapping with the green pixels (corresponding to *LdActin* epitopes), resulted in an estimation of $59 \pm 14\%$ ($n=49$) of *LdTyrPIP₂₂* signal superimposed with the *LdActin* signal in all the morphological forms of promastigotes' culture. Higher levels of pixel co-localization were observed in procyclic-like/dividing and metacyclic-like parasites (60 ± 12 , 63 ± 10 and $65 \pm 11\%$ respectively) while for the leptomonad- and nectomonad-like forms the overlapping pixels ranged from 50 ± 11 - $52 \pm 14\%$. Therefore, from this pixel intensity analysis, a molecular proximity of *LdTyrPIP₂₂* with *LdActin* is inferred with the possibility of a direct or indirect interaction.

Additional sites where *LdTyrPIP₂₂* was detected in axenic promastigote, regardless the α -*LdTyrPIP₂₂* pAb used were: 1) next to or surrounding the kinetoplast (the mass of concatenated mitochondrial DNA) (**Figure S5**, arrowheads), 2) the base or the sides of the flagellar pocket (invagination of the cell membrane forming a vase-like structure at the base of the flagellum) and 3) the proximal end of the flagellum (**Figures 5 and S5**, short arrowheads). Often the entire flagellar pocket was decorated by the α -*LdTyrPIP₂₂* Ab staining (**Figures S5Ac and S5Ba,b** insets). In newly divided (**Figure S5Ac**) and dividing promastigote, identified by the two nuclei (**Figure S5Ad**), we also

observed staining of vesicular-like structures. Co staining with the α -GAPDH antibody, GAPDH was used as a glycosome marker, showed that the LdTyrPIP₂₂ vesicular staining was excluded from the structures highlighted by this Ab (**Figure S8**). The punctate staining observed around large compartments (**S5A a inset, c**) could mark acidocalcisomes or megasomes (Rodrigues et al., 2014).

Overall, LdTyrPIP₂₂ epitopes were detected in multiple sites in the *L. donovani* axenic promastigote with the most prominent ones being 1) the periphery of the cell body, 2) adjacent to the kinetoplast, 3) intracellular small vesicles, 4) the proximal end of the flagellum, and 5) the flagellar pocket area.

A Shift to 37°C and pH 5.5 Triggered a Pronounced Recruitment of LdTyrPIP₂₂ at the Flagellar Pocket Region and a Perinuclear Redistribution

In the *in vivo* situation, the differentiation process converting the *Leishmania* promastigote to amastigote takes place within the mammalian host macrophages when the infective metacyclic promastigote is phagocytosed and enclosed in the parasitophorous phagolysosome (Sunter and Gull, 2017). The metacyclic promastigote (MP) to the amastigote transition involves dramatic changes in cell shape and results in a minimized cell surface to volume ratio, hence reducing the area over which the cell is exposed to the harsh environment of the parasitophorous vacuole reformatting of the flagellum and also occurs. These changes require substantial membrane and cytoskeleton remodeling in which, from what is known for higher eukaryotes (Schink et al., 2016; Senju et al., 2017), PI metabolism and signaling play central roles. Therefore, we decided to monitor by microscopy the localization of the LdTyrPIP₂₂ over time under conditions resembling those experienced by the promastigote when enclosed in the parasitophorous phagolysosome.

To this end, a stationary phase promastigote culture, 8 days post subculturing, was subjected to a temperature shift at 37°C while the pH was adjusted to 5.5. The conversion of the promastigotes' population to amastigotes in most protocols begins 4 h after the temperature and pH shift. In the first 24 h of incubation of the axenic parasites' culture at 37°C and pH 5.5, a mixed population of flagellated promastigotes and amastigote-like parasites with short flagella coexist. (Doyle et al., 1991; Debrabant et al., 2004; Zilberstein, 2020). Imaging of promastigotes from this population using immunofluorescence and confocal microscopy showed a systematic and drastic recruitment of the LdTyrPIP₂₂ towards the base of the flagellum and the flagellar pocket (**Figures 6 and 7**). The other two prominent localizations observed were: 1) a perinuclear punctate staining (**Figures 6A, 7A–C**) and 2) a vesicular staining throughout the cell body (**Figure 6B**). Of note, in this axenic promastigote culture we also observed LdActin in the nucleus (**Figures 6A, 7A, B**) as it has already been reported (Sahasrabudhe et al., 2004).

To refine the conditions that induce accumulation of the LdTyrPIP₂₂ at the promastigote's flagellar pocket, we tested separately the effect of temperature and pH. We found that as

early as 30 min after transferring the promastigote to 37°C we could detect the distinct accumulation of LdTyrPIP₂₂ at the promastigote's flagellar pocket (**Figure S7**, arrowhead). A similar LdTyrPIP₂₂ distribution was observed in extracellular promastigotes in an *in vitro* infection assay of J744 murine macrophages exposed only to 37°C but not to low pH shift 4 h post-infection (**Figure 6C**, insets).

In this case the promastigotes were promastigotes grown at 25°C and pH 5.5 for 24 h did not show this characteristic recruitment of LdTyrPIP₂₂ at the flagellar pocket (data not shown). Moreover, in amastigote-like forms, observed in the axenic culture grown at 37°C and pH 5.5 for 24 h up to 144 h, LdTyrPIP₂₂ epitopes were detected at the flagellar pocket near the kinetoplast (**Figures 7A inset, 7B and S9B**), in vesicles (**Figure S9A**) or at the tip of the small flagellum barely emerging from the flagellar pocket (**Figures 7B and S9B**).

Concluding, at 37°C and pH 5.5, conditions resembling the ones encountered by *Leishmania* parasites in the mammalian hosts where the developmental transition of the MPs to amastigotes is initiated, LdTyrPIP₂₂ is strongly recruited to the flagellar pocket and redistributes perinuclearly.

DISCUSSION

This study provides the first experimental evidence documenting the expression of the *L. donovani* LDBPK_{220120.1} gene product in the *L. donovani* parasites, a *Leishmania* spp. highly pathogenic to humans. The ortholog gene *LmjF_22_0250* from *L. major*, shown to be upregulated in metacyclic *L. major* promastigote (Dillon et al., 2015; Inbar et al., 2017), was earlier reported to encode a protein which when expressed as recombinant in bacteria exhibited PTP and PI phosphatase activities (Beresford et al., 2010).

We cloned the LDBPK_{220120.1} gene from a Sudanese *L. donovani* (LG13) strain and showed that its protein product, when expressed heterologously in bacteria, dephosphorylated P-Tyr peptides and monophosphorylated PIs [PI(3)P and PI(4)P], similarly to its *L. major* ortholog LM1 (Beresford et al., 2010), properties that classify both as atypical Dual Specificity Lipid-like phosphatases (Brenchley et al., 2007). The *L. donovani* aDSP, that we named LdTyrPIP₂₂, together with its *L. major* ortholog, represent to our knowledge the first PI phosphatases characterized in *Leishmania* spp. to date. With specific antibodies that we generated we analyzed the subcellular localization of LdTyrPIP₂₂ using detergent based subcellular fractionation and immunofluorescence microscopy. An array of intracellular localizations, comprising membrane and cytoskeleton associated elements, were observed by both approaches, suggesting that LdTyrPIP₂₂ has multiple cellular partners/substrates participating thereby in multiple cellular functions which are consistent with its identity as a dual specificity P-Tyr/PI phosphatase.

Interestingly, the recombinant LdTyrPIP₂₂ used in this study has a narrower substrate preference than its bacterial homologs MptpB and LipA from the ALP family (Beresford

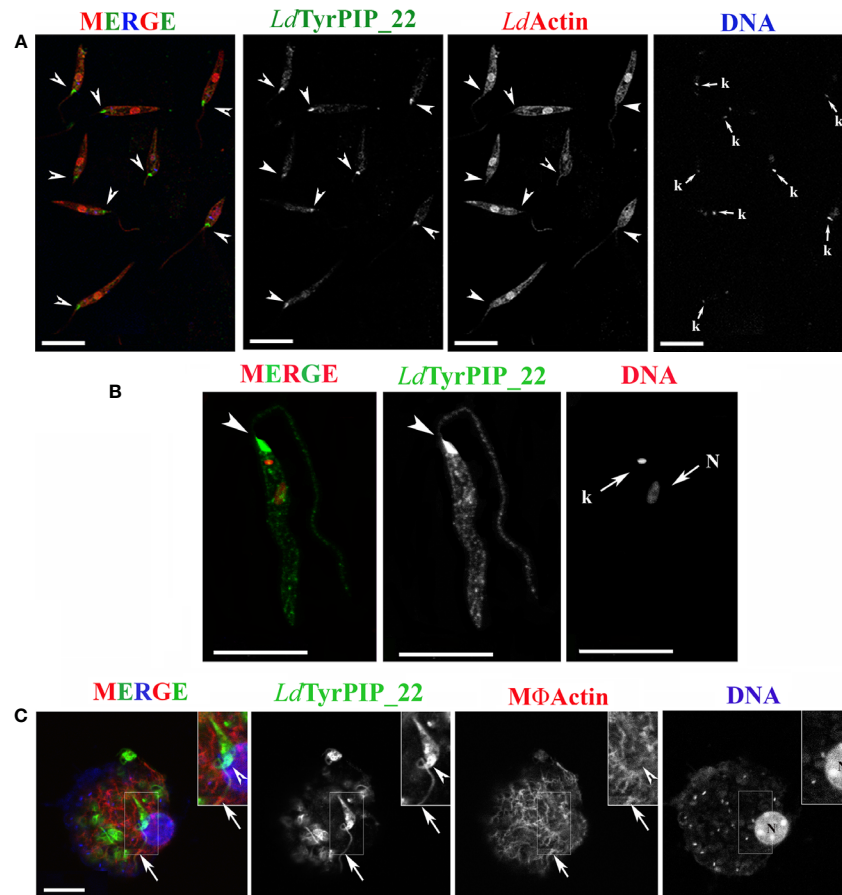


FIGURE 6 | Localization of LdTyrPIP₂₂ epitopes in axenic *L. donovani* promastigotes after 24 h exposure at 37°C and pH 5.5 or during a 4 h *in vitro* infection of J774 macrophages. **(A, B)** Confocal microscopy images of *L. donovani* stationary phase promastigotes incubated for 24 h at 37°C and pH 5.5. Images were acquired with a Leica SP8 confocal microscope by z-scanning with 0.3 μ m step size. Images in **(A)** were acquired at 1X digital magnification while in **B** at 4X. **(A)** Double IF staining of fixed cells permeabilized with 0.1% (v/v) Triton X-100 was performed with the α -LdTyrPIP₂₂ mouse pAb (1:100) and α -LdActin rabbit pAb (1:1,000) followed by secondary Abs conjugated to Alexa Fluor[®] 488 or Alexa Fluor[®] 546. Nuclear and kinetoplast DNA was stained with Hoechst 33342 (1:5,000). Images (max projections) of several promastigotes are presented. In the DNA stain the kinetoplast (small arrow, k) is more intensely stained than the nucleus. **(B)** An image of a promastigote (single z section of a z-series) acquired with a 4X magnification factor. IF staining for LdTyrPIP₂₂ and DNA staining were performed as in **(A)**. The nuclear (N) and kinetoplast (k) DNA staining is presented here in red pseudo color for better contrast in merged image. **(C)** A J774 murine macrophage 4 h post-infection *in vitro* with *L. donovani* promastigotes imaged by confocal microscopy. Stationary phase promastigotes were added to adhered macrophages at a 20:1 ratio. IF staining of fixed cells permeabilized with 0.1% (v/v) Triton X-100 was performed with the α -LdTyrPIP₂₂ mouse pAb (1:100) followed by secondary Ab conjugated to Alexa Fluor[®] 488. Macrophage polymerized actin was stained with phalloidine conjugated to Alexa Fluor[®] 546. Images were acquired with a Leica TCS SP5 confocal microscope by z-scanning performed at 1 μ m step size. A single optical section from the top of the cell is presented. A promastigote, still extracellular in most part but in the process of being phagocytosed is shown in the insets (1.5X magnification). Single FL and phase contrast images are presented in BW while images of the three merged FL signals are shown in color. The molecule highlighted in the BW images with single color FL is indicated at the top in the same color as the respective FL signal. In **(A)**, **(B)**, and **(C)** arrowheads point to the flagellar pocket/base of flagellum. Small arrows in **(A)** and **(B)** point to the kinetoplast (k) and nucleus (N) while large arrows in **(C)** point to polymerized actin surrounding part of the phagocytosed parasites' flagellum. Scale bar size in **(A–C)**: 10 μ m.

et al., 2010). MptpB from *Mycobacterium tuberculosis* has triple specificity, dephosphorylating P-Ser, P-Thr, and P-Tyr peptides as well as mono- and di-phosphorylated PIs (i.e., PI(3)P, P(4)P, PI(5)P, and PI(4,5)P₂), (Beresford et al., 2010). LipA, from *Listeria monocytogenes* although it has similar substrate preference to the PIs with MptpB, it dephosphorylates only P-Tyr peptides (Beresford et al., 2010). The P-loop sequence in the catalytic site of the three proteins is almost identical with

only one aa difference at position 2 (i.e., Phe¹⁶¹ in MptpB instead of Thr¹⁴⁸ in rLdTyrPIP₂₂ and Thr¹⁸⁸ in LipA). Point mutation studies in the MptpB (Beresford et al., 2007) showed that the nature of this aa plays an important role in the substrate specificity for PIs as well as in the levels of enzymatic activity. However, other determinants in the 3D structure of the three proteins must play critical role in the substrate preference. The bacterially expressed ortholog of

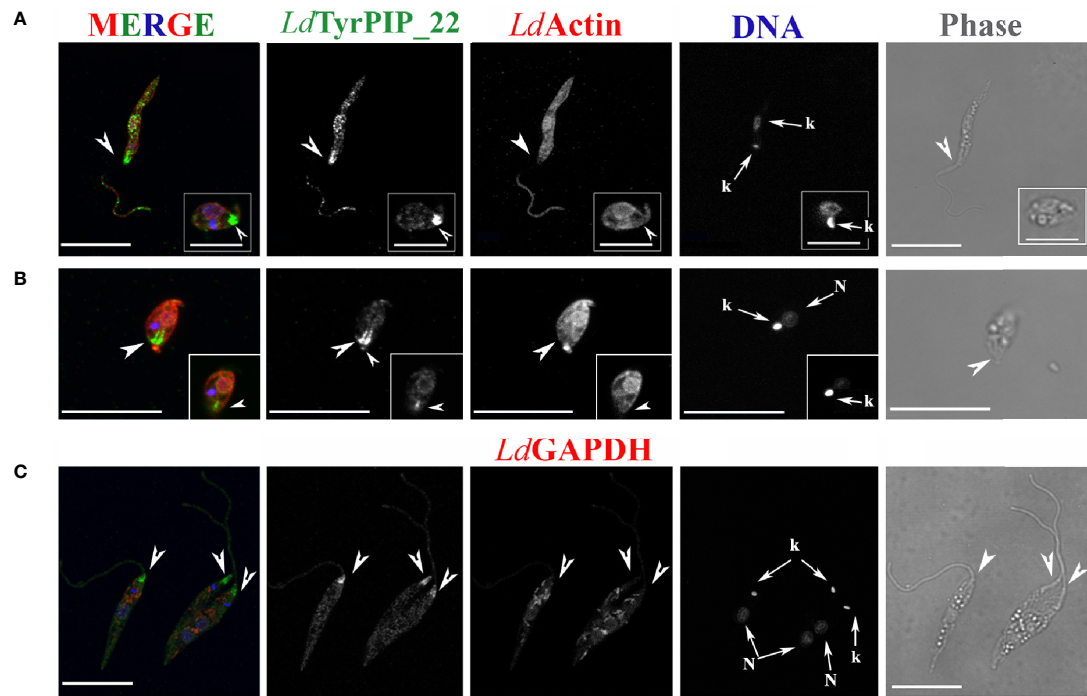


FIGURE 7 | Localization of *LdTyrPIP₂₂* epitopes in tationary phase *L. donovani* parasites after 24 h exposure at 37°C and pH 5.5. Co staining with *LdActin* and *LdGAPDH*. Confocal microscopy images of *L. donovani* promastigote- and amastigote-like forms. Double IF staining of fixed cells permeabilized with 0.1% (v/v) TritonX-100 was performed with the anti-*LdTyrPIP₂₂* mouse pAb (1:100) and the anti-*LdActin* rabbit pAb (1:1,000) in (A, B) or the anti-GAPDH rabbit pAb (1:100) in (C) followed by secondary Abs conjugated to Alexa Fluor® 488 or Alexa Fluor® 546. Nuclear and kinetoplast DNA was stained with Hoechst 33342 (1:5,000). In (A, C), single z-sections of axenic promastigote-like forms. Inset in (A): an amastigote-like parasite from the same field at a 2X magnification. In (B), the maximum intensity projection of an amastigote-like parasite (i.e., smaller than promastigotes, ovoid, with retracted/short flagellum). Inset in (B): a single z-section at the same magnification as the maximum intensity projection. Single FL and phase contrast images are presented in BW while images of the three FL signals merged are shown in color. The molecule highlighted in the BW images with single color FL is indicated at the top in the same color of the respective FL signal. Images were acquired with a Leica TCS SP8 confocal microscope by z-scanning performed at 0.3 µm step size. Large arrowheads point to the flagellar pocket/base of flagellum. Small arrowhead in inset (B), shows the small flagellum. Small arrows in (A–C) point to the kinetoplast (k) and nucleus (N). Scale bar size in A–C: 10 µm. Inset (A) scale bar size: 5 µm.

LdTyrPIP₂₂ from *L. major* (i.e., LM1), additionally to the PI (3)P and PI(4)P, was shown to also dephosphorylate PI(5)P (Beresford et al., 2010). The predicted primary structures of the two proteins differ in 7 aa (Figure 1). Whether these differences play a critical role on the two enzymes' substrate preferences remains to be shown.

Phosphorylation and dephosphorylation are well-documented post translational modifications regulating the developmental transitions of *Leishmania* spp. along their biological cycle (Chow et al., 2011; Tsigankov et al., 2013; Tsigankov et al., 2014; Dillon et al., 2015). Especially, phosphorylation on tyrosine residues, although comprising a small fraction of all protein phosphorylation events, plays a pivotal role in signaling, cell-cycle control, and differentiation (Cool and Blum, 1993; Nascimento et al., 2006). Indeed, inhibition of tyrosine phosphorylation in *Leishmania* promotes partial differentiation from promastigote to amastigote forms (Nascimento et al., 2003). Therefore tyrosine kinases and P-Tyr phosphatases can be viewed as master regulators of the *Leishmania* developmental cycle. The *LdTyrPIP₂₂*

phosphatase represents a putative player in these regulations with its P-Tyr phosphatase activity. The finding that the *LDBPK_220120.1* ortholog gene transcription in *L. major* is significantly upregulated in both cultured and sandfly metacyclic promastigotes (Dillon et al., 2015; Inbar et al., 2017) suggests a need for this enzyme's activity over the developmental transition of *Leishmania* from the forms adapted in the blood feeding insects' midgut/foregut to the ones living in the mammal dermis and skin-distant organs. Moreover, the substantial upregulation (5.92 fold vs 2.63 fold) of this *L. major* transcript in the sandfly living metacyclics (Inbar et al., 2017) versus the cultured metacyclics (Dillon et al., 2015), points to its importance in the survival of the parasite under the stress and nutrient scarcity conditions in the anterior midgut of the fly where metacyclogenesis occurs. Moreover, the MP to the amastigote transition involves dramatic changes in cell size and shape and a reformatting of the flagellum. These changes require substantial membrane and cytoskeleton remodeling and dynamics in which, from what is known for higher eukaryotes (Schink et al., 2016; Senju et al., 2017), PI signaling and metabolism play central roles.

LdTyrPIP₂₂ with its PI dephosphorylating activity may contribute to events resulting in these developmental transitions of *Leishmania* promastigotes.

In this study, the microscopy imaging of promastigotes growing at 25°C revealed LdTyrPIP₂₂ epitopes at the flagellar pocket region (Figures S5A small arrows, B and Ba,b insets), adjacent to the kinetoplast (Figure S5A arrowheads) where the Golgi apparatus is located (Halliday et al., 2019) and occasionally in vesicular (Figure S5A), and tubular structures (Figures S5b and S7b) resembling MTV endosomes (Wang et al., 2020). All these localizations, considering that 1) the flagellar pocket region in protozoans of the *Leishmania* genus is highly specialized for uptake of macromolecular nutrients and secretion via the conventional exocytic route (Landfear and Ignatushchenko, 2001) and 2) the LdTyrPIP₂₂ dephosphorylates selectively PI(3)P and PI(4)P, are compatible with a role for this phosphatase in endocytosis/exocytosis event(s) and/or membrane trafficking in *Leishmania* promastigotes. Diverse functions of PI(3)P and PI(4)P PIs in the regulation of membrane traffic and cell signaling pathways are based, at least in part, on their spatiotemporally controlled formation and turnover at defined subcellular sites (Marat and Haucke, 2016). In metazoan cells, PI 3-phosphates such as PI(3)P and PI(3,5)P₂ are found predominantly in membranes of early and late endosomes or lysosomes with key importance for their function (Balla, 2013). Endosomal recycling to the cell surface requires PI(3)P hydrolysis and the concomitant generation of PI(4)P is required for exocytosis to occur (Wallroth and Haucke, 2018). PI(4)P is mainly concentrated in the exocytic pathway, in particular in the Golgi complex, the trans-Golgi network (TGN), and the plasma membrane (Balla, 2013; Hanes et al., 2017; Wallroth and Haucke, 2018). However, the *Leishmania* cell is largely an unmapped territory with respect to its PIs' localization, metabolism and signaling pathways (Zhang and Beverley, 2010; Velasquez et al., 2015). In *Trypanosoma brucei*, one of the closest relatives of *Leishmania* spp. in the Trypanosomatidae family, it is known that PIs and their related kinases and phosphatases function as a regulatory system in addition to their role in the synthesis of membrane or glycoconjugate structures (Cestari, 2020). This is evidenced by the numerous cellular processes affected when genes encoding PI-related proteins or proteins generating PI metabolites are mutated or knocked out (reviewed in (Cestari, 2020)). Interestingly, in *Trypanosoma brucei*, PIs have diversified in function with respect to their role in metazoans to control specialized processes (Cestari and Stuart, 2018; Cestari et al., 2019). If we extrapolate from the localizations of PI(3)P and PI(4)P in metazoans and what is known for *Trypanosoma brucei*, LdTyrPIP₂₂ may be involved in endocytosis/exocytosis event(s) and/or membrane trafficking in *Leishmania* promastigotes.

The distinct, although not prominent, detection of LdTyrPIP₂₂ epitopes along the flagellum could support the hypothesis that this enzyme may also be involved in the regulation of intraflagellar transport or the flagellum's remodeling during MP to amastigote differentiation. This could be another explanation for the LdTyrPIP₂₂ epitopes detected to sites adjacent to the kinetoplast, known to be

connected via a tripartite attachment complex (TAC) to the flagellum basal body (Gluenz et al., 2010). Recent studies on mammalian epithelial cells have shown that PI(4)P homeostasis, coordinated by a pair of PI kinase and phosphatase at the centrosome/ciliary base, is vital for ciliogenesis (Xu et al., 2016). It is possible that a similar mechanism also exists in *Leishmania* cells.

Finally, the observed localization of LdTyrPIP₂₂ in regions enriched in LdActin, mainly at the periphery of the cell body of promastigotes growing at 25°C (Figure 5), suggests a possible role of this phosphatase in the regulation of actin cytoskeleton properties, as it is the case for a number of other phosphatases in lower (Delorme et al., 2003; Schuler and Matuschewski, 2006; Fernandez-Pol et al., 2013) and higher eukaryotes (Larsen et al., 2003; Nakashima and Lazo, 2010). From the quantitative analysis on the microscopy images of promastigotes co stained with the a-LdTyrPIP₂₂ and the a-LdActin specific Abs, a molecular proximity of these two proteins was inferred with the possibility of a direct or indirect interaction. This could drive a working hypothesis on a dynamic interplay between the LdTyrPIP₂₂ phosphatase and actin via its PI or its P-Tyr dephosphorylating activities. Interestingly, actin controls the motile behavior of the *Leishmania* promastigote and is involved in intracellular vesicular trafficking and flagellar-pocket organization in *Trypanosomatids* (Sahasrabudhe et al., 2004; Katta et al., 2010). Both functions are compatible with the LdTyrPIP₂₂ localizations in the *L. donovani* promastigotes.

One of the most novel findings of this study was the pronounced recruitment of LdTyrPIP₂₂ in the flagellar pocket region when stationary phase promastigotes were subjected to temperature 37°C and pH 5.5 for 24 h (Figures 6, 7). This accumulation did not seem to be due to higher expression levels of LdTyrPIP₂₂ since quantification by Western Blot of the LdTyrPIP₂₂ protein levels in axenic *L. donovani* promastigotes treated as above did not show a significant difference with the levels observed in stationary phase promastigotes growing at 25°C and pH 7 (Figures 4Ba and d). Environmental signals like elevated temperature and acidity have already been shown to be crucial in triggering the developmental transition from the motile MP to the immotile amastigote inside the mammalian host macrophage (Zilberstein and Shapira, 1994; Sereno and Lemesre, 1997; Barak et al., 2005). This differentiation marked by a dramatic change in the parasite's cell shape from the elongated slender cell body to a small ovoid shape one and from a long motile flagellum with a 9 + 2 axoneme arrangement to a short non motile flagellum with a 9 + 0 axoneme arrangement (Gluenz et al., 2010). Additionally, a large restructuring of the flagellar pocket and neck region takes place. This associates with changes in the localization of the flagellum attachment zone proteins. As a consequence, the flagellar pocket neck closes to fit tightly around the remaining short flagellum end (Sunter and Gull, 2017) the tip of which is considered to play a sensory role in the interaction with the host (Kelly et al., 2020). Moreover, the growth rate and the metabolism of the amastigotes slow down considerably (McConville et al., 2007) by the expression of stage specific survival factors (Leifso et al., 2007; Biyani and Madhubala, 2012).

If the *ldtyrpip*₂₂ gene transcription is upregulated in metacyclogenesis as for its ortholog *LmjF.22.0250* in *L. major* (Inbar et al., 2017), it may be involved in a process preparing the parasite for adaptation to the mammalian host microenvironment, part of which is the transformation to the amastigote form. Interestingly, in this study, LdTyrPIP₂₂ was recruited to the flagellar pocket soon after the stationary axenic promastigote culture was shifted from 25°C to 37°C (**Figure S8**). This recruitment was more dramatic in axenic amastigote-like *L. donovani* forms (**Figures 7A inset, 7B, and S9B**) identified in *L. donovani* culture subjected to temperature and low pH stress conditions for 24–144 h, pointing to a role of this phosphatase in the MP to amastigote transition. In that sense, LdTyrPIP₂₂ could be involved in the regulation of endo/exocytosis processes, upregulated when parasites are subjected to temperature stress (Hassani et al., 2011) but, also in mechanisms regulating flagellum disassembly with flagellar pocket maintenance through remodeling. The latter is a process that follows the demands of minimizing the amastigote cell's total surface area as an adaptation in the phagolysosome environment (Wheeler et al., 2016). Moreover, the presence of LdTyrPIP₂₂ epitopes in the short flagellum tip of amastigote-like parasites (**Figures 7B and S9B** small arrowheads) suggests a possible role in the communication of the parasite with the parasitophorous phagosome membrane (Gluenz et al., 2010). All the above stated hypotheses merit further extensive investigation in *Leishmania* cells genetically engineered to overexpress LdTyrPIP₂₂ or dominant negative mutants of LdTyrPIP₂₂ or in KO parasites with the *ldtyrpip*₂₂ gene deleted.

The punctate perinuclear redistribution of LdTyrPIP₂₂, consistently observed at different levels, resembles nuclear pores' staining pattern. In metazoans, a large number of phosphatases have been shown to localize at the Nuclear envelope and this membrane is attracting attention as a cell's compartment for the control and transduction of several signaling pathways (Sales Gil et al., 2018). Moreover, PIs are localized inside the nucleus and are shown to play important roles in chromatin remodeling, gene transcription, and RNA processing (Castano et al., 2019). PI kinases, phosphatases and phospholipases have also been shown to localize in the nucleus (Barlow et al., 2010). Moreover, given that LdTyrPIP₂₂ is a P-Tyr phosphatase as well, its nuclear localization may imply a regulatory role through P-Tyr dephosphorylation in nuclear processes, as shown for certain mammalian PTPs. Multiple evidence exists for a turnover of phosphotyrosine at the nuclear envelope of intact metazoan cells (Otto et al., 2001).

An unexpected result of this study was the detection of higher amount of LdTyrPIP₂₂ protein in total lysates of logarithmically growing promastigotes as compared to promastigotes in stationary phase. The latter constitute the promastigotes' population enriched in metacyclic forms in which the gene transcript of the *L. major* ortholog of *ldtyrpip*₂₂ (i.e., the *LmjF.22.0250* gene) was observed to be upregulated 2.6 fold (Dillon et al., 2015) in axenic parasites. However, the metacyclic forms in the stationary phase promastigotes of the *L. donovani* complex *Leishmania* spp.

constitute a small pool (below 6%–7%) of the total population (Santarem et al., 2014). Even if this small pool of *L. donovani* metacyclics expressed higher levels of LdTyrPIP₂₂ this would not affect significantly the levels of this protein in the total population of stationary phase promastigotes, mostly consisting of leptomonad- and nectomonad-like forms (Sunter and Gull, 2017). It remains however an interesting finding that the amount of LdTyrPIP₂₂ protein detected in the promastigotes' population enriched in dividing *L. donovani* is ~ 2 fold higher as compared to the non-dividing population, a result that merits further investigation.

Before concluding, it worths mentioning a recent interesting study which showed that *L. mexicana* knock out parasites in the *LmxM.22.0250* gene (i.e., the *ldtyrpip*₂₂ *L. mexicana* ortholog) presented severely attenuated virulence in the infection of primary mouse macrophages *in vitro* (Kraeva et al., 2019). This finding highlights further the importance of our study given that the LdTyrPIP₂₂ homologs from the pathogenic bacteria *M. tuberculosis* and *L. monocytogenes*, MptpB and LipA, are known virulence factors (Beresford et al., 2009; Kastner et al., 2011). If LdTyrPIP₂₂ is shown to play a role in *L. donovani* virulence it will gain a value as a candidate drug target, especially because it does not have a homolog in higher eukaryotes (Brenchley et al., 2007; Beresford et al., 2010). Other enzymes of PI metabolism in kinetoplastids have already gained attention as candidate antiparasitic drugs (Cestari, 2020).

To sum up, this work describing the enzymatic substrate specificity and subcellular localization of the LdTyrPIP₂₂ P-Tyr/PI phosphatase, the first such aDSP to be described in *L. donovani*, forms the basis and will serve as a compass for more detailed studies toward the exploration of this phosphatase's functional role(s). The results of this study point to an involvement of LdTyrPIP₂₂ in the regulation of the endocytic/exocytic pathways and in the MP to amastigote differentiation, key processes for the parasite's fitness to complete its life cycle. The Blast analysis we performed showing that LdTyrPIP₂₂ is highly conserved amongst several *Leishmania* spp. also highlights the importance of this phosphatase in the parasite's life cycle. Further follow up studies using *L. donovani* strains with genetic modifications in the *ldtyrpip*₂₂ gene will enable exploration of the LdTyrPIP₂₂ putative role(s) in PI signaling in *Leishmania* cells. Although PIs constitute 10% of the total phospholipid content of *Leishmania* promastigotes (Zhang and Beverley, 2010), PI metabolism and signaling in these protozoans remain understudied and PI regulatory molecules identified by bioinformatics analyses (Velasquez et al., 2015) (Brenchley et al., 2007) remain poorly characterized. To conclude, this study emphasizes the importance of *Leishmania* phosphatases classified as aDSPs Lipid-like in the Trypanosomatids' phosphatome (Brenchley et al., 2007) and as Atypical Lipid phosphatases (Beresford et al., 2010) which, given that they are highly divergent from human homologs or have no human homologs at all, may prove to be valuable candidate drug targets for human leishmaniasis treatment, a goal of strong urgency.

DATA AVAILABILITY STATEMENT

The datasets presented in this study can be found in online repositories. The names of the repository/repositories and accession number(s) can be found in the article/**Supplementary Material**.

ETHICS STATEMENT

The animal study was reviewed and approved by the Hellenic Pasteur Institute's Institutional Animal Bioethics Committee following the EU Directive 2010/63 and the National Law 2013/56.

AUTHOR CONTRIBUTIONS

Conceived and designed the experiments: HB, AP, PR, OT, MK, and IT. Performed the experiments: AP, AK, OT, PK, and AD. Analyzed the data: AP, AK, PR, PK, MK, and HB. Contributed reagents/materials/analysis tools: HB, MK, and IT. Wrote the paper: AP and HB. Edited the paper: MK, IT, OT, and PK. Revised the paper: HB and OT. All authors contributed to the article and approved the submitted version.

FUNDING

This work was a Bilateral Research & Technology Collaboration Greece-France 2013 grant (no 1811) funded by the Greek General Secretariat for Research and Technology (<http://www.gsrt.gr/central.aspx?slid=119I428I1089I323I488743>) (HB and IT); IKYDA, the bilateral research promotion program, concluded between the DAAD with Greece and the Greek State Scholarship Foundation (IKY) (2014-2015) (HB and MK); KRIPIS I & II (2013-2019) Development Grants for Research Institutions, funded by the Greek General Secretariat for Research and Technology (HB), the Hellenic Foundation for Research and Innovation (HFRI) under the HFRI PhD Fellowship grant (Fellowship Number: 606) and the "BIOIMAGING-GR: A Greek Research Infrastructure for Visualizing and Monitoring Fundamental Biological Processes (MIS 5002755)", funded by the Operational Program "Competitiveness, Entrepreneurship and Innovation" (NSRF 2014-2020), co-financed by Greece and the European Union (European Regional Development Fund). The funders had no role in study design, data collection, and analysis, decision to publish, or preparation of the manuscript.

ACKNOWLEDGMENTS

Microscopy work was performed in the Light Microscopy unit of the Hellenic Pasteur Institute (HPI-LMU). The technical help of Dr Evangelia Xingi and Mrs Virginie Gonzalez is highly acknowledged. Special thanks to Dr Marios Zouridakis for his

assistance with the FPLC experiments. The polyclonal Abs were generated in the Department of Animal Models for Biomedical Research of the Hellenic Pasteur Institute. We thank Dr Amogh Sahasrabudhe (Division of Molecular and Structural Biology Central Drug Research Institute Lucknow, India) for the a-LdActin rabbit pAb and Dr Frédéric Bringaud (U. of Bordeaux/CNRS, France) for the a-GAPDH pAb. Special thanks to Dr Genevieve Milon for fruitful discussions and critical editing suggestions for this manuscript.

SUPPLEMENTARY MATERIAL

The Supplementary Material for this article can be found online at: <https://www.frontiersin.org/articles/10.3389/fcimb.2021.591868/full#supplementary-material>

Supplementary Figure 1 | Bioinformatics analysis of the LdTyrPIP₂₂ active site including the P-loop region HCXXGKDR. **(A)** ClustalW multiple sequence alignment of the *L. donovani* including the P-loop (strain LG13) sequence with homologs from *Mycobacterium tuberculosis* (MtpB, GenBank: CCC62750.1), *Listeria monocytogenes* [lmo1800, NP_465325; lmo1935, NP_465459], *Yersinia pestis* KIM10+ (WP_002228183), and *Bacillus anthracis* strain Ames (NP_845680). The aa sequences were obtained from the Genbank database and were analyzed/edited using the software BioEdit Sequence Alignment Editor. P-loop signature amino acids are framed by a blue box; **(B)** Rooted phylogenetic tree (UPGMA) from a multiple sequence alignment of the LdTyrPIP₂₂ orthologs from pathogenic bacteria.

Supplementary Figure 2 | Assessment of solubility of the LdTyrPIP₂₂-His and 15N-LdTyrPIP₂₂-His recombinant proteins in *E. coli* BL21 lysates. **(A)** The solubility of the rLdTyrPIP₂₂-His produced in bacteria was tested after 16 h induction with 0.1 mM IPTG at 20 °C, 25 °C and 37 °C. At the end of the induction, bacteria were lysed by sonication, soluble and insoluble fractions were separated by centrifugation (14 000×g, 30 min, 4 °C) and the insoluble fraction was resuspended in the same volume of lysis buffer. Equal volumes from total bacteria lysates (lane 1), soluble fraction (lane 2) and insoluble fraction (lane 3) were analyzed by SDS-PAGE (12% w/v) followed by WB using the a-LdTyrPIP₂₂ mouse serum (1:1200). The positions of the MW markers (kDa) are indicated on the left and right of the panels. Two protein species were revealed to be induced, recovered mostly in the insoluble fraction at all 3 temperatures; **(B)** The solubility of 15N-LdTyrPIP₂₂ produced by bacteria was tested after 16 h induction at 25 °C without IPTG. Equal volumes from total bacteria lysates (lane 1) soluble fraction (lane 2) and insoluble fraction (lane 3) were analyzed by SDS-PAGE (12% w/v) followed by WB using the a-His mAb (1.0 µg/mL). The arrow indicates the protein band corresponding to 15N-LdTyrPIP₂₂ in the part of the blot within the 30-45 kDa range; **(C)** Testing the effect of the length of induction to the solubility of 15N-LdTyrPIP₂₂ in bacteria lysates. WB of the soluble and pellet fractions from BL21-pTriEx-N15-LdtyrPIP₂₂ after incubation at 25 °C for 16 h and addition of IPTG (0.5 mM) for the indicated hours. Proteins were analyzed on 12% w/v SDS PAGE and transferred to nitrocellulose which was subsequently incubated with the a-His mAb (1.0 µg/mL). S: soluble supernatant, P: insoluble pellet. Arrow indicates the protein band corresponding to 15N-LdTyrPIP₂₂.

Supplementary Figure 3 | (A, B), Time course of dephosphorylation of four different PIs by the bacterially expressed recombinant human PRL-3 phosphatase (A), or two P-Tyr peptides (1 mM) by the bacterially expressed recombinant human PTP1B (B). The aa sequences for the pTyr2 and pTyr4 peptides are shown in Table S3. The assays were performed as described in **Figure 2**. **(C)**, Effect of pH in the rN15-LdTyrPIP₂₂-8His phosphatase activity at 37°C. The rN15-LdTyrPIP₂₂-8His phosphatase activity was assayed in 1 ml reaction volume with pNPP as substrate at 37°C (pH 4-8) and at 25°C (pH 6) in parallel as described in *Materials and Methods*. The absorbance of the reaction product (*p*-nitrophenolate = *p*NP) in the supernatant was measured at λ=405 nm. Error bars represent standard

deviations calculated from results acquired from four independent experiments performed in duplicates with three different batches of purified recombinant protein.

Supplementary Figure 4 | Testing of *a-LdTyroP₂₂* Abs' reactivity **(A)** Western Blot analysis of the *a-LdTyroP₂₂* pAbs reactivity (rabbit and mouse polyclonals) in detecting the rN15-*LdTyroP₂₂*-His protein produced in *E. coli* BL21 cells carrying the pTriEx1.1-rN15-*LdtyrP₂₂* plasmid. Bacteria were grown at 25°C for 16 h and induced with 0.5 mM IPTG (4 h, 25°C) to express the rN15-*LdTyroP₂₂*-His protein. Subsequently, the rN15-*LdTyroP₂₂*-His protein was affinity purified on Ni²⁺ NTA agarose beads from the bacteria lysates (Materials and Methods). Bacteria lysates (lane 1, left panel) or Ni²⁺ NTA beads with rN15-*LdTyroP₂₂*-His bound on them (lane 2, left panel) were analyzed by 12% SDS-PAGE and transferred on nitrocellulose membranes. Membrane strips with bacteria lysates were probed with the affinity purified rabbit pAb [0.2 & 0.1 µg/ml from the 5th and 1st bleed, (i & ii respectively, middle panel)]. Additionally strips with rN15-*LdTyroP₂₂*-His (material shown in lane 2 of left panel) were probed with the mouse pAb [dilution 1:100 (iii) & 1:1000 (iv) right panel]. HRP conjugated a-rabbit and a-mouse pAbs were used as secondary Abs. In all the panels the Ab's reactivity was revealed by the chromogenic DAB method. Arrow heads point to the rN15-*LdTyroP₂₂*-His band. **(B)** The *a-LdTyroP₂₂* pAbs (rabbit and mouse) were used to detect *LdTyroP₂₂* epitopes in axenic *L. donovani* static phase promastigotes by IF and confocal microscopy. IF staining of fixed cells permeabilized with 0.1% (v/v) Triton X-100 was performed with the *a-LdTyroP₂₂* mouse pAb (1:250) and the *a-LdTyroP₂₂* rabbit pAb (1:70) used together. As secondary Abs were used a-mouse Ab conjugated to Alexa Fluor[®] 633 and an a-rabbit Alexa Fluor 546 respectively. Nuclear and kinetoplast DNA was stained with DAPI. Images were acquired with a TCS SP confocal microscope by z-scanning performed at 0.3 µm step size. Single optical sections from representative images are shown. Single FL and phase contrast images are presented in Black and White (BW) while merged FL images are shown in color. The 1st Ab used in each case or the dye used for staining are shown at the top in color corresponding to the respective FL signal. Arrow heads point to the flagellar pocket/beginning of flagellum while arrows point to kinetoplast (k) and Nucleus (N). Scale bar size: 8 µm.

Supplementary Figure 5 | Localization of *LdTyroP₂₂* epitopes in different cell cycle morphological forms of axenic *L. donovani* promastigotes growing at 25°C, pH 7. Confocal microscopy images of *L. donovani* promastigotes. IF staining of fixed cells permeabilized with 0.1% (v/v) Triton X-100 was performed with the *a-LdTyroP₂₂* mouse (1:250) **(A)** or rabbit (1:70) **(B)** pAbs followed by the corresponding secondary Abs conjugated to Alexa Fluor[®] 488. Nuclear and kinetoplast DNA was stained with PI. Images were acquired by z-scanning with the TCS-SP confocal microscope at 0.5 µm step size. Single z sections are shown; Details in **B** depict 2X magnifications of the framed areas. Phase contrast and FL images are presented in BW. Merged images of FL or Phase and FL are shown in color. The molecule highlighted in each image or the dye used for staining is indicated at the top in the same color of the respective FL signal. Arrow heads point to the kinetoplast while short arrows point to the flagellar pocket. Long arrows point to the kinetoplast (k) and Nucleus (N). Scale bar size: 8 µm

Supplementary Figure 6 | Localization of *LdTyroP₂₂* epitopes in promastigotes growing at 25°C, pH 7; co staining for *LdTubulin*. Confocal microscopy images of axenic *L. donovani* promastigotes from logarithmic **(A)** and stationary phase **(B, C)** cultures growing at 25°C and pH 7. IF staining of fixed cells permeabilized with 0.1% (v/v) Triton X-100 was performed with the *a-LdTyroP₂₂* rabbit pAb (2 µg/ml) and *a-LdTubulin* mouse mAb (1:2000) followed by an a-rabbit Alexa Fluor 546 and an a-mouse Ab conjugated to Alexa Fluor[®] 488 respectively. Nuclear and kinetoplast DNA was stained

with Hoechst 33342 (1:5000). Images were acquired with the Leica TCS SP8 confocal microscope by z-scanning performed at 0.3 µm step size. A single optical section of a procyclic-like promastigote with two flagella is presented in **(A)** while in **(B)** and **(C)** are shown max projections of 7 optical sections from a leptomonad-like **(B)** and a nectomonad-like **(C)** promastigotes. Insets in **(A)**: the framed area with the FL signal intensified so that the two flagella are distinguished. Single FL images are shown in BW and merged in color. The molecule highlighted in each image or the dye used for staining is indicated at the top in the color of the respective FL signal. Arrowheads point to the beginning of flagellum/flagellar pocket region. Arrows point to kinetoplast (k) and Nucleus (N). Scale bar size: 10 µm.

Supplementary Figure 7 | Localization of *LdTyroP₂₂* in stationary phase *L. donovani* promastigotes stained with the FM4-64FX marker of the endocytic pathway. Confocal microscopy images of axenic *L. donovani* promastigotes grown for 192 h at 25°C, (pH 7) and stained alive with the FM4-64FX red fluorescent dye (20 µg/ml, Molecular Probes F34653) for 1 min at 4°C **(A)** or 5 min at 25°C **(B)**. After removing the dye, promastigotes were washed with ice-cold PBS and fixed with PFA 2% w/v in PBS for 10 min on ice. IF staining of fixed cells permeabilized with 0.1% (v/v) Triton X-100 was performed with the *a-LdTyroP₂₂* mouse pAb (1:200) followed by an a-mouse Ab conjugated to Alexa Fluor[®] 488. The molecule highlighted in each image or the dye used for staining is indicated at the top in the same color as the respective FL signal. Nuclear and kinetoplast DNA was stained with Hoechst 33342 (1:5000). Images were acquired with the Leica TCS SP8 confocal microscope by z-scanning performed at 0.3 µm step size. Single z-sections are shown. Arrowheads point to the beginning of flagellum/flagellar pocket region. Arrows point to kinetoplast (k) and Nucleus (N). Scale bar size: 10 µm.

Supplementary Figure 8 | Localization of *LdTyroP₂₂* in axenic stationary phase *L. donovani* promastigotes after a quick thermal shift at 37°C. Confocal microscopy images of *L. donovani* grown for 192 h at 25°C (pH 7) and after a 15 min incubation at 37°C (pH 7). IF staining of fixed cells permeabilized with 0.1% (v/v) TritonX-100 was performed with the *a-LdTyroP₂₂* mouse pAb (1:200) and a-GAPDH rabbit pAb (1:200) followed by an a-mouse Ab conjugated to Alexa Fluor[®] 488 and an a-rabbit Alexa Fluor 633 respectively (here presented in red pseudocolor in the merged image). Nuclear and kinetoplast DNA was stained with Hoechst 33342 (1:5000). Single color FL images are presented in BW while merged FL or Phase-FL signals are shown in color. The molecule highlighted in each image or the dye used for staining is indicated at the top in the same color as the respective FL signal. Images were acquired with the Leica TCS SP8 confocal microscope by z-scanning performed at 0.3 µm step size. Single optical sections are shown. Arrowheads point to the beginning of flagellum/flagellar pocket region. Arrows point to kinetoplast (k) and Nucleus (N). Scale bar size: 10 µm.

Supplementary Figure 9 | Localization of *LdTyroP₂₂* epitopes in axenic amastigote-like forms; co staining for *LdTubulin*. Confocal microscopy images of *L. donovani* grown for 5 days at 37°C and pH 5.5. IF staining of fixed cells permeabilized with 0.1% (v/v) TritonX-100 was performed as described in Figure S6. The molecule highlighted in each image or the dye used for staining is indicated at the top in the same color as the respective FL signal. Single FL and phase contrast images are presented in BW. Images were acquired with a Leica TCS SP5 confocal microscope by z-scanning performed at 0.3 µm step size. Single z-sections are shown. **(A a, b)**: Two different z sections of the same parasite. Arrow heads point to the remaining short flagellum. **(B)** A dividing parasite with amastigote-like morphology. Arrow head points to the tip of the short flagellum. Scale bar size: 5 µm.

REFERENCES

- Akhoundi, M., Kuhls, K., Cannet, A., Votpyka, J., Marty, P., Delaunay, P., et al. (2016). A Historical Overview of the Classification, Evolution, and Dispersion of Leishmania Parasites and Sandflies. *PLoS Negl. Trop. Dis.* 10 (3), e0004349. doi: 10.1371/journal.pntd.0004349
- Akhoundi, M., Downing, T., Votpyka, J., Kuhls, K., Lukes, J., Cannet, A., et al. (2017). Leishmania infections: Molecular targets and diagnosis. *Mol. Aspects Med.* 57, 1–29. doi: 10.1016/j.mam.2016.11.012

- Balla, T. (2013). Phosphoinositides: tiny lipids with giant impact on cell regulation. *Physiol. Rev.* 93 (3), 1019–1137. doi: 10.1152/physrev.00028.2012
- Barak, E., Amin-Spector, S., Gerliak, E., Goyard, S., Holland, N., and Zilberstein, D. (2005). Differentiation of Leishmania donovani in host-free system: analysis of signal perception and response. *Mol. Biochem. Parasitol.* 141 (1), 99–108. doi: 10.1016/j.molbiopara.2005.02.004
- Barlow, C. A., Laishram, R. S., and Anderson, R. A. (2010). Nuclear phosphoinositides: a signaling enigma wrapped in a compartmental conundrum. *Trends Cell Biol.* 20 (1), 25–35. doi: 10.1016/j.tcb.2009.09.009

- Bates, P. A., Robertson, C. D., Tetley, L., and Coombs, G. H. (1992). Axenic cultivation and characterization of *Leishmania mexicana* amastigote-like forms. *Parasitology* 105 (Pt 2), 193–202. doi: 10.1017/s0031182000074102
- Bates, P. A. (1994). The developmental biology of *Leishmania* promastigotes. *Exp. Parasitol.* 79 (2), 215–218. doi: 10.1006/expr.1994.1084
- Bates, P. A. (2007). Transmission of *Leishmania* metacyclic promastigotes by phlebotomine sand flies. *Int. J. Parasitol.* 37 (10), 1097–1106. doi: 10.1016/j.ijpara.2007.04.003
- Beresford, N., Patel, S., Armstrong, J., Soor, B., Fordham-Skelton, A. P., and Taberner, L. (2007). MptpB, a virulence factor from *Mycobacterium tuberculosis*, exhibits triple-specificity phosphatase activity. *Biochem. J.* 406 (1), 13–18. doi: 10.1042/BJ20070670
- Beresford, N. J., Mulhearn, D., Szczepankiewicz, B., Liu, G., Johnson, M. E., Fordham-Skelton, A., et al. (2009). Inhibition of MptpB phosphatase from *Mycobacterium tuberculosis* impairs mycobacterial survival in macrophages. *J. Antimicrob. Chemother.* 63 (5), 928–936. doi: 10.1093/jac/dkp031
- Beresford, N., Saville, C., Bennett, H., Roberts, I., and Taberner, L. (2010). A new family of phosphoinositide phosphatases in microorganisms: identification and biochemical analysis. *BMC Genomics* 11 (1), 457. doi: 10.1186/1471-2164-11-457
- Biyani, N., and Madhubala, R. (2012). Quantitative proteomic profiling of the promastigotes and the intracellular amastigotes of *Leishmania donovani* isolates identifies novel proteins having a role in *Leishmania* differentiation and intracellular survival. *Biochim. Biophys. Acta* 1824 (12), 1342–1350. doi: 10.1016/j.bbapap.2012.07.010
- Brenchley, R., Tariq, H., McElhinney, H., Soor, B., Huxley-Jones, J., Stevens, R., et al. (2007). The TriTryp phosphatome: analysis of the protein phosphatase catalytic domains. *BMC Genomics* 8, 434. doi: 10.1186/1471-2164-8-434
- Burza, S., Croft, S. L., and Boelaert, M. (2018). Leishmaniasis. *Lancet* 392 (10151), 951–970. doi: 10.1016/S0140-6736(18)31204-2
- Castano, E., Yildirim, S., Faberova, V., Krausova, A., Ulicna, L., Paprckova, D., et al. (2019). Nuclear Phosphoinositides-Versatile Regulators of Genome Functions. *Cells* 8 (7):649. doi: 10.3390/cells8070649
- Cestari, I., and Stuart, K. (2018). Inositol phosphate pathway controls transcription of telomeric expression sites in trypanosomes. *Proc. Natl. Acad. Sci. U. S. A.* 112 (21), E2803–E2812. doi: 10.1073/pnas.1501206112
- Cestari, I., McLeland-Wieser, H., and Stuart, K. (2019). Nuclear Phosphatidylinositol 5-Phosphatase Is Essential for Allelic Exclusion of Variant Surface Glycoprotein Genes in Trypanosomes. *Mol. Cell Biol.* 39 (3), e00395-18. doi: 10.1128/MCB.00395-18
- Cestari, I. (2020). Phosphoinositide signaling and regulation in *Trypanosoma brucei*: Specialized functions in a protozoan pathogen. *PLoS Pathog.* 16 (1), 1–8. doi: 10.1371/journal.ppat.1008167
- Chow, C., Cloutier, S., Dumas, C., Chou, M. N., and Papadopoulos, B. (2011). Promastigote to amastigote differentiation of *Leishmania* is markedly delayed in the absence of PERK eIF2alpha kinase-dependent eIF2alpha phosphorylation. *Cell Microbiol.* 13 (7), 1059–1077. doi: 10.1111/j.1462-5822.2011.01602.x
- Cool, D. E., and Blum, J. J. (1993). Protein tyrosine phosphatase activity in *Leishmania donovani*. *Mol. Cell Biochem.* 127–128, 143–149. doi: 10.1007/BF01076765
- Costes, S. V., Daelemans, D., Cho, E. H., Dobbin, Z., Pavlakis, G., and Lockett, S. (2004). Automatic and quantitative measurement of protein-protein colocalization in live cells. *Biophys. J.* 86 (6), 3993–4003. doi: 10.1529/biophysj.103.038422
- Coutinho-Abreu, I. V., Serafim, T. D., Meneses, C., Kamhawi, S., Oliveira, F., and Valenzuela, J. G. (2020). Distinct gene expression patterns in vector-residing *Leishmania* infantum identify parasite stage-enriched markers. *PLoS Negl. Trop. Dis.* 14 (3), e0008014. doi: 10.1371/journal.pntd.0008014
- De Pablos, L. M., Ferreira, T. R., and Walrad, P. B. (2016). Developmental differentiation in *Leishmania* lifecycle progression: post-transcriptional control conducts the orchestra. *Curr. Opin. Microbiol.* 34, 82–89. doi: 10.1016/j.mib.2016.08.004
- de Souza, W., and Barrias, E. S. (2020). Membrane-bound extracellular vesicles secreted by parasitic protozoa: cellular structures involved in the communication between cells. *Parasitol Res.* 119 (7), 2005–2023. doi: 10.1007/s00436-020-06691-7
- Debrabant, A., Joshi, M. B., Pimenta, P. F., and Dwyer, D. M. (2004). Generation of *Leishmania donovani* axenic amastigotes: their growth and biological characteristics. *Int. J. Parasitol.* 34 (2), 205–217. doi: 10.1016/j.ijpara.2003.10.011
- Delorme, V., Cayla, X., Faure, G., Garcia, A., and Tardieux, I. (2003). Actin dynamics is controlled by a casein kinase II and phosphatase 2C interplay on *Toxoplasma gondii* Toxofilin. *Mol. Biol. Cell* 14 (5), 1900–1912. doi: 10.1091/mbc.e02-08-0462
- Depledge, D. P., Evans, K. J., Ivens, A. C., Aziz, N., Maroof, A., Kaye, P. M., et al. (2009). Comparative expression profiling of *Leishmania*: modulation in gene expression between species and in different host genetic backgrounds. *PLoS Negl. Trop. Dis.* 3 (7), e476. doi: 10.1371/journal.pntd.0000476
- Desjardins, M., and Descoteaux, A. (1997). Inhibition of phagolysosomal biogenesis by the *Leishmania* lipophosphoglycan. *J. Exp. Med.* 185 (12), 2061–2068. doi: 10.1084/jem.185.12.2061
- Dillon, L. A., Okrah, K., Hughitt, V. K., Suresh, R., Li, Y., Fernandes, M. C., et al. (2015). Transcriptomic profiling of gene expression and RNA processing during *Leishmania* major differentiation. *Nucleic Acids Res.* 43 (14), 6799–6813. doi: 10.1093/nar/gkv656
- Dong, G., Filho, A. L., and Olivier, M. (2019). Modulation of Host-Pathogen Communication by Extracellular Vesicles (EVs) of the Protozoan Parasite *Leishmania*. *Front. Cell Infect. Microbiol.* 9, 100. doi: 10.3389/fcimb.2019.00100
- Dostalova, A., and Volf, P. (2012). *Leishmania* development in sand flies: parasite-vector interactions overview. *Parasit. Vectors* 5, 276. doi: 10.1186/1756-3305-5-276
- Doukas, A., Karena, E., Botou, M., Papakostas, K., Papadaki, A., Tziouvara, O., et al. (2019). Heterologous expression of the mammalian sodium-nucleobase transporter rSNBT1 in *Leishmania tarentolae*. *Biochim. Biophys. Acta Biomembr.* 1861 (9), 1546–1557. doi: 10.1016/j.bbmem.2019.07.001
- Doyle, P. S., Engel, J. C., Pimenta, P. F., da Silva, P. P., and Dwyer, D. M. (1991). *Leishmania donovani*: long-term culture of axenic amastigotes at 37 degrees C. *Exp. Parasitol.* 73 (3), 326–334. doi: 10.1016/0014-4894(91)90104-5
- Fernandes, A. C. S., Soares, D. C., Neves, R. F. C., Koeller, C. M., Heise, N., Adade, C. M., et al. (2020). Endocytosis and Exocytosis in *Leishmania amazonensis* Are Modulated by Bromoenol Lactone. *Front. Cell Infect. Microbiol.* 10, 39. doi: 10.3389/fcimb.2020.00039
- Fernandez-Pol, S., Slouka, Z., Bhattacharjee, S., Fedotova, Y., Freed, S., An, X., et al. (2013). A bacterial phosphatase-like enzyme of the malaria parasite *Plasmodium falciparum* possesses tyrosine phosphatase activity and is implicated in the regulation of band 3 dynamics during parasite invasion. *Eukaryot. Cell* 12 (9), 1179–1191. doi: 10.1128/EC.00027-13
- Foucher, A. L., Papadopoulos, B., and Ouellette, M. (2006). Prefractionation by digitonin extraction increases representation of the cytosolic and intracellular proteome of *Leishmania infantum*. *J. Proteome Res.* 5 (7), 1741–1750. doi: 10.1021/pr060081j
- Ghedini, E., Debrabant, A., Engel, J. C., and Dwyer, D. M. (2001). Secretory and endocytic pathways converge in a dynamic endosomal system in a primitive protozoan. *Traffic* 2 (3), 175–188. doi: 10.1034/j.1600-0854.2001.020304.x
- Ghorbani, M., and Farhoudi, R. (2018). Leishmaniasis in humans: drug or vaccine therapy? *Drug Des. Devel. Ther.* 12, 25–40. doi: 10.2147/DDDT.S146521
- Glaser, T. A., Wells, S. J., Spithill, T. W., Pettitt, J. M., Humphris, D. C., and Mukkada, A. J. (1990). *Leishmania* major and *L. donovani*: a method for rapid purification of amastigotes. *Exp. Parasitol.* 71 (3), 343–345. doi: 10.1016/0014-4894(90)90039-f
- Gluenz, E., Ginger, M. L., and McKean, P. G. (2010). Flagellum assembly and function during the *Leishmania* life cycle. *Curr. Opin. Microbiol.* 13 (4), 473–479. doi: 10.1016/j.mib.2010.05.008
- Goldstein, B. J. (2001). Protein-tyrosine phosphatase 1B (PTP1B): a novel therapeutic target for type 2 diabetes mellitus, obesity and related states of insulin resistance. *Curr. Drug Targets Immune Endocr. Metabol. Disord.* 1 (3), 265–275. doi: 10.2174/1568008013341163
- Gupta, N., Goyal, N., and Rastogi, A. K. (2001). In vitro cultivation and characterization of axenic amastigotes of *Leishmania*. *Trends Parasitol.* 17 (3), 150–153. doi: 10.1016/S1471-4922(00)01811-0
- Halliday, C., Billington, K., Wang, Z., Madden, R., Dean, S., Sunter, J. D., et al. (2019). Cellular landmarks of *Trypanosoma brucei* and *Leishmania mexicana*. *Mol. Biochem. Parasitol.* 230, 24–36. doi: 10.1016/j.molbiopara.2018.12.003
- Handman, E., and Bullen, D. V. (2002). Interaction of *Leishmania* with the host macrophage. *Trends Parasitol.* 18 (8), 332–334. doi: 10.1016/S1471-4922(02)02352-8
- Hanes, C. M., D'Amico, A. E., Ueyama, T., Wong, A. C., Zhang, X., Hynes, W. F., et al. (2017). Golgi-Associated Protein Kinase C-epsilon Is Delivered to Phagocytic Cups: Role of Phosphatidylinositol 4-Phosphate. *J. Immunol.* 199 (1), 271–277. doi: 10.4049/jimmunol.1700243

- Harlow, E., and Lane, D. (1988). *Antibodies. A laboratory manual* (Cold Spring Harbor Lab) 17, 220.
- Hassani, K., Antoniaki, E., Jardim, A., and Olivier, M. (2011). Temperature-induced protein secretion by *Leishmania mexicana* modulates macrophage signalling and function. *PLoS One* 6 (5), e18724. doi: 10.1371/journal.pone.0018724
- Herman, M., Perez-Morga, D., Schtickzelle, N., and Michels, P. A. (2008). Turnover of glycosomes during life-cycle differentiation of *Trypanosoma brucei*. *Autophagy* 4 (3), 294–308. doi: 10.4161/auto.5443
- Iantorno, S. A., Durrant, C., Khan, A., Sanders, M. J., Beverley, S. M., Warren, W. C., et al. (2017). Gene Expression in *Leishmania* Is Regulated Predominantly by Gene Dosage. *mBio* 8 (5). doi: 10.1128/mBio.01393-17
- Inbar, E., Hughitt, V. K., Dillon, L. A., Ghosh, K., El-Sayed, N. M., and Sacks, D. L. (2017). The Transcriptome of *Leishmania major* Developmental Stages in Their Natural Sand Fly Vector. *MBio* 8 (2), 00029-17. doi: 10.1128/mBio.00029-17
- Karamysheva, Z. N., Gutierrez Guarnizo, S. A., and Karamyshev, A. L. (2020). Regulation of Translation in the Protozoan Parasite *Leishmania*. *Int. J. Mol. Sci.* 21 (8), 2981. doi: 10.3390/ijms21082981
- Kastner, R., Dussurget, O., Archambaud, C., Kernbauer, E., Soulat, D., Cossart, P., et al. (2011). LipA, a tyrosine and lipid phosphatase involved in the virulence of *Listeria monocytogenes*. *Infect. Immun.* 79 (6), 2489–2498. doi: 10.1128/IAI.05073-11
- Katta, S. S., Tammana, T. V., Sahasrabudhe, A. A., Bajpai, V. K., and Gupta, C. M. (2010). Trafficking activity of myosin XXI is required in assembly of *Leishmania* flagellum. *J. Cell Sci.* 123 (Pt 12), 2035–2044. doi: 10.1242/jcs.064725
- Kelly, F. D., Sanchez, M. A., and Landfear, S. M. (2020). Touching the Surface: Diverse Roles for the Flagellar Membrane in Kinetoplastid Parasites. *Microbiol. Mol. Biol. Rev.* 84 (2), e00079-19. doi: 10.1128/MMBR.00079-19
- Koul, A., Choudas, A., Treder, M., Tyagi, A. K., Drlica, K., Singh, Y., et al. (2000). Cloning and characterization of secretory tyrosine phosphatases of *Mycobacterium tuberculosis*. *J. Bacteriol.* 182 (19), 5425–5432. doi: 10.1128/JB.182.19.5425-5432.2000
- Kraeva, N., Lestina, T., Ishemgulova, A., Majerova, K., Butenko, A., Vaselek, S., et al. (2019). LmxM.22.0250-Encoded Dual Specificity Protein/Lipid Phosphatase Impairs *Leishmania mexicana* Virulence In Vitro. *Pathogens* 8 (4), 241–255. doi: 10.3390/pathogens8040241
- Landfear, S. M., and Ignatushchenko, M. (2001). The flagellum and flagellar pocket of trypanosomatids. *Mol. Biochem. Parasitol.* 115 (1), 1–17. doi: 10.1016/S0166-6851(01)00262-6
- Larsen, M., Tremblay, M. L., and Yamada, K. M. (2003). Phosphatases in cell-matrix adhesion and migration. *Nat. Rev. Mol. Cell Biol.* 4 (9), 700–711. doi: 10.1038/nrm1199
- Leifso, K., Cohen-Freue, G., Dogra, N., Murray, A., and McMaster, W. R. (2007). Genomic and proteomic expression analysis of *Leishmania* promastigote and amastigote life stages: the *Leishmania* genome is constitutively expressed. *Mol. Biochem. Parasitol.* 152 (1), 35–46. doi: 10.1016/j.molbiopara.2006.11.009
- Marat, A. L., and Haucke, V. (2016). Phosphatidylinositol 3-phosphates-at the interface between cell signalling and membrane traffic. *EMBO J.* 35 (6), 561–579. doi: 10.15252/embj.201593564
- Maue, J. (1996). Intracellular survival of protozoan parasites with special reference to *Leishmania* spp., *Toxoplasma gondii* and *Trypanosoma cruzi*. *Adv. Parasitol.* 38, 1–51. doi: 10.1016/S0065-308X(08)60032-9
- McConville, M. J., de Souza, D., Saunders, E., Likic, V. A., and Naderer, T. (2007). Living in a phagolysosome; metabolism of *Leishmania* amastigotes. *Trends Parasitol.* 23 (8), 368–375. doi: 10.1016/j.pt.2007.06.009
- McNicoll, F., Drummelsmith, J., Muller, M., Madore, E., Boilard, N., Ouellette, M., et al. (2006). A combined proteomic and transcriptomic approach to the study of stage differentiation in *Leishmania infantum*. *Proteomics* 6 (12), 3567–3581. doi: 10.1002/pmic.200500853
- McParland, V., Varsano, G., Li, X., Thornton, J., Baby, J., Aravind, A., et al. (2006). The metastasis-promoting phosphatase PRL-3 shows activity toward phosphoinositide. *Biochemistry* 45 (35), 7579–7590. doi: 10.1021/bi201095z
- Moore, I., and Murphy, A. (2009). Validating the location of fluorescent protein fusions in the endomembrane system. *Plant Cell* 21 (6), 1632–1636. doi: 10.1105/tpc.109.068668
- Morales, M. A., Pescher, P., and Spath, G. F. (2010). *Leishmania major* MPK7 protein kinase activity inhibits intracellular growth of the pathogenic amastigote stage. *Eukaryot. Cell* 9 (1), 22–30. doi: 10.1128/EC.00196-09
- McParland, V., Varsano, G., Li, X., Thornton, J., Baby, J., Aravind, A., et al. (2011). The metastasis-promoting phosphatase PRL-3 shows activity toward phosphoinositides. *Biochemistry* 50 (35), 7579–7590. doi: 10.1021/bi201095z
- Nakashima, M., and Lazo, J. S. (2010). Phosphatase of regenerating liver-1 promotes cell migration and invasion and regulates filamentous actin dynamics. *J. Pharmacol. Exp. Ther.* 334 (2), 627–633. doi: 10.1124/jpet.110.167809
- Nascimento, M., Abourjeily, N., Ghosh, A., Zhang, W. W., and Matlashewski, G. (2003). Heterologous expression of a mammalian protein tyrosine phosphatase gene in *Leishmania*: effect on differentiation. *Mol. Microbiol.* 50 (5), 1517–1526. doi: 10.1046/j.1365-2958.2003.03811.x
- Nascimento, M., Zhang, W. W., Ghosh, A., Houston, D. R., Berghuis, A. M., Olivier, M., et al. (2006). Identification and characterization of a protein-tyrosine phosphatase in *Leishmania*: Involvement in virulence. *J. Biol. Chem.* 281 (47), 36257–36268. doi: 10.1074/jbc.M606256200
- Nayak, A., Akpunarlieva, S., Barrett, M., and Burchmore, R. (2018). A defined medium for *Leishmania* culture allows definition of essential amino acids. *Exp. Parasitol.* 185, 39–52. doi: 10.1016/j.exppara.2018.01.009
- Otto, H., Dreger, M., Bengtsson, L., and Hucho, F. (2001). Identification of tyrosine-phosphorylated proteins associated with the nuclear envelope. *Eur. J. Biochem.* 268 (2), 420–428. doi: 10.1046/j.1432-1033.2001.01901.x
- Papadaki, A., and Boleti, H. (2019). Measurement of Acid Ecto-phosphatase Activity in Live *Leishmania donovani* Parasites. *Bio-protocol* 9 (19), e3384 doi: 10.21769/BioProtoc.3384
- Papadaki, A., Politou, A. S., Smirlis, D., Kotini, M. P., Kourou, K., Papamarcaki, T., et al. (2015). The *Leishmania donovani* histidine acid ecto-phosphatase LdMACP: insight into its structure and function. *Biochem. J.* 467, 473–486. doi: 10.1042/BJ20141371
- Rodrigues, J. C., Godinho, J. L., and de Souza, W. (2014). Biology of human pathogenic trypanosomatids: epidemiology, lifecycle and ultrastructure. *Subcell Biochem.* 74, 1–42. doi: 10.1007/978-94-007-7305-9_1
- Rogers, M. E., Chance, M. L., and Bates, P. A. (2002). The role of promastigote secretory gel in the origin and transmission of the infective stage of *Leishmania mexicana* by the sandfly *Lutzomyia longipalpis*. *Parasitology* 124 (Pt 5), 495–507. doi: 10.1017/S0031182002001439
- Sahasrabudhe, A. A., Bajpai, V. K., and Gupta, C. M. (2004). A novel form of actin in *Leishmania*: molecular characterisation, subcellular localisation and association with subpellicular microtubules. *Mol. Biochem. Parasitol.* 134 (1), 105–114. doi: 10.1016/j.molbiopara.2003.11.008
- Sales Gil, R., de Castro, I. J., Berihun, J., and Vagnarelli, P. (2018). Protein phosphatases at the nuclear envelope. *Biochem. Soc. Trans.* 46 (1), 173–182. doi: 10.1042/BST20170139
- Santarem, N., Cunha, J., Silvestre, R., Silva, C., Moreira, D., Ouellette, M., et al. (2014). The impact of distinct culture media in *Leishmania infantum* biology and infectivity. *Parasitology* 141 (2), 192–205. doi: 10.1017/S0031182013001388
- Schink, K. O., Tan, K. W., and Stenmark, H. (2016). Phosphoinositides in Control of Membrane Dynamics. *Annu. Rev. Cell Dev. Biol.* 32, 143–171. doi: 10.1146/annurev-cellbio-111315-125349
- Schuler, H., and Matuschewski, K. (2006). Regulation of apicomplexan microfilament dynamics by a minimal set of actin-binding proteins. *Traffic* 7 (11), 1433–1439. doi: 10.1111/j.1600-0854.2006.00484.x
- Senju, Y., Kalimeri, M., Koskela, E. V., Somerharju, P., Zhao, H., Vattulainen, I., et al. (2017). Mechanistic principles underlying regulation of the actin cytoskeleton by phosphoinositides. *Proc. Natl. Acad. Sci. U. S. A.* 114 (43), E8977–E8986. doi: 10.1073/pnas.1705032114
- Sereno, D., and Lemesre, J. L. (1997). Axenically cultured amastigote forms as an in vitro model for investigation of antileishmanial agents. *Antimicrob. Agents Chemother.* 41 (5), 972–976. doi: 10.1128/AAC.41.5.972
- Silverman, J. M., Chan, S. K., Robinson, D. P., Dwyer, D. M., Nandan, D., Foster, L. J., et al. (2008). Proteomic analysis of the secretome of *Leishmania donovani*. *Genome Biol.* 9 (2), R35. doi: 10.1186/gb-2008-9-2-r35
- Soulat, D., and Bogdan, C. (2017). Function of Macrophage and Parasite Phosphatases in Leishmaniasis. *Front. Immunol.* 8, 1838. doi: 10.3389/fimmu.2017.01838

- Sunter, J., and Gull, K. (2017). Shape, form, function and Leishmania pathogenicity: from textbook descriptions to biological understanding. *Open Biol.* 7 (9), 170165–170178. doi: 10.1098/rsob.170165
- Tsigankov, P., Gherardini, P. F., Helmer-Citterich, M., Spath, G. F., and Zilberstein, D. (2013). Phosphoproteomic analysis of differentiating Leishmania parasites reveals a unique stage-specific phosphorylation motif. *J. Proteome Res.* 12 (7), 3405–3412. doi: 10.1021/pr4002492
- Tsigankov, P., Gherardini, P. F., Helmer-Citterich, M., Spath, G. F., Myler, P. J., and Zilberstein, D. (2014). Regulation dynamics of Leishmania differentiation: deconvoluting signals and identifying phosphorylation trends. *Mol. Cell Proteomics* 13 (7), 1787–1799. doi: 10.1074/mcp.M114.037705
- Velasquez, V., Ochoa, R., and Muskus, C. (2015). [Detection of molecular targets on the phosphatidylinositol signaling pathway of Leishmania spp. through bioinformatics tools and mathematical modeling]. *Biomedica* 35 (2), 235–246. doi: 10.1590/S0120-41572015000200012
- Vince, J. E., Tull, D. L., Spurck, T., Derby, M. C., McFadden, G. I., Gleeson, P. A., et al. (2008). Leishmania adaptor protein-1 subunits are required for normal lysosome traffic, flagellum biogenesis, lipid homeostasis, and adaptation to temperatures encountered in the mammalian host. *Eukaryot. Cell* 7 (8), 1256–1267. doi: 10.1128/EC.00090-08
- Wallroth, A., and Haucke, V. (2018). Phosphoinositide conversion in endocytosis and the endolysosomal system. *J. Biol. Chem.* 293 (5), 1526–1535. doi: 10.1074/jbc.R117.000629
- Wang, Z., Wheeler, R. J., and Sunter, J. D. (2020). Lysosome assembly and disassembly changes endocytosis rate through the Leishmania cell cycle. *Microbiologyopen* 9 (2), e969. doi: 10.1002/mbo3.969
- Wassef, M. K., Fioretti, T. B., and Dwyer, D. M. (1985). Lipid analyses of isolated surface membranes of Leishmania donovani promastigotes. *Lipids* 20 (2), 108–115. doi: 10.1007/BF02534216
- Wheeler, R. J., Gluenz, E., and Gull, K. (2011). The cell cycle of Leishmania: morphogenetic events and their implications for parasite biology. *Mol. Microbiol.* 79 (3), 647–662. doi: 10.1111/j.1365-2958.2010.07479.x
- Wheeler, R. J., Gluenz, E., and Gull, K. (2015). Basal body multipotency and axonemal remodelling are two pathways to a 9+0 flagellum. *Nat. Commun.* 6, 8964. doi: 10.1038/ncomms9964
- Wheeler, R. J., Sunter, J. D., and Gull, K. (2016). Flagellar pocket restructuring through the Leishmania life cycle involves a discrete flagellum attachment zone. *J. Cell Sci.* 129 (4), 854–867. doi: 10.1242/jcs.183152
- WHO/PAHO (2020). *Leishmaniasis. Communication materials/ Fact sheets.*
- Xu, Q., Zhang, Y., Wei, Q., Huang, Y., Hu, J., and Ling, K. (2016). Phosphatidylinositol phosphate kinase PIPK γ and phosphatase INPP5E coordinate initiation of ciliogenesis. *Nat. Commun.* 7, 10777. doi: 10.1038/ncomms10777
- Young, J., and Kima, P. E. (2019). The Leishmania Parasitophorous Vacuole Membrane at the Parasite-Host Interface. *Yale J. Biol. Med.* 92 (3), 511–521.
- Zakai, H. A., Chance, M. L., and Bates, P. A. (1998). In vitro stimulation of metacyclogenesis in Leishmania braziliensis, L. donovani, L. major and L. mexicana. *Parasitology* 116 (Pt 4), 305–309. doi: 10.1017/S0031182097002382
- Zhang, K., and Beverley, S. M. (2010). Phospholipid and sphingolipid metabolism in Leishmania. *Mol. Biochem. Parasitol.* 170 (2), 55–64. doi: 10.1016/j.molbiopara.2009.12.004
- Zhou, Y., Bhattacharjee, H., and Mukhopadhyay, R. (2006). Bifunctional role of the leishmanial antimonate reductase LmACR2 as a protein tyrosine phosphatase. *Mol. Biochem. Parasitol.* 148 (2), 161–168. doi: 10.1016/j.molbiopara.2006.03.009
- Zilberstein, D., and Shapira, M. (1994). The role of pH and temperature in the development of Leishmania parasites. *Annu. Rev. Microbiol.* 48, 449–470. doi: 10.1146/annurev.mi.48.100194.002313
- Zilberstein, D. (2020). In Vitro Culture for Differentiation Simulation of Leishmania spp. Protocol for Axenic Promastigote-to Amastigote Differentiation, Springer Protocols. *Methods Mol. Biol.* 2116, 39–47. doi: 10.1007/978-1-0716-0294-2_3

Conflict of Interest: The authors declare that the research was conducted in the absence of any commercial or financial relationships that could be construed as a potential conflict of interest.

Copyright © 2021 Papadaki, Tziouvara, Kotopouli, Koumariou, Doukas, Rios, Tardieux, Köhn and Boleti. This is an open-access article distributed under the terms of the Creative Commons Attribution License (CC BY). The use, distribution or reproduction in other forums is permitted, provided the original author(s) and the copyright owner(s) are credited and that the original publication in this journal is cited, in accordance with accepted academic practice. No use, distribution or reproduction is permitted which does not comply with these terms.



Involvement of *Leishmania* Phosphatases in Parasite Biology and Pathogeny

Anita Leocadio Freitas-Mesquita^{1,2*}, André Luiz Araújo Dos-Santos^{1,2}
and José Roberto Meyer-Fernandes^{1,2*}

¹ Instituto de Bioquímica Médica Leopoldo De Meis, Universidade Federal do Rio de Janeiro, Rio de Janeiro, Brazil, ² Instituto Nacional de Ciência e Tecnologia em Biologia Estrutural e Bioimagem, Universidade Federal do Rio de Janeiro, Rio de Janeiro, Brazil

OPEN ACCESS

Edited by:

Juan David Ramirez,
Rosario University, Colombia

Reviewed by:

Juliana Ide Aoki,
University of São Paulo, Brazil
Maria Aguirre-Garcia,
Universidad Nacional Autónoma de
México, Mexico

*Correspondence:

Anita Leocadio Freitas-Mesquita
anitaleocadio2@gmail.com
José Roberto Meyer-Fernandes
meyer@bioqmed.ufrj.br

Specialty section:

This article was submitted to
Parasite and Host,
a section of the journal
Frontiers in Cellular and
Infection Microbiology

Received: 24 November 2020

Accepted: 06 April 2021

Published: 22 April 2021

Citation:

Freitas-Mesquita AL, Dos-Santos ALA
and Meyer-Fernandes JR (2021)
Involvement of *Leishmania*
Phosphatases in Parasite
Biology and Pathogeny.
Front. Cell. Infect. Microbiol. 11:633146.
doi: 10.3389/fcimb.2021.633146

In the *Leishmania* lifecycle, the motile promastigote form is transmitted from the sand fly vector to a mammalian host during a blood meal. Inside vertebrate host macrophages, the parasites can differentiate into the amastigote form and multiply, causing leishmaniasis, one of the most significant neglected tropical diseases. *Leishmania* parasites face different conditions throughout their development inside sand flies. Once in the mammalian host, the parasites have to overcome the microbicide repertoire of the cells of the immune system to successfully establish the infection. In this context, the expression of protein phosphatases is of particular interest. Several members of the serine/threonine-specific protein phosphatase (STP), protein tyrosine phosphatase (PTP), and histidine acid phosphatase (HAcP) families have been described in different *Leishmania* species. Although their physiological roles have not been fully elucidated, many studies suggest they have an involvement with parasite biology and pathogeny. Phosphatases play a role in adaptation to nutrient starvation during parasite passage through the sand fly midgut. They are also important to parasite virulence, mainly due to the modulation of host cytokine production and impairment of the microbiocidal potential of macrophages. Furthermore, recent whole-genome expression analyses have shown that different phosphatases are upregulated in metacyclic promastigotes, the infective form of the mammalian host. *Leishmania* phosphatases are also upregulated in drug-resistant strains, probably due to the increase in drug efflux related to the activation of ABC transporters. Throughout this review, we will describe the physiological roles that have been attributed to *Leishmania* endogenous phosphatases, including their involvement in the adaptation, survival, and proliferation of the parasites inside their hosts.

Keywords: *Leishmania* spp, phosphatases, phosphate metabolism, parasite virulence, parasite infection

INTRODUCTION

Leishmania spp. are trypanosomatid parasites that infect humans and other mammals (Chang, 1983). Leishmaniasis may be asymptomatic or it may manifest as cutaneous or mucocutaneous disease or even as a visceral form that can be lethal if untreated. The course of infection depends on the complex interaction between the infecting species and the host immune response (Pace, 2014). In the *Leishmania* lifecycle, promastigote forms are transmitted from the sand fly vector to the mammalian host during a blood meal. Inside the host macrophages, the parasites differentiate into the amastigote form (Chang, 1983). During their lifecycle, *Leishmania* parasites are exposed to diverse environmental stimuli. Protein phosphorylation and dephosphorylation are crucial events in cell recognition of external and internal signals, leading to specific responses (Cosentino-Gomes and Meyer-Fernandes, 2011; Freitas-Mesquita and Meyer-Fernandes, 2014).

The majority of eukaryotic proteins (96–99%) are phosphorylated at serine and threonine residues. Thus, serine/threonine-specific protein phosphatases (STPs) are of great importance for crucial dephosphorylation events. STPs are divided into three groups: phosphoprotein phosphatases (PPPs), metallo-dependent protein phosphatases (PPM/PP2C), and aspartate-based phosphatases (FCP/SCP) (Cohen, 1997; Szöör, 2010; Soulat and Bogdan, 2017). PPP and PPM depend on metal ions for catalysis through the activation of a water molecule for the dephosphorylation reaction, while FCPs/SCPs use an aspartate-based (DxDxT/V) catalytic core to dephosphorylate phospho Ser/Thr residues (Szöör, 2010).

Different STPs expressed by *Leishmania* parasites have been identified and characterized by biochemical and molecular means, including protein phosphatase 5 (PP5) (Norris-Mullins et al., 2018), protein phosphatase 1 (PP1) (Qureshi et al., 2019), protein phosphatase 2C (PP2C) (Jakkula et al., 2018), and protein phosphatase 2B (PP2B) (Banerjee et al., 1999) of *Leishmania donovani*; PP2B (Naderer et al., 2011), protein phosphatase with EF-Hand (PPEF) (Mills et al., 2007), and arsenate reductase 2 (ACR2) (Zhou et al., 2004; Zhou et al., 2006) of *Leishmania major*; PP2C (Escalona-Montaña et al., 2016) of *Leishmania mexicana*; and PP2C (Burns et al., 1993) of *Leishmania chagasi*.

Although phosphorylation on tyrosine residues comprises a small fraction of all protein phosphorylation events, it plays an important role in signaling involved in cell cycle control and differentiation (Andreeva and Kutuzov, 2008). Protein tyrosine phosphatases (PTPs) share a consensus sequence motif, and their catalytic site is surrounded by cysteine and arginine (CX₅R) (Soulat and Bogdan, 2017). Based on their catalytic domains and substrate specificity, PTPs are classified as Class I, Class II, Class III, or Class IV (Alonso et al., 2004). The great majority of *Leishmania* PTPs belong to the Class I group, which is subdivided into classical and dual-specificity PTPs (Szöör, 2010). Classical PTPs include phosphatases homologous to human protein tyrosine phosphatase 1B (PTP1B). Contrary to those found in higher eukaryotes, in *Leishmania* and other kinetoplastid parasites, this group does not contain any PTP-

receptors (Soulat and Bogdan, 2017). Dual-specificity phosphatases (DUSPs) are able to dephosphorylate a wide variety of phospho-substrates in addition to phospho-tyrosine (Soulat and Bogdan, 2017).

PTP1B homologs were identified and characterized in *L. mexicana* (Escalona-Montaña et al., 2010), *L. infantum* (Nascimento et al., 2006), *L. major* (Nascimento et al., 2006), and *L. donovani* (Nascimento et al., 2006). Phosphatase activity assays performed with living cells revealed the presence of a phosphohydrolase ectoenzyme with phosphotyrosine phosphatase activity in *L. amazonensis* (de Almeida-Amaral et al., 2006).

The histidine acid phosphatase (HAcP) superfamily is a large family of proteins with a conserved catalytic histidine residue in the motif RHG present at the N-terminus, which becomes phosphorylated during the reaction (Rigden, 2008; Coker et al., 2013). Their substrate specificity has not been ascertained; therefore, they do not belong to the classical STP or PTP families (Soulat and Bogdan, 2017). Recently, *in silico* analysis of the genome of different *Leishmania* species revealed the presence of several genes encoding HAcP, including membrane-bound acid phosphatases (also known as ectophosphatases) and secreted acid phosphatases (Soulat and Bogdan, 2017). The most studied *Leishmania* HAcPs are the membrane-bound acid phosphatases of *L. donovani* (LdMAcP) (Shakarian et al., 2002) and *L. mexicana* (LmxMBAP) (Wiese, 1996) and the secreted acid phosphatases of *L. donovani* (LdSACP-1 and LdSACP-2) (Shakarian et al., 1997) and *L. mexicana* (LmxSAP-1 and LmxSAP-2) (Wiese et al., 1995).

The present review aims to describe the occurrence of STPs, PTPs, and HAcPs in *Leishmania* species, highlighting their physiological roles. In the following sections, we will discuss in detail the information available in the literature concerning the involvement of *Leishmania* phosphatases during parasite infection. We will also provide an overview of the differential expression of phosphatases throughout the *Leishmania* lifecycle, particularly in response to stress conditions.

INVOLVEMENT OF PHOSPHATASES IN LEISHMANIA PATHOGENY

The success of *Leishmania* infection in mammalian hosts is related to its prompt adaptation to new and hostile environments, in addition to its ability to impair the main microbicidal functions of macrophages (Shio et al., 2012; Soulat and Bogdan, 2017). Through the secretion of virulence factors, parasites interfere in host signaling pathways, modulating the production of cytokines and inhibiting the generation of nitric oxide (NO) and reactive oxygen species (ROS) (Remaley et al., 1984; Remaley et al., 1985; Forget et al., 2006; Soulat and Bogdan, 2017). The involvement of kinase and phosphatase proteins is crucial for the tight control of phosphorylation events that govern these signaling pathways (Soulat and Bogdan, 2017). It is well known that *Leishmania* parasites can activate host PTPs such as src homology 2 domain-

containing tyrosine phosphatase 1 (SHP-1), impairing the microbicidal capacity of macrophages (Blanchette et al., 1999; Shio et al., 2012). However, the participation of *Leishmania* phosphatases is also relevant during the infection process. Throughout this section, we will describe studies reporting the occurrence of STP, PTP, and HAcP in different *Leishmania* species and their involvement in the adaptation, survival, and proliferation of the parasites inside the host cells. **Figure 1** presents a schematic summary of the physiological roles that have been attributed to *Leishmania* endogenous phosphatases so far.

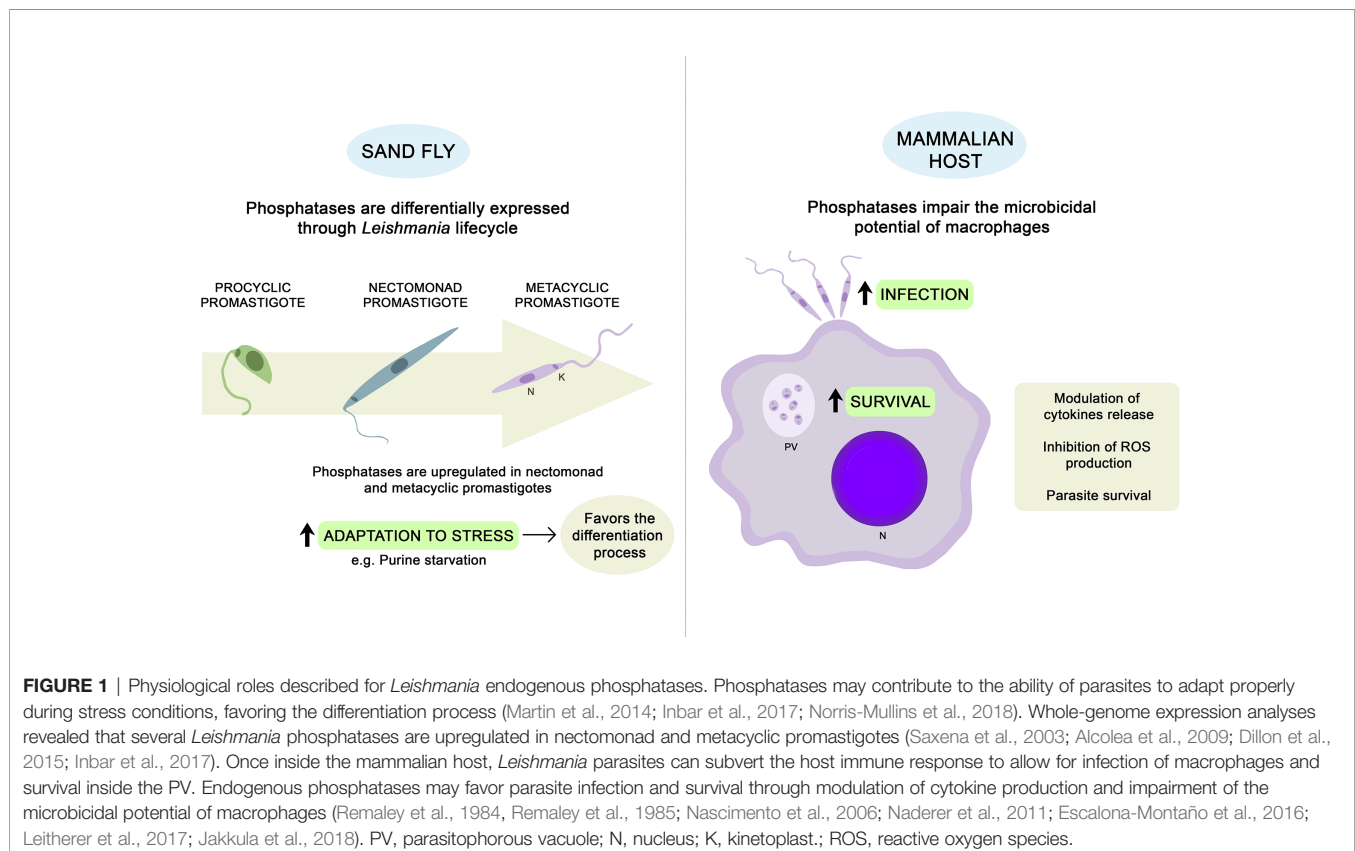
Serine/Threonine Specific Protein Phosphatases (STPs)

PP5 is a unique member of the PPP family due to the presence of an N-terminal tetratricopeptide repeat (TPR) domain that is involved in protein-protein interactions (Borthwick et al., 2001). Recently, it was observed that PP5 plays a role in the metacyclogenesis and virulence of *Leishmania* parasites (Norris-Mullins et al., 2018). *L. donovani* axenic metacyclic promastigotes present an increase in PP5 expression when compared to procyclic promastigote and amastigote stages. Further analyses, performed using PP5-overexpressing and PP5 null mutants (Δ PP5), revealed that the absence of PP5 impairs the ability of the parasites to adapt properly during stress conditions. Although Δ PP5 promastigotes retain the ability to differentiate, a significant increase in premature cell death was observed. The relevance of PP5 during the differentiation process

seems to be related to its interaction with the heat-shock protein HSP83 (Norris-Mullins et al., 2018). To investigate the potential consequences of the abolishment of PP5 on the pathobiology of *Leishmania*, *in vitro* and *in vivo* assays were performed with *L. donovani* and *L. major*, respectively. Although Δ PP5 *L. donovani* parasites have been able to successfully invade murine macrophages, an attenuation in the virulence of Δ PP5 *L. major* parasites was demonstrated through a well-established cutaneous leishmaniasis model system (Norris-Mullins et al., 2018).

Recently, a PP1 of *L. donovani* (LdPP1) was purified to study its structural properties as well as its effectiveness as an immunomodulator (Qureshi et al., 2019). Sequence analysis showed great similarity between LdPP1 and the PP1 of other trypanosomatids and even with human PP1. Such conservation during the course of evolution may be related to its indispensable involvement in vital functions (Qureshi et al., 2019). Cultured macrophages were treated with the purified LdPP1 protein to investigate possible immunomodulatory effects by ELISA and qRT-PCR analyses. LdPP1 was found to upregulate the Th1-type immune response due to the increase in the proinflammatory cytokines TNF- α and IL-6 and the levels of NO and NF- κ B in macrophages (Qureshi et al., 2019).

Calcineurin (PP2B) is a Ca^{2+} and calmodulin-activated protein phosphatase that is comprised of a catalytic (CnA) and regulatory (CnB) subunit. The catalytic site of calcineurin, usually autoinhibited, is released by calmodulin binding, which occurs due to the increase in intracellular levels of Ca^{2+} (Rodríguez et al., 2009). The requirement of calcium uptake



for parasite thermotolerance at 34–37°C has motivated the investigation of the role played by calcineurin in this process (Naderer et al., 2011). Through the generation of an *L. major* mutant lacking the essential CbN subunit (Δ cnb), it was observed that calcineurin plays a role in both early and long-term adaptive parasite responses to environmental stresses faced during their lifecycle in the mammalian host (Naderer et al., 2011). Although Δ cnb mutants have been internalized by macrophages, their differentiation into heat-adapted amastigotes was impaired, and consequently, they failed to proliferate. To investigate the role of calcineurin during infection *in vivo*, susceptible BALB/c mice were subcutaneously infected with wild-type, Δ cnb mutant or complemented (Δ cnb + CnB) *L. major* promastigotes. Δ cnb parasites were completely cleared by the susceptible BALB/c mice; however, complementation with CnB restored virulence almost to wild-type levels, confirming that calcineurin signaling is essential for the survival of *L. major* (Naderer et al., 2011).

The involvement of secreted proteins in the evasion of the host immune response has been described in different microorganisms. Proteins with phosphatase activities were identified in the secretion medium of both promastigote (PSM) and amastigote (ASM) *L. mexicana* parasites. The occurrence of a PP2C in both secretion media was confirmed through recognition by an antibody against PP2C of *L. major*. The incubation of human macrophages with PSM and ASM led to an increase in the production of several inflammatory cytokines, including TNF- α , IL-1 β , IL-12p70, and IL-10 (Escalona-Montano et al., 2016). In *L. donovani*, a PP2C (*Ld*PP2C) was also shown to elicit innate immune functions through upregulation of proinflammatory cytokines (TNF- α and IL-6) as well as NO generation by macrophages (Jakkula et al., 2018). The full-length ORF of *Ld*PP2C was cloned into an expression vector to obtain the purified protein. In addition to an analysis of its immunomodulation, its biochemical and structural parameters were evaluated. The amino acid sequence of *Ld*PP2C showed high conservation to its counterparts in other *Leishmania* species, such as *L. infantum*, *L. major*, and *L. mexicana* (Jakkula et al., 2018).

Protein Tyrosine Phosphatases (PTPs)

In higher eukaryotic cells, a large number of studies have demonstrated that PTPs are involved in the regulation of multiple cell processes, including proliferation and differentiation (Tonks, 2003). The involvement of PTPs in inducing differentiation and increasing virulence was first demonstrated through the heterologous expression of a prototype human protein-tyrosine phosphatase 1B (hPTP1B) in *L. donovani* (Nascimento et al., 2003). Genes encoding PTP were identified in *L. major* (LmPTP1), *L. infantum* (LiPTP1), and *L. donovani* (LdPTP1) due to their homology with hPTP1B (Nascimento et al., 2006). *In silico* structural analysis confirmed that LiPTP1 and hPTP1B share remarkable conservation, mainly in their active sites. The generation of LdPTP1 null mutants showed that PTP1 is dispensable for the growth and development of the parasite in culture, in contrast with previous observations that suggested the participation of PTP in the differentiation process. However, the deletion of the gene

severely impaired the survival of amastigotes in BALB/c mice (Nascimento et al., 2006).

Another PTP was recently identified in *L. major* parasites and named Lm-PRL-1 due to its strong similarity to the human phosphatases of regenerating liver (PRL), as confirmed by structural analysis and a similar profile of their biochemical parameters (Leitherer et al., 2017). The presence of LmPRL-1 was detected in exosomes released by *L. major* promastigotes. Exosomes are vesicles secreted by parasites that are loaded with cytoplasmic and membrane-bound proteins, including virulence factors. To investigate the fate of the LmPRL-1 released during infection, further analyses were performed using *L. major* parasites that ectopically expressed hemagglutinin (HA₃)-tagged LmPRL-1 (Leitherer et al., 2017). HA₃-LmPRL-1 was detected not only in the amastigotes but also in the cytoplasm of the infected macrophages. Colocalization with the late phagosomal marker LAMP-1 confirmed its occurrence on the surface of parasitophorous vacuoles (PVs), where it is prone to modulate host cell signaling pathways that may favor parasite survival. *In vitro* interaction assays have confirmed that the expression of HA₃-LmPRL-1 significantly increased parasite survival after 72 h of infection (Leitherer et al., 2017).

A dual specificity protein/lipid phosphatase of *L. mexicana* (LmDUSP1) has also been recently identified as a virulence factor (Kraeva et al., 2019). The *Lm*DUSP1-encoding gene (*LmxM.22.0250*), acquired from bacteria via horizontal gene transfer, presents orthologs that have been implicated in virulence (Beresford et al., 2010; Soulat and Bogdan, 2017). To investigate the role of LmDUSP1 in parasite infection, knockout of *LmxM.22.0250* (LmDUSP1 KO) was obtained using the CRISPR-Cas9 approach. The ablation of *LmxM.22.0250* leads to a significant decrease in the parasite's ability to infect or develop in primary murine macrophages *in vitro* (Kraeva et al., 2019).

Histidine Acid Phosphatase (HAcPs)

The passage of *L. donovani* promastigotes through susceptible Balb/c mice increased the levels of parasite HAcP activities. This was the first evidence that acid phosphatase could be considered a marker of virulence (Katakura and Kobayashi, 1988). A few years later, a study tested seven isolates of *L. donovani* and showed a correlation between the degree of virulence and the membrane-bound acid phosphatase activity of the parasites (Singla, 1992).

Preincubation of neutrophils stimulated by the chemoattractant peptide N-formyl-methionyl-leucyl-phenylalanine with a purified preparation of the tartrate-resistant membrane-bound HAcP of *L. donovani* decreased oxygen consumption and the generation of superoxide and hydrogen peroxide. These effects were abolished by the incorporation of an HAcP inhibitor in the preincubation medium, indicating that they are related to the catalytic activity of the enzyme (Remaley et al., 1984; Remaley et al., 1985). Both the membrane-bound and the secreted acid phosphatases were resistant to exposure to the toxic oxygen metabolites (e.g., superoxide anions, hydrogen peroxide, and hypochlorite) generated by the phagocytic cells. The stability of

their catalytic activity enables HACPs to compromise other host cell functions during the course of infection (Saha et al., 1985).

The association between murine peritoneal macrophages and *L. amazonensis* parasites in the presence of protein kinase C (PKC) agonists suggests that PKC activation may modulate the parasite-macrophage association via secreted HACP in the early stage of a 60-min interaction (Vannier-Santos et al., 1995). By extending the analysis over a total period of 24 h postinfection, it was observed that *L. amazonensis*-secreted HACP also mediates the maturation of PVs (Fernandes et al., 2013). Previous studies using bacteria as models suggested the involvement of microorganism-secreted phosphatases in both PV biogenesis and bacterial growth via an unknown mechanism (Hussain et al., 2010). Indeed, it has also been shown in *L. donovani* and *L. major* that secreted HACP leaves the PV and becomes concentrated in compartments distributed in the cytoplasm of infected macrophages (McCall and Matlashewski, 2010).

A recent study promoted the overexpression of *LdMacP* in *L. donovani* promastigotes and showed an increase in transgenic parasite survival during *in vitro* infection of macrophages (Papadaki et al., 2015). These data suggest a possible similar role for endogenous *LdMacP*, consistent with previous observations indicating that this enzyme may play a role in parasite virulence (Katakura and Kobayashi, 1988; Singla, 1992; Papadaki et al., 2015; Soulat and Bogdan, 2017). On the other hand, the deletion of the membrane-bound HACP gene of *L. mexicana* did not affect the virulence of these parasites (Benzel et al., 2000). Comparing wild-type and *LmxMBAP*-deficient parasites, no significant differences were observed in survival during *in vitro* infection in macrophages or *in vivo* infection of susceptible BALB/c mice (Benzel et al., 2000). Although this result may rule out the involvement of the membrane-bound HACP in *L. mexicana* virulence, a definitive statement is not possible because of potential compensatory mechanisms, as *Leishmania* parasites carry a minimum of four genes encoding HACPs (Soulat and Bogdan, 2017).

The unique tartrate-resistant membrane-bound acid phosphatase seems to be specifically expressed in the *L. donovani* complex, responsible for visceralization, the most severe manifestation of leishmaniasis. It is possible that this enzyme modulates the secretion of cytokines by macrophages, thereby affecting the pathophysiology of the disease. Further studies are needed to deepen the knowledge in this area. If this hypothesis is confirmed, *LdMacP* could be proven useful in diagnosis or epidemiological studies (Papadaki et al., 2015).

TRANSCRIPTOME AND PROTEOMIC ANALYSES REVEALED THE DIFFERENTIAL EXPRESSION OF SEVERAL *LEISHMANIA* PHOSPHATASES

Recent advances in sequencing techniques have shown the global changes in gene expression during the lifecycle of *Leishmania* parasites. The following section presents several whole-genomic

analyses showing the differential expression of *Leishmania* phosphatases according to parasite stage of life or in drug-resistant strains, as summarized in **Table 1**.

Differential Expression of Phosphatases During the *Leishmania* Lifecycle

Leishmania parasites shift their lifecycle between the PV of their mammalian host mononuclear phagocytes and the alimentary tract of their sand fly vector. Briefly, when a sand fly takes a blood meal from an infected mammalian host, the acquired amastigotes differentiate into promastigotes and colonize the insect midgut. The *Leishmania* promastigotes are subjected to several microenvironments with different conditions, such as a lack of nutrient availability (Inbar et al., 2017). In response to these specific conditions, the parasite can differentiate into several distinct forms. Beyond the proliferative procyclic and infective metacyclic forms, there are also intermediate forms of promastigotes, such as nectomonads, leptomonads and haptomonads. This adaptation ability has motivated several studies comparing the global variations in gene expression of the different parasite stages during their lifecycle (Inbar et al., 2017).

The first genome-scale quantitative analysis of gene expression during the differentiation from promastigotes to amastigotes was performed with *L. donovani* in a host-free system that mimics this process. Microarray-based expression profiling revealed that several hundred genes were transiently or permanently up- and downregulated during differentiation, including protein phosphatases that may be important in signal transduction (Saxena et al., 2007). Four morphological phases can be distinguished until 120 hours after the exposure of promastigotes to the differentiation signal: signal perception (phase I); movement cessation and aggregation (phase II); amastigote morphogenesis (phase III) and maturation (phase IV) (Barak et al., 2005). Shotgun phosphopeptide analysis has revealed that in axenic *L. donovani*, there is more stage-specific than constitutive protein phosphorylation (Tsigankov et al., 2013). To investigate the protein phosphorylation dynamics during promastigote to amastigote differentiation, a proteomic analysis was performed employing isobaric tags for relative and absolute quantitation (iTRAQ). Several proteins, including kinases and phosphatases, change their phosphorylation profiles during differentiation. The increase in phosphorylation predominated during phases I and III, whereas phases II and IV were characterized by greater dephosphorylation (Tsigankov et al., 2014).

Transcriptome analysis of different stages of *L. infantum* revealed that the upregulation rate is lower in intracellular amastigotes after infection of the U937 cell line compared to promastigotes of axenic cultures or metacyclic promastigotes anterior to the stomodeal valves (Pro-Pper) isolated from sand flies (Alcolea et al., 2010; Alcolea et al., 2016). This profile corroborates the hypothesis of preadaptation from promastigote forms toward life in the intracellular environment. However, the set of differentially regulated genes is notably different with respect to promastigotes from Pro-Pper instead of axenic cultures (Alcolea

TABLE 1 | Differential expression of *Leishmania* endogenous phosphatases during their lifecycle and in drug-resistant strains.

| Leishmania spp. | Compared to | Upregulates Phosphatase (s) | Fold-change | Ref. |
|--|--|--|--------------------|------------------------|
| <i>L. infantum</i> logarithmic-phase promastigotes | Amastigote isolated from <i>in vitro</i> infected macrophages ^a | PP2C, putative (LinJ32_V3.1770) | 5.08-fold | (Alcolea et al., 2010) |
| <i>L. infantum</i> Pro-Pper | Amastigote isolated from <i>in vitro</i> infected macrophages ^a | MBAP2 (LinJ23_V3.1430) | 2.20-fold | (Alcolea et al., 2014) |
| | | PP2C (LinJ.36.0560) | 2.72-fold | (Alcolea et al., 2014) |
| | | STP (LinJ.22.134) | 7.23-fold | (Saxena et al., 2003) |
| <i>L. major</i> axenic metacyclic promastigotes | Axenic procyclic promastigotes ^a | MBAP (Im26a07) | 1.60-fold | (Saxena et al., 2003) |
| | | STP (Im34d12) | 1.20-fold | (Saxena et al., 2003) |
| | | STP (Im74g05) | 2.20-fold | (Saxena et al., 2003) |
| <i>L. major</i> axenic metacyclic promastigotes | Axenic procyclic promastigotes ^b | PP2C-like protein (LmjF.34.2500) | 2.49-fold | (Dillon et al., 2015) |
| <i>L. infantum</i> axenic metacyclic promastigotes | Axenic procyclic promastigotes ^a | PP2C (LinJ15_V3.0170) | 2.12-fold | (Alcolea et al., 2009) |
| <i>L. infantum</i> ProPper | Axenic procyclic promastigotes ^a | PP1 (LinJ.34.0840) | 2.09-fold | (Alcolea et al., 2016) |
| | | PP2B (LinJ.36.2090; catalytic subunit A2) | 3.12-fold | (Alcolea et al., 2016) |
| | | DUSP (LinJ.28.0850; referred as DualPP) | 2.28-fold | (Alcolea et al., 2016) |
| <i>L. major</i> four distinct stages of development ^b | NP versus AM, PP, and MP | MBAP2 (LmjF.28.2650) | N/A | (Inbar et al., 2017) |
| Purine-starved | Purine-replete | MBAP2 (LmjF.23.1170) | N/A | (Inbar et al., 2017) |
| <i>L. donovani</i> promastigotes | <i>L. donovani</i> promastigotes ^b | MPAP2-36 (LinJ.36.2720) | 4.47-fold | (Martin et al., 2014) |
| <i>L. infantum</i> Sb ^{III} -resistant promastigotes | Sb ^{III} -sensitive promastigotes ^b | DUSP (LINF_340027100) | 8.93-fold | (Andrade et al., 2020) |
| | | PPP (LINF_130020500) | 2.28-fold | (Andrade et al., 2020) |
| | | PP2C (LINF_340030800) | 17.52-fold | (Andrade et al., 2020) |
| <i>L. amazonensis</i> Sb ^{III} -resistant promastigotes | Sb ^{III} -sensitive promastigotes ^b | MBAP2 (LmxM.23.1170) | 1.55-fold | (Patino et al., 2019) |
| <i>L. donovani</i> PMM-resistant promastigotes | PMM-sensitive promastigotes ^a | PP2C-like protein (LinJ14_V3.0960) | 3.02-fold | (Verma et al., 2017) |
| | | STP, putative (LinJ30_V3.3330) | 2.97-fold | (Verma et al., 2017) |

^aDNA microarray analysis.^bRNA-seq analysis.

PP2C, protein phosphatase 2C; MBAP2, membrane-bound acid phosphatase 2; ProPper, metacyclic promastigotes anterior to the stomodeal valves obtained from sand fly; STP, serine/threonine specific protein phosphatases; N/A, data not available; PP1, protein phosphatase 1; PP2B, protein phosphatase 2B; DUSP, dual-specificity phosphatase; NP, nectomonad promastigotes obtained from sand fly; AM, lesion-derived amastigotes; PP, procyclic promastigotes obtained from sand fly; MP, metacyclic promastigotes obtained from sand fly; Sb^{III}, trivalent stibogluconate (antimony); PPP, phosphoprotein phosphatase; PMM, paromomycin.

Bold titles refers to the proteins which expression have been evaluated.

et al., 2016). In both cases, the upregulation of several phosphatases was described. Comparing amastigotes with logarithmic-phase culture promastigotes, putative PP2C (LinJ32_V3.1770) and membrane-bound acid phosphatase 2 (MBAP2) (LinJ23_V3.1430) were upregulated in promastigotes by 5.08- and 2.20-fold, respectively (Alcolea et al., 2010). With respect to Pro-Pper, an upregulation of 2.72-fold of a PP2C (LinJ.36.0560) and of 7.23-fold of a STP (LinJ.22.134) was observed (Alcolea et al., 2014).

The final development phase of *Leishmania* parasites found in sand flies is metacyclic promastigotes. The differentiation process named metacyclogenesis naturally occurs at the stomodeal valve of the insect; however, it is possible to mimic this process *in vitro* to obtain metacyclic promastigotes in axenic culture (Sacks et al., 1985; McConville et al., 1992). Studies with *L. major* have evaluated the global changes in gene expression during the maturation of axenic promastigotes from procyclic to metacyclic forms. DNA microarray analysis revealed an upregulation of a membrane-bound HAcP (Im26a07; 1.6-fold) and two STPs (Im34d12 and Im74g05; 1.2- and 2.2-fold, respectively) (Saxena et al., 2003). Posterior RNA-seq analysis showed that a PP2C-like protein (LmjF.34.2500) was 2.49-fold upregulated in *L. major* metacyclic promastigotes (Dillon et al., 2015).

The usual method to isolate metacyclic promastigotes from stationary phase cultures is negative selection with *Arachis hypogaea* lectin (peanut agglutinin, PNA). Using this approach, both fractions of procyclic (PNA⁺) and metacyclic (PNA⁻) *L. infantum* promastigotes can be simultaneously isolated from the same population to compare their expression profiles by whole-genome shotgun DNA microarrays. It was observed that a PP2C (LinJ15_V3.0170) was upregulated in PNA⁻ metacyclic promastigotes (Alcolea et al., 2009). Notably, several genes previously related to infectivity are upregulated in PNA⁻ metacyclic promastigotes, which is consistent with their increased infection rate confirmed by U937 human cell line infection experiments (Alcolea et al., 2009).

Although the promastigote culture model is stable, reproducible, and widely used for various purposes, some parasite properties are affected by culture passaging, such as infectivity and virulence. The difficulty of studying promastigotes in their natural environment is mainly related to the reduced amount of available biomass; however, it is possible to overcome this limitation by mRNA amplification for transcriptome analysis (Alcolea et al., 2014). Studies with *L. infantum* have revealed significant differences when comparing metacyclic promastigotes isolated from the sand fly midgut (Pro-Pper) to metacyclic promastigotes obtained in

axenic culture by negative selection with PNA (Pro-PNA[−]) (Alcolea et al., 2016). The genes encoding a PP1 (LinJ.34.0840), a PP2B catalytic subunit A2 and a DUSP are upregulated in Pro-Pper (Alcolea et al., 2016). Consistent with the increase in *in vitro* infectivity, phosphoglycan β -1,3-galactosyltransferase (PG β 1, 3GalT), which is involved in the biosynthesis of lipophosphoglycan (LPG) and proteophosphoglycans (PPG), is also upregulated in Pro-Pper. These glycoconjugates, which include membrane-bound and secreted HACp, are abundant on the parasite's surface (Alcolea et al., 2016).

Recently, global changes in gene expression were evaluated based on RNASeq from distinct insect stages of *L. major* during their cyclical development *in vivo*. The upregulation of membrane-bound HACps (LmjF.28.2650, LmjF.23.1170) was observed in nectomonad promastigotes. Together with the increase in autophagy-related genes, these observations suggest that differentiation to nectomonads and to metacyclic promastigotes involves a response to stress conditions, which triggers protein recycling (Inbar et al., 2017). Indeed, putative membrane-bound acid phosphatase 2-36 (MAP2-36; LinJ.36.2720) was one of the first and most significantly upregulated proteins in response to purine starvation, as described by proteome and transcriptome analysis in *L. donovani* axenic promastigotes (Martin et al., 2014).

Differential Expression of Phosphatases in Drug-Resistant Parasites

There are currently no effective vaccines to prevent leishmaniasis; thus, the control of this disease relies essentially on chemotherapy (Singh and Sundar, 2012). Although several different drugs are available, pentavalent antimony-containing compounds, including sodium stibogluconate (Pentostam[®]), are used as standard treatments against all forms of leishmaniasis, especially in Latin America (Herwaldt and Berman, 1992; Berman, 1997; Ashutosh et al., 2007). However, in the last decade, the emergence of parasites resistant to antimonials has led to an increase in therapeutic failure (Croft and Olliaro, 2011). Understanding drug resistance is essential to guarantee the efficacy of the available treatments and the development of new treatments (Hefnawy et al., 2017). In this context, several studies have been performed to elucidate the mechanisms of resistance and parasite biology in response to different drugs.

By using high-throughput RNA sequencing to analyze the transcriptome profiles, significant differences were identified between wild-type and potassium antimonite tartrate (Sb^{III})-resistant *L. infantum* lines (abbreviated as LiWTS and LiSbR, respectively) (Andrade et al., 2020). The LiSbR line showed an upregulation of thirty-seven transcripts belonging to the protein phosphorylation category, which includes a DUSP that was 8.93-fold upregulated. In addition, a PPP and a PP2C were 2.28- to 17.52-fold upregulated, respectively (Andrade et al., 2020). This is consistent with a previous proteomic analysis that found a major abundance of both enzymes in the Sb^{III}-resistant line (Matrangolo et al., 2013).

Similar analyses were performed using Sb^{III}-resistant and Sb^{III}-sensitive *L. amazonensis* promastigotes (La-Sb^{III}-R and La-Sb^{III}-S,

respectively). Global transcriptomic changes point to an upregulation of genes encoding autophagy proteins in La-Sb^{III}-R cells, suggesting a possible strategy of survival or induced cell death (Patino et al., 2019). The autophagy protein ATG9 is involved in cytoplasm-to-vacuole transport vesicle formation (Patino et al., 2019), while MBAP2 plays a role in endosomal trafficking (Inbar et al., 2017; Patino et al., 2019). Transcripts encoding APG9 (LmxM.27.0390) and MBAP2 (LmxM.23.1170) were both upregulated in La-Sb^{III}-R (Patino et al., 2019).

Paromomycin (PMM) is an aminoglycoside antibiotic that has already been approved for the treatment of visceral leishmaniasis in Southeast Asia (Coser et al., 2021). Antimony-resistant and sensitive isolates of *L. donovani* are equally susceptible to PMM, making it a valid alternative treatment (Kulshrestha et al., 2011). To elucidate the mechanisms of resistance and parasite biology, a PMM-resistant strain was generated in the laboratory, and the expression of genes encoding the proteins of interest was determined by real-time PCR (Bhandari et al., 2014). A marked increase in the levels of the ATP-binding cassette (ABC) transporters MDR1 (6.83 ± 3.01 -fold) and MRPA (11.47 ± 0.22 -fold) and of PP2A (4.47 ± 0.71 -fold) was observed in PMM-resistant *L. donovani* promastigotes. PP2A seems to be involved in activating the expression of those transporters, culminating in increased drug efflux (Bhandari et al., 2014). Comparing the genes differentially modulated in PMM-resistant and PMM-sensitive *L. donovani* promastigotes by transcriptome analysis, a PP2C-like protein (LinJ14_V3.0960) and a putative STP (LinJ30_V3.3330) were upregulated 3.02- and 2.97-fold, respectively, in the PMM-resistant parasites (Verma et al., 2017).

CONCLUDING REMARKS

The successful establishment of parasite infection depends on many factors. *Leishmania* parasites have evolved different features that allow them to survive and proliferate within their host cells. To impair the microbicidal function of macrophages, parasites can interfere with host signaling pathways. In this context, protein phosphatases play an important role. It is well known that the activation of host phosphatases is crucial for parasite survival (Shio et al., 2012). The participation of endogenous *Leishmania* phosphatases in the infection process has been an object of study for many years. Although their roles have not been fully elucidated, many studies suggest their involvement not only in parasite virulence but also in resistance to stress conditions during the *Leishmania* lifecycle.

Since the 1980s, phosphatases have been considered possible virulence factors. Previously, it was demonstrated that *L. donovani* HACp was able to decrease ROS production by host immune cells (Remaley et al., 1984; Remaley et al., 1985). Furthermore, studies with *L. amazonensis* showed that HACp was related to an increase in the parasite-macrophage association index (Vannier-Santos et al., 1995) and the survival of the amastigote form inside PVs (Fernandes et al., 2013).

More recently, several studies performed with *L. donovani*, *L. major*, and *L. mexicana* have confirmed the involvement of

different phosphatases in parasite survival through the ablation and/or overexpression of specific genes (Nascimento et al., 2006; Naderer et al., 2011; Papadaki et al., 2015; Leitherer et al., 2017; Norris-Mullins et al., 2018; Kraeva et al., 2019). These endogenous phosphatases are able to favor infection mainly due to the modulation of cytokine production by macrophages (Leitherer et al., 2017; Kraeva et al., 2019). STPs seem to be particularly relevant for the ability of parasites to adapt properly during stress conditions (Naderer et al., 2011; Norris-Mullins et al., 2018). These physiological roles that have been attributed to *Leishmania* phosphatases are summarized in **Figure 1**.

Whole-genome expression analyses performed throughout the lifecycle of different *Leishmania* species revealed that phosphatases are generally upregulated in metacyclic promastigotes, the infective form of the mammalian host (Saxena et al., 2003; Alcolea et al., 2009; Dillon et al., 2015). While STPs and PTPs are related to cell signaling (Saxena et al., 2007; Dillon et al., 2015; Alcolea et al., 2016), membrane-bound HACPs seem to play a role in the response to protein recycling during stress conditions, such as nutrient starvation (Martin et al., 2014; Inbar et al., 2017). *Leishmania* phosphatases are also upregulated in drug-resistant strains (Matrangolo et al., 2013; Bhandari et al., 2014; Verma et al., 2017; Patino et al., 2019; Andrade et al., 2020). STPs may contribute to parasite resistance by activating ABC transporters, leading to an increase in drug efflux (Bhandari et al., 2014; Verma et al., 2017). **Table 1** presents the main findings related to the differential expression of *Leishmania* endogenous phosphatases during their lifecycle and in drug-resistant strains.

REFERENCES

- Alcolea, P. J., Alonso, A., Degayón, M. A., Moreno-Paz, M., Jiménez, M., Molina, R., et al. (2016). *In Vitro* Infectivity and Differential Gene Expression of *Leishmania Infantum* Metacyclic Promastigotes: Negative Selection With Peanut Agglutinin in Culture Versus Isolation From the Stomodaeal Valve of *Phlebotomus Perniciosus*. *BMC Genomics* 17, 1–14. doi: 10.1186/s12864-016-2672-8
- Alcolea, P. J., Alonso, A., Gómez, M. J., Moreno, I., Domínguez, M., Parro, V., et al. (2010). Transcriptomics Throughout the Life Cycle of *Leishmania Infantum*: High Down-Regulation Rate in the Amastigote Stage. *Int. J. Parasitol.* 40, 1497–1516. doi: 10.1016/j.ijpara.2010.05.013
- Alcolea, P. J., Alonso, A., Gómez, M. J., Postigo, M., Molina, R., Jiménez, M., et al. (2014). Stage-Specific Differential Gene Expression in *Leishmania Infantum*: From the Foregut of *Phlebotomus Perniciosus* to the Human Phagocyte. *BMC Genomics* 15, 1–16. doi: 10.1186/1471-2164-15-849
- Alcolea, P. J., Alonso, A., Sánchez-Gorostiaga, A., Moreno-Paz, M., Gómez, M. J., Ramos, I., et al. (2009). Genome-Wide Analysis Reveals Increased Levels of Transcripts Related With Infectivity in Peanut Lectin Non-Agglutinated Promastigotes of *Leishmania Infantum*. *Genomics* 93, 551–564. doi: 10.1016/j.ygeno.2009.01.007
- Alonso, A., Sasín, J., Bottini, N., Friedberg, I., Friedberg, I., Osterman, A., et al. (2004). Protein Tyrosine Phosphatases in the Human Genome. *Cell* 117, 699–711. doi: 10.1016/j.cell.2004.05.018
- Andrade, J. M., Gonçalves, L. O., Liarte, D. B., Lima, D. A., Guimarães, F. G., de Melo Resende, D., et al. (2020). Comparative Transcriptomic Analysis of Antimony Resistant and Susceptible *Leishmania Infantum* Lines. *Parasites. Vectors* 13, 1–15. doi: 10.1186/s13071-020-04486-4
- Andreeva, A. V., and Kutuzov, M. A. (2008). Protozoan Protein Tyrosine Phosphatases. *Int. J. Parasitol.* 38, 1279–1295. doi: 10.1016/j.ijpara.2008.04.003
- Ashutosh, S., Sundar, S., and Goyal, N. (2007). Molecular Mechanisms of Antimony Resistance in *Leishmania*. *J. Med. Microbiol.* 56, 143–153. doi: 10.1099/jmm.0.46841-0
- Banerjee, C., Sarkar, D., and Bhaduri, A. (1999). Ca²⁺ and Calmodulin-Dependent Protein Phosphatase From *Leishmania Donovanii*. *Parasitology* 118, 567–573. doi: 10.1017/S0031182099004308
- Barak, E., Amin-Spector, S., Gerliak, E., Goyard, S., Holland, N., and Zilberstein, D. (2005). Differentiation of *Leishmania Donovanii* in Host-Free System: Analysis of Signal Perception and Response. *Mol. Biochem. Parasitol.* 141, 99–108. doi: 10.1016/j.molbiopara.2005.02.004
- Benzel, I., Weise, F., and Wiese, M. (2000). Deletion of the Gene for the Membrane-Bound Acid Phosphatase of *Leishmania Mexicana*. *Mol. Biochem. Parasitol.* 111, 77–86. doi: 10.1016/S0166-6851(00)00306-6
- Beresford, N. J., Saville, C., Bennett, H. J., Roberts, I. S., and Taberner, L. (2010). A New Family of Phosphoinositide Phosphatases in Microorganisms: Identification and Biochemical Analysis. *BMC Genomics* 11, 1–12. doi: 10.1186/1471-2164-11-457
- Berman, J. D. (1997). Human Leishmaniasis: Clinical, Diagnostic, and Chemotherapeutic Developments in the Last 10 Years. *Clin. Infect. Dis.* 24, 684–703. doi: 10.1093/clind/24.4.684
- Bhandari, V., Sundar, S., Dujardin, J. C., and Salotra, P. (2014). Elucidation of Cellular Mechanisms Involved in Experimental Paromomycin Resistance in *Leishmania Donovanii*. *Antimicrob. Agents Chemother.* 58, 2580–2585. doi: 10.1128/AAC.01574-13
- Blanchette, J., Racette, N., Faure, R., Siminovich, K. A., and Olivier, M. (1999). *Leishmania*-Induced Increases in Activation of Macrophage SHP-1 Tyrosine Phosphatase are Associated With Impaired IFN- γ -Triggered JAK2 Activation. *Eur. J. Immunol.* 29, 3737–3744. doi: 10.1002/(SICI)1521-4141(199911)29:11<3737::AID-IMMU3737>3.0.CO;2-S
- Borthwick, E. B., Zeke, T., Prescott, A. R., and Cohen, P. T. (2001). Nuclear Localization of Protein Phosphatase 5 is Dependent on the Carboxy-Terminal Region. *FEBS Lett.* 491, 279–284. doi: 10.1016/S0014-5793(01)02177-9
- Burns, J. M., Parsons, M., Rosman, D. E., and Reed, S. G. (1993). Molecular Cloning and Characterization of a 42-KDa Protein Phosphatase of *Leishmania Chagasi*. *J. Biol. Chem.* 268, 17155–17161.

AUTHOR CONTRIBUTIONS

AF-M, AD-S, and JM-F wrote the manuscript. AF-M prepared the figure. All authors contributed to the article and approved the submitted version.

FUNDING

This work was supported by grants from the Brazilian agencies Conselho Nacional de Desenvolvimento Científico e Tecnológico (CNPq - Grant Number: 401134/2014–8), Coordenação de Aperfeiçoamento de Pessoal de Nível superior (CAPES - Grant Number: 0012017), and Fundação Carlos Chagas Filho de Amparo à Pesquisa do Estado do Rio de Janeiro (FAPERJ - Grant Number: e-26/201.300/2014) to JM-F. AD-S was supported by Fundação Carlos Chagas Filho de Amparo à Pesquisa do Estado do Rio de Janeiro (FAPERJ - Grant Number: 202.378/2017).

- Chang, K. P. (1983). Cellular and Molecular Mechanisms of Intracellular Symbiosis in Leishmaniasis. *Int. Rev. Cytol. Suppl.* 14, 267–305.
- Cohen, P. T. W. (1997). Novel Protein Serine/Threonine Phosphatases: Variety is the Spice of Life. *Trends Biochem. Sci.* 22, 245–251. doi: 10.1016/S0968-0004(97)01060-8
- Coker, O., Warit, S., Rukseer, K., Sumppun, P., Prammananan, T., and Palittapongarnpim, P. (2013). Functional Characterization of Two Members of Histidine Phosphatase Superfamily in *Mycobacterium Tuberculosis*. *BMC Microbiol.* 13, 292. doi: 10.1186/1471-2180-13-292
- Cosentino-Gomes, D., and Meyer-Fernandes, J. R. (2011). Ecto-Phosphatases in Protozoan Parasites: Possible Roles in Nutrition, Growth and ROS Sensing. *J. Bioenerg. Biomembr.* 43, 89–92. doi: 10.1007/s10863-011-9334-y
- Coser, E. M., Ferreira, B. A., Yamashiro-Kanashiro, E. H., Lindoso, J. A. L., and Coelho, A. C. (2021). Susceptibility to Paromomycin in Clinical Isolates and Reference Strains of *Leishmania* Species Responsible for Tegumentary Leishmaniasis in Brazil. *Acta Trop.* 215, 105806. doi: 10.1016/j.actatropica.2020.105806
- Croft, S. L., and Ollario, P. (2011). Leishmaniasis Chemotherapy—Challenges and Opportunities. *Clin. Microbiol. Infect.* 17, 1478–1483. doi: 10.1111/j.1469-0691.2011.03630.x
- de Almeida-Amaral, E. E., Belmont-Firpo, R., Vannier-Santos, M. A., and Meyer-Fernandes, J. R. (2006). *Leishmania Amazonensis*: Characterization of an Ecto-Phosphatase Activity. *Exp. Parasitol.* 114, 334–340. doi: 10.1016/j.exppara.2006.04.011
- Dillon, L. A. L., Okrah, K., Hughitt, K. V., Suresh, R., Li, Y., Fernandes, M. C., et al. (2015). Transcriptomic Profiling of Gene Expression and RNA Processing During *Leishmania Major* Differentiation. *Nucleic Acids Res.* 43, 6799–6813. doi: 10.1093/nar/gkv656
- Escalona-Montaño, A. R., Ortiz-Lozano, D. M., Rojas-Bernabé, A., Wilkins-Rodriguez, A. A., Torres-Guerrero, H., Mondragón-Flores, R., et al. (2016). *Leishmania Mexicana*: Promastigotes and Amastigotes Secrete Protein Phosphatases and This Correlates With the Production of Inflammatory Cytokines in Macrophages. *Parasitology* 143, 1409–1420. doi: 10.1017/S0031182016000949
- Escalona-Montaño, A. R., Pardavé-Alejandre, D., Cervantes-Sarabia, R., García-López, P., Gutiérrez-Quiroz, M., Gutiérrez-Kobeh, L., et al. (2010). *Leishmania Mexicana* Promastigotes Secrete a Protein Tyrosine Phosphatase. *Parasitol. Res.* 107, 309–315. doi: 10.1007/s00436-010-1863-5
- Fernandes, A. C. S., Soares, D. C., Saraiva, E. M., Meyer-Fernandes, J. R., and Souto-Pradón, T. (2013). Different Secreted Phosphatase Activities in *Leishmania Amazonensis*. *FEMS Microbiol. Lett.* 340, 117–128. doi: 10.1111/1574-6968.12080
- Forget, G., Gregory, D. J., Whitcombe, L. A., and Olivier, M. (2006). Role of Host Protein Tyrosine Phosphatase SHP-1 in *Leishmania Donovanii*-Induced Inhibition of Nitric Oxide Production. *Infect. Immun.* 74, 6272–6279. doi: 10.1128/IAI00853-05
- Freitas-Mesquita, A. L., and Meyer-Fernandes, J. R. (2014). Ecto-Nucleotidases and Ecto-Phosphatases From *Leishmania* and *Trypanosoma* Parasites. *Subcell. Biochem.* 74, 217–252. doi: 10.1007/978-94-007-7305-9_10
- Hefnawy, A., Berg, M., Dujardin, J.-C., and De Muylder, G. (2017). Exploiting Knowledge on *Leishmania* Drug Resistance to Support the Quest for New Drugs. *Trends Parasitol.* 33, 162–174. doi: 10.1016/j.pt.2016.11.003
- Herwaldt, B. L., and Berman, J. D. (1992). Recommendations for Treating Leishmaniasis With Sodium Stibogluconate (Pentostam) and Review of Pertinent Clinical Studies. *Am. J. Trop. Med. Hyg.* 46, 296–306. doi: 10.4269/ajtmh.1992.46.296
- Hussain, S. K., Broderdorf, L. J., Sharma, U. M., and Voth, D. E. (2010). Host Kinase Activity is Required for *Coxiella Burnetii* Parasitophorous Vacuole Formation. *Front. Microbiol.* 1, 1–10. doi: 10.3389/fmicb.2010.00137
- Inbar, E., Hughitt, V. K., Dillon, L. A. L., Ghosh, K., El-Sayed, N. M., and Sacks, D. L. (2017). The Transcriptome of *Leishmania Major* Developmental Stages in Their Natural Sand Fly Vector. *MBio* 8, 1–18. doi: 10.1128/mBio.00029-17
- Jakkula, P., Qureshi, R., Iqbal, A., Sagurthi, S. R., and Qureshi, I. A. (2018). *Leishmania Donovanii* PP2C: Kinetics, Structural Attributes and in Vitro Immune Response. *Mol. Biochem. Parasitol.* 223, 37–49. doi: 10.1016/j.molbiopara.2018.06.005
- Katakura, K., and Kobayashi, A. (1988). Acid Phosphatase Activity of Virulent and Avirulent Clones of *Leishmania Donovanii* Promastigotes. *Infect. Immun.* 56, 2856–2860. doi: 10.1128/IAI.56.11.2856-2860.1988
- Kraeva, N., Leštinová, T., Ishemgulova, A., Majerová, K., Butenko, A., Vaselek, S., et al. (2019). Lmxm.22.0250-Encoded Dual Specificity Protein/Lipid Phosphatase Impairs *Leishmania Mexicana* Virulence in Vitro. *Pathogens* 8, 1–14. doi: 10.3390/pathogens8040241
- Kulshrestha, A., Singh, R., Kumar, D., Negi, N. S., and Salotra, P. (2011). Antimony-Resistant Clinical Isolates of *Leishmania Donovanii* are Susceptible to Paromomycin and Sitamaquine. *Antimicrob. Agents Chemother.* 55, 2916–2921. doi: 10.1128/AAC.00812-10
- Leitherer, S., Clos, J., Liebler-Tenorio, E. M., Schleicher, U., Bogdan, C., and Soulat, D. (2017). Characterization of the Protein Tyrosine Phosphatase Lmp1-1 Secreted by *Leishmania Major* Via the Exosome Pathway. *Infect. Immun.* 85, 1–19. doi: 10.1128/IAI.00084-17
- Martin, J. L., Yates, P. A., Soysa, R., Alfaro, J. F., Yang, F., Burnum-Johnson, K. E., et al. (2014). Metabolic Reprogramming During Purine Stress in the Protozoan Pathogen *Leishmania Donovanii*. *PLoS Pathog.* 10, 1–21. doi: 10.1371/journal.ppat.1003938
- Matrangola, F. S. V., Liarte, D. B., Andrade, L. C., de Melo, M. F., Andrade, J. M., Ferreira, R. F., et al. (2013). Comparative Proteomic Analysis of Antimony-Resistant and -Susceptible *Leishmania Braziliensis* and *Leishmania Infantum Chagasi* Lines. *Mol. Biochem. Parasitol.* 190, 63–75. doi: 10.1016/j.molbiopara.2013.06.006
- McCall, L.-I., and Matlashewski, G. (2010). Localization and Induction of the A2 Virulence Factor in *Leishmania*: Evidence That A2 is a Stress Response Protein. *Mol. Microbiol.* 77, 518–530. doi: 10.1111/j.1365-2958.2010.07229.x
- McConville, M. J., Turco, S. J., Ferguson, M. A., and Sacks, D. L. (1992). Developmental Modification of Lipophosphoglycan During the Differentiation of *Leishmania Major* Promastigotes to an Infectious Stage. *EMBO J.* 11, 3593–3600.
- Mills, E., Price, H. P., Johnner, A., Emerson, J. E., and Smith, D. F. (2007). Kinetoplastid PPEF Phosphatases: Dual Acylated Proteins Expressed in the Endomembrane System of *Leishmania*. *Mol. Biochem. Parasitol.* 152, 22–34. doi: 10.1016/j.molbiopara.2006.11.008
- Naderer, T., Dandash, O., and McConville, M. J. (2011). Calcineurin is Required for *Leishmania Major* Stress Response Pathways and for Virulence in the Mammalian Host. *Mol. Microbiol.* 80, 471–480. doi: 10.1111/j.1365-2958.2011.07584.x
- Nascimento, M., Abourjeily, N., Ghosh, A., Zhang, W. W., and Matlashewski, G. (2003). Heterologous Expression of a Mammalian Protein Tyrosine Phosphatase Gene in *Leishmania*: Effect on Differentiation. *Mol. Microbiol.* 50, 1517–1526. doi: 10.1046/j.1365-2958.2003.03811.x
- Nascimento, M., Zhang, W., Ghosh, A., Houston, D. R., Berghuis, A. M., Olivier, M., et al. (2006). Identification and Characterization of a Protein-Tyrosine Phosphatase in *Leishmania* 281, 36257–36268. doi: 10.1074/jbc.M606256200
- Norris-Mullins, B., Krivda, J. S., Smith, K. L., Ferrell, M. J., and Morales, M. A. (2018). *Leishmania* Phosphatase PP5 is a Regulator of HSP83 Phosphorylation and Essential for Parasite Pathogenicity. *Parasitol. Res.* 117, 2971–2985. doi: 10.1007/s00436-018-5994-4
- Pace, D. (2014). Leishmaniasis. *J. Infect.* 69, S10–S18. doi: 10.1016/j.jinf.2014.07.016
- Papadaki, A., Politou, A. S., Smirlis, D., Kotini, M. P., Kourou, K., Papamarcaki, T., et al. (2015). The *Leishmania Donovanii* Histidine Acid Ecto-Phosphatase Ldmacp: Insight Into Its Structure and Function. *Biochem. J.* 467, 473–486. doi: 10.1042/BJ20141371
- Patino, L. H., Muskus, C., and Ramírez, J. D. (2019). Transcriptional Responses of *Leishmania (Leishmania) Amazonensis* in the Presence of Trivalent Sodium Stibogluconate. *Parasites. Vectors.* 12, 1–15. doi: 10.1186/s13071-019-3603-8
- Qureshi, R., Jakkula, P., Sagurthi, S. R., and Qureshi, I. A. (2019). Protein Phosphatase 1 of *Leishmania Donovanii* Exhibits Conserved Catalytic Residues and Pro-Inflammatory Response. *Biochem. Biophys. Res. Commun.* 516, 770–776. doi: 10.1016/j.bbrc.2019.06.085
- Remaley, A. T., Glew, R., Kuhns, D. B., Basford, R. E., Waggoner, A., Ernst, A., et al. (1985). *Leishmania Donovanii*: Surface Membrane Acid Phosphatase Oxidative Metabolite Production. *Exp. Parasitol.* 60, 331–341. doi: 10.1016/0014-4894(85)90039-6
- Remaley, A. T., Kuhns, D. B., Basford, R. E., Glew, R. H., and Kaplan, S. S. (1984). Leishmanial Phosphatase Blocks Neutrophil O₂⁻ Production. *J. Biol. Chem.* 259, 11173–11175.
- Rigden, D. J. (2008). The Histidine Phosphatase Superfamily: Structure and Function. *Biochem. J.* 409, 333–348. doi: 10.1042/BJ20071097

- Rodríguez, A., Roy, J., Martínez-Martínez, S., López-Maderuelo, M. D., Niño-Moreno, P., Ortí, L., et al. (2009). A Conserved Docking Surface on Calcineurin Mediates Interaction With Substrates and Immunosuppressants. *Mol. Cell.* 33, 616–626. doi: 10.1016/j.molcel.2009.01.030
- Sacks, D. L., Hieny, S., and Sher, A. (1985). Identification of Cell Surface Carbohydrate and Antigenic Changes Between Noninfective and Infective Developmental Stages of *Leishmania Major* Promastigotes. *J. Immunol.* 135, 564–569.
- Saha, A. K., Das, S., Glew, R. H., and Gottlieb, M. (1985). Resistance of Leishmanial Phosphatases to Inactivation by Oxygen Metabolites. *J. Clin. Microbiol.* 22, 329–332. doi: 10.1128/jcm.22.3.329-332.1985
- Saxena, A., Lahav, T., Holland, N., Aggarwal, G., Anupama, A., Huang, Y., et al. (2007). Analysis of the *Leishmania Donovanii* Transcriptome Reveals an Ordered Progression of Transient and Permanent Changes in Gene Expression During Differentiation. *Mol. Biochem. Parasitol.* 152, 53–65. doi: 10.1016/j.molbiopara.2006.11.011
- Saxena, A., Worthey, E. A., Yan, S., Leland, A., Stuart, K. D., and Myler, P. J. (2003). Evaluation of Differential Gene Expression in *Leishmania Major* Friedlin Procyclics and Metacyclics Using DNA Microarray Analysis. *Mol. Biochem. Parasitol.* 129, 103–114. doi: 10.1016/S0166-6851(03)00100-2
- Shakarian, A. M., Ellis, S. L., Mallinson, D. J., Olafson, R. W., and Dwyer, D. M. (1997). Two Tandemly Arrayed Genes Encode the (Histidine) Secretory Acid Phosphatases of *Leishmania Donovanii*. *Gene* 196, 127–137. doi: 10.1016/S0378-1119(97)00218-7
- Shakarian, A. M., Joshi, M. B., Ghedin, E., and Dwyer, D. M. (2002). Molecular Dissection of the Functional Domains of a Unique, Tartrate-Resistant, Surface Membrane Acid Phosphatase in the Primitive Human Pathogen *Leishmania Donovanii*. *J. Biol. Chem.* 277, 17994–18001. doi: 10.1074/jbc.M200114200
- Shio, M. T., Hassani, K., Isnard, A., Ralph, B., Contreras, I., Gomez, M. A., et al. (2012). Host Cell Signalling and *Leishmania* Mechanisms of Evasion. *J. Trop. Med.* 2012, 1–14. doi: 10.1155/2012/819512
- Singh, B., and Sundar, S. (2012). Leishmaniasis: Vaccine Candidates and Perspectives. *Vaccine* 30, 3834–3842. doi: 10.1016/j.vaccine.2012.03.068
- Singla, N. (1992). Acid Phosphatase Activity of Promastigotes of *Leishmania Donovanii*: A Marker of Virulence. *FEMS Microbiol. Lett.* 94, 221–225. doi: 10.1016/0378-1097(92)90634-Z
- Soulat, D., and Bogdan, C. (2017). Function of Macrophage and Parasite Phosphatases in Leishmaniasis. *Front. Immunol.* 8, 1–21. doi: 10.3389/fimmu.2017.01838
- Szöör, B. (2010). Trypanosomatid Protein Phosphatases. *Mol. Biochem. Parasitol.* 173, 53–63. doi: 10.1016/j.molbiopara.2010.05.017
- Tonks, N. K. (2003). PTP1B: From the Sidelines to the Front Lines! *FEBS Lett.* 546, 140–148. doi: 10.1016/S0014-5793(03)00603-3
- Tsigankov, P., Gherardini, P. F., Helmer-Citterich, M., Späth, G. F., Myler, P. J., and Zilberstein, D. (2014). Regulation Dynamics of *Leishmania* Differentiation: Deconvoluting Signals and Identifying Phosphorylation Trends. *Mol. Cell. Proteomics.* 13, 1787–1799. doi: 10.1074/mcp.M114.037705
- Tsigankov, P., Gherardini, P. F., Helmer-Citterich, M., Späth, G. F., and Zilberstein, D. (2013). Phosphoproteomic Analysis of Differentiating *Leishmania* Parasites Reveals a Unique Stage-Specific Phosphorylation Motif. *J. Proteome Res.* 12, 3405–3412. doi: 10.1021/pr4002492
- Vannier-Santos, M. A., Martiny, A., Meyer-Fernandes, J. R., and de Souza, W. (1995). Leishmanial Protein Kinase C Modulates Host Cell Infection Via Secreted Acid Phosphatase. *Eur. J. Cell Biol.* 67, 112–119.
- Verma, A., Bhandari, V., Deep, D. K., Sundar, S., Dujardin, J. C., Singh, R., et al. (2017). Transcriptome Profiling Identifies Genes/Pathways Associated With Experimental Resistance to Paromomycin in *Leishmania Donovanii*. *Int. J. Parasitol. Drugs Drug Resist.* 7, 370–377. doi: 10.1016/j.ijpddr.2017.10.004
- Wiese, M. (1996). Gene Cloning and Cellular Localization of a Membrane-Bound Acid Phosphatase of *Leishmania Mexicana*. *Mol. Biochem. Parasitol.* 82, 153–165. doi: 10.1016/0166-6851(96)02729-6
- Wiese, M., Ilg, T., Lottspeich, F., and Overath, P. (1995). Ser/Thr-Rich Repetitive Motifs as Targets for Phosphoglycan Modifications in *Leishmania Mexicana* Secreted Acid Phosphatase. *EMBO J.* 14, 1067–1074.
- Zhou, Y., Bhattacharjee, H., and Mukhopadhyay, R. (2006). Bifunctional Role of the Leishmanial Antimonate Reductase Lmacr2 as a Protein Tyrosine Phosphatase. *Mol. Biochem. Parasitol.* 148, 161–168. doi: 10.1016/j.molbiopara.2006.03.009
- Zhou, Y., Messier, N., Ouellette, M., Rosen, B. P., and Mukhopadhyay, R. (2004). *Leishmania Major* Lmacr2 is a Pentavalent Antimony Reductase That Confers Sensitivity to the Drug Pentostam. *J. Biol. Chem.* 279, 37445–37451. doi: 10.1074/jbc.M404383200

Conflict of Interest: The authors declare that the research was conducted in the absence of any commercial or financial relationships that could be construed as a potential conflict of interest.

Copyright © 2021 Freitas-Mesquita, Dos-Santos and Meyer-Fernandes. This is an open-access article distributed under the terms of the Creative Commons Attribution License (CC BY). The use, distribution or reproduction in other forums is permitted, provided the original author(s) and the copyright owner(s) are credited and that the original publication in this journal is cited, in accordance with accepted academic practice. No use, distribution or reproduction is permitted which does not comply with these terms.



Characterization and Follow-Up of *Trypanosoma cruzi* Natural Populations Refractory to Etiological Chemotherapy in Oral Chagas Disease Patients

Arturo Muñoz-Calderón¹, Zoraida Díaz-Bello², Belkisyolé Alarcón de Noya², Oscar O. Noya-González² and Alejandro G. Schijman^{1*}

OPEN ACCESS

Edited by:

Gustavo Benaim,
Fundación Instituto de Estudios
Avanzados (IDEA), Venezuela

Reviewed by:

Sergio Andres Castañeda,
Rosario University, Colombia
Rodrigo Andrés López-Muñoz,
Austral University of Chile, Chile

*Correspondence:

Alejandro G. Schijman
schijman@dna.uba.ar

Specialty section:

This article was submitted to
Parasite and Host,
a section of the journal
Frontiers in Cellular
and Infection Microbiology

Received: 07 February 2021

Accepted: 12 April 2021

Published: 28 April 2021

Citation:

Muñoz-Calderón A,
Díaz-Bello Z, Alarcón de Noya B,
Noya-González OO and Schijman AG
(2021) Characterization and
Follow-Up of *Trypanosoma cruzi*
Natural Populations Refractory
to Etiological Chemotherapy in
Oral Chagas Disease Patients.
Front. Cell. Infect. Microbiol. 11:665063.
doi: 10.3389/fcimb.2021.665063

¹ Laboratorio de Biología Molecular de la Enfermedad de Chagas, Instituto de Investigaciones en Ingeniería Genética y Biología Molecular (INGEBI), Consejo Nacional de Investigaciones Científicas y Técnicas (CONICET), Buenos Aires, Argentina, ² Instituto de Medicina Tropical "Dr Félix Pifano", Universidad Central de Venezuela, Caracas, Venezuela

We aimed to characterize the genetic constitution of natural *T. cruzi* populations involved in an Oral Chagas Disease (OCD) outbreak at a rural school of the community of Chichiriviche de la Costa, Venezuela, which affected patients did not respond to the etiological treatment. Peripheral blood samples and/or hemocultures were obtained from twenty-nine OCD patients at time of diagnosis or along nine years of Post-treatment (Tx) follow-up. The IgG serology, *T. cruzi* discrete typing units (DTU), satellite DNA-qPCR parasitic loads, and minicircle signatures were determined at Pre-Tx and after Tx. The serological titles and parasitic loads changed after treatment, with a significant decrease of IgG titers (Spearman's r value = -0.961) and median parasite loads from 2.869 [IQR = 2.113 to 3.720] to 0.105 [IQR = -1.147 to 1.761] log₁₀ par eq. /mL at Pre-Tx and Post-Tx, respectively, suggesting infection evolution from acute to chronic phase, without seroconversion or parasitological eradication, which was indicative of treatment failure. All patients were infected with *T. cruzi* DTU I populations. At Pre-Tx their median Jaccard genetic distances were 0.775 [IQR = 0.708 to 0.882], decreasing in genetic variability towards the end of follow-up (Mann-Whitney U test p = 0.0031). Interestingly, no Post-Tx minicircle signature was identical to its Pre-Tx counterpart population in a same patient, revealing selection of parasite subpopulations between the primary infection and Post-Tx. The parasitic populations isolated from hemocultures showed a lower number of bands in the minicircle signatures with respect to the signatures obtained directly from the patients' blood samples, demonstrating a process of parasitic selection and reduction of the population variability that initially infected the patients. Decrease of parasitic loads after treatment as well as Pre- and Post-Tx intra-Tcl diversity might be a consequence of both,

natural evolution of the acute infection to the chronic phase and persistence of refractory populations due to Tx selection.

Keywords: *Trypanosoma cruzi*, Oral Chagas disease, trypanocidal chemotherapy, therapeutic failure, genetic diversity, restriction fragment length polymorphism, parasite load, minicircle signature

INTRODUCTION

Chagas disease (CD), caused by *Trypanosoma cruzi* affects mostly populations living in poor housing conditions in Latin America (Pereiro, 2019). Although initially considered transmitted mostly by triatomine bugs, the parasite can be transmitted by other routes, one of the most important in recent decades being oral transmission, as a result of contamination of food with feces of wild triatomines or secretions from reservoirs in endemic regions (Rueda et al., 2014; Alarcón de Noya et al., 2015).

Venezuela is the third country with oral Chagas disease (OCD) reports since 2007, and the first one with the most numerous OCD micro-epidemics (Alarcón de Noya et al., 2015). The first outbreaks were associated with consumption of guava (*Psidium guajava*) juice in an urban school in the Chacao Municipality (Caracas, Capital District) in 2007 (Alarcon de Noya et al., 2010) and the second in a rural school in the community of Chichiriviche de la Costa (Vargas State) (Alarcon de Noya et al., 2016) in 2009, with varied degree of disease severity and mortality (Alarcón de Noya et al., 2015; Alarcon de Noya et al., 2016).

In Chichiriviche de la Costa, a small tourist town nestled between mountains and on the shores of the Caribbean Sea, located on the north-central coast of Venezuela, there were simultaneous cases of fever and myocarditis in students, teachers, and administrative staff of the local school (10°31' 53.97"N - 67°15'36.02"W). These clinical findings led to the serological screening of specific anti-*T. cruzi* IgM and IgG reactivities to 441 people, resulting in 89 infected people and mortality associated with acute *T. cruzi* infection in 5.6% of them (Alarcón de Noya and Martinez, 2009; Alarcon de Noya et al., 2016).

In these patients, the outcome observed by serological, parasitological and PCR-based monitoring two years after treatment with Benznidazole (Bnz) was disappointing. Around 70% of patients still had positive lytic antibodies; some presented anti-*T. cruzi* IgG antibody titers and positive *T. cruzi* PCR findings (Alarcón de Noya et al., 2011). Considering that Bnz is highly effective in the acute phase and during childhood in other endemic regions where other parasite DTUs prevail (Bianchi et al., 2015; Moscatelli et al., 2019), these data suggested therapeutic failure and consequently a second treatment was administered to people with persistence of lytic antibodies and/or positive PCR results, however without outcome improvement (Garcia-Bournissen, 2019; Molina-Morant et al., 2020).

It is crucial to carry out genetic studies on parasitic populations involved in OCD aiming to seek an explanation

for the differences in Bnz efficacy with respect to other epidemiological settings. In assessing drug efficacy, *in vitro* susceptibility tests carried out in parasite isolates obtained at pre-treatment (Pre-Tx) and Post-treatment (Post-Tx) from these outbreaks displayed clones naturally less susceptible to Bnz and Nfx (Muñoz-Calderón et al., 2012; Muñoz-Calderón et al., 2019). Indeed, the genetic polymorphism of *T. cruzi* may be involved in its susceptibility to anti-parasitic drugs. However, genetic studies of natural parasite populations in CD patients exhibiting treatment failure have not been done so far. In this context, peripheral blood samples and hemocultures obtained from OCD patients at Chichiriviche de la Costa outbreak were analyzed at time of diagnosis and after Tx, attempting to detect and characterize fluctuations of *T. cruzi* genetic diversity and parasitic loads along the follow-up.

METHODS

Ethics Statement

The study was approved by the Ethical Review Board of the Instituto de Medicina Tropical “Dr Félix Pifano”-Universidad Central de Venezuela, Caracas, Venezuela (CEC-IMT 019/2010 - December 10, 2010); following the principles expressed in the Declaration of Helsinki.

Written informed consent forms were signed by each participant or from their legal guardians (minor subjects were included). Samples were anonymized before being processed.

Patients and Samples

The study population consisted of students, teachers, school workers and outsiders involved in the preparation or transportation of food consumed in schools, and anyone considered as a potential at-risk “school contact”. The participants eligible for the study were 29 patients who presented positive anti-*T. cruzi* IgG antibody titers or kinetoplastid DNA-PCR amplification after nine years of Post-Tx follow-up, according to data provided by the Instituto de Medicina Tropical “Dr Félix Pifano”- Universidad Central de Venezuela, Caracas, Venezuela.

Table 1 shows epidemiological features of the study patients from the Chichiriviche de la Costa outbreak, hemocultures obtained, number of blood samples analyzed and Post-Tx time period of each sample. Additionally, the distribution of the number of samples for each of the variables studied in this work (Pre-treatment and Post-treatment points), is outlined in **Figure 1**.

TABLE 1 | Description of the Oral Chagas Disease patients' cohort with Pre and Post treatment follow-up samples for 9 years.

| Code | Origin of <i>T. cruzi</i> gDNA | Age (years) | Gender | DTU | Pre-treatment clinical status | Primary Treatment | Secondary Treatment | Number of Post-treatment samples evaluated | Culture isolate period |
|------|--------------------------------|-------------|--------|-----|-------------------------------|-------------------|---------------------|--|------------------------|
| P1 | Blood | 10 | F | Tcl | Severe | Bnz | | 5 | N/A |
| P2 | Blood | 7 | F | Tcl | Severe | Bnz | | 5 | N/A |
| P3 | Blood | 8 | F | Tcl | Moderate | Bnz | | 4 | N/A |
| P4 | Blood | 9 | F | Tcl | Severe | Bnz | | 3 | N/A |
| P5 | Blood | 9 | F | Tcl | Severe | Bnz | Bnz ⁺ | 5 | N/A |
| P6 | Blood | 7 | F | Tcl | Severe | Bnz | | 4 | N/A |
| P7 | Blood/ Hemoculture | 8 | M | Tcl | Moderate | Bnz | Bnz ⁺ | 5 | Pre-Tx |
| P8 | Blood | 10 | F | Tcl | Severe | Bnz | | 4 | N/A |
| P9 | Blood | 9 | F | Tcl | Severe | Bnz | | 4 | N/A |
| P10 | Blood | 10 | M | Tcl | Moderate | Bnz | | 4 | N/A |
| P11 | Blood | 10 | M | Tcl | Severe | Bnz | Bnz ⁺ | 4 | N/A |
| P12 | Blood | 9 | M | Tcl | Severe | Bnz | | 4 | N/A |
| P13 | Blood | 6 | M | Tcl | Severe | Bnz | | 4 | N/A |
| P14 | Blood | 7 | M | Tcl | Severe | Bnz | | 3 | N/A |
| P15 | Blood | 7 | M | Tcl | Severe | Bnz | Bnz ⁺ | 4 | N/A |
| P16 | Blood | 8 | M | Tcl | Severe | Bnz | | 4 | N/A |
| P17 | Blood | 9 | M | Tcl | Severe | Bnz | | 4 | N/A |
| P18 | Blood | 11 | F | Tcl | Severe | Bnz | | 4 | N/A |
| P19 | Blood | 16 | M | Tcl | Severe | Bnz | | 4 | N/A |
| P20 | Blood | 11 | F | Tcl | Severe | Bnz | | 4 | N/A |
| P21 | Blood/ Hemoculture | 36 | M | Tcl | Severe | Bnz | | 4 | Pre-Tx |
| P22 | Blood | 11 | F | Tcl | Severe | Bnz | | 4 | N/A |
| P23 | Blood | 47 | F | Tcl | Severe | Bnz | Bnz ⁺ | 4 | N/A |
| P24 | Blood | 11 | M | Tcl | Severe | Bnz | | 4 | N/A |
| P25 | Blood | 11 | M | Tcl | Severe | Bnz | | 4 | N/A |
| P26 | Hemoculture | 5 | F | Tcl | Severe | Bnz | Bnz ⁺ | N/A | Pre-Tx |
| P27 | Hemoculture | 9 | M | Tcl | Severe | Bnz | Bnz ⁺ | N/A | 1 year Post-Tx |
| P28 | Hemoculture | 10 | M | Tcl | Severe | Bnz | Bnz ⁺ | N/A | 1 year Post-Tx |
| P29 | Hemoculture | 7 | F | Tcl | Severe | Bnz | Bnz ⁺ | N/A | 2 years Post-Tx |

Bnz⁺ - Second treatment with Benznidazole given 1 year post infection.

Bnz⁺⁺ - Second treatment with Benznidazole given 4 years post infection.

N/A, Not Applicable.

Bzn, Benznidazole.

Clinical Classification

Patients with acute OCD were clinically classified with i) moderate symptoms whose clinical situation allowed them to continue with work activities (facial edema; dyspnea; abdominal pain; headache; arthralgia; myalgia; asthenia; drowsiness; headache; intraocular pain; rash; echocardiogram (ECHO): Supraventricular hypertrophy), and ii) severe symptoms who had to be hospitalized or deceased (ECHO: pericardial effusion or myocarditis; electrocardiogram (EKG): supraventricular arrhythmia or supraventricular hypertrophy; adenomegaly; cardiomegaly; tachycardia).

Antiparasitic Treatment

Patients were treated with Bnz (6 mg/kg/day) during 60 continuous days in three daily doses (Alarcón de Noya et al., 2011; Alarcon de Noya et al., 2016). During follow-up, nine treated patients who remained with evidence of parasite persistence (high values in anti-*T. cruzi* IgG titers, presence of lytic antibodies, and/or persistence of positive PCR) received a new course of treatment with Bnz (Amato Neto, 1999).

Laboratory Diagnosis

At each visit, a single peripheral blood sample was withdrawn by venipuncture. Five milliliters were dedicated to serum collection to perform IgG-based serological analyses. The remaining volume was used for molecular biology studies.

Immunoenzymatic Assay

An in-house immunoenzymatic assay (ELISA) was performed using a delipidized antigenic lysate obtained from the epimastigote stage of the *T. cruzi* "PM" strain (Tcl) and processed using Maxisorp plates. ELISA tests involving anti-human IgG alkaline phosphatase conjugates were carried out simultaneously in all sera. ELISA IgG cut-off line was defined as an optical density (OD) value equal to 0.200 to determine a positive sample (Alarcón de Noya et al., 2011).

Preparation of Samples for Molecular Biology Studies

Five mL of patients' peripheral blood was mixed with an equal volume of 6M Guanidine HCl/0.2 mM EDTA, pH 8.00 (GEB)

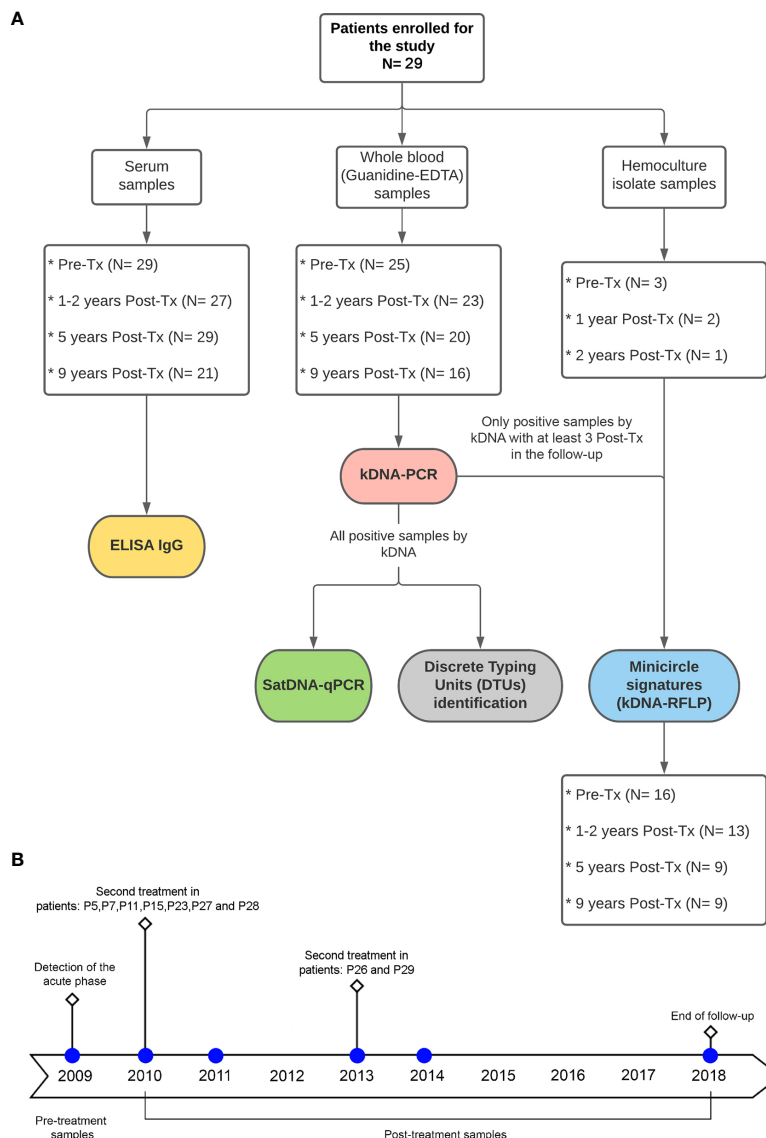


FIGURE 1 | (A) Flowchart for the distribution of study patients' samples and type of analysis performed. Tx: Treatment. **(B)** timeline of blood sample collection at follow-up time.

and boiled according to Diaz-Bello et al. (2008). The GEB mixture was stored at 4°C; DNA was extracted from 300 μ L aliquots using the High Pure PCR Template Preparation kit (Roche Diagnostics, Indianapolis, IN) and eluted in 100 μ L elution buffer (Duffy et al., 2013).

Parasite Cultures

Epimastigote forms obtained from patients' hemocultures and four TcI reference strains (Dm28c, SilvioX10, gal4, and CMA) were cultured in LIT medium (supplemented with 5% bovine fetal serum) and sub-cultured every 15 days during the exponential growth phase.

DNA Extraction and Quantitative Analysis

Parasites were collected at logarithmic phase and centrifuged at $3000 \times g$. The High Pure PCR Template Preparation kit (Roche Diagnostic, Indianapolis, IN) was used for DNA extraction following the manufacturer's recommendations. The genomic DNA was then preserved at 4°C until use. DNA purity and concentration were determined in a Nanodrop ND-1000 (NanoDrop Technologies, Houston, TX, USA) at 260/280 nm wavelengths.

kDNA-PCR Amplification

A 330 bp sequence belonging to the hypervariable region of *T. cruzi* kDNA was amplified as reported (Schijman et al., 2011). Briefly, the master mix was composed by 1X Taq platinum

amplification buffer, 200 μ M dNTPs, 3 mM MgCl₂ solution, 1.5 U Taq Platinum (Invitrogen, Brazil), 10 μ M kDNA specific primers 121 (AAATAATGTACGGGKGAGATGCATGA) and 122 (GGTTCGATTGGGGTTGGTGTAAATATA), 5 μ l of template DNA, and a quantity of water sufficient to give a final volume of 50 μ l. Cycling parameters were one step of 3 min denaturation at 94°C; 2 cycles of 1 min at 97.5°C, 2 min at 64°C; 33 cycles of 1 min at 94°C, 1 min at 62°C and one final extension step of 10 min at 72°C. The kDNA-PCR products were analyzed in 2% agarose gels stained with ethidium bromide.

Estimation of Parasitic Loads

A standardized duplex quantitative real-time PCR (qPCR) targeted to *T. cruzi* Satellite (Sat) DNA and Internal Amplification control (IAC) was used, under the reported conditions (Duffy et al., 2013). Standard curves were plotted with 1/10 serial dilutions of total DNA obtained from the same stock of a GEB seronegative sample spiked with 1×10^5 par.eq./mL of Silvio X10 (TcI) cultured epimastigotes. The reportable linear range of this qPCR was 1 to 6 log₁₀par eq./mL for TcI-infected samples (Duffy et al., 2013).

Identification of *Trypanosoma cruzi* Discrete Typing Units (DTUs)

A Real-Time PCR-based algorithm for identification of *T. cruzi* DTUs was done by means of amplification of spliced-leader genes, 24S α rRNA, 18S α rRNA and COII genomic markers using TaqMan probes, as described (Cura et al., 2015).

Minicircle Signatures

To identify minicircle signatures (Ms) of bloodstream parasite populations, kDNA-PCR samples were studied. The 330 bp purified amplicon was subjected to HindFI, RsaI, and MspI digestions as reported (Burgos et al., 2010). Signatures were visualized and digitized using a Syngene ultraviolet light transilluminator (Synoptics Ltd., Cambridge, UK), at 498 nm. The sizes of the bands of each signature were determined by comparison with molecular weight markers included in each electrophoresis, using the GelAnalyzer v2010a program (<http://www.gelanalyzer.com>). To assess the reproducibility of the Ms, three independent kDNA-PCR experiments from a same DNA preparation were performed, and each product was digested on triplicate.

Genetic Distance Determination

Binary matrices were created from each Ms. Only sharp bands resolved by gel electrophoresis were used in the analysis. Visible amplified bands were scored as “1”, whereas the absence of bands of the same molecular weight was scored as “0”. All samples from a same patient were analyzed in a same gel. The degree of similarity, i.e. frequency of co-occurrence, between clinical samples was measured using the Jaccard's coefficient (JC) between Pre-Tx and Post-Tx samples for each patient.

In order to estimate the overall variability of the Pre-Tx parasite populations using as marker the minicircle signatures, a median value of the Jaccard genetic distances among the pre-Tx samples was determined, and the profiles obtained from each

sample at the different Post-Tx points were compared against that pre-Tx median value.

In addition, the minicircle profiles obtained from the hemocultures were compared among them, in order to obtain an overall JC sight of the cultured parasite strains and compare their JCs with those obtained among laboratory reference clones belonging to Tc I.

Statistical Analysis

A data analysis was performed on the follow-up panel to evaluate the change in parasite loads, IgG antibody values, Jaccard's coefficient, and/or the clinical classification of the patients. The graphic comparisons between the different variables obtained from each patient: IgG serology (optical density), parasite load (Par.eq/mL) and JC, were carried out with a Z score data transformation. The continuous measurements were expressed and plotted as the median and interquartile range of 25–75%, whereas dichotomous variables were expressed and plotted as a percentage.

For all variables, the normal distributions were evaluated using the Shapiro-Wilks test. The Spearman's rank correlation coefficient was calculated to assess correlations among the variables under study (parasitemia levels, ELISA IgG values and patients' clinical classification). Correlation is stronger as the value of *r* approaches 1 for positive correlations or -1 for negative correlations. To evaluate the differences between Pre-Tx and Post-Tx follow-up points, the Mann-Whitney U test was used.

All analyses were performed with the RStudio Team software (2020), and calculations were determined with a *p*-value of <0.05 for significant statistical differences.

RESULTS

Peripheral blood samples and/or hemocultures obtained from 29 OCD patients at Pre-Tx and/or at different Post-Tx visits were included in the study (Table 1). From each patient (except P26 to P29, in which only hemocultures were obtained), one Pre-Tx sample and Post-Tx samples collected at at least two different visits were analyzed by serological and molecular tools.

IgG-based Serological Findings and Parasitic Loads

All study patients were seropositive at Pre-Tx. The Post-Tx accumulated seropositivity was 82.26% (*n* = 21) (Figure 2A). After nine years of Post-Tx, seropositivity was 71.43% (*n*=15), with a median in optical density of 0.320 [IQR = 0.174 to 0.507]. Although there was not seroconversion, a trend towards antibodies titers decrease was observed (Figure 2C).

Out of the 29 study patients, whole blood samples were collected in 25. In patient P7 and P21 whole blood and a Pre-Tx hemoculture isolate were obtained. In patients P26 to P29, hemocultures but not blood were obtained at different follow-up stages, so qPCR quantification of parasitic loads was not performed.

Overall, 92.06% (116 out of 126 samples) agreement between kDNA-PCR and satDNA-qPCR findings was found

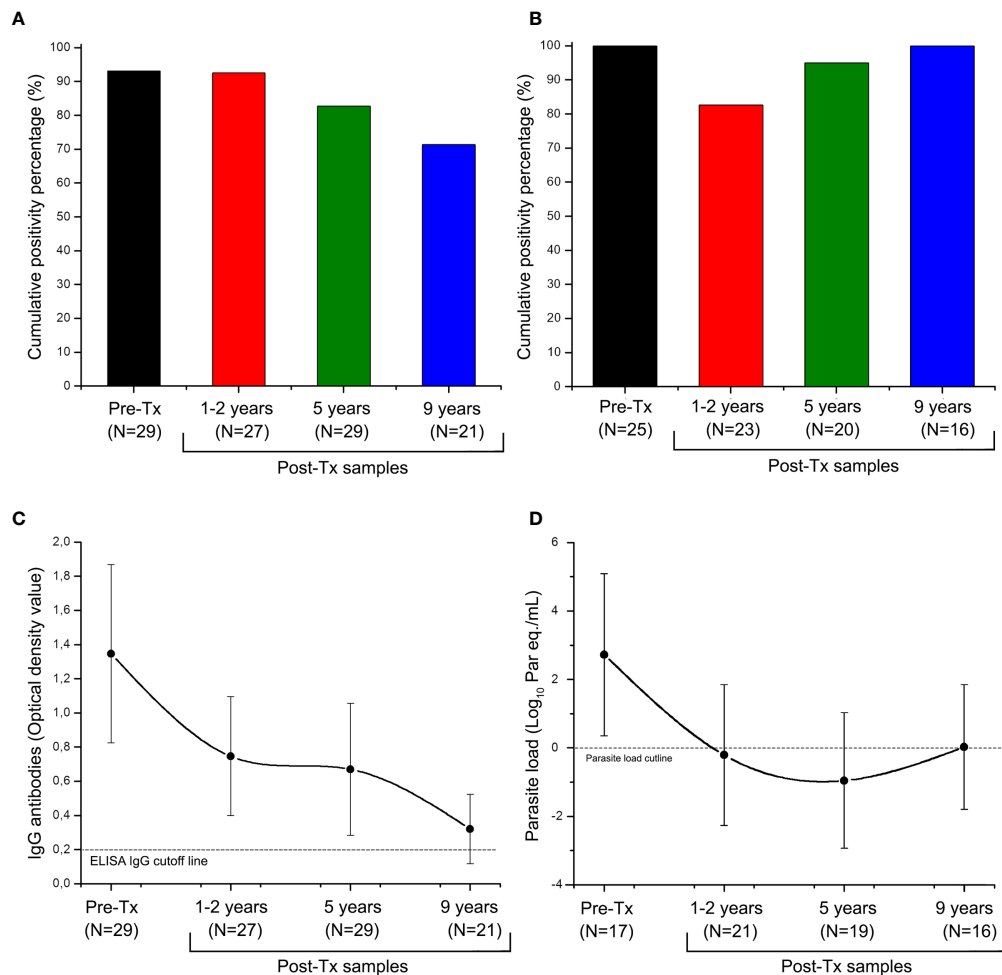


FIGURE 2 | Distribution of anti-*Trypanosoma cruzi* ELISA-IgG reactivity and SatDNA-qPCR positivity during the follow-up of patients of the Chichiriviche de la Costa oral Chagas disease outbreak. **(A)** Cumulative positivity percentage of ELISA-IgG; **(B)** satDNA-qPCR cumulative positivity percentage; **(C)** Trend of optical density values for the ELISA-IgG; **(D)** Trend of parasitic load values for the satDNA-qPCR. Tx: Treatment. ELISA IgG cutoff line: Optical Density (OD) value reportable by a positive sample (Díaz-Bello et al., 2008); TcI load cutoff line: 1 par eq./mL, lowest value of linear reportable range of qPCR (Duffy et al., 2013). The data in Figures **(C)** and **(D)** are presented as median and interquartile range from 25 to 75%.

(Supplementary Data). The percentage of positivity for Pre-Tx samples was 100% ($n=25$), with a median parasite load of 2.869 [IQR = 2.113 to 3.720] \log_{10} par eq./mL (**Figures 2B, D**). In approximately one-third of patients, parasitic load fluctuations above and below the lower reportable range were detected during follow-up. Despite this, a 92.5% ($n=14$) cumulative qPCR positivity was obtained up to nine years Post-Tx (**Figure 2B**). During Post-Tx monitoring, a median of the parasite load of 0.105 [IQR = -1.147 to 1.761] \log_{10} par eq./mL was obtained, which is close to qPCR detection limit (**Figure 2D**). At 9 years Post-Tx, 50% ($n=8$) of the samples remained quantifiable by qPCR, with a median of the parasite load of 0.028 [IQR = -0.502 to 1.783] \log_{10} par eq./mL. Thus, SatDNA-qPCR was more sensitive than serological analysis to detect treatment failure, allowing detection of 28.57% ($n=5$) more cases of patients who did not respond to treatment. In sum, treatment failure of around 85% ($n=16$) was obtained.

Serological reactivity decreased during Post Tx follow-up (Spearman's r value = -0.961, **Figure 3A**), whereas parasitic load showed a slight tendency to decrease at the end of follow-up (Spearman's r value = -0.400), however, this trend was not statistically significant (P value of the Spearman's rank correlation coefficient >0.05). Post-Tx parasitic loads showed a median of 0.105 [IQR = -1.147 to 1.761] \log_{10} par eq./mL along monitoring (**Figure 3B**).

Characterization of DTUs and Minicircle Signatures

Bloodstream DTUs were identified in kDNA-PCR positive samples, resulting all TcI (**Table 1**). The intra-TcI genetic composition was characterized by RFLP-PCR of kDNA amplicons obtained in 41 blood samples from 12 patients at different follow-up time points, and in the hemocultures isolated from 6 patients. The Ms exhibited between five and 14 digestion

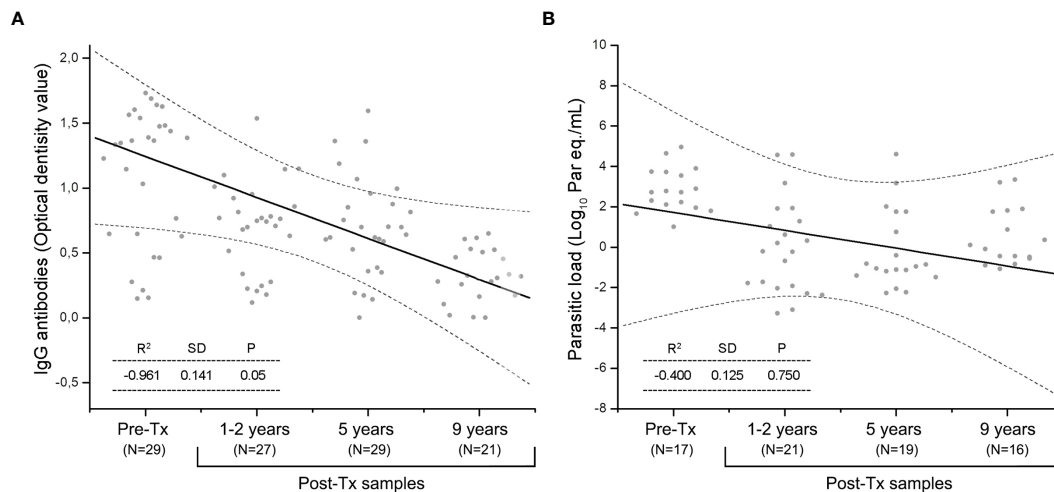


FIGURE 3 | The Spearman's rank correlation coefficient during Post-Tx follow-up in patients of the Chichiriviche de la Costa oral Chagas disease outbreak. **(A)** IgG serology; **(B)** SatDNA-qPCR parasitic loads. Dotted lines indicate the 95% confidence interval. P value <0.05 indicates the significance of the correlation between the variables.

bands from ~30 to 330 bp of length (**Figure 4A**). A high degree of heterogeneity was observed among different patients' populations and between Pre-Tx and Post-Tx Ms signatures in the same patients.

Comparing the JC values, a slight difference in median values, 0.775 [IQR = 0.708 to 0.882] and 0.857 [IQR = 0.798 to 0.941] were observed in Pre-Tx populations analyzed from clinical samples or culture isolates, respectively (**Figures 5A, B**). However, the Mann-Whitney U test did not show differences between both types of samples. Out of the 25 Post-Tx Ms profiles evaluated, none presented 100% homology with the corresponding Pre-Tx Ms (**Supplementary Data**), revealing that parasite populations changed between the time of diagnosis and times of follow-up. When analyzing the overall *T. cruzi* variability between Pre-Tx and Post-Tx follow-up samples, fluctuations in the degree of polymorphism were observed.

The JC distances decreased respect to Pre-Tx values at 1-2 years and five years Post-Tx (Mann-Whitney U test $p < 0.0001$, respectively). At 9 years Post-Tx, a slight increase in the JC values could be observed compared to those obtained in previous Post-Tx points, however, the difference in values was only significant when comparing the JC values against the Pre-Tx samples (Mann-Whitney U test $p = 0.0031$). The median of the JC among the three parasite isolates obtained at Pre-Tx was 0.92 and the JC values among the three isolates tested 1-2 years Post-Tx was 0.84 (Mann-Whitney U test $p > 0.05$). Finally, the JC values among the Pre-Tx hemocultures obtained from this outbreak, suggested greater heterogeneity with respect to the JC values obtained in the four TcI reference strains, without reaching significant difference (Mann-Whitney U test $p > 0.05$).

The number of Ms restriction fragments from the tested patients' parasite populations was counted as an indirect measure of the degree of clonality of those populations along follow-up. Different patterns were observed (**Figure 6**). In four

patients, the number of Ms bands persisted or showed a slight decrease between Pre-Tx and two years Post-Tx and decreased in complexity when tested five years Post-Tx (pattern 1), suggesting clonal selection. The parasitic populations of other four patients showed an increase in kDNA fragments (pattern 2), which suggests proliferation of a higher number of parasite clones. Finally, two patients (P4 and P21) showed no variation in the number and molecular weights of the Ms restriction fragments of their parasitic populations, except for differences in the intensity of some bands (**Figure 4**).

DISCUSSION

This is the first study showing the dynamics of parasitic burden and genetic diversity of natural *T. cruzi* populations infecting OCD patients who did not respond to Bnz treatment after nine years of follow-up.

The fluctuations in ELISA-IgG titers and parasitic loads after etiological treatment showed negative Pearson correlation coefficients with a tendency to negativization. Parasite load values at nine years Post-Tx were very close to the lowest value of the qPCR reportable range (**Figure 2D**). However, no seroconversion nor persistent PCR negativization was observed, suggesting a partial parasitological response to Tx, which was even observed in the nine patients who received two rounds of Bnz.

When analyzing parasite loads, the first stands out was the heterogeneity observed in Post-Tx values. This could be associated with the evolution of the infection from its acute phase at time of diagnosis, to the chronic phase during the follow-up period. Low bloodstream parasitic loads are typical of the chronic stage, when parasite persists in tissues according to their clonal histotropism (Macedo and Segatto, 2010). The immune system plays a fundamental role in the control of circulating parasite levels

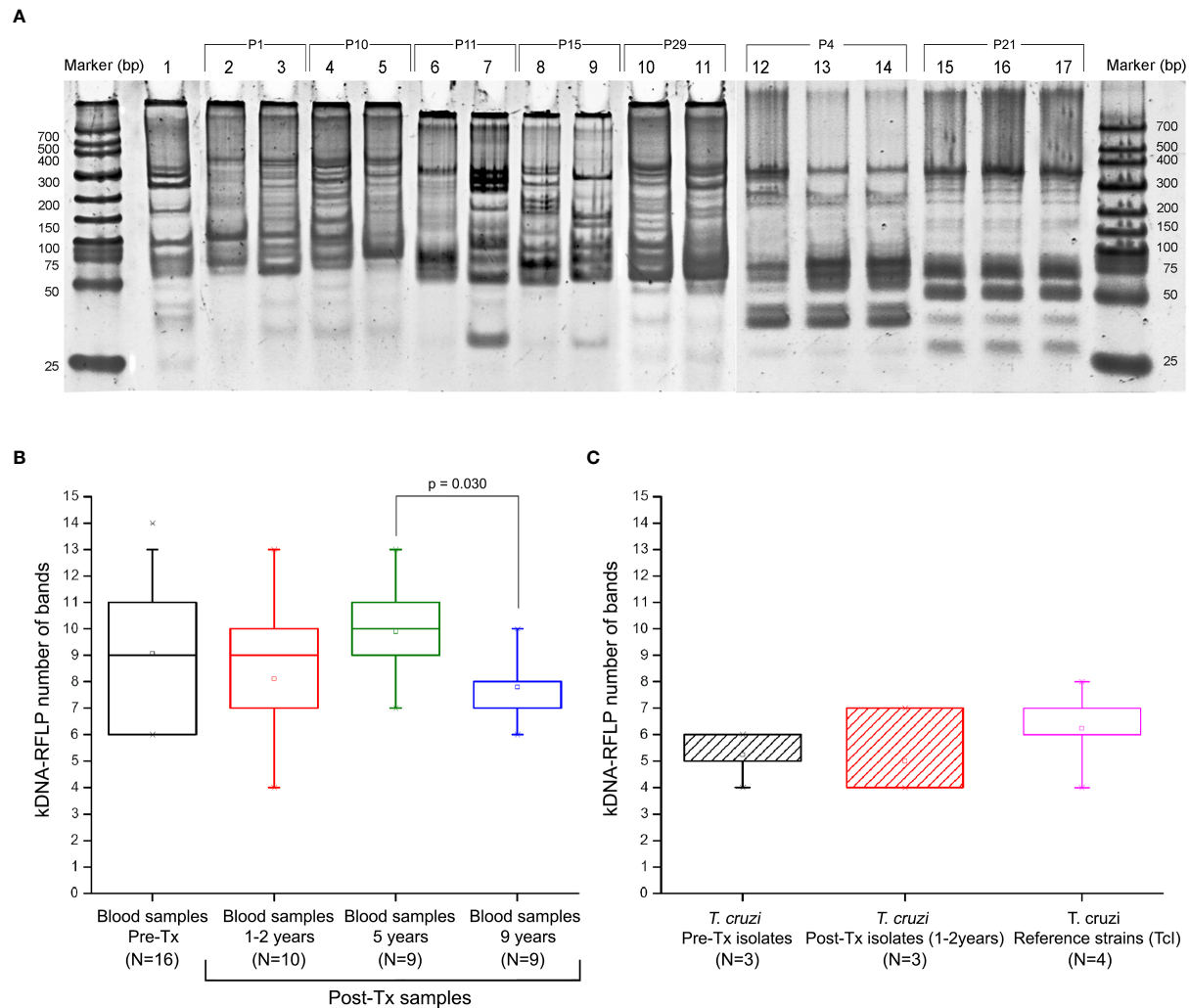


FIGURE 4 | Profile of minicircle signatures in parasite populations by kDNA-PCR restriction fragment polymorphism (RFLP). **(A)** Example of comparative band analysis of minicircle profiles obtained by RFLP-PCR between patients' parasite populations; **(B)** Boxplot distribution of number bands obtained by RFLP-PCR throughout the follow-up in the blood samples. **(C)** Distribution of the boxplot of number of digestion fragments obtained by RFLP-PCR in *Trypanosoma cruzi* isolates obtained from hemocultures and TcI reference strains. 1: Reference strain (DTU I - Dm28c); 2-3: Sample P1 (Pre-Tx and 5 years Post-Tx); 4-5: Sample P10 (Pre-Tx and 5 years Post-Tx); 6-7: Sample P11 (Pre-Tx and 5 years Post-Tx); 8-9: Sample P15 (Pre-Tx and 5 years Post-Tx); 10-11: Sample P29 (Pre-Tx culture isolate and 1 year Post-Tx culture isolate); 12-14: Sample P4 (Pre-Tx, 5 years and 9 years Post-Tx); 15-17: Sample P21 (Pre-Tx, 5 years and 9 years Post-Tx). The JC results shown in the box "reference strains" were obtained from the comparison of the Ms from the Dm28c, SilvioX10, gal4, and CMA strains. P value indicates significant differences between populations (Mann-Whitney U test; $p < 0.05$). Data in the boxplot are presented as median and interquartile range of 25 to 75%.

once intracellular amastigotes replicate and differentiate into trypomastigotes that are released to the bloodstream (Macedo and Segatto, 2010), and this can be reflected in the bloodstream qPCR quantifications. Thus, the observed changes may be more related to the passage from one infection phase to the other one than to a selective pressure exerted by chemotherapy, or to a mixture of both factors.

Following the hypothesis proposed by Alarcón de Noya and co-authors, that "all individuals were infected by a common source for each outbreak, based in eco-epidemiological and molecular genetics studies" (Alarcon de Noya et al., 2010; Munoz-Calderon et al., 2013; Diaz-Bello et al., 2014; Alarcon de Noya et al., 2016),

and identification of TcI DTU in all patients, similarly to what has been detected in other surveys in Venezuela (Carrasco et al., 2012), parasite genetic heterogeneity in patients from Chichiriviche de la Costa was revealed at the intra DTU level and between Pre-Tx and Post-Tx in a same patient. This is indicative of polyclonal populations as sources of oral infection in this outbreak. In fact, in food contaminated with triatomines feces, all metacyclic trypomastigotes present in the intestinal content of the triatomines are involved. It is estimated that a single fecal sample may contain between 3000 to 4000 trypomastigotes per microliter, thus a high clonal complexity may exist (Schaub, 1989).

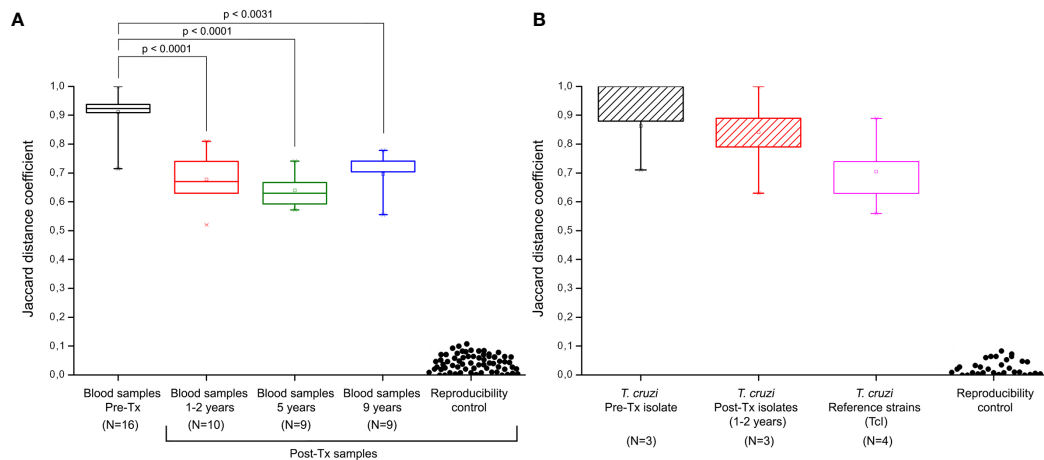


FIGURE 5 | Jaccard distances of minicircle signatures in parasite populations by kDNA-PCR restriction fragment length polymorphism (RFLP). **(A)** Jaccard distances from bloodstream parasites populations in patients of the Chichiriviche de la Costa outbreak. **(B)** Jaccard distances of the hemocultures from the Chichiriviche de la Costa outbreak and TcI reference strains. Reproducibility controls were obtained by comparison of signatures between duplicate samples. Tx: treatment. The JC results shown in the box “reference strains” were obtained from the comparison of the Ms from the Dm28c, SilvioX10, gal4, and CMA strains. P values indicate significant differences between populations (Mann-Whitney U test; $p < 0.05$). Data in the boxplot are presented as median and interquartile range of 25 to 75%.

Wild populations of *T. cruzi* may contain both susceptible and resistant clones to chemotherapeutic drugs, therefore destruction of susceptible forms by drugs leads to the selection and proliferation of resistant subpopulations (Noya et al., 2015). In a subgroup of patients whose parasite populations decreased or persisted in clonal complexity after Tx, suggested by the quantity of minicircle restriction fragments of different lengths, it is tempting to speculate that some drug-driven selection pressure could have played a role in subpopulations selection. (Ms patterns 1 and 3; **Figure 6**). Interestingly, parasite culture isolate from patient P21 harbored a truncated Nitroreductase protein sequence, with a putative role in drug resistance (Unpublished data).

In vitro susceptibility studies carried out with *T. cruzi* strains isolated from the patients of the Chacao outbreak showed high heterogeneity in IC_{50} values against Nfx, suggesting that the therapeutic failure could be due in part to a phenotypic variability extant in the original parasite source of oral transmission (Muñoz-Calderón et al., 2019). These findings, together with the high heterogeneity found between Pre-Tx and Post-Tx follow-up bloodstream *T. cruzi* populations of this outbreak are compatible to the existence of drug-driven selective pressure.

On the other side, clonal selection may occur in the natural development of *T. cruzi* infection from its acute to its chronic phase. Indeed, clones capable to escape from the host's immune system are the ones to proliferate in the chronic phase. The median of the parasitic loads of 0.105 [IQR = -1.147 to 1.761] \log_{10} par eq./mL observed during follow-up are typical of chronic infection. In four patients (P10, P11, P17, and P25) an increase in Ms polymorphism at some point in the Post-Tx follow-up was observed. In general, it is assumed that a higher number of minicircle bands is indicative of a higher level of clonality (Burgos et al., 2010). In all cases, as the JC value with

respect to the Pre-Tx Ms is high, it can be hypothesized that the subpopulations proliferating after treatment were hidden into the tissues during treatment. In these particular cases, it could be attributed to possible reinfections, since the area is a region with a risk of active vector transmission (Noya et al., 2015).

A point to be highlighted is that the characterized parasitic populations correspond to bloodstream parasites. However, it is not possible to analyze the genetic diversity of parasites housed in tissues. Sánchez-Valdéz et al. (2018) showed for the first time that *T. cruzi* enters a dormant state, i.e. some amastigotes can interrupt their cellular replication during an *in vitro* infection (Thomas et al., 2018; Alonso-Padilla et al., 2020). This characteristic in bacteria and other protozoa has been related to the recurrence of infection or drug resistance (Sánchez-Valdéz et al., 2018). Therefore, the appearance of different parasite populations in the Post-Tx samples of OCD patients respect to their Pre-Tx populations could also be associated with this feature. Accordingly, we could have been identifying the genetic diversity of intracellular parasite populations that survived in an environment where the drug concentration was lower and they were not necessarily resistant clones. This could be the case for those patients who showed an increase in parasite variability after Tx. On the other hand, dormancy would not be so relevant in TcI strains, at least compared to other DTUs, as reported by Resende et al. (2020).

The limited sample size of the patients for each of the time points evaluated (Pre-Tx, 1-2 years, 5 years and 9 years Post-Tx) has been a study limitation, mainly influenced by the difficulty of extracting parasitic gDNA from blood samples in patients at the chronic phase of Chagas disease. Additionally, the lack of a placebo group limits the analysis of the genetic variability of parasitic populations when evolving from the acute phase to the chronic phase of the disease. The inclusion of a placebo group

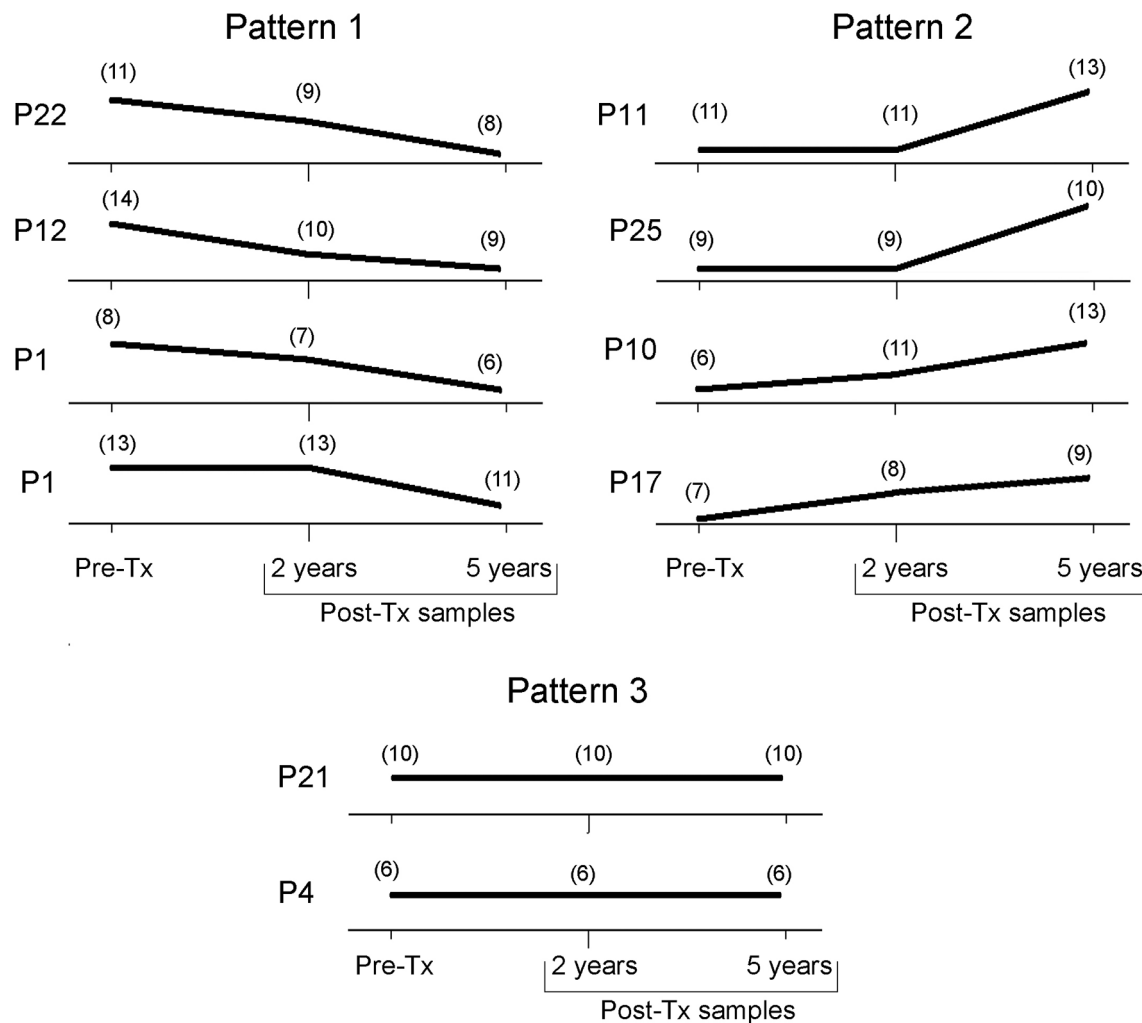


FIGURE 6 | Trend of the genetic variability of natural *T. cruzi* populations by kDNA-RFLP. Each panel represents the count of the number of bands present at each time point along follow-up. Tx, treatment.

would have also allowed us to evaluate in greater detail the response of these parasitic populations after the etiological treatment. These limitations must be taken in account when designing future studies. In conclusion, our serological and molecular parasitological findings suggest that synergistic multiple factors, such as the existence of clones with natural drug resistance, selective pressure exerted by trypanocidal treatment, existence of dormant subpopulations, and evolution of acute oral infection to its chronic phase may account for the persistence of seroreactivity and parasite diversity in this patient cohort after almost a decade of follow-up.

DATA AVAILABILITY STATEMENT

The original contributions presented in the study are included in the article/**Supplementary Material**. Further inquiries can be directed to the corresponding author.

ETHICS STATEMENT

The studies involving human participants were reviewed and approved by Ethical Review Board of the Instituto de Medicina Tropical “Dr Félix Pifano”-Universidad Central de Venezuela, Caracas, Venezuela (CEC-IMT 019/2010 - December 10, 2010). Written informed consent to participate in this study was provided by the participants’ legal guardian/next of kin.

AUTHOR CONTRIBUTIONS

AM-C and AS were responsible for study design, data analysis, and writing up of the manuscript. ZD-B, BA, and ON-G were responsible for recruitment and clinical care of the patients. AM-C and ZD-B were responsible for the laboratory analysis. AS and BA supervised the molecular and serological related experiments.

All authors contributed to the article and approved the submitted version.

FUNDING

This work was supported by a Fellowship given by the Programme for biotechnology in Latin America and the Caribbean of the United Nations University (UNU-BIOLAC) [to AM-C], funds from the ANPCyT through PICT 2014-0274 [to AS] and financial support from the Immunology Section - Instituto de Medicina Tropical – Universidad Central de Venezuela.

REFERENCES

- Alarcon de Noya, B., Colmenares, C., Diaz-Bello, Z., Ruiz-Guevara, R., Medina, K., Munoz-Calderon, A., et al. (2016). Orally-Transmitted Chagas Disease: Epidemiological, Clinical, Serological and Molecular Outcomes of a School Microepidemic in Chichiriviche De La Costa, Venezuela. *Parasite Epidemiol. Control* 1 (2), 188–198. doi: 10.1016/j.parepi.2016.02.005
- Alarcón de Noya, B., Diaz-Bello, Z., Colmenares, C., Muñoz-Calderón, A., Ruiz-Guevara, R., Balzano, L., et al. (2011). Eficacia Terapéutica En El Primer Brote De Transmisión Oral De La Enfermedad De Chagas En Venezuela. *Biomédica* 31 (sup 3), 3–315. doi: 10.7705/biomedica.v31i0.525
- Alarcón de Noya, B., Diaz-Bello, Z., Colmenares, C., Ruiz-Guevara, R., Mauriello, L., Muñoz-Calderón, A., et al. (2015). Update on Oral Chagas Disease Outbreaks in Venezuela: Epidemiological, Clinical and Diagnostic Approaches. *Memórias do Instituto Oswaldo Cruz* 110 (3), 377–386. doi: 10.1590/0074-02760140285
- Alarcon de Noya, B., Diaz-Bello, Z., Colmenares, C., Ruiz-Guevara, R., Mauriello, L., Zavala-Jaspe, R., et al. (2010). Large Urban Outbreak of Orally Acquired Acute Chagas Disease At a School in Caracas, Venezuela. *J. Infect. Dis.* 201 (9), 1308–1315. doi: 10.1086/651608
- Alarcón de Noya, B., and Martínez, J. (2009). Transmisión Oral De La Enfermedad De Chagas En Venezuela: Un Segundo Brote Escolar. *Salus* 13 (2), 9.
- Alonso-Padilla, J., Abril, M., Alarcón de Noya, B., Almeida, I. C., Angheben, A., Araujo Jorge, T., et al. (2020). Target Product Profile for a Test for the Early Assessment of Treatment Efficacy in Chagas Disease Patients: An Expert Consensus. *PLoS Neglected Trop. Dis.* 14 (4), e0008035. doi: 10.1371/journal.pntd.0008035
- Amato Neto, V. (1999). Etiological Treatment for Infection by *Trypanosoma Cruzi*. *Memórias do Instituto Oswaldo Cruz* 94, 337–339. doi: 10.1590/S0074-02761999000700065
- Bianchi, F., Cucunubá, Z., Guhl, F., González, N. L., Freilij, H., Nicholls, R. S., et al. (2015). Follow-Up of an Asymptomatic Chagas Disease Population of Children After Treatment With Nifurtimox (Lampit) in a Sylvatic Endemic Transmission Area of Colombia. *PLoS neglected Trop. Dis.* 9 (2), e0003465. doi: 10.1371/journal.pntd.0003465
- Burgos, J. M., Diez, M., Vigliano, C., Bisio, M., Risso, M., Duffy, T., et al. (2010). Molecular Identification of *Trypanosoma Cruzi* Discrete Typing Units in End-Stage Chronic Chagas Heart Disease and Reactivation After Heart Transplantation. *Clin. Infect. Dis.* 51 (5), 485–495. doi: 10.1086/655680
- Carrasco, H. J., Segovia, M., Llewellyn, M. S., Morocoima, A., Urdaneta-Morales, S., Martínez, C., et al. (2012). Geographical Distribution of *Trypanosoma Cruzi* Genotypes in Venezuela. *PLoS neglected Trop. Dis.* 6 (6), e1707. doi: 10.1371/journal.pntd.0001707
- Cura, C. I., Duffy, T., Lucero, R. H., Bisio, M., Peneau, J., Jimenez-Coello, M., et al. (2015). Multiplex Real-Time Pcr Assay Using Taqman Probes for the Identification of *Trypanosoma Cruzi* Dts in Biological and Clinical Samples. *PLoS Negl. Trop. Dis.* 9 (5), e0003765. doi: 10.1371/journal.pntd.0003765
- Diaz-Bello, Z., Thomas, M. d. C., Egui, A., Pérez-Antón, E., López López, M. C., et al. (2014). *Trypanosoma Cruzi* Genotyping Supports a Common Source of Infection in a School-Related Oral Outbreak of Acute Chagas Disease in Venezuela. *Epidemiol. Infect.* 142 (1), 156–162. doi: 10.1017/S0950268813000757
- Diaz-Bello, Z., Zavala-Jaspe, R., Diaz-Villalobos, M., Mauriello, L., Maekelt, A., and de Noya, B. A. (2008). A Confirmatory Diagnosis of Antibodies Anti-*Trypanosoma Cruzi* in Donors Referred by Blood Banks in Venezuela. *Investigacion clinica* 49 (2), 141–150.
- Duffy, T., Cura, C. I., Ramirez, J. C., Abate, T., Cayo, N. M., Parrado, R., et al. (2013). Analytical Performance of a Multiplex Real-Time PCR Assay Using Taqman Probes for Quantification of *Trypanosoma Cruzi* Satellite DNA in Blood Samples. *PLoS Negl. Trop. Dis.* 7 (1), e2000. doi: 10.1371/journal.pntd.0002000
- Garcia-Bournissen, F. (2019). “Clinical Pharmacology of Drugs for the Treatment of Chagas Disease,” in *Chagas Disease*, vol. 299–312. (Cham, New York: Springer).
- Macedo, A. M., and Segatto, M. (2010). “Implications of *Trypanosoma Cruzi* Intraspecific Diversity in the Pathogenesis of Chagas Disease,” in *American Trypanosomiasis* (Amsterdam: Elsevier), 489–522.
- Molina-Morant, D., Fernández, M., Bosch-Nicolau, P., Sulleiro, E., Bangher, M., Salvador, F., et al. (2020). Efficacy and Safety Assessment of Different Dosage of Benznidazol for the Treatment of Chagas Disease in Chronic Phase in Adults (Multibenz Study): Study Protocol for a Multicenter Randomized Phase II Non-Inferiority Clinical Trial. *Trials* 21, 1–10. doi: 10.1186/s13063-020-4226-2
- Moscattelli, G., Moroni, S., García Bournissen, F., González, N., Ballering, G., Schijman, A., et al. (2019). Longitudinal Follow Up of Serological Response in Children Treated for Chagas Disease. *PLoS neglected Trop. Dis.* 13 (8), e0007668. doi: 10.1371/journal.pntd.0007668
- Muñoz-Calderón, A., Diaz-Bello, Z., Ramírez, J. L., Noya, O., and Alarcón de Noya, B. (2019). Nifurtimox Response of *Trypanosoma Cruzi* Isolates From an Outbreak of Chagas Disease in Caracas, Venezuela. *J. Vector Borne Dis.* 56 (3), 237–243. doi: 10.4103/0972-9062.289397
- Munoz-Calderon, A., Diaz-Bello, Z., Valladares, B., Noya, O., Lopez, M. C., Alarcon de Noya, B., et al. (2013). Oral Transmission of Chagas Disease: Typing of *Trypanosoma Cruzi* From Five Outbreaks Occurred in Venezuela Shows Multiclonal and Common Infections in Patients, Vectors and Reservoirs. *Infect. Genet. Evol.* 17, 113–122. doi: 10.1016/j.meegid.2013.03.036
- Muñoz-Calderón, A., Santaniello, A., Pereira, A., Yannuzzi, J., Diaz-Bello, Z., and Alarcón de Noya, B. (2012). Susceptibilidad *in Vitro* a Nifurtimox Y Benznidazol De Aislados De *Trypanosoma Cruzi* Obtenidos De Pacientes Venezolanos Con Enfermedad De Chagas Infectados Por Mecanismos De Transmisión Oral Y Vectorial. *Rev. Ibero-Latinoam Parasitol* 71 (1), 14–22.
- Noya, O., Ruiz-Guevara, R., Diaz-Bello, Z., and Alarcón de Noya, B. (2015). “Epidemiología Y Clínica De La Transmisión Oral De *Trypanosoma Cruzi*,” in *Rev Esp Epidemiol: XI Workshop on Chagas Disease* (Barcelona Spain: Rev Esp Epidemiol), 23–34.
- Pereiro, A. C. (2019). Guidelines for the Diagnosis and Treatment of Chagas Disease. *Lancet* 393 (10180), 1486–1487. doi: 10.1016/S0140-6736(19)30288-0
- Resende, B. C., Oliveira, A. C. S., Guañabens, A. C. P., Repolés, B. M., Santana, V., Hiraiwa, P. M., et al. (2020). The Influence of Recombinational Processes to Induce Dormancy in *Trypanosoma Cruzi*. *Front. Cell. Infection Microbiol.* 10, 5. doi: 10.3389/fcimb.2020.00005
- Rueda, K., Trujillo, J. E., Carranza, J. C., and Vallejo, G. A. (2014). Transmisión Oral De *Trypanosoma Cruzi*: Una Nueva Situación Epidemiológica De La Enfermedad De Chagas En Colombia Y Otros Países Suramericanos. *Biomédica* 34 (4), 631–641. doi: 10.7705/biomedica.v34i4.2204

ACKNOWLEDGMENTS

This is a collaborative article of the Network NHEPACHA.

SUPPLEMENTARY MATERIAL

The Supplementary Material for this article can be found online at: <https://www.frontiersin.org/articles/10.3389/fcimb.2021.665063/full#supplementary-material>

- Sánchez-Valdéz, F. J., Padilla, A., Wang, W., Orr, D., and Tarleton, R. L. (2018). Spontaneous Dormancy Protects *Trypanosoma Cruzi* During Extended Drug Exposure. *Elife* 7, e34039. doi: 10.7554/eLife.34039
- Schaub, G. (1989). *Trypanosoma Cruzi*: Quantitative Studies of Development of Two Strains in Small Intestine and Rectum of the Vector *Triatoma Infestans*. *Exp. parasitology* 68 (3), 260–273. doi: 10.1016/0014-4894(89)90108-2
- Schijman, A. G., Bisio, M., Orellana, L., Sued, M., Duffy, T., Jaramillo, A. M. M., et al. (2011). International Study to Evaluate Pcr Methods for Detection of *Trypanosoma Cruzi* DNA in Blood Samples From Chagas Disease Patients. *PLoS Negl. Trop. Dis.* 5 (1), e931. doi: 10.1371/journal.pntd.0000931
- Team, R. (2020). *Rstudio: Integrated Development for R* Vol. 42 (Boston, MA, USA: RStudio, Inc).
- Thomas, M. d. C., Egui, A., Pérez-Antón, E., and López López, M. C. (2010). “Biomarcadores para la valoración del impacto terapéutico en pacientes crónicos de Chagas: ensayo clínico multi-Centro NHEPACHA.” in *Publicación XIV Taller sobre la Enfermedad de Chagas* (ISGlobal), 14–17.
- Conflict of Interest:** The authors declare that the research was conducted in the absence of any commercial or financial relationships that could be construed as a potential conflict of interest.

Copyright © 2021 Muñoz-Calderón, Díaz-Bello, Alarcón de Noya, Noya-González and Schijman. This is an open-access article distributed under the terms of the Creative Commons Attribution License (CC BY). The use, distribution or reproduction in other forums is permitted, provided the original author(s) and the copyright owner(s) are credited and that the original publication in this journal is cited, in accordance with accepted academic practice. No use, distribution or reproduction is permitted which does not comply with these terms.



Guide RNA Repertoires in the Main Lineages of *Trypanosoma cruzi*: High Diversity and Variable Redundancy Among Strains

OPEN ACCESS

Edited by:

Juan David Ramírez,
Rosario University, Colombia

Reviewed by:

Philipp Schwabl,
Harvard University, United States
Carlos Robello,
Universidad de la República, Uruguay
Rodrigo Baptista,
University of Georgia, United States

*Correspondence:

Nicolás Tomasini
nicolas.tomasini@conicet.gov.ar
Patricio Diosque
patricio.diosque@unsa.edu.ar

[†]These authors have contributed
equally to this work and
share senior authorship

Specialty section:

This article was submitted to
Parasite and Host,
a section of the journal
Frontiers in Cellular and
Infection Microbiology

Received: 02 February 2021

Accepted: 12 May 2021

Published: 31 May 2021

Citation:

Rusman F, Floridia-Yapur N,
Tomasini N and Diosque P (2021)
Guide RNA Repertoires in the Main
Lineages of *Trypanosoma cruzi*:
High Diversity and Variable
Redundancy Among Strains.
Front. Cell. Infect. Microbiol. 11:663416.
doi: 10.3389/fcimb.2021.663416

Fanny Rusman, Noelia Floridia-Yapur, Nicolás Tomasini^{*†} and Patricio Diosque^{*†}

Unidad de Epidemiología Molecular (UEM), Instituto de Patología Experimental, Universidad Nacional de Salta-CONICET,
Salta, Argentina

Trypanosoma cruzi, as other kinetoplastids, has a complex mechanism of editing of mitochondrial mRNAs that requires guide RNAs (gRNAs) coded in DNA minicircles in the kinetoplast. There are many variations on this mechanism among species. mRNA editing and gRNA repertoires are almost unknown in *T. cruzi*. Here, gRNAs were inferred based on deep-sequenced minicircle hypervariable regions (mHVRs) and editing cascades were rebuilt in strains belonging to the six main *T. cruzi* lineages. Inferred gRNAs were clustered according to their sequence similarity to constitute gRNA classes. Extreme diversity of gRNA classes was observed, which implied highly divergent gRNA repertoires among different lineages, even within some lineages. In addition, a variable gRNA class redundancy (i.e., different gRNA classes editing the same mRNA region) was detected among strains. Some strains had upon four times more gRNA classes than others. Such variations in redundancy affected gRNA classes of all mRNAs in a concerted way, i.e., there are correlated variations in the number of gRNAs classes editing each mRNA. Interestingly, cascades were incomplete for components of the respiratory complex I in several strains. Finally, gRNA classes of different strains may potentially edit mitochondrial mRNAs from other lineages in the same way as they edit their own mitochondrial mRNAs, which is a prerequisite for biparental inheritance of minicircle in hybrids. We propose that genetic exchange and biparental inheritance of minicircles combined with minicircle drift due to (partial) random segregation of minicircles during kDNA replication is a suitable hypothesis to explain the divergences among strains and the high levels of gRNA redundancy in some strains. In addition, our results support that the complex I may not be required in some stages in the life cycle as previously shown and that linkage (in the same minicircle) of gRNAs that edit different mRNAs may prevent gRNA class lost in such stage.

Keywords: Chagas disease, kinetoplastids, minicircles, RNA editing, DTU

INTRODUCTION

Kinetoplastids are a phylogenetic group of flagellate protozoa that include the genus *Leishmania* and *Trypanosoma*, with three species causing neglected diseases: Leishmaniasis, Chagas disease and sleeping sickness. Interestingly, kinetoplastids have a single large mitochondrion with a disk shape structure called kinetoplast. This structure has a complex network of concatenated DNA rings (Cavalcanti and de Souza, 2018). Two different kinds of DNA rings are contained in such network: maxicircles and minicircles. Maxicircles are large molecules (20–30 kb) that appear in a few dozens of almost identical copies. They code for two mitochondrial ribosomal subunits and eighteen mitochondrial proteins (most of them participating in the respiratory chain) (Simpson et al., 1987; Ruvalcaba-Trejo and Sturm, 2011; Lin et al., 2015). Several of such genes require post-transcriptional modifications in their pre-mRNA to generate functional open reading frames. The process is known as mRNA editing and it is made by inserting or deleting uridines (U) (Benne et al., 1986; Koslowsky et al., 1991; Stuart, 1993; Kim et al., 1994; Simpson et al., 1996; Hajduk et al., 1997; Hajduk and Ochsenreiter, 2010; Ammerman et al., 2012; Aphasizheva et al., 2016). Some mRNAs require extensive editing, a phenomenon known as pan-editing [e.g. more than six hundred edited bases to generate the cytochrome c oxidase subunit III (COIII) open reading frame in *T. brucei* (Feagin et al., 1988)]. Instead, other mRNAs are just partially or non-edited.

Uridine insertion/deletion is directed by short RNAs called guide RNAs (gRNAs) and it works as a cascade of steps. Basically, the first gRNA binds the pre-mRNA at a specific and complementary site (non-canonic G:U base pairing is allowed) in the 3' extreme of the mRNA. Then, it determines the editing of the adjacent sites at the 5' based on mismatches (Estevez and Simpson, 1999). This modified region is recognized by another gRNA which drives the editing of the next adjacent region, and successively up to generate the initial codon in the 5' end. If gRNAs that edit a region are lost, the editing is stopped, and no translation is made (Estevez and Simpson, 1999; Lukes et al., 2005). Most editing cascades have been identified for *T. brucei* (Ochsenreiter et al., 2007; Koslowsky et al., 2014; Kirby et al., 2016), *T. vivax* (Greif et al., 2015) and *L. tarentolae* (Simpson et al., 2015). Different evolutionary hypotheses have been proposed to explain the origin and persistence of this expensive editing system, although no consensus has been achieved yet (Gray et al., 2010; Speijer, 2010; Flegontov et al., 2011).

Guide RNAs are coded in the minicircles. In *T. cruzi* there are about 20–30 thousand minicircles per parasite, 1.4 kb each one. Each minicircle contains four hypervariable regions (mHVRs) interspersed by four conserved regions located 90° apart each other. Every mHVR potentially encodes one gRNA (Degraeve et al., 1988; Velazquez et al., 2008).

Most of our knowledge on mitochondrial mRNA editing in trypanosomatids comes from studies in *T. brucei* and *L. tarentolae*, while little is known about editing in *T. cruzi* (Thomas et al., 2007). This parasite is a very diverse species and seven different lineages (also called Discrete Typing Units or

simply DTUs) have been described: the six main lineages TcI–TcVI (Zingales et al., 2009) plus TcBat (Marcili et al., 2009; Pinto et al., 2012; Lima et al., 2015). Strains belonging to the six main lineages of *T. cruzi* can be classified in three different mitochondrial clades according to their maxicircle sequences (Machado and Ayala, 2001; de Freitas et al., 2006; Westenberger et al., 2006; Ruvalcaba-Trejo and Sturm, 2011).

Recently, we deep-sequenced the mHVRs from 9 strains of this parasite at millions of paired-end reads (Rusman et al., 2019). The number of mHVR sequence clusters (according to pairwise identity) was quite different among most strains and the different DTUs shared few mHVR clusters. These results suggest that different DTUs, and even strains, may have different gRNA repertoires. In addition, such differences in the number of mHVR clusters may imply redundant gRNAs (gRNAs with relatively different sequences that edit the same region) or mHVRs not encoding gRNAs. We proposed that minicircle inheritance is biparental in hybrid DTUs (Rusman et al., 2019) and hybrid strains (Rusman et al., 2020) despite the uniparental inheritance of maxicircles (Tomasini, 2018). This scenario opens the question on how mixing minicircles from different parents could still lead to correct editing of mitochondrial mRNAs, since maxicircles are inherited from one parental. The mHVR sequences have previously been used to identify gRNAs and to build editing cascades by comparing them with edited mRNAs (Thomas et al., 2007; Simpson et al., 2015). Here, based on mHVR reads previously obtained, an algorithm was developed to identify and cluster gRNA sequences from big datasets. The aims of this study were to describe and compare editing cascades for representative strains of the *T. cruzi* diversity, to address differences in mRNA editing and to infer how gRNA repertoires evolve.

MATERIAL AND METHODS

mHVR Sequences

The strains analyzed in this study are listed in **Table 1**. The paired-end mHVR amplicon sequences were obtained by Rusman et al. (2019). Reads are available at the Sequence Read Archive (SRA) under the BioProject ID: PRJNA514922. Raw sequence reads for all samples were pre-processed. First, reads were quality filtered using the pair-end mode of Trimmomatic v0.36 (Bolger et al., 2014). Posteriorly, the preserved paired reads were merged into consensus sequences with their associated quality score and chimeras were removed using LeeHom software with default parameters (Renaud et al., 2014).

Mitochondrial mRNA Estimation

Predicted edited mRNA sequences for strains Sylvio (mitochondrial clade A, TcI), CL Brener (mitochondrial clade B, TcVI) and Esmeraldo (mitochondrial clade C, TcII) (Ruvalcaba-Trejo and Sturm, 2011) were generated by manually inserting or deleting uridines (U's) into the unedited sequences of their genes as proposed by (Greif et al., 2015). Briefly, unedited sequences corresponding to Sylvio (FJ203996.1), CL Brener (DQ343645.1) and Esmeraldo (DQ343646.1) obtained from the

TABLE 1 | Datasets used in this study.

| Accession | Strain | DTU | Mitochondrial clade | Origin | Host |
|------------|--------------|-------|---------------------|-------------------------|------------------------------|
| SRX5245771 | PalDa20cl3 | Tcl | A | El Palmar, Argentina | <i>Didelphis albiventris</i> |
| SRX5245770 | TEV55cl1 | Tcl | A | Tres Estacas, Argentina | <i>Triatoma infestans</i> |
| SRX5245773 | Esmeraldo | Tcll | C | Sao Felipe, Brazil | <i>Homo sapiens</i> |
| SRX5245772 | TU18cl93 | Tcll | C | Potosí, Bolivia | <i>Triatoma infestans</i> |
| SRX5245767 | X109/2 | Tclll | B | Makthlawaiya, Paraguay | <i>Canis familiaris</i> |
| SRX5245766 | CANlllcl1 | TclV | B | Belém, Brazil | <i>Homo sapiens</i> |
| SRX5245769 | MNcl2 | TcV | B | Región IV, Chile | <i>Homo Sapiens</i> |
| SRX5245768 | LL014R1 | TcV | B | Las Leonas, Argentina | <i>Triatoma infestans</i> |
| SRX5245774 | L015P68R0cl4 | TcVI | B | Las Leonas, Argentina | <i>Canis familiaris</i> |

NCBI database were aligned using MEGA v7 software (Kumar et al., 2016). Then, the alignment was manually manipulated by inserting or deleting uridines (U's) at specific sites into the unedited sequences following the editing patterns of the corresponding *T. brucei* and *T. vivax* edited mRNAs, meanwhile the resulting amino acid sequence was preserved. Predicted sequences were generated for *mitochondrial unidentified reading frame 2* (MURF2), *NADH dehydrogenase subunit 3* (ND3) and *C-rich region 4* (CR4) following the known edited mRNAs for *T. vivax* and *T. brucei* (**Supplementary File 1**). On the other hand, sequence data of predicted edited mRNAs for the following genes were obtained from Ruvalcaba-Trejo et al. (Ruvalcaba-Trejo and Sturm, 2011) for the same three *T. cruzi* strains: *ATPase6*, *C-rich region 3* (CR3), *cytochrome b* (CyB), *ribosomal protein S12* (RPS12), *NADH dehydrogenase subunit 7* (ND7), *NADH dehydrogenase subunit 8* (ND8) and *NADH dehydrogenase subunit 9* (ND9). CL Brener *cytochrome oxidase subunit 3* (COIII) mRNA was downloaded from GenBank (accession number: EF058194.1). In addition, Sylvio and Esmeraldo COIII edited mRNA sequences were manually generated (**Supplementary File 1**). Additional maxicircle sequences described by Reis-Cunha et al. (2018) were downloaded from GenBank, manually edited, and also used for gRNA search. Predicting gRNAs based on such sequences (shown in **Table S1**) had similar results to the obtained by using Sylvio, Esmeraldo or CL-Brener edited mRNAs.

gRNA Detection

An algorithm using c++ and the SeqAn library (Reinert et al., 2017) was built to detect potential gRNA in the mHVR reads. First, a hash-table was built from the reads by storing position of all the possible k-mers (seeds) of 15 bases. However, due to non-canonical base pair a hash-table was used considering just purines (R) and pyrimidines (Y) instead the four bases. Although C::A pairing is allowed with this approach, it is considered a mismatch in the following steps. An algorithm scheme is provided in **Figure S1**. The hash table only allows to reduce the search time in the next steps. The mRNA sequence for each edited gene was used to identify gRNAs. The estimated edited mRNA of the corresponding mitochondrial clade was used to infer gRNA for each strain. First, a window of 15 bases was selected at the 5' end in the mRNA and the reverse complement of the purine/pyrimidine pattern was used to determine which mHVRs contains a potential gRNA by using the hash-table. Then, the potential site was evaluated considering

canonical and non-canonical base pairing (G::U) with the mRNA and allowing only one mismatch. Finally, the pairing is extended to both sides using an x-drop extension allowing one mismatch. Mismatches were allowed considering some flexibility in editing and considering that mRNAs are estimated and minimal errors in estimations are possible (Thomas et al., 2007). A filter was then applied to discard the predicted gRNA if it has fewer bases than the parameter *f*. This parameter is the minimum number of bases that a gRNA candidate must have to be accepted. This parameter is required because short sequences with complementarity to mRNAs are expected by simple random. Then, the window is moved over the mRNA one base at a time and the process is repeated until the entire mRNA is scanned. Different values for *f* were evaluated in order to discard sequences that are not gRNAs. In a first approach, gRNAs with <40 bases were discarded (*f* = 40). This filter was too stringent but allowed to identify the most probable regions of the mHVR that contain the gRNA, that is the gRNA cassette. Then, the filter was lowered looking for hits outside the cassette and the minimum filter that had as maximum as 5% of the gRNA hits out of the cassette was selected (*f* = 30) (**Figure S3**). Alternatively, other approaches for gRNA detection were evaluated. The first one was based on (Kosłowsky et al., 2014). Briefly, after looking for 15 bp seeds, the algorithm scored canonical (score = 2) and non-canonical (score = 1) base pairings and gRNAs with scores <45 were discarded. The second approach was based on (Cooper et al., 2019) by looking for gRNAs with 6 bp-anchors (canonical base pairing) in the 5' end and then discarding gRNAs with less than 25 bp (canonical plus non-canonical base pairing). Both approaches were too stringent, they recovered reduced gRNA coverage in ATPase 6 mRNA and a smaller number of gRNAs than using the above approach *f* = 40 (**Figure S1**). Consequently, *f* = 30 was established given its higher sensitivity than *f* = 40, and a reasonable rate of gRNA hits out of the cassette. The c++ source code for gRNA detection in mHVRs and example datasets are stored in <https://osf.io/kn34z/>.

gRNA Clustering Analyses

Identified gRNAs were clustered according to sequence similarity and overlapping in the edited-mRNA target region. A SWARM-like algorithm (Mahe et al., 2014) was implemented to cluster gRNAs. SWARM is a fast unsupervised (*de novo*) single-linkage-clustering algorithm. An algorithm scheme is provided in **Figure S2**. The modified algorithm also included an overlapping threshold (*o*) in addition to a threshold of the

maximum number of base mismatches between sequences (d). Basically, the algorithm selects one gRNA as a cluster seed and then it iteratively looks for gRNAs with a number of mismatches lower than d and an overlapping $> o$ and adds them to the cluster. Then, it iteratively looks for unclustered gRNAs with less than d mismatches and overlapping $> o$ to every gRNA previously included in the cluster. When no new gRNAs can be added to the cluster a new cluster is seeded using a gRNA that was not previously clustered. The process is iterated until the all gRNAs were joined to a cluster. $o = 0.7$ and $d = 4$ were implemented. This is a relaxed threshold to cluster moderately different gRNAs in the same cluster considering divergency in such kind of sequences. Considering the overlapping region of two gRNAs of ~30–50bp, $d = 4$ implies 85–92% pairwise similarity. Similar percentages were used to cluster mHVRs in (Rusman et al., 2019). The second phase of breakage in the original SWARM algorithm was not required (Mahe et al., 2014) because of the high distances and reduced overlapping among clusters. Identified gRNA clusters based on SWARM were termed as gRNA classes here. Finally, a consensus gRNA was built for every gRNA class to represent editing cascades. In order to fast calculation, the consensus gRNA was built using a base-by-base majority-rule criterium (i.e. the most abundant base in each position of gRNA alignment was used to build the consensus gRNA). Because artifactual gRNA may be generated by this method the algorithm also calculated the number of gRNAs sharing such sequence and informed it in the output file to manual inspection. The consensus gRNAs were graphed aligned to the edited mRNA and the cluster abundance was represented with a color scale.

In order to assess linkage disequilibrium as a measure of genetic structuring among strains, the index of association (I_a) and the proportion of compatible pairs of loci with strict clonality (PrCompat) were calculated. Briefly, gRNA classes were coded as present (>20 reads) or absent (≥ 20 reads) emulating RFLP pattern data for each strain and the coded matrix was analyzed as haploid data in Mulilocus v1.3 (Agapow and Burt, 2001) with 10,000 iterations to calculate statistical significance.

A subset of gRNA classes was selected to predict secondary structure. Briefly, gRNA classes with more than 200 reads (high abundance), with more than 90% of the reads being identical to the consensus sequence of the class and with at least 40 bases were selected. The selected class representative gRNAs were analyzed using RNAstructure software (Reuter and Mathews, 2010). The maximum accuracy structures were calculated using default parameters but considering a temperature of 27°C (optimal to temperature for epimastigotes and previously used in *T. brucei* analysis of gRNA secondary structure) (Schmid et al., 1995).

mHVR Clustering and Comparison With gRNA Classes

mHVR reads were processed and clustered according to (Rusman et al., 2019) using a UCLUST algorithm with a threshold of 85% of identity for cluster definition. Clustering at

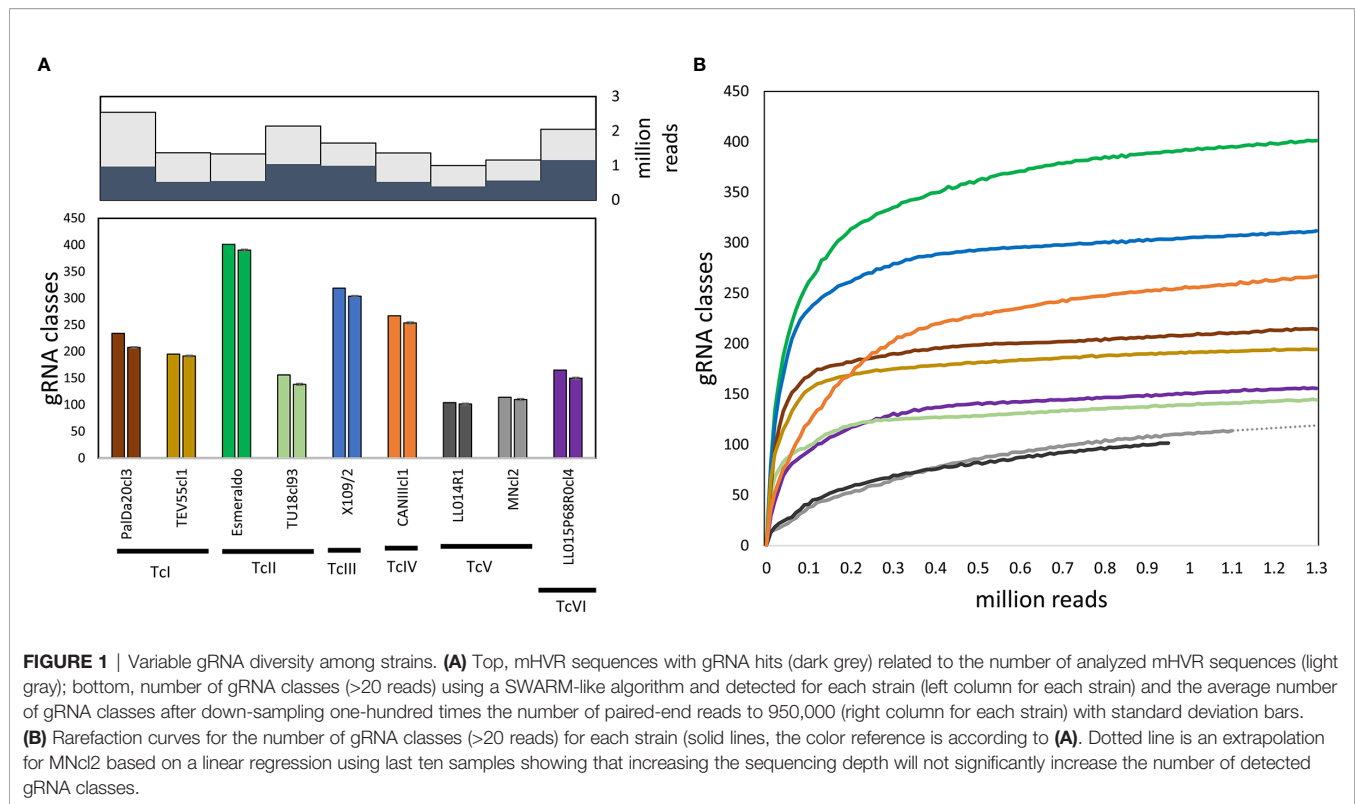
85% was previously used to define mHVR clusters (Rusman et al., 2019) and such clusters were used to determine relationships between mHVR clusters and gRNA classes. Briefly, a c++ algorithm was designed to add a string with the mHVR cluster ID to each read name in the raw fastq file. Then, this fastq file was used to determine gRNAs using the above-described algorithm. This way, each identified gRNA could be assigned to an mHVR cluster. After clustering gRNAs in classes using the SWARM algorithm, it was evaluated whether each mHVR cluster coded none, one or more than one gRNA. Around 9.5% of the clusters corresponded to two gRNA classes in the same mHVR cluster. Although it is expected none or just one gRNA in an mHVR, such possible method inaccuracy was allowed in order to gain sensitivity to obtain the maximum coverage on mRNA editing cascades.

RESULTS

Fast Evolutionary Changes in gRNA Repertoires

Guide RNAs coded in mHVRs were inferred based on the available sequences or predicted edited mRNAs of *T. cruzi*. A total of 7,476,003 gRNAs were detected for nine *T. cruzi* strains belonging to the six DTUs. The percentage of detected gRNAs from the total number of mHVR reads for each studied strain varied from 38% to 60% (Figure 1A), suggesting that some mHVRs would not encode gRNAs. Posteriorly, the gRNAs were clustered in gRNA classes according to the editing region and their sequence similarity (Supplementary File 2). A total of 1334 gRNA classes were identified (every class with >20 reads). The number of gRNA classes *per* strain was variable ranging from 104 (LL014R1-TcV) to 401 (Esmeraldo-TcII). Particularly, TcV strains had up to three or four times fewer gRNA classes than other DTUs (Figure 1). The number of gRNA classes was also variable within DTUs (Figure 1 and Figure 2) suggesting fast changes in gRNA repertoires and probably gRNA redundancy (i.e., different gRNA classes editing the same mRNA region). Rarefactions of each dataset showed that these differences between strains are not the effect of different sequencing depths (Figure 1B).

Just 22.8% of the whole identified gRNA classes in all strains were shared among two or more of them and only four gRNA classes were shared among all strains (sequences provided in Supplementary File 2) revealing high divergence. However, the percentage of shared gRNA classes between strains of the same DTU was variable (Figure 2). TcI strains shared a relatively low number of gRNA classes (19.2%) despite that the studied strains are very close phylogenetically (according to nuclear genes) (Schmid et al., 1995) and they were isolated in the same geographical area and time (Diosque et al., 2003). In addition, TcII strains shared even few gRNA classes (9.1%) (Figure 2). Instead, TcV strains (LL014R1 and MNcl2) shared a high proportion of gRNA classes (73.8%) despite they were isolated in geographically distant places and with a difference of around 30 years between the isolation dates. All these results suggest



significant changes in gRNA repertoires in relatively short evolutionary times. In addition, linkage disequilibrium was analyzed to address the structuring of such diversity. The index of association (I_a) was 49.3 and showed high significance ($p < 0.001$). Furthermore, the ratio of pairs of gRNA classes compatible (PrCompat) with unmixed gRNA classes was 0.98 suggesting structuring of diversity among strains. Finally, it was addressed whether probable predicted secondary structures are common in such gRNA sequence diversity. A subset of 89 gRNA classes defined by a stringent criterion (see Material and methods) was studied. Although variable structures were observed (**Supplementary File 4**), 70.7% of the gRNAs have a stem region intercalated by one or two internal loops (or less frequently bulges) and ending in a hairpin loop (**Figure S4**). Only 26% of the structures have a double hairpin (**Figure S4**).

Silent mHVRs

In a previous work, entire mHVR sequences were clustered according to sequence identity (Rusman et al., 2019). Here, the gRNA classes were assigned to mHVR clusters. First, most (97.1%) mHVR clusters of all strains had one of two states: (i) high proportion (> 75%) of the sequences in the mHVR cluster coding one gRNA class; or (ii) low proportion (< 10%) of sequences in the mHVR cluster coding a gRNA class (**Table S2**). Most exceptions to the rule were observed in TcV strains (**Table S1**). The term “silent” mHVR clusters was used for those in which less than 20 gRNAs were identified. Silent mHVR clusters were from 25% to 54% of the total mHVR clusters in the studied strains (**Table 2**). Curiously, strains with the lowest

number of gRNA classes (TcV and TcVI strains) also had the lowest percentage of silent mHVR clusters (**Table 2**).

Furthermore, the analyses showed there is no clear relationship between mHVR cluster size and whether it encodes a gRNA or not since silent mHVR clusters were of quite different abundances (**Figure 3**).

Concerted Changes in the Number of gRNA Classes

The gRNA classes identified for each strain were aligned with the edited mRNAs of the corresponding mitochondrial clade. The number of gRNA classes editing each gene for all strains is represented in **Figure 4** and **Table S3**. Most gRNA classes (more than 50%) edit ATPase 6 and COIII mRNAs in all strains (**Figure 4A**). Interestingly, the percentage of gRNA classes editing each mRNA was nearly conserved among strains (**Figure 4B**). This implies correlated variations in the number of gRNAs classes editing each mRNA (see correlation coefficients in **Table S4**). These results show that observed variations in the number of gRNA classes are balanced, i.e., if one strain decreased gRNA classes for one mRNA also decreased the number of gRNAs classes for editing other mRNAs. This would be an expected result whether each minicircle codes for different gRNAs, each one editing different mRNAs.

Editing mRNA Cascades for ATPase6 and COIII

The algorithms identified a complete or almost complete set of gRNA classes necessary to edit the mRNAs for the ATPase6

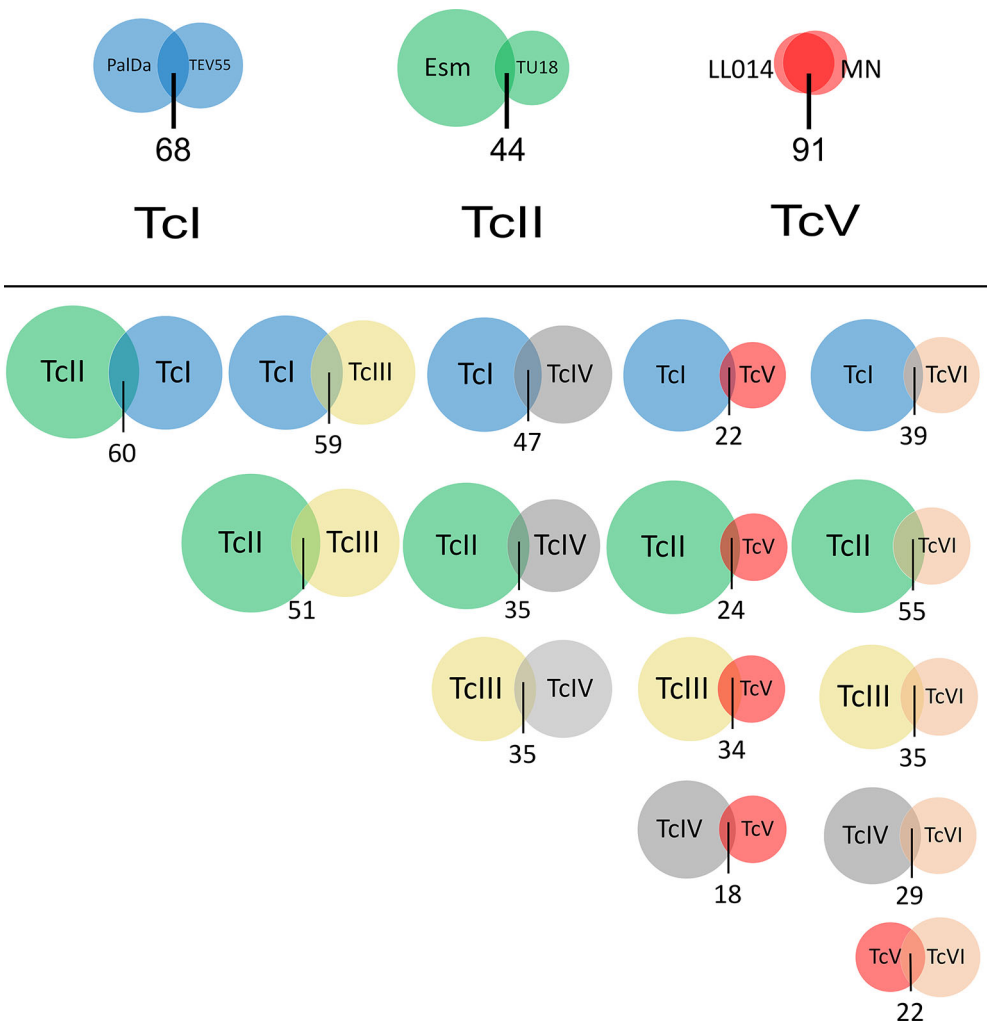


FIGURE 2 | Venn diagrams showing overlapping gRNA repertoires between strains of the same DTU and between DTUs. Circle size represents the number of gRNA classes identified in a strain (above) or in a DTU (below). The overlapping area among circles indicates gRNA classes with more than 20 reads that are shared between strains or DTUs. The number below circles represents the percentage of shared gRNA classes. PalDa=PalDa20c3, TEV=TEV55c1, Esm=Esmeraldo, X109=X109/2, Tu18=Tu18c93, MN=MNc12 and LL014=LL014R1.

(complex V) and COIII (complex IV) in every strain despite the highly variable number of gRNA classes editing such mRNAs. This clearly shows redundant gRNA classes for some strains. The editing mRNA cascades for ATPase6 and COIII pan-edited genes are shown in **Figure 5** and **Figure S5**, respectively.

Aligned gRNAs-mRNAs are provided in the **Supplementary File 2**. Strains PalDa20c3, Esmeraldo, X109/2 and CANIICl1 showed a greater redundancy of gRNA classes than other strains which implied strong variations among and within some DTUs, mainly TcII strains (**Figure 5** and **Figure S5**). On the other side,

TABLE 2 | Relationship between mHVR clusters and gRNA classes.

| | TcI | | TcII | | TcIII | TcIV | TcV | | TcVI |
|-----------------------------------|-----------|---------|-----------|---------|--------|----------|---------|-------|---------------|
| | PalDa20c3 | TEV55c1 | Esmeraldo | TU18c93 | X109/2 | CANIICl1 | LL014R1 | MNc12 | LL015P68R0c14 |
| mHVR clusters ¹ | 324 | 234 | 347 | 151 | 373 | 149 | 72 | 71 | 108 |
| Silent mHVR clusters ² | 47% | 39% | 42% | 37% | 43% | 54% | 32% | 34% | 25% |

¹mHVR clusters were defined in Rusman et al. (2019).
²mHVR clusters for which less than 20 gRNAs were detected.

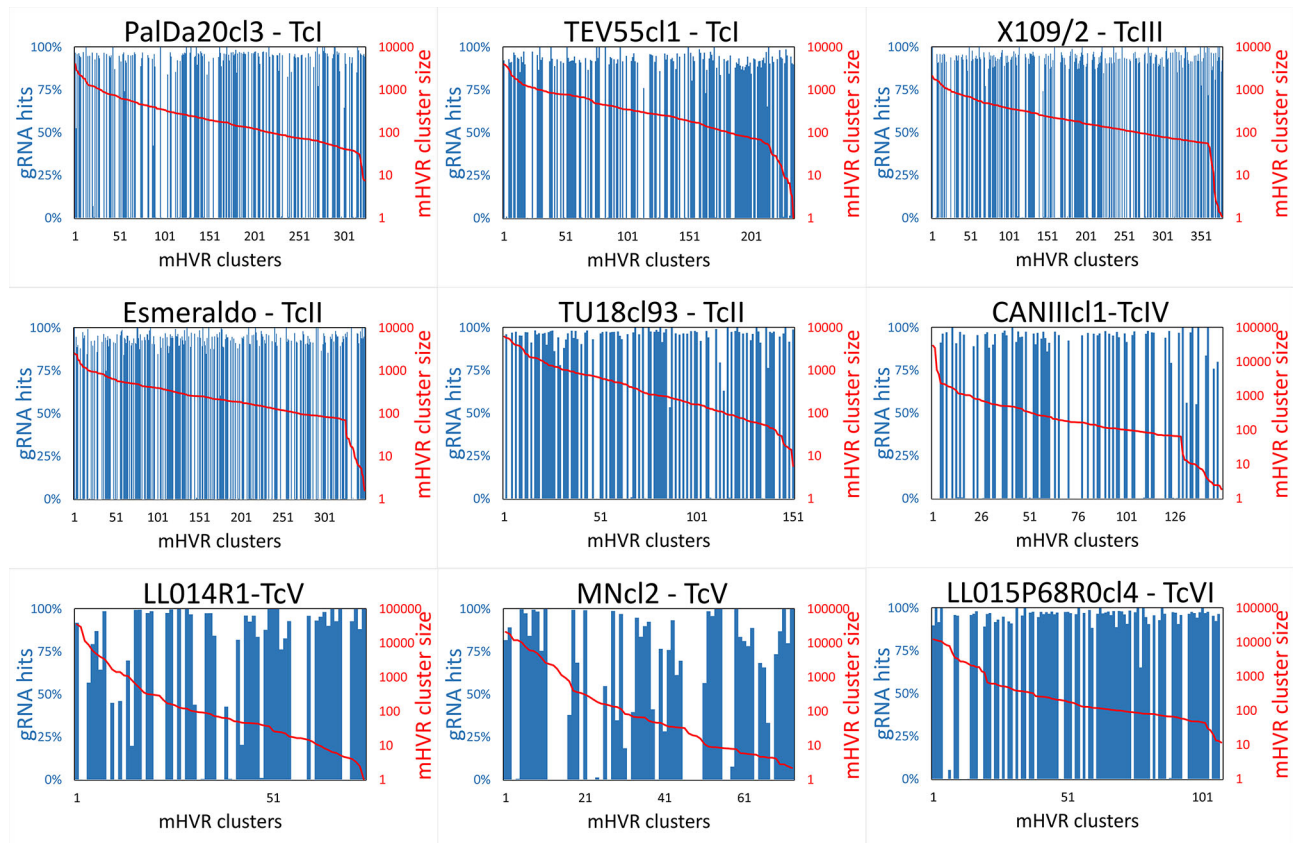


FIGURE 3 | The number of mHVR sequences in a cluster is not related to the coding of gRNAs. mHVR clusters were graphed in decreasing order according to their size (mHVR cluster size is indicated with a solid redline). Each blue bar indicates the percentage of reads in the mHVR cluster in which a gRNA was identified (gRNA hits). Red color indicates percentage of reads in the mHVR cluster where gRNAs were not detected.

TcV strains - MNcl2 and LL014R1 - had the lowest redundancy of gRNA classes (Figure 5 and Figure S5).

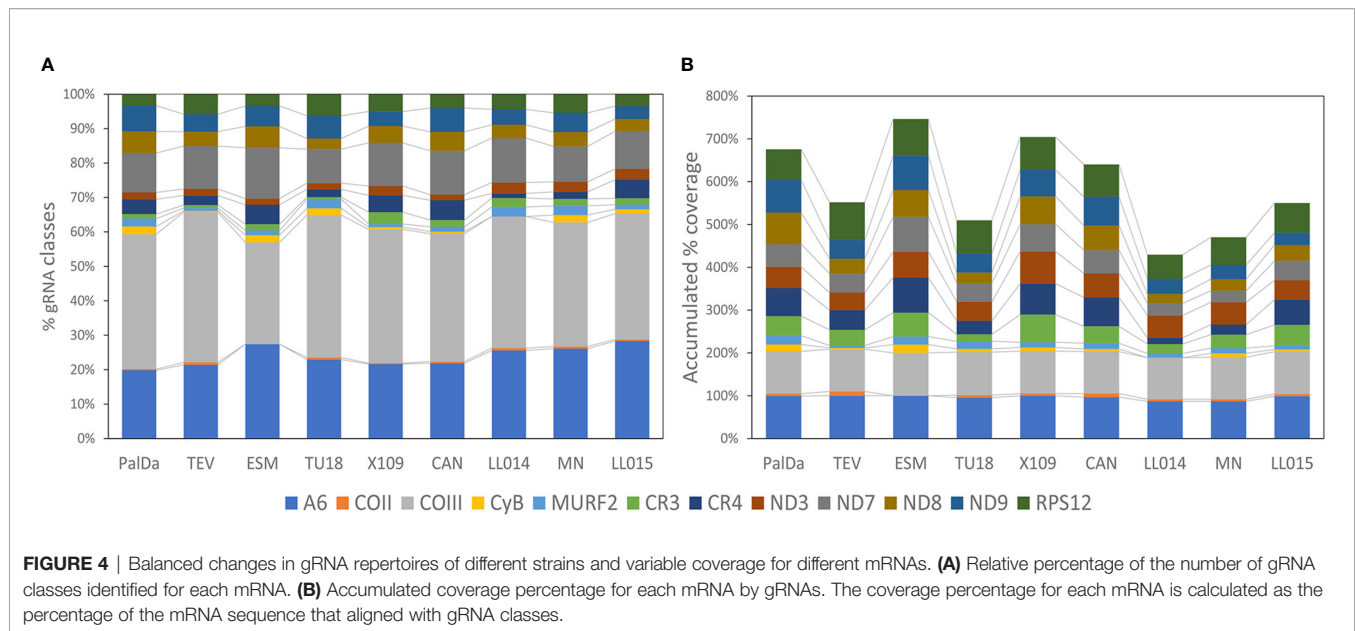
Respiratory Complex I: Incomplete Editing Cascades

The percentage of coverage by gRNAs for each mRNA is shown in Figure 4B and Table S5. Interestingly, the coverage was almost complete for ATPase6 and COIII mRNAs but highly variable for the remaining mRNAs, especially in the complex I members (Figure 4B). The editing cascades of the mRNAs coding complex I members —ND9, CR3, CR4, ND3, ND7, ND8— of the respiratory chain are shown in Figure 6 and Figures S6–S10. Even strains showing high mRNA class redundancy in COIII and ATPase6, such as Esmeraldo and X109/1, have incomplete cascades for complex I members. The exception was ND9 mRNA, in which both strains (X109/2 and Esmeraldo) presented almost a complete coverage (Table S5), although most of the gRNA classes (82.1% and 74.8%, respectively) had less than 20 reads (see also Table S6). Breaking points in ND3, ND7 and ND8 editing cascades in these two strains were also observed. Interestingly, TcV strains —LL014R1 and MNcl2— presented

relatively few gRNA classes that edit the complex I components messengers (Table S3, Figure 6 and Figures S6–S10) and relatively low coverage of the mRNAs (Table S5 and Table S6).

Potential Cross-Editing of Mitochondrial mRNAs Among Different DTUs

Biparental inheritance of minicircles in hybrid DTUs was previously proposed (Rusman et al., 2019). Here, it was analyzed whether gRNAs from one strain may potentially edit mRNAs from a strain from another DTU, particularly another mitochondrial clade. This ability for “cross-editing” is a requirement in hybrid DTUs, where minicircles come from both parentals but maxicircles come from just one parent. Editing cascades were again generated for Esmeraldo gRNAs and X109/2 gRNAs but based on mRNAs of different mitochondrial clades. mRNA coverage by gRNAs was evaluated and both gRNA repertoires have similar coverages on mRNAs from different mitochondrial clades (Figure 7). Cross-editing was also evaluated in more stringent conditions by lowering the allowed number of mismatches in cluster definition ($d = 3$, $d = 2$ and $d = 1$) and it was not detected a significant difference in mRNA coverage percentage. Minor differences were observed in the mRNA



coverage percentages for genes *CyB* and *ND9* in $d = 1$ settings (Figure S11). These results suggest that biparental inheritance of the kDNA would not generate mRNA editing problems even among phylogenetically distant DTUs.

DISCUSSION

mRNA editing in kinetoplastids is an intriguing evolutionary mechanism. Questions about how and why such complex and energy-expensive mechanism has evolved are still controversial (Covello and Gray, 1993; Gray et al., 2010; Flegontov et al., 2011). The elucidation of editing cascades in mRNA is a prerequisite to start filling the gaps around such questions. We have previously reported the DNA sequence diversity of the hypervariable region of kinetoplastid minicircles (mHVR) in the main lineages of *T. cruzi*, which were virtually unknown until then (Rusman et al., 2019). Here, we deeply addressed gRNA repertoires (coded in the mHVRs) of nine *T. cruzi* strains belonging to the main lineages of this parasite.

Our results showed that gRNA diversity was enormous, with more than 1,300 different gRNA classes, each one detected in >20 reads. Such diversity was structured among the strains according to linkage disequilibrium indexes. However, further analyses are required to address how good the linkage disequilibrium measures perform on this kind of data. In addition, the number of gRNA classes was highly variable among strains. In addition, it was addressed whether shared common secondary structures exist despite the high sequence diversity for gRNAs, as it has been described for *T. brucei* (Schmid et al., 1995). Double-hairpin structures observed in *T. brucei* were not the most frequent structures in *T. cruzi* predictions. However, the predictions should be considered cautiously because they do not include the poly-U commonly added to 3' of gRNAs (Schmid et al., 1995) and

predictions could change if constraints based on experimental data are added to the analysis (Reuter and Mathews, 2010). Finally, despite this study analyzed the mitochondrial editomes of different strains in a comparative and large scale, experimental studies are needed to determine gRNA complete sequences and the abundances of each one. Nevertheless, studies in *T. vivax* and *T. brucei* have revealed that gRNA abundance is related to the coding minicircle abundance (Koslowsky et al., 2014; Greif et al., 2015) although such correlation is not so clear in *Leishmania tarentolae* (Simpson et al., 2015).

As expected from mHVR sequence analyses (Telleria et al., 2006; Rusman et al., 2019), different DTUs shared a relatively low number of gRNA classes, but it was surprising that even strains of the same DTU (here TcI and TcII) shared few gRNA classes. Such strains showed not only different gRNA classes but also very divergent abundances in shared gRNA classes.

The TcI strains analyzed here are phylogenetically close according to nuclear and mitochondrial sequences (Tomasini et al., 2014; Rusman et al., 2020). However, they shared just 19.2% of their gRNA classes. Such results suggest that gRNA repertoires may vary extremely fast. Even TcV strains which are identically at most nuclear analyzed DNA sequences have a poor correlation in the abundances of shared gRNAs, even though TcV strains share most of their mHVR clusters at 95% identity threshold (Rusman et al., 2019) and most of their gRNA classes. Such results suggest that fast changes in minicircle repertoires are not mainly caused by mutation. It is important to mention that the variations in gRNA classes between strains described above would not be a result of minicircle loss after long periods in culture. The strain with more gRNA diversity (Esmeraldo, TcII) was isolated in the eighties and maintained in culture for several years; whereas, for example, LL015P68R0cl4 (TcVI) was isolated ten years ago, cultured for less than a year and then frozen until this study. In addition, LL014R1 (TcV) which showed the lowest

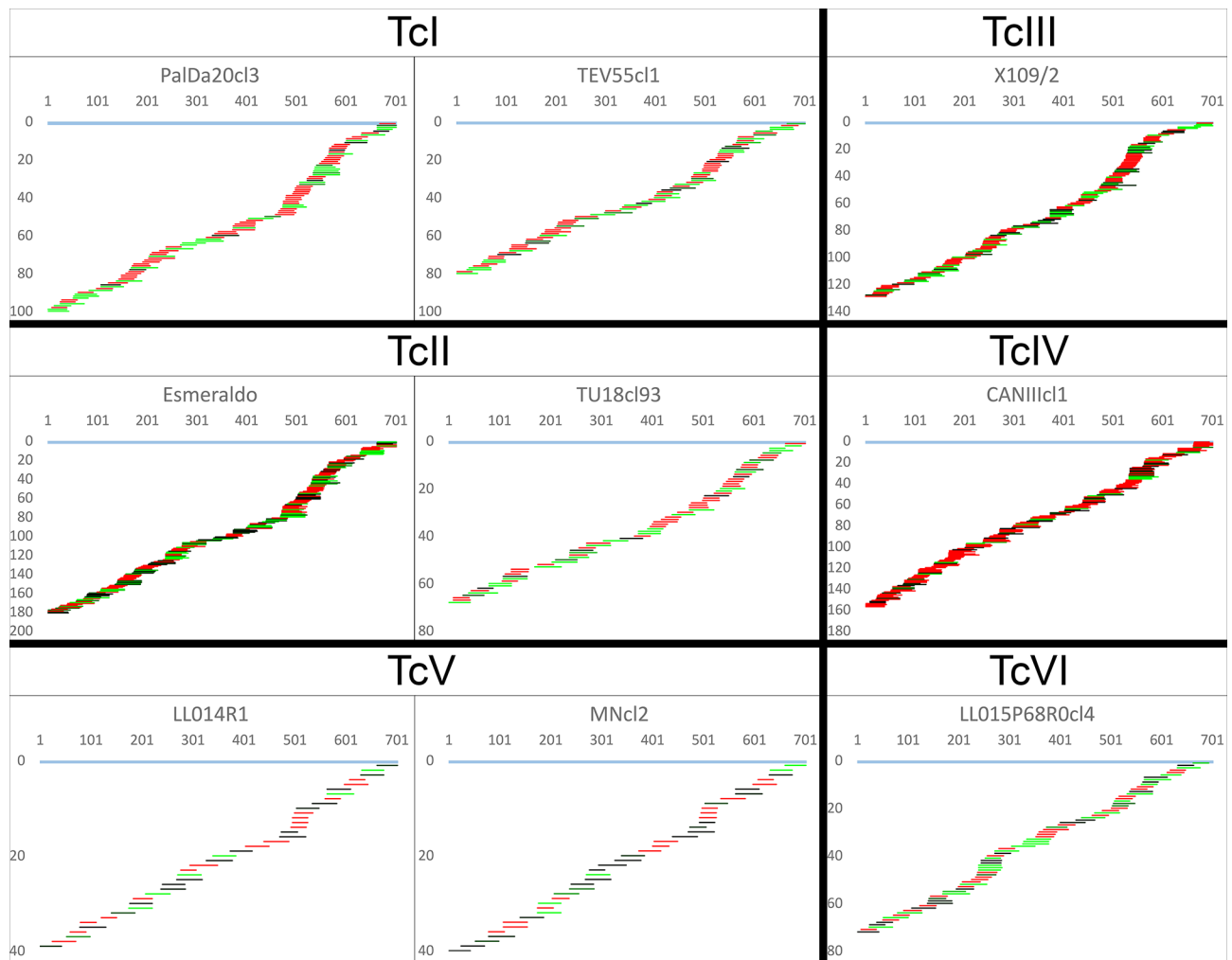


FIGURE 5 | Canonical ATPase6 mRNA editing cascade inferred from mHVR reads. gRNA classes are shown aligned below the fully edited mRNA (light blue). The x-axis indicates mRNA position, and the y-axis indicates the accumulated number of gRNA classes until such mRNA position. gRNA classes are colored based on sequence abundance as follow: red (1-19 reads), black to green (20-1,000 reads), light-green (>1,000 reads).

number of gRNA classes, was maintained mostly through mouse-triatomine passages since isolation in 2009. In addition, such variations in gRNA class diversity between strains correlate well with mHVR cluster diversity. This result supports that changes in gRNA diversity among strains is not caused by differences in gRNA estimation for different DTUs (caused by edited mRNA prediction).

The models of random or partially random segregation of minicircles (minicircle drift) during kDNA division predicts changes in gRNA composition by variations in gRNA class abundance (Savill and Higgs, 1999). “Minicircle drift” is caused by an error during kDNA network division resulting in the two copies of a replicated minicircle being inherited to the same descendant kinetoplast. Such random changes are analogous to genetic drift in populations (e.g., allele frequency varies randomly until fixation or lost, reducing allele diversity in absence of any other

evolutionary force). In the same way, partially random segregation of minicircles predicts loss of gRNA redundancy (Savill and Higgs, 1999). Linkage of gRNA classes (that is, their presence in the same minicircle) may conserve some redundancy. This would occur in the case that redundant gRNA classes were linked with different essential gRNAs (i.e., gRNA classes without redundancy). However, gRNA linkage is still not compatible with spread redundancy observed in some strains because it is expected that the greater the number of redundant classes the greater the number of essential gRNA classes necessary to support them, which strongly limits redundancy.

Since the model of (partial) random segregation as the unique evolutionary force does not fit the high levels of gRNA class redundancy observed in some strains, the genetic exchange would be the most probable force generating gRNA class redundancy. In a previous paper, we proposed biparental

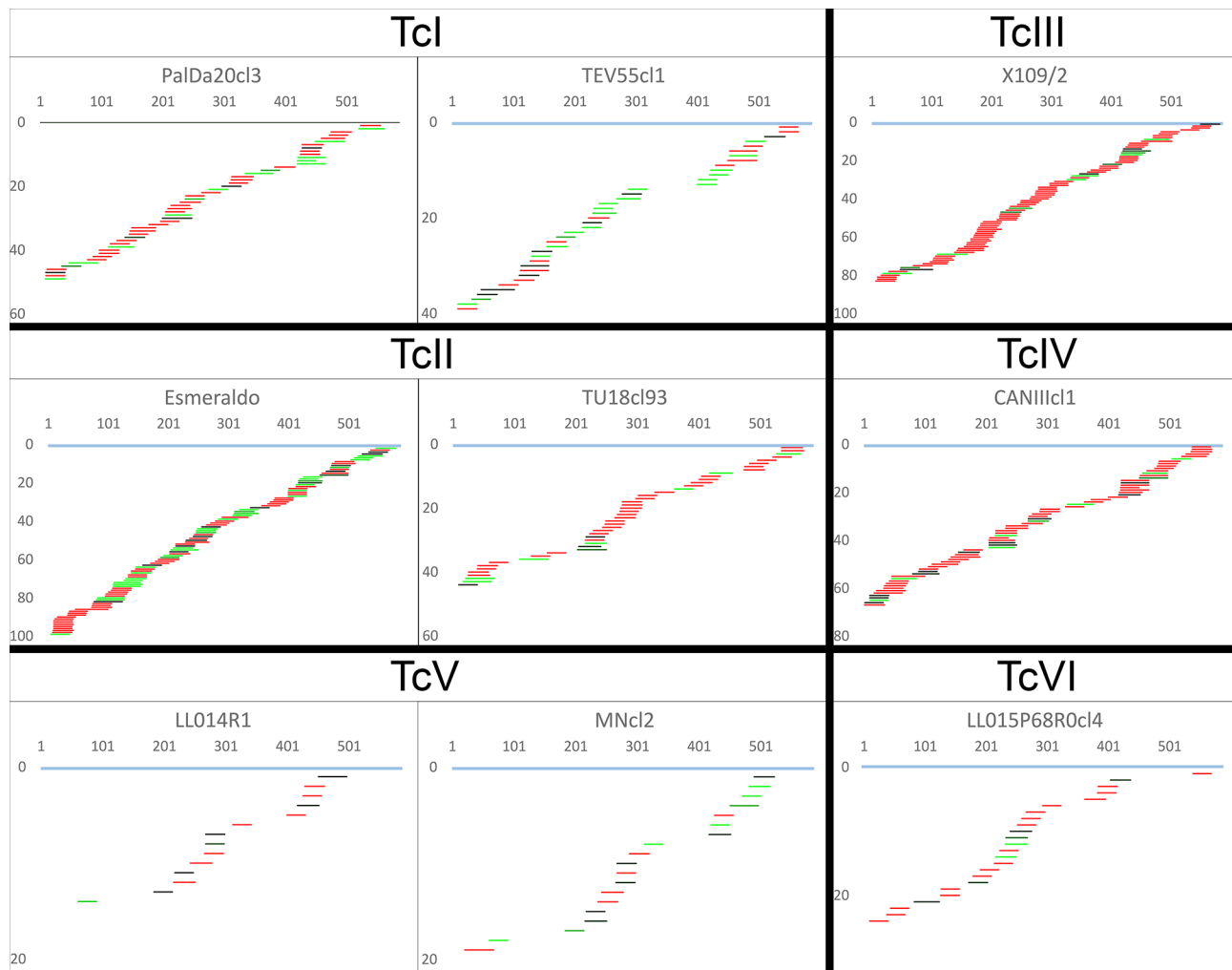
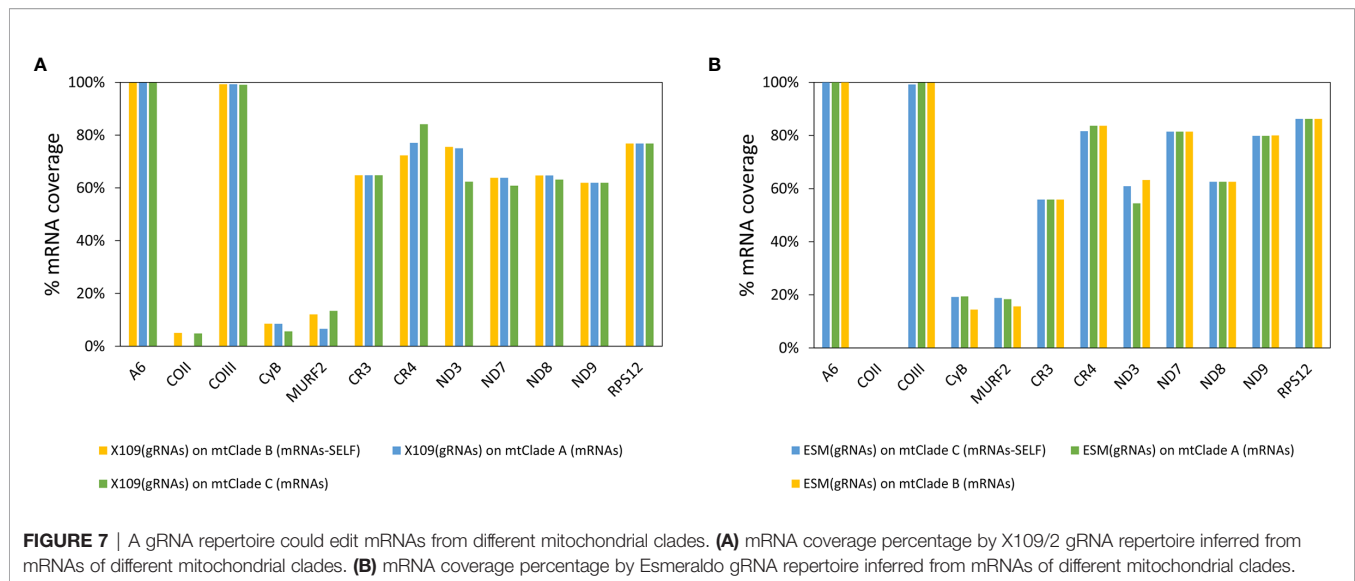


FIGURE 6 | Incomplete editing cascades for NADH dehydrogenase subunit 9. gRNA classes are shown aligned below the fully edited mRNA (light blue). The x-axis indicates mRNA position, and the y-axis indicates the accumulated number of gRNA classes until such mRNA position. gRNA classes are colored based on sequence abundance as follow: red (1-19 reads), black to green (20-1,000 reads), light-green (>1,000 reads).

inheritance of minicircles in hybrid DTUs of *T. cruzi* (Rusman et al., 2019) and in an intra TcI hybrid (Rusman et al., 2020). Biparental inheritance has also been proposed for *T. brucei* (Turner et al., 1995; Gibson et al., 2008). Maxicircles and minicircles may be biparentally inherited but maxicircles of one parent are lost by drift in few generations (Turner et al., 1995). Despite, minicircles of both parents are maintained by many more generations. In this sense, genetic exchange may generate gRNA redundancy (Savill and Higgs, 1999). In addition, the observed correlated variations in the number of gRNAs classes editing each mRNA (see **Tables 2** and **S4**) may also be explained by a biparental inheritance of minicircles which is a bulky change in gRNA classes. Conversely, clonal propagation would generate a loss of gRNA classes by minicircle drift. Under this hypothetical dynamic, DTUs with less gRNA redundancy (i.e. TcV and TcVI) should have a typical clonal propagation (Lewis et al., 2011;

Diosque et al., 2014; Tomasini and Diosque, 2015); while, most gRNA class redundancy has been observed in lineages in which genetic exchange has been reported (TcI, TcII and TcIII) (Llewellyn et al., 2009; Ocana-Mayorga et al., 2010; Baptista Rde et al., 2014; Tomasini and Diosque, 2015; Berry et al., 2019).

Biparental inheritance of minicircles has another challenge, i.e., to make the right editing of mRNA when maxicircles come from just one parent. However, *in silico* analyses showed that gRNA classes from one strain may edit mRNAs from the other mitochondrial clades in a similar way than in the self-clade. This result suggests that genetic exchange and biparental inheritance of minicircles should not cause editing conflicts. In this sense, genetic exchange may increase gRNA class redundancy, avoiding that an editing site being near to lost gRNAs, even restoring broken editing cascades. Consequently, strict clonal lineages would not persist in long evolutionary times (a Muller ratchet).



Interestingly, gRNA class redundancy was mainly detected in ATPase subunit 6 and Cytochrome c oxidase subunit III. Editing cascades of both mRNAs were complete or almost complete in all strains suggesting that such genes are essential for the parasite. However, editing cascades of the complex I subunits have less gRNA class redundancy and even interrupted cascades at several positions in some strains. Functions of the complex I are debatable in trypanosomatids (Oppendoes and Michels, 2008) and it has been proposed that electrons bypass this complex in the respiratory chain of *T. cruzi* epimastigotes (Denicola-Seoane et al., 1992; Carranza et al., 2009). In addition, the absence of two key subunits suggests that if functional for electron transport, the complex I cannot pump protons to intermembranous space and may function to renewing NAD⁺ (Oppendoes and Michels, 2008) although other studies showed that this activity has no differences between ND mutants and wild type strains in *T. cruzi* epimastigotes (Carranza et al., 2009) although only log-phase epimastigotes were evaluated. Considering the fast evolutionary rates shown for gRNA class frequencies, a completely non-functional complex I should imply highly impaired cascades of gRNA elements editing such sequences. Instead, almost complete editing cascades recovered for some complex I elements do not fit with the hypothesis of non-functional complex I at least in some strains like Esmeraldo or X109 (Figure 6). Despite, it is a more suitable hypothesis that time in culture without infecting a mammal allowed that some gRNA classes were lost, or they reduced their abundance as observed. However, it cannot be discarded that some DTUs like TcV may have lost complex I components since the cascades are highly incomplete in both strains in a similar manner. Further studies on this topic are required, especially because deletions in genes coding the complex I subunits were associated with the indeterminate form of the Chagas disease in TcII (Baptista et al., 2006). Nevertheless, our results support that complex I is not required in all stages of the parasite. In this sense, the linkage of different gRNA classes editing different mRNAs may help to protect

against gRNA class loss in stages where the complex I is not required.

Another interesting observation was the high frequency of mHVR clusters without gRNA hits. Such “silent” mHVR has been observed in *L. tarentolae* (Simpson et al., 2015) and *T. brucei* (Hajduk et al., 1997) although in minor proportions. There are several potential non-exclusive explanations. Some mHVR clusters may code for gRNAs involved in alternative editing of the mRNAs (which cannot be detected by our current algorithm), or code gRNAs that accumulated mutations or even code for shorter gRNAs (less than 30 bp). Alternatively, many mHVRs may not code for gRNAs and such mHVRs persist by linkage to others that code for essential gRNAs (Savill and Higgs, 2000). However, it is not clear if such situations are enough to explain that around a half of the mHVR clusters did not code for gRNAs in some strains. Interestingly, TcV and TcVI strains, which have relatively less redundancy in gRNA classes, also have relatively less silent mHVR clusters, although the percentage is still not negligible. Consequently, unknown functions of these silent mHVR sequences it is a possibility that cannot be ruled out.

Finally, a model is proposed based on data presented here, from which hypotheses can be derived for further testing. Each minicircle in *T. cruzi* has mHVRs coding for different gRNAs that edit different regions and probably (by random) from different mRNAs (which is also supported by the correlated variations in the number of gRNAs classes editing each mRNA). Such linkage may reduce the chances of losing a gRNA class which is only required in some stages of the lifecycle. Such linkage may also explain the existence of silent mHVRs (although other functions cannot be discarded). In addition, minicircle drift cause loss of gRNA classes and low levels of gRNA class redundancy. Consequently, genetic exchange and biparental inheritance of minicircles may restore gRNA abundances for editing each mRNA site and redundancy which may reduce the chances of lethal loss of essential gRNA

classes. The conjunction of minicircle drift and occasional biparental inheritance of kDNA may explain the divergence of gRNA repertoires among strains even within the same DTU.

DATA AVAILABILITY STATEMENT

The datasets analyzed for this study can be found in the Sequence Read Archive at NCBI with the following accession number PRJNA514922. The source code for gRNA inference is stored at the Open Science Framework <https://osf.io/kn34z/>.

AUTHOR CONTRIBUTIONS

FR: Bioinformatic Analysis, Writing – original draft. NF-Y: Bioinformatic Analysis, Writing – Review and Editing. NT: Conceptualization, Programming, Bioinformatic analysis, Supervision, Writing – Review and Editing. PD: Conceptualization, Funding acquisition, Writing – Review and Editing. All authors contributed to the article and approved the submitted version.

REFERENCES

- Agapow, P. M., and Burt, A. (2001). Indices of Multilocus Linkage Disequilibrium. *Mol. Ecol. Notes* 1, 101–102. doi: 10.1046/j.1471-8278.2000.00014.x
- Ammerman, M. L., Downey, K. M., Hashimi, H., Fisk, J. C., Tomasello, D. L., Faktorova, D., et al. (2012). Architecture of the Trypanosome RNA Editing Accessory Complex, MRB1. *Nucleic Acids Res.* 40 (12), 5637–5650. doi: 10.1093/nar/gks211
- Aphasizheva, I., Zhang, L., and Aphasizhev, R. (2016). Investigating RNA Editing Factors From Trypanosome Mitochondria. *Methods* 107, 23–33. doi: 10.1016/j.jmeth.2016.03.020
- Baptista Rde, P., D'Avila, D. A., Segatto, M., do Valle, I. F., Franco, G. R., Valadares, H. M., et al. (2014). Evidence of Substantial Recombination Among *Trypanosoma Cruzi* II Strains From Minas Gerais. *Infect. Genet. Evol.* 22, 183–191. doi: 10.1016/j.jmeegid.2013.11.021
- Baptista, C. S., Vencio, R. Z., Abdala, S., Carranza, J. C., Westenberger, S. J., Silva, M. N., et al. (2006). Differential Transcription Profiles in *Trypanosoma Cruzi* Associated With Clinical Forms of Chagas Disease: Maxicircle NADH Dehydrogenase Subunit 7 Gene Truncation in Asymptomatic Patient Isolates. *Mol. Biochem. Parasitol* 150 (2), 236–248. doi: 10.1016/j.molbiopara.2006.08.008
- Benne, R., Van den Burg, J., Brakenhoff, J. P., Sloof, P., Van Boom, J. H., and Tromp, M. C. (1986). Major Transcript of the Frameshifted coxII Gene From Trypanosome Mitochondria Contains Four Nucleotides That are Not Encoded in the DNA. *Cell* 46 (6), 819–826. doi: 10.1016/0092-8674(86)90063-2
- Berry, A. S. F., Salazar-Sanchez, R., Castillo-Neyra, R., Borrini-Mayori, K., Chipana-Ramos, C., Vargas-Maquera, M., et al. (2019). Sexual Reproduction in a Natural *Trypanosoma Cruzi* Population. *PLoS Negl. Trop. Dis.* 13 (5), e0007392. doi: 10.1371/journal.pntd.0007392
- Bolger, A. M., Lohse, M., and Usadel, B. (2014). Trimmomatic: A Flexible Trimmer for Illumina Sequence Data. *Bioinformatics* 30 (15), 2114–2120. doi: 10.1093/bioinformatics/btu170
- Carranza, J. C., Kowaltowski, A. J., Mendonca, M. A., de Oliveira, T. C., Gadelha, F. R., and Zingales, B. (2009). Mitochondrial Bioenergetics and Redox State are Unaltered in *Trypanosoma Cruzi* Isolates With Compromised Mitochondrial Complex I Subunit Genes. *J. Bioenerget Biomembranes* 41 (3), 299–308. doi: 10.1007/s10863-009-9228-4
- Cavalcanti, D. P., and de Souza, W. (2018). The Kinetoplast of Trypanosomatids: From Early Studies of Electron Microscopy to Recent Advances in Atomic Force Microscopy. *Scanning* 2018:9603051. doi: 10.1155/2018/9603051

FUNDING

The current study is funded by Bunge and Born foundation and the National Scientific and Technical Research Council (D.2555/16.22920160100063CO) (CONICET, Argentina) to Patricio Diosque.

SUPPLEMENTARY MATERIAL

The Supplementary Material for this article can be found online at: <https://www.frontiersin.org/articles/10.3389/fcimb.2021.663416/full#supplementary-material>

Supplementary File 1 | Zip file containing fasta formatted files with mRNA sequences used for gRNA inference.

Supplementary File 2 | Zip file containing gRNA classes aligned to different mRNAs for each strain in this study.

Supplementary File 3 | **Tables S1–S6** and **Figures S1–S11**.

Supplementary File 4 | Zip file containing predicted gRNA structures in postscript format and the gRNA sequences used for the analysis.

- Cooper, S., Wadsworth, E. S., Ochsenreiter, T., Ivens, A., Savill, N. J., and Schnauffer, A. (2019). Assembly and Annotation of the Mitochondrial Minicircle Genome of a Differentiation-Competent Strain of *Trypanosoma Brucei*. *Nucleic Acids Res.* 47 (21), 11304–11325. doi: 10.1093/nar/gkz928
- Covello, P. S., and Gray, M. W. (1993). On the Evolution of RNA Editing. *Trends Genet.* 9 (8), 265–268. doi: 10.1016/0168-9525(93)90011-6
- de Freitas, J. M., Augusto-Pinto, L., Pimenta, J. R., Bastos-Rodrigues, L., Gonçalves, V. F., Teixeira, S. M., et al. (2006). Ancestral Genomes, Sex, and the Population Structure of *Trypanosoma Cruzi*. *PLoS Pathog.* 2 (3), e24. doi: 10.1371/journal.ppat.0020024
- Degrave, W., Fragoso, S. P., Britto, C., van Heuverswyn, H., Kidane, G. Z., Cardoso, M. A., et al. (1988). Peculiar Sequence Organization of Kinetoplast DNA Minicircles From *Trypanosoma Cruzi*. *Mol. Biochem. Parasitol* 27 (1), 63–70. doi: 10.1016/0166-6851(88)90025-4
- Denicola-Seoane, A., Rubbo, H., Prodanov, E., and Turrens, J. F. (1992). Succinate-Dependent Metabolism in *Trypanosoma Cruzi* Epimastigotes. *Mol. Biochem. Parasitol* 54 (1), 43–50. doi: 10.1016/0166-6851(92)90093-Y
- Diosque, P., Barnabe, C., Padilla, A. M., Marco, J. D., Cardozo, R. M., Cimino, R. O., et al. (2003). Multilocus Enzyme Electrophoresis Analysis of *Trypanosoma Cruzi* Isolates From a Geographically Restricted Endemic Area for Chagas' Disease in Argentina. *Int. J. Parasitol* 33 (10), 997–1003. doi: 10.1016/s0020-7519(03)00139-5
- Diosque, P., Tomasini, N., Lauthier, J. J., Messenger, L. A., Monje Rumi, M. M., Ragone, P. G., et al. (2014). Optimized Multilocus Sequence Typing (MlSt) Scheme for *Trypanosoma Cruzi*. *PLoS Negl. Trop. Dis.* 8 (8), e3117. doi: 10.1371/journal.pntd.0003117
- Estevez, A. M., and Simpson, L. (1999). Uridine Insertion/Deletion RNA Editing in Trypanosome Mitochondria—a Review. *Gene* 240 (2), 247–260. doi: 10.1016/s0378-1119(99)00437-0
- Feagin, J. E., Abraham, J. M., and Stuart, K. (1988). Extensive Editing of the Cytochrome C Oxidase III Transcript in *Trypanosoma Brucei*. *Cell* 53 (3), 413–422. doi: 10.1016/0092-8674(88)90161-4
- Flegontov, P., Gray, M. W., Burger, G., and Lukes, J. (2011). Gene Fragmentation: A Key to Mitochondrial Genome Evolution in Euglenozoa? *Curr. Genet.* 57 (4), 225–232. doi: 10.1007/s00294-011-0340-8
- Gibson, W., Peacock, L., Ferris, V., Williams, K., and Bailey, M. (2008). The Use of Yellow Fluorescent Hybrids to Indicate Mating in *Trypanosoma Brucei*. *Parasit Vectors* 1 (1):4. doi: 10.1186/1756-3305-1-4
- Gray, M. W., Lukes, J., Archibald, J. M., Keeling, P. J., and Doolittle, W. F. (2010). Cell Biology. Irremediable Complexity? *Science* 330 (6006), 920–921. doi: 10.1126/science.1198594

- Greif, G., Rodriguez, M., Reyna-Bello, A., Robello, C., and Alvarez-Valin, F. (2015). Kinetoplast Adaptations in American Strains From *Trypanosoma Vivax*. *Mutat. Res.* 773, 69–82. doi: 10.1016/j.mrfmmm.2015.01.008
- Hajduk, S. L., Adler, B., Madison-Antenucci, S., McManus, M., and Sabatini, R. (1997). Insertional and Deletional RNA Editing in Trypanosome Mitochondria. *Nucleic Acids Symposium Ser.* 36, 15–18.
- Hajduk, S., and Ochsenreiter, T. (2010). RNA Editing in Kinetoplastids. *RNA Biol.* 7 (2), 229–236. doi: 10.4161/rna.7.2.11393
- Kim, K. S., Teixeira, S. M., Kirchhoff, L. V., and Donelson, J. E. (1994). Transcription and Editing of Cytochrome Oxidase II RNAs in *Trypanosoma Cruzi*. *J. Biol. Chem.* 269 (2), 1206–1211. doi: 10.1016/S0021-9258(17)42243-5
- Kirby, L. E., Sun, Y., Judah, D., Nowak, S., and Koslowsky, D. (2016). Analysis of the *Trypanosoma Brucei* EATRO 164 Bloodstream Guide RNA Transcriptome. *PLoS Negl. Trop. Dis.* 10 (7), e0004793. doi: 10.1371/journal.pntd.0004793
- Koslowsky, D. J., Bhat, G. J., Read, L. K., and Stuart, K. (1991). Cycles of Progressive Realignment of gRNA With mRNA in RNA Editing. *Cell* 67 (3), 537–546. doi: 10.1016/0092-8674(91)90528-7
- Koslowsky, D., Sun, Y., Hindenach, J., Theisen, T., and Lucas, J. (2014). The Insect-Phase gRNA Transcriptome in *Trypanosoma Brucei*. *Nucleic Acids Res.* 42 (3), 1873–1886. doi: 10.1093/nar/gkt973
- Kumar, S., Stecher, G., and Tamura, K. (2016). Mega7: Molecular Evolutionary Genetics Analysis Version 7.0 for Bigger Datasets. *Mol. Biol. Evol.* 33 (7), 1870–1874. doi: 10.1093/molbev/msw054
- Lewis, M. D., Llewellyn, M. S., Yeo, M., Acosta, N., Gaunt, M. W., and Miles, M. A. (2011). Recent, Independent and Anthropogenic Origins of *Trypanosoma Cruzi* Hybrids. *PLoS Negl. Trop. Dis.* 5 (10), e1363. doi: 10.1371/journal.pntd.0001363
- Lima, L., Espinosa-Alvarez, O., Ortiz, P. A., Trejo-Varon, J. A., Carranza, J. C., Pinto, C. M., et al. (2015). Genetic Diversity of *Trypanosoma Cruzi* in Bats, and Multilocus Phylogenetic and Phylogeographical Analyses Supporting TcBat as an Independent DTU (Discrete Typing Unit). *Acta Trop.* 151, 166–177. doi: 10.1016/j.actatropica.2015.07.015
- Lin, R. H., Lai, D. H., Zheng, L. H., Wu, J., Lukes, J., Hide, G., et al. (2015). Analysis of the Mitochondrial Maxicircle of *Trypanosoma Lewisi*, a Neglected Human Pathogen. *Parasit Vectors* 8, 665. doi: 10.1186/s13071-015-1281-8
- Llewellyn, M. S., Lewis, M. D., Acosta, N., Yeo, M., Carrasco, H. J., Segovia, M., et al. (2009). *Trypanosoma Cruzi* IIc: Phylogenetic and Phylogeographic Insights From Sequence and Microsatellite Analysis and Potential Impact on Emergent Chagas Disease. *PLoS Negl. Trop. Dis.* 3 (9), e510. doi: 10.1371/journal.pntd.0000510
- Lukes, J., Hashimi, H., and Zikova, A. (2005). Unexplained Complexity of the Mitochondrial Genome and Transcriptome in Kinetoplastid Flagellates. *Curr. Genet.* 48 (5), 277–299. doi: 10.1007/s00294-005-0027-0
- Machado, C. A., and Ayala, F. J. (2001). Nucleotide Sequences Provide Evidence of Genetic Exchange Among Distantly Related Lineages of *Trypanosoma Cruzi*. *Proc. Natl. Acad. Sci. U.S.A.* 98 (13), 7396–7401. doi: 10.1073/pnas.121187198
- Mahe, F., Rognes, T., Quince, C., de Vargas, C., and Dunthorn, M. (2014). Swarm: Robust and Fast Clustering Method for Amplicon-Based Studies. *PeerJ* 2, e593. doi: 10.7717/peerj.593
- Marcili, A., Lima, L., Cavazzana, M., Junqueira, A. C., Veludo, H. H., Maia Da Silva, F., et al. (2009). A New Genotype of *Trypanosoma Cruzi* Associated With Bats Evidenced by Phylogenetic Analyses Using SSU rDNA, Cytochrome B and Histone H2B Genes and Genotyping Based on ITS1 rDNA. *Parasitology* 136 (6), 641–655. doi: 10.1017/S0031182009005861
- Ocana-Mayorga, S., Llewellyn, M. S., Costales, J. A., Miles, M. A., and Grijalva, M. J. (2010). Sex, Subdivision, and Domestic Dispersal of *Trypanosoma Cruzi* Lineage I in Southern Ecuador. *PLoS Negl. Trop. Dis.* 4 (12), e915. doi: 10.1371/journal.pntd.0000915
- Ochsenreiter, T., Cipriano, M., and Hajduk, S. L. (2007). KISS: The Kinetoplastid RNA Editing Sequence Search Tool. *RNA* 13 (1), 1–4. doi: 10.1261/rna.232907
- Opperdoes, F. R., and Michels, P. A. (2008). Complex I of Trypanosomatidae: Does it Exist? *Trends Parasitol* 24 (7), 310–317. doi: 10.1016/j.pt.2008.03.013
- Pinto, C. M., Kalko, E. K., Cottontail, L., Wellinghausen, N., and Cottontail, V. M. (2012). TcBat a Bat-Exclusive Lineage of *Trypanosoma Cruzi* in the Panama Canal Zone, With Comments on its Classification and the Use of the 18S rRNA Gene for Lineage Identification. *Infect. Genet. Evol.* 12 (6), 1328–1332. doi: 10.1016/j.meegid.2012.04.013
- Reinert, K., Dadi, T. H., Ehrhardt, M., Hauswedell, H., Mehringer, S., Rahn, R., et al. (2017). The SeqAn C++ Template Library for Efficient Sequence Analysis: A Resource for Programmers. *J. Biotechnol.* 261, 157–168. doi: 10.1016/j.jbiotec.2017.07.017
- Reis-Cunha, J. L., Baptista, R. P., Rodrigues-Luiz, G. F., Coqueiro-Dos-Santos, A., Valdivia, H. O., de Almeida, L. V., et al. (2018). Whole Genome Sequencing of *Trypanosoma Cruzi* Field Isolates Reveals Extensive Genomic Variability and Complex Aneuploidy Patterns Within TcII DtU. *BMC Genomics* 19 (1), 816. doi: 10.1186/s12864-018-5198-4
- Renaud, G., Stenzel, U., and Kelso, J. (2014). leeHom: Adaptor Trimming and Merging for Illumina Sequencing Reads. *Nucleic Acids Res.* 42 (18), e141. doi: 10.1093/nar/gku699
- Reuter, J. S., and Mathews, D. H. (2010). Rnastructure: Software for RNA Secondary Structure Prediction and Analysis. *BMC Bioinf.* 11:129. doi: 10.1186/1471-2105-11-129
- Rusman, F., Florida-Yapur, N., Ragone, P. G., Diosque, P., and Tomasini, N. (2020). Evidence of Hybridization, Mitochondrial Introgression and Biparental Inheritance of the kDNA Minicircles in *Trypanosoma Cruzi* I. *PLoS Negl. Trop. Dis.* 14 (1), e0007770. doi: 10.1371/journal.pntd.0007770
- Rusman, F., Tomasini, N., Yapur, N. F., Puebla, A. F., Ragone, P. G., and Diosque, P. (2019). Elucidating Diversity in the Class Composition of the Minicircle Hypervariable Region of *Trypanosoma Cruzi*: New Perspectives on Typing and kDNA Inheritance. *PLoS Negl. Trop. Dis.* 13 (6), e0007536. doi: 10.1371/journal.pntd.0007536
- Ruvalcaba-Trejo, L. I., and Sturm, N. R. (2011). The *Trypanosoma Cruzi* Sylvio X10 Strain Maxicircle Sequence: The Third Musketeer. *BMC Genomics* 12:58. doi: 10.1186/1471-2164-12-58
- Savill, N. J., and Higgs, P. G. (1999). A Theoretical Study of Random Segregation of Minicircles in Trypanosomatids. *Proc. Biol. Sci.* 266 (1419), 611–620. doi: 10.1098/rspb.1999.0680
- Savill, N. J., and Higgs, P. G. (2000). Redundant and non-Functional Guide RNA Genes in *Trypanosoma Brucei* are a Consequence of Multiple Genes Per Minicircle. *Gene* 256 (1–2), 245–252. doi: 10.1016/S0378-1119(00)00345-0
- Schmid, B., Riley, G. R., Stuart, K., and Goring, H. U. (1995). The Secondary Structure of Guide RNA Molecules From *Trypanosoma Brucei*. *Nucleic Acids Res.* 23 (16), 3093–3102. doi: 10.1093/nar/23
- Simpson, L., Douglass, S. M., Lake, J. A., Pellegrini, M., and Li, F. (2015). Comparison of the Mitochondrial Genomes and Steady State Transcriptomes of Two Strains of the Trypanosomatid Parasite, *Leishmania Tarentolae*. *PLoS Negl. Trop. Dis.* 9 (7), e0003841. doi: 10.1371/journal.pntd.0003841
- Simpson, L., Frech, G. C., and Maslov, D. A. (1996). RNA Editing in Trypanosomatid Mitochondria. *Methods Enzymol.* 264, 99–121. doi: 10.1016/S0076-6879(96)64012-9
- Simpson, L., Neckelmann, N., de la Cruz, V. F., Simpson, A. M., Feagin, J. E., Jasmer, D. P., et al. (1987). Comparison of the Maxicircle (Mitochondrial) Genomes of *Leishmania Tarentolae* and *Trypanosoma Brucei* at the Level of Nucleotide Sequence. *J. Biol. Chem.* 262 (13), 6182–6196. doi: 10.1016/S0021-9258(18)45555-X
- Speijer, D. (2010). Constructive Neutral Evolution Cannot Explain Current Kinetoplastid Panediting Patterns. *Proc. Natl. Acad. Sci. U.S.A.* 107 (7), E25. doi: 10.1073/pnas.0909867107
- Stuart, K. (1993). The RNA Editing Process in *Trypanosoma Brucei*. *Semin. Cell Biol.* 4 (4), 251–260. doi: 10.1006/scel.1993.1030
- Telleria, J., Lafay, B., Virreira, M., Barnabe, C., Tibayrenc, M., and Svoboda, M. (2006). *Trypanosoma Cruzi*: Sequence Analysis of the Variable Region of Kinetoplast Minicircles. *Exp. Parasitol* 114 (4), 279–288. doi: 10.1016/j.exppara.2006.04.005
- Thomas, S., Martinez, L. L., Westenberg, S. J., and Sturm, N. R. (2007). A Population Study of the Minicircles in *Trypanosoma Cruzi*: Predicting Guide RNAs in the Absence of Empirical RNA Editing. *BMC Genomics* 8:133. doi: 10.1186/1471-2164-8-133
- Tomasini, N. (2018). Introgression of the Kinetoplast Dna: An Unusual Evolutionary Journey in *Trypanosoma Cruzi*. *Curr. Genomics* 19 (2), 133–139. doi: 10.2174/1389202918666170815124832
- Tomasini, N., and Diosque, P. (2015). Evolution of *Trypanosoma Cruzi*: Clarifying Hybridisations, Mitochondrial Introgressions and Phylogenetic Relationships Between Major Lineages. *Mem Inst Oswaldo Cruz* 110 (3), 403–413. doi: 10.1590/0074-02760140401

- Tomasini, N., Lauthier, J. J., Monje Rumi, M. M., Ragone, P. G., Alberti D'Amato, A. M., Brandan, C. P., et al. (2014). Preponderant Clonal Evolution of *Trypanosoma Cruzi* I From Argentinean Chaco Revealed by Multilocus Sequence Typing (Mlst). *Infect. Genet. Evol.* 27C, 348–354. doi: 10.1016/j.meegid.2014.08.003
- Turner, C. M., Hide, G., Buchanan, N., and Tait, A. (1995). *Trypanosoma Brucei*: Inheritance of Kinetoplast DNA Maxicircles in a Genetic Cross and Their Segregation During Vegetative Growth. *Exp. Parasitol.* 80 (2), 234–241. doi: 10.1006/expr.1995.1029
- Velazquez, M., Diez, C. N., Mora, C., Diosque, P., and Marcipar, I. S. (2008). *Trypanosoma Cruzi*: An Analysis of the Minicircle Hypervariable Regions Diversity and its Influence on Strain Typing. *Exp. Parasitol.* 120 (3), 235–241. doi: 10.1016/j.exppara.2008.07.016
- Westenberger, S. J., Cerqueira, G. C., El-Sayed, N. M., Zingales, B., Campbell, D. A., and Sturm, N. R. (2006). *Trypanosoma Cruzi* Mitochondrial Maxicircles Display Species- and Strain-Specific Variation and a Conserved Element in the non-Coding Region. *BMC Genomics* 7:60. doi: 10.1186/1471-2164-7-60
- Zingales, B., Andrade, S. G., Briones, M. R., Campbell, D. A., Chiari, E., Fernandes, O., et al. (2009). A New Consensus for *Trypanosoma Cruzi* Intraspecific Nomenclature: Second Revision Meeting Recommends TcI to TcVI. *Mem Inst Oswaldo Cruz* 104 (7), 1051–1054. doi: 10.1590/s0074-02762009000700021

Conflict of Interest: The authors declare that the research was conducted in the absence of any commercial or financial relationships that could be construed as a potential conflict of interest.

Copyright © 2021 Rusman, Floridia-Yapur, Tomasini and Diosque. This is an open-access article distributed under the terms of the Creative Commons Attribution License (CC BY). The use, distribution or reproduction in other forums is permitted, provided the original author(s) and the copyright owner(s) are credited and that the original publication in this journal is cited, in accordance with accepted academic practice. No use, distribution or reproduction is permitted which does not comply with these terms.



Development of a Fluorescent Assay to Search New Drugs Using Stable tdTomato-*Leishmania*, and the Selection of Galangin as a Candidate With Anti-Leishmanial Activity

María Fernanda García-Bustos^{1,2,3}, Agustín Moya Álvarez², Cecilia Pérez Brandan², Cecilia Parodi², Andrea Mabel Sosa², Valeria Carolina Buttazzoni Zuñiga¹, Oscar Marcelo Pastrana¹, Paula Manghera¹, Pablo Alejandro Peñalva¹, Jorge Diego Marco² and Paola Andrea Barroso^{2*}

OPEN ACCESS

Edited by:

Alberto Enrique Paniz Mondolfi,
Icahn School of Medicine at Mount
Sinai, United States

Reviewed by:

John Mina,
Teesside University, United Kingdom
Isabel Mauricio,
New University of Lisbon, Portugal

*Correspondence:

Paola Andrea Barroso
paolabarroso@conicet.gov.ar;
barrosopaola75@gmail.com

Specialty section:

This article was submitted to
Parasite and Host,
a section of the journal
Frontiers in Cellular
and Infection Microbiology

Received: 11 February 2021

Accepted: 17 May 2021

Published: 04 June 2021

Citation:

García-Bustos MF, Moya Álvarez A, Pérez Brandan C, Parodi C, Sosa AM, Buttazzoni Zuñiga VC, Pastrana OM, Manghera P, Peñalva PA, Marco JD and Barroso PA (2021) Development of a Fluorescent Assay to Search New Drugs Using Stable tdTomato-*Leishmania*, and the Selection of Galangin as a Candidate With Anti-Leishmanial Activity. *Front. Cell. Infect. Microbiol.* 11:666746. doi: 10.3389/fcimb.2021.666746

¹ Escuela Universitaria en Ciencias de la Salud y Facultad de Ciencias Agrarias y Veterinarias, Universidad Católica de Salta, Salta, Argentina, ² Instituto de Patología Experimental, Consejo Nacional de Investigaciones Científicas y Técnicas (CONICET) - Universidad Nacional de Salta, Salta, Argentina, ³ Facultad de Ciencias de la Salud, Universidad Nacional de Salta, Salta, Argentina

Antimonials continue to be considered the first-line treatment for leishmaniasis, but its use entails a wide range of side effects and serious reactions. The search of new drugs requires the development of methods more sensitive and faster than the conventional ones. We developed and validated a fluorescence assay based in the expression of tdTomato protein by *Leishmania*, and we applied this method to evaluate the activity *in vitro* of flavonoids and reference drugs. The pIR1SAT/tdTomato was constructed and integrated into the genome of *Leishmania (Leishmania) amazonensis*. Parasites were selected with nourseothricin (NTC). The relation of *L. amaz*/tc3 fluorescence and the number of parasites was determined; then the growth *in vitro* and infectivity in BALB/c mice was characterized. To validate the fluorescence assay, the efficacy of miltefosine and meglumine antimoniate was compared with the conventional methods. After that, the method was used to assess *in vitro* the activity of flavonoids; and the mechanism of action of the most active compound was evaluated by transmission electron microscopy and ELISA. A linear correlation was observed between the emission of fluorescence of *L. amaz*/tc3 and the number of parasites ($r^2 = 0.98$), and the fluorescence was stable in the absence of NTC. No differences were observed in terms of infectivity between *L. amaz*/tc3 and wild strain. The efficacy of miltefosine and meglumine antimoniate determined by the fluorescence assay and the microscopic test showed no differences, however, *in vivo* the fluorescence assay was more sensitive than limiting dilution assay. Screening assay revealed that the flavonoid galangin (GAL) was the most active compound with IC₅₀ values of 53.09 μ M and 20.59 μ M in promastigotes and intracellular amastigotes, respectively. Furthermore, GAL induced mitochondrial swelling, lipid inclusion bodies and vacuolization in promastigotes; and up-modulated the production of IL-12 p70 in infected

macrophages. The fluorescence assay is a useful tool to assess the anti-leishmanial activity of new compounds. However, the assay has some limitations in the macrophage-amastigote model that might be related with an interfere of flavanol aglycones with the fluorescence readout of tdTomato. Finally, GAL is a promising candidate for the development of new treatment against the leishmaniasis.

Keywords: tdTomato, *L. (L.) amazonensis*, flavonoids, galangin, fluorescence

INTRODUCTION

The leishmaniasis are a group of diseases caused by parasites of the genus *Leishmania*, which are transmitted to humans through the bite of infected female phlebotomine sandflies. These diseases in all their clinical expressions are endemic in 98 countries (Alvar et al., 2012), affecting mainly low income populations of the tropical and subtropical belt worldwide. According to the WHO report (2016), over one billion people live in endemic areas at risk of infection (World Health Organization, 2016), and an estimated 900.000 – 1.6 million new cases and 20.000 to 40.000 deaths occur annually (Alvar et al., 2012).

Depending on the infecting *Leishmania* species and the immune response of the host, leishmaniasis can exhibit a disease spectrum that includes visceral leishmaniasis or “kala-azar”, affecting mainly the mononuclear phagocytic system; as well as cutaneous (cutaneous leishmaniasis, CL) and mucosal forms (mucosal leishmaniasis, ML), which are characterized by involvement of skin and mucous membranes, respectively (McGwire and Satoskar, 2014).

The development of new therapeutic approaches for leishmaniasis treatment requires as well new high throughput screening methodologies for searching compounds with anti-leishmanial activity. Reporter gene (RG) technology has become one of the most promissory and widely used tool for drug screening in several models since it offers live imaging, high sensibility, specificity and flexibility (Pulido et al., 2012). These genes typically encode a gene product that has a readily measurable phenotype and is easily distinguishable over endogenous cellular background (Dube et al., 2009). Depending on the application, an ideal RG should be: (i) absent from the host; (ii) inert (should not affect the physiology of the parasite cell); and (iii) should represent a simple, sensitive, and inexpensive assay for quantification of reporter expression (Dube et al., 2009). The choice of a RG depends on the cell line used, the nature of the experiment, and the adaptability of the assay to the appropriate detection method (New et al., 2003).

Fluorescent RGs have been applied in the developing of new methods less laborious and more sensitive than the classical microscopy method for drug screening. The family of green fluorescent protein (GFP and multimeric gfp) was the most studied, but the main disadvantage of these RGs was the low level of fluorescence of transgenic parasites (Ha et al., 1996). Moreover, a background noise was observed, when *L. (L.) donovani* expressing the episomal GFP was used for the screening in intracellular

amastigotes and promastigotes generating a problem to automatize the technique (Dube et al., 2005). Another approach was to use the enhanced GFP (egfp) trying to improve the fluorescent signals. The transfected parasites showed stable expression of the fluorescent protein and the assay provided a more accurate approach in drug sensitivity profile, but it was not automated as a high-throughput (Bolhassani et al., 2011). Then, GFP integrated into the *Leishmania* genome was evaluated, the expression was very stable and homogeneous reducing the noise generated by similar episomal genetic manipulation (Pulido et al., 2012). This allows the development of automatized methodologies with the least background. Another RG, is tandem dimer Tomato (tdTomato), a variant of DsRed, derived from the coral *Discosoma* sp, which has demonstrated photostability and a high brightness (283% of eGFP) (Shaner et al., 2004; Morris et al., 2010). TdTomato has been used successfully in transgenic mouse models, fusion protein applications, and as a promoter-reporter (Morris et al., 2010). It also demonstrated to be useful in the generation of *Trypanosoma cruzi* parasite lines that express this fluorescent protein and the use of these lines to establish accurate and simple *in vitro* as well as *in vivo* systems to screen and test anti-*T. cruzi* compounds (Canavaci et al., 2010).

On the other hand, chemotherapy remains the major control strategy for leishmaniasis with meglumine antimoniate (Ma) enduring as the first-line treatment (Pan American Health Organization, 2013). However, its use in the clinical setting exhibits several limitations, given that they require an aggressive administration schedule (one or two intramuscular daily injections for 21 to 35 days), and often exhibit a wide range of local and systemic side effects. On the other hand, Pan American Health Organization (PAHO) recognizes that currently none of the drugs available for the treatment of leishmaniasis in the Americas completely eradicates the infection (PAHO, 2013). Given the above-mentioned reasons, the development of new, less toxic and more cost-effective drugs with greater efficacy as well as more accessible alternative therapeutic strategies that could become available for low-income populations to treat the disease has become a necessity (PAHO, 2013; Oryan, 2015).

In recent years, there has been growing interest in alternative natural products and plant compounds for the treatment of leishmaniasis (Chouhan et al., 2014). The anti-leishmanial activity of some plant extracts has been attributed to flavonoids (Wong et al., 2014). These are a group of polyphenolic compounds that naturally present in fruits and vegetables and are known as antioxidants and anticancer with a significant protective effect against membrane damage (Sifaoui et al., 2014).

Recently, we reported the activity of several catechins from *Camellia sinensis* against *L. (L.) amazonensis*, being EGCG the most active one (Sosa et al., 2020). This group of compound can form complexes with the parasite cell wall to influence processes requiring cell linking, and hence inhibit the parasite growth (Ogeto et al., 2013). In a research work carried out by Manjolin et al. (2013), it has been shown that dietary flavonoids with low cytotoxicity characteristics such as fisetin, quercetin, luteolin and 7,8-hydroxyflavone can inhibit arginase enzyme from *L. (L.) amazonensis*. Arginase plays a central role in the biosynthesis of polyamine which is very important and essential for protecting the parasite against oxidative stress and ROS produced by the host's defense system (Oryan, 2015). Therefore, natural compounds as flavonoids are an interesting group to search potential candidate with anti-leishmanial activity.

For all the aforementioned, the aims of this work were to develop and validate a fluorescence assay based in the expression of tdTomato protein by *Leishmania (L.) amazonensis*, and to apply this method to evaluate *in vitro* the activity of flavonoids and reference drugs. In addition, we studied the mechanism of action of one active compound selected through the *in vitro* screening assay.

MATERIALS AND METHODS

Compounds

Flavonoids: Flavonol: Galangin (GAL) – ≥95% (HPLC) (Sigma-Aldrich 282200), fisetin (FI) – P90% (HPLC) (PhytoLab PHL82542), rutin (RU) – ≥95.0% (HPLC) (PhytoLab PHL89270), morin (MO) – ≥95.0% (HPLC) (PhytoLab PHL82601). Flavanol: (-)-epigallocatechin gallate (EGCG) – >98% (HPLC) was kindly supplied by Mitsui Norin (Shizuoka, Japan).

Reference drugs: Pentamidine isethionate (PE) (Sigma-Aldrich P0547) and Miltefosine (MI) – ≥98.0% (perchloric acid titration) (Sigma-Aldrich M5571) were purchased from Sigma-Aldrich. Meglumine antimoniate (Ma) (Glucantime®, Aventis-Sanofi, São Paulo, Brazil) was kindly supplied by Ministerio de Salud de la Nación (Buenos Aires, Argentina).

Parasites

Parasites of *L. (L.) amazonensis* (MHOM/BR/73/M2269) were isolated from an infected mouse. First, the isolated parasites were cultured in Difco agar containing 20% defibrinated rabbit blood (USMARU medium) plus sterile proline balanced salts solution (PBSS) with 100 U/mL penicillin and 50 µg/mL streptomycin (P-S) at 23°C. After four days, the parasites were passaged to RPMI-1640 medium (Gibco, Grand Island, NY, USA) supplemented with 10% (v/v) heat-inactivated fetal bovine serum (FBS) and P-S.

PIR1SAT/tdTomato Plasmid Construction

The tandem dimeric tomato red fluorescent reporter gene (tdTomato, 1464 bp) was obtained by restriction enzyme digestion from the pTREX-tdTomato plasmid constructed for *Trypanosoma cruzi* (Canavaci et al., 2010). The fragment was

then gel purified and cloned into the expression site of pIR1SAT plasmid (Xba and Sal1). Correct insertion of the tdTomato gene was corroborated by digestion with selected restriction enzymes. For transfection, pIR1SAT-tdTomato plasmid was linearized with SmaI enzyme, gel purified and quantified. This plasmid integrates into the *Leishmania* genome by replacing one copy of the SSU rRNA gene which is transcribed by pol1 (Buckner and Wilson, 2005). pTREX-tdTomato and pIR1SAT plasmids were kindly provided by Dr. R.L. Tarleton (University of Georgia, USA) and Dr. S. Beverley (Washington University, USA), respectively. Additional information about tdTomato and its sequence can be found at the following link <https://www.fpbase.org/protein/tdtomato/>.

Transfection of *Leishmania*

Mid-log promastigotes of *L. (L.) amazonensis* were collected by centrifugation and washed once with phosphate buffer saline (PBS; pH 7.4) plus P-S. Then, parasites were resuspended in cold OPTI-MEM reduced serum medium (Gibco) at 1×10^8 /ml and the pIR1SAT-tdTomato (10 µg/ml) was added. The parasites and the plasmid were placed in a 2 mm gap electroporation cuvette (BTX Inc., San Diego, CA). The cuvette was chilled on ice for 10 min, then parasites were electroporated using an Electro Cell Manipulator 630 (BTX Inc.) set at 450 V, 0.025 Ω, and 500 µF. After electroporation, the cuvette was placed on ice for 10 min, then the parasites were transferred to USMARU medium for 24 h. One-day post-electroporation, nourseothricin (NTC) (50 µg/ml) was added to select parasites expressing the streptothricin acetyltransferase (SAT) gene. Resistant parasites were cloned in a Petri dish in USMARU medium plus RPMI-1640 with 10% SFB and NTC (50 µg/ml). A diagnostic PCR was carried out in 6 clones (C2, C3, C5, C11, C12 and C21) to confirm the insertion of tdTomato gene into the *Leishmania* genome. The sequence of the primers used is detailed in **Supplementary Material**.

Detection of Fluorescence Signal in Transfected Parasites and Its Correlation With the Number of Parasites

The fluorescence emission was measured in C2, C3, C5, C11, C12 and C21. Briefly, promastigotes in the log phase (1×10^6 /0.1ml) of each clone and promastigotes of the wild-type strain (*L. amaz/ wt*) were plated in a 96-well black culture plate with clear bottom (Nunc, USA) and incubated at 23°C. After 24 h of incubation, the fluorescence was measured in a fluorimeter plate reader Infinite F200 (Tecan, Männedorf, Switzerland) with the optics positioned under the bottom of the plate and the filters 535/25 for excitation and 595/35 for emission. A clone (*L. amaz/tc3*) was selected for subsequent *in vitro* and *in vivo* experiments.

To determine the correlation between the fluorescence signal and the number of parasites, *L. amaz/tc3* promastigote in the mid-log phase (3×10^7 , 1×10^7 , 3×10^6 , 1×10^6 , 3×10^5 , 1.2×10^5 , 4×10^4 cells/well) and *L. amaz/tc3* amastigotes (3×10^6 , 1×10^6 , 3×10^5 , 1×10^5 , 3×10^4 , 1.2×10^4 , 4×10^3 cells/well) were plated in 0.1 ml in a 96-well black culture plate with clear bottom (Nunc, USA). In the case of amastigotes, the parasites were isolated from a macrophage culture as was described previously (Chang, 1980).

Un-transfected parasites (*L. amaz/*wt) were the negative control. The fluorescence was measured in a fluorimeter plate reader (Tecan, Männedorf, Switzerland).

In Vitro Assessment of Transfected Parasites Growth

In order to evaluate if the growth of *L. amaz/tc3* was modified by the transfection with the RG, promastigotes (5×10^5 p/ml) were plated in triplicate in RPMI-1640 medium in a 96-well culture plate and the positive control was *L. amaz/*wt. At the 1st, 3rd and 7th day of incubation, the density (parasites/ml) was determined using a Neubauer chamber in an optic microscope (40x) (Leitz Wetzlar, Germany).

Then, the growth of intracellular amastigotes of *L. amaz/tc3* was evaluated. Raw 264.7 cells (5×10^4 /well) were cultured in complete RPMI-1640 and plated in 96-well black plate (Nunc, USA) for 3 h at 37°C in a 5% CO₂ for macrophage adherence. After that, macrophages were infected with promastigotes of *L. amaz/tc3* at different ratios, 1:5, 1:10 and 1:20 (macrophage: promastigotes), and incubated at 34°C in a 5% CO₂ overnight. Infected cultures were washed with pre-warmed PBS to remove free parasites. Macrophages without infection were the negative controls. The fluorescent was measured in a plate reader (Tecan, Männedorf, Switzerland) at 1st, 2nd, 3rd and 4th day of culture.

In Vitro, Fluorescent Assay Validation

Then, we evaluated the efficacy of MI, a reference drug for leishmaniasis by the fluorescence method (*L. amaz/tc3*) and by the conventional method based in counting the parasite at the optic microscope (*L. amaz/*wt). Mid-log promastigotes of *L. amaz/tc3* and *L. amaz/*wt were harvest and seeded (1×10^6 /0.1 ml) with different concentrations of MI (40 to 0.6 µg/ml) in a 96-well plate at 23°C. Promastigotes cultured only in medium were the controls. Parasite viability was determined by measuring the fluorescence of *L. amaz/tc3* in a plate reader (Tecan, Männedorf, Switzerland) and by counting the mobile promastigotes in a Neubauer chamber at the optic microscope (40x) (Leitz Wetzlar, Germany) at 48 h of incubation with MI. Viability was calculated with the formula: $Viability_{L. amaz/tc3} = \frac{FLt}{FLc} \times 100$ where, FLt is the fluorescence of treated culture, and FLc is the fluorescence of control; $Viability_{L. amaz/wt} = \frac{NPt}{NPc} \times 100$ where, NPt is the number of promastigotes in the treated culture, and NPc is the number of promastigotes in control culture. Then, the 50% inhibitory concentration (IC₅₀) of MI was estimated.

Furthermore, the efficacy of MI was also determined against intracellular amastigotes of *L. amaz/tc3* and *L. amaz/*wt. Raw 264.7 macrophages were plated in 96-well black plate (5×10^4 cells/well) and in eight well Lab-Tek tissue culture slides (6.6×10^4 cells/ml) (Nunc, USA). The cells were infected with promastigotes in stationary phase of *L. amaz/tc3* and *L. amaz/*wt (1:20 ratio) at 33°C, 5% CO₂. After incubation, the infected macrophages were washed to remove non-internalized parasites with PBS plus P-S. New RPMI-1640 medium with different concentrations of MI (20 to 0.62 µg/ml) was added to each well and incubated at 33°C, 5% CO₂ during 48 h. The anti-leishmanial activity of MI was determined by measuring the

fluorescence of intracellular amastigotes of *L. amaz/tc3* in a plate reader (Tecan, Männedorf, Switzerland). The viability was calculated as mentioned above, and the IC₅₀ was also estimated. Simultaneously, the leishmanicidal activity of MI against *L. amaz/*wt was determined by the microscopy test. In this case, the infected macrophages were stained with Diff Quik (Biopur S.R.L., Rosario, Argentina) and the number of intracellular amastigotes was determined in 200-500 macrophages in treated and control cultures per slide under the immersion lens microscope (100x) (Leitz Wetzlar, Germany). The infection index (II) and the % infectivity (I) were calculated by the following formulas: $II = IM \times A$, where IM= infected macrophages (%), A= number of amastigotes per infected macrophages; and $I(\%) = \frac{IIT}{IIC} \times 100$, where IIT= infection index in treated cultures, IIC= infection index in control cultures (Ayres et al., 2008). The IC₅₀ of MI was calculated.

Course of Infection of *L. amaz/tc3* in Mice

Mice were bred at the mouse facility of the Faculty of Health Sciences, National University of Salta (Salta, Argentina). Female BALB/c mice ($n = 5$) of 6 weeks of age were infected in their hind right footpad with the stationary phase promastigotes (5×10^6 parasites/0.05 ml) to evaluate the infectivity of *L. amaz/tc3*; animals infected with *L. amaz/*wt were the controls ($n = 5$). The footpad swelling was measured weekly with a digital caliper (150 mm; Digimess).

Efficacy of Ma in Mice Infected With *L. amaz/tc3*

Female BALB/c mice were infected in their hind right footpad with the stationary phase of promastigotes (5×10^6 parasites/0.05 ml) of *L. amaz/tc3*. Once a week the footpad swelling was measured with the digital caliper. Mice ($n = 5$) were treated with Ma in PBS (120 mg Sb/kg/day) starting at week 9 post-infection; the antimonial was administered by intraperitoneal injection (ip) once a day for 21 days. Control group ($n = 5$) received only PBS (ip). Within a week of finishing the Ma treatment, the parasite load was quantified by three methods, fluorescence (FL), optic microscope (OM) and limiting dilution assay (LD) in treated and control group. The FL method was carried out as follows, the hind right footpad was excised and weighed; then the tissue was homogenized using a glass grinder with 5 ml of complete RPMI-1640 medium and the intracellular amastigotes of *L. amaz/tc3* were released. A sample (0.1 ml) of the homogenate was centrifuged to replace the medium for PBS, then it was plated in duplicates in a 96-well black culture plate with clear bottom (Nunc, USA) and the fluorescence was measured in a plate reader (Tecan, Männedorf, Switzerland). Besides, a calibration curve was used to extrapolate the sample fluorescence to the number of amastigotes. For that, a pool of amastigotes from control samples was used; amastigotes (1×10^6 to 1.5×10^4) were plated in duplicates in a 96-well black culture plate with clear bottom, and the fluorescence was measured in a plate reader (Tecan, Männedorf, Switzerland). The number of amastigotes was adjusted to the weight of the sample.

Another sample of the tissue homogenate was used to quantify the parasite loads by direct counting in a Neubauer chamber under an optical microscope (40X) (Leitz Wetzlar, Germany), and the concentration of parasites (amastigotes/ml) of each homogenate was determined (Hill et al., 1983). The total number of parasites was adjusted to the weight of each tissue sample.

Finally, a sample of the tissue homogenate was also used to quantify the parasite loads by the LD assay (Lima et al., 1997). After serial dilutions in 96-well plates, the samples were incubated at 23°C for 14 days and the number of viable promastigotes was determined from the highest dilution at which the parasite could grow.

Drug Screening Against Promastigotes and Intracellular Amastigotes by the Fluorescence Assay

After fluorescence assay validation as it is described above, the method was used to evaluate *in vitro* the flavonoids anti-leishmanial activity. Mid-log promastigotes of *L. amaz/tc3* were harvest and seeded with different concentrations of GAL (1,200 to 18.75 μ M), MO, FI and RU (40 to 1.25 μ M), and EGCG (300 to 18.75 μ M). Positive control were promastigotes treated with PE (4 to 0.25 μ M), the negative control were promastigotes cultured with medium only, and the blank was the culture medium. The parasites were incubated at 23°C for 48 h. The anti-leishmanial activity was determined by measuring the parasite fluorescence in a plate reader (Tecan, Männedorf, Switzerland). The viability was estimated as was described above for MI (fluorescent assay). The IC₅₀ was calculated for each compound.

The flavonoids anti-leishmanial activity was also evaluated against intracellular amastigotes. Macrophages (Raw 264.7) were plated in 96-well black plate (5 x 10⁴ cell/well) and infected with promastigotes in stationary phase of *L. amaz/tc3* (1:20 ratio) at 33°C, 5% CO₂. After incubation, the infected macrophages were washed to remove non-internalized parasites with PBS plus P-S. New RPMI-1640 medium with different concentrations of GAL (30 to 3.75 μ M), MO (300 to 37.5 μ M), FI (65 to 8.12 μ M), RU (300 to 37.5 μ M) and EGCG (30 to 7.5 μ M) was added to each well and incubated at 33°C, 5% CO₂ for 48 h. Infected cells treated with Ma (136.6 to 34.1 μ M) were the positive controls, and cells incubated only with RPMI-1640 were the negative control. The infected macrophages were incubated during 48 h at 33°C, 5% CO₂. After treatment, the fluorescence of intracellular amastigotes of *L. amaz/tc3* was measured in a plate reader (Tecan, Männedorf, Switzerland). The viability was determined as was described for MI (fluorescent assay). The selectivity index (SI) (CC₅₀ for macrophages/IC₅₀ for *Leishmania*) was calculated. A SI higher than one, was considered more selective for activity against *Leishmania*, whereas a value lower than one was considered more selective for the activity against the macrophages (Tiuman et al., 2005).

All experiments in promastigotes and intracellular amastigotes were performed in duplicate or triplicate wells for each condition and repeated at least twice.

Drug Toxicity in a Macrophage Cell Line

The cytotoxicity against a cell line of macrophages (Raw 264.7) of GAL, MO, FI, RU, EGCG, PE, MI and MA was determined by the MTT method. Cells (3.3 x 10⁵/ml) cells were treated with different concentrations of each compound during 48 h at 37°C, 5% CO₂. The controls were incubated with RPMI-1640 medium. Briefly, 50 μ l of MTT (2 mg/mL) was added to each well and, after 4 h of incubation at 37°C, 5% CO₂, the reaction was stopped dissolving the formazan crystals with 100 μ l/well of dimethyl sulfoxide. The relative amount of formazan produced by viable macrophages was determined using a spectrophotometer at 595 nm. The percentage of viable cells was calculated according to the formula $\frac{(OD_{treated\ culture} - OD_{blank})}{(OD_{control} - OD_{blank})} \times 100$ as was described previously (Adinehbeigi et al., 2017). The cytotoxicity concentration 50% (CC₅₀) was calculated for each compound.

Analysis by Transmission Electron Microscopy

Ultrastructural alterations in *Leishmania* induced by flavonoids with anti-leishmanial activity were analyzed by transmission electron microscopy (TEM). Promastigotes of *L. amaz/tc3* (1 x 10⁶ parasites/ml) were exposed to the IC₅₀ of most active flavonoids selected in the drug screening. The control was a culture of *L. amaz/tc3* incubated in complete RPMI-1640 medium. After 48 h of incubation, samples of *L. amaz/tc3* promastigotes from each culture were fixed in modified Karnovsky's solution (formaldehyde [2.66%], glutaraldehyde [1.66%]) and PBS 0.1M (pH 7.4), and incubated overnight at 4°C. The fixed samples were post-fixed with a 1/1 solution of PBS/2% osmium tetroxide (OsO₄), overnight. Then the material was dehydrated and included in Spurr (Pelco, USA). Ultrathin sections were cut with an ultramicrotome (MT1, Sorvall, USA), mounted on copper grids, and contrasted with uranyl acetate (PELCO, USA) and lead citrate. The samples were observed with a Zeiss EM109 (Carl Zeiss, Oberkochen, Germany) transmission electron microscope, at CIME (Centro Integral de Microscopía Electrónica, CONICET-UNT-Tucumán, Argentina) and electron micrographs were taken.

Cytokine Production by Activated Macrophages

To evaluate if the most active flavonoid against *Leishmania* can active infected macrophages to produce IL-12p70 and IL-10 cytokines, macrophages (Raw 264.7) were infected with promastigotes (ratio 1:20) of *L. amaz/tc3* as was described previously in "Drug Screening Against Promastigotes and Intracellular Aastigotes by The Fluorescence Assay" section, and cultured in a 5% CO₂ incubator. Non-infected cells (2 x 10⁵ cells/mL) were cultured in RPMI-1640 medium plus 10% FCS and 1% antibiotics (P-S) and placed into 24 well plates. Cells were exposed to 5 μ g/ml of phytohaemagglutinin (PHA) (Sigma Aldrich, Missouri, USA), 5 μ g/ml of concanavalin A (CONA) (Sigma Aldrich, Missouri, USA); and the most active flavonoid selected against *Leishmania* (20 μ M) during 48 h. Then, the culture supernatant was recovered and maintained at -80°C until use. The culture supernatant concentrations of IL-12p70 and

IL-10 (BD Biosciences, San Diego, USA) were determined by ELISA following the specifications of the supplier. Each condition was performed in quadruplicate.

Statistical Analysis

The GraphPad Prism 5.0 software (GraphPad Software Inc., San Diego, CA, USA) was used to calculate the IC_{50} and CC_{50} values by nonlinear regression. Multiple comparisons of the parasite burden between groups were made with a one-way analysis of variance (ANOVA) followed by Tukey test. Comparisons between two groups were performed by Mann-Whitney (non-parametric t-test). The parasite loads obtained by the LD assay were estimated with the ELIDA software (Taswell, 1986). $p < 0.05$ was considered significant. For the analyses of culture supernatants by ELISA, continuous variables between two groups were compared with the Mann-Whitney U-test. A nonparametric Kruskal-Wallis test with Dunn's post-test was used to compare differences among multiple groups.

RESULTS

Generation of *L. (L.) Amazonensis* Expressing the tdTomato Protein

The pIR1SAT-tdTomato plasmid was linearized with *Swa*I restriction enzyme before transfection of *L. (L.) amazonensis*

parasites (**Figure 1A**). The linearized plasmid integrates into the *Leishmania* genome by replacing one copy of the SSU rRNA gene which is transcribed by pol1 (Buckner and Wilson, 2005). After the selection of transfected parasites with NTC, 6 clones out of the 23 (C2, C3, C5, C11, C12 and C21) were chosen randomly to confirm the genomic integration by PCR. The **Figure 1B** shows a schematic representation of the expected genomic loci after transfection and the primers used for PCR of selected clones. The pair of primers 3001-F and 3002-R hybridized outside the expression cassette and were used to corroborate insertion of the linearized plasmid. As we expected, PCR fragments of 1.1 kb (**Figure 1C**) and 2.1-2.9 kb (**Figure 1D**) were obtained when primers sets 3001-F/TOMA-R and F2999/3002-R were used respectively in the analysis of the 6 clones selected.

Detection of Fluorescence Signal in Transfected Parasites and Its Correlation With the Number of Parasites

The fluorescence signal was detected in the six clone selected (C2, C3, C5, C11, C12 and C21) after 24 h of incubation at 23°C (**Figure 1E**). Clone 11 was the only one that showed a lower fluorescence with respect to the others ($p < 0.05$) (**Figure 1E**); this could be related with the kinetic of different clone cultures, i.e. parasites in different stages of growth could be slightly different in its metabolism, affecting the transcriptional activity of the reporter gene.

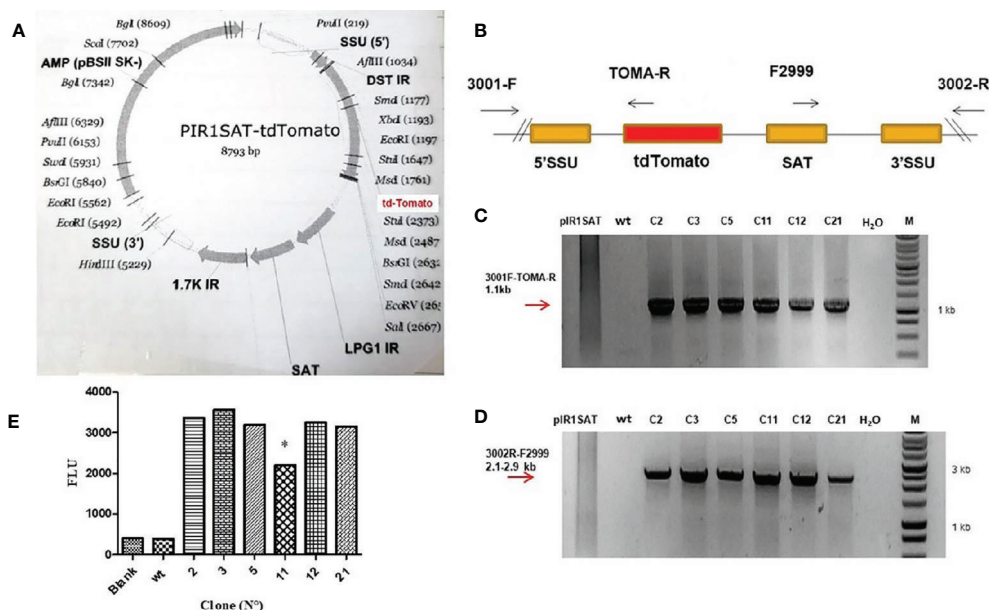


FIGURE 1 | (A) Map of the PIR1SAT-tdTomato plasmid indicating the enzyme used for cloning and linearization for *L. (L.) amazonensis* transfection assays.

(B) Schematic representation of expected genomic loci of transfected *Leishmania* after replacement of one copy of the SSU rRNA gene. **(C)** PCR genotyping analysis with primers 3001-F/TOMA-R confirming the expected gene insertion. **(D)** PCR genotyping analysis with primers 3002-R/F2999 also corroborating the correct insertion and replacement of SSU rRNA gene. Line 1: pIR1SAT-tdTomato plasmid, line 2: wild type parasites, lines 3-8: transfected clones, line 9: no template control (-), line 10: molecular weight and marker. Diagrams are not to scale. Numbers are sizes (kb) of expected products. **(E)** Detection of fluorescence emission in six clone selected (C2, C3, C5, C11, C12 and C21) after 24 h of incubation at 23°C ($p < 0.05$). Parasite wild-type (wt). Statistical significance was assessed using ANOVA ($*p < 0.05$).

The clone number 3 (*L. amaz/tc3*) was selected to carry out the subsequent *in vitro* and *in vivo* experiments. Promastigotes and amastigotes of *L. amaz/tc3* showed a good correlation between the fluorescence signal and the number of parasites ($p < 0.0001$) (Figures 2A, B).

In Vitro Assessment of Transfected Parasites Growth

On the first day of culture, the density of both, *L. amaz/tc3* and *L. amaz/wt*, increased almost 20 times (approximately to 1×10^7 p/ml). Then, from day 3 to 7, the density of fluorescent parasites and wild-type was stable showing the cultures were in the stationary phase (Figure 2C). No statistical differences were observed between the curve of growth of *L. amaz/tc3* and *L. amaz/wt*, indicating that transfection with the RG did not modified the normal parasite growth.

In addition, the growth of intracellular amastigotes of *L. amaz/tc3* was evaluated at different times and ratios of infection. The fluorescence signal increased with the infection time and reached a peak on the second day post-infection (pi) (Figure 2D). Besides, the fluorescence was significantly higher in macrophages infected at ratio 1:20 with respect to those infected at ratio 1:5 ($p < 0.001$) and 1:10 ($p < 0.05$) (Figure 2D). After that, the fluorescence started to decrease in all the infected cultures (4th day pi, data not shown).

Validation of the Fluorescence Assay

Once the fluorescence was detected in promastigote and amastigote of *L. amaz/tc3*, we evaluated if the fluorescence was a good indicator of the parasite viability after treatment with an anti-leishmanial drug. For that, MI was selected since it showed activity against promastigotes and amastigotes of several species

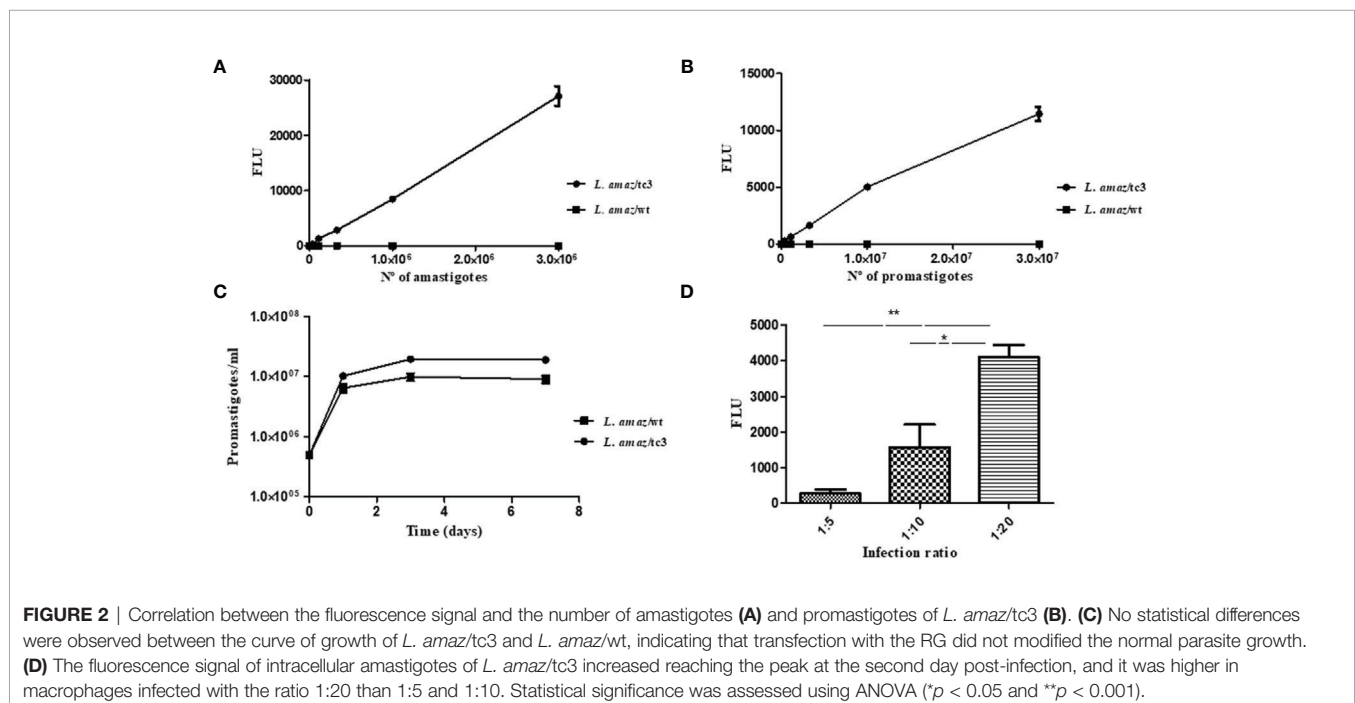
of *Leishmania*, and the efficacy of MI was determined by the fluorescent assay and by the conventional methods. After, 48 h of incubation with MI, promastigotes viability decrease, and no difference was observed between the values of IC_{50} determined by the fluorescence and microscopic test ($IC_{50} = 5.25 \pm 0.05 \mu\text{g/ml}$). In the same manner, MI inhibited the growth of intracellular amastigotes, and both methods showed similar results ($IC_{50} = 1.65 \pm 0.75 \mu\text{g/ml}$).

Course of Infection of *L. amaz/tc3* in Mice

The infectivity of *L. amaz/tc3* was evaluated in BALB/c mice. After infection, the footpad swelling increased weekly as did the wild strain. At week 5 pi, no differences in the footpad swelling were observed (Figure 3A).

Efficacy of Ma in Mice Infected With *L. amaz/tc3*

BALB/c mice were infected with *L. amaz/tc3* to evaluate the efficacy of Ma. The animals were treated with the antimonial for 21 days, once a day. After one week of treatment, the footpad swelling started to decrease and it still continued after ended the treatment (week 12-13) (Figure 3B). At week 13 of the experiment, a significant difference in the footpad swelling was observed between Ma and the control group ($p < 0.05$) (Figure 3B). In addition, differences highly significant were observed in the parasite burden between Ma and control group ($p < 0.001$) for FL and OM showing 55% and 75% of inhibition, respectively. On the other hand, we observed the parasite burden determined by LD assay was significantly lower ($p < 0.001$) in both groups, Ma and control, than those quantified by FL and OM; despite this, the inhibition percentage obtained by this assay was 54%, similar to those obtained for FL (Figures 3C, D).



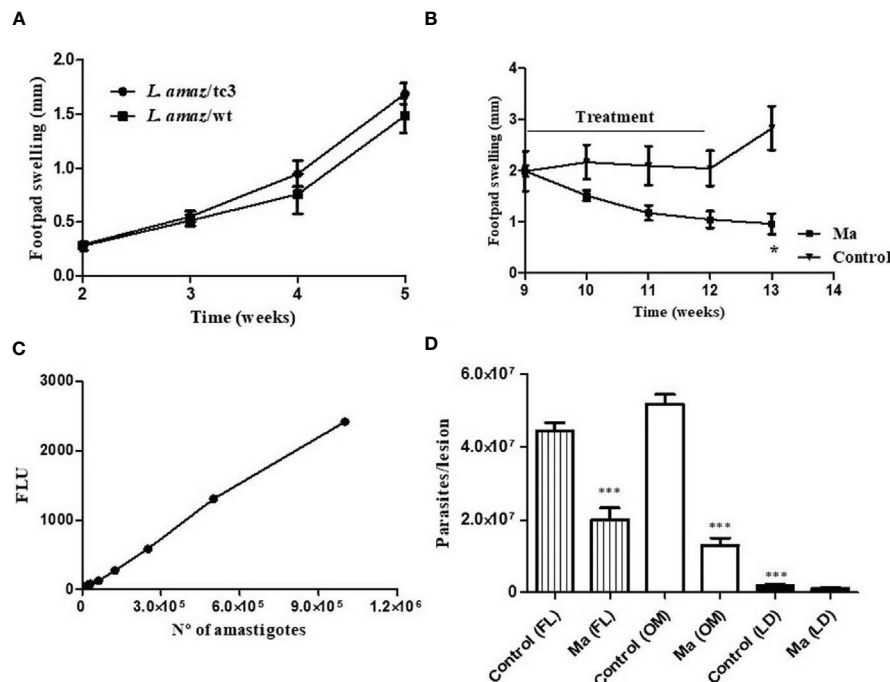


FIGURE 3 | (A) The infectivity of *L. amaz/tc3* in BALB/c mice was similar to the wild strain (*L. amaz/wt*). **(B)** Reduction in the footpad swelling in BALB/c mice infected with *L. amaz/tc3* and treated with meglumine antimoniate (MA) (120 mg Sb/kg/day) ($p < 0.05$). **(C)** Calibration curve, fluorescence and number of amastigotes isolated from mice infected with *L. amaz/tc3* ($r^2 = 0.99$, $p < 0.0001$). **(D)** Parasite load quantified, at week 13 of the experiment in mice treated with Ma and control group, by fluorescence method (FL), optic microscope (OM) and limiting dilution (LD). Statistical significance was assessed using Mann-Whitney U-test ($*p < 0.05$) and ANOVA ($***p < 0.001$). Data (mean \pm SD) are from a representative experiment ($n = 5$ mice).

Drug Screening Against Promastigotes and Intracellular Amastigotes by the Fluorescence Assay

First, the anti-leishmanial activity of a group of flavonols (GAL, MO, FI and RU) was assessed in promastigotes cultures. Also, we compared the activity of this group with EGCG, a catechin flavanol with leishmanicidal activity that we reported previously (Sosa et al., 2020). GAL showed activity on *L. amaz/tc3* and the IC_{50} value was 2.2 fold lower ($53.09 \pm 16.56 \mu\text{M}$) than EGCG ($119.8 \pm 17.6 \mu\text{M}$); while no inhibition in the parasite growth was observed for MO, FI and RU with doses $\leq 40 \mu\text{M}$. The reference drug PE, used as the positive control, was highly active against promastigotes ($IC_{50} = 0.67 \pm 0.18 \mu\text{M}$) after 48 h of incubation.

Then, we evaluated the efficacy of flavonols (GAL, MO, FI and RU), EGCG and the reference drug (Ma) in the

macrophage-amastigote model by the fluorescent assay. After treatment, the fluorescence was measured in the plate reader. The results caught our attention, since no relationship between the drug concentrations and the fluorescence was observed in GAL, MO and FI. The background fluorescence increased with concentrations $\geq 30 \mu\text{M}$ (GAL and FI) or $\geq 75 \mu\text{M}$ (MO), and it could neither be subtracted from the blank nor be eliminated by washing the cell culture. It is important to mention, the auto-fluorescence of macrophage cells and culture medium was very low compared to the fluorescence of td-tomato (data not shown). Therefore, we could not determine the IC_{50} for GAL, MO and FI by the fluorescent assay; instead, we estimated the percentage of amastigotes inhibition in those concentrations where the background did not interfere the fluorescence readout. GAL and FI showed a similar percentage of inhibition on the parasites (29–31%) with $15 \mu\text{M}$ (Table 1). On the other hand,

TABLE 1 | *In vitro* anti-leishmanial activity and cytotoxicity of flavonoids and the reference drug, MA.

| METHOD | | GAL | MO | RU | FI | EGCG | Ma |
|--------------------------|----------------------------|----------------------|----------------------|--------------------|----------------------|----------------------|----------------------|
| Microscopic Fluorescence | $IC_{50} \mu\text{M}$ (SE) | 20.59 (± 4.47) | 122.4 (± 2.55) | 133 (± 8.25) | > 60 | 130 (± 10.01) | ND |
| | $IC_{50} \mu\text{M}$ (SE) | ND | ND | 171 | ND | ND | 80.31 (± 14.7) |
| | Inhibition (%) | 29 | 13.5 | ND | 31 | 20 | ND |
| Colorimetric | $CC_{50} \mu\text{M}$ (SE) | 22.75 (± 2.87) | > 230.2 | > 240 | 52.57 (± 6.14) | 193.9 (± 23.8) | > 1,000 |
| | SI | 1.1 | > 1.8 | > 1.8 | < 1 | 1.5 | > 12.5 |

ND, Not determined; SE, Standard error; SI, Selectivity index = CC_{50} for macrophages/ IC_{50} for *Leishmania*.

MO showed a low inhibition (13.5%) against amastigotes at 37.5 μM . In the case of RU and Ma, not background fluorescence was detected, and the IC_{50} values were 171 μM and 80.31 μM , respectively (Table 1).

Then, to estimate the IC_{50} values of GAL, FI and MO; and to confirm the IC_{50} of RU, the activity was evaluated quantifying the intracellular amastigotes at the optic microscope. We followed the same methodology described for MI (microscopic assay) in “*In Vitro, Fluorescent Assay Validation*” section and the range of concentrations were for GAL (30 to 7.5 μM), FI (60 to 15 μM), RU and MO (200 to 50 μM), EGCG (142 a 17.7 μM). The IC_{50} of GAL ($20.59 \pm 4.47 \mu\text{M}$) was 5.9 and 6.4 times lower than the IC_{50} of MO ($122.4 \pm 2.55 \mu\text{M}$) and RU ($133 \pm 8.25 \mu\text{M}$), respectively. Furthermore, GAL was more active than the flavanol EGCG ($\text{IC}_{50} = 130 \pm 10.01 \mu\text{M}$) (Table 1).

Referred to the toxicity, GAL (SI = 1.1), MO (SI > 1.8), RU (SI > 1.8), EGCG (SI = 1.5) and Ma (SI > 12.5) were more selective against the parasites than the host cells with SI values higher than 1. Instead, FI was more selective against the host cells than the parasite (SI < 1) (Table 1).

GAL and EGCG Induced Ultrastructural Alterations in *Leishmania*

Through the *in vitro* drug screening, we found GAL was the most active compound against *Leishmania*. Thus, we investigated the effects of this compound on the ultrastructure of *L. amaz/tc3* promastigotes by transmission electron microscopy (TEM). In addition, we analyzed the effects of EGCG, another compound that also showed anti-leishmanial activity. As controls we used untreated *L. amaz/tc3* promastigotes. As we expected, control promastigotes presented a typical elongated morphology with normal cellular structures such as nucleus, lipid inclusion, mitochondrion, and flagellar pocket (Figure 4A). Both GAL and EGCG induced different alterations in the ultrastructure of

promastigotes, showing intense cellular damage (Figures 4B, C). GAL produced dramatic changes in the mitochondrial structure, with the formation of enlarged and swollen mitochondria compared to the untreated control, cytoplasmic lipid bodies as well an increase in plasma membrane blebs (surface blebbing) (Figure 4C). EGCG induced intense cytoplasmic vacuolization and also the presence of nuclear membrane detachment, chromatin condensation, and marginalization (Figure 4B). Moreover, the morphology of the parasites exposed to the drugs became visibly altered, with loss of most of the cytoplasmic organelles and a predominant round shape, confirming cellular death.

GAL Induced the Production of Th1 Cytokine in Infected Cultured Macrophages

We determined in the culture supernatant the concentration of two cytokines produced by activated macrophages: IL-12 p70, required for the induction of IFN- γ production; and IL-10, which is known to diminish the production of inflammatory mediators. We compared the production of IL-12 p70 and IL-10 between the different culture treated cells: infected and non-infected macrophages alone (RPMI medium) or exposed to PHA, CONA, and GAL. GAL was evaluated in this assay since this compound was the most active against *Leishmania*. Infected cells treated with GAL showed higher production of IL-12 p70 [mean (range) 232.2 pg/ml (137.5–331.7 pg/ml)] compared to infected non-stimulated controls (RPMI medium) [72.11 pg/ml (56.38–84.20 pg/ml)] ($p < 0.01$) (Figure 5A). Moreover, the addition of GAL to infected macrophages induced a significant increase of IL-12 p70 in comparison to non-infected macrophages treated with the same stimulus ($p < 0.05$) (Figure 5B). IL-10 concentration did not show significant differences between the different treated groups (data not shown).

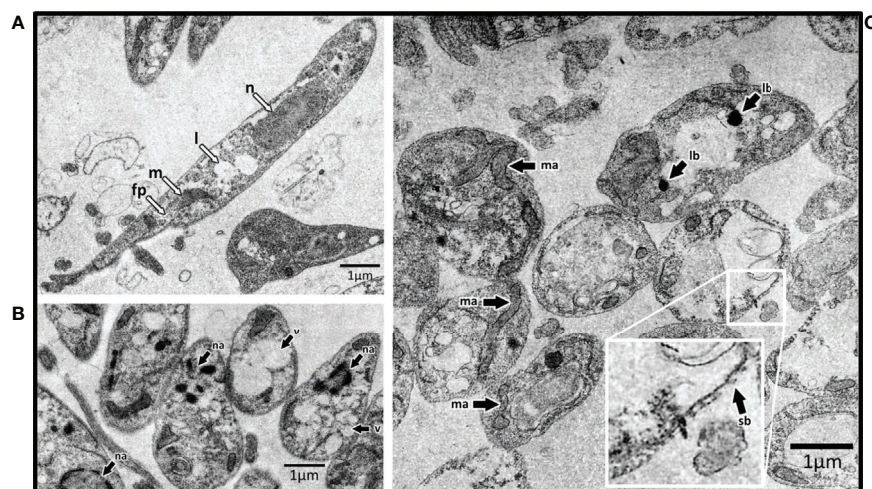


FIGURE 4 | Transmission electron microscopy of *L. amaz/tc3* promastigotes. (A) Untreated culture with normal cellular structures: nucleus (n), lipid inclusion (l), mitochondrion (m), and flagellar pocket (fp). Black arrows indicate ultrastructural alterations in parasites exposed to EGCG (B) and GAL (C) nuclear alterations (na), vacuolization (v), alterations in mitochondrial structure (ma), lipid-storage bodies (lb), and surface blebbing (sb).

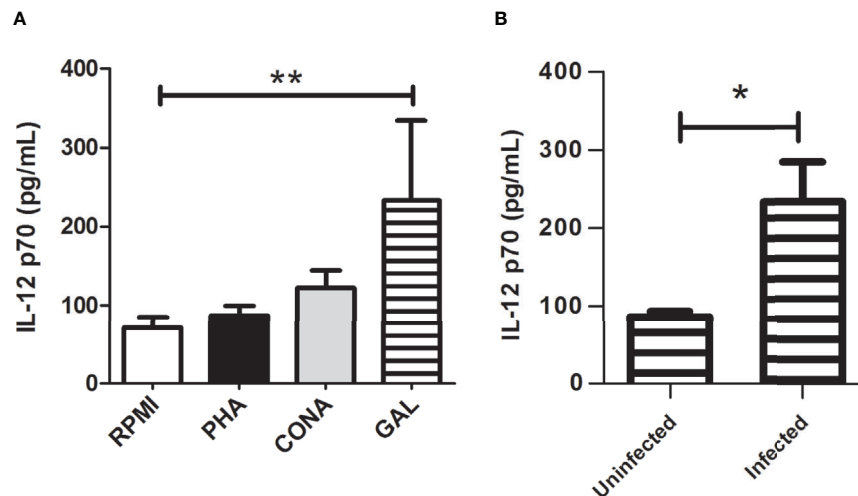


FIGURE 5 | Culture supernatant production of IL-12 p70 by *Leishmania* infected macrophages treated with GAL. **(A)** The amount of IL-12p70 was assessed in infected cultured RAW 264.7 macrophages maintained alone (RPMI) or treated with phytohemagglutinin (PHA), concanavalin A (CONA) and galangin (GAL). Each variable was performed in quadruplicate. Comparison among groups were assessed by Kruskal-Wallis test and Dunn's post-test (** $p < 0.01$). **(B)** Production of IL-12p70 after the addition of GAL to uninfected vs. infected cultured macrophages. Analysis performed by Mann Whitney test (* $p < 0.05$).

DISCUSSION

A search for new chemotherapeutic compounds for leishmaniasis diseases is still a challenge as well as the development of new methods to evaluate potential anti-leishmanial drugs. Moreover, the emergence of drug resistance and the treatment failure to antimonial make this search imperative (Agnew et al., 2001; García-Bustos et al., 2021).

In this sense, we obtained a clone of *L. (L.) amazonensis* (*L. amaz/tc3*) expressing the tdTomato. Its tandem dimer structure plays an important role in the exceptional brightness of this protein (283% of eGFP and 160% of DsRed) (Shaner et al., 2004). It is important to mention, that tdTomato gene was integrated into *Leishmania* genome by replacing a copy of SSU rRNA gene; this region has a high expression level since it is transcribed by polymerase 1, and it is highly conserved among *Leishmania* species (Buckner and Wilson, 2005).

As was expected, promastigotes and amastigotes of *L. amaz/tc3* showed a strong fluorescence signal, and it was correlated with the number of parasites. On the other hand, the genetic manipulation of parasites did not alter either, the *in vitro* growth, or the infectivity in BALB/c mice showing similar behavior to the wild-type strain (*L. amaz/wt*).

In vitro, the fluorescence assay was validated with MI since promastigote are not sensitive to MA (Robert et al., 1995). MI showed a similar efficacy against both *L. amaz/tc3* and the wild type (*L. amaz/wt*), indicating that transfection and the constitutive tdTomato expression did not affect the anti-leishmanial activity of the drug. The IC_{50} values determined for MI by the fluorescence assay in our study was consistent with the published data that demonstrated an effective dose of 1.31 μ g/ml and 7.54 μ g/ml for amastigotes and promastigotes of *L. (L.) amazonensis*, respectively (Escobar et al., 2002; Morais-Teixeira et al., 2011).

Then, the fluorescence assay was validated *in vivo*. BALB/c mice were infected with *L. amaz/tc3* and *L. amaz/wt* and treated with Ma, the drug efficacy was determined by fluorescence and LD assay. Both methods showed a similar percentage of inhibition in the parasite load (54-55%) at the end of treatment, but the fluorescence assay was more sensitivity than the LD. The sensitivity difference observed between the methods might be because LD assay only detect amastigotes capable of transforming into promastigotes and surviving in the medium culture; instead, the fluorescence assay quantifies all the amastigotes present in the crude extract of lesion macerate able of expressing the tdTomato protein. Besides, the parasite load determined by the fluorescent assay was consistent with the optic microscope indicating the amastigotes were viable. In agreement with our results, the luminescence assay in *ex vivo* tissue also showed a higher sensitivity than the LD (Reimão et al., 2013).

The fluorescence assay developed in this work, through the expression of tdTomato RG, was a simple system for drug screening. This method, unlike those based on catalytic reporter genes (β -lactamase, luciferase, β -galactosidase) (Okuno et al., 2003; Ashutosh et al., 2005; Buckner and Wilson, 2005), has the advantage that not require an addition of reagent, and the fluorescence readout can be done at different times of incubation. Besides, we highlight the stability of the fluorescence of *L. amaz/tc3*. We observed that transfected parasites showed fluorescence 6 months' post-infection in BALB/c mice (data not shown). The fluorescence stability in infected animals is important in studies that require a long period of evaluation like relapses of treatments or in vaccines studies. Furthermore, these transgenic parasites can be used at *in-vivo* experiments taking advantage of the tdTomato emission range, which is easily detected at 620 nm, outside of the range of most of the animal tissue auto-fluorescence (Canavaci et al., 2010).

Several fluorescent proteins, applied in drug screening assay, have been studied during the last three decades. The GFP was the most studied, but the main disadvantage of this RG was the low level of fluorescence of transgenic parasites (Ha et al., 1996). Then, trying to improve the fluorescent signals, egfp was studied. The transfected parasites showed stable expression of the fluorescent protein and the assay provided a more accurate approach in drug sensitivity profile, but it was not automated as a high-throughput (Bolhassani et al., 2011). On the contrary, our system was automatized using a plate reader, to measure the fluorescence in promastigotes drug screening and in amastigotes isolated from treated animals.

Through the fluorescence assay, we selected the flavonol GAL as the most active compound against promastigotes of *L. amaz/tc3*. Another work reported the activity of GAL isolated from *Alpinia galanga* rhizomes against promastigotes of *L. (L.) donovani*, the causal agent of visceral leishmaniasis, but the parasite inhibition was reached at 100 μ M (IC₅₀), (Kaur et al., 2010) almost twice the IC₅₀ in *L. amaz/tc3* determined in this work. The differences in the sensitivity might be related to the species of *Leishmania* as it was showed by Escobar et al. (2002).

It is worth to mention that in the macrophage-amastigote model, we observed an interference in the tdTomato fluorescence readout, and it increased with drug concentrations of GAL, MO and FI. This interference was not associated with the auto-fluorescence of macrophages and culture medium because they were very low compared to the tdTomato. Mukai et al. (2009) demonstrated that flavonol aglycones like GAL, MO, isorhamnetin and quercetin, presented auto-fluorescence (ex 488 nm and em 515–535 nm) in Hepa-1c1c7 cells treated with these compounds; moreover, it was concentration-dependent. They suggested the auto-fluorescence might be related with the hydroxyl group at the C3-position in the flavonol skeleton since no fluorescence was observed in the cells treated with compounds belonging to the flavone, flavanone and catechin subclasses. Therefore, we hypothesized the interference in the tdTomato readout might be due to an overlap between the extremes of the emission spectra of tdTomato and green fluorescence of the flavonol aglycones when they are excited at 535 nm. On the other hand, we did not observe interference in the tdTomato fluorescence readout when infected macrophages were treated with RU and Ma and we could determine the IC₅₀ of these compound. The activity of GAL, MO, FI and EGCG was determined by optic microscopy.

After all, GAL was the most active compound against promastigotes and amastigotes of *L. amaz/tc3*. GAL produced morphological alterations on mitochondria and plasma membrane of promastigotes of *L. amaz/tc3* with loss of the cytoplasmic organelles. Moreover, the ability of GAL to induce IL-12p70 up-regulation by *Leishmania* infected macrophages *in vitro* indicates that this natural compound could play an important role in the eradication of the invading parasites. Optimal production of both fractions of IL-12 (p40 and p70) is required to drive a predominant T helper 1 response with the subsequent IFN- γ production, macrophage activation and NO-mediating effects needed to kill the pathogens (Mattner et al., 1996; Guler et al., 2011).

All these data demonstrates that the fluorescence assay, based on the stable expression of the tdTomato protein by *L. (L.) amazonensis*, is a useful tool to assess the anti-leishmanial activity of new drugs. However, some interference in the tdTomato readout can occur in the macrophage-amastigote model when flavonol aglycones are been testing. Further studies are necessary to identify if there are others natural compounds that might affect the performance of the fluorescence assay. Besides, the present study demonstrated the potential inhibitory effect of GAL against *L. (L.) amazonensis* and its capacity to induce the production of IL-12 p70, a cytokine related to a Th1 response (cure); therefore, these results encourage us to study its efficacy in animal model in near future.

DATA AVAILABILITY STATEMENT

The original contributions presented in the study are included in the article/**Supplementary Material**. Further inquiries can be directed to the corresponding author.

ETHICS STATEMENT

The animal study was reviewed and approved by Animal Ethics Committee of the Faculty of Health Sciences, National University of Salta, Salta, Argentina (Resolution N° 309–18).

AUTHOR CONTRIBUTIONS

MG-B, PB, CPB, AM, CP, JM, AS, VB, OP, PM, and PP performed experiments. MG-B, PB, CPB, CP, and JM analyzed data. MG-B and PB designed experiments. MG-B and PB drafted the manuscript. All authors contributed to the article and approved the submitted version.

FUNDING

This work was funded by Agencia Nacional de Promoción Científica y Tecnológica and by GLAXO, PICT-O 2011-0017 (PB), by the Research Council of the Catholic University of Salta, Argentina (Grant Resolution 1494/16) and by the Research Council of the National University of Salta (Type B Project No. 2411) (MG-B).

ACKNOWLEDGMENTS

The authors thank to Med. Vet. Maria Celia Mora and to the technicians Alejandro Uncos, Federico Ramos and Renato Uncos for the technical supports *in vivo* assays; and to the technicians Cecilia Gallardo, Walter Ferrari and Manuel Siñeriz Louis for technical assistance in the TEM experiments. We also thank to Dr. Carl Taswell who kindly provided us the ELIDA software, to

Dr. Stephen Beverley for providing us the pIRISAT plasmid, and to Dr. R.L. Tarleton who provide us the pTREX-tdTomato plasmid. Finally, we thank to Mitsui Norin (Shizuoka, Japan) for providing us the EGCG, and to the Ministerio de Salud de la Nación (Buenos Aires, Argentina) for supplying us the MA.

REFERENCES

- Adinehbeigi, K., Razi Jalali, M. H., Shahriari, A., and Bahrami, S. (2017). *In Vitro* Antileishmanial Activity of Fisetin Flavonoid Via Inhibition of Glutathione Biosynthesis and Arginase Activity in *Leishmania Infantum*. *Pathog. Glob. Health* 111, 176–185. doi: 10.1080/20477724.2017.1312777
- Agnew, P., Holzmüller, P., Michalakakis, Y., Sereno, D., Lemesre, J. L., and Renaud, F. (2001). *In Vitro* Growth of *Leishmania Amazonensis* Promastigotes Resistant to Pentamidine Is Dependent on Interactions Among Strains. *Antimicrob. Agents Chemother.* 45, 1928–1929. doi: 10.1128/AAC.45.6.1928-1929.2001
- Alvar, J., Vélez, I. D., Bern, C., Herrero, M., Desjeux, P., Cano, J., et al. (2012). Leishmaniasis Worldwide and Global Estimates of its Incidence. *PLoS One* 7, e35671. doi: 10.1371/journal.pone.0035671
- Ashutosh, Gupta, S., Ramesh, S., Sundar, S., and Goyal, N. (2005). Use of *Leishmania Donovanii* Field Isolates Expressing the Luciferase Reporter Gene in *In Vitro* Drug Screening. *Antimicrob. Agents Chemother.* 49 (9), 3776–3783. doi: 10.1128/AAC.49.9.3776-3783.2005
- Ayres, D. C., Pinto, L. A., and Giorgio, S. (2008). Efficacy of Pentavalent Antimony, Amphotericin B, and Miltefosine in *Leishmania Amazonensis*-Infected Macrophages Under Normoxic and Hypoxic Conditions. *J. Parasitol.* 94, 1415–1417. doi: 10.1645/GE-1613.1
- Bolhassani, A., Taheri, T., Taslimi, Y., Zamanilui, S., Zahedifard, F., Seyed, N., et al. (2011). Fluorescent *Leishmania* Species: Development of Stable GFP Expression and its Application for *In Vitro* and *In Vivo* Studies. *Exp. Parasitol.* 127 (3), 637–645. doi: 10.1016/j.exppara.2010.12.006
- Buckner, F. S., and Wilson, A. J. (2005). Colorimetric Assay for Screening Compounds Against *Leishmania* Amastigotes Grown in Macrophages. *Am. J. Trop. Med. Hyg.* 72, 600–605. doi: 10.4269/ajtmh.2005.72.600
- Canavaci, A. M. C., Bustamante, J. M., Padilla, A. M., Perez Brandan, C. M., Simpson, L. J., Xu, D., et al. (2010). *In Vitro* and *In Vivo* High-Throughput Assays for the Testing of Anti-*Trypanosoma Cruzi* Compounds. *PLoS Negl. Trop. Dis.* 4, e740. doi: 10.1371/journal.pntd.0000740
- Chang, K. P. (1980). Human Cutaneous Leishmania in a Mouse Macrophage Line: Propagation and Isolation of Intracellular Parasites. *Science* 209, 1240–1242. doi: 10.1126/science.7403880
- Chouhan, G., Islamuddin, M., Sahal, D., and Afrin, F. (2014). Exploring the Role of Medicinal Plant-Based Immunomodulators for Effective Therapy of Leishmaniasis. *Front. Immunol.* 5, 193. doi: 10.3389/fimmu.2014.00193
- Dube, A., Gupta, R., and Singh, N. (2009). Reporter Genes Facilitating Discovery of Drugs Targeting Protozoan Parasites. *Trends Parasitol.* 25, 432–439. doi: 10.1016/j.pt.2009.06.006
- Dube, A., Singh, N., Sundar, S., and Singh, N. (2005). Refractoriness to the Treatment of Sodium Stibogluconate in Indian Kala-Azar Field Isolates Persist in *In Vitro* and *In Vivo* Experimental Models. *Parasitol. Res.* 96, 216–223. doi: 10.1007/s00436-005-1339-1
- Escobar, P., Matu, S., Marques, C., and Croft, S. L. (2002). Sensitivities of *Leishmania* Species to Hexadecylphosphocholine (Miltefosine), ET-18-OCH₃ (Edelfosine) and Amphotericin B. *Acta Trop.* 81, 151–157. doi: 10.1016/S0001-706X(01)00197-8
- García-Bustos, M. F., González-Prieto, G., Pániz-Mondolfi, A. E., Parodi, C., Becker, J., Monroig, S., et al. (2021). Risk Factors for Antimony Treatment Failure in American Cutaneous Leishmaniasis in Northwestern-Argentina. *PLoS Negl. Trop. Dis.* 15, e0009003. doi: 10.1371/journal.pntd.0009003
- Guler, R., Afshar, M., Arendse, B., Parihar, S. P., Revaz-Breton, M., Leitges, M., et al. (2011). PKC δ Regulates IL-12p40/p70 Production by Macrophages and Dendritic Cells, Driving a Type 1 Healer Phenotype in Cutaneous Leishmaniasis. *Eur. J. Immunol.* 41, 706–715. doi: 10.1002/eji.201040985
- Ha, D. S., Schwarz, J. K., Turco, S. J., and Beverley, S. M. (1996). Use of the Green Fluorescent Protein as a Marker in Transfected *Leishmania*. *Mol. Biochem. Parasitol.* 77, 57–64. doi: 10.1016/0166-6851(96)02580-7
- Hill, J. O., North, R. J., and Collins, F. M. (1983). Advantages of Measuring 833 Changes in the Number of Viable Parasites in Murine Models of Experimental Cutaneous Leishmaniasis. *Infect. Immun.* 39, 1087–1094. doi: 10.1128/IAI.39.3.1087-1094.1983
- Kaur, A., Singh, R., Dey, C. S., Sharma, S. S., Bhutani, K. K., and Singh, I. P. (2010). Antileishmanial Phenylpropanoids From *Alpinia Galanga* (Linn.) Willd. *Indian J. Exp. Biol.* 48, 314–317.
- Lima, H. C., Bleyenbergh, J. A., and Titus, R. G. (1997). A Simple Method for Quantifying *Leishmania* in Tissues of Infected Animals. *Parasitol. Today* 13, 80–82. doi: 10.1016/S0169-4758(96)40010-2
- Manjolin, L. C., dos Reis, M. B., Maquiaveli do Carmo, C., Santos-Filho, O. A., and da Silva, E. R. (2013). Dietary Flavonoids Fisetin, Luteolin and Their Derived Compounds Inhibit Arginase, A Central Enzyme in *Leishmania (Leishmania) Amazonensis* Infection. *Food. Chem.* 141, 2253–2262. doi: 10.1016/j.foodchem.2013.05.025
- Mattner, F., Magram, J., Ferrante, J., Launois, P., Di Padova, K., Behin, R., et al. (1996). Genetically Resistant Mice Lacking Interleukin-12 Aresusceptible to Infection With *Leishmania Major* and Mount a Polarized Th2cell Response. *Eur. J. Immunol.* 26, 1553–1559. doi: 10.1002/eji.1830260722
- McGwire, B. S., and Satoskar, A. R. (2014). Leishmaniasis: Clinical Syndromes and Treatment. *QJM* 107, 7–14. doi: 10.1093/qjmed/hct116
- Morais-Teixeira, E., Damasceno, Q., Galuppo, M., Kolos, R., Romanha, A. J., and Rabello, A. (2011). The *In Vitro* Leishmanicidal Activity of Hexadecylphosphocholine (Miltefosine) Against Four Medically Relevant *Leishmania* Species of Brazil. *Mem. Inst. Oswaldo Cruz* 106, 475–478. doi: 10.1590/S0074-02762011000400015
- Morris, L. M., Klanke, C. A., Lang, S. A., Lim, F. Y., and Crombleholme, T. M. (2010). TdTomato and EGFP Identification in Histological Sections: Insight and Alternatives. *Biotech. Histochem.* 85, 379–387. doi: 10.3109/10520290903504753
- Mukai, R., Shirai, Y., Saito, N., Yoshida, K., and Ashida, H. (2009). Subcellular Localization of Flavonol Aglycone in Hepatocytes Visualized by Confocal Laser Scanning Fluorescence Microscope. *Cytotechnology* 59, 177–182. doi: 10.1007/s10616-009-9206-z
- New, D. C., Miller-Martini, D. M., and Wong, Y. H. (2003). Reporter Gene Assays and Their Applications to Bioassays of Natural Products. *Phytother. Res.* 17, 439–448. doi: 10.1002/ptr.1312
- Ogato, T. K., Odhiambo, R. A., Shivairo, R. S., Muleke, C. I., Osero, B. O., Anjili, C., et al. (2013). Antileishmanial Activity of *Aloe Secundiflora* Plant Extracts Against *Leishmania Major*. *Adv. Life. Sci. Technol.* 13, 9–18.
- Okuno, T., Goto, Y., Matsumoto, Y., Otsuka, H., and Matsumoto, Y. (2003). Applications of Recombinant *Leishmania Amazonensis* Expressing Egfp or the Beta-Galactosidase Gene for Drug Screening and Histopathological Analysis. *Exp. Anim.* 52 (2), 109–118. doi: 10.1538/expanim.52.109
- Oryan, A. (2015). Plant-Derived Compounds in Treatment of Leishmaniasis. *Iran J. Vet. Res.* 16, 1–19.
- Pan American Health Organization (2013) *Leishmaniasis in the Americas. Recommendations for Treatment*. Available at: <http://iris.paho.org/xmlui/handle/123456789/7704> (Accessed December 18, 2020).
- Pulido, S. A., Muñoz, D. L., Restrepo, A. M., Mesa, C., Alzate, J. F., Vélez, I. D., et al. (2012). Improvement of the Green Fluorescent Protein Reporter System in *Leishmania* Spp. for the *In Vitro* and *In Vivo* Screening of Antileishmanial Drugs. *Acta Trop.* 122 (1), 36–45. doi: 10.1016/j.actatropica.2011.11.015
- Reimão, J. Q., Trinconi, C. T., Yokoyama-Yasunaka, J. K., Miguel, D. C., Kalil, S. P., and Uliana, S. R. B. (2013). Parasite Burden in *Leishmania (Leishmania) Amazonensis*-Infected Mice: Validation of Luciferase as a Quantitative Tool. *J. Microbiol. Methods* 93, 95–101. doi: 10.1016/j.mimet.2013.02.007
- Robert, W. L., Berman, J. D., and Rainey, P. M. (1995). *In Vitro* Antileishmanial Properties of Tri- and Pentavalent Antimonial Preparations. *Antimicrob. Agents Chemother.* 39, 1234–1239. doi: 10.1128/aac.39.6.1234

SUPPLEMENTARY MATERIAL

The Supplementary Material for this article can be found online at: <https://www.frontiersin.org/articles/10.3389/fcimb.2021.666746/full#supplementary-material>

- Shaner, N. C., Campbell, R. E., Steinbach, P. A., Giepmans, B. N. G., Palmer, A. E., and Tsien, R. Y. (2004). Improved Monomeric Red, Orange and Yellow Fluorescent Proteins Derived From *Discosoma Sp.* Red Fluorescent Protein. *Nat. Biotechnol.* 22, 1567–1572. doi: 10.1038/nbt1037
- Sifaoui, I., Lopez-Arencibia, A., Martin-Navarro, C. M., Chammem, N., Reyes-Battle, M., Mejri, M., et al. (2014). Activity of Olive Leaf Extracts Against the Promastigote Stage of *Leishmania* Species and Their Correlation With the Antioxidant Activity. *Exp. Parasitol.* 141, 106–111. doi: 10.1016/j.exppara.2014.03.002
- Sosa, A. M., Moya Álvarez, A., Bracamonte, E., Korenaga, M., Marco, J. D., and Barroso, P. A. (2020). Efficacy of Topical Treatment With (–)-Epigallocatechin Gallate, a Green Tea Catechin, in Mice With Cutaneous Leishmaniasis. *Molecules* 25, 1741. doi: 10.3390/molecules25071741
- Taswell, C. (1986). “Limiting Dilution Assays for the Separation, Characterization and Quantification of Biologically Active Particles and Their Clonal Progeny”, in *Cell Separation: Methods and Selected Applications*. Eds. T. G. Pretlow and T. P. Pretlow (New York, NY, USA: Academic Press), 109–145.
- Tiuman, T. S., Ueda-Nakamura, T., Garcia Cortez, D. A., Dias Filho, B. P., Morgado-Díaz, J. A., de Souza, W., et al. (2005). Antileishmanial Activity of Parthenolide, A Sesquiterpene Lactone Isolated From *Tanacetum Parthenium*. *Antimicrob. Agents Chemother.* 49, 176–182. doi: 10.1128/AAC.49.11.176-182.2005
- Wong, I. L., Chan, K. F., Chen, Y. F., Lun, Z. R., Chan, T. H., and Chow, L. M. (2014). *In Vitro* and *In Vivo* Efficacy of Novel Flavonoid Dimers Against Cutaneous Leishmaniasis. *Antimicrob. Agents Chemother.* 58, 3379–3388. doi: 10.1128/AAC.02425-13
- World Health Organization (2016) *Leishmaniasis in High-Burden Countries: An Epidemiological Update Based on Data Reported in 2014*. Available at: <https://www.who.int/wer/2016/wer9122.pdf?ua=1> (Accessed November 15, 2020).

Conflict of Interest: The authors declare that the research was conducted in the absence of any commercial or financial relationships that could be construed as a potential conflict of interest.

Copyright © 2021 García-Bustos, Moya Álvarez, Pérez Brandan, Parodi, Sosa, Buttazzoni Zuñiga, Pastrana, Manghera, Peñalva, Marco and Barroso. This is an open-access article distributed under the terms of the Creative Commons Attribution License (CC BY). The use, distribution or reproduction in other forums is permitted, provided the original author(s) and the copyright owner(s) are credited and that the original publication in this journal is cited, in accordance with accepted academic practice. No use, distribution or reproduction is permitted which does not comply with these terms.



The Complete Mitochondrial DNA of *Trypanosoma cruzi*: Maxicircles and Minicircles

OPEN ACCESS

Francisco Callejas-Hernández^{1†‡}, Alfonso Herreros-Cabello^{1‡}, Javier del Moral-Salmoral¹, Manuel Fresno^{1,2*§} and Núria Gironès^{1,2*§}

Edited by:

Emilia Mia Sordillo,
Icahn School of Medicine
at Mount Sinai, United States

Reviewed by:

Sergio Schenkman,
Federal University of São Paulo,
Brazil
Veronica Jimenez,
California State University, Fullerton,
United States
Lissa Cruz Saavedra,
Rosario University, Colombia

*Correspondence:

Núria Gironès
ngirones@cbm.csic.es
Manuel Fresno
mfresno@cbm.csic.es

†Present address:

Francisco Callejas-Hernández,
Center for Genomics and Systems
Biology, Department of Biology,
New York University, New York,
NY, United States

[‡]These authors have contributed
equally to this work and
share first authorship

[§]These authors have contributed
equally to this work and
share last authorship

Specialty section:

This article was submitted to
Parasite and Host,
a section of the journal
Frontiers in Cellular and
Infection Microbiology

Received: 25 February 2021

Accepted: 04 June 2021

Published: 29 June 2021

¹ Centro de Biología Molecular Severo Ochoa, Consejo Superior de Investigaciones Científicas, Universidad Autónoma de Madrid, Madrid, Spain, ² Instituto Sanitario de Investigación de la Princesa, Group 12, Madrid, Spain

The mitochondrial DNA of Trypanosomatids, known as the kinetoplast DNA or kDNA or mtDNA, consists of a few maxicircles and thousands of minicircles concatenated together into a huge complex network. These structures present species-specific sizes, from 20 to 40 Kb in maxicircles and from 0.5 to 10 Kb in minicircles. Maxicircles are equivalent to other eukaryotic mitochondrial DNAs, while minicircles contain coding guide RNAs involved in U-insertion/deletion editing processes exclusive of Trypanosomatids that produce the maturation of the maxicircle-encoded transcripts. The knowledge about this mitochondrial genome is especially relevant since the expression of nuclear and mitochondrial genes involved in oxidative phosphorylation must be coordinated. In *Trypanosoma cruzi* (*T. cruzi*), the mtDNA has a dual relevance; the production of energy, and its use as a phylogenetic marker due to its high conservation among strains. Therefore, this study aimed to assemble, annotate, and analyze the complete repertoire of maxicircle and minicircle sequences of different *T. cruzi* strains by using DNA sequencing. We assembled and annotated the complete maxicircle sequence of the Y and Bug2148 strains. For Bug2148, our results confirm that the maxicircle sequence is the longest assembled to date, and is composed of 21 genes, most of them conserved among Trypanosomatid species. In agreement with previous results, *T. cruzi* minicircles show a conserved structure around 1.4 Kb, with four highly conserved regions and other four hypervariable regions interspersed between them. However, our results suggest that the parasite minicircles display several sizes and numbers of conserved and hypervariable regions, contrary to those previous studies. Besides, this heterogeneity is also reflected in the three conserved sequence blocks of the conserved regions that play a key role in the minicircle replication. Our results using sequencing technologies of second and third-generation indicate that the different consensus sequences of the maxicircles and minicircles seem to be more complex than previously described indicating at least four different groups in *T. cruzi* minicircles.

Keywords: kinetoplast DNA, maxicircle, minicircle, strain, *Trypanosoma cruzi*

INTRODUCTION

Trypanosoma cruzi is a unicellular eukaryotic organism that causes the Chagas disease or American Trypanosomiasis, a chronic endemic illness of Latin America, and a neglected tropical disease (Pérez-Molina and Molina, 2018). Nowadays, it has been estimated that there are around 6–7 million of chronically infected people (World Health Organization). This parasite has a very complex life cycle that includes an invertebrate hematophagous triatomine vector and a broad range of mammalian hosts (Clayton, 2010). Also, *T. cruzi* has different biological stages (de Souza et al., 2010; Rodrigues et al., 2014). The non-infective epimastigotes are present in the midgut of triatomines where they differentiate into infective metacyclic trypomastigotes, that after the infection of host cells are differentiated into the replicative amastigote stages and subsequently into infective trypomastigotes that reach the bloodstream (Echeverría and Morillo, 2019). Chagas disease presents an acute phase with low mortality and symptomatology. Then, the patients can remain in an asymptomatic chronic phase for life or in the 30–40% of them will produce after 10–30 years chronic myocarditis, megavisceras, or both (Rassi et al., 2012).

T. cruzi is characterized for showing a great genomic heterogeneity and plasticity across strains (Reis-Cunha et al., 2015; Callejas-Hernández et al., 2018; Herreros-Cabello et al., 2020). This diversity at the genomic level, has promoted the creation of different methods for the classification of hundreds of strains described to date (Zingales et al., 2009; Zingales et al., 2012; Barnabé et al., 2016). These classifications have been established based on some conserved genetic sequences (genomic, mitochondrial and microsatellite DNA). Besides, some researchers have suggested that both the parasite and host genetic variability could be the causes of differential clinical manifestations of Chagas disease (Manoel-Caetano Fda and Silva, 2007). Also, transcriptomic analysis revealed differences between virulent and non-virulent strains (Belew et al., 2017; Oliveira et al., 2020). Indeed, some *T. cruzi* strains highly differ in pathogenicity. Some are acute lethal strains as Y, whereas others, such as VFRA can produce a chronic infection in BALB/c mice (Rodríguez et al., 2014). Furthermore, proteomic analysis, comparing strains with different pathogenicity, indicates that strains inducing chronic infection have enriched antioxidant defenses, while those inducing acute infections produce nucleotides and proteins involved in parasite replication and lethality (Herreros-Cabello et al., 2019).

All the Trypanosomatids have a single large mitochondrion per cell (Maslov et al., 2019). Its mitochondrial DNA is a network of concatenated circular molecules of maxicircles and minicircles that is called the kinetoplast (kDNA). This structure contains dozens of maxicircles (20–40 Kb) and thousands of minicircles (0.5–10 Kb) with varying sizes depending on species (Shapiro, 1993; Lukes et al., 2002; Thomas et al., 2007).

Kinetoplasts may play a role in the pathogenicity of *T. cruzi*, and some researchers suggest the minicircles can integrate into the host genome generating autoimmune events (Simoes-Barbosa et al., 2006; Hecht et al., 2010). Also, maxicircle gene

deletions have been associated with asymptomatic patients of Chagas disease (Baptista et al., 2006). Both maxicircles and minicircles have been proposed as targets for molecular detection of *T. cruzi* DNA (Morel et al., 1980; Schijman et al., 2011; Rusman et al., 2019).

Maxicircles contain the characteristic mitochondrial genes of other eukaryotes (Simpson, 1987) and it has been shown that their sequence is characterized by two main regions: the coding region, highly conserved across strains and the divergent/variable region, very difficult to sequence due to its repetitive nature and length variability. Recent findings of maxicircles using third-generation sequencing technologies have revealed that the sequence length may differ across strains, but more importantly, for some strains, its complete sequence is longer than previous estimations (Gerasimov et al., 2020).

Minicircles are exclusive to Trypanosomatids and they are directly involved in U-insertion/deletion editing system as they encode guide RNAs (gRNAs) (Simpson et al., 2003; Aphasizhev and Aphasizheva, 2014; Smith et al., 2020). Moreover, it is suggested that both molecule populations are heterogeneous in the cell, showing strain-specific variations (Westenberger et al., 2006; Messenger et al., 2012).

Several studies have elucidated that the set of minicircles in *T. cruzi* presents a conserved structure among strains of approximately 1.4 Kb, being organized into four highly conserved regions (mHCRs) of 120 bp located 90 degrees apart from each other, and an equal number of hypervariable regions (mHVRs) of 330 bp interspersed between these conserved regions (Leon et al., 1980; Gonzalez, 1986; Macina et al., 1986; Degraeve et al., 1988; Avila et al., 1990; Shapiro and Englund, 1995; Guhl et al., 2002; Junqueira et al., 2005). Also, mHVRs diversity have gained attention since they are involved in specific functions that are unique for Trypanosomatids. mHVRs code for gRNAs that direct the edition of several mitochondrial mRNAs converting these primary transcripts into functional messages (Simpson et al., 2003).

The presence of three conserved sequence blocks (CSB) in Trypanosomatids minicircles. CSB-1 (10 bp sequence) and CSB-2 (8 bp sequence) show lower interspecies homology, while CSB-3 (12 bp sequence), known as the Universal Minicircle Sequence (UMS), is conserved within most Trypanosomatids and constitutes the minicircle replication origin (Ray, 1989). Also, the number, size, and location of these CSBs in minicircles seem to differ between species (Ponzi et al., 1984; Sugisaki and Ray, 1987; Degraeve et al., 1988; Botero et al., 2018). Concretely, the CSB-3 or UMS is the specific binding site of the UMS binding protein (UMSBP), which has been related with the minicircle replication and kDNA segregation (Milman et al., 2007). UMSBP has been widely studied in *Crithidia fasciculata* (Tzfati et al., 1995; Abu-Elneel et al., 1999; Abu-Elneel et al., 2001; Onn et al., 2006), but its presence has been revealed in other Trypanosomatids such as *T. cruzi* (Milman et al., 2007; Herreros-Cabello et al., 2019), *Leishmania donovani* (Singh et al., 2016) or *T. brucei* (Milman et al., 2007). According to these studies the consensus sequence for each CSB, including *T. cruzi*, would be: CSB-1=AGGGGCGTTC, CSB-2=CCCCGTAC and CSB-3=GGGGTTGGTGTA.

However, a similar analysis is lacking in *T. cruzi*. Therefore, our study aimed to assemble, annotate, and analyze the complete repertoire of maxicircle and minicircle sequences of different *T. cruzi* strains.

MATERIALS AND METHODS

Parasite Cultures and DNA Isolation

Y strain was obtained from Dr. J. David (Harvard Medical School, Boston, Massachusetts, USA), originally isolated back in 1953 (Amato Neto, 2010). Bug2148 strain was obtained from Dr. M. Miles (London School of Hygiene and Tropical Medicine, London, UK) through the European program ChagasEpiNet.

Vero cells were culture with complete Roswell Park Memorial Institute (RPMI, Thermo Fisher Scientific) medium containing 2 mM L-glutamine, 100 UI/ml of antibiotics mixture, 10 µg/ml streptomycin and 0.1 mM non-essential amino acids and supplemented with 5% Fetal Bovine Serum (FBS, Gibco Life Technologies, Grand Island, NY) at 37°C in an atmosphere of 5% CO₂ until the cells reached 80% confluence in biosafety level 3 (BSL3) cell culture laboratories. The cell monolayer was subsequently infected with previously infected Vero cell-derived trypomastigotes (Bug2148 and Y strains). After 4 days, the supernatant medium was collected, dead cells and amastigotes were removed by centrifugation at 1000 g by 5 min and trypomastigotes were collected by centrifugation at 1600 g for 10 min.

DNA from Y strain was isolated using the “High Pure PCR Template Preparation Kit” (Roche). DNA from Bug2148 strain was isolated using the Phenol-Chloroform method to obtain larger fragments for sequencing as needed for PacBio technology. Samples for sequencing were treated with DNase-free RNase I (Roche) and quantified by absorbance at 260 nm using the Nanodrop ND-1000 (Thermo Scientific). All samples showed an A260/A280 ratio higher than 2.0 and DNA integrity was assessed by agarose gel electrophoresis.

Maxicircle and Minicircle Sequencing

DNA from Bug2148 was sequenced using Pacific Biosciences (PacBio) technologies at the Norwegian Sequencing Centre (www.sequencing.uio.no), a national technology platform hosted by the University of Oslo and supported by the “Functional Genomics” and “Infrastructure” programs of the Research Council of Norway and the Southeastern Regional Health Authorities. PacBio library preparation includes a fragment length filtering (>8Kb). DNA from the Y strain was sequenced with Illumina MiSeq series by the Genomics facility at the *Parque Científico de Madrid* (PCM, Madrid, Spain). Both are described in Callejas-Hernández et al., (2018). Integrity from two samples was analyzed in Bioanalyzer (Agilent 2100) to confirm DNA fragmentation level larger than 20 Kb for PacBio and 900 bp for Illumina sequencing. No overlapping Paired-end reads of 2 × 300 format and 8–15 Kb of read length were obtained from Illumina and PacBio, respectively. Raw reads were subject to quality-filtering using standard processes and analyzed

using FASTQC tool. Reads with quality lower to 25 (phred score based) and mapped to nuclear genomic DNA references were discarded.

Assembly and Gene Annotation of *Trypanosoma cruzi* Maxicircle and Minicircle Sequences

Reads from the Y strain were assembled using SPADes (v3.9.0). Bug2148 maxicircle was assembled using HGAP v3 (Pacific Biosciences, SMRT Analysis Software v2.3.0), seed sequence length and minimal coverage values were set to 6 Kb and 15X, respectively. Assembled maxicircles were annotated in a semi-automatic mode. We checked the synteny of maxicircle genes described by Ruvalcaba-Trejo and Sturm (2011) using Blastn searches.

Maxi and minicircle sequences were further tested for circularity, manifested by the presence of directly repeated ends in the assembled molecule. Briefly, contigs were split into two halves, and then Minimus2 [from to Amos (version 3.1.0)] tool was used to identify repeated ends as described by Camacho et al. (2019) and Treangen et al. (2011).

Maxicircle synteny between strains was analyzed using Artemis Comparison Tool (ACT) and R using the genoPlotR package.

Analysis of Conserved and Variable Motifs in Minicircles

Multiple alignments of the minicircle sequences of Y strain were performed using MUSCLE software (<https://www.ebi.ac.uk/Tools/msa/muscle/>). The conserved regions of the Y strain minicircles were analyzed using the WebLogo 3 (version 3.7.4) tool (Crooks et al., 2004).

Validation of Minicircles by PCR Amplification and Sequencing

Experimental validation of some minicircles of Y strain was performed by PCR amplification. Primers were manually designed and then checked *in silico* by Primer Blast, NCBI Blast and TriTrypDB Blast to check the predicted PCR amplicon length and their specificity to *T. cruzi*. Primers for each minicircle are described in **Supplementary Table S1**. The same primers were tested in DNA sample of Bug2148 strain. Amplification was carried out in a 25 µL-final volume using Q5 High-Fidelity DNA Polymerase protocol (New England BioLabs) and 30 ng of DNA. PCR was run on a MyCycler Thermal Cycler (BioRad) using the following profile: initial denaturation at 95°C for 3 min followed by 20 cycles of 30 s at 95°C, 30 s at 58°C and 30 s at 72°C, completed by a final incubation of 5 min at 72°C. Amplification products were analyzed by agarose gel electrophoresis and sequenced using Sanger technology by the *Plataforma de Genómica* of the *Parque Científico de Madrid*.

RESULTS

Maxicircles of Y and Bug2148 Strains

In agreement with previous estimations, the total length of the Y strain maxicircle is about 24 Kb. However, in the case of Bug2148

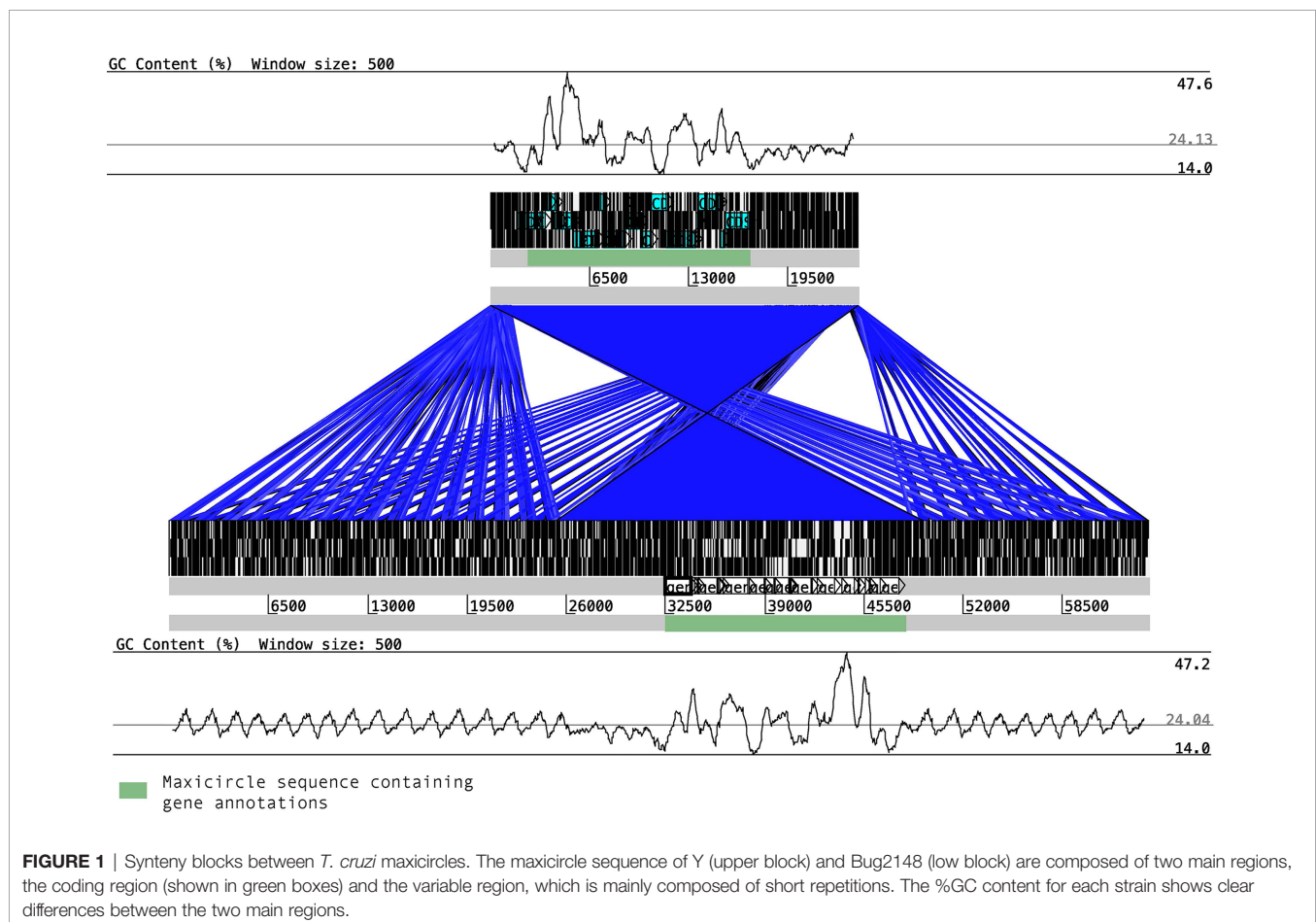
strain, the sequence length is the largest obtained to date with 64.11 Kb, suggesting that an unknown level of complexity may exist for some *T. cruzi* strains. Both maxicircles are available in **Supplementary Data S1, S2**, and accessible in GenBank. However, the complete repertoire of 21 genes listed by Ruvalcaba-Trejo and Sturm (2011) was confirmed in both strains (**Supplementary Table S2**) with minimum sequence length variations (about 15 Kb of the coding sequence in both strains), confirming that the well-documented differences between strains in the maxicircle only depends on the divergent sequence, in agreement to Gerasimov et al. findings (Gerasimov et al., 2020).

Synteny between the two maxicircles showed a highly conserved block, corresponding to the coding sequence, perfectly flanked by the variable sequence (**Figure 1**). Besides, for the first time in *T. cruzi*, we found clear differences in %GC content of the two main regions. The variable region is highly enriched with AT (up to 76%) nucleotides while the coding sequences are composed with a more proportional composition of nucleotides (about 47.6% of GC content). Multiple whole maxicircle synteny maps confirm the high conservation of the coding sequence between different *T. cruzi* strains (**Supplementary Figure S1**).

Validation of *T. cruzi* Minicircles

We were able to assembly minicircle sequences of the Y strain using Illumina (sequences < 1Kb), but it was not possible to assembly Bug2148 strain minicircles using PacBio since library preparation includes a fragment length filtering discarding DNA fragments below 8Kb. We assembled and confirmed the circularity (*in silico*) of 286 different minicircles belonging to the Y strain. Sequences and assembly statistics for all these minicircles are summarized in the **Supplementary Data S3** grouped by size. We designed primers to confirm the sequence and circularity of some of these Y strain minicircles. Primers were designed to amplify a specific band around 200-500 bp (depending on the minicircle total length). The methodology followed to confirm sequence circularity predicted *in silico* is described in **Figure 2A**. We designed primers with opposite directions at 5' and 3' ends; in this way, we obtained amplified sequences just for circular and completely assembled minicircles.

We confirmed the sequence and circularity of 9 different minicircles from the Y strain (**Figure 2B**). Sequencing results of the PCR products are shown in **Supplementary Figure S2**. However, we decided to test the same set of primers with the Bug2148 strain (**Figure 2C**). Our results showed one minicircle specific of the Y strain, confirming previous suggestions that the



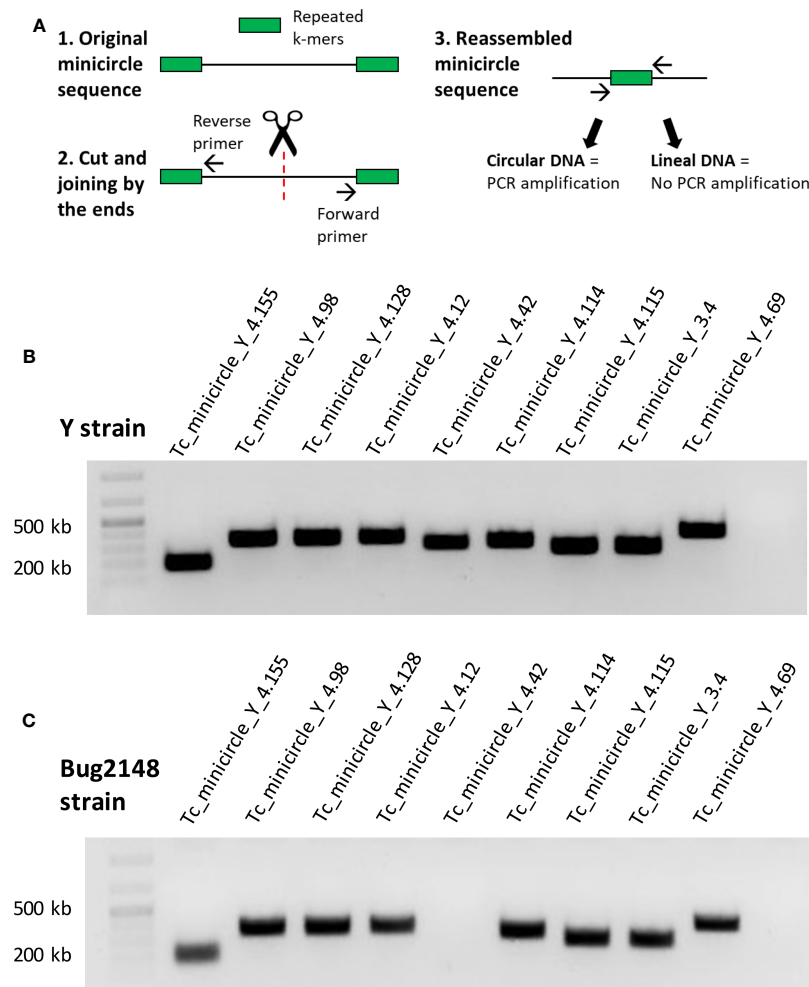


FIGURE 2 | (A) Strategy followed to confirm sequence and circularity of the Y strain minicircles. **(B)** PCR products of nine minicircles of the Y strain. **(C)** PCR products with the primers designed against the Y strain, tested in Bug2148 strain.

number and sequence of these short molecules may differ between strains.

Minicircles of Y Strain Display Heterogeneity in Size

Previous studies have proposed that the *T. cruzi* minicircles are highly conserved among strains with a regular size around 1.4 Kb and the same number and length of conserved (mHCR) and variable (mHVR) regions (Degraeve et al., 1988; Avila et al., 1990; Guhl et al., 2002; Junqueira et al., 2005).

However, despite Y strain was analyzed in these original studies, we have elucidated that different sizes of minicircles exist in this strain with a variable number of mHCRs and mHVRs. Contrary to other Trypanosomatids where the minicircle sequences have a more uniform length, we found that *T. cruzi* minicircles sizes vary from 300 bp to 1400 bp, as we can see in **Figure 3**.

We identified 42 minicircles with sizes between 336–376 bp, the smallest interval. Just 9 minicircles were found between 698–769

bp. 47 had a size between 1051–1095 bp and finally, 188 minicircles belonged to the largest group with 1357–1448 bp. This result gives us a clear classification in 4 groups according to the range of sizes, being each group separated from the next one by around 300 bp.

Analysis of Conserved and Variable Motifs of the Y Strain Minicircle

We analyzed the presence and composition of the mHCRs and mHVRs in the Y strain minicircles. Multiple alignments for each group of size were performed: 336–376 (group 1), 698–769 (group 2), 1051–1095 (group 3) and 1357–1448 bp (group 4).

In group 1 all the minicircles present a unique mHCR, and therefore a unique mHVR (**Figure 4A**). CSB-1, CSB-2, and CSB-3 sequences can be seen in the mHCR and the consensus logo of each one is also displayed. Interestingly, in the three CSBs the conserved sequence is longer than the consensus sequence described for Trypanosomatids, suggesting for the first time a larger conserved signature in both ends.

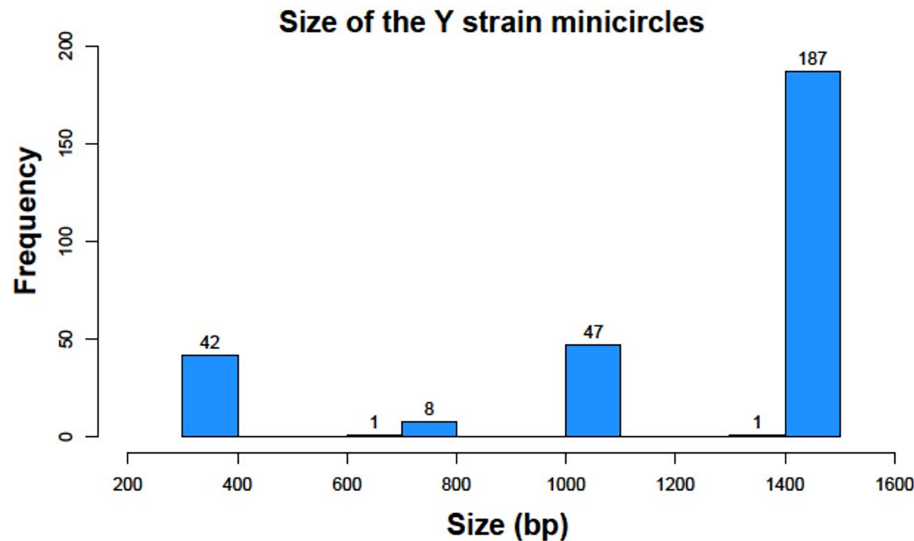


FIGURE 3 | Histogram representation of minicircle sizes of the Y strain in base pairs (bp).

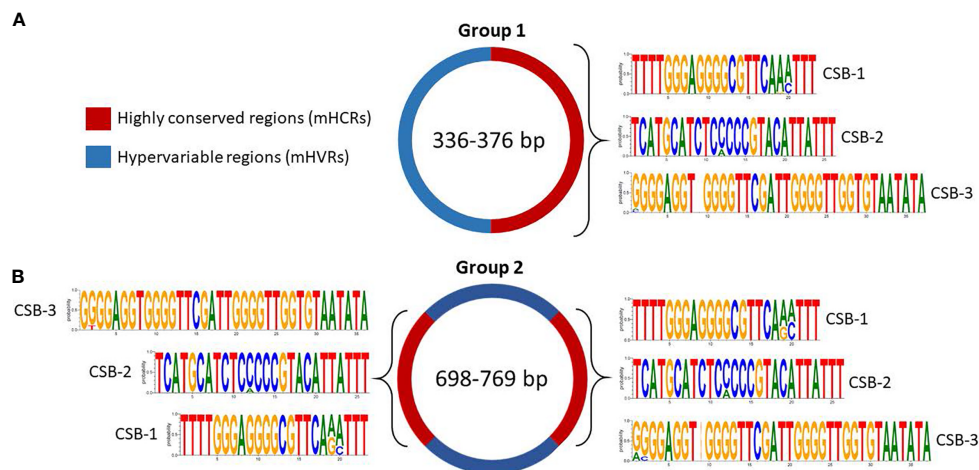


FIGURE 4 | Sequence structure of mHCRs (red) and mHVRs (blue) in group 1 (A) and group 2 (B) of the Y strain minicircles. Logos of the CSB regions are displayed in each mHCR.

Regarding group 2, the multiple alignment analysis displayed 2 mHCRs and 2 mHVRs (**Figure 4B**). Interestingly, minicircles in group 2 double the size of group 1, and the same occurs with the number of mHCRs and mHVRs. Besides, the logo of each CSB is extremely similar to the respective logo in group 1, showing an increase in the number of conserved nucleotides compared to the theoretical consensus sequence of the *T. cruzi* Y strain CSBs (CSB-1 = AGGGGCGTTC, CSB-2 = CCCCCTAC, CSB-3 = GGGGTTGGTGTA).

For group 3, we discovered 3 mHCRs and 3 mHVRs in these minicircles (**Figure 5**). Logos of the CSBs showed a similar

distribution to those in groups 1 and 2, although logos of the same CSB in each one of these three mHCRs are not exactly the same. There are minimal differences, as the insertion of a nucleotide in a specific minicircle or a variation in the proportion of a nucleotide in a specific position. However, in all the mHCRs the conservation of the principal nucleotide in each position is evident.

And finally, minicircles from group 4 contain 4 mHCRs and 4 mHVRs (**Figure 6**). Logos of CSBs were highly similar to the other groups in analysis, although there were specific differences as the insertion of a nucleotide or changes in the nucleotide proportion in some positions.

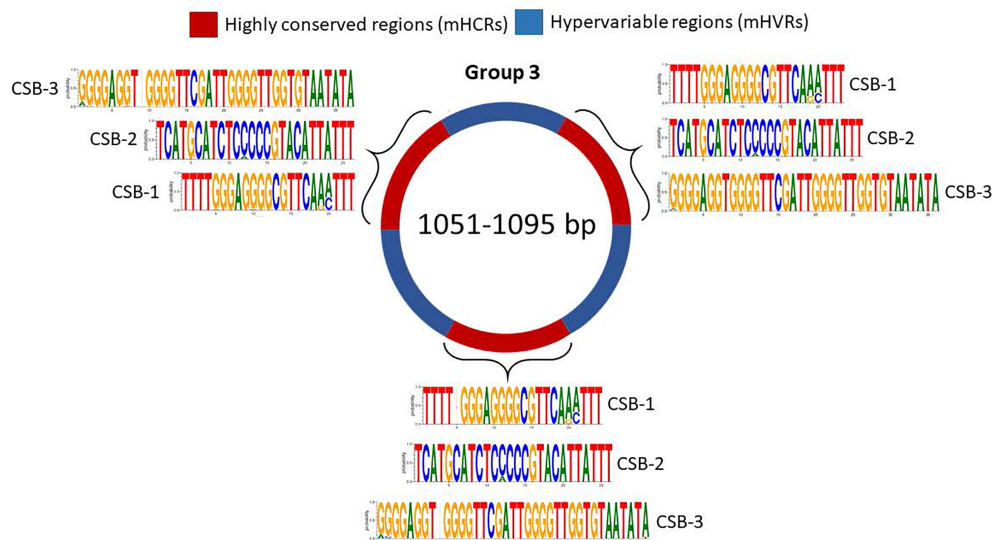


FIGURE 5 | Sequence structure of group 3 minicircles (1051-1095 bp). mHCRs are shown in red and mHVRs in blue. Logos of each CSB region are displayed in each mHCR.

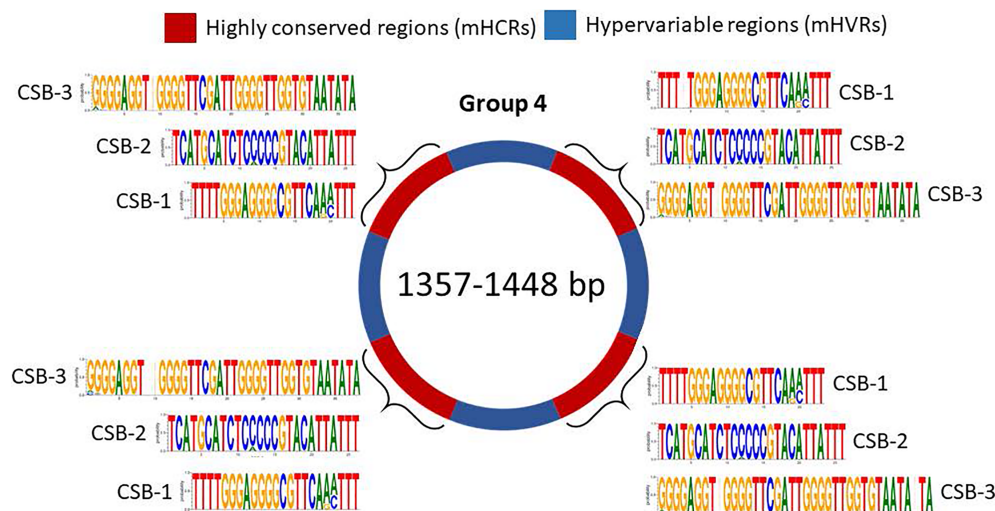


FIGURE 6 | Sequence structure of minicircles from group 4 (1357-1448 bp). mHCRs are shown in red and mHVRs in blue. Logos of each CSB region are displayed in each mHCR.

Interestingly, each group in the analysis had an increment of around 300 bp in size with respect to the immediately shorter. According to our results, it seems like the minicircle needs a new mHCR each 300 bp. Minicircles in group 1 have only a mHCR, while minicircles in group 4 have four mHCRs, one every 90 degrees in the circular structure as it has been well documented (Degraeve et al., 1988; Junqueira et al., 2005). Also, in all the minicircle groups the consensus sequence of each CSB seems to be longer than those previously described (Botero et al., 2018).

DISCUSSION

We report relevant information regarding maxicircles and minicircles kinetoplast DNA isolated from cell-derived parasites. Using second and third generation sequencing techniques we unraveled more complexity than previously reported. Being aware of the limitations of dealing with this complex parasite we were able to obtain valuable results by comparing data from different technologies.

Contrary to the first maxicircles assembled and described in *T. cruzi* (Westenberger et al., 2006), our results suggest that their total length may be larger than previous suggestions, at least for some strains as one analyzed here. Interestingly, this work indicated that the mitochondrial genes are highly conserved between strains and the coding region is about 16 Kb long, independently of the maxicircle length. The main difference between strains (at maxicircle level) corresponds to the variable/divergent sequence length, which also does not have conserved motifs or repetitive patterns. Besides, clear differences in %GC content between the coding and variable regions were found, suggesting, on one hand, the importance of the maxicircle stability and structure and on the other hand, that the transcription efficiency in *T. cruzi* is highly correlated with a proportional sequence composition.

We detected a total of 286 different minicircles. This is the first time that the complete repertoire of different minicircles of a particular *T. cruzi* strain is described. The general structural organization of some *T. cruzi* minicircles was described (Degraeve et al., 1988; Avila et al., 1990; Guhl et al., 2002; Junqueira et al., 2005). Their common scheme would be a minicircle with a size around 1.4 Kb, in which four mHCRs of 120 bp are interspersed with four 330 bp regions that would correspond to the mHVRs. However, our results suggest that this organization, at least in some strains, is more complex, suggesting a new potential aggrupation in at least four main groups of minicircles according to their size and the number of mHCRs and mHVRs: 336-376 bp (group 1), 698-769 bp (group 2), 1051-1095 bp (group 3) and 1357-1448 bp (group 4). Minicircles of group 1 have only one mHCR and mHVR. Group 2 minicircles have two mHCRs and mHVRs. Those belonging to group 3 present three mHCRs and mHVRs. And finally, minicircles of group 4 have four mHCRs and mHVRs. The most abundant was group 4, with 188 members, and the less abundant the group 2 with just 9.

The circularity of minicircles was validated by PCR amplification using specific primers of different groups that amplified the common regions detected at both 3' and 5' ends of the reads. Primers were designed for the Y strain, but were also amplified in the Bug2148 strain, except for one set of primers, suggesting that these minicircles may be also present in this strain.

Interestingly, the four groups we have described here in Y strain differ in size by about 300 bp, and this distance is always conserved between the mHCRs in all the groups. Also, the size of the mHCRs is around 120 bp in all of the groups. Therefore, the common patterns of distance are the same as those previously described, which may explain the number of mHCRs depending on the size of the minicircle. Previous analysis detected minicircles around 1.4 Kb (Degraeve et al., 1988; Avila et al., 1990; Guhl et al., 2002; Junqueira et al., 2005), as those ascribed to our group 4 (the group with more members). Thus, the new techniques of Next Generation Sequencing used here have likely improved the detection of all minicircles regardless of their abundance.

Also, we analyzed the presence and number of the CSB-1, CSB-2, and CSB-3 in the mHCRs of the Y strain minicircles.

Previous studies had determined a consensus sequence for each CSB in other Trypanosomatids, although little differences in length and nucleotide composition have been described between species for the CSB-1 and CSB-2 (Barrois et al., 1981; Jasmer and Stuart, 1986; Nasir et al., 1987; Botero et al., 2018). However, in our study of the Y strain of *T. cruzi* we have highlighted that this theoretical consensus sequence for *T. cruzi* is larger than the previous one, with more conserved nucleotides in both ends in all the CSBs of the Y strain minicircles. Interestingly, there are even small differences as changes in the nucleotide proportion in a position or nucleotide insertions between mHCRs of distinct minicircle groups and between the mHCRs of the same minicircle group.

For decades, many researchers have used for their experiments this standard organization of 1.4 Kb and 4 mHCRs and 4 mHVRs of the *T. cruzi* minicircles, although sequences in the NCBI databases of some minicircles suggest a variety of sizes between less than 100 bp and more than 1000 bp. However, the vast majority of submitted sequences correspond to unpublished data, partial or only the hypervariable regions of specific minicircles sequences (Telleria et al., 2006; Velazquez et al., 2008). Therefore, our contribution with the new full complement of different 286 minicircles of the Y strain supposes a great advance in the knowledge and current data that we have of this type of circular structures.

While *T. cruzi* has four groups of minicircles, other species as *Trypanosoma rangeli* (*T. rangeli*) display three different classes of minicircle sequences that are known as KP1, KP2, and KP3 according to the number of conserved regions. They may present one conserved region (KP1), two conserved regions located at 180 degrees (KP2), or four conserved regions, located at 90 degrees (KP3) (Recinos et al., 1994; Vallejo et al., 2002). However, while in *T. cruzi* the size of the minicircles varies between 336 and 1448 bp, *T. rangeli* displays a less size variation in minicircles with a range of 1.6-1.8 Kb (Vallejo et al., 1994). In *Trypanosoma copemani*, minicircles have 2048 bp of size and two classes were suggested considering the number of conserved and variable regions: the G1M1 minicircles with two conserved and two variable regions, and the G1M2 minicircles with four conserved and four variable regions (Botero et al., 2018).

In *Leishmania major* 97 different minicircles were detected, and 49 in *Leishmania infantum*, although in these species the size of their minicircles is very uniform, between 660-876 bp and 775-832 bp respectively (Camacho et al., 2019), while *T. cruzi* presents a bigger size minicircle heterogeneity. Moreover, the researchers described the minicircles of *Leishmania* with only one conserved region, while for the same minicircle size *T. cruzi* displays two, and the CSBs present differences in sequence length and nucleotide composition between both species. Taking into account that these conserved regions contain the replication origin, it seems that *Leishmania* only needs one to perform the completed minicircle replication, while *T. cruzi* needs one each 300 bp, probably due to the different efficiency in this biological process between both Trypanosomatids.

Mitochondrial metabolism and gene expression are highly regulated to deal with all those complicated environmental changes across the complete life cycle alternating between the

mammalian host and insect vector, including regulation of mRNAs that require extensive uridine insertion/deletion (U-indel) editing for their maturation, as has been described in other closely related Trypanosomatids (Smith et al., 2020). To our knowledge, it is the first time describing a large repertoire of complete *T. cruzi* minicircle sequences.

We sequenced DNA from cell-derived trypomastigotes while in previous reports used epimastigotes. It could be argued that kinetoplast DNA may change from one stage to another. According to Riou and Gutteridge (1978), there should not be differences in DNA content between different stages of *T. cruzi*. On the other hand, Schwabl et al. (2019) found genomic changes over the same stage just by culture passage. Thus, it would be interesting to further investigate whether the increase in complexity could be due to changes in DNA content between epimastigotes and trypomastigotes.

Finally, considering that there are minicircles conserved among strains and their relevant role for the maturation of the maxicircle-encoded transcripts, critical for the replication and survival of the parasite, their analysis may contribute to the understanding of the mitochondrial transcription and translation processes potentially related to the Chagas disease.

DATA AVAILABILITY STATEMENT

The complete maxicircle sequences for Y and Bug2148 strains are available from the Genbank database accession numbers MW732647, and MW732648, respectively.

AUTHOR CONTRIBUTIONS

FC-H, MF, and NG conceived the idea, MF and NG acquired funding. FC-H, AH-C, and JM-S performed the experiments. FC-H and AH-C wrote the first version of the manuscript.

REFERENCES

- Abu-Elneel, K., Kapeller, I., and Shlomai, J. (1999). Universal Minicircle Sequence-Binding Protein, A Sequence-Specific DNA-Binding Protein That Recognizes the Two Replication Origins of the Kinetoplast DNA Minicircle. *J. Biol. Chem.* 274, 13419–13426. doi: 10.1074/jbc.274.19.13419
- Abu-Elneel, K., Robinson, D. R., Drew, M. E., Englund, P. T., and Shlomai, J. (2001). Intramitochondrial Localization of Universal Minicircle Sequence-Binding Protein, A Trypanosomatid Protein That Binds Kinetoplast Minicircle Replication Origins. *J. Cell Biol.* 153, 725–734. doi: 10.1083/jcb.153.4.725
- Amato Neto, V. (2010). Origin of the “Y Strain” of *Trypanosoma cruzi*. *Rev. Inst. Med. Trop. Sao Paulo* 52, 171. doi: 10.1590/s0036-46652010000300012
- Aphasizhev, R., and Aphasizheva, I. (2014). Mitochondrial RNA Editing in Trypanosomes: Small RNAs in Control. *Biochimie* 100, 125–131. doi: 10.1016/j.biochi.2014.01.003
- Avila, H., Goncalves, A. M., Nehme, N. S., Morel, C. M., and Simpson, L. (1990). Schizodeme Analysis of *Trypanosoma cruzi* Stocks From South and Central America by Analysis of PCR-Amplified Minicircle Variable Region Sequences. *Mol. Biochem. Parasitol.* 42, 175–187. doi: 10.1016/0166-6851(90)90160-n
- Baptista, C. S., Vencio, R. Z., Abdala, S., Carranza, J. C., Westenberger, S. J., Silva, M. N., et al. (2006). Differential Transcription Profiles in *Trypanosoma cruzi*

All authors reviewed and edited the manuscript. All authors contributed to the article and approved the submitted version.

FUNDING

This work was supported by: “Ministerio de Economía y competitividad” and “Fondo Europeo de Desarrollo Regional” (SAF2015-63868-R (MINECO/FEDER) to NG, and SAF2016-75988-R (MINECO/FEDER) to MF); “Ministerio de Ciencia, Innovación y Universidades-Agencia Estatal de Investigación” and “Fondo Europeo de Desarrollo Regional” (PGC2018-096132-B-I00 (MICINN/FEDER) to NG); “Red de Investigación de Centros de Enfermedades Tropicales” (RICET RD12/0018/0004 to MF); Comunidad de Madrid (S-2010/BMD-2332 to MF); FC-H was recipient of a Ph.D. studentship number 411595 (“Consejo Nacional de Ciencia y Tecnología” (CONACYT, Mexico) and the “Consejo de Ciencia, Tecnología e Innovación de Hidalgo” (CITNOVA, Mexico)); AH-C was recipient of a FPU contract of the “Ministerio de Ciencia, Innovación y Universidades”; JM-S was recipient of a “Garantía Juvenil” predoctoral fellowship (Comunidad de Madrid); and Institutional grants from “Fundación Ramón Areces” and “Banco de Santander”.

ACKNOWLEDGMENTS

The authors would like to thank Maria. A. Chorro for their excellent technical assistance.

SUPPLEMENTARY MATERIAL

The Supplementary Material for this article can be found online at: <https://www.frontiersin.org/articles/10.3389/fcimb.2021.672448/full#supplementary-material>

- Associated With Clinical Forms of Chagas Disease: Maxicircle NADH Dehydrogenase Subunit 7 Gene Truncation in Asymptomatic Patient Isolates. *Mol. Biochem. Parasitol.* 150, 236–248. doi: 10.1016/j.molbiopara.2006.08.008
- Barnabé, C., Mobarec, H. I., Jurado, M. R., Cortez, J. A., and Brenière, S. F. (2016). Reconsideration of the Seven Discrete Typing Units Within the Species *Trypanosoma cruzi*, A New Proposal of Three Reliable Mitochondrial Clades. *Infect. Genet. Evol.* 39, 176–186. doi: 10.1016/j.meegid.2016.01.029
- Barrois, M., Riou, G., and Galibert, F. (1981). Complete Nucleotide Sequence of Minicircle Kinetoplast DNA From *Trypanosoma equiperdum*. *Proc. Natl. Acad. Sci. U. S. A.* 78, 3323–3327. doi: 10.1073/pnas.78.6.3323
- Belew, A. T., Junqueira, C., Rodrigues-Luiz, G. F., Valente, B. M., Oliveira, A. E. R., Polidoro, R. B., et al. (2017). Comparative Transcriptome Profiling of Virulent and Non-Virulent *Trypanosoma cruzi* Underlines the Role of Surface Proteins During Infection. *PLoS Pathog.* 13 (12), e1006767. doi: 10.1371/journal.ppat.1006767
- Botero, A., Kapeller, I., Cooper, C., Clode, P. L., Shlomai, J., and Thompson, R. C. A. (2018). The Kinetoplast DNA of the Australian Trypanosome, *Trypanosoma copemani*, Shares Features With *Trypanosoma cruzi* and *Trypanosoma lewisi*. *Int. J. Parasitol.* 48, 691–700. doi: 10.1016/j.ijpara.2018.02.006
- Callejas-Hernández, F., Rastrojo, A., Poveda, C., Gironès, N., and Fresno, M. (2018). Genomic Assemblies of Newly Sequenced *Trypanosoma cruzi* Strains

- Reveal New Genomic Expansion and Greater Complexity. *Sci. Rep.* 8, 14631. doi: 10.1038/s41598-018-32877-2
- Camacho, E., Rastrojo, A., Sanchiz, A., González-de la Fuente, S., Aguado, B., and Requena, J. M. (2019). Leishmania Mitochondrial Genomes: Maxicircle Structure and Heterogeneity of Minicircles. *Genes (Basel)* 10 (10), 758. doi: 10.3390/genes10100758
- Clayton, J. (2010). Chagas Disease 101. *Nature* 465, S4–S5. doi: 10.1038/nature09220
- Crooks, G. E., Hon, G., Chandonia, J.-M., and Brenner, S. E. (2004). Weblogo: A Sequence Logo Generator. *Genome Res.* 14, 1188–1190. doi: 10.1101/gr.849004
- Degrave, W., Fragos, S. P., Britto, C., van Heuverswyn, H., Kidane, G. Z., Cardoso, M. A., et al. (1988). Peculiar Sequence Organization of Kinetoplast DNA Minicircles From Trypanosoma Cruzi. *Mol. Biochem. Parasitol.* 27, 63–70. doi: 10.1016/0166-6851(88)90025-4
- de Souza, W., de Carvalho, T. M. U., and Barrias, E. S. (2010). Review on Trypanosoma Cruzi: Host Cell Interaction. *Int. J. Cell Biol.* 2010, 295394. doi: 10.1155/2010/295394
- Echeverría, L. E., and Morillo, C. A. (2019). American Trypanosomiasis (Chagas Disease). *Infect. Dis. Clin. North Am.* 33, 119–134. doi: 10.1016/j.idc.2018.10.015
- Gerasimov, E. S., Zamyatnina, K. A., Matveeva, N. S., Rudenskaya, Y. A., Kraeva, N., Kolesnikov, A. A., et al. (2020). Common Structural Patterns in the Maxicircle Divergent Region of Trypanosomatidae. *Pathogens* 9 (2), 100. doi: 10.3390/pathogens9020100
- Gonzalez, A. (1986). Nucleotide Sequence of a Trypanosoma Cruzi Minicircle. *Nucleic Acids Res.* 14:9217. doi: 10.1093/nar/14.22.9217
- Guhl, F., Jaramillo, C., Carranza, J. C., and Vallejo, G. A. (2002). Molecular Characterization and Diagnosis of Trypanosoma Cruzi and T. Rangeli. *Arch. Med. Res.* 33, 362–370. doi: 10.1016/S0188-4409(02)00380-6
- Hecht, M. M., Nitz, N., Araujo, P. F., Sousa, A. O., Rosa Ade, C., Gomes, D. A., et al. (2010). Inheritance of DNA Transferred From American Trypanosomes to Human Hosts. *PLoS One* 5, e9181. doi: 10.1371/journal.pone.0009181
- Herreros-Cabello, A., Callejas-Hernández, F., Fresno, M., and Gironès, N. (2019). Comparative Proteomic Analysis of Trypomastigotes From Trypanosoma Cruzi Strains With Different Pathogenicity. *Infect. Genet. Evol.* 76, 104041. doi: 10.1016/j.meegid.2019.104041
- Herreros-Cabello, A., Callejas-Hernández, F., Gironès, N., and Fresno, M. (2020). Trypanosoma Cruzi Genome: Organization, Multi-Gene Families, Transcription, and Biological Implications. *Genes* 11, 1196. doi: 10.3390/genes11101196
- Jasmer, D. P., and Stuart, K. (1986). Conservation of Kinetoplastid Minicircle Characteristics Without Nucleotide Sequence Conservation. *Mol. Biochem. Parasitol.* 18, 257–269. doi: 10.1016/0166-6851(86)90084-8
- Junqueira, A. C., Degrave, W., and Brandao, A. (2005). Minicircle Organization and Diversity in Trypanosoma Cruzi Populations. *Trends Parasitol.* 21, 270–272. doi: 10.1016/j.pt.2005.04.001
- Leon, W., Frasch, A. C., Hoeijmakers, J. H., Fase-Fowler, F., Borst, P., Brunel, F., et al. (1980). Maxi-Circles and Mini-Circles in Kinetoplast DNA From Trypanosoma Cruzi. *Biochim. Biophys. Acta* 607, 221–231. doi: 10.1016/0005-2787(80)90075-1
- Lukes, J., Guilbride, D. L., Votýpka, J., Zíková, A., Benne, R., and Englund, P. T. (2002). Kinetoplast DNA Network: Evolution of an Improbable Structure. *Eukaryot. Cell* 1, 495–502. doi: 10.1128/ec.1.4.495-502.2002
- Macina, R. A., Sanchez, D. O., Gluschkof, D. A., Burrone, O. R., and Frasch, A. C. (1986). Sequence Diversity in the Kinetoplast DNA Minicircles of Trypanosoma Cruzi. *Mol. Biochem. Parasitol.* 21, 25–32. doi: 10.1016/0166-6851(86)90075-7
- Manoel-Caetano Fda, S., and Silva, A. E. (2007). Implications of Genetic Variability of Trypanosoma Cruzi for the Pathogenesis of Chagas Disease. *Cad Saude Publ.* 23, 2263–2274. doi: 10.1590/S0102-311X2007001000002
- Maslov, D. A., Opperdoes, F. R., Kostygov, A. Y., Hashimi, H., Lukes, J., and Yurchenko, V. (2019). Recent Advances in Trypanosomatid Research: Genome Organization, Expression, Metabolism, Taxonomy and Evolution. *Parasitology* 146, 1–27. doi: 10.1017/S0031182018000951
- Messenger, L. A., Llewellyn, M. S., Bhattacharyya, T., Franzén, O., Lewis, M. D., Ramírez, J. D., et al. (2012). Multiple Mitochondrial Introgression Events and Heteroplasmy in Trypanosoma Cruzi Revealed by Maxicircle MLST and Next Generation Sequencing. *PLoS Negl. Trop. Dis.* 6, e1584. doi: 10.1371/journal.pntd.0001584
- Milman, N., Motyka, S. A., Englund, P. T., Robinson, D., and Shlomai, J. (2007). Mitochondrial Origin-Binding Protein UMSBP Mediates DNA Replication and Segregation in Trypanosomes. *Proc. Natl. Acad. Sci. U. S. A.* 104, 19250–19255. doi: 10.1073/pnas.0706858104
- Morel, C., Chiari, E., Camargo, E. P., Mattei, D. M., Romanha, A. J., and Simpson, L. (1980). Strains and Clones of Trypanosoma Cruzi can be Characterized by Pattern of Restriction Endonuclease Products of Kinetoplast DNA Minicircles. *Proc. Natl. Acad. Sci. U. S. A.* 77, 6810–6814. doi: 10.1073/pnas.77.11.6810
- Nasir, A., Cook, G. A., and Donelson, J. E. (1987). Sequences of Two Kinetoplast Minicircle DNAs for Trypanosoma (Nannomona) Congolense. *Mol. Biochem. Parasitol.* 24, 295–300. doi: 10.1016/0166-6851(87)90162-9
- Oliveira, A. E. R., Pereira, M. C. A., Belew, A. T., Ferreira, L. R. P., Pereira, L. M. N., Neves, E. G. A., et al. (2020). Gene Expression Network Analyses During Infection With Virulent and Avirulent Trypanosoma Cruzi Strains Unveil a Role for Fibroblasts in Neutrophil Recruitment and Activation. *PLoS Pathog.* 16 (8), e1008781. doi: 10.1371/journal.ppat.1008781
- Onn, I., Kapeller, I., Abu-Elneel, K., and Shlomai, J. (2006). Binding of the Universal Minicircle Sequence Binding Protein at the Kinetoplast DNA Replication Origin. *J. Biol. Chem.* 281, 37468–37476. doi: 10.1074/jbc.M606374200
- Pérez-Molina, J. A., and Molina, I. (2018). Chagas Disease. *Lancet* 391, 82–94. doi: 10.1016/S0140-6736(17)31612-4
- Ponzi, M., Birago, C., and Battaglia, P. A. (1984). Two Identical Symmetrical Regions in the Minicircle Structure of Trypanosoma Lewisi Kinetoplast DNA. *Mol. Biochem. Parasitol.* 13, 111–119. doi: 10.1016/0166-6851(84)90105-1
- Rassi, A., Rassi, A., and Marcondes de Rezende, J. (2012). American Trypanosomiasis (Chagas Disease). *Infect. Dis. Clin. North Am.* 26, 275–291. doi: 10.1016/j.idc.2012.03.002
- Ray, D. S. (1989). Conserved Sequence Blocks in Kinetoplast Minicircles From Diverse Species of Trypanosomes. *Mol. Cell Biol.* 9, 1365–1367. doi: 10.1128/mcb.9.3.1365
- Recinos, R. F., Kirchhoff, L. V., and Donelson, J. E. (1994). Characterization of Kinetoplast DNA Minicircles in Trypanosoma Rangeli. *Mol. Biochem. Parasitol.* 63, 59–67. doi: 10.1016/0166-6851(94)90008-6
- Reis-Cunha, J. L., Rodrigues-Luiz, G. F., Valdivia, H. O., Baptista, R. P., Mendes, T. A. O., de Moraes, G. L., et al. (2015). Chromosomal Copy Number Variation Reveals Differential Levels of Genomic Plasticity in Distinct Trypanosoma Cruzi Strains. *BMC Genomics* 16 (1), 499. doi: 10.1186/s12864-015-1680-4
- Riou, G. F., and Gutteridge, W. E. (1978). Comparative Study of Kinetoplast DNA in Culture, Blood and Intracellular Forms of Trypanosoma Cruzi. *Biochimie* 60, 365–379. doi: 10.1016/S0300-9084(78)80670-1
- Rodrigues, J. C. F., Godinho, J. L. P., and de Souza, W. (2014). Biology of Human Pathogenic Trypanosomatids: Epidemiology, Lifecycle and Ultrastructure. *Subcell. Biochem.* 74, 1–42. doi: 10.1007/978-94-007-7305-9_1
- Rodriguez, H. O., Guerrero, N. A., Fortes, A., Santi-Rocca, J., Gironès, N., and Fresno, M. (2014). Trypanosoma Cruzi Strains Cause Different Myocarditis Patterns in Infected Mice. *Acta Tropica* 139, 57–66. doi: 10.1016/j.actatropica.2014.07.005
- Rusman, F., Tomasini, N., Yapur, N. F., Puebla, A. F., Ragone, P. G., and Diosque, P. (2019). Elucidating Diversity in the Class Composition of the Minicircle Hypervariable Region of Trypanosoma Cruzi: New Perspectives on Typing and kDNA Inheritance. *PLoS Negl. Trop. Dis.* 13, e0007536. doi: 10.1371/journal.pntd.0007536
- Ruvalcaba-Trejo, L. I., and Sturm, N. R. (2011). The Trypanosoma Cruzi Sylvio X10 Strain Maxicircle Sequence: The Third Musketeer. *BMC Genomics* 12:58. doi: 10.1186/1471-2164-12-58
- Schijman, A. G., Bisio, M., Orellana, L., Sued, M., Duffy, T., Mejia Jaramillo, A. M., et al. (2011). International Study to Evaluate PCR Methods for Detection of Trypanosoma Cruzi DNA in Blood Samples From Chagas Disease Patients. *PLoS Negl. Trop. Dis.* 5, e931. doi: 10.1371/journal.pntd.0000931
- Schwabl, P., Imamura, H., Van den Broeck, F., Costales, J. A., Maiguashca-Sánchez, J., Miles, M. A., et al. (2019). Meiotic Sex in Chagas Disease Parasite Trypanosoma Cruzi. *Nat. Commun.* 10 (1), 3972. doi: 10.1038/s41467-019-11771-z
- Shapiro, T. A. (1993). Kinetoplast DNA Maxicircles: Networks Within Networks. *Proc. Natl. Acad. Sci. U. S. A.* 90, 7809–7813. doi: 10.1073/pnas.90.16.7809
- Shapiro, T. A., and Englund, P. T. (1995). The Structure and Replication of Kinetoplast DNA. *Annu. Rev. Microbiol.* 49, 117–143. doi: 10.1146/annurev.mi.49.100195.001001

- Simoes-Barbosa, A., Arganaraz, E. R., Barros, A. M., Rosa Ade, C., Alves, N. P., Louvandini, P., et al. (2006). Hitchhiking Trypanosoma Cruzi Minicircle DNA Affects Gene Expression in Human Host Cells Via LINE-1 Retrotransposon. *Mem Inst. Oswaldo Cruz* 101, 833–843. doi: 10.1590/s0074-02762006000800003
- Simpson, L. (1987). The Mitochondrial Genome of Kinetoplastid Protozoa: Genomic Organization, Transcription, Replication, and Evolution. *Annu. Rev. Microbiol.* 41, 363–382. doi: 10.1146/annurev.mi.41.100187.002051
- Simpson, L., Sbicego, S., and Aphasizhev, R. (2003). Uridine Insertion/Deletion RNA Editing in Trypanosome Mitochondria: A Complex Business. *RNA* 9, 265–276. doi: 10.1261/rna.2178403
- Singh, R., Purkait, B., Abhishek, K., Saini, S., Das, S., Verma, S., et al. (2016). Universal Minicircle Sequence Binding Protein of Leishmania Donovanii Regulates Pathogenicity by Controlling Expression of Cytochrome-B. *Cell Biosci.* 6, 13. doi: 10.1186/s13578-016-0072-z
- Smith, J. J. T., Doleželová, E., Tylec, B., Bard, J. E., Chen, R., Sun, Y., et al. (2020). Developmental Regulation of Edited CYB and COIII Mitochondrial mRNAs is Achieved by Distinct Mechanisms in Trypanosoma Brucei. *Nucleic Acids Res.* 48, 8704–8723. doi: 10.1093/nar/gkaa641
- Sugisaki, H., and Ray, D. S. (1987). DNA Sequence of Crithidia Fasciculata Kinetoplast Minicircles. *Mol. Biochem. Parasitol.* 23, 253–263. doi: 10.1016/0166-6851(87)90032-6
- Telleria, J., Lafay, B., Virreira, M., Barnabé, C., Tibayrenc, M., and Svoboda, M. (2006). Trypanosoma Cruzi: Sequence Analysis of the Variable Region of Kinetoplast Minicircles. *Exp. Parasitol.* 114, 279–288. doi: 10.1016/j.exppara.2006.04.005
- Thomas, S., Martinez, L. L. I. T., Westenberger, S. J., and Sturm, N. R. (2007). A Population Study of the Minicircles in Trypanosoma Cruzi: Predicting Guide RNAs in the Absence of Empirical RNA Editing. *BMC Genomics* 8, 133. doi: 10.1186/1471-2164-8-133
- Treangen, T. J., Sommer, D. D., Angly, F. E., Koren, S., and Pop, M. (2011). Next Generation Sequence Assembly With AMOS. *Curr. Protoc. Bioinf.* 33, 11.8.1–11.8.18. doi: 10.1002/0471250953.bi1108s33
- Tzfati, Y., Abeliovich, H., Avrahami, D., and Shlomai, J. (1995). Universal Minicircle Sequence Binding Protein, a CCHC-type Zinc Finger Protein That Binds the Universal Minicircle Sequence of Trypanosomatids. Purification and Characterization. *J. Biol. Chem.* 270, 21339–21345. doi: 10.1074/jbc.270.36.21339
- Vallejo, G. A., Guhl, F., Carranza, J. C., Lozano, L. E., Sánchez, J. L., Jaramillo, J. C., et al. (2002). kDNA Markers Define Two Major Trypanosoma Rangeli Lineages in Latin-America. *Acta Tropica* 81, 77–82. doi: 10.1016/S0001-706X(01)00186-3
- Vallejo, G. A., Macedo, A. M., Chiari, E., and Pena, S. D. (1994). Kinetoplast DNA From Trypanosoma Rangeli Contains Two Distinct Classes of Minicircles With Different Size and Molecular Organization. *Mol. Biochem. Parasitol.* 67, 245–253. doi: 10.1016/0166-6851(94)00137-5
- Velazquez, M., Diez, C. N., Mora, C., Diosque, P., and Marcipar, I. S. (2008). Trypanosoma Cruzi: An Analysis of the Minicircle Hypervariable Regions Diversity and its Influence on Strain Typing. *Exp. Parasitol.* 120, 235–241. doi: 10.1016/j.exppara.2008.07.016
- Westenberger, S. J., Cerqueira, G. C., El-Sayed, N. M., Zingales, B., Campbell, D. A., and Sturm, N. R. (2006). Trypanosoma Cruzi Mitochondrial Maxicircles Display Species- and Strain-Specific Variation and a Conserved Element in the Non-Coding Region. *BMC Genomics* 7, 60. doi: 10.1186/1471-2164-7-60
- World Health Organization. *Chagas disease (American trypanosomiasis)*. Available at: https://www.who.int/health-topics/chagas-disease#tab_1 (Accessed January 15, 2021).
- Zingales, B., Andrade, S. G., Briones, M. R. S., Campbell, D. A., Chiari, E., Fernandes, O., et al. (2009). A New Consensus for Trypanosoma Cruzi Intraspecific Nomenclature: Second Revision Meeting Recommends TcI to Tcvi. *Memórias do Inst. Oswaldo Cruz* 104, 1051–1054. doi: 10.1590/S0074-02762009000700021
- Zingales, B., Miles, M. A., Campbell, D. A., Tibayrenc, M., Macedo, A. M., Teixeira, M. M. G., et al. (2012). The Revised Trypanosoma Cruzi Subspecific Nomenclature: Rationale, Epidemiological Relevance and Research Applications. *Infect. Genet. Evol.* 12, 240–253. doi: 10.1016/j.meegid.2011.12.009

Conflict of Interest: The authors declare that the research was conducted in the absence of any commercial or financial relationships that could be construed as a potential conflict of interest.

Citation: Callejas-Hernández F, Herreros-Cabello A, del Moral-Salmoral J, Fresno M and Gironès N (2021) The Complete Mitochondrial DNA of Trypanosoma cruzi: Maxicircles and Minicircles. *Front. Cell. Infect. Microbiol.* 11:672448. doi: 10.3389/fcimb.2021.672448

Copyright © 2021 Callejas-Hernández, Herreros-Cabello, del Moral-Salmoral, Fresno and Gironès. This is an open-access article distributed under the terms of the Creative Commons Attribution License (CC BY). The use, distribution or reproduction in other forums is permitted, provided the original author(s) and the copyright owner(s) are credited and that the original publication in this journal is cited, in accordance with accepted academic practice. No use, distribution or reproduction is permitted which does not comply with these terms.



Molecular and Functional Characteristics of DNA Polymerase Beta-Like Enzymes From Trypanosomatids

Edio Maldonado^{1††}, Sebastian Morales-Pison^{2†}, Fabiola Urbina¹ and Aldo Solari^{1*}

OPEN ACCESS

Edited by:

Juan David Ramirez,
Rosario University, Colombia

Reviewed by:

Elisa Azuara-Liceaga,
Universidad Autónoma
de la Ciudad de México, Mexico
Laurence A. Marchat,
Instituto Politécnico Nacional,
Mexico

*Correspondence:

Edio Maldonado
emaldona@med.uchile.cl
Aldo Solari
asolari@med.uchile.cl

^{††}These authors share first authorship

Specialty section:

This article was submitted to
Parasite and Host,
a section of the journal
Frontiers in Cellular and
Infection Microbiology

Received: 21 February 2021

Accepted: 08 June 2021

Published: 05 August 2021

Citation:

Maldonado E, Morales-Pison S,
Urbina F and Solari A (2021)
Molecular and Functional
Characteristics of DNA
Polymerase Beta-Like Enzymes
From Trypanosomatids.
Front. Cell. Infect. Microbiol. 11:670564.
doi: 10.3389/fcimb.2021.670564

¹ Programa de Biología Celular y Molecular, Instituto de Ciencias Biomédicas, Facultad de Medicina, Universidad de Chile, Santiago, Chile, ² Laboratorio de Genética Molecular Humana, Programa de Genética Humana, Instituto de Ciencias Biomédicas, Facultad de Medicina, Universidad de Chile, Santiago, Chile

Trypanosomatids are a group of primitive unicellular eukaryotes that can cause diseases in plants, insects, animals, and humans. Kinetoplast genome integrity is key to trypanosomatid cell survival and viability. Kinetoplast DNA (kDNA) is usually under attack by reactive oxygen and nitric species (ROS and RNS), damaging the DNA, and the cells must remove and repair those oxidatively generated lesions in order to survive and proliferate. Base excision repair (BER) is a well-conserved pathway for DNA repair after base damage, single-base loss, and single-strand breaks, which can arise from ROS, RSN, environmental genotoxic agents, and UV irradiation. A powerful BER system has been described in the *T. cruzi* kinetoplast and it is mainly carried out by DNA polymerase β (pol β) and DNA polymerase β -PAK (pol β -PAK), which are kinetoplast-located in *T. cruzi* as well as in other trypanosomatids. Both pol β and pol β -PAK belong to the X-family of DNA polymerases (pol X family), perform BER in trypanosomatids, and display intrinsic 5-deoxyribose phosphate (dRP) lyase and DNA polymerase activities. However, only Pol β -PAK is able to carry out trans-lesion synthesis (TLS) across 8oxoG lesions. *T. cruzi* cells overexpressing pol β are more resistant to ROS and are also more efficient to repair 8oxoG compared to control cells. Pol β seems to play a role in kDNA replication, since it associates with kinetoplast antipodal sites in those development stages in trypanosomatids which are competent for cell replication. ROS treatment of cells induces the overexpression of pol β , indicating that plays a role in kDNA repair. In this review, we will summarize the main features of trypanosomatid minicircle kDNA replication and the biochemical characteristics of pol β -like enzymes and their involvement in BER and kDNA replication. We also summarize key structural features of trypanosomatid pol β compared to their mammalian (human) counterpart.

Keywords: *Trypanosoma cruzi*, DNA polymerase beta, kinetoplast DNA, trypanosomatids, BER

TRYPANOSOMATIDAE

Kinetoplastae, Trypanosomatidae, is a group of single flagellated parasites found in a wide range of geographic areas. All members in this group are exclusively parasitic and found primarily in insects, although a few genera have life cycles involving a secondary host, which might be vertebrates, and plants. Their presence can cause a considerable economic impact and several species can cause diseases in plants, insects, animals, and humans. The three main sicknesses caused by trypanosomatids in humans are African trypanosomiasis (caused by *Trypanosoma brucei* and transmitted by the vector tsetse flies), Chagas disease (caused by *Trypanosoma cruzi* and transmitted by triatomine bugs), and leishmaniasis (caused by several species of *Leishmania* transmitted by sandflies) (Nussbaum et al., 2010). Three parasite genera are dioxenous (two hosts in the life cycle), *Leishmania*, *Phytomonas*, and *Trypanosoma*, while all the rest are monoxenous (one host in the life cycle) (Overath et al., 2001). *Trypanosoma* species can employ two different forms of development inside the invertebrate host vector. The Salivary species are characterized by parasites that can develop in the initial portion of the invertebrate digestive system and transmitted to the vertebrate host through the insect bite (Stevens and Gibson, 1990; Haag et al., 1998). Meanwhile, the Stercorary species are characterized by their development in the invertebrate posterior region of the digestive system and transmitted to the vertebrate host through urine-feces excretion (Stevens and Gibson, 1990; Haag et al., 1998).

Trypanosomatids can cause agricultural and non-agricultural economical losses. The honeybee *Apis mellifera* can pollinate crop fields and fruit trees, however, the trypanosomatid pathogen *Crithidia mellificae* can infect the honeybees, causing economical losses in terms of honey production and the agriculture for food production (Ravoet et al., 2013; Runckel et al., 2014).

Phytomonas is a ubiquitous and diverse genus of plant parasites distributed in a wide range of tropical and subtropical geographic areas (Sturm et al., 2007; Votýpka et al., 2010). *Phytomonas* spp were first described from the latex of the Mediterranean spurge *Euphorbia pilulifera* (Lafont, 1909). They can grow and develop in latex tubes, phloem, fruit sap, seeds, and nectar of many plant families (Sturm et al., 2007; Votýpka et al., 2010). Currently, the *Phytomonas* genus includes more than two hundred species, which can colonize more than twenty plant families and are pathogenic in the phloem of the coffee tree, coconut palms, and oil palms (Camargo, 1999; Dollet et al., 2000). In those plants, this can cause lethal diseases and destruction of plantations in Central and South America. *Phytomonas* are transmitted by the nocturne coreid spurge bug *Dicranocephalus agilis*, which is the natural vector.

Leishmanias is a very diverse genus distributed worldwide, and over 20 different species have different animal hosts, which are transmitted by over 90 sandfly insect vectors. Leishmaniasis is one of the seven most important neglected tropical and subtropical diseases, which is found in all continents, apart from Oceania (Torres-Guerrero et al., 2017). It is endemic to Asia, Africa, the Mediterranean region, and the Americas.

Leishmania species can generate three different forms of disease that are cutaneous, mucocutaneous, and visceral with a potentially fatal outcome (Torres-Guerrero et al., 2017). Diagnosis (case finding) and treatment of leishmaniasis can cost \$11-22 as measured by the disability-adjusted life-years (DALY) measure averted in developing countries (Conteh et al., 2010). Parasite identification is clinically relevant since it is known that there exists a link between the *Leishmania* species and disease severity, which can influence the treatment outcome (Arevalo et al., 2007).

The *T. brucei* causes African trypanosomiasis or sleeping sickness, which is restricted to tropical Africa, mainly in rural areas, where wild and domestic animals act as a reservoir of the disease. The parasite develops in the salivary gland of the tsetse fly and it is transmitted by the insect bite (Nussbaum et al., 2010). Diagnosis and treatment of the African trypanosomiasis cost \$12-24 per DALY averted in developing countries (Conteh et al., 2010). This treatment cost is mainly due to private drug donations or preferentially priced medicaments.

Chagas disease or American trypanosomiasis is caused by *T. cruzi* and has two phases (Bern, 2015). The initial acute phase can last several weeks and then some patients can develop a chronic phase which might continue for decades and can generate mega-organ syndrome, cardiomyopathy, and sudden death (Bern, 2015). This disease remains as the most important parasitic disease in the Western hemisphere with an estimated disease burden, as measured by DALY, that is 7.5 times bigger than malaria (Lee et al., 2013). *T. cruzi* is transmitted to vertebrate hosts by Stercorary triatomine bugs, which are distributed mainly in rural areas from South USA to Argentina and North Chile (Nussbaum et al., 2010).

It is thought that trypanosomatids have a single origin, exclusively as insect-borne parasites, and then become digenic when vertebrates appeared in the Mesozoic era about 230 million years ago (Hamilton et al., 2004). Despite being evolutionarily primitives and mainly asexually reproduced, however, they have developed genetic recombination mechanisms as evolution driving forces. After the fusion of two diploid cells (a kind of asexual mating) and later nuclear erosion, the tetraploid cell eventually tends to return to the diploid stage after genetic exchanging, as described for *T. cruzi* hybrid strains (Westenberger et al., 2005). It is currently accepted that reproduction involving asexual meiosis can explain *T. brucei* variability, a process that occurs in the salivary gland of the insect vector (Gibson, 1990). This parasexual pathway is also observed in axenic cultures of *Leishmania*, although seems to be unlikely or rare in nature (Chogas, 1986; Cruz et al., 1993; Laurent et al., 2007). This genetic exchange mechanism has been also observed in some fungi (Heitman et al., 2014). On the other hand, in other parasites, such as *Plasmodium falciparum* (which causes malaria), sexual reproduction is an obligatory part of the life cycle, and mating must occur during every transmission cycle through the mosquito vector (Rono et al., 2018).

Trypanosomatids can respond rapidly and efficiently to quick environmental changes, though cannot regulate gene expression at the transcriptional level as higher eukaryotes do (De Pablos et al., 2016). However, they can mainly regulate gene product

functions at the post-transcription or post-translational levels (De Pablos et al., 2016). Also, *Leishmania* under conditions of severe stress can amplify single-copy genes to obtain a high amount of those gene products (De Pablos et al., 2016). In experimentally induced drug-resistant *Leishmania* strains, it is common to find circular episomes, which are the result of the amplification of short chromosomal regions containing key enzymes involved in DNA nucleotide metabolism and overexpression (by gene amplification) of specific genes involved in drug resistance, such as against antimonial drugs, which are used to treat leishmaniasis (De Pablos et al., 2016). Trypanosomatids must respond to extracellular and intracellular signals as they should adapt quickly to new environments inside their various hosts. Transcriptional responses are absent in trypanosomatids as their transcriptional units are polycistronic and their promoters do not contain gene regulatory sequences as in higher eukaryotes (De Pablos et al., 2016). Therefore, the regulation must be through mRNA processing, mRNA translation, mRNA stability, protein stability, and modification. Interestingly, after heat shock in *T. brucei*, changes in mRNA compartmentalization are observed (Minia et al., 2016). The untranslated mRNA of the zinc-finger protein ZC3H11 is present in the cytosol, however, after heat shock, it moves to a polysomal fraction and escapes sequestration into the granules and the mRNAs bound for ZC3H11 remained in the polysomal fraction to be translated (Minia et al., 2016). The function of ZC3H11 has been shown to be regulated by protein kinases. Interestingly, another example of rapid protein regulation to oxidative stress is the *T. cruzi* pol β , which can be overexpressed and quickly activated by protein kinases after acute exposition to hydrogen peroxide (Rojas et al., 2018).

Considering the importance of trypanosomatids as pathogens of humans, animals, plants, and insects is important to know the basic biological process that controls their complex life cycle. Trypanosomatids are early-branching eukaryotes, and their primitive lineage has revealed unusual biological features, and probably their most notable characteristic is the mitochondrial DNA, named kinetoplast DNA (kDNA). Therefore, we will describe the kDNA repair and minicircle kDNA replication processes of those parasites with an emphasis on the function and involvement of pol β -like enzymes in DNA repair and replication.

BASE EXCISION REPAIR

The eukaryotic cell possesses mitochondrial and nuclear genomes, which can replicate and accumulate mutations. Nuclear damaged DNA is repaired by multiple, often overlapping, DNA repair systems, however, mitochondrial DNA has a more restricted repair system. Since reactive oxygen species (mtROS) are produced in the mitochondria, the genome is altered; therefore, this organelle must possess a DNA repair system to deal with oxidative damage. The DNA repair systems are essential to maintain genome integrity and can therefore avoid mutations to ensure cell survival. In the

nucleus, DNA lesions are frequently generated; abasic sites and DNA strand breaks that are oxidized, deaminated, and alkylated are repaired mainly by the BER system (for a comprehensive review see references 28 and 29). The BER system has been extensively studied in mammalian cells and starts with a DNA glycosylase that removes the damaged base, producing an apurinic/apyrimidinic site (AP site) followed by an incision of the phosphodiester backbone 5' to the abasic site by an AP endonuclease (Krokan and Bjørås, 2013; Beard et al., 2019; Mullins et al., 2019). This step leaves a single-nucleotide gap with 3'-hydroxyl and 5'-deoxyribose phosphate at the gap margins. Afterward, pol β incorporates the missing nucleotide according to the template instructions and removes the 5'-deoxyribose-5-phosphate (intrinsic dRP lyase activity), and the chain is sealed by a DNA ligase (Krokan and Bjørås, 2013; Beard et al., 2019). In the short-patch pathway (SP-BER) a unique nucleotide is inserted by pol β , but in the long-patch pathway (LP-BER) two or more nucleotides can be incorporated by pol β or pol λ (García-Díaz et al., 2001; Braithwaite et al., 2005; Braithwaite et al., 2005; Krokan and Bjørås, 2013). Both the SP- and LP-BER are sub-pathways of BER, and they have common steps. One of the most common lesions caused by ROS is the formation of 7,8-dihydro-8-oxoguanine lesions (8-oxoG), which if left unrepaired can lead to mutagenic GC-TA transversions during cell replication (Krokan and Bjørås, 2013; Beard et al., 2019). In the nuclei of mammalian cells, most of the DNA oxidative damage is repaired by BER, and pol β is the principal polymerase involved in this process (Krokan and Bjørås, 2013; Beard et al., 2019). However, pol λ also plays a minor role in BER during the repair of oxidative DNA damage and possesses a domain with dRP lyase activity (García-Díaz et al., 2001; Braithwaite et al., 2005; Braithwaite et al., 2005). Mammalian pol β is a small 335-amino-acid-residues-long polypeptide possessing two domains that correspond to an N-terminal 90-amino-acid-residues-long domain (8 kDa amino-terminal domain) and a 265-amino-acid-residues-long C-terminal domain (31 kDa carboxy-terminal domain) (Beard and Wilson, 2019). The amino-terminal domain has intrinsic lyase activity and can remove the 5'-deoxyribose phosphate, which is left after incision by an apurinic/apyrimidinic endonuclease (AP) in the course of BER. The C-terminal domain has DNA polymerase activity and is involved in template-directed gap-filling of DNA. Although it was thought that mammalian pol β was located exclusively into the nucleus, it has been recently found that pol β is associated with mouse and human mitochondria of brain and kidney cells, indicating a role of this enzyme in mitochondrial DNA repair (Sykora et al., 2017; Prasad et al., 2017; Kaufman and Van Houten, 2017). The size of pol β detected in mitochondria and nuclei is the same, indicating that both are identical proteins.

DNA POLYMERASE X-FAMILY

The pol X family can be found in all life kingdoms and are phylogenetically conserved. In mammals, the pol X family is

comprised of pol β , pol μ , pol λ , and terminal deoxynucleotidyl transferase (TdT) (Bienstock et al., 2014). Plants, fungi, and simpler organisms (bacteria) possess only one or two family members, and a pol X member has been also found in the African swine fever virus (Bienstock et al., 2014). Surprisingly, in some metazoan organisms, such as *Caenorhabditis elegans* and *Drosophila melanogaster*, pol X family members are not present. Pol X family members are mainly involved in DNA repair pathways, such as BER, nonhomologous end joining (NHEJ), and V(D)J recombination. Typically, the members of this family show low fidelity; contrastingly, family A and B members are highly accurate and function in DNA replication and repair of replication errors. In mammals, the pol X family are rather small proteins ranging from 35–75 kDa, and they share a common domain structure, which is a BRCT domain (BRCA1 C-terminal) at the N-terminus (with exception of pol β), a Ser/Pro-rich domain (exclusively in pol λ), a middle lyase domain, and a C-terminal polymerase domain with three subdomains: DNA-binding (D), catalytic (C), and nucleotide binding (N) (Bienstock et al., 2014). The BRCT domain is essential for interactions with functional partner proteins of the NHEJ system, such as Ku antigen, DNA ligase IV, and XRCC4 in vertebrates. The lyase domain is involved in dRP lyase activity and is only active in pol β and pol λ , which are involved in BER (Bienstock et al., 2014). On the other hand, the polymerase domain is involved in DNA synthesis.

Fungi, such as *Schizosaccharomyces pombe*, contain a pol X (SpPol4) closely related to mammalian pol μ , whereas *Saccharomyces cerevisiae* pol X (Scpol4) is related to mammalian pol λ (Bienstock et al., 2014). On the other hand, plants have only a pol λ orthologue. Trypanosomatids are unusual since they have two pol β -like enzymes, which are named pol β and pol β -PAK. Those polymerases in most of the trypanosomatids are mitochondrial, although in *Leishmania* pol β is nuclear as well as in higher eukaryotes. Interestingly, trypanosomatid pol β is related to vertebrate pol β , as they share the same ancestor gene (Bienstock et al., 2014). Both, pol β and pol β -PAK are involved in kDNA replication and kDNA repair. Therefore, we will focus mainly on the biological functions of trypanosomatid pol β and pol β -PAK.

KINETOPLAST DNA REPLICATION

Trypanosomatids contain a single and large mitochondrion, with a specialized region of the mitochondria containing an unusual DNA, which is named kinetoplast and is a characteristic structure of the Kinetoplastida order. The kinetoplast contains several discrete domains and those are described in **Figure 1A** (Cavalcanti and de Souza, 2018). The kDNA is a network of circular DNA, consisting of thousands of interlocked DNA circles. Those DNA circles are of two types, the maxicircles (20–40 Kb, depending on the species) and the minicircles, which are 1.0–2.5 Kb in size and depend upon the species (Jensen and Englund, 2012; Botero et al., 2018; Cavalcanti and de Souza, 2018). The minicircles and maxicircles can be observed in **Figure 2**.

There are only a few dozen identical copies of maxicircles, which are analogous to the mitochondrial DNA of higher eukaryotes, and several thousand minicircles, which can differ in size and sequence between species. The DNA maxicircles encode the mitochondrial gene products, whereas the DNA minicircle encodes guide RNAs (gRNAs), which contain the genetic information to edit mitochondrial RNA transcripts (Benne, 1990; Jensen and Englund, 2012).

The replication mechanism of the kDNA is not well understood yet, however, the minicircle replication has been more studied than the maxicircle replication and is better understood. It is important to note that the proteins involved in this process have different locations within the kinetoplast with respect to the kDNA disk (see **Figure 1A**). The location of the proteins and enzymes involved in kDNA replication indicates that the events of replication of the kDNA are spatially regulated, and they proceed in an orderly fashion (Jensen and Englund, 2012). Minicircles contain a conserved region, with three highly conserved sequence blocks (CSB), namely, CBS-1, CBS-2, and CBS-3 (Ray, 1989). The sequences of those regions in *T. cruzi* are CBS-1 (AGGGGCGTTC; 10 bp), CSB-2 (CCCCGTAC; 8 bp), and CBS-3 (GGGGTTGGTGTA; 12 bp) (Botero et al., 2018). Both CBS-1 and CBS-2 present lower interspecies homology, however, CBS-3 is highly conserved in most of the trypanosomatids, also named Universal Minicircle Sequence (UMS), and is part of the minicircle replication origin (Ray, 1989; Jensen and Englund, 2012; Botero et al., 2018). The number of UMS in each minicircle depends on the species and the *T. cruzi* minicircles contain four UMS, whereas the *T. brucei* minicircles contain a single UMS (Botero et al., 2018). UMS is the specific DNA binding site for the protein UMS binding protein (UMSBP), which is involved in kDNA replication and segregation (Abeliovich et al., 1993; Milman et al., 2007). This protein has been well studied in *Crithidia fasciculata* and is also present in other trypanosomatids such as *T. brucei* and *Leishmania donovani* (Milman et al., 2007; Jensen and Englund, 2012; Englund, 2014). The importance of the USBP has been demonstrated in *T. brucei* in which the knockdown of both USBP genes affects the kDNA minicircles replication initiation, segregation of the daughter networks, and also blocks nuclear division (Milman et al., 2007; Englund, 2014). USBP is a single-stranded sequence-specific DNA binding protein that can bind to the UMS and an octameric sequence conserved at the replication origin of *C. fasciculata* kDNA minicircles (Tzfati et al., 1995; Singh et al., 2016). USBP is a small conserved protein that contains five tandemly arranged zinc knuckle motifs. Each motif forms a compact zinc finger containing the core motif CysX2CysX4HisX4Cys (X represents any amino acid). USBP orthologues have been described in *T. brucei* (TbUMSBP1) (Wang et al., 2000) and in *T. cruzi* (PDZ5; TcUMSBP1) (Coelho et al., 2003) and they can be found in most of the trypanosomatid genomes listed at the NCBI Genbank by using the BLASTP bioinformatic tool.

Moreover, *C. fasciculata* USBP binding to UMS is regulated by the redox potential. It has been shown that USBP activity cycles throughout the trypanosomatid cell cycle and the activity

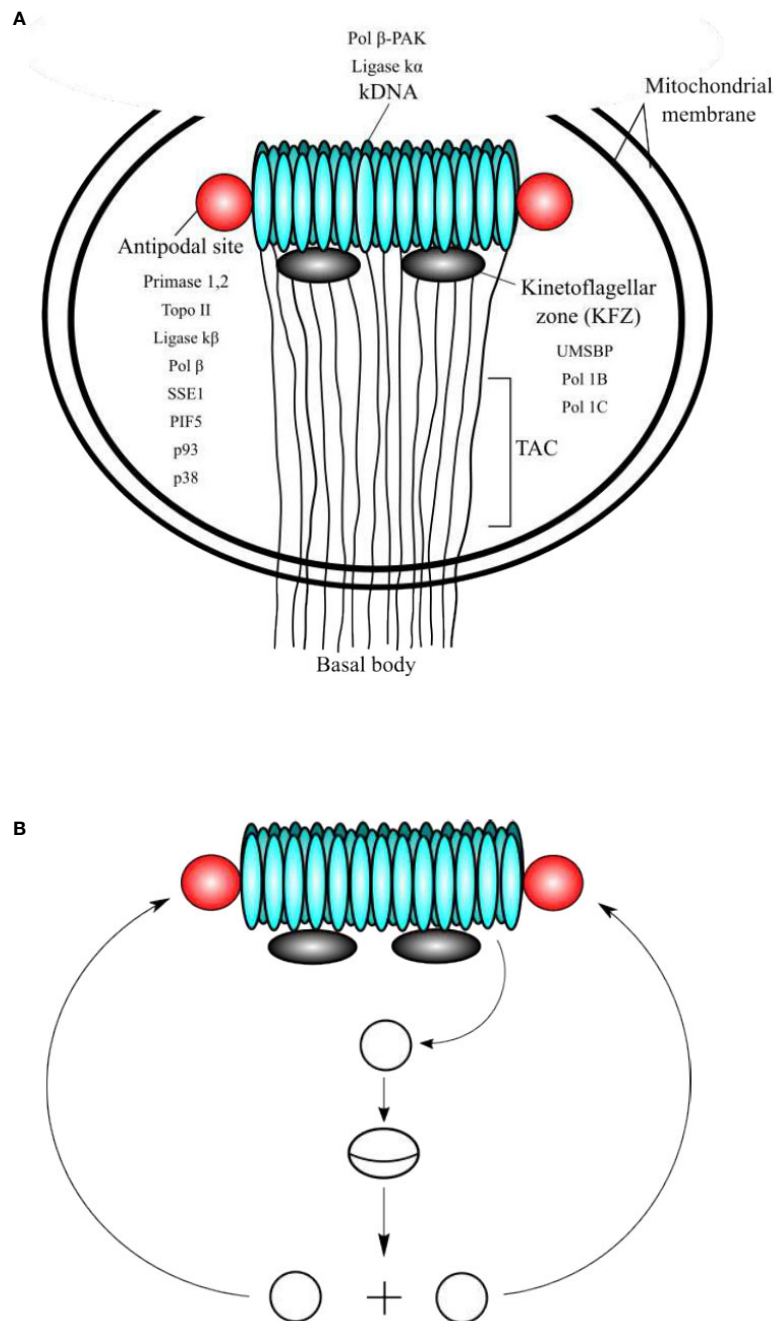


FIGURE 1 | (A) Schematic representation of the domains of kinetoplast. **(A)** The kinetoplast domains include the kDNA disc, the antipodal sites, the kinetoflagellar zone (KFZ), the tripartite attachment complex (TAC), and the basal body, which is located outside of the mitochondrial membrane. The locations of critical proteins involved in minicircle kDNA replication are shown. **(B)** At the beginning of replication, the minicircles are released into the KFZ from the network through decatenation by a type II DNA topoisomerase (yet to be identified), where proteins that initiate replication locate. Replication proceeds as a theta structure and the newly replicated sister minicircles migrate to the antipodal sites. The next steps of kDNA replication occur at the antipodal sites, which contain a set of proteins involved in kDNA replication. Minicircles are attached to the network by topo II, where RNA primers are removed by SSE1/PIF5 and gaps are filled by pol β and nicks are sealed ligase $\kappa\beta$. Those minicircles that contain at least one gap are repaired at the kDNA disc by pol β -PAK and ligase $\kappa\alpha$.

tightly correlates with the UMSBP redox state (Sela and Shlomai, 2009). The oxidation of UMSBP can result in dimerization with inhibition of its binding activity to the UMS, while the reduction

of UMSBP can produce monomers that can easily bind to the UMS (Sela and Shlomai, 2009). However, the binding of UMSBP to the replication origin is not regulated by the protein

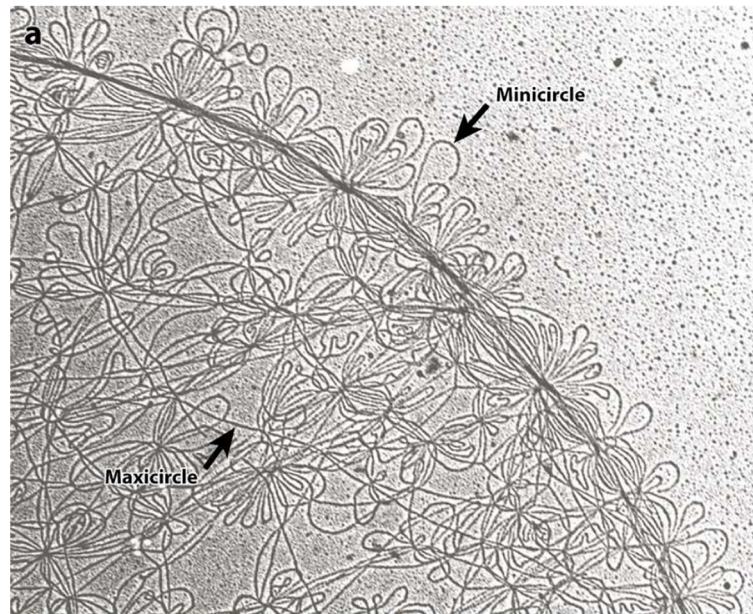


FIGURE 2 | Electron microscopy photographs of the isolated kDNA network from *C. fasciculata* show the minicircles (small DNA loops) and maxicircles (long strands). Both, minicircles and maxicircles are indicated by the arrows. This figure was reproduced from reference 40. Each minicircle has a contour length of 0.7 microns.

oligomerization state. It has been shown that loss of UMSBP DNA-binding activity by oxidation is a consequence of intramolecular generation of disulfide bonds, and this event does not affect oligomerization (Sela and Shlomai, 2009). UMSBP oligomerization occurs in zinc-depleted unfolded zinc finger domains, but the zinc presence is essential for UMSBP binding to the replication origin of kDNA minicircles (Sela and Shlomai, 2009). This indicates that the binding of UMSBP to the UMS depends on intact properly folded zinc finger domains. The trypanothione-dependent trypanredoxin is able to activate the binding of UMSBP to the UMS DNA sequence, indicating that binding of the UMSBP at the replication origin of the kDNA minicircles is regulated by a redox mechanism (Sela and Shlomai, 2009).

Prior to the replication, the minicircles are released from the network into the kinetoplast flagellar zone (KFZ) by a type II DNA topoisomerase and the UMSBP should bind to the UMS (CBS-3) of the minicircle replication origin and start the recruitment of the other protein components needed for replication to proceed. The UMSBP locates at two sites in the KFZ whereupon minicircle replication begins (Benne, 1990; Jensen and Englund, 2012; Englund, 2014). It is still unknown the number of components involved in the replication of kDNA minicircles, but this might be 50 or 100, due to the complexity of the process since the kDNA network has an unusual organization, which imposes constraints to the process. The knowledge of the functions of the proteins involved in the process can lead to a partial model of kDNA replication as proposed by Englund and colleagues (Benne, 1990; Jensen and Englund, 2012; Englund, 2014) and detailed here (**Figures 1A, B**). Once the UMSBP is bound to the kDNA replication origin (UMS) of the minicircles, a

Pol I-like and a DNA primase should bind to the replication origin, recruited by UMSBP (**Figure 3**) and perhaps other auxiliary proteins as well, to start the synthesis of the daughter strands (Benne, 1990; Jensen and Englund, 2012; Botero et al., 2018). The replication of the leading strand starts near the UMS, and the replication of the lagging strand begins near the CBS-2 block. The CBS-1 block lies downstream and close to CBS-2. The replicative DNA polymerase seems to be pol IB (and perhaps pol IC in the leading strand), which could replicate both the leading and the lagging strand of the minicircle (Bruhn et al., 2010). However, the involvement of another pol I-like, such as pol IC, cannot be ruled out, and it might be possible that pol IB replicates the lagging strand and pol IC could replicate the leading strand as proposed in **Figure 3**. The replication proceeds unidirectionally from the UMS in a theta structure intermediate, resulting in a single gap in the leading strand and multiple gaps between Okazaki fragments in the lagging strand. The sister minicircles are believed to migrate to the antipodal sites, where RNA primers must be removed from the Okazaki fragments by PIF5 a DNA helicase that functions in primer removal from Okazaki fragments together with structure-specific endonuclease 1 (SSE1), an enzyme with RNAase H activity (Jensen and Englund, 2012; Englund, 2014). Thereafter, most of the gaps are filled by pol β to be sealed by DNA ligase $\kappa\beta$ (ligase $\kappa\beta$), and the newly replicated minicircle is attached to the periphery of the kDNA network by DNA topoisomerase II (topo II) (Jensen and Englund, 2012). However, one or two gaps are maintained on some of the newly replicated minicircles after attachment to the network and they are probably filled by pol β -PAK" and sealed by DNA ligase $\kappa\alpha$, most likely at the kDNA disk, where pol β -PAK and DNA ligase $\kappa\alpha$ (ligase $\kappa\alpha$) locate (Jensen and Englund, 2012). After the whole process is

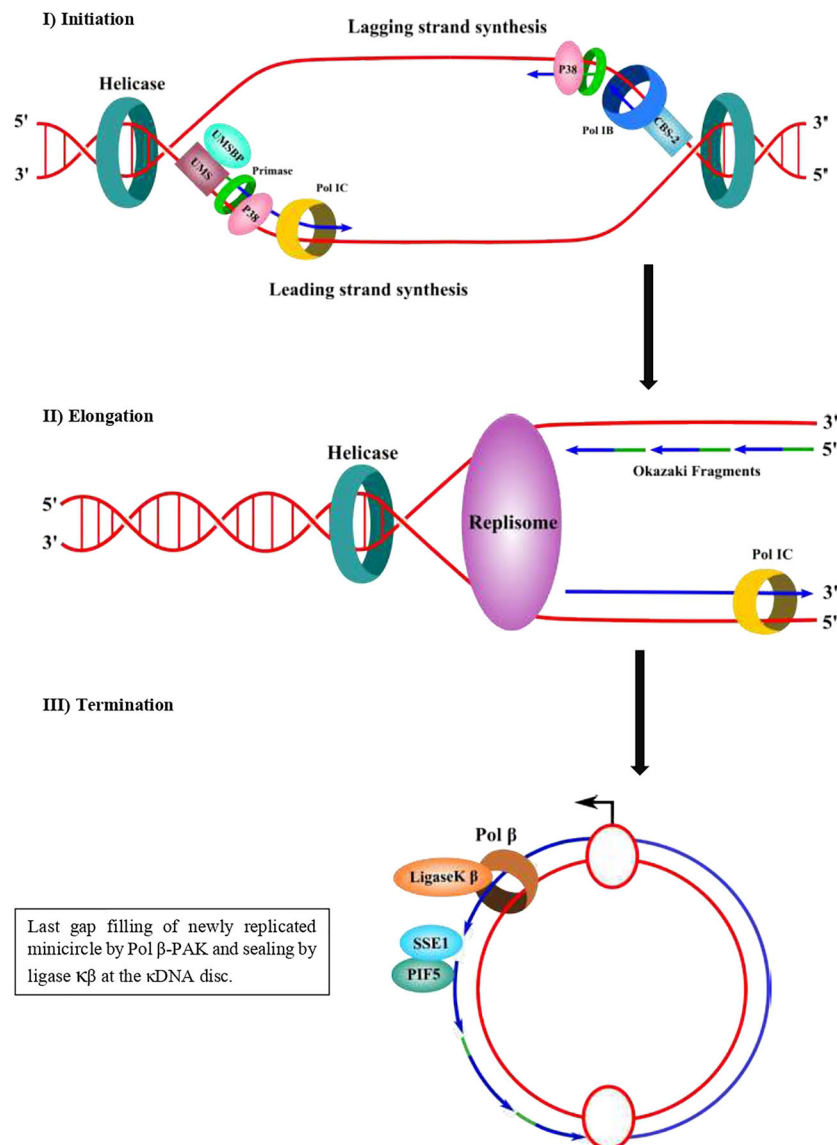


FIGURE 3 | Proposed molecular mechanism of minicircle kDNA replication. In a first step (initiation), UMSBP binds to the CBS-3 (UMS) at the replication origin and recruits a helicase/p38 complex, which in a complex with a DNA helicase can open the replication origin using ATP hydrolysis and recruits a primase/pol I complex. The leading strand synthesis starts near the UMS and the lagging strand synthesis starts near CBS-2 (former hexamer). CBS-1 lies downstream and close to CBS-2. In a second step (elongation), a replisome elongates the DNA daughter strands of both the leading strand (continuous) and the lagging strand as Okazaki fragments. The lagging strand can be synthesized by pol IB and the leading strand could be replicated either by pol IB or pol IC. It is not clear yet whether pol IB synthesizes both strands and whether another pol I (pol IC) could synthesize the other strand. A DNA helicase should separate the DNA strands and DNA topoisomerase should manage the supercoiling produced during the movement of the replisome. In a third step (termination) and after synthesis of both strands, the sister minicircles migrate to the antipodal sites and primers from Okazaki fragments are eliminated by SSE1/PIF5, followed by gap-filling by pol β and sealed by ligase κβ and then attached to the network periphery by topo II. Some of the newly replicated minicircles might contain one or two gaps and they are gap-filled by pol β-PAK and sealed by ligase κα to terminate the replication process. Primers of the Okazaki fragments are shown in green. Newly synthesized DNA is shown in blue.

finished, the progeny networks are segregated into the daughter cells. The supercoiling produced during minicircle DNA replication should be managed by mitochondrial DNA topoisomerase IA to allow the replisome to progress and for proper segregation of the progeny molecules (Sococa and Shapiro, 2008; Jensen and Englund, 2012). The

current model of minicircle kDNA replication is displayed in **Figures 1A, B**, and we propose a molecular model of minicircle kDNA replication in **Figure 3**. The main proteins that have been identified and that participate in minicircle kDNA replication are listed in **Table 1**.

TABLE 1 | Main proteins involved in minicircle kDNA replication that have been identified.

| Name | Accession Genbank | Function |
|-----------------------|-------------------|------------------------------------|
| Primase 2 | RHW74362* | Minicircle primase |
| Topo II | CAA42182 | Minicircle attachment to kDNA disc |
| Ligase $\kappa\beta$ | AAQ88427 | Gap sealing |
| Pol β | AAA68599 | Gap filling |
| p93 | RHW73544* | kDNA replication |
| p38 | AAQ39843 | Binds replication origin |
| UMSBP | AAC32813 | Binds UMS |
| Pol IB | AAM81963* | kDNA synthesis |
| Pol IC | AAM81964* | kDNA synthesis |
| Pol β -PAK | AAQ516190* | Gap filling |
| Ligase $\kappa\alpha$ | AAY22182 | Gap sealing |
| SSE1 | AF124228 | RNA primer removal |
| PIF5 | RHW71036* | Helicase for RNA primer removal |

For each identified protein, name, accession number, and function are indicated. Those proteins labeled with * have been identified from *Trypanosoma brucei* and the rest from *Crithidia fasciculata*.

MOLECULAR CHARACTERISTICS OF TRYPANOSOMATID POL β

As stated earlier, trypanosomatids have two DNA pol β -like enzymes. Pol β locates at the mitochondria, together with another DNA pol β -like polymerase, which is named pol β -PAK. Both DNA polymerases function in the BER pathway of the kDNA repair of oxidative lesions and in replication of the kDNA minicircles.

The pol β from *C. fasciculata* was the first trypanosomatid mitochondrial DNA polymerase of this family to be purified and its encoding gene was cloned (Torri et al., 1994; Torri and Englund, 1995). Later, by searching the genome database of *T. brucei*, two genes encoding two pol β -like enzymes were discovered (Saxowsky et al., 2003). One is the homolog of *C. fasciculata* pol β and the other was distantly related, and it was named pol β -PAK. Both enzymes are mitochondrial, however, their location into the kinetoplast is different. Pol β locates at the antipodal sites, whereas pol β -PAK locates at the kDNA disk (Saxowsky et al., 2003). Pol β -PAK from *T. brucei* has unusual structural features, such as a long N-terminal domain, which is rich in Proline, Alanine, and Lysine residues (PAK domain); however, this domain is absent in homologues from *T. cruzi* and *L. infantum*, although they are also called pol β -PAK.

On the other hand, *T. cruzi* pol β was first purified by our group from *T. cruzi* epimastigotes cell extracts. The major polypeptide of the purified fractions had a 50 kDa molecular weight and a minor polypeptide of 45 kDa after analysis by SDS-PAGE (Venegas and Solari, 1995). Only the 50 kDa polypeptide had polymerase activity in a colorimetric activity in a gel technique. The purified enzyme was highly sensitive to inhibition by the dideoxythymidine triphosphate analog, and it is active in DNA synthesis using DNAase I-activated DNA as a template (Venegas and Solari, 1995). Also, a cDNA encoding for *T. cruzi* pol β was cloned by our group from a TcI lineage by using information from peptides obtained from the purification described earlier (Venegas et al., 2009). The cDNA encodes a protein of 403 amino acid residues, and it is similar to the one from a *T. cruzi* TcVI lineage (CL Brener), however, it differs in

three amino acid residues in highly conserved segments of the polypeptide (Venegas et al., 2009). From the published sequence of *T. cruzi* CL Brener genome, a pol β -related polymerase was found, named pol β -PAK, since it shares a high homology amino acid sequence with *T. brucei* pol β -PAK, and they are related at the level of amino acid sequence with mammalian pol β (Venegas et al., 2009). The mRNA encoding pol β is highly expressed in both proliferative and non-proliferative developmental forms of *T. cruzi*, indicating that the enzyme performs important functions through the complete life cycle of the parasite (Venegas et al., 2009).

The cDNA encoding *T. cruzi* pol β from TcI and TcVI lineages have been cloned and expressed in a recombinant form from bacteria and their biochemical properties were described by Machado and colleagues (de Oliveira Lopes et al., 2008) and by our group (Maldonado et al., 2015). Also, a cDNA encoding pol β -PAK has been cloned and expressed in *E. coli* (de Oliveira Lopes et al., 2008). The biochemical and molecular functions of both pol β and pol β -PAK were compared (de Oliveira Lopes et al., 2008). Both have some similar molecular functions, but they differ in some others. The main functional characteristics of pol β and pol β -PAK will be summarized in the next section.

As mentioned earlier, trypanosomatid pol β is multitasking and one of the smallest DNA polymerases belonging to the pol X family of DNA polymerases. This polymerase has two main domains, which can be defined based on the structure of the homolog human pol β . The N-terminus contains an 8 kDa domain with lyase activity, whereas the second domain contains three subdomains, namely, the DNA binding (D), catalytic (C), and nucleotide-binding (N) subdomains (Garcia-Diaz et al., 2001; Braithwaite et al., 2005; Prasad et al., 2017), which comprise the polymerase domain. Those domains allow pol β to perform its role in BER and to carry out other roles such as replication of the kDNA. The lyase domain can remove the 5'-deoxyribose phosphate (dRP lyase) left after incision for the AP endonuclease during BER, and afterward the missing nucleotide is inserted by pol β itself and the nick can be sealed by a ligase. Also, the lyase domain of human Pol β participates in the processive search for DNA damage by interacting nonspecifically with DNA during the processive search process (Howard et al., 2017; Howard and Wilson, 2017; Howard et al., 2020). The functions of the other three subdomains are the binding to the DNA (D), template-guided incorporation of the missing nucleotide (C), and binding of the nucleotide for catalysis (N). The role of trypanosomatid pol β in kDNA replication and repair of oxidative lesions has been demonstrated in *T. cruzi* (Schamber-Reis et al., 2012; Rajao et al., 2014). On the other hand, it is most likely that pol β in *T. cruzi* is always bound to the DNA, even in the absence of DNA damage, as it can be crosslinked to kDNA (Rojas et al., 2018) and we speculate that carries out a similar role in processive searching as the lyase domain in human pol β . In *T. cruzi* pol β there is an extra domain, located at the C-terminus, which we named CK2-regulatory domain, since possesses several consensus sites for Casein Kinase 2 (CK2) phosphorylation, and perhaps this

domain regulates its DNA synthesis activity. This domain is absent in human pol β , and it is shorter in *C. fasciculata* and *L. infantum* pol β , whereas only a single CK2 phosphorylation site is conserved in *T. brucei* pol β . The domain organization of those enzymes is described in **Figure 4A**. A phylogenetic analysis of the different polymerases is displayed in **Figure 4B**.

The *T. cruzi* pol β -PAK is larger than pol β and contains 629 amino acids, which can be divided into four domains (**Figure 4A**). A N-terminal variable domain (NTVD) and a second domain with dRP lyase activity. The third domain is the DNA polymerase and contains the three subdomains D-C-N and a fourth C-terminal extra domain (CTVD). Also, it has an insertion in between the dRP lyase domain and the DNA polymerase domain. The function of this insertion is currently unknown, however, is Glycine-rich and might function as a hinge region. The fourth CTVD extra domain, located at the C-terminal end of the polypeptide, contains phosphorylation consensus sites for Casein Kinase 1 (CK1) and Protein Kinase A (PKA). Both pol β and β -PAK have dRP lyase and DNA polymerase activities, however, only pol β -PAK possesses *in vitro* trans-lesion synthesis (TLS) activity, since it can perform DNA synthesis through an 8oxoG lesion (de Oliveira Lopes et al., 2008). *T. brucei* and *L. infantum* pol β -PAK are large

polypeptides, however, their domain organization is similar to the other DNA polymerases displayed in **Figure 4A**.

Although, pol β and pol β -PAK locate at the mitochondria, they have different locations inside the kinetoplast, while pol β locates at the antipodal sites, pol β -PAK is located at the kDNA disk (Saxowsky et al., 2003; de Oliveira Lopes et al., 2008; Schamber-Reis et al., 2012). These observations indicate that the two enzymes perform distinct and non-redundant roles in kDNA repair and replication. The fact that pol β -PAK can replicate through 8oxoG lesions (de Oliveira Lopes et al., 2008) might indicate that this polymerase is more error-prone than pol β itself, and this feature could be a mechanism to generate mutations in the minicircles in sites away from the CBS to generate diverse gRNAs involved in mitochondrial mRNA editing.

The cellular functions of *T. cruzi* pol β have been studied by overexpressing the protein in epimastigote cells and then exposing the cells to high concentrations of genotoxic agents in the absence or presence of BER inhibitors. The results indicate that the overexpression of pol β protects the cells from the effects of those agents, and the presence of BER inhibitors greatly reduces the protective effects of the overexpression of pol β (Schamber-Reis et al., 2012). It has been shown by

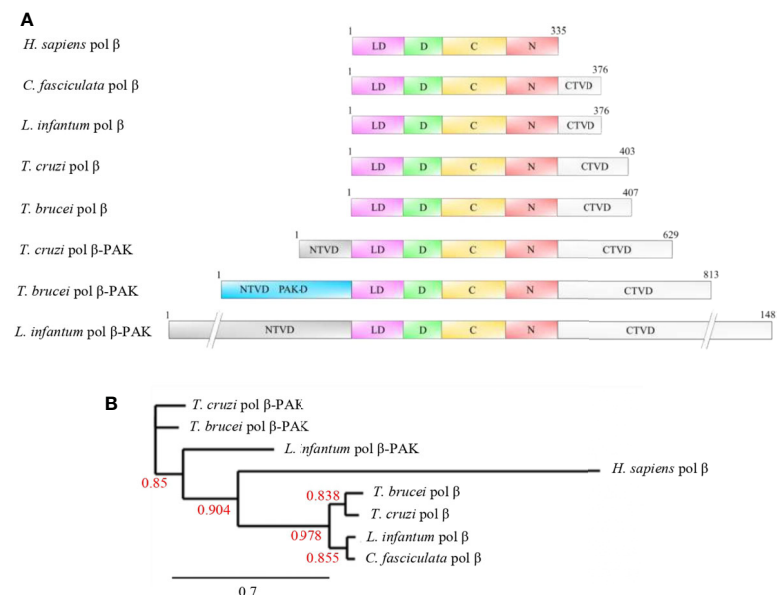


FIGURE 4 | (A) Domain organization of selected pol β and pol β -PAK enzymes from different trypanosomatid species compared to human pol β . Pol β -PAKs are large polypeptides of variable length and contain N-terminal variable (NTVD; grey) and C-terminal variable (CTVD; white) domains with a central core, which contains the conserved lyase and polymerase domains. *T. cruzi* pol β -PAK contains the PAK-D (light blue), which is rich in Proline, Alanine, and Lysine residues. The functions of those variable domains are largely unknown, but we speculate that might contain modification sites to regulate protein function or might be engaged in species-specific protein-protein interactions. On the other hand, pols β are smaller polypeptides compared to pol β -PAK and contain the conserved lyase and polymerase domains to complement their biological role in BER and replication. They contain an extra short C-terminal domain, which most likely could modulate their biological activities. The lyase domain (LD; pink), D-subdomain (green), and C-N-subdomains (red). **(B)** Phylogenetic tree of the selected trypanosomatid pol β -like enzymes and human pol β . It can be observed that human pol β is closer to the trypanosomatid pol β as they arose from the same ancestor, while pol β -PAK is rather distant compared to pol β . The Phylogenetic tree was constructed using the phylogeny.fr program and bootstrap values are given (red numbers). The bootstrap values show high confidence. The accession numbers of each polymerase are PBJ75947.1 (*T. Cruzi* pol β -PAK), AAQ56190.1 (*T. brucei* pol β -PAK), XP_001463421.1 (*L. infantum* pol β -PAK), NP_002681.1 (*H. sapiens* pol β), AAX79362.1 (*T. brucei* pol β), RNC61524.1 (*T. cruzi* pol β), AAF00495.1 (*L. infantum* pol β), and AAA68599.2 (*C. fasciculata* pol β). Dashes were introduced in the NTVD and CTVD in *L. infantum* pol β -PAK to fit into the figure.

immunofluorescence studies that *T. cruzi* pol β is found at the antipodal sites of kDNA in the epimastigotes in the replication stage from G1/S until the early G2 phase (Schamber-Reis et al., 2012). However, in the late G2 phase, pol β spreads and it is no longer associated with the antipodal sites and this pattern is maintained until the end of mitosis. Pol β is also located at the antipodal sites in amastigote developmental stages. Moreover, pol β is found in the mitochondrial matrix of trypomastigote cells (Schamber-Reis et al., 2012). When pol β is overexpressed in parasites, the levels of 8oxoG are reduced compared to normal cells (Schamber-Reis et al., 2012). Also, those pol β overexpressing-parasites showed increased resistance to hydrogen peroxide treatment, when compared with normal parasites (Schamber-Reis et al., 2012). Treatment of the pol β -overexpressing parasites with methoxyamine, which reacts to the apurinic/apyrimidinic sites inhibiting BER, prevents resistance to hydrogen peroxide treatment (Schamber-Reis et al., 2012). When epimastigote cells are treated with hydrogen peroxide, pol β forms a third focus in the kDNA in addition to those located at the antipodal sites (Schamber-Reis et al., 2012). Overexpression of pol β in epimastigote cells confers resistance to the drug benznidazole, which is one of the drugs used to treat patients with Chagas disease (Rajao et al., 2014). Since pol β is located into the mitochondria of *T. cruzi* cells, those observations indicate that benznidazole also induces damage to the kDNA (Rajao et al., 2014). We recently showed that *T. cruzi* epimastigote and trypomastigote cells exposed to hydrogen peroxide during short periods of time showed increased levels of pol β enzyme and two forms of the polymerase were identified and overexpressed after treatment with hydrogen peroxide (Rojas et al., 2018). The smaller one (L) was unphosphorylated, whereas the bigger one (H) was phosphorylated and active in DNA synthesis. Those results indicate that *in vivo* pol β must be phosphorylated to perform its function and is overexpressed in response to a genotoxic insult. pol β is associated physically with kDNA since it can be crosslinked to the kDNA; however, it is not associated with nuclear DNA (Rojas et al., 2018).

In both *T. cruzi* and *T. brucei*, pol β and pol β -PAK are nuclear-encoded enzymes, however, they are located in the mitochondrion (Saxowsky et al., 2003; Schamber-Reis et al., 2012). Also, in *C. fasciculata* pol β locates at the mitochondria, however, in other *Crithidia* species a pol β or pol β -PAK homologs cannot be found using BLAST searches. This indicates that a pol β encoding gene was deleted in the other *Crithidia* species during the speciation process or alternatively a pol β encoding gene was transferred from another trypanosomatid species into the *C. fasciculata* genome. Interestingly enough, in *Leishmania* species, the pol β enzyme is nuclear-located (Taladriz et al., 2001), however, a pol β -PAK encoding gene is found in the genome of these species. The pol β -PAK in *Leishmania* species is predicted to locate at the mitochondria; however, a biochemical characterization of this enzyme has not been done yet. This pol β -PAK homologue gene could fulfill the function of both pol β and pol β -PAK in the mitochondria of *Leishmania* species.

It is clear the role of pol β in *T. cruzi* and in other trypanosomatids is the kDNA replication and the repair, *via*

BER, of oxidative DNA damage, which is produced by genotoxic agents, such as hydrogen peroxide and benznidazole. It is still unknown whether trypanosomatid pol β can repair short or long patches of DNA and the processivity of this polymerase is largely unknown. Also, the signals that regulate the levels and activity of pol β remain to be studied.

KEY FEATURES OF TRYPANOSOMATID POL β STRUCTURE

As noted earlier, mammalian pol β has two enzymatic activities that contribute to the BER process. The activities are contained in two domains: the N-terminal 8 kDa lyase domain and the 31 kDa C-terminal polymerase domain. Trypanosomatid pol β display a similar domain structure, although the *T. cruzi* enzyme contains an extra CTVD domain which is rich in protein kinase CK2 phosphorylation sites, however, only one CK2 phosphorylation site is conserved in the *T. brucei* pol β .

The tridimensional structure of mammalian pol β has been solved with a variety of substrates, which has provided a wealth of structural information. For over 40 years, Wilson and colleagues have studied mammalian pol β at the biological and molecular level (for a review see reference Whitaker and Freudenthal, 2020). Structures of mammalian pol β and others derived from the pol X family of polymerases indicate that they have the same modular domain organization (Yamtich and Sweasy, 2010; Bienstock et al., 2014). Those members involved in DNA repair contain the N-terminal lyase domain and the polymerase domain, which is composed of three functionally different subdomains, including the DNA-binding (D), catalytic (C), and nucleotide-binding (N) subdomains (**Figure 5A**). The D subdomain is involved in the proper positioning of the template base, whereas the C subdomain coordinates two divalent metal cations and is responsible for the DNA synthesis. The N subdomain is involved in the binding of the deoxynucleotide triphosphate substrate. The D and N subdomains are spatially located on opposite sides of the C subdomain in the apoenzyme (**Figure 5A**), however, in the presence of substrates, the tridimensional structure shows that the lyase domain physically interacts with the N subdomain (Yamtich and Sweasy, 2010; Beard and Wilson, 2019) (**Figure 5B**).

As noted earlier, usually trypanosomatids possess more than one pol β -like enzymes. These enzymes are mitochondria-located in most of them, except in *Leishmania* species, where pol β is localized to the nucleus. Unfortunately, only one pol β crystal structure from trypanosomatids has been reported and derives from *Leishmania infantum* pol β , which is in a complex with a single-nucleotide gap substrate and a dNTP (Mejia et al., 2014). This crystal structure could shed light on the structure of *T. cruzi* and *T. brucei* pol β since they are highly conserved (70% sequence identity). The structural characterization reveals that *L. infantum* pol β conserves the overall conserved domain organization of pol X family of enzymes interacting with DNA in a similar manner to human pol β (Beard and Wilson, 2014) (**Figure 5C**). Modeling of the tridimensional structure of *T. cruzi* pol β indicates that adopts the

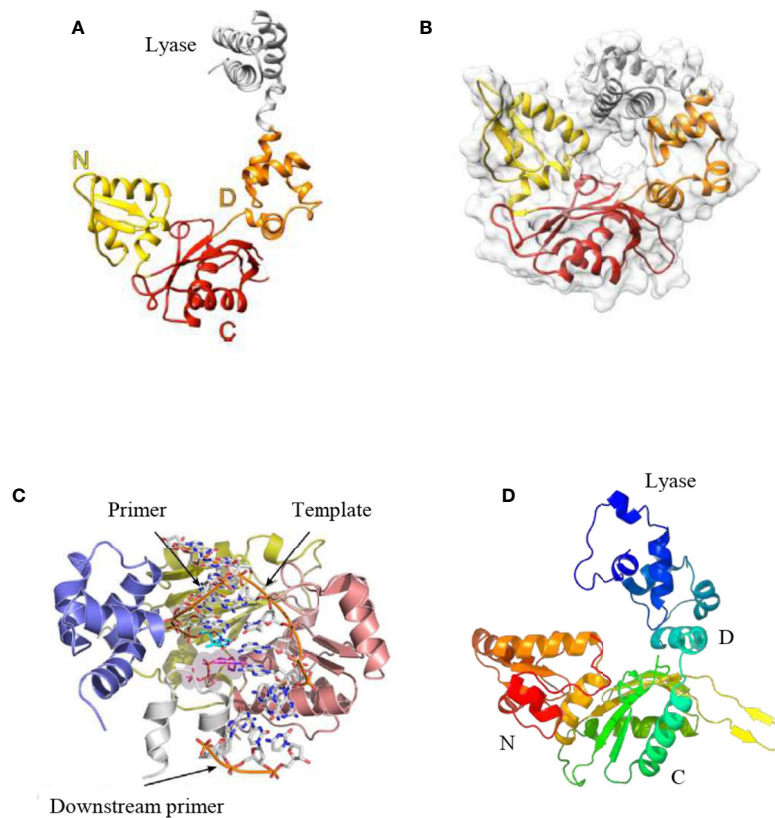


FIGURE 5 | (A) Tridimensional structure of the human pol β apoenzyme. The apoenzyme can form an extended structure, in which the lyase domain and polymerase subdomains can be seen. (B) The tridimensional structure of human pol β in a ternary complex displays a doughnut-like structure in which the lyase domain and the N-subdomain interact. (C) The crystal structure of *L. infantum* pol β in the ternary complex adopts a similar structure as the human pol β in the ternary complex. (D). Predicted tridimensional structure of *T. cruzi* pol β. The overall fold of this polymerase is similar to the structure of the human pol β apoenzyme (A). The modeling was performed with the Phyre2 Program. In (A, D), the domains are shown. Figures (A–C) were reproduced from references Mejia et al., 2014 and Beard and Wilson, 2014.

common pol X family fold as it is expected (Figure 5D). The overall predicted structure is similar to *L. infantum* and human pol β. It is important to state that family-X polymerases contain variable regions in between β-strands, which can form variable loops (Delarue et al., 2002; Mejia et al., 2014; Beard and Wilson, 2014). These loops are important to the pol X family of polymerases to perform specific functions. In *L. infantum* pol β, there is a variable loop at the C-terminus (loop 3) which interacts with the template strand upstream of the nascent base pair (Mejia et al., 2014). The deletion of this loop results in the higher catalytic activity of the *L. infantum* DNA pol β (Mejia et al., 2014). In *T. cruzi* pol β, this loop is longer as compared to the *L. infantum* enzyme and most likely plays a similar role, besides that contains several protein kinase CK2 phosphorylation sites.

We have done an extensive comparative analysis of the amino acid residues critical for pol β function and it shows that most of them are conserved in both *T. cruzi* and *L. infantum* pol β with respect to human DNA pol β (Yamtich and Sweasy, 2010; Bienstock et al., 2014; Mejia et al., 2014; Beard and Wilson, 2014).

Those key conserved residues are shown in Figure 6. The dRP lyase nucleophile Lys72 of human pol β is conserved in *T. cruzi* (Lys74) and *L. infantum* (Lys72) enzymes and Lys68, which corresponds to Lys70 in *T. cruzi* pol β and Lys68 in the *L. infantum* enzyme. Another conserved residue is Lys84 of human pol β, which corresponds to Lys86 in *T. cruzi* DNA pol β and Lys84 in pol β from *L. infantum*. Lys68 is important for the binding of the 5'-PO₄ (5'-dRP) moiety of the gap and Lys72 acts as the primary amine forming a Schiff-base intermediate for excision of the 5'-dRP moiety during the BER process. Lys84 acts as an alternative nucleophile in human pol β and most likely has the same function in trypanosomatid pol β. The 8-kDa lyase domain of *L. infantum* pol β is engaged in the binding of the 5'-PO₄ of the gapped DNA, however, the tridimensional structure of this domain was not completely resolved due to disorder in the structure of the lyase domain (Mejia et al., 2014).

The active site of *L. infantum* pol β shows the same structural features as those observed in human DNA pol β (Yamtich and Sweasy, 2010; Bienstock et al., 2014; Beard and Wilson, 2014).

| | | |
|--|--|-----|
| <i>T. cruzi</i> Pol β | MFRRTFRWNPDSRENIIRIFKEMADLNALGEKYKVQSYIRALNSLKTNDLPLRTVED | 60 |
| <i>L. infantum</i> Pol β | MLRRTFLR--RDHRENIIRIFQEMADLNALGEKYKVSSYHRSIESLKTNDKPLNTPQD | 58 |
| <i>H. sapiens</i> Pol β | MSKRKAPQ--ETLNGGITDMLTELANFEKNVSAIHKNYAKAASVIAKYPHKIKSGAE | 58 |
| * : * . : : * . * : : * : : : : : : : : * : : : : : : : : : | | |
| <i>T. cruzi</i> Pol β | LERFPGFGSKLLKAAEEIIMTGRLEELKKTTP-KLKAIQELTQVHGFGPRAAAALFDRE | 119 |
| <i>L. infantum</i> Pol β | LKAFSGFGAKLLKAAEIMATGRLEELKKTTP-KLKAIQELTQVHGFGPRAAAALFDRE | 117 |
| <i>H. sapiens</i> Pol β | AKKLPGVGTIAEKIDEFLATGKLRKLEIRQDDTSSINFLTRVSGIGPSAARK-FVDE | 117 |
| : : * . * : : * : : : * : : : * : : : * : : : * : : : * : : : | | |
| <i>T. cruzi</i> Pol β | GIFTVEELIEKADRI-QLTQQRVGVKYFHDINEIPMHESVLHENFLRESVQARLTSQDY | 178 |
| <i>L. infantum</i> Pol β | GIFTVEELLQKADSIPLTDQQRVGKIFYDINEIPMQESVLHENFLREKCEVLGKDF | 177 |
| <i>H. sapiens</i> Pol β | GIKTLEDLRKNE--KLNHHQRIGLKYFGDFEKRIPREEMLMQDIVLNE-VKKVDSEY | 173 |
| ** * : : * : : * . * . : : * : : * : : : * : : * : : : : : : : : | | |
| <i>T. cruzi</i> Pol β | EIQVCGSYRRHPFSGDVDAIARTLSAPPLDCPVNTGVLGTLDVYLQERNYLEATMAQ | 238 |
| <i>L. infantum</i> Pol β | SILICGSYRRHPFSGDVDAIARTLSAPPLDCPVNTGVLGTLDVYLQERNYLEATMAQ | 237 |
| <i>H. sapiens</i> Pol β | IATVCGSFRGAESSGDVLLTHPSFT---SESTKQKLLHQVVEQLQKVHFTITDLSK | 230 |
| : * : : * : : * : : * : : * : : * : : * : : * : : * : : * : : : | | |
| <i>T. cruzi</i> Pol β | GPLKYMGMGRLLPRTTN----GTTKHYKARRVIRLIEARSVPTALLTFTGSKNFNVIM | 293 |
| <i>L. infantum</i> Pol β | GPLKYMGMGRLLPRTNVRDKAGRENTKVYKARRVIRLIEKTSVPTAMLTFTGSKNFNVIM | 297 |
| <i>H. sapiens</i> Pol β | GETKFMGVCLPSK-----NDEKEYPHRRIRLIPKDYCYGVLYTFTGSDIFNKNM | 282 |
| * * : : * : : * : : * : : * : : * : : * : : * : : * : : * : : * | | |
| <i>T. cruzi</i> Pol β | RQAATISKGYLLNEGLFKLGSPEEVKALQERVRANKIAGTKNSPTDAASDPTVEEGVDFV | 353 |
| <i>L. infantum</i> Pol β | RQAATISKGYLLNEGLFKLGTPEEARALYERIGRK----- | 334 |
| <i>H. sapiens</i> Pol β | RAHALEKGTINEITIRPLGVTGVAG----- | 308 |
| * * : : * : : * : : * : : * : : * : : * : : * : : * : : * : : * | | |
| <i>T. cruzi</i> Pol β | VSVISGHSAMETLGLTKEELVKRVHVTCEKDVFDVLGMPFAKFNENRDP | 403 |
| <i>L. infantum</i> Pol β | -----NAGEELGVPKDELEDKRVEVRSEQDVFDVLGMPYAKFNENRDP | 376 |
| <i>H. sapiens</i> Pol β | -----EPLFVDSKIDFDYIQWKYREPKDRSE | 335 |
| : : * . * : : * : : * : : * : : * : : * : : * : : * : : * : : : | | |

FIGURE 6 | Protein sequence alignment of *T. cruzi*, *L. infantum*, and human pol β shows the key conserved residues involved in BER (yellow shaded). Those residues are also conserved in other trypanosomatid pol β enzymes as well. The alignment was done using the Clustal Omega program.

The active site is the DXD motif, which corresponds to Asp190 and Asp192 in human pol β and to Asp194 and Asp196 in the *L. infantum* enzyme. In *T. cruzi* pol β, those catalytic residues correspond to Asp195 and Asp197. The other important catalytic residue in human pol β is Asp256, which corresponds to Asp271 in the *L. infantum* enzyme and Asp267 in *T. cruzi* pol β. In human pol β Asp192 can coordinate two active-site Mg²⁺ metal ions required for DNA synthesis (Yamtich and Sweasy, 2010; Bienstock et al., 2014; Beard and Wilson, 2014). Also, Arg283 in the human polymerase is conserved as is key for fidelity since it functions in the proper positioning of the templating base and corresponds to Arg298 in *L. infantum* pol β and to Arg294 in the *T. cruzi* enzyme.

Residues important for dNTP binding of human pol β are in part contained in the YFTGSDIFNK motif (residues 271–280; 38,70), whereas in *T. cruzi* and *L. infantum* pol β is TFTGSKNFNV (residues 286–295 and 282–291 in the *T. cruzi* enzyme). That motif contains Asp276, which forms hydrogen bonds with O3' of the incoming nucleotide. Other important residues are Arg183, which coordinates non-bridging oxygens on the α-phosphate (Pα) and β-phosphate (Pβ) of the incoming nucleotide, while Arg149 and Gly189 coordinate the γ-phosphate (Pγ) of the incoming nucleotide. Asp276 in the human enzyme is substituted by Lys291 in *L. infantum* pol β and by Lys287 in the *T. cruzi* polymerase. Arg183 is conserved in *L. infantum* pol β (Arg187) and in the *T. cruzi* enzyme (Arg188). Gly189 in the human enzyme is also conserved and correspond to Gly193 in the *L. infantum* polymerase and to Gly194 in *T. cruzi* pol β, while Arg149 is replaced by Lys152 in *L. infantum* and for Lys153 in *T. cruzi* pol β. A detailed tridimensional structure of *L. infantum* pol β in a ternary complex (enzyme-DNA template-nucleotide) can be found in the paper by Mejia et al. (2014).

The structure of human pol β in the ternary complex is in a doughnut-like structure (**Figure 5B**), where the N-terminal lyase domain interacts with the N-subdomain of the polymerase domain and those interactions are key during the processing of the 5' and 3'-ends of the gapped DNA during BER (Beard and Wilson, 2014; Beard and Wilson, 2019). When it is compared the binary complex (enzyme-DNA template) with the ternary complex (enzyme-DNA template-dNTP) it is seen that the N-subdomain repositions itself and closes around the nascent base pair on the DNA (Beard and Wilson, 2014; Beard and Wilson, 2019). The lyase domain also closes and the interactions between the lyase domain and N-subdomain are enhanced, stabilizing a closed conformation. The transition from an open binary complex to a closed ternary complex can induce changes in the local hydrogen bonding involving a critical Asp192 of the catalytic site, which is required to coordinate two Mg²⁺ metal ions involved in DNA synthesis (**Figure 7**; Beard and Wilson, 2014; Beard and Wilson, 2019). The transition from an open to a closed form is induced by the binding of dNTP-Mg²⁺, since the binding of a dNTP without a coordinating metal does not induce a conformational change. During the open to closed transition state, an altered hydrogen bonding interaction occurs between key residues of the D and C-subdomains (Beard and Wilson, 2014; Beard and Wilson, 2019). Those changes involve Asp192, Arg258, Phe272, Glu295, Tyr296, and Arg283. In the open conformation, Asp192 interacts with Arg258; however, in the closed conformation, the interaction between these two residues is interfered by Phe272, and Arg258 can now interact with Glu295 and Tyr296, which in turn can interact with Arg283, which can interact with the template strand. Therefore, the position of the N-subdomain can be structurally transmitted to the active catalytic site and enables Asp192 to coordinate two Mg²⁺ metal ions (**Figure 7**; Beard and Wilson, 2014; Beard and Wilson, 2019). As mentioned

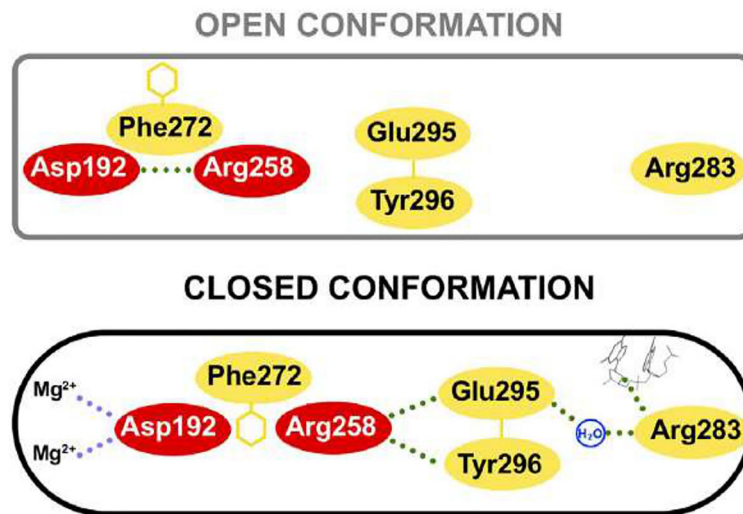


FIGURE 7 | Key residue interactions during the open and closed conformation of human pol β . In the open conformation Arg258 does not interact with Glu295 and Tyr296, however, in the closed conformation, Arg258 can interact with those residues and Glu295 can interact with Arg283, which in turn interacts with the templating coding base. Also, the closed conformation can coordinate two Mg^{2+} metal ions. Residues of the C-subdomain are red. This figure was reproduced from reference Beard and Wilson, 2014.

earlier, Asp192 and Arg258 from human pol β are conserved in trypanosomatid pol β and the rest of the residues are also conserved as well, including Phe272 (Phe282 in *T. cruzi* and Phe287 in *L. infantum* pol β), Glu295 (Glu306 in *T. cruzi* and Glu310 in *L. infantum* pol β), and Tyr296 (Tyr307 in *T. cruzi* and Tyr311 in the *L. infantum* enzyme). Arg283 of human pol β is also conserved in the tripanosomatid DNA pol β and corresponds to Arg294 in *T. cruzi* pol β and Arg298 in the *L. Infantum* polymerase.

CONCLUDING REMARKS

The minicircle kDNA replication is an extremely complex process that requires several proteins to be completed. Moreover, the architecture of the kDNA is unusual, and replication proteins are located at discrete domains into the kinetoplast. We expect that many other components of the replication machinery will be uncovered and the functions of those components studied. It is still unknown how the sister minicircles are moved to the antipodal sites and which are the motors and the mechanisms. Unfortunately, *in vitro* systems for kDNA replication and kDNA repair have not been developed yet, perhaps due to the complexity of the whole process. Studies using a biochemical assay would provide many answers, such as the minimal components required for minicircle kDNA replication and the function of each component.

The pol β -like enzymes in trypanosomatids play a fundamental role in the repair of oxidative lesions in the mitochondria and kDNA replication as they are mitochondria-located in most trypanosomatids, apart from *L. infantum* and other *Leishmania* species. However, their biological functions have not been as deeply studied as their mammalian

counterparts. It is probable that many other functions will be discovered in the future as biochemical and cellular studies can progress. Also, very little is known about the regulation of its activity, which most likely is regulated at the post-translational modification level, such as phosphorylation for example. This is another interesting field to investigate.

Structural and biological studies of trypanosomatid pol β -like enzymes are limited even though they are necessary for the development of new drugs to target this enzyme family since they are key players for parasite survival. Also, other proteins of the replication machinery or kDNA repair could be targeted to treat the different diseases caused by parasites of this order. Any attempt to design drugs against components of the parasite replication machinery will necessarily require structural and biological studies of those components. We expect that soon biological and structural studies can provide fundamental molecular details on kDNA repair and kDNA replication carried out by this polymerase family in trypanosomatids.

AUTHOR CONTRIBUTIONS

Both SM-P and FU performed the bibliographical search and wrote the first draft for the manuscript. EM and AS wrote the final manuscript. All authors contributed to the article and approved the submitted version.

FUNDING

This work was funded by Grant FONDECYT 1190392 to AS and an internal Grant from the ICBM, Faculty of Medicine, the University of Chile to EM.

REFERENCES

- Abeliovich, H., Tzfati, Y., and Shlomai, J. (1993). A Trypanosomal CCHC-Type Zinc Finger Protein Which Binds the Conserved Universal Sequence of Kinetoplast DNA Minicircles: Isolation and Analysis of the Complete cDNA From *Crithidia Fasciculata*. *Mol. Cell. Biol.* 13 (12), 7766–7773. doi: 10.1128/MCB.13.12.7766
- Arevalo, J., Ramirez, L., Adai, V., Zimic, M., Tulliano, G., Miranda-Verástegui, C., et al. (2007). Influence of *Leishmania* (Viannia) Species on the Response to Antimonial Treatment in Patients With American Tegumentary Leishmaniasis. *J. Infect. Dis.* 195 (12), 1846–1851. doi: 10.1086/518041
- Beard, W. A., Horton, J. K., Prasad, R., and Wilson, S. H. (2019). Eukaryotic Base Excision Repair: New Approaches Shine Light on Mechanism. *Annu. Rev. Biochem.* 88, 137–162. doi: 10.1146/annurev-biochem-013118-111315
- Beard, W. A., and Wilson, S. H. (2014). Structure and Mechanism of DNA Polymerase β . *Biochemistry* 53 (17), 2768–2780. doi: 10.1021/bi500139h
- Beard, W. A., and Wilson, S. H. (2019). DNA Polymerase Beta and Other Gap-Filling Enzymes in Mammalian Base Excision Repair. *Enzymes* 45, 1–26. doi: 10.1016/bs.enz.2019.08.002
- Benne, R. (1990). RNA Editing in Trypanosomes: Is There a Message? *Trends Genet.* 6, 177–181. doi: 10.1016/0168-9525(90)90173-4
- Bern, C. (2015). Chagas' Disease. *N. Engl. J. Med.* 373 (5), 456–466. doi: 10.1056/NEJMr1410150
- Bienstock, R. J., Beard, W. A., and Wilson, S. H. (2014). Phylogenetic Analysis and Evolutionary Origins of DNA Polymerase X-Family Members. *DNA Repair* 22, 77–88. doi: 10.1016/j.dnarep.2014.07.003
- Botero, A., Kapeller, I., Cooper, C., Clode, P. L., Shlomai, J., and Thompson, R. A. (2018). The Kinetoplast DNA of the Australian Trypanosome, *Trypanosoma Copemani*, Shares Features With *Trypanosoma Cruzi* and *Trypanosoma Lewisi*. *Int. J. Parasitol.* 48 (9–10), 691–700. doi: 10.1016/j.ijpara.2018.02.006
- Braithwaite, E. K., Kedar, P. S., Lan, L., Polosina, Y. Y., Asagoshi, K., Poltoratsky, V. P., et al. (2005). DNA Polymerase λ Protects Mouse Fibroblasts Against Oxidative DNA Damage and Is Recruited to Sites of DNA Damage/Repair. *J. Biol. Chem.* 280 (36), 31641–31647. doi: 10.1074/jbc.C500256200
- Braithwaite, E. K., Prasad, R., Shock, D. D., Hou, E. W., Beard, W. A., and Wilson, S. H. (2005). DNA Polymerase λ Mediates a Back-Up Base Excision Repair Activity in Extracts of Mouse Embryonic Fibroblasts. *J. Biol. Chem.* 280 (18), 18469–18475. doi: 10.1074/jbc.M411864200
- Bruhn, D. F., Mozeleski, B., Falkin, L., and Klingbeil, M. M. (2010). Mitochondrial DNA Polymerase POLIB Is Essential for Minicircle DNA Replication in African Trypanosomes. *Mol. Microbiol.* 75 (6), 1414–1425. doi: 10.1111/j.1365-2958.2010.07061.x
- Camargo, E. P. (1999). Phytomonas and Other Trypanosomatid Parasites of Plants and Fruit. *Adv. Parasitol.* 42, 29–112. doi: 10.1016/S0065-308X(08)60148-7
- Cavalcanti, D. P., and de Souza, W. (2018). The Kinetoplast of Trypanosomatids: From Early Studies of Electron Microscopy to Recent Advances in Atomic Force Microscopy. *Scanning* 2018, 9603051. doi: 10.1155/2018/9603051
- Chogas, E. (1986). Molecular Biology of *Leishmania*. *Parasitol Today* 2 (2), 45.
- Coelho, E. R., Úrményi, T. P., da Silva, J. F., Rondinelli, E., and Silva, R. (2003). Identification of PDZ5, a Candidate Universal Minicircle Sequence Binding Protein of *Trypanosoma Cruzi*. *Int. J. Parasitol.* 33 (8), 853–858. doi: 10.1016/S0020-7519(03)00107-3
- Conteh, L., Engels, T., and Molyneux, D. H. (2010). Socioeconomic Aspects of Neglected Tropical Diseases. *Lancet* 375 (9710), 239–247. doi: 10.1016/S0140-6736(09)61422-7
- Cruz, A. K., Titus, R., and Beverley, S. M. (1993). Plasticity in Chromosome Number and Testing of Essential Genes in *Leishmania* by Targeting. *Proc. Natl. Acad. Sci.* 90 (4), 1599–1603. doi: 10.1073/pnas.90.4.1599
- Delarue, M., Boule, J. B., Lescar, J., Expert-Bezançon, N., Jourdan, N., Sukumar, N., et al. (2002). Crystal Structures of a Template-Independent DNA Polymerase: Murine Terminal Deoxynucleotidyltransferase. *EMBO J.* 21 (3), 427–439. doi: 10.1093/emboj/21.3.427
- de Oliveira Lopes, D., Schamber-Reis, B. L. F., Regis-da-Silva, C. G., Rajão, M. A., DaRocha, W. D., Macedo, A. M., et al. (2008). Biochemical Studies With DNA Polymerase β and DNA Polymerase β -PAK of *Trypanosoma Cruzi* Suggest the Involvement of These Proteins in Mitochondrial DNA Maintenance. *DNA Repair* 7 (11), 1882–1892. doi: 10.1016/j.dnarep.2008.07.018
- De Pablos, L. M., Ferreira, T. R., and Walrad, P. B. (2016). Developmental Differentiation in *Leishmania* Lifecycle Progression: Post-Transcriptional Control Conducts the Orchestra. *Curr. Opin. Microbiol.* 34, 82–89. doi: 10.1016/j.mib.2016.08.004
- Dollet, M., Sturm, N. R., Sánchez-Moreno, M., and Campbell, D. A. (2000). 5s Ribosomal RNA Gene Repeat Sequences Define at Least Eight Groups of Plant Trypanosomatids (Phytomonas Spp.): Phloem-Restricted Pathogens Form a Distinct Section. *J. Eukaryotic Microbiol.* 47 (6), 569–574. doi: 10.1111/j.1550-7408.2000.tb00091.x
- Englund, P. T. (2014). A Passion for Parasites. *J. Biol. Chem.* 289 (49), 33712–33729. doi: 10.1074/jbc.X114.620666
- García-Díaz, M., Bebenek, K., Kunkel, T. A., and Blanco, L. (2001). Identification of an Intrinsic 5'-Deoxyribose-5-Phosphate Lyase Activity in Human DNA Polymerase λ : A Possible Role in Base Excision Repair. *J. Biol. Chem.* 276 (37), 34659–34663. doi: 10.1074/jbc.M106336200
- Gibson, W. (1990). *Trypanosoma* Diversity in Lambwe Valley, Kenya-Sex or Selection? *Parasitol Today* 6 (11), 342–343. doi: 10.1016/0169-4758(90)90408-v
- Haag, J., O'hugin, C., and Overath, P. (1998). The Molecular Phylogeny of Trypanosomes: Evidence for an Early Divergence of the Salivaria. *Mol. Biochem. Parasitol.* 91 (1), 37–49. doi: 10.1016/S0166-6851(97)00185-0
- Hamilton, P. B., Stevens, J. R., Gaunt, M. W., Gidley, J., and Gibson, W. C. (2004). Trypanosomes Are Monophyletic: Evidence From Genes for Glyceraldehyde Phosphate Dehydrogenase and Small Subunit Ribosomal RNA. *Int. J. Parasitol.* 34 (12), 1393–1404. doi: 10.1016/j.ijpara.2004.08.011
- Heitman, J., Carter, D. A., Dyer, P. S., and Soll, D. R. (2014). Sexual Reproduction of Human Fungal Pathogens. *Cold Spring Harbor Perspect. Med.* 4 (8), a019281. doi: 10.1101/cshperspect.a019281
- Howard, M. J., Horton, J. K., Zhao, M. L., and Wilson, S. H. (2020). Lysines in the Lyase Active Site of DNA Polymerase β Destabilize Nonspecific DNA Binding, Facilitating Searching and DNA Gap Recognition. *J. Biol. Chem.* 295 (34), 12181–12187. doi: 10.1074/jbc.RA120.013547
- Howard, M. J., Rodriguez, Y., and Wilson, S. H. (2017). DNA Polymerase β Uses its Lyase Domain in a Processive Search for DNA Damage. *Nucleic Acids Res.* 45 (7), 3822–3832. doi: 10.1093/nar/gkx047
- Howard, M. J., and Wilson, S. H. (2017). Processive Searching Ability Varies Among Members of the Gap-Filling DNA Polymerase X Family. *J. Biol. Chem.* 292 (42), 17473–17481. doi: 10.1074/jbc.M117.801860
- Jensen, R. E., and Englund, P. T. (2012). Network News: The Replication of Kinetoplast DNA. *Annu. Rev. Microbiol.* 66, 473–491. doi: 10.1146/annurev-micro-092611-150057
- Kaufman, B. A., and Van Houten, B. (2017). POLB: A New Role of DNA Polymerase Beta in Mitochondrial Base Excision Repair. *DNA Repair* 60, A1–A5. doi: 10.1016/j.dnarep.2017.11.002
- Krokan, H. E., and Bjørås, M. (2013). Base Excision Repair. *Cold Spring Harbor Perspect. Biol.* 5 (4), a012583. doi: 10.1101/cshperspect.a012583
- Lafont, A. (1909). Sur La Présence D'un Parasite De La Classe Des Flagellés Dans Le Latex De *Euphorbia Pilulifera*. *CR Soc. Biol.* 66, 1011–1013.
- Laurent, T., Rijal, S., Yardley, V., Croft, S., De Doncker, S., Decuypere, S., et al. (2007). Epidemiological Dynamics of Antimonial Resistance in *Leishmania* Donovanii: Genotyping Reveals a Polyclonal Population Structure Among Naturally-Resistant Clinical Isolates From Nepal. *Infect. Genet. Evol.* 7 (2), 206–212. doi: 10.1016/j.meegid.2006.08.005
- Lee, B. Y., Bacon, K. M., Bottazzi, M. E., and Hotez, P. J. (2013). Global Economic Burden of Chagas Disease: A Computational Simulation Model. *Lancet Infect. Dis.* 13 (4), 342–348. doi: 10.1016/S1473-3099(13)70002-1
- Maldonado, E., Rojas, D. A., Moreira-Ramos, S., Urbina, F., Miralles, V. J., Solari, A., et al. (2015). Expression, Purification, and Biochemical Characterization of Recombinant DNA Polymerase Beta of the *Trypanosoma Cruzi* TcI Lineage: Requirement of Additional Factors and Detection of Phosphorylation of the Native Form. *Parasitol. Res.* 114 (4), 1313–1326. doi: 10.1007/s00436-014-4308-8
- Mejia, E., Burak, M., Alonso, A., Larraga, V., Kunkel, T. A., Bebenek, K., et al. (2014). Structures of the *Leishmania Infantum* Polymerase Beta. *DNA Repair* 18, 1–9. doi: 10.1016/j.dnarep.2014.03.001
- Milman, N., Motyka, S. A., Englund, P. T., Robinson, D., and Shlomai, J. (2007). Mitochondrial Origin-Binding Protein UMSBP Mediates DNA Replication and Segregation in Trypanosomes. *Proc. Natl. Acad. Sci.* 104 (49), 19250–19255. doi: 10.1073/pnas.0706858104

- Minia, I., Merce, C., Terrao, M., and Clayton, C. (2016). Translation Regulation and RNA Granule Formation After Heat Shock of Procyclic Form *Trypanosoma Brucei*: Many Heat-Induced mRNAs Are Also Increased During Differentiation to Mammalian-Infective Forms. *PLoS Negl. Trop. Dis.* 10 (9), e0004982. doi: 10.1371/journal.pntd.0004982
- Mullins, E. A., Rodriguez, A. A., Bradley, N. P., and Eichman, B. F. (2019). Emerging Roles of DNA Glycosylases and the Base Excision Repair Pathway. *Trends Biochem. Sci.* 44 (9), 765–781. doi: 10.1016/j.tibs.2019.04.006
- Nussbaum, K., Honek, J., Cadmus, C. M. C., and Efferth, T. (2010). Trypanosomatid Parasites Causing Neglected Diseases. *Curr. Med. Chem.* 17 (15), 1594–1617. doi: 10.2174/092986710790979953
- Overath, P., Haag, J., Lischke, A., and O'hugin, C. (2001). The Surface Structure of Trypanosomes in Relation to Their Molecular Phylogeny. *Int. J. Parasitol.* 31 (5–6), 468–471. doi: 10.1016/s0020-7519(01)00152-7
- Prasad, R., Çağlayan, M., Dai, D. P., Nadalutti, C. A., Zhao, M. L., Gassman, N. R., et al. (2017). DNA Polymerase β : A Missing Link of the Base Excision Repair Machinery in Mammalian Mitochondria. *DNA Repair* 60, 77–88. doi: 10.1016/j.dnarep.2017.10.011
- Rajao, M. A., Furtado, C., Alves, C. L., Passos-Silva, D. G., de Moura, M. B., Schamber-Reis, B. L., et al. (2014). Unveiling Benznidazole's Mechanism of Action Through Overexpression of DNA Repair Proteins in *Trypanosoma Cruzi*. *Environ. Mol. Mutagen.* 55 (4), 309–321. doi: 10.1002/em.21839
- Ravoet, J., Maharrov, J., Meeus, I., De Smet, L., Wenseleers, T., Smaghe, G., et al. (2013). Comprehensive Bee Pathogen Screening in Belgium Reveals *Crithidia Mellificae* as a New Contributory Factor to Winter Mortality. *PLoS One* 8 (8), e72443. doi: 10.1371/journal.pone.0072443
- Ray, D. S. (1989). Conserved Sequence Blocks in Kinetoplast Minicircles From Diverse Species of Trypanosomes. *Mol. Cell. Biol.* 9 (3), 1365–1367. doi: 10.1128/MCB.9.3.1365
- Rojas, D. A., Urbina, F., Moreira-Ramos, S., Castillo, C., Kemmerling, U., Lapier, M., et al. (2018). Endogenous Overexpression of an Active Phosphorylated Form of DNA Polymerase β Under Oxidative Stress in *Trypanosoma Cruzi*. *PLoS Neglected Trop. Dis.* 12 (2), e0006220. doi: 10.1371/journal.pntd.0006220
- Rono, M. K., Nyonda, M. A., Simam, J. J., Ngoyi, J. M., Mok, S., Kortok, M. M., et al. (2018). Adaptation of *Plasmodium Falciparum* to its Transmission Environment. *Nat. Ecol. Evol.* 2 (2), 377–387. doi: 10.1038/s41559-017-0419-9
- Runkel, C., DeRisi, J., and Flenniken, M. L. (2014). A Draft Genome of the Honey Bee Trypanosomatid Parasite *Crithidia Mellificae*. *PLoS One* 9 (4), e95057. doi: 10.1371/journal.pone.0095057
- Saxowsky, T. T., Choudhary, G., Klingbeil, M. M., and Englund, P. T. (2003). *Trypanosoma Brucei* has Two Distinct Mitochondrial DNA Polymerase β Enzymes. *J. Biol. Chem.* 278 (49), 49095–49101. doi: 10.1074/jbc.M308565200
- Schamber-Reis, B. L. F., Nardelli, S., Régis-Silva, C. G., Campos, P. C., Cerqueira, P. G., Lima, S. A., et al. (2012). DNA Polymerase Beta From *Trypanosoma Cruzi* Is Involved in Kinetoplast DNA Replication and Repair of Oxidative Lesions. *Mol. Biochem. Parasitol.* 183 (2), 122–131. doi: 10.1016/j.molbiopara.2012.02.007
- Scocca, J. R., and Shapiro, T. A. (2008). A Mitochondrial Topoisomerase IA Essential for Late Theta Structure Resolution in African Trypanosomes. *Mol. Microbiol.* 67 (4), 820–829. doi: 10.1111/j.1365-2958.2007.06087.x
- Sela, D., and Shlomai, J. (2009). Regulation of UMSBP Activities Through Redox-Sensitive Protein Domains. *Nucleic Acids Res.* 37 (1), 279–288. doi: 10.1093/nar/gkn927
- Singh, R., Purkait, B., Abhishek, K., Saini, S., Das, S., Verma, S., et al. (2016). Universal Minicircle Sequence Binding Protein of *Leishmania Donovanii* Regulates Pathogenicity by Controlling Expression of Cytochrome-B. *Cell Biosci.* 6 (1), 1–17. doi: 10.1186/s13578-016-0072-z
- Stevens, J., and Gibson, W. (1990). The Evolution of Salivarian Trypanosomes. *Memórias do Instituto Oswaldo Cruz* 94 (2), 225–228. doi: 10.1590/s0074-02761999000200019
- Sturm, N. R., Dollet, M., Lukeš, J., and Campbell, D. A. (2007). Rational Sub-Division of Plant Trypanosomes (*Phytomonas* Spp.) Based on Minicircle Conserved Region Analysis. *Infection Genet. Evol.* 7 (5), 570–576. doi: 10.1016/j.meegid.2007.04.002
- Sykora, P., Kanno, S., Akbari, M., Kulikowicz, T., Baptiste, B. A., Leandro, G. S., et al. (2017). DNA Polymerase Beta Participates in Mitochondrial DNA Repair. *Mol. Cell. Biol.* 37 (16). doi: 10.1128/MCB.00237-17
- Taladriz, S., Hanke, T., Ramiro, M. J., García-Díaz, M., García de Iacoba, M., Blanco, L., et al. (2001). Nuclear DNA Polymerase Beta From *Leishmania Infantum*. Cloning, Molecular Analysis and Developmental Regulation. *Nucleic Acids Res.* 29 (18), 3822–3834. doi: 10.1093/nar/29.18.3822
- Torres-Guerrero, E., Quintanilla-Cedillo, M. R., Ruiz-Esmerjand, J., and Arenas, R. (2017). Leishmaniasis: A Review. *F1000Research* 6. doi: 10.12688/f1000research.11120.1
- Torri, A. F., and Englund, P. T. (1995). A DNA Polymerase β in the Mitochondrion of the Trypanosomatid *Crithidia Fasciculata*. *J. Biol. Chem.* 270 (8), 3495–3497. doi: 10.1074/jbc.270.8.3495
- Torri, A. F., Kunkel, T. A., and Englund, P. T. (1994). A Beta-Like DNA Polymerase From the Mitochondrion of the Trypanosomatid *Crithidia Fasciculata*. *J. Biol. Chem.* 269 (11), 8165–8171. doi: 10.1016/S0021-9258(17)37175-2
- Tzfati, Y., Abeliovich, H., Avrahami, D., and Shlomai, J. (1995). Universal Minicircle Sequence Binding Protein, a CCHC-Type Zinc Finger Protein That Binds the Universal Minicircle Sequence of Trypanosomatids: Purification and Characterization. *J. Biol. Chem.* 270 (36), 21339–21345. doi: 10.1074/jbc.270.36.21339
- Venegas, J. A., Åslund, L., and Solari, A. (2009). Cloning and Characterization of a DNA Polymerase β Gene From *Trypanosoma Cruzi*. *Parasitol. Int.* 58 (2), 187–192. doi: 10.1016/j.parint.2009.01.007
- Venegas, J., and Solari, A. (1995). Purification and Characterization of a β -Like DNA Polymerase From *Trypanosoma Cruzi*. *Mol. Biochem. Parasitol.* 73 (1–2), 53–62. doi: 10.1016/0166-6851(94)00091-Z
- Votýpka, J., Maslov, D. A., Yurchenko, V., Jirků, M., Kment, P., Lun, Z. R., et al. (2010). Probing Into the Diversity of Trypanosomatid Flagellates Parasitizing Insect Hosts in South-West China Reveals Both Endemism and Global Dispersal. *Mol. Phylogenet. Evol.* 54 (1), 243–253. doi: 10.1016/j.jympev.2009.10.014
- Wang, Z., Morris, J. C., Drew, M. E., and Englund, P. T. (2000). Inhibition of *Trypanosoma Brucei* Gene Expression by RNA Interference Using an Integratable Vector With Opposing T7 Promoters. *J. Biol. Chem.* 275 (51), 40174–40179. doi: 10.1074/jbc.M008405200
- Westenberger, S. J., Barnabé, C., Campbell, D. A., and Sturm, N. R. (2005). Two Hybridization Events Define the Population Structure of *Trypanosoma Cruzi*. *Genetics* 171 (2), 527–543. doi: 10.1534/genetics.104.038745
- Whitaker, A. M., and Freudenthal, B. D. (2020). History of DNA Polymerase β X-Ray Crystallography. *DNA Repair*, 93, 102928. doi: 10.1016/j.dnarep.2020.102928
- Yamlich, J., and Sweasy, J. B. (2010). DNA Polymerase Family X: Function, Structure, and Cellular Roles. *Biochim. Biophys. Acta (BBA)-Proteins Proteomics* 1804 (5), 1136–1150. doi: 10.1016/j.bbapap.2009.07.008

Conflict of Interest: The authors declare that the research was conducted in the absence of any commercial or financial relationships that could be construed as a potential conflict of interest.

Publisher's Note: All claims expressed in this article are solely those of the authors and do not necessarily represent those of their affiliated organizations, or those of the publisher, the editors and the reviewers. Any product that may be evaluated in this article, or claim that may be made by its manufacturer, is not guaranteed or endorsed by the publisher.

Copyright © 2021 Maldonado, Morales-Pison, Urbina and Solari. This is an open-access article distributed under the terms of the Creative Commons Attribution License (CC BY). The use, distribution or reproduction in other forums is permitted, provided the original author(s) and the copyright owner(s) are credited and that the original publication in this journal is cited, in accordance with accepted academic practice. No use, distribution or reproduction is permitted which does not comply with these terms.

Advantages of publishing in Frontiers



OPEN ACCESS

Articles are free to read
for greatest visibility
and readership



FAST PUBLICATION

Around 90 days
from submission
to decision



HIGH QUALITY PEER-REVIEW

Rigorous, collaborative,
and constructive
peer-review



TRANSPARENT PEER-REVIEW

Editors and reviewers
acknowledged by name
on published articles

Frontiers

Avenue du Tribunal-Fédéral 34
1005 Lausanne | Switzerland

Visit us: www.frontiersin.org

Contact us: frontiersin.org/about/contact



REPRODUCIBILITY OF RESEARCH

Support open data
and methods to enhance
research reproducibility



DIGITAL PUBLISHING

Articles designed
for optimal readership
across devices



FOLLOW US

@frontiersin



IMPACT METRICS

Advanced article metrics
track visibility across
digital media



EXTENSIVE PROMOTION

Marketing
and promotion
of impactful research



LOOP RESEARCH NETWORK

Our network
increases your
article's readership